OPTICAL TECHNOLOGY
APOLLO EXTENSION SYSTEM
PART I

FINAL TECHNICAL REPORT

VOLUME II

Section 3 - Systems Integration

CONTRACT NAS 8-20256

GPO PRICE $ _____

CFSTI PRICE(S) $ _____

Hard copy (HC) 2.00

Microfiche (MF) 1.75

ff 653 July 65

FACILITY FORM 602

N67 12056 (ACCESSION NUMBER)

355 (PAGES)

CR-79477 (NASA CR OR TMX OR AD NUMBER)

(THRU)

1 (CODE)

14 (CATEGORY)

SPACE DIVISION CHRYSLER CORPORATION

OPTICAL TECHNOLOGY
APOLLO EXTENSION SYSTEM
PART I

FINAL TECHNICAL REPORT

VOLUME II

Section 3 - SYSTEMS INTEGRATION

CONTRACT NAS 8-20256
October 21, 1966

Approved by: William W Kloepfer
William W. Kloepfer
Program Manager

CHRYSLER CORPORATION SPACE DIVISION, MICHOUD ASSEMBLY FACILITY
P.O. BOX 29200, NEW ORLEANS, LA. 70129

2857A-10-18-66

MASTER

TABLE OF CONTENTS

Volume	Title
I	Section I - Introduction Section II - Experiment Development
II	Section III - Systems Integration
III	Section IV - Technology Development Plan

PRECEDING PAGE BLANK NOT FILMED.

VOLUME II

TABLE OF CONTENTS

Section	Title	Page
III	SYSTEMS INTEGRATION	2-1
	7.0 Experiment Grouping	2-1
	7.1 Manning Requirements	2-1
	7.2 Orbital Requirements	2-7
	7.3 Experiment Groups	2-8
	8.0 Optical Propagation Experiment Group	2-12
	8.1 Telescope Requirements	2-12
	8.2 One Meter Telescope	2-18
	8.3 Strapped Down Telescope	2-46
	8.4 Gimballed Telescope	2-50
	9.0 Stellar Oriented Experiment Group	2-61
	9.1 Telescope Requirements	2-61
	9.2 Fine Guidance Telescope	2-65
	10.0 OTAES Mission Development	2-71
	10.1 Candidate Missions	2-77
	10.2 Recommended Missions	2-92
	10.3 AAP Mission Constraints	2-100
	10.4 Ground Station Concepts	2-103
	11.0 Supporting Spacecraft Subsystems	2-116
	11.1 Candidate Spacecraft Concept	2-116
	11.2 Recommended Spacecraft Concept	2-163
	11.3 Structural and Mechanical	2-171
	11.4 Stabilization and Control	2-202
	11.5 Power	2-257
	11.6 Environmental Control	2-308
	12.0 Experiment/Mission Time Phasing	2-327
	13.0 Typical OTAES Subsystem/Component Summary	2-347

PRECEDING PAGE BLANK NOT FILMED.

SECTION III

SYSTEMS INTEGRATION

7.0 EXPERIMENT GROUPING

The principle objective of this study was to develop optical technology experiments which would support an overall technology development program. Once these experiments were identified and conceptually designed the next objective was to consider the problems associated with performing these experiments integrated into a space mission. To do so involved arranging the experiments into groups which were compatible from the standpoint of manning requirements, orbital requirements and equipment. These groups were then used as a basis for developing OTAES mission and spacecraft concepts.

7.1 MANNING REQUIREMENTS

It is the objective of this section to assess the criticality of the flight crew's participation in the selected optical technology experiments. Therefore, each experiment is discussed individually. After these discussions, a matrix summary is presented on man's criticality for all experiments.

Identification of the flight crew's activites within the content of mission phases, events and necessary CSM/OM spacecraft system sequences will be treated in section 12.0, Volume II, on experiment/mission time phasing.

7.1.1 Optical Heterodyne Detection on Earth

For this experiment and subsequent eight laser experiments, man will be useful in turning on and stabilizing the three laser telescopes and associated electronics, prior to experiment operations. He will align the applicable telescopes, conduct tests on laser transmitter performance and make optical and electrical adjustments.

For this particular experiment, man will also be useful for diagnostic and remedial maintenance, such as, detection and replacement of burnt-out laser cathode heaters and switchover from an automatic laser acquisition mode to a manual backup mode. In case of telescope failure, the basic 0.6328 experiment can still be performed by man switching over to the backup 0.6328 transmitter.

During the operation of the experiment, it may be necessary to restrain the crew so as not to induce motions.

7.1.2 Optical Heterodyne Detection on the Spacecraft

From the standpoint of man's utility in space, this experiment is similar to the Optical Heterodyne Detection on Earth experiment. However, man will perform precise alignment of the Heterodyne receivers.

7.1.3 Direct Detection from Space to Ground

The nature of man's inflight activities will be similar to the Optical Heterodyne Detection on Earth experiment. Both experiments will use the same equipment, but operating requirements will be relaxed for the Direct Detection experiment, e.g., wider beam widths and less stringent pointing accuracy. Thus the flight crew can perform restrained or unrestrained body movements during the operation of this experiment, but the ground station should be informed when these movements occur.

7.1.4 Communication with 10 Megahertz Bandwidth

Man will be highly desirable for aligning the pick-off optics following shifts to lasers of different frequency. He will also make minor adjustments in frequency to overcome doppler effects.

In addition, man will select different combinations of digital, sinusoidal, voice, television dot or television picture signal sources to match analog and digital coding forms for FM, PL, or AM modulation. For real-time video ground coverage and concurrent ground analyses of inflight operational events, the flight crew will be able to direct television cameras for ground monitoring during IVA and EVA.

7.1.5 Precision Tracking of a Ground Beacon

In this experiment, as in the two subsequent experiments, man's participation will be useful, and on the other hand, his motions (inducing spacecraft perturbations) can be undesirable. This situation arises because the experiment's purpose is to determine the laser optical systems' ability for fine pointing. Initially, measures of tracking accuracy should be obtained in stably oriented spacecraft, with the restrained crew minimizing their motions. However, it will be necessary to measure the impact of crew motion disturbances upon tracking accuracy in order to answer questions for operational system design. Man will be necessary for monitoring his own unprogrammed motions in the spacecraft. He will also act as a source of intentional disturbance, undertaking a programmed series of motions. During these unprogrammed and programmed motions, tracking accuracy is to be determined.

Man will monitor the cloud cover, earthshine and weather conditions in the atmosphere.

In addition, he will perform periodic system checks, and, when necessary, remedial repairs or replacements of accessible malfunctioning components. In case of a partial failure of the Precision Tracking system, man will be able to override the system and obtain partial information.

7.1.6 Point-Ahead and Space to Ground Loop Closure

This experiment employs the same equipment as the Precision Tracking experiment, but in a different operational mode, and the usefulness of man's involvement is similarly assessed.

7.1.7 Transfer Tracking from One Ground Station to Another

This experiment employs the same equipment as the Precision Tracking experiment, but in a different operational mode, and the usefulness of man's involvement is similarly assessed.

7.1.8 Phase Correlation Measurements

Man will be highly desirable in setting up requisite conditions in the spacecraft for conducting the experiment. He will have to align the laser transmitter. He will be useful in placing the transmitter in a single frequency, continuous wave mode for correlation with obtained results from the 10.6 micron transmitter.

During equipment operations, man's motions may be restrained in order for the lasers to maintain tracking with the ground.

7.1.9 Pulse Distortion Measurements

The importance and nature of man's contribution to this experiment are similar to those described for the Phase Correlation Experiment. The exception is that the 0.6328 transmitter will be placed in a pulsing mode lock.

7.1.10 Primary Mirror Figure Test and Correction

Man will be most efficient in setting up the instrumentation for the experiment. His participation will be essential in conducting large portions of the experiment, since the man-machine loop will form a continuous information interpretation, decision-making, and processing channel with the human element often allocated the major role, e.g., employment of the Foucault knife-edge test.

Furthermore, man can assist in encoding and transmitting experimental results to ground stations and replenishing film.

He will also be essential for removing and replacing optical instrumentation, since an in-space handling operation is difficult to perform by remote control from the earth.

7.1.11 Thin Mirror Nesting Verification

Man is essential in this experiment, since its objective is to investigate the feasibility of a man to assembly, align and test a 50 inch optical system in orbit. His participation in this experiment is similar in many respects to his activities in the Primary Mirror Figure Test and Correction Experiment.

7.1.12 Fine Guidance

Man will be a highly desirable tool in aligning the fine guidance optics in the telescope. His presence will offer the capability for switching between presently conceived alternate modes of operation, e.g., selecting between two fine error sensors. However, spacecraft perturbation due to man's motions can be a serious impediment to the successful completion of the experiment.

He will also be highly desirable in evaluating the fine guidance performance in space.

7.1.13 Comparison of Isolation Techniques

The objective of the experiment is to compare suspension systems for isolating spacecraft telescopes from man-produced disturbances.

It is possible to attempt to simulate man's disturbances in an unmanned spacecraft, but this is not an attractive approach. There is scanty empirical data on human body segment motions (i.e., direction, magnitude, duration, rate and force/torque application) under simulated and actual weightlessness in shirtsleeves, vented spacesuit and pressurized spacesuit conditions. Exact ground-based empirical studies of man-produced spacecraft disturbances under simulated weightlessness are difficult and have not been conducted. It is not feasible to endeavor to verify the results of analytical ground efforts on man-produced spacecraft disturbances without actual experimentation aboard an inflight spacecraft. Therefore, man's involvement in performing unprogrammed and programmed body motions is highly desirable in the experiment.

A high desirable rating also applies to the real-time recording and monitoring of the experiment.

Furthermore, if malfunctioning of the automatic suspension system control instrumentation would occur, man can be useful as a manual backup to install and remove the telescope suspension systems components.

7.1.14 Interferometer System

Man's participation will be useful in EVA assembly and deployment of the short and long interferometer beams. He will be essential in positioning the flat mirrors on the outboard beams, since it will be necessary for him to interpret interference patterns. Present electromechanical sensors would yield ambiguous results.

As a continuous information interpretation, decision-making and processing channel in the man-machine loop, man will be essential in conducting interferometer experiment operations. During these operations, man will bring the interferometer displayed pencils into the field of view, check optical alignments, adjust for equality of path length with double wedges, adjust for coincidence of the pencils with the mirror, and adjust for equality of path length in the pencils.

Man will also be essential in performing unprogrammed and programmed body motions to subject the optical beam to disturbance influences, measure the resulting beam motion, and observe the effect on image quality.

Furthermore, man will be useful in data communications and management function by switching on recording and telemetry modes which will initiate storage and transmission to the ground of experimental information.

7.1.15 Segmented Optics

Man will be essential in aligning the three segments of the 24 inch diameter mirror in the telescope, such that the Ronchi test pattern lines appear continuous.

After perceiving line continuity, he will be useful in actuating spacecraft pitch, roll and yaw attitude slewing controls and acquiring either a planetary or stellar target in the telescope field of view, while monitoring a display through an eyepiece.

7.1.16 Degradation of Optical Materials and Coatings

Man will be useful in retrieving the test panel from the Cumulative Exposure Experiment Box prior to earth return. Man can also emplace a substitute test panel in the Experiment Box. This new test panel would be exposed to the space environment during the unmanned portion of the spacecraft flight after post-CSM separation. After a specified period of lapsed time, man could return in another vehicle to the unmanned spacecraft, rendezvous with the spacecraft, and retrieve the second emplaced test panel.

Experiment Summary

It is this sections' intent to summarize man's criticality in the individual optical technology experiments. To accomplish this, table 7.1-1 has been constructed to serve as an overview of man's participation in the mission experiments.

In the table, four categories of clustered human functions are rated. The categories are based on current concepts for experiment setup and alignment, operations communication and data management, and preventive and remedial maintenance.

The criticality rating entries for each experiment-category cell consist of either A, B, C, D, or E or a combination thereof. The determination of the criticality level for each cell (applying to A, B. and C) is set by the highest rating for a component human function associated with the cell.

The rationale for the criticality ratings are as follows: a) a rating of "A" indicates that man's functions are essential, i.e., the experiment, as presently conceived, cannot be carried out in an unmanned mode; b) a rating

TABLE 7.1-1

CRITICALITY OF MAN'S PARTICIPATION

EXPERIMENT \ HUMAN FUNCTION CLUSTER	PREPARATION & SET-UP	EXPERIMENT OPERATIONS	COMMUNICATION AND DATA MANAGEMENT	PREVENTIVE & REMEDIAL MAINTENANCE
Optical Heterodyne Detection on Earth	C	CD	C	C
Optical Heterodyne Detection on the Spacecraft	C	CD	C	C
Communication with 10 Megahertz Bandwidth	B	CD	B	C
Direct Detection from Space to Ground	B	CD	E	C
Precision Tracking of a Ground Beacon	C	CD	E	C
Point Ahead and Space-to-Ground-to-Space Loop Closure	C	CD	E	C
Transfer Tracking from One Ground Station to Another	C	CD	C	C
Phase Correlation Measurements	B	CD	C	C
Pulse Distortion Measurements	B	CD	C	C
Primary Mirror Figure Test and Correction	B	A	A	C
Thin Mirror Nesting Verification	A	BD	C	C
Fine Guidance	B	BD	C	C
Comparison of Isolation Techniques	B	B	B	C
Interferometer System	A	A	C	C
Segmented Optics	A	C	A	C
Degradation of Optical Materials and Coatings	C	E	E	C

KEY: A = Man is essential.
B = Man is best, most efficient and/or hightly desirable.
C = Man can perform useful tasks.
D = Man could be undesirable.
E = Man is not involved.

of "B" means that the performance of one or more experiment-related functions could best or most efficiently be carried out with man's participation. Unmanned operation is feasible, but would entail severe penalties in terms of such factors as equipment complexity, weight, reliability, system life, comprehensiveness of data collection; c) a rating of "C" indicates that man's presence is not specifically justified by the functions required for a particular experiment, but that he could perform certain useful tasks and might prove desirable in the interests of design simplicity and experiment flexibility; d) a rating of "D" indicates experiment functions could be negatively effected by man, such as, crew motions inducing spacecraft attitude disturbances; and e) a rating "E" indicates that man's participation is not required or useful for a particular function.

7.2 ORBITAL REQUIREMENTS

Mission variables which affect performance of a given OTAES experiment and which are functions of orbit parameters include maximum lengths of uninterrupted observation times, orbital velocities, sun shadow times, and contact profiles for given ground stations.

Orbital velocities accrue doppler shifts which can be detrimental if the doppler shift range is significant during the operating time of the experiment. For heterodyne laser communications experiments, doppler shift tolerance is dictated by the laser resonance envelope. The OTAES Helium-Neon laser systems, for example, can tolerate shifts of 600 MHz, which obtain for closing velocities of about 360 m/sec. This would reduce useable portions of near earth orbits since closing velocities of up to 6600 m/sec result for these orbits. The direct detection systems are limited only by the front-end filters of 2 to 200Å bandpass which are useable over the range of doppler shifts for any of the candidate missions.

For the laser communications point-ahead experiments and station transfer experiments, it is important that the angle between the lines-of-sight from the spacecraft to two ground stations should remain constant, or at most should vary slowly such as for synchronous orbits of moderate or no inclinations.

If the experiment runs are reduced by system constraints towards fractions of an hour, then the value of the data collected degrades very rapidly due to time required for such preparatory processes as acquisition. The laser experiments which rely on a ground station link techniques are particularly affected due to the nature of contact profiles related to each orbit/ground-net combinations.

Contact profiles degrade significantly for the near earth orbits, as compared to synchronous orbits. For a single ground station, long-time average of contact duty cycle would be 14 per cent for an equatorial station and equatorial orbit. This maximum of 14 per cent duty cycle quickly reduces

to less than a few per cent for a ground station at 35° latitude. When acquisition times and minimum depression angles for optical links are considered, the use of near earth orbits for the optical communications experiments becomes extremely limited.

In general, it can be concluded that laser experiments are best effected from a synchronous orbit. This will allow measurements over a sufficiently long time to obtain statistically meaningful data, as well as to monitor minute-by-minute changes in atmospheric conditions with a fixed line-of-sight. In addition to this, measurements from lower altitude vehicles would be complicated by large angular tracking rates.

The interferometer system experiment requiring long term dimensional stability is sensitive to thermal unbalance. This makes the synchronous orbit preferable over the near earth orbit due to the associated shadow time effects.

The fine pointing experiment may require continuous observation times of the order of one hour or more. However, the uninterrupted observational time lengths generally are not a severe constraint in that proper choice of stellar targets relative to the orbit plane can permit continuous observations. Figure 7.2-1, "Observation Time as a Function of View Angle", shows this increase in view time as the target line of sight is chosen to have increasingly greater angle with the orbit plane.

The following experiments are not sensitive to the parameters discussed above: Primary Mirror Figure Test and Correction, Thin Mirror Nesting Verification, Comparison of Isolation Techniques, Segmented Optics, Cryogenic Cooling Experiment, Degradation of Optical Materials and Coatings, and the Interference Spectrometer. For these and other experiment, of course, the final trade-off will involve the launch vehicle costs associated with each orbital choice. However, these cost trade-offs aren't treated in this part of the study.

The elliptical orbits have been discarded at this time due to the high radiation dosages associated with the daily traverses of the trapped radiation belts. This radiation environment is intolerable by the astrionic black boxes and also by the crew and other subsystems, especially solar cell power systems.

7.3 EXPERIMENT GROUPS

Table 7.3-1 summarizes the manning and orbital requirements for the Optical Technology Experiments now being recommended.

It can be seen that the experiments can be separated into two basic groups. For the laser oriented experiments, synchronous orbits are preferred and the manning is optional. Manned operations is preferred for the mirror figure and stellar-oriented experiments. Also, each of these experiments,

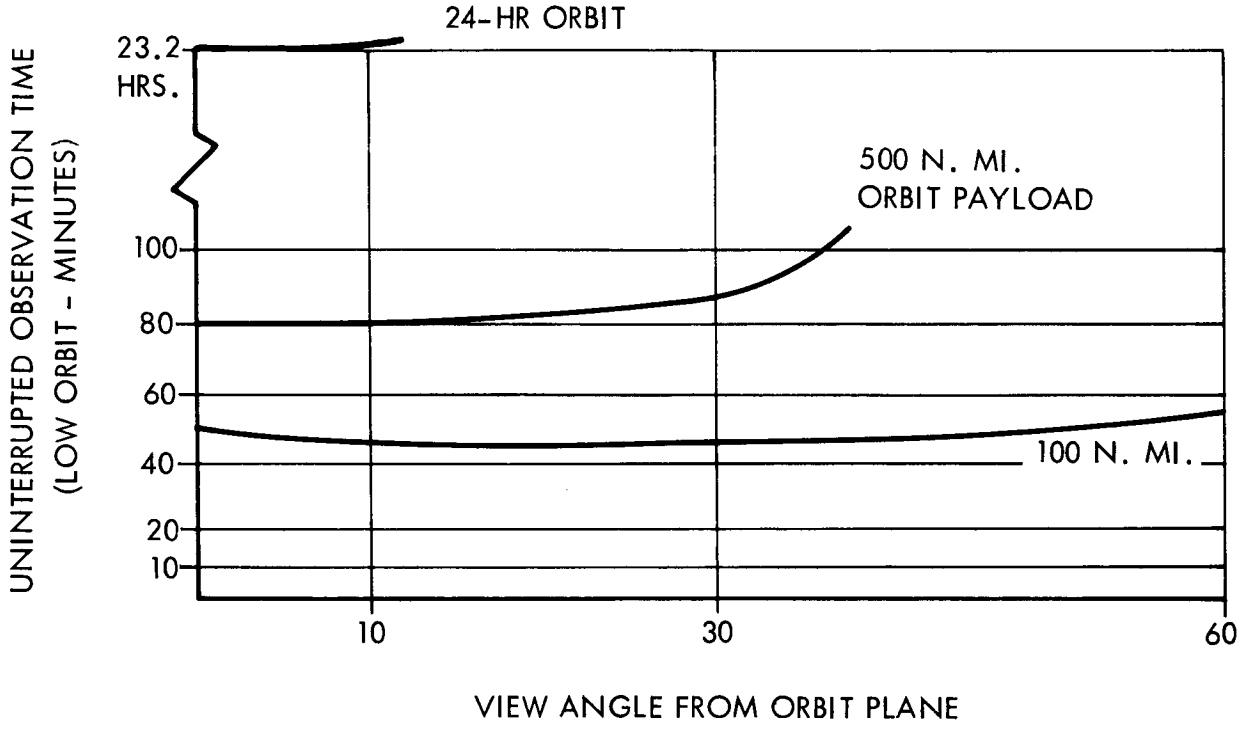


Figure 7.2-1. Observation Time as a Function of View Angle

TABLE 7.3-1

ORBIT AND MANNING REQUIREMENTS

Experiment	Manning	Orbit
1. Heterodyne Detection	O	S
2. Direct Detection	O	S
3. 10 Megahertz Communication	O	S
4. Precision Tracking	O	S
5. Point Ahead	O	S
6. Transfer Tracking	O	S
7. Phase Correlation Measurements	O	S
8. Pulse Distortion Measurements	O	S
9. Primary Mirror Figure Correction	M	N
10. Thin Mirror Nesting	M	N
11. Fine Guidance	M	N
12. Comparison of Isolation Techniques	M	N
13. Interferometer System	M	S
14. Segmented Optics	M	N
15. Degradation of Optical Materials	M	N

O - Manning Optinal
M - Manned Preferred
S - Synchronous Orbit Preferred
N - Orbit Optional

could be performed in a manned synchronous mission. Further, the optical communication experiments, might be performed on an unmanned synchronous mission. The remaining experiments, excepting the interferometer experiment could be performed on a manned low earth orbit mission.

With respect to equipment compatibility it was decided to perform the optical communication experiments on a common set of telescope independent of all other experiments. Three telescopes were selected for these experiments. The criteria of this selection is presented in section 8.1. The two primary mirror experiments, primary mirror figure correction and thin mirror testing were combined into a single telescope well. Finally, it was attempted to combine the fine guidance, comparison of isolation techniques and interferometer system experiments into a single telescope. This proved to be the most difficult task and several integration problems remain to be solved.

As a result of these ground rules it was concluded that five telescopes and two primary mirrors were required to perform all of the experiments.

The following sections of this report discuss the optical communication telescopes and the stellar oriented telescope.

8.0 OPTICAL PROPAGATION EXPERIMENT GROUP

There are nine OTAES experiments which are predicated upon the transmission of energy at visible or infrared frequencies. In each of these experiments, the effects of propagation path variables will be analyzed on the basis of received signal characteristics:

a. Optical Heterodyne Detection on Earth

b. Optical Heterodyne Detection in the Spacecraft

c. Direct Detection on Earth

d. Communication with 10 MHz Bandwidth

e. Precision Tracking of a Ground Beacon

f. Point-Ahead and Space-to-Ground-to-Space Loop Closure

g. Transfer Tracking from One Ground Station to Another

h. Phase Correlation

i. Pulse Distortion Measurements.

8.1 TELESCOPE REQUIREMENTS

The OTAES laser experiments, which were initially defined to gather optical propagation data and to further the atmospheric sciences, can also be designed to provide engineering data for future operational system designers. The obvious operational application for lasers is deep space communication for which the near-term example may be wide-band data transmission from Mars. In this context, it is possible to consider OTAES as a Mars mission simulator on which: (a) laser communication technology can be exercised, (b) realistic enviornmental disturbances can be introduced, (c) the significant communication parameters can be measured, and (d) a valid comparison can be made with conventional techniques. Although scientific objectives establish the nature of the laser telescopes, the particular configuration concept can be determined by this Mars mission simulation objective, and by general experiment design practice.

Good practice, and the very difficulty of the precision pointing and optical signal analysis experiments to be attempted, suggests the need for high reliability in the laser subsystems. There are two such subsystems which

can be considered acceptable in this context. These alternatives are based on the argon (0.488-micron) and helium neon (0.6328-micron) lasers, both of which are coherent, CW sources suitable for heterodyne communication applications. All necessary components and their coatings are adequately developed; have been demonstrated reliably in a variety of configurations; and, in the case of optical elements and beam splitters, have already been proven in space. Furthermore, neither alternative imposes complicating requirements such as pumping, q-switching, or cryogenic cooling. However, the high power argon laser exhibits a high input power threshold requirement, making helium neon the logical choice for space-to-ground experiments. It follows that the 0.488-micron subsystem will be used as the fundamental ground-to-space link since an argon local oscillator can operate in the lowest power mode. These choices lead to specific primary mirror diameter and telescope pointing requirements.

8.1.1 Mirror Diameter and Pointing

Certain of the laser experiments are predicated on phase coherence measurements. A diffraction-limited aperture will preserve the coherence of the source and conserve the transmitted energy. Size and mass are secondary, but important, considerations. Acceptance of the diffraction limit leads to the smallest possible aperture requirement with attendant easing of spacecraft packaging and of pointing actuator drive power problems.

Taking the ratio of the well-known Friis transmission expressions for optical and microwave communication gives:

$$\frac{\left(\frac{S}{N}\right)_o}{\left(\frac{S}{N}\right)_m} = \frac{\epsilon_{to} A_{to} \lambda_m^2 A_{ro} kT}{\epsilon_m A_{tm} \lambda_o^2 A_{rm} h\nu/q}$$

which relates transmitter efficiencies, ϵ; aperture areas, A; wavelengths, λ; detector quantum efficiency, q; noise temperature, T; frequency, ν; and the familiar constants of Planck, h, and Boltzmann, k. The subscripts t, r, m, and o denote transmitter, receiver, microwave, and optical, respectively.

In Table 8.1-1, the various terms of this relation are evaluated from the viewpoint of microwave optimism (e.g., a 100-meter diameter, X-band receiving aperture on the Earth; a 30-meter diameter X-band transmitter on the spacecraft; a 100° receiver noise temperature; a 50 percent, X-band transmitter efficiency, etc.) These assumed characteristics are contrasted with 0.6328-micron laser communication components which could be fabricated today. The noise, receiving aperture, and transmitter efficiency ratios (23.5 + 20.0 + 20.5 = 64.0 db) are inherently advantageous to the microwave technology. Only the wavelength (93.5 db) term favors the optical technique. For equivalence between the microwave and optical techniques, the ratio of transmitting apertures on the spacecraft must give no more than a 29.5 db advantage to the microwave technique. Thus, a favorable comparison of optical communication with microwave communication cannot be made with apertures less than one meter; and this choice results in a 0.14 arc second

beamwidth, imposing a 0.1 arc second pointing requirement. This one-meter aperture gives adequate signal strength for the pulse distortion experiment and permits the use of 2-cm apertures on Earth for the phase correlation experiment.

The helium-neon, single frequency laser, the one-meter diffraction-limited aperture, and the 0.1 arc second pointing system combined in a single Earth orbital test, will make a significant comparison of wide-band planetary communication capability at optical frequencies.

TABLE 8.1-1

MARS MISSION COMMUNICATION COMPARISON PARAMETERS

	$\frac{kT}{h\nu/q}$	$\frac{A_{ro}}{A_{rm}}$	$\frac{\epsilon_o}{\epsilon_m}$	$\frac{\lambda_m}{\lambda_o}$	$\frac{A_{to}}{A_{tm}}$
OPTICAL	At $6328^{\circ}A$ $h\nu = 3.12 \times 10^{-19}$ Joules $q = 0.05$	D=10 Meter $A_{ro} = 78.5 m^2$	0.0045	$\lambda_o^2 = 4 \times 10^{-13}$ m^2	D=1 Meter 0.785 m^2
MICRO-WAVE	AT $100^{\circ}K$ 1.38×10^{-21} Joules	D=100m $A_{rm} = 785 m^2$	0.5	$\lambda_m^2 =$ $9 \times 10^{-4} m^2$	D=30 Meters $A_{rm} = 706 m^2$
db:	+23.5	+20	+20.5	-93.5	+29.5

8.1.2 Auxiliary Telescopes

The 0.6328-micron link offers reliability and can be used in a simulated planetary mission context to generate system engineering data. However, the HeNe laser is not the ultimate device for operational applications. Its efficiency appears limited to a maximum in the order of 0.004, and there is little hope of increasing its maximum output power beyond 200 milliwatts. It was selected here for its advanced state of development, proven operation, and flexibility (e.g., its adaptability for single frequency, super-mode, and mode-locked operation). There are other lasers which exhibit better operational potential.

Furthermore, the atmospheric physics experiments would be better served by including at least two transmitter wavelengths on the spacecraft. In fact, the phase correlation experiment is predicated on the use of widely separated wavelengths to establish coherence scaling laws. Thus, a second transmitter frequency is not only desirable in all of the propagation experiments, it is essential in some.

The nitrogen carbon-dioxide (N_2-CO_2) laser is a new form showing great promise because of its high power and efficiency and favorable wavelength for operation in the atmosphere. Significant advances in detection and modulation devices will be required before this laser can be applied in operational wide-band systems. However, its threshold of oscillation is about one tenth that of argon lasers of comparable power.

The laser will not be massive since a solenoid is not required, but additional space may be needed to carry reservoirs of the N_2 and CO_2 gases. For the proposed optical heterodyne detection experiment at a long optical wavelength, the transmitter is aboard the spacecraft and the receiver is at the ground station, where it is practical to use cryogenically cooled detectors. Because of the longer wavelength, the tuning and alignment problems are less severe than for the helium-neon local oscillator. However, the output will have to be maintained at specified frequency in a single TEM_{00} mode.

Such a wide separation in frequency (0.488 micron to 10.6 microns) imposes very stringent requirements on the laser telescope design. Conventional materials which transmit at one of the wavelength extremes are opaque at the opposite extreme. Three avenues of solution are evident: (a) develop a new refracting material, (b) restrict the laser telescope to an all-reflecting configuration, or (c) use a separate telescope for the 10.6-micron transmitter. The latter solution is the simplest and the lowest-risk alternative.

To compare a 10.6-micron link with a 0.6328-micron link, consider the transmission equations once again. Equating signal-to-noise ratio, prime power, receiving aperture, and bandwidth:

$$\left(\frac{D_{t_1}}{D_{t_2}}\right)^2 = \left(\frac{q_2}{q_1}\right)\left(\frac{\epsilon_2}{\epsilon_1}\right)\left(\frac{\lambda_1}{\lambda_2}\right) \quad .$$

Comparison of 0.6328-micron and 10.6-micron links on a detector quantum efficiency basis is not rigorous. In the visible region, photoemissive detectors apply. These are customarily compared on a quantum efficiency basis. Infrared detectors are photoconductive, hence should be compared on a detectivity basis. However, for a gross comparison, the equivalent infrared detector quantum efficiency can be postulated as approximately twice that of visible light detectors. Thus, an order of magnitude comparison of the spacecraft transmitting aperture requirement can be made as:

$$\left(\frac{D_{t_1}}{D_{t_2}}\right)^2 < \frac{1}{2}\,\frac{\epsilon_2}{\epsilon_1}\,\frac{\lambda_1}{\lambda_2} = 0.067 \quad ,$$

since at $\lambda_2 = 0.6328$ micron, $\epsilon_2 < 0.0004$; and at $\lambda_1 = 10.6$ microns, $\epsilon_1 > 0.1$. It follows that a 10.6-micron link with a 0.3-meter aperture should give equivalent, or slightly superior, received signal characteristics.

For a 0.3-meter aperture, 10.6-micron transmitter, the diffraction-limited half power beamwidth is 6 arc seconds, allowing an absolute alignment error of ± 3 arc seconds. Using the 3σ probability criterion for circular errors, this translates into an error budget of $\sigma_\theta = 1$ arc second. Such a tolerance is large enough to consider slaving the 0.3-meter telescope to the 1.0-meter telescope, thereby eliminating the need for a second precision tracking system in the smaller telescope. Preliminary structural analysis of a strap-together 1.0-meter/0.3-meter telescope configuration indicates that angular deflections will be less than one arc second for typical spacecraft attitude disturbances. It follows that, if 0.1 arc second error tolerances are assigned to boresight parallelism, the 1.0-meter telescope tracking error, and the 0.3-meter telescope point-ahead device, respectively, adequate pointing accuracy can be assured for the slaved, strap-together telescope.

8.1.3 Separately Gimbaled Telescopes

It is desirable, from the viewpoint of atmospheric physics experiment design, to provide an Earth-to-space propagation link at the same wavelength as one of the down-links. This stratagem serves to correlate observed effects and, in some instances, to isolate test variables. Thus far, the logic for including a 0.488-micron up-link, a 0.6328-micron down-link, and a 10.6-micron down-link has been developed. The needed coincidence of up-link and down-link frequency can be obtained by adding a reverse direction link at one of these frequencies. The simplest solution might be a corner reflector on the spacecraft - but this approach violates the desire to correlate observed effects.

To add a 0.488-micron down-link imposes the same threshold power penalty which was avoided in the initial choice of spaceborne transmitter. Addition of a 10.6-micron up-link introduces a high degree of risk into the experiment recommendation since the development of some necessary 10.6-micron system components is just beginning. For these, availability on Earth is not assured; to make them available in orbit is even more difficult, Furthermore, present 10.6-micron detectors require cryogenic cooling. While it is possible to meet this requirement, it is a cumbersome imposition, if avoidable - and the 0.6328-micron up-link would not induce such a requirement. Once again, the availability of proven components, many of them previously tested in space, makes the 0.6328-micron up-link a desirable choice.

However, to incorporate both transmitter and receiver of the same frequency for simultaneous operation in the same telescope would result in obvious isolation problems. If such problems are solvable, the solution would surely add complexity with attendant reliability implications and would probably degrade experiments (such as Phase Correlation) to which signal power is critical. Installation in a different telescope is clearly indicated.

A ground-based helium-neon transmitter need not be constrained in size, power consumption, and environmental qualification as a spaceborne transmitter. Existing designs now operate with 100-milliwatt output power - in contrast with the 10-milliwatt output contemplated for the one-meter aperture, helium-neon spaceborne transmitter (i.e., $\frac{P_2}{P_1} = 10$). Once again returning to the transmission equation, recall that:

$$\left(\frac{D_{t_1}}{D_{t_2}}\right)^2 = \left(\frac{D_{r_2}}{D_{r_1}}\right)\left(\frac{P_2}{P_1}\right) \quad .$$

For the coherent light experiments, the same diameter limitations apply to an Earth-based transmitting aperture as to an Earth-based receiving aperture: $D_{t_2} = D_{r_1}$. Then,

$$D_{r_2} = \frac{D_{t_1}}{\sqrt{10}} = 0.3 \text{ meter} \quad .$$

Again, a 0.3-meter auxiliary telescope aperture would be adequate. But, in this case, the reasons previously given for optically dissociating the 0.6328-micron and 10.6-micron energy processing still hold. Combination in the 0.3-meter, 10.6-micron telescope is undesirable. Furthermore, the corresponding diffraction-limited beamwidth is less than half of an arc second - an order of magnitude smaller error budget for a 0.3-meter, 0.6328-micron strap-on configuration than for the 10.6-micron, 0.3-meter telescope. It follows that the 0.3-meter, 0.6328-micron receiving telescope should contain a separate fine tracking device.

There are secondary bonuses to a separately gimbaled 0.3-meter telescope. In transferring tracking from one ground station to another, a separation of at least 11 arc seconds is contemplated. If handled within the one-meter telescope, the tracking transfer experiment would impose additional field-of-view and defocusing requirements. These requirements are relaxed when two separately gimbaled telescopes are used.

Finally, there can be space behind the separately gimbaled 0.3-meter telescope to install a back-up 0.6328-micron laser transmitter. This back-up laser is redundant. It will not be operated under normal experiment conditions. It is included to assure qualified success in the event of a debilitating or catastrophic failure of key elements housed in the 1.0-meter telescope well. Each of the space-to-Earth propagation experiments can be conducted with the back-up laser transmitter on the 0.3-meter telescope - compromised by reduction in signal strength and pointing accuracy as compared to the 1.0-meter telescope.

8. ONE METER TELESCOPE

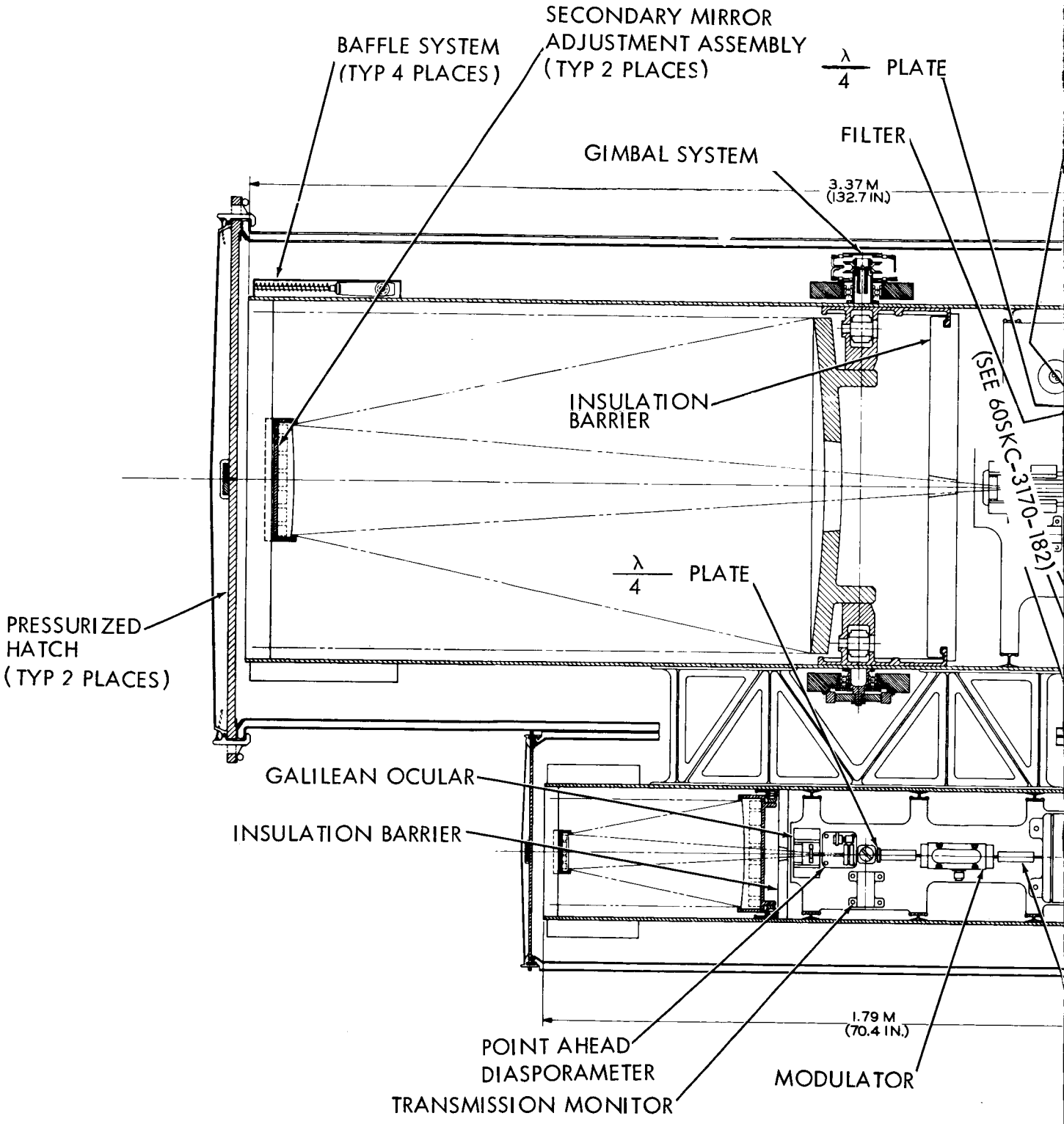
The one meter telescope is an optical frequency transmitter-receiver with tracking capability operating through a common Cassegrainian telescope which serves as a highly directional collector and collimator of light energy. The transmitter operates at a wavelength of 6328 Å and the receiver and tracker at 4880 Å. The telescope contains provisions for modulating the transmitter carrier, detecting the modulation on the receiver carrier, centering its beam on the ground station, compensating for transit time differences and making certain alignment adjustments.

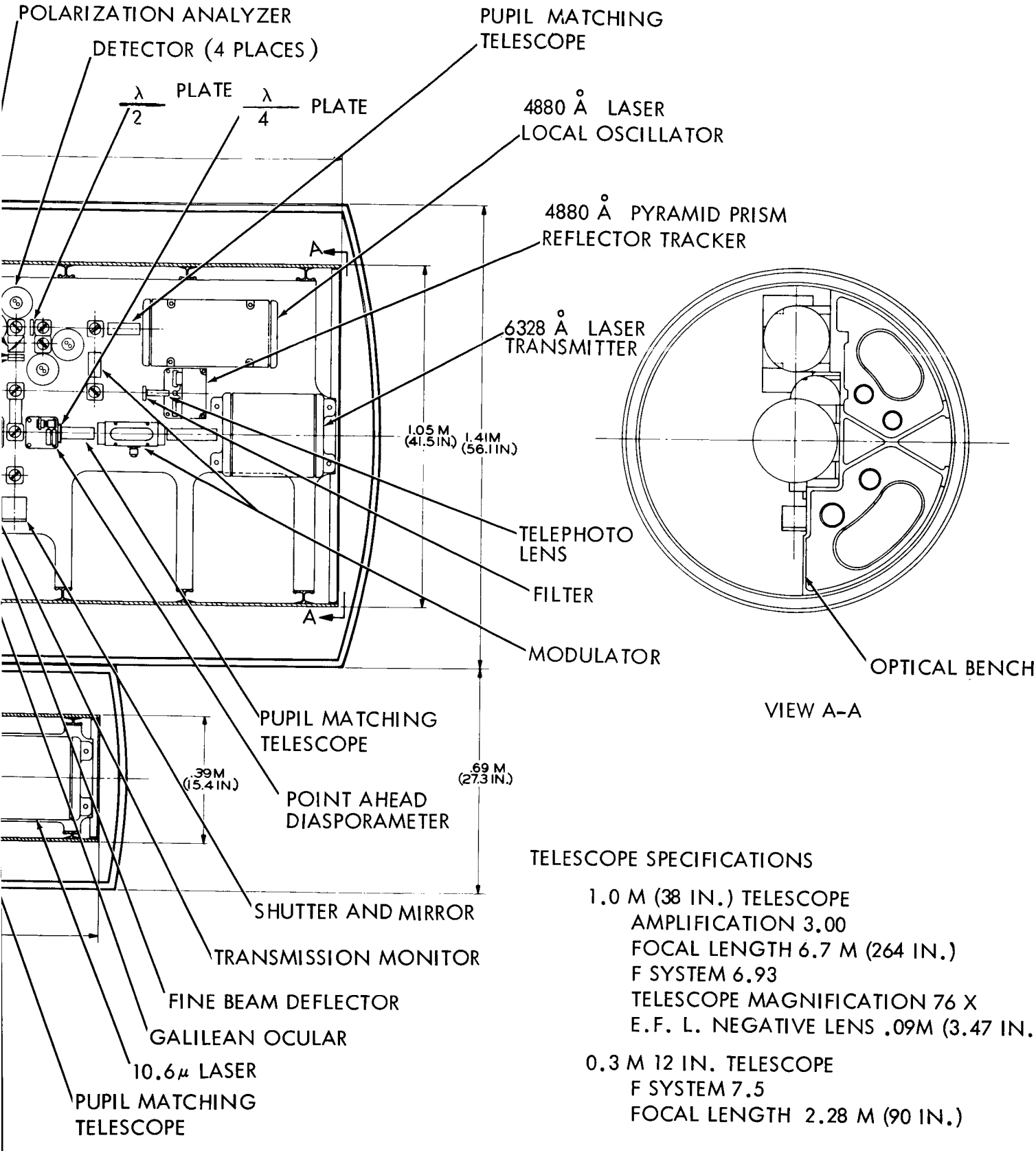
Rigidly mounted to the one meter telescope is a 0.3 meter transmitter telescope which will be described in Subsection 8.3. These telescopes are illustrated in Figure 8.2-1.

8.2.1 Transmitter

The transmitter of the one meter telescope is illustrated in figures 8.2-2a and 8.2-2b. The oscillator-amplifier of the transmitter is a helium neon laser operating at the 6328A wavelength with an output power of 10 milliwats. The output beam has a diameter of 2 millimeters. The laser feeds into a pupil matching telescope (PMT-1) to reduce the beam to a diameter of 1 millimeter to be compatible with the electro-optical modulator (MOD-1). This telescope consists of a positive lens of 150 mm focal length and a negative lens of -75 mm focal length with the positive lens toward the transmitter. The clear aperture of the lenses can be very small, in the order of 3 mm. The electro optic modulator serves the function of impressing the information signal on the carrier generated by the laser. The details of the modulator are discussed in subsection 4.4. After the modulator is another pupil matching telescope (PMT-2), this one increasing the aperture from 1 millimeter to 12.7 millimeters (1/2 inch) to provide a reasonable pupil size and magnification factor for the beam deflection mechanisms, the point ahead diasporameter and fine beam deflector, which fall between this telescope and the main telescope. The pupil matching telescope consists of a positive lens of 102 mm focal length and a negative lens of -8 mm focal length. The required clear apertures are 13 mm for the positive lens and 2mm for the negative lens. The negative lens is at the end closer to the modulator. It is possible, by judicious use of aspheric surfaces or other techniques on one or both of the pupil matching telescopes in the transmitter line of sight, to increase the transmitter efficiency by redistributing the energy over the pupil in a more uniform fashion rather than in the Gaussian distribution produced by the laser. The purpose of this is to take some of the energy that would be occulted by the secondary mirror and move it slightly off axis where it would fall in the outer zones of the telescope primary. Further details relating to redistribution of the laser energy are given in Section 8.2.1.1.

After the pupil matching telescope is a quarter wave plate ($\lambda/4$) which, together with the polarization analyzer in the modulator produces a circularly polarized amplitude modulated signal suitable for detection at the ground station receiver. Because of the distance covered by the ground station


BAFFLE SYSTEM
(TYP 4 PLACES)
SECONDARY MIRROR
ADJUSTMENT ASSEMBLY
(TYP 2 PLACES)
λ/4 PLATE
FILTER
GIMBAL SYSTEM
3.37 M
(132.7 IN.)
INSULATION
BARRIER
(SEE 60SKC-3170-182)
λ/4 PLATE
PRESSURIZED
HATCH
(TYP 2 PLACES)
GALILEAN OCULAR
INSULATION BARRIER
1.79 M
(70.4 IN.)
POINT AHEAD
DIASPORAMETER
TRANSMISSION MONITOR
MODULATOR

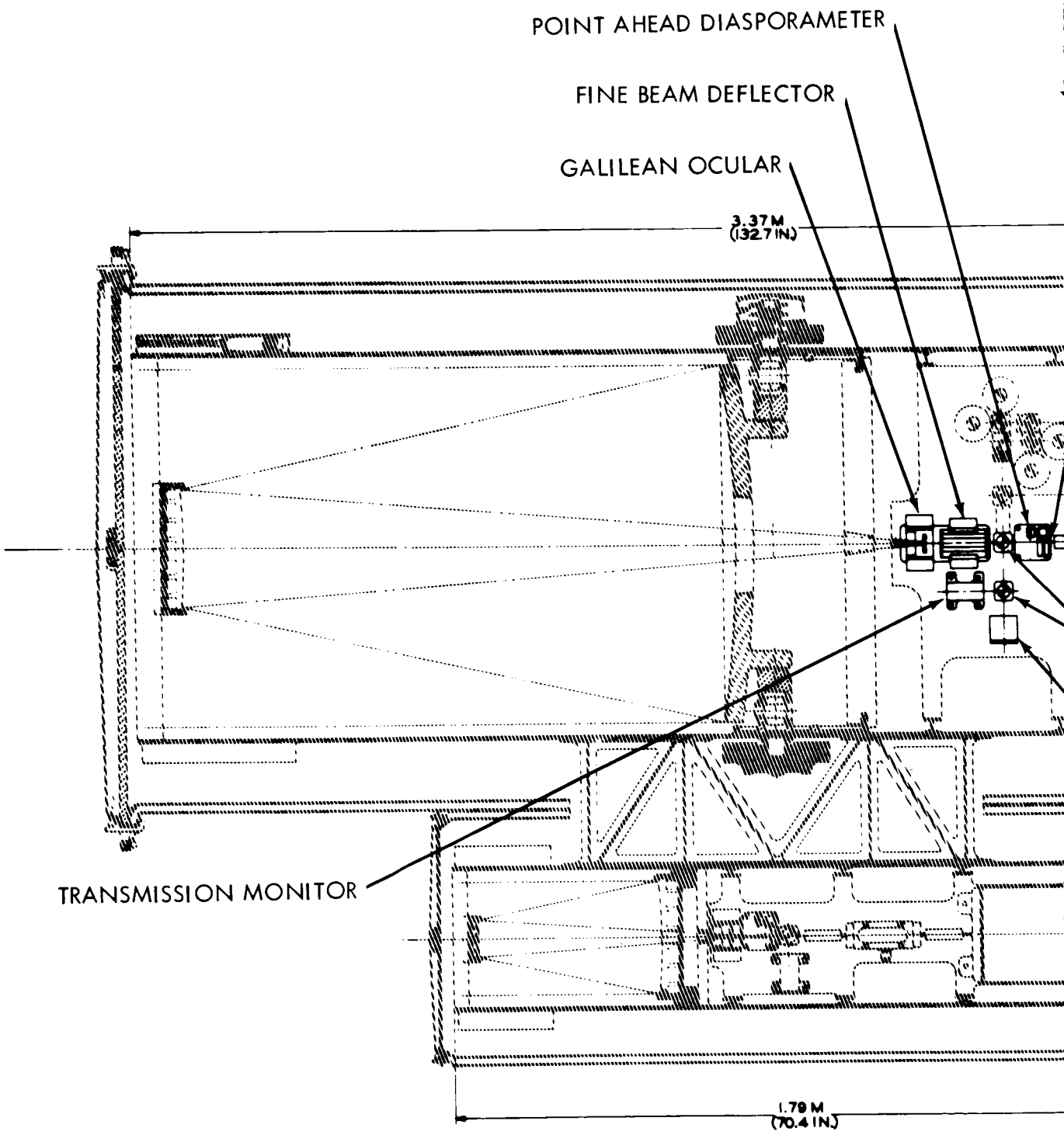


TELESCOPE SPECIFICATIONS

1.0 M (38 IN.) TELESCOPE
- AMPLIFICATION 3.00
- FOCAL LENGTH 6.7 M (264 IN.)
- F SYSTEM 6.93
- TELESCOPE MAGNIFICATION 76 X
- E.F. L. NEGATIVE LENS .09M (3.47 IN.)

0.3 M 12 IN. TELESCOPE
- F SYSTEM 7.5
- FOCAL LENGTH 2.28 M (90 IN.)

Figure 8.2-1. 0.3 and 1.0 Meter Telescope


POINT AHEAD DIASPORAMETER
FINE BEAM DEFLECTOR
GALILEAN OCULAR
3.37 M
(132.7 IN.)
TRANSMISSION MONITOR
1.79 M
(70.4 IN.)

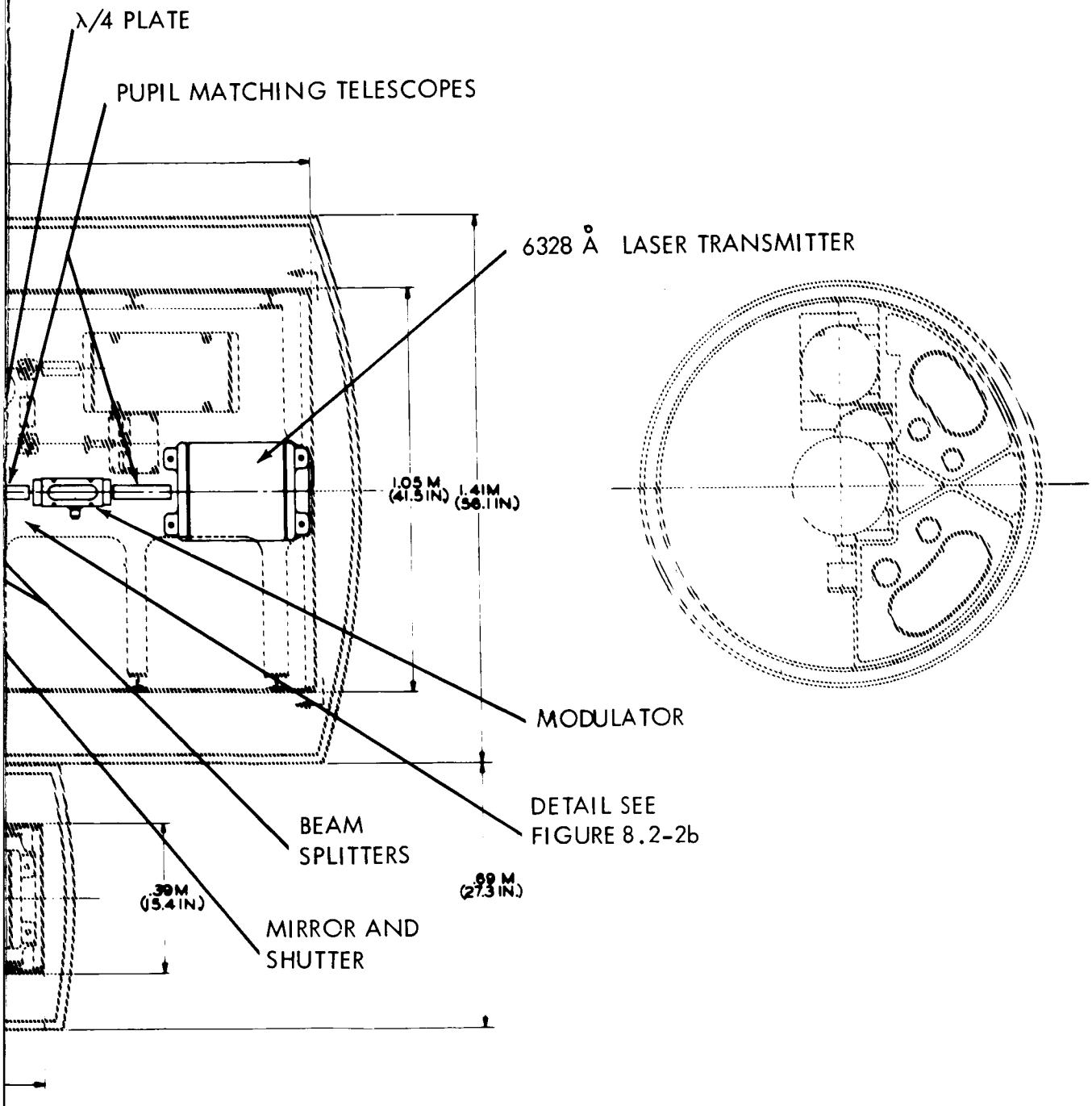


Figure 8.2-2a. 1.0 Meter Telescope Transmitter

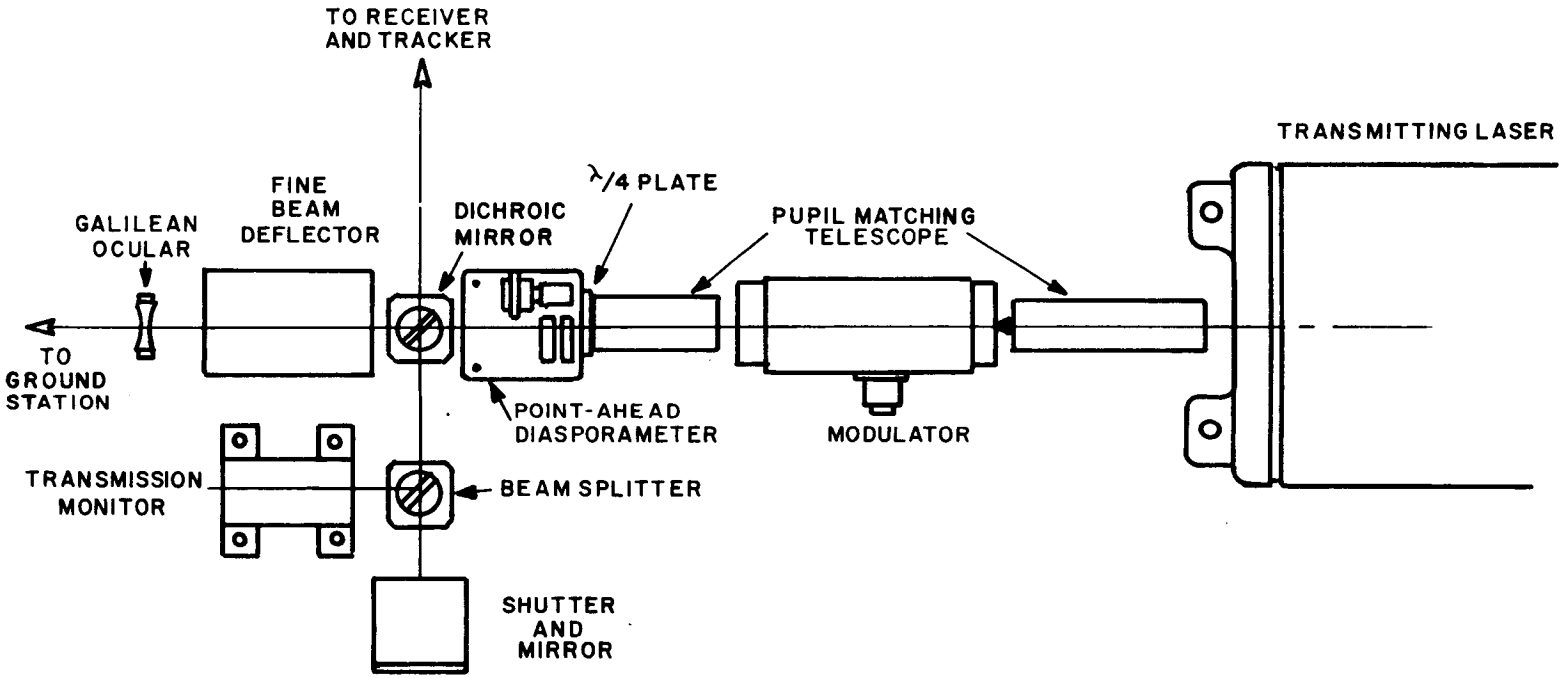


Figure 8.2-2b 1.0 Meter Telescope Transmitter

during the time required for the signal to transmit from the earth to the space probe and back, a small offset angle must be provided between the received and transmitted line of sight. This is accomplished by interposing a pair of beam deflecting wedges in the transmitter line of sight. This is referred to as the point-head diasporameter (PAD-1). A general discussion of diasporameters can be found in Section 8.2.1.2.1. If the wedges were to be mounted normal to the line of sight the beam would be deviated and start diverging from the axis of the main telescope so as to cause about 25% vignetting of the transmitted beam at maximum point ahead angle. This effect can be compensated by introducing the appropriate tilt angle and thickness into the wedges to translate the beam in the opposite sense to the deviation so that the combined displacement and deflection will cause the beam to follow a path identical to that traced by an incoming ray off axis by the proper angle. A more detailed discussion of diasporameter compensation is given in Subsection 8.2.1.2.2.

The diasporameter wedges must be driven in counterrotation to provide the deflection for point ahead, and in unison to provide orientation. This can be accomplished with two motors, a differential and two rotation sensors. The sensor for deflection angle should be a resolver or a similar sinusoidal transducer and the sensor for the azimuth angle should be linear with angle.

An alternate method for point-ahead generation is the use of four wedges arranged in two pairs with orthogonal axes, the two members of each pair being driven in counterrotation. This has the advantage of isolation of two axes and elimination of the differential from the drive. At the same time it is burdened by the requirement of added optical surfaces and additional length of optical path, involving as it does an increase in volume. Either technique could serve the required function and a tradeoff analysis may be indicated before a choice is decided upon.

After the point ahead diasporameter, which is required to deflect the transmitted beam only, and before the fine beam deflection device which operates on both the transmitted and received beam is a dichroic mirror (D C) which passes the 6328 Å energy and reflects 4880 Å energy. Its function is to separate out the received energy and direct it toward the receiver and tracker while not materially diminishing the transmitted energy. Less than one percent of transmitter energy is reflected and utilized for monitoring and boresight adjustment as described in a later paragraph.

The fine beam deflector, (FBD) the next item in the transmitter chain serves the function of compensating for small disturbances that can occur in the spacecraft and telescope and for a vernier adjustment superimposed on the telescope gimbals. As presently conceived this fine beam deflector consists of two eight element cascades of piezo-electrically driven shear plate mirrors in series, one for each axis. This technique exhibits the advantage of very high speed of response, but is severely burdened by the number of reflecting surfaces required, with the consequent high loss of optical energy, to provide adequate beam deflection. For this reason alternate

schemes embodying bimorph bender crystals and galvanometer driven mirrors are receiving serious consideration. Either of these techniques should be able to perform the required deflection with a maximum of four reflecting surfaces in place of sixteen at the expense of moderate sacrifice in high frequency response. These are discussed at greater detail in subsection 8.2.1.3.

The principal telescope is a 76 power telescope consisting of a Cassegrainian objective of 0.965 meter aperture and 6.705 meters effective focal length, and a Galilean ocular (G O - 1) of -88 mm focal length and a clear aperture of 16 millimeters. The eypiece is achromatized for the two wavelengths of interest, namely 6328 A and 4880 A, and corrected for reasonable image quality over a field of $\pm$ one minute. The objective consists of a primary mirror (PM-1) with a focal length of 2.235 meters and an aperture of 0.965 meter. The secondary (SM-1) is separated from the primary by 1.524 meters and has an aperture of 0.318 meter and a focal length of -1.067 meter. With the extremely small field of view requirements these can be in the classical Cassagrainian configuration with a paraboloidal primary and a hyperboloidal secondary. The principal telescope has two functions: It matches the 12.7 mm pupil of the transmitted beam at the fine beam deflector to a one meter pupil for transmission to earth in a highly directional beam; at the same time it collects the received energy from earth and collimates it into a half inch pencil for transmission to the receiver.

The transmitter energy which is reflected by the dichroic mirror (DC), which amounts to less than one percent of the total, is directed towards beamsplitter BS-1 where it is divided between the transmission monitor and the boresight shutter and mirror. The transmission monitor is a photomultiplier which detects the transmitter energy received and continuously checks the transmitter output level and modulation. The remaining energy is used for the transmitter boresight adjustment which is described in subsection 8.2.3.

8.2.1.1 Effect of Central Obscuration on Transmitter Beam

The combination of a laser transmitter and a collimating telescope of Cassegrainian configuration has a mismatch which could conceivably cause a serious loss in efficiency. This is due to the fact that the aperture of the Cassegrainian telescope has a central obscuration through which nothing can be transmitted, while the output of the laser is Gaussian in distribution, which makes the central part of the beam carry the densest concentration of energy. Therefore the richest part of the beam is blocked by the central obscuration.

There are several approaches to the solution of this problem which will be discussed in order. They include refractive optics, Herschelian telescope, refractive compensation and reflective redistribution of energy.

8.2.1.1.1 Refractive Optics

The first and most obvious method of correcting the mismatch is to eliminate the central obscuration. One way in which this can be accomplished is by the use of refractive optics. While this is quite feasible for small optics, the likelihood of success decreases rapidly as the aperture increases. As a matter of fact, the optical design described in this report uses refractive optics for all elements whose apertures are less than one inch. This serves to delay the problem until the principal telescope is reached, at which point, because of the larger size of the elements, the fraction of the aperture obscured can be kept to a minimum. The use of refractive elements for the main objectives of the telescopes is out of the question for several reasons including the weight penalty of such a large piece of optical glass, the difficulty and expense of manufacturing such a large lens and the difficulty of supporting it adequately to survive the launch environment. Any lingering suspicion that this is a practical solution should be dispelled by the fact that the largest refractive astronomical telescope in the world has an objective no larger than the one required for the 1.0 meter telescope.

8.2.1.1.2 Herschelian Telescope

There is a type of reflecting telescope which also avoids the central obscuration. This is the Herschelian telescope, shown in Figure 8.2-3a whose objective is a portion of an off-axis paraboloid and whose secondary mirror is outside of the field of the primary. This configuration not only eliminates the central obscuration but it also eliminates the diffraction effects of the support structure for the secondary. The disadvantages of the Herschelian telescope are three.

a. It is non-symmetrical, thus eliminating any balancing of aberrations that can be derived from a symmetrical telescope;

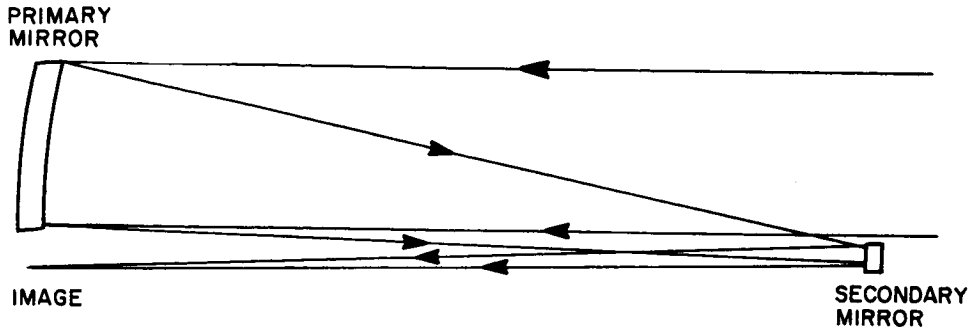
b. The extreme rays are twice as far off-axis in a Herschelian telescope than in a Cassegrainian; and, in the case of the 1.0 meter telescope approach, a focal ratio of 1.16 rather than 2.32, thus making correction to a diffraction limit more difficult;

c. The manufacture of an off-axis mirror frequently requires finishing one twice the required size, cutting out the part desired and discarding the remainder. Making a two meter mirror is many times more difficult than making a one meter mirror.

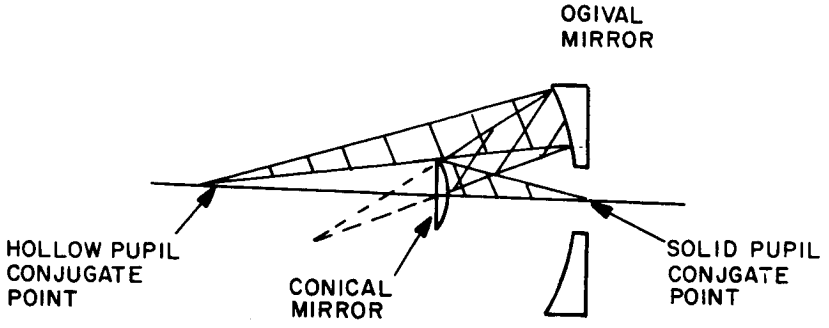
Therefore, the Herschelian telescope is not recommended as the answer.

8.2.1.1.3 Refractive Compensation

Another approach is to redistribute the energy in the laser output beam to change the Gaussian distribution of the output to uniform distribution, or even to over-compensate and put the bulk of the energy into an annular zone where it will be free of central obscuration. Two media present themselves



(a) Herschelian Telescope



(b) Reflective Redistribution of Energy (1)

Figure 8.2-3 Central Obscuration Correction

(1) Journal of the Optical Society of America, Vol. 45, p. 398

whereby this might be accomplished within the pupil matching telescope at the modulator output. One mechanism is the use of aspheric surfaces on the telescope lenses designed to deviate the central rays more sharply at the center of the field than at the edge. A corresponding aspheric in the re-collimating lens is required to maintain a collimated beam. A method not using aspherics is also available. Coma is an aberration which is characterized by differential magnification as a function of displacement from axis. If the lens has higher magnification in the outer zones, the coma is said to be positive; if the magnification is greater in the center, the coma is negative. Using the above definitions, consider the short focal length lens to possess negative coma, and then long focal length lens to possess positive coma, some of the energy should be redistributed out of the central zone and into the outer zones, producing effects similar to those described for the aspheric lenses. To determine the actual effectiveness of these schemes, a ray trace program must be conducted.

8.2.1.1.4 Reflective Redistribution of Energy

A mechanism has been described (Ref. Seymour Rosin - JOSA Volume 45 P398, "Mirror Condenser for Spectrographs") whose function is "to create or eliminate holes in the pupil of a beam of light". It consists of a conical mirmirror and an ogival mirror. See Figure 8.2-3b. When used to create the hole as in the present requirement, the incoming light strikes the conical mirror and is diverged in a hollow cone. The light is recollected and reimaged or recollimated in a beam of annular cross section. While the device illustrated shows finite conjugates, the text indicates that it can also be corrected for collimated light. Such a device has been constructed and used, but as in the prior case, further investigation in the form of a ray trace analysis is recommended.

In summary, it may be stated that a laser and a Cassegrainian telescope make poor companions; it may be possible to reduce and, perhaps, even eliminate the incompatibility so that they can perform quite efficiently when teamed together.

8.2.1.2 Point-Ahead Deflector

Several mechanisms have been studied as the preferable way of achieving the point-ahead correction for transit time to the ground station. Since the magnitude of deflection required for point-ahead is comparable with that of the fine beam deflection, the use of the same type of mechanism for both deflections was entertained. However, the bandwidth requirements are vastly different and it became evident that the sophisticated approach required to get the high speed of response in the fine beam deflector is entirely unnecessary in the point-ahead function. For the comparatively static correction required, and the low speed of response the diasporameter is adequate, and its efficiency, stability and reliability highly recommended its use for point-ahead deflection.

8.2.1.2.1 Diasporameter

A diasporameter consists of a pair of optical wedges, each effecting a small angular deviation on an incident light ray. As generally applied, the deviation is the same in each wedge, although there are specific cases where they may not be equal. In this discussion, only matched pairs are considered.

An optical wedge, as shown in Figure 8.2-4a, deflects an incident ray by bending it toward the normal on entering the wedge and away from the normal on leaving the wedge. For small angles:

$$\rho = a(n-1)$$

where

ρ is the angular deviation

a is the apex angle of the wedge

n is the refractive index of the wedge material

The deviation can be resolved into components as follows: (Figure 8.2-4b)

$$\rho_x = \rho \cos \theta$$
$$\rho_y = \rho \sin \theta$$

where

ρ_x and ρ_y are the x and y components of ρ

θ is the angle between the thick end of the wedge and the positive x axis

When two wedges are used in a diasporameter, the effect of both wedges is summed. If θ is the same in both wedges, as shown in Figure 8.2-4c,

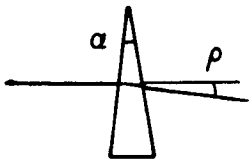
$$\rho_x = \rho \cos\theta + \cos\theta = 2\ \rho \cos\theta$$
$$\rho_y = \rho \sin\theta + \sin\theta = 2\ \rho \sin\theta$$

Hence, the net effect of two wedges with the same orientation is double the effect of a single wedge.

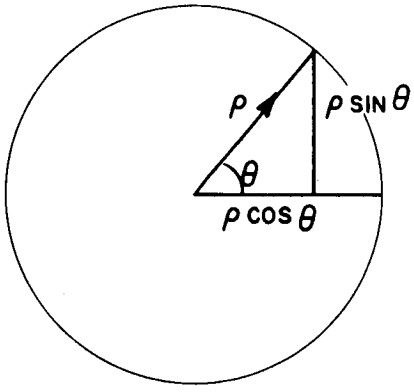
Next, consider the effect when the angles are separated by 180°.

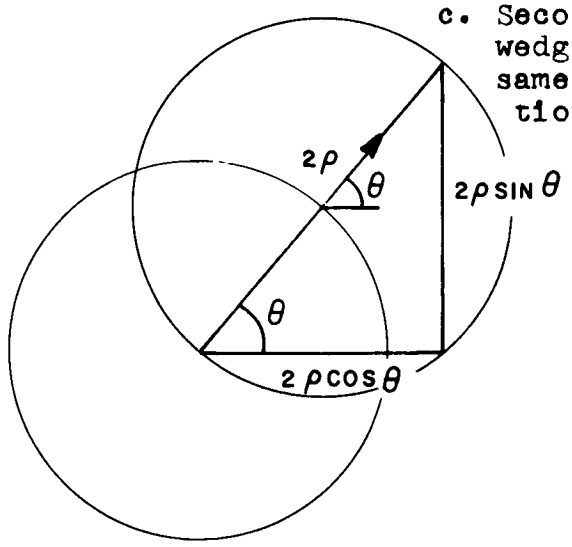
$$\rho x = \rho \cos\theta + \rho \cos\ (180^\circ + \theta) = 0$$
$$\rho y = \rho \sin\theta + \rho \sin\ (180^\circ + \theta) = 0$$

Hence, the effect is a net cancellation.



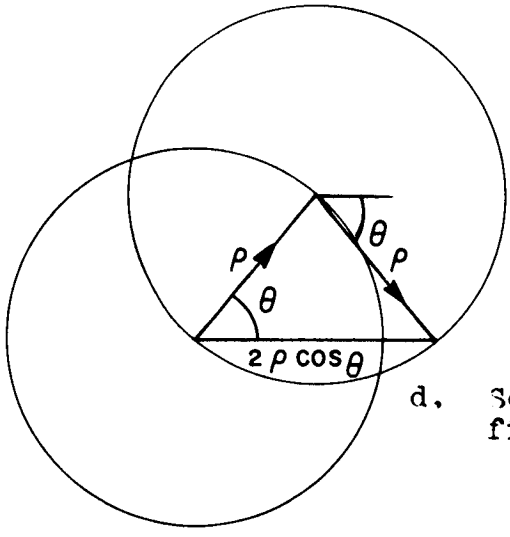
a. Deviation by single wedge





c. Second wedge with same rotation as first

b. Resolved components of deviation by single wedge



d. Second wedge rotated counter to first.

Figure 8.2-4 Beam Deviation by Diasporameter

The third case of special interest is the situation where the angles are equal but opposite. See Figure 8.2-4d.

$$\rho x = \rho \cos \theta + \rho \cos(-\theta) = 2 \rho \cos \theta$$

$$\rho y = \rho \sin \theta + \rho \sin(-\theta) = 0$$

Hence the x components are additive, the deviation bears a cosine relation to the wedge rotation, and the y components cancel.

From the foregoing, it can be concluded that any displacement between zero and 2ρ can be achieved by counterrotating the wedges by a specific amount between 0° and 90° and that the orientation of the displacement angle can be adjusted by moving the two wedges in unison.

8.2.1.2.2 Compensation for Point Ahead Diasporameters

The diasporameters used in the point ahead device produce the required beam deflection, but in so doing, they introduce a possible cause of severe vignetting of the output beam. This is due to the comparatively large separation between the diasporameter and the Galilean ocular of the principal telescope. To be free of vignetting, an exit beam should follow, in reverse, the path of an incoming beam that is off axis by the desired amount. Figure 8.2-5 shows such an incoming beam, and the effect of an uncompensated diasporameter on an exiting beam. Because of the very small angles of point ahead deflection, the sketch is greatly exaggerated.

An undeflected central ray follows the optical axis of the telescope throughout, going from Point A to A^1 for a transmitted ray and from A^1 to A for a received ray. An off axis incoming central ray (which actually does not exist because of the central obscuration) enters the telescope via Line OP and is reflected at an equal angle to its off axis focus position at F. It is intercepted by the secondary mirror at Point S and is reflected to its position in the secondary image plane at F^1. But it is again intercepted by the Galilean eyepiece at Point E and is refracted outward by an angle appropriate to the off axis angle in object space and the magnification of the telescope system, and the ray exits into the collimated space along Line EC. The standard diasporameter, on the other hand, deflects the central ray along Line AA", which although parallel to Line EC, is displaced from it by a measurable amount which may be sufficient to cause serious vignetting.

There are two readily available approaches that can be applied to remedy the situation by bringing the ray leaving the diasporameter AA" into coincidence with the ray as it should enter the telescope, Ray CE. One is preferable for use where there is ample space between the diasporameter and the Galilean ocular, as is the case in the 0.3 meter gimbaled telescope, and the other where the distance between them is small.

In the first case, an aperture transfer telescope is used to bring the two lines into alignment. As shown in Figure B, this telescope consists of two identical lenses separated by twice their focal length and centered midway

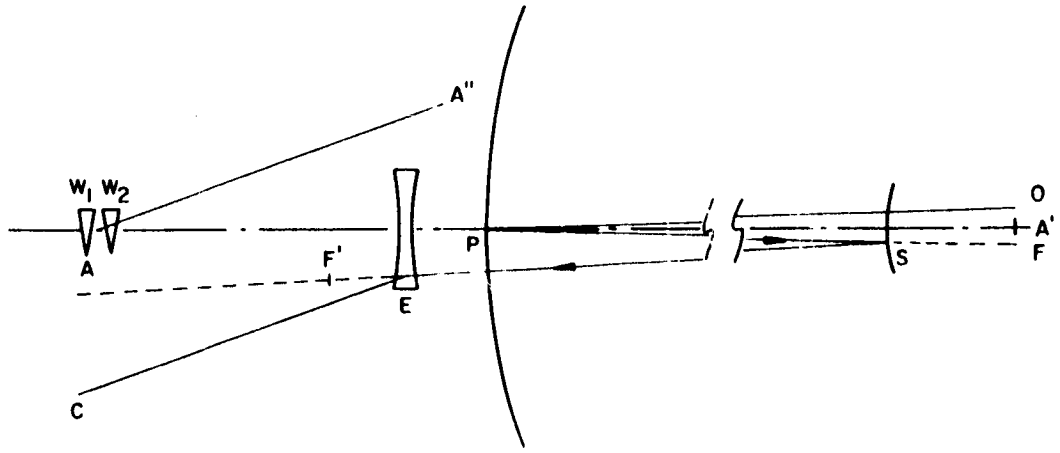


FIGURE A. PATH OF OFF AXIS CENTRAL RAY

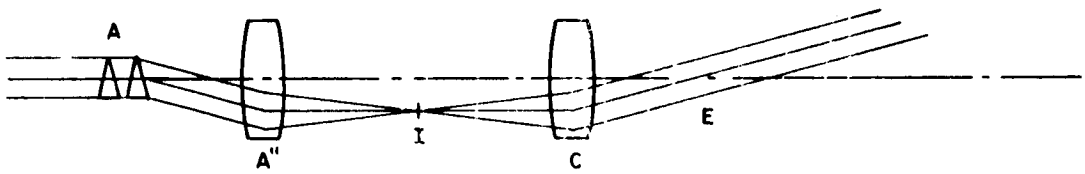


FIGURE B. APERTURE TRANSFER TELESCOPE

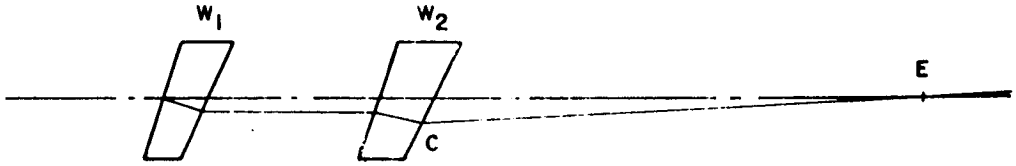


FIGURE C. COMPENSATED DIASPORAMETER

Figure 8.2-5 Diasporameter Compensation

between the diasporameter and the desired crossover point (beyond the Galilean ocular). The ideal configuration is to have the focal length equal to one-fourth the distance between the diasporameter and the cross-over, but a reasonable approximation to this condition is satisfactory. The first lens accepts the collimated light along Line AA" and forms an image at I which is off axis by an amount proportional to the disaporameter deflection. The second lens recollimates the energy and directs it along Line CE toward the crossover point on the axis. In generating the relayed crossover point, the lenses also serve as an image inverter. In so doing, they reverse the sense of the diasporameter. This is readily corrected at the diasporameter itself by putting a 180° offset into both wedges and causing them to generate an output diametrically opposite to the end result desired. This approach to vignetting reduction is applicable to the 0.3 meter gimbaled telescope where the distance between the diasporameter and the Galilean lens is large and there is ample free space between the dichroic mirror and the fine beam deflector.

The other approach is to build the compensation into the diasporameter wedges themselves. As shown in Figure C, this is done by providing the wedges with considerable thickness and inclining them at an angle which will displace the rays in a direction opposite to the deflection. W_1 and W_2 are the two diasporameter wedges shown in an additive configuration. With the broad side of the wedges toward the top of the figure, the beam is deflected toward the top. Likewise with the wedges tilted to the right, the beam is displaced toward the bottom of the figure. Thus the emerging beam is directed as desired along Line CE toward a crossover point.

In the 1.0 meter telescope and the 0.3 meter strapped-down telescope where there is a reasonably short distance separating the diasporameter from the principal telescope, this technique is applicable.

In the fine beam deflector, the same considerations apply, but since these elements are so close to the principal telescope, their effect is expected to be minimal and no special precautions against vignetting are anticipated.

8.2.1.3 Fine Beam Deflectors

The choice of a beam deflector for an optical tracking system depends upon the requirements set for resolution, speed of response, optical attenuation and the optical configuration of the rest of the system. If it is to be launched the unit must also be rugged, and weight and power consumption become important considerations. Those beam steering devices which will be discussed herein will be limited to three reflection type devices, the shear-plate-mirror, the bender-mode-mirror, and the mirror galvanometer. Each of these is basically a transducer driven mirror. Other beam steering techniques are not being considered since they fail to meet the resolution requirement of ± 300 spot diameters.

Wideband reflection scanning may be achieved by using mirrors attached to piezoelectric shear transducers, as shown in Figure 8.2-6. These transducers develop a shear strain in response to an electric field applied perpendicular

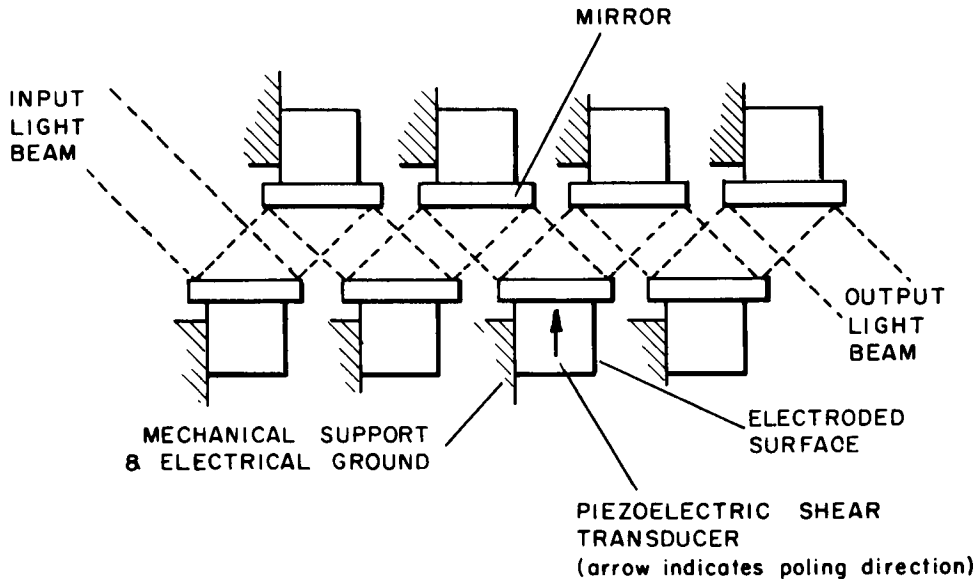


Figure 8.2-6 Shear-Plate Mirror Deflector Uses Shear-Mode Transducers To Tilt The Mirrors

to their poling direction. The induced shearing action causes the mirrors to tilt through an angle proportional to the applied field. Multiple mirror structures are employed to increase the scan angle, and hence the resolution of the device. With presently available piezoelectric materials, peak-to-peak angular mirror motions of 0.05^{o} are possible. The relative sizes of the mechanical components govern the operating bandwidth by determining the mechanical resonance frequency of the mirror-driver combination. Units with half inch mirrors have been made to operate over a bandwidth of dc to 17 kHz, however, 18 mirrors are needed to obtain 400 spot resolution and optical attenuation becomes excessive. This same problem is present in designs for lower frequency, higher resolution operation due to the large number of reflections needed.

There is another type piezoelectric transducer which can be designed to give much larger angular deflections, but which is more compliant than the shear transducer. This element is the piezoelectric bender and is illustrated in Figure 8.2-7. The bender construction and action is similar to that of a bimetallic thermometer. Two piezoelectric expanders are bonded together and energized so that one expands as the other contracts. This causes the entire unit to bend. If the bender is mounted as a cantilever beam with a mirror on the free end, the tilting of this end may be used to steer a light beam. Since the deflection and compliance of the bender are both proportional to its length, large scan angles in a single element are achieved only at the expense of bandwidth. Because of this, and the fact that the maximum deflection is not inherently limited, the bender seems more suited than the shear transducer to low frequency scanning up to a few hundred Hertz.

The mechanism of the traditional optical galvanometer consists of a mirror attached to a coil which is suspended in a steady magnetic field. Passing a current through the coil causes the mirror-coil assembly to twist on the suspension. The magnitude of the current governs the twist angle while the suspension provides the restoring force. Systems of this type may be constructed to give 400 spots resolution at a few kHz from a single mirror. Because of the need for a magnet to provide the dc field the weight of a one-dimensional scanner may reach 10 lbs. or more and require many times the volume of the previous devices. These factors will most likely limit its usefulness for spaceborn applications.

8.2.2 Receiver

The first two elements of the receiver optics are the principal telescope and the fine beam deflector described above. They serve to collect the incoming energy, compress it into a 12.7 mm bundle of light and make the necessary beam adjustments to keep the received bundle on axis. At the dichroic mirror the receiver line of sight is separated from the transmitter line of sight as shown in Figure 8.2-8. It is then put through a pupil matching telescope (PMT-3) to reduce the diameter from 12.7 mm to two millimeters. This is accomplished with a positive lens of 75 mm focal length and a negative lens of -12 mm focal length. The positive lens is placed adjacent to the dichroic mirror. The clear apertures of the lenses need not

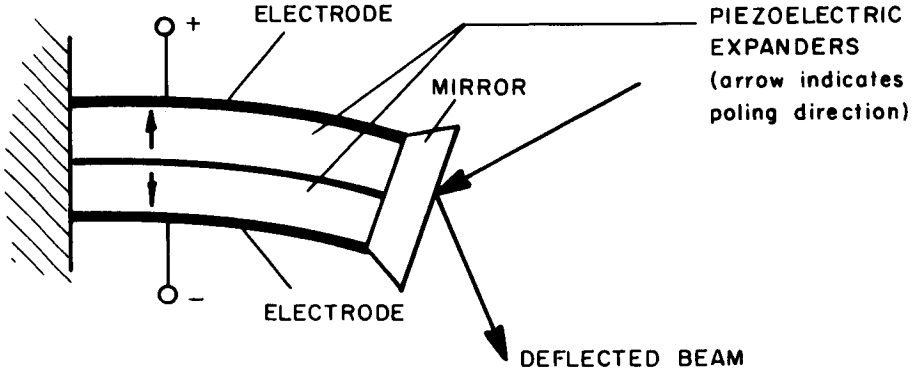


Figure 8.2-? Cantilever-Mounted Piezoelectric Bimorph

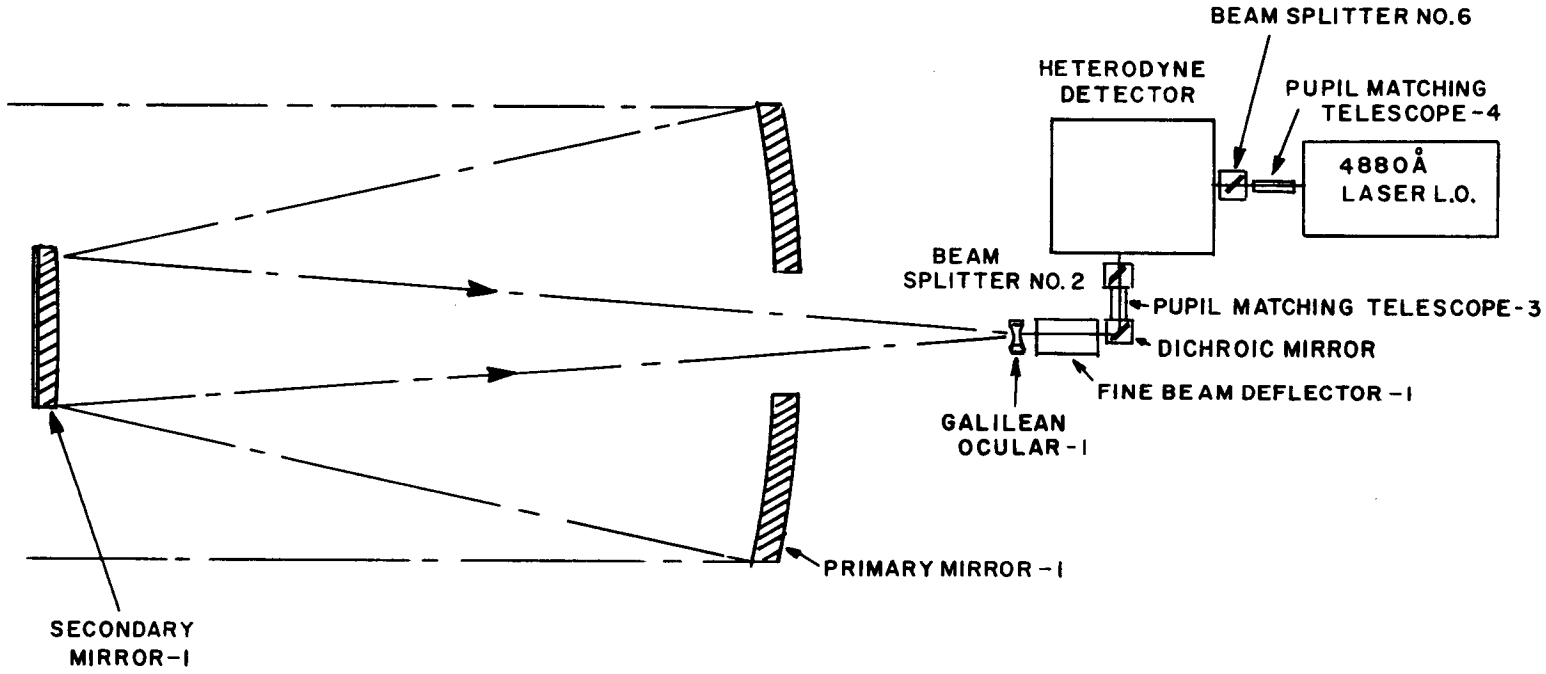


Figure 8.2-8 1.0 Meter Telescope Receiver

be greater than 16 mm and 3 mm for the positive and negative lenses respectively.

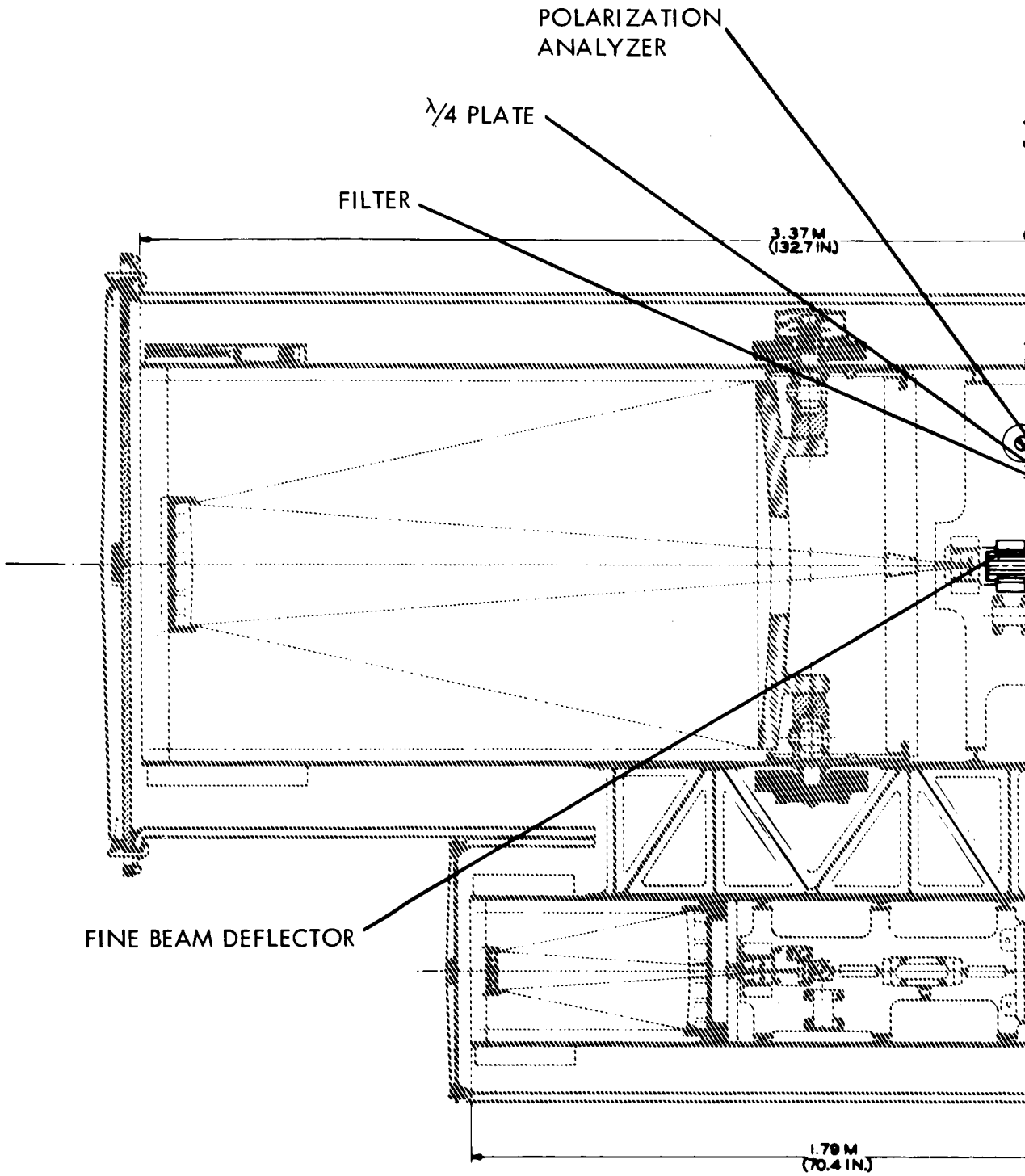
Immediately after the telescope is a beamsplitter (BS-2) which divides the incoming energy equally for the purposes of heterodyne detection and tracking. The receiver energy is then passed through a narrow band filter to reduce background radiation and its associated noise. For a detailed view of the detector part of the receiver, see Figures 8.2-9a and 8.2-9b.

Next the beam passes throguh a quarter wave plate to take the incoming light which is circularly polarized and render it plane polarized in preparation for passing it through the polarization analyzer (PA) that follows. The polarization analyzer separates the light into two polarized components, the vertically polarized light being transmitted through the analyzer and the horizontally polarized light being deflected to the side. Each of the polarized components is then combined at a beam splitter (BS-3 and 5) with a similarly polarized bundle originating at the local oscillator. Both beams from each beam splitter are heterodyne detected and the outputs of all four detector (D-1, 2,3,4) are processed to reconstitute the received signal modulation.

The local oscillator mentioned above is a 4880 Å laser whose output is a beam 1 mm in diameter and plane polarized horizontally. The output is fed through a pupil matching telescope (PMT-4) to increase the beam diameter to two millimeters. This telescope is identical to PMT-1 except that the negative lens is turned toward the laser. The excess power (not needed for the heterodyne detectors) is tapped off by means of a beam splitter (BS-6) for a tracker electronic balancing which is described in subsection 8.2.3. The remaining energy is then equally divided by a beam splitter (BS-4) and directed toward the beam splitters (BS-3 and 5) where it is combined with the received signal. The light going toward the detectors for horizontally polarized light already possesses the proper polarization. However, the light destined for the other detectors must have its plane of polarization changed to agree with that of the incoming beam. This is accomplished by placing a suitably oriented halfwave plate immediately after beamsplitter BS-4.

8.2.3 Tracker

As shown in figures 8.2-10a and 8.2-10b the incoming signal for the tracker is picked off the receiver line of sight by means of the beamsplitter BS-2. This is followed by another beamsplitter (BS-7) which couples in less than one per cent of energy from the local oscillator for electronically balancing the tracker detectors. This beamsplitter in turn is followed by a very narrow band filter whose band pass is in the order of 1 Å. This filter reduces the noise into the tracker by limiting its optical bandwidth. A telephoto lens with an effective focal length of 182 mm forms an image of the ground station source on the apex of the tracker pyramid mirror. In conjunction with the 6.35X magnification of the pupil matching telescope and the 76X magnification of the principal telescope, an effective focal length is produced of 87.4 meters and a scale factor of 2.36 seconds per millimeter (1 minute per inch) at the image plane. The image is split into four quadrants by


POLARIZATION
ANALYZER
λ/4 PLATE
FILTER
3.37 M
(132.7 IN.)
FINE BEAM DEFLECTOR
1.79 M
(70.4 IN.)

21200

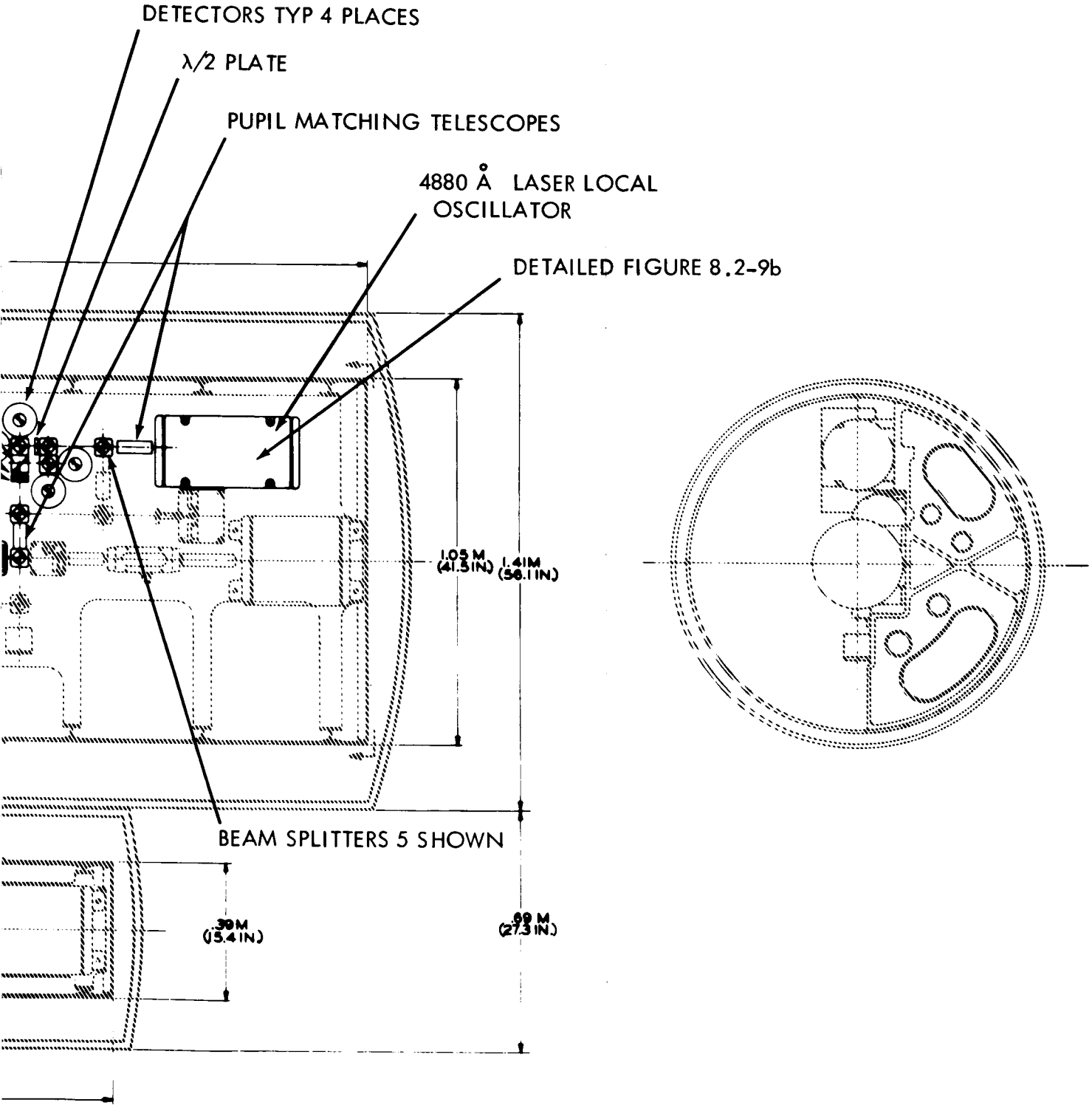


Figure 8.2-9a. 1.0 Meter Laser Telescope - Heterodyne Detector

~~2-39~~

2-40

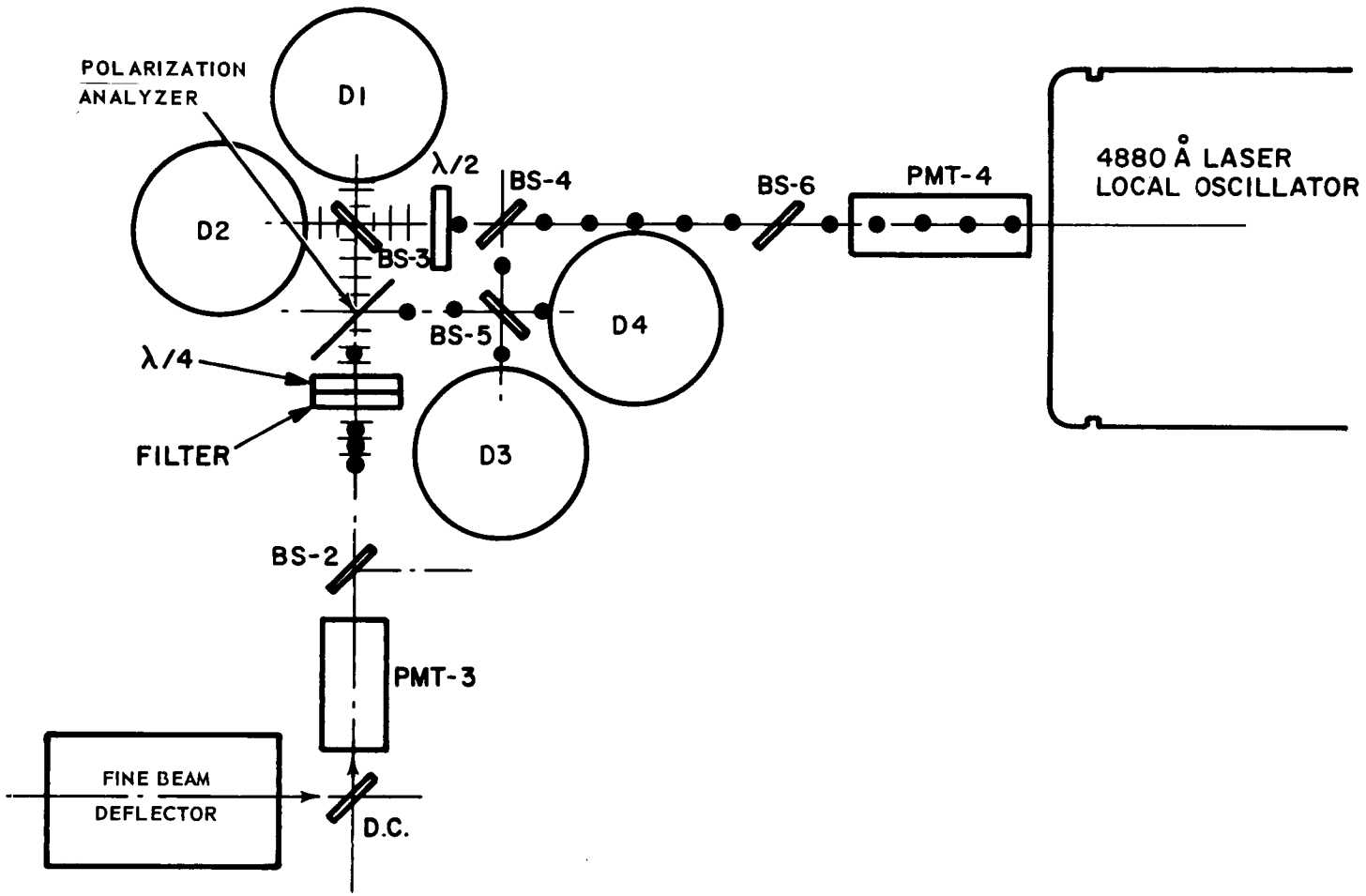
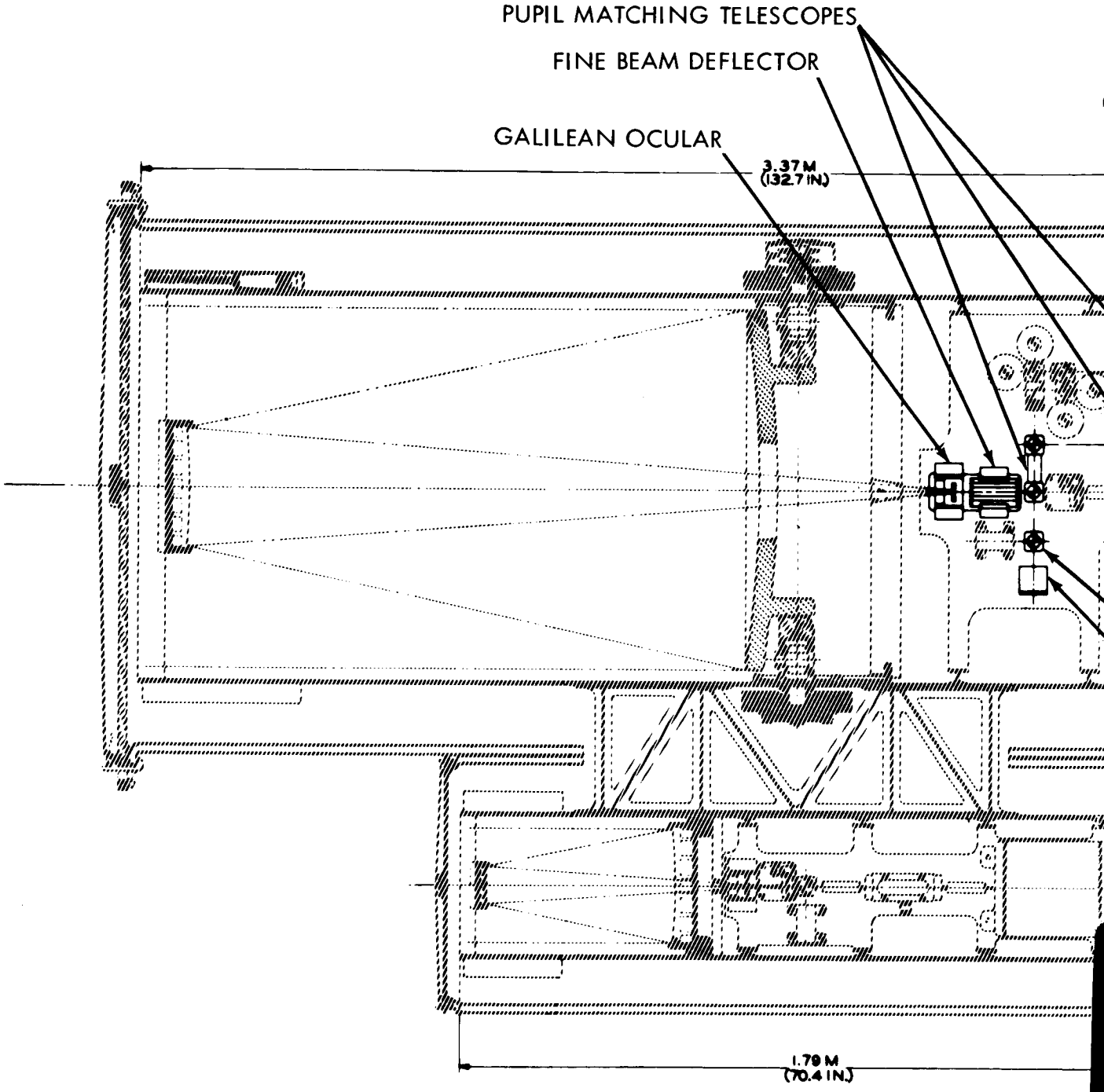


Figure 8.2-9b Heterodyne Detector



2-43

PRECEDING PAGE BLANK NOT FILMED.

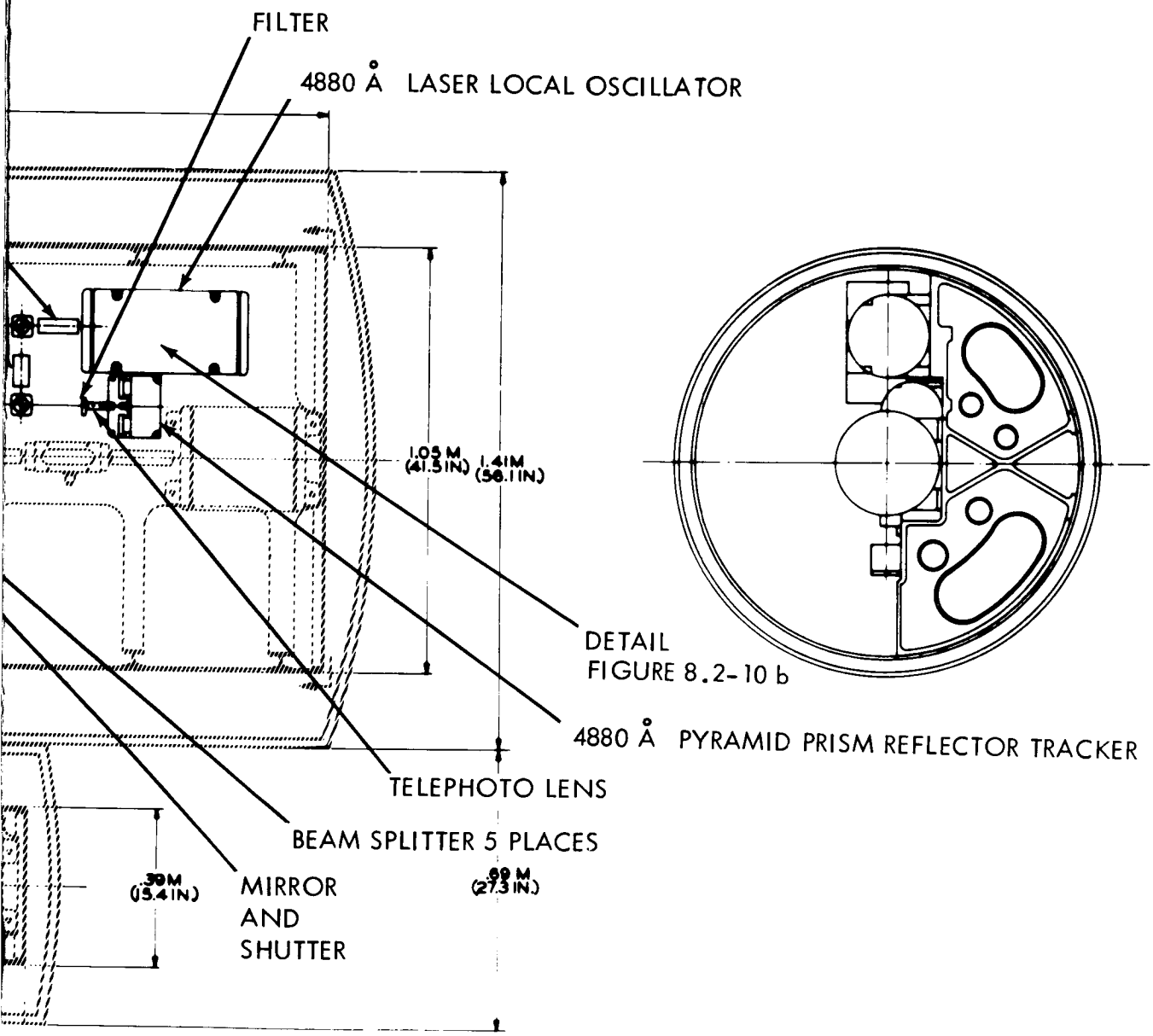


Figure 8.2-10a. 1.0 Meter Laser Telescope Tracker

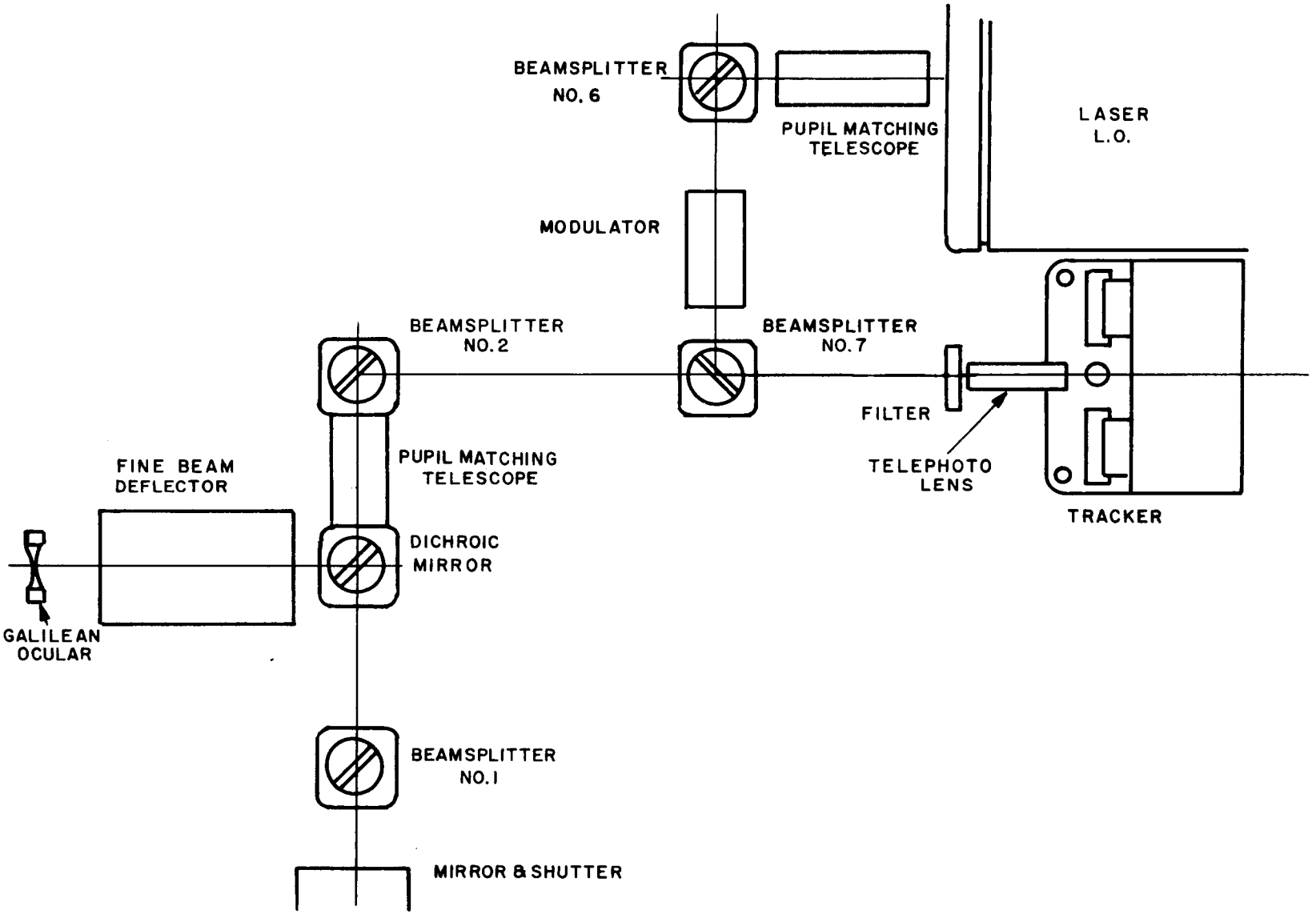


Figure 8.2-10b 1.0 Meter Telescope Tracker

the pyramid, and the energy from each quadrant is collected by its proper photomultiplier tube. The outputs from the four photomultiplier tubes are processed to determine the tracking error and a correcting signal is transmitted to the fine beam deflector to null the error.

To balance the tracker detector a test signal originating at the receiver local oscillator is provided. The energy not needed for the heterodyne receiver is picked off by a beam splitter BS-5, is fed through a modulator (MOD-2) to impress a reference signal on the local oscillator carrier. Sufficient signal to drive the tracker is coupled into the tracker line of sight by means of another beam splitter BS-7 in front of the tracker objective lens. Any output of the tracker when operating in this configuration indicates a condition of unbalance. The output signal is used to adjust the gain of the appropriate tube or tubes to return the tracker to a condition of balance.

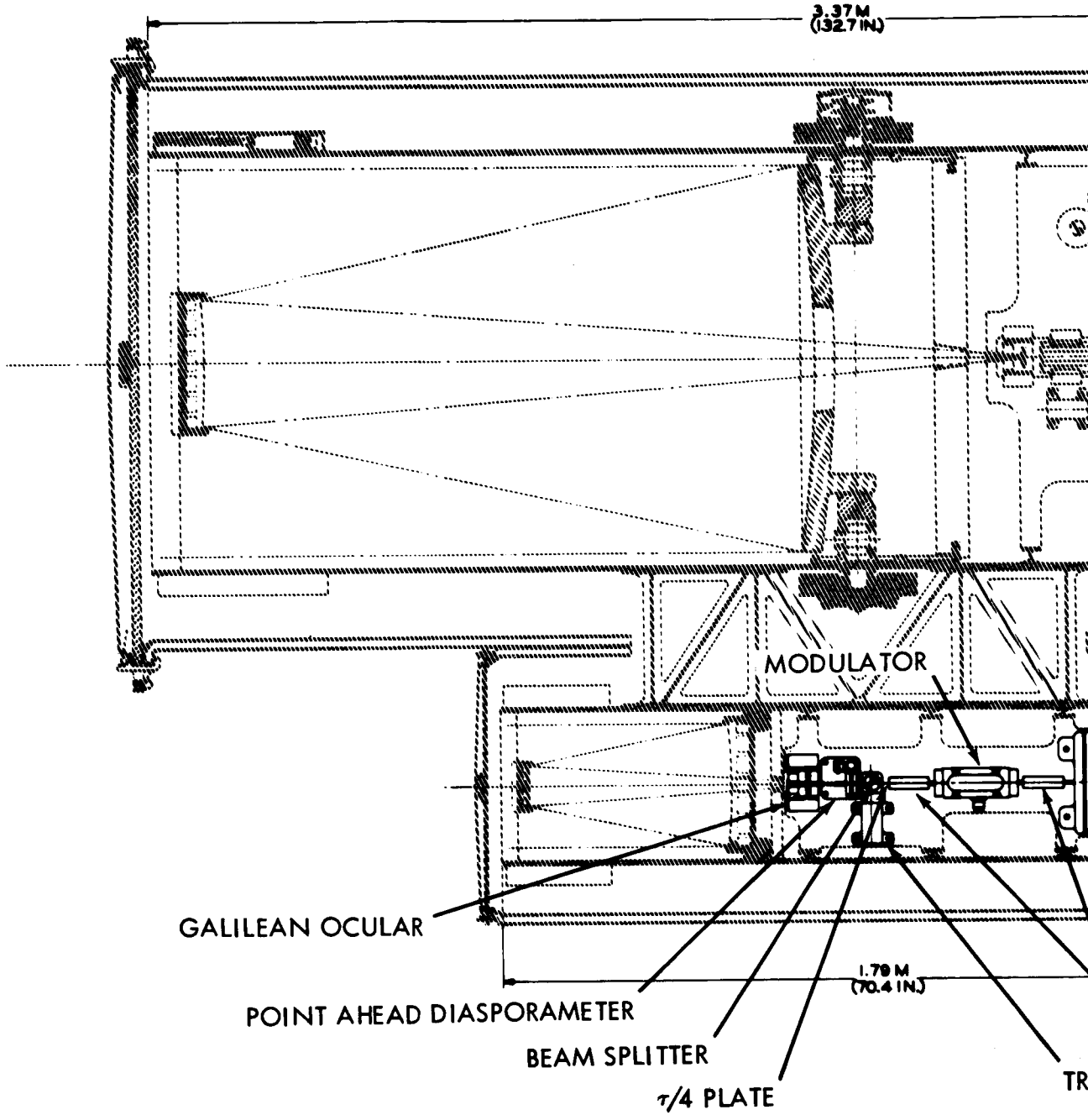
Another test provided is a transmitter boresight adjustment. This is accomplished by scavenging the transmitter energy that is reflected by the dichroic mirror, reflecting it back on itself by means of a plane mirror. It passes through the dichroic mirror and some of it is reflected by the beamsplitter to the tracker. To perform the check, the shutter adjacent to the redirecting mirror is opened and the tracker output analyzed. Any signal indicates a boresighting error. Small errors can be nulled out by means of the point ahead diasporameter. Closing the shutter turns off the boresight signal so it cannot interfere with the tracker or receiver under operating conditions. This operation is described in detail in subsection 4.5.5.3.

8.3 STRAPPED DOWN TELESCOPE

The 0.3 meter strapped down telescope is essentially a scaled down version of the transmitting equipment of the 1 meter telescope with the following changes: it operates at a wavelength of 10.6 u rather than 6328Å; it has no receiving equipment, and it has no fine beam pointing capability. It is illustrated in Figures 8.3-1a and 8.3-1b.

Again, starting at the transmitter laser, the component parts are as follows: The oscillator-amplifier is a Nitrogen-Carbon Dioxide laser operating at 10.6 u with an output beam 5 millimeters in diameter. The beam is matched to the aperture of the electro optic modulator by a 5 power telescope consisting of a positive lens of 100 mm focal length and a negative lens of -20 mm focal length with the positive element adjacent to the laser. The clear apertures need be no greater than 6 mm for the positive lens and 3 mm for the negative. Because of the wave length of the transmitter the lenses are made of germanium or some other suitable infrared transmitting material.

The electro optical modulator is similar in function to the modulator in the 1 meter telescope except that due notice is taken of the optical bandpass of the refractive materials used. After the modulator the beam is again changed in diameter, this time being expanded from 1 to 7.5 millimeters by means of a pupil matching telescope. This telescope consists of


3.37 M
(132.7 IN.)
MODULATOR
GALILEAN OCULAR
1.79 M
(70.4 IN.)
POINT AHEAD DIASPORAMETER
BEAM SPLITTER
τ/4 PLATE
TR

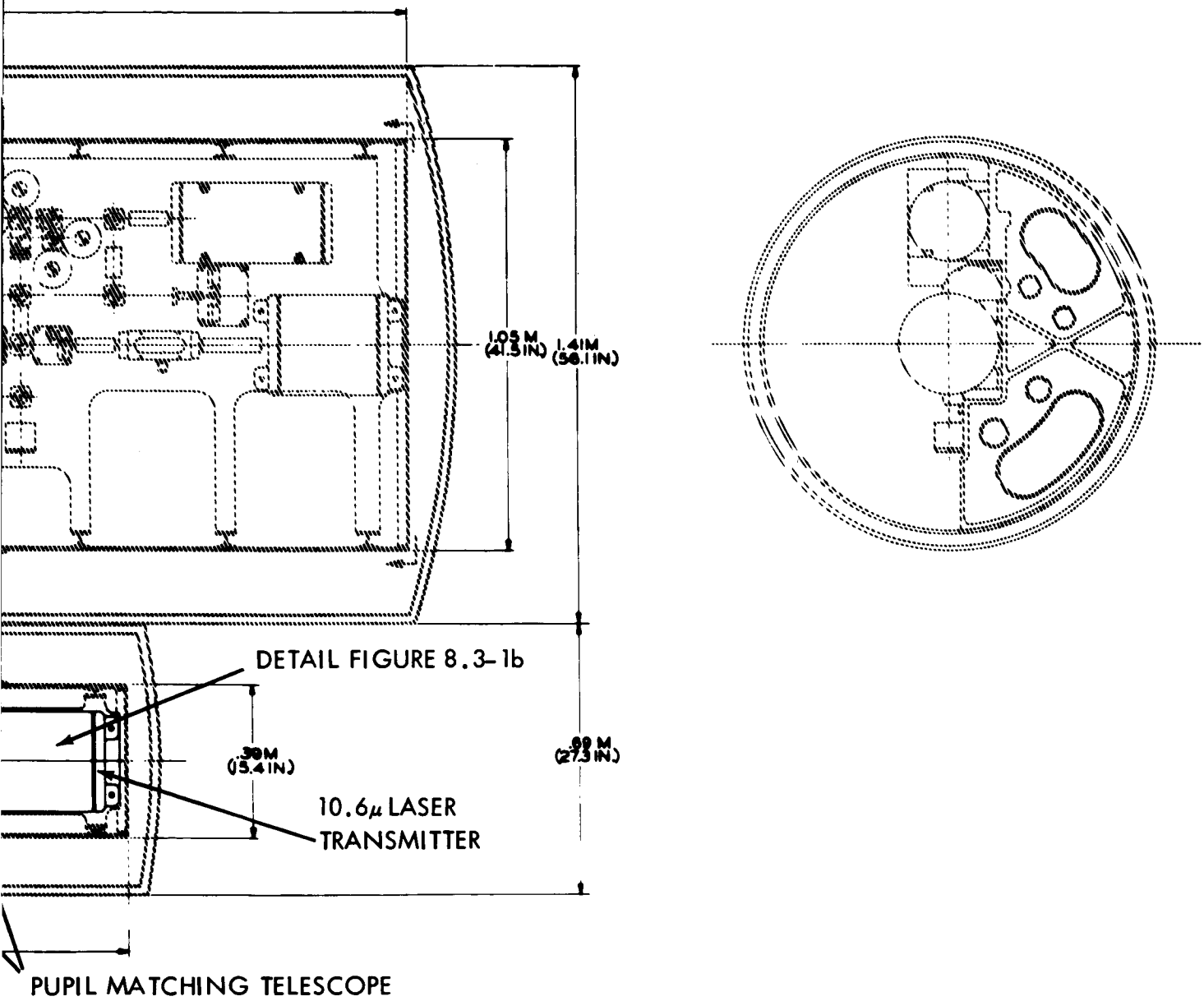


Figure 8.3-1a. 0.3 Meter Laser Telescope

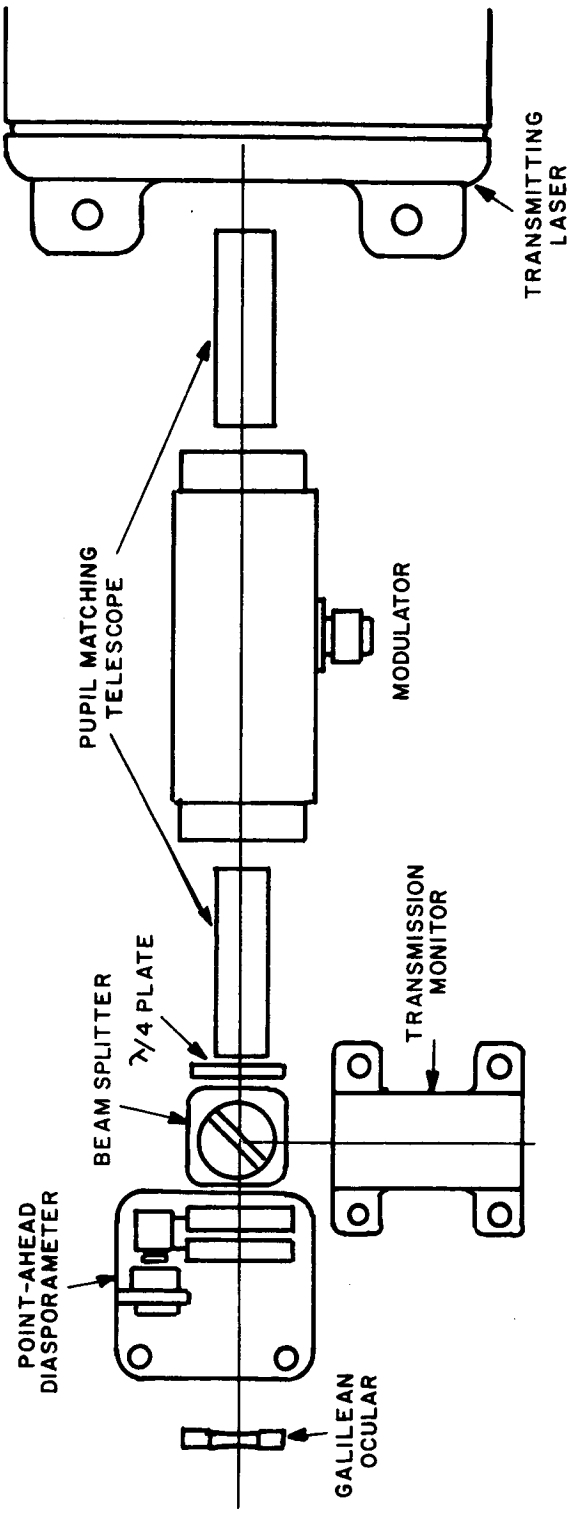


Figure 8.3-1b 0.3 Meter Strapped Down Telescope

a positive lens of 105 mm focal length, a clear aperture of 13 mm and a negative lens of 14 mm inches focal length and 3 mm clear aperture. The negative lens is closest to the modulator.

A beam splitter picks off a small portion of the transmitter energy and directs it toward a detector to monitor the transmission. The bulk of the energy is transmitted through the beam splitter and encounters the point-ahead diasporameter where it is deflected up to 0.5 degree (40 seconds in object space) by the diasporameter wedges. Compensation is much less in this telescope than in the one meter telescope because of the combined effects of lower magnifying power and closer spacing of the diasporameter to the telescope ocular element.

After the diasporameter there remains only the 0.3 meter telescope which consists of a Cassegrainian objective made up of a paraboloidal mirror 0.762 meter focal length and 0.3 meter aperture and a hyperboloidal secondary mirror of -0.381 meter focal length and 100 mm aperture with 0.508 meter separation between them, and a Galilean ocular with a focal length of -57.15 mm and 13 mm clear aperture. This results in a telescope with a magnification of 40 X due to the effective focal length of 2.286 meters for the objective and -57.15 mm for the ocular. The telescope accepts the transmitted beam at an aperture of 7.5 mm, and with its magnification factor of 40, recollimates it in a beam of 0.3 meters diameter.

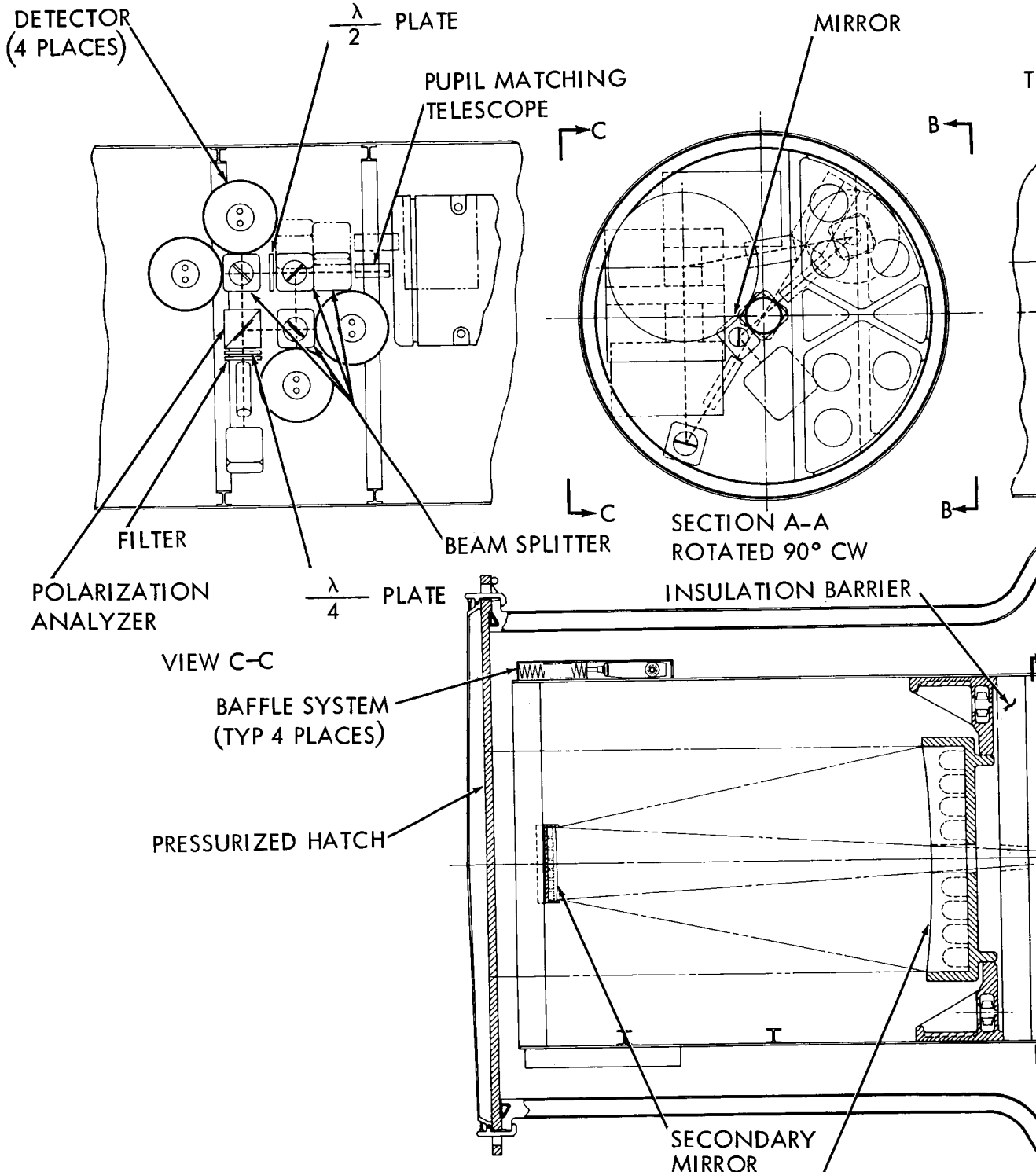
8.4 THREE TENTHS METER GIMBALLED TELESCOPE

The 0.3 meter gimballed telescope (Figure 8.4-1) is basically a scaled down version of the 1.0 meter telescope (Figure 8.2-1) insofar as it incorporates the same functions, (transmitting, receiving and tracking) and performs them generally in the same fashion. The difference between the two instruments stem from three factors: the receiver operates on a wavelength of 6328 Å instead of 4880 Å; the entrance pupil of the telescope is smaller, so different magnification ratios are convenient, and finally, the smaller size envelope of the telescope calls for different packaging techniques for more efficient use of the available space. Since the drawing of the optical system involves several out of plane views due to the physical arrangement, a schematic diagram Figure 8.4-2 showing all functions in plane is provided as an adjunct to the description that follows. A perspective diagram is also provided in Figure 8.4-3.

As with the other instruments the description starts with the transmitter laser, follows the transmitter line of sight through to the principal telescope, and then picks up the receiver and tracker in turn and finally the auxiliary equipment. Since the function of the major elements has been described in detail in the discussion of the 1.0 Meter Telescope, they will be mentioned in more general terms in the present discussion.

8.4.1 Transmitter

The transmitter laser, first pupil matching telescope and electro optical modulator are identical with those of the 1.0 meter telescope as shown in



TELESCOPE SPECIFICATIONS
0.3 M 12 IN. TELESCOPE
F SYSTEM 7.5
FOCAL LENGTH 2.28 M (90 IN.)

GALILEAN OCULAR

FINE BEAM D

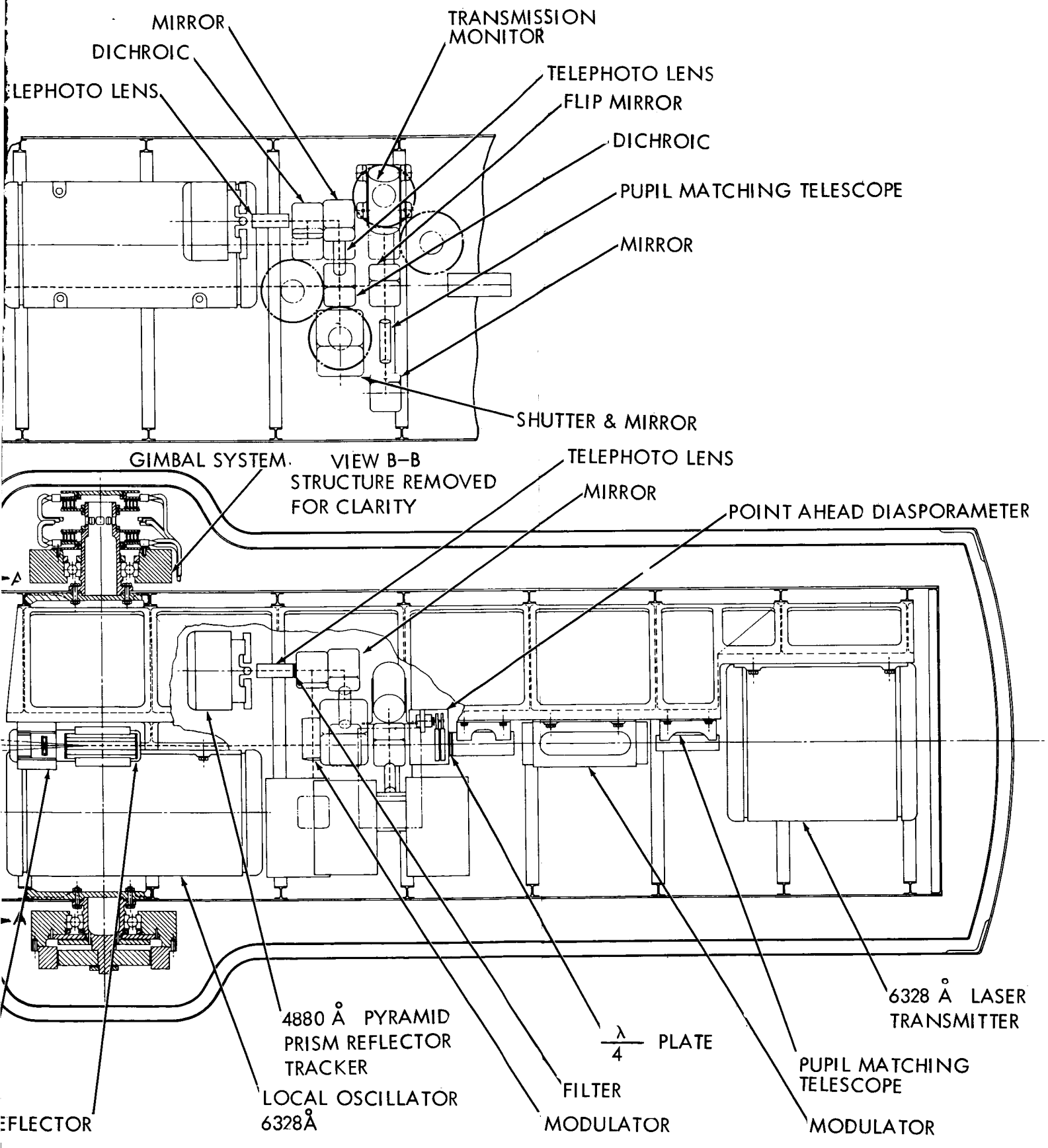


Figure 8.4-1. 0.3 Meter Laser Telescope

~~2-51~~
2-52

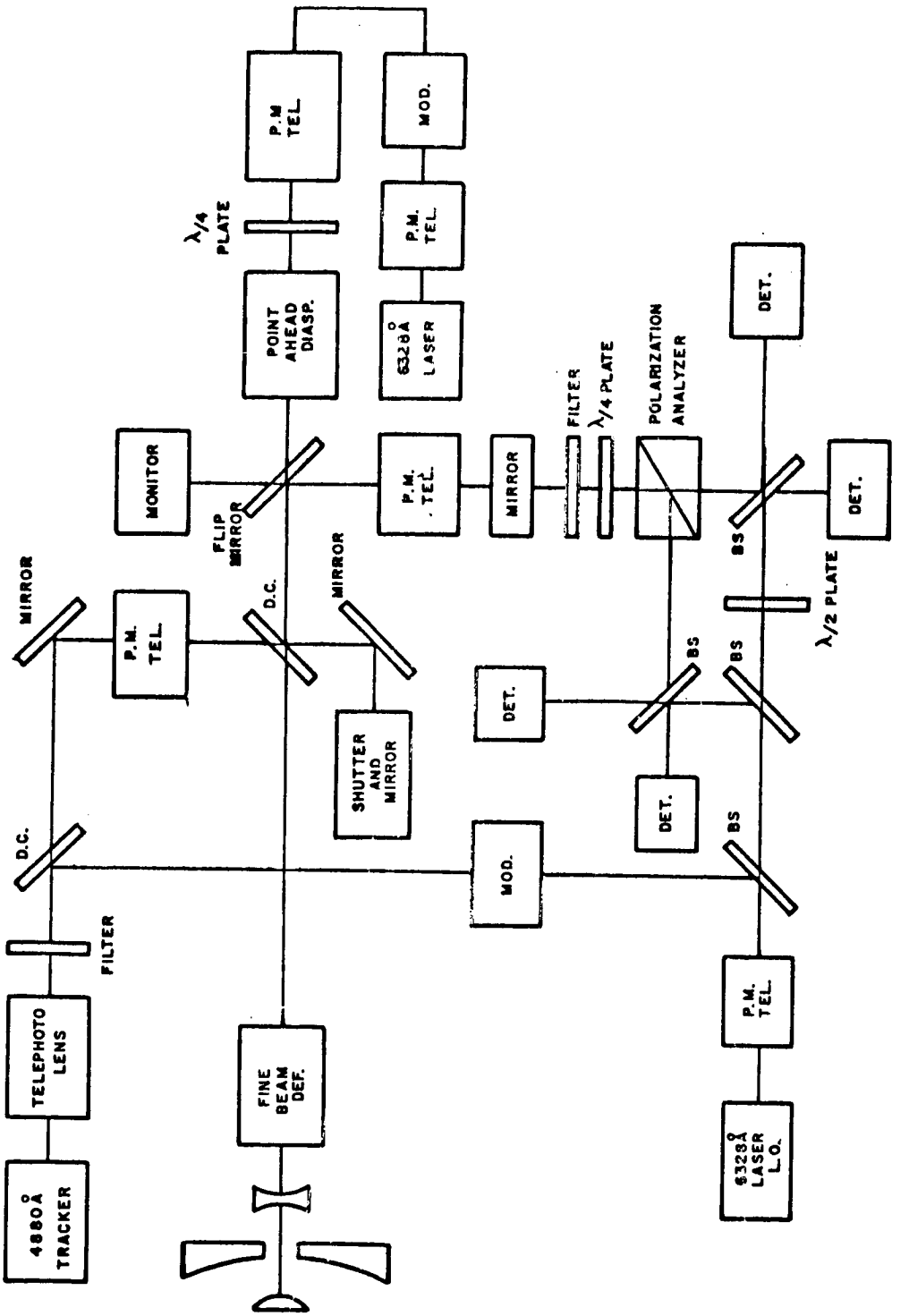


Figure 8.4-2 0.3 Meter Gimbaled Telescope

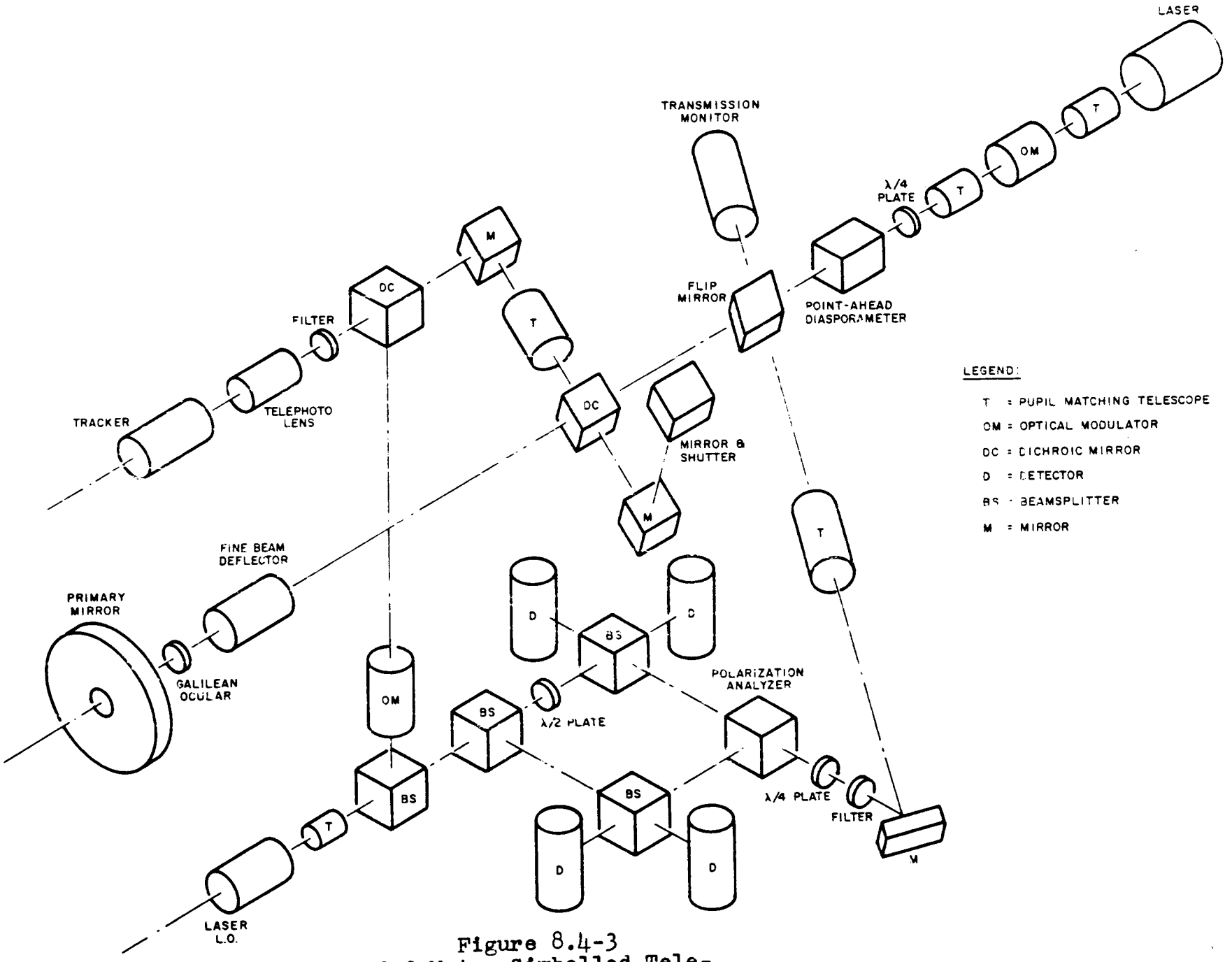


Figure 8.4-3
0.3 Meter Gimballed Telescope, Perspective View

Figure 8.4-4. The second pupil matching telescope increases the beam diameter from 1 millimeter to 7.5 millimeters instead of from 1 millimeter to 12.7 millimeters as in the 1.0 meter telescope. This is accomplished by a telescope consisting of a positive lens of 97.5 mm focal length and 13 mm clear aperture and a negative lens of -13 mm inch focal length and clear aperture of 3 mm, the negative lens being closer to the modulator. The quarter wave plate that is placed immediately after the pupil matching telescope serves the function of circularly polarizing the plane polarized modulator output. The point-ahead diasporameter performs the same adjustment for transit time correction but is required to provide a deflection of only 15 minutes per wedge instead of the 26 minutes needed in the 1.0 meter diasporameter. The compensation required of this diasporameter is slightly greater than in the 1.0 meter telescope, because of the long throw between the diasporameter and the Galilian eyepiece. It may be preferable in this case to use an aperture transfer telescope in lieu of the diasporameter compensation as indicated in Section 8.2.1.2.2.

After the point-ahead diasporameter there is a movable (flip) mirror, half of which is fully silvered and half a very weak beam splitter. The latter half is used in the transmit position, reflecting a small portion of the energy to a transmission monitor and passing the bulk of the beam. In the receiving mode the mirror is shifted so that the fully silvered half deflects all the incoming 6328 Å energy toward the heterodyne detector.

A dichroic mirror transmitting 6328 Å and reflecting 4880 Å is the next element in the transmitter line of sight. The bulk of the transmitter energy passes through the mirror, but as in the case of the 1.0 meter telescope a small amount is reflected and used intermittently in a receiver axis transmitter axis boresight check. See Subsection 8.4.3.

The requirement for a flip mirror in addition to the dichroic mirror is dictated by the fact that the receiver and transmitter operate in the same wavelength band (6328 Å) and the tracker operates at 4880 Å, whereas in the 1.0 meter telescope the receiver and tracker operate in the same band (4880 Å) and the transmitter alone operates at 6328 Å. A flip mirror is used in preference to a beamsplitter in the interest of efficiency and is made possible by the fact that the receiver and transmitter do not operate simultaneously. Finally the use of a very weak beamsplitter at the flip mirror position during transmission is necessitated by packaging requirements which make it awkward to take the monitor signal off the dichroic mirror.

The function of the dichroic mirror is to separate the ground transmitted signal for the tracker from the main telescope axis of the instrument. The transmitter energy is then put through the fine beam deflector to compensate for vehicle disturbances and to act as a vernier for the mechanical gimbals. (The upcoming beams from the ground are acted upon in the same manner and thus are compensated for vehicle disturbance). Because of the smaller magnification of the principal telescope and the narrower pupil, this deflector can be less elaborate than the one used in the 1.0 meter telescope. Assuming the same cascaded piezoelectrically driven mirror system, it

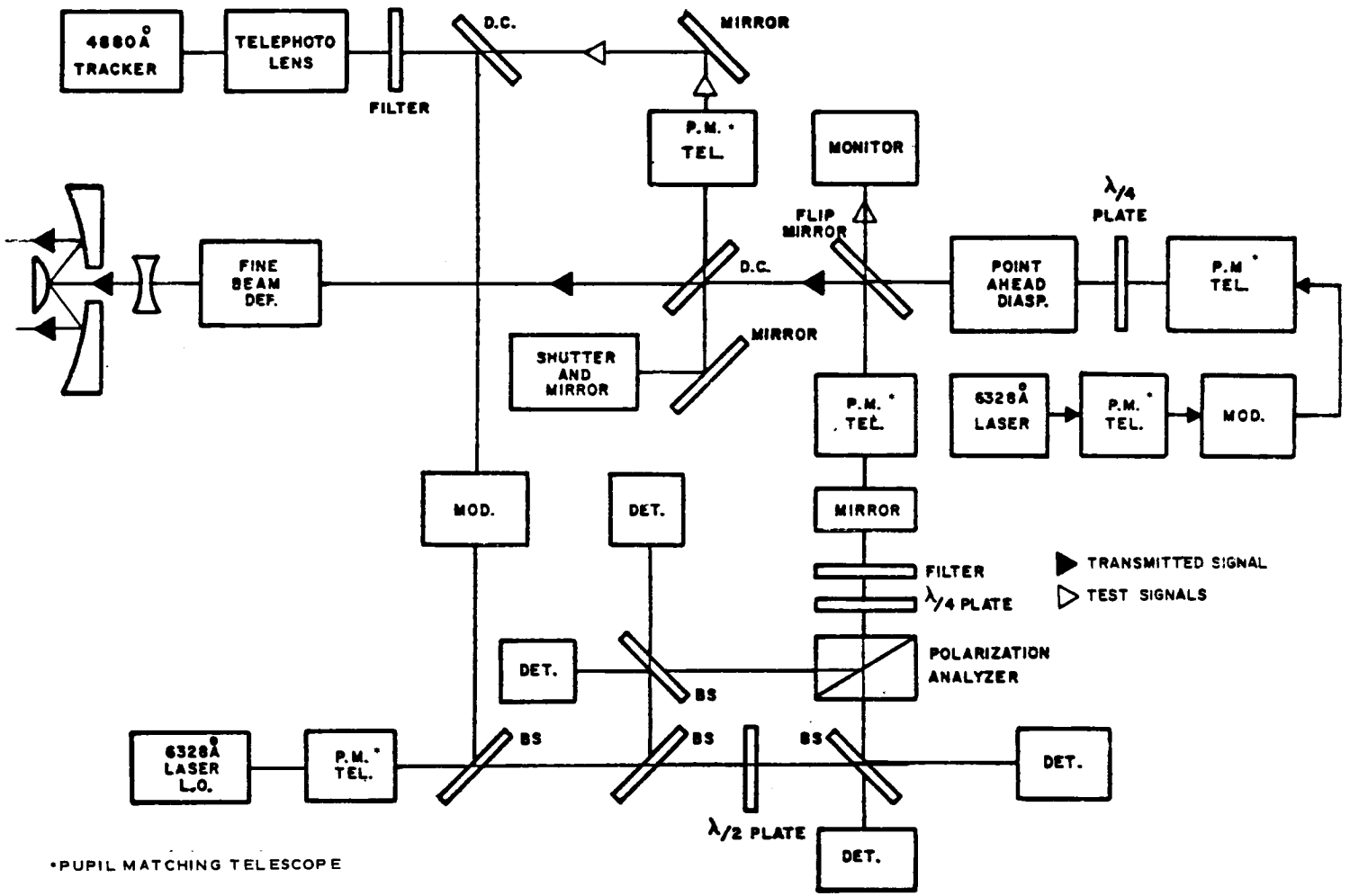


Figure 8.4-4 Transmitter

is possible to use four mirrors in each axis instead of eight. Using the other techniques which are mentioned in subsection 8.2.1.3 there would be no obvious change except a reduction in the required aperture and deflection angle.
From the fine beam deflector the signal is fed through the principal telescope which is a copy of the telescope used in the 0.3 meter strapped down instrument except that the Galilean lens is fabricated of glass and achromatized for 6328 Å and 4880 Å. The telescope serves to expand the transmitted beam from 7.5 millimeters to 0.3 meters. The telescope consists of a primary and secondary mirror in cassegrainian configuration providing an effective focal length of 2.29 meters and an aperture of 0.305 meters.

8.4.2 RECEIVER

The incoming 6328 Å energy is collected and recollimated into an exit beam of 7.5 millimeters diameter by the principal telescope, passed through the fine beam deflector and the dichroic mirror and is reflected off the flip mirror which is put into the circuit for the receiving function. See Figure 8.4-5. From the mirror the beam is passed through another pupil matching telescope to reduce the beam to a two millimeter diameter. The telescope that does this consists of a positive lens of 120 mm focal length and a negative lens of -32 mm focal length. The clear apertures can be 13 mm and 3 mm respectively. The positive lens is closer to the flip mirror. This narrowed beam is then redirected by a mirror toward the filter, quarter wave plate, polarization analyzer, beam splitters and heterodyne detectors. These elements are the same as those used in the 1.0 meter telescope except that the filter pass band is centered at 6328 Å instead of 4880 Å and the other elements are selected or treated for optimum performance at this wavelength. For details refer to subsection 8.2.2.

The local oscillator part of the receiver is a copy of the corresponding portion of the 1.0 meter instrument except that the oscillator is a 6328 Å laser instead of 4880 Å. The beam splitters and half wave plate are arranged in the same configuration to provide the required energy for the heterodyne detectors and the tracker balance check.

8.4.3 TRACKER

The incident 4880 Å light is collected, collimated and stabilized by the principal telescope and fine beam deflector as described for the transmitter. It is separated from the instrument axis by means of a dichroic filter which transmits 6328 Å light and reflects 4880 Å. The diameter of the tracking beam is reduced from 7.5 millimeters to 2 millimeters by means of a pupil matching telescope identical to that used in the receiver line of sight.

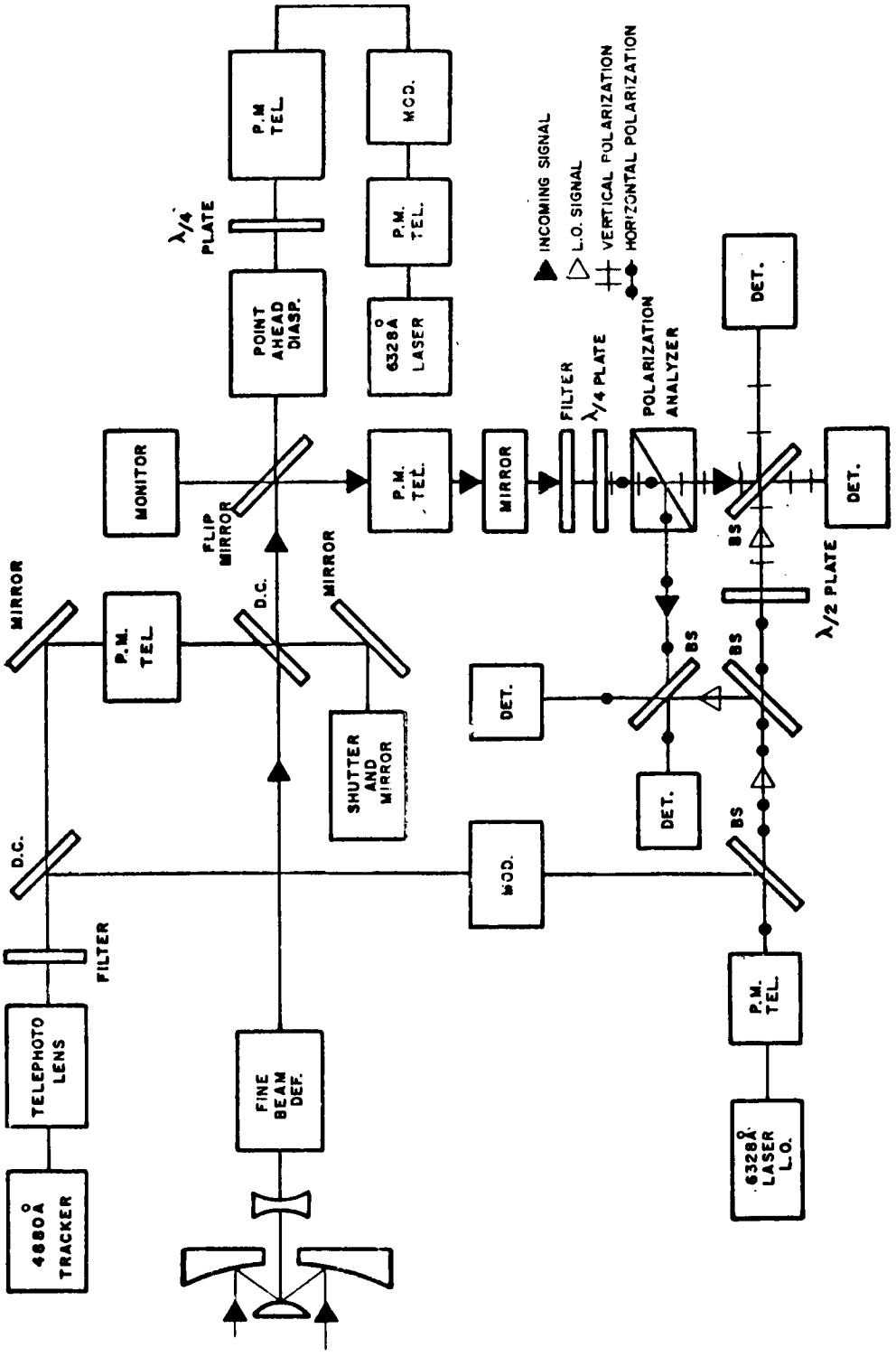


Figure 8.4-5 Receiver

See Fig. 8.4-6. It is then deflected by a mirror toward a dichroic mirror which transmits 4880 Å and reflects 6328 Å. This dichroic mirror permits the incoming tracker signal to pass through to the tracker and couples in the modulated local oscillator signal for the tracker balance test, without significant loss to either signal.

The light then passes through the narrow bandwidth filter, which serves to reduce the ambient noise for the tracker and as an attenuator for the balance test. A telephoto lens of 195 mm effective focal length is used to form an image of the target on the apex of the prism reflector of the tracker, where its energy is divided among its four detectors as a function of displacement from the center of the field. The focal length cited provides an image plane scale factor of 1.5 minutes per inch. The telephoto lens consists of a positive element of 127 mm focal length and a negative element of 120 mm focal length separated by 89 mm. In this configuration the negative lens provides a magnification factor of 1.53 and gives an effective focal length of 195 mm for the telephoto lens.

The 0.3 meter telescope also incorporates means for electronically balancing the tracker detector and adjusting the boresight of the transmitter. The balancing is accomplished by picking off a portion of the local oscillator output not needed for the heterodyne detectors, passing the energy through a modulator and feeding it into the tracker via the dichroic mirror. The narrow band filter will attenuate the 6328 Å signal to about 10^{-5} of its original strength, but this amount is adequate for detection. The signal is detected and the gain of the photomultipliers is adjusted to null the signal. When this condition is achieved the detectors are balanced. The transmitter boresight is adjusted by using the transmitter energy reflected from the dichroic mirror in the main axis of the telescope. The energy is then reflected from a mirror to a shutter and redirected along the same path to and through the dichroic mirror from which it follows the path of the 4880 Å received beam to the tracker. Error signals from the tracker are fed to the point ahead diasporameter if necessary to null out the error. These procedures follow those used in the 1.0 meter telescope with the modifications required by the change in receiver frequency.

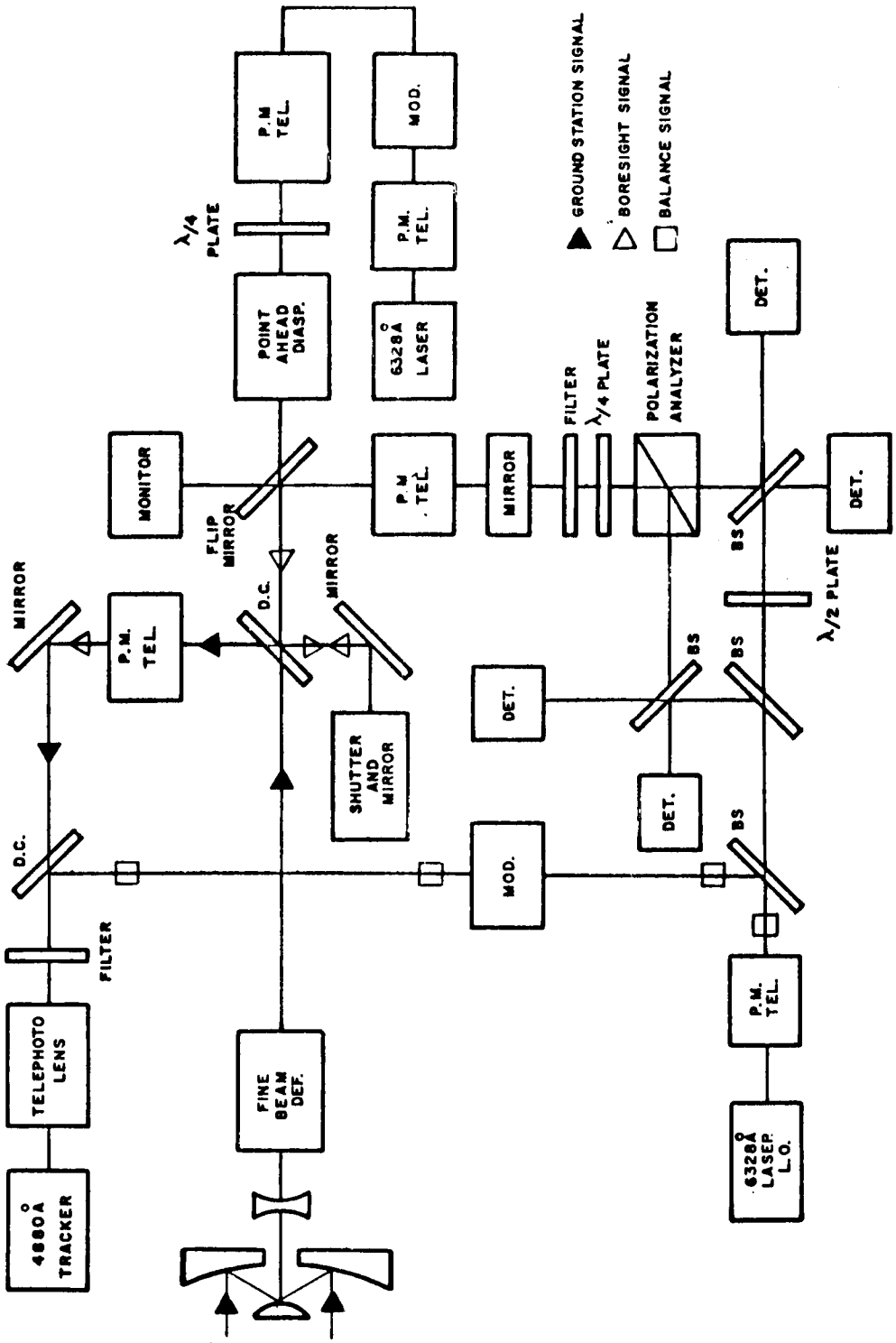


Figure 8.4.-6 Tracker

9.0 STELLAR ORIENTED EXPERIMENT GROUP

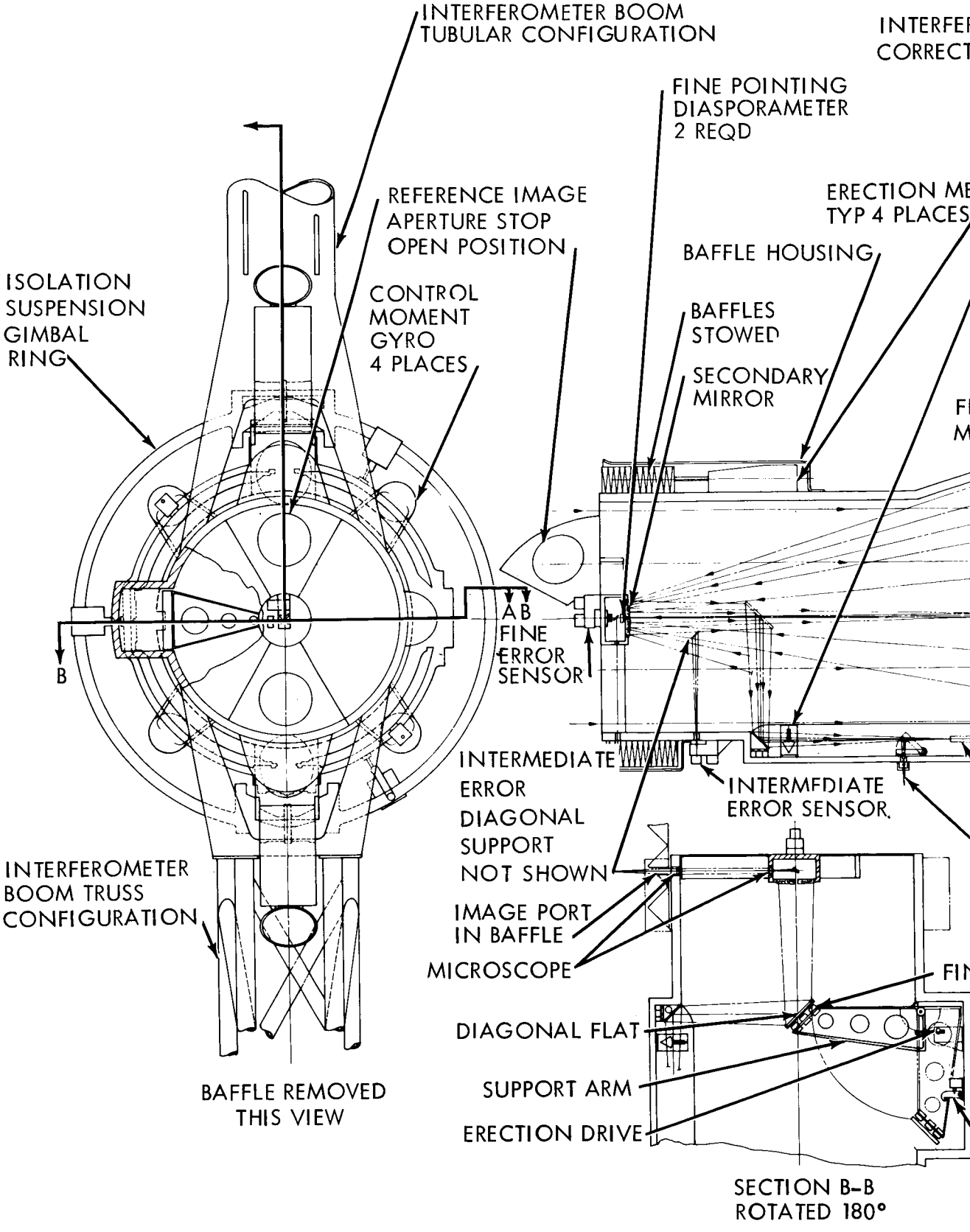
There are four recommended OTES experiments which are classified in the stellar oriented experiment group. These are the Fine Guidance, Comparison of Isolation Techniques, Interferometer System and Segmented Optics. The first three of these four experiments were designed to be performed on a single 0.6 meter (approx. 24 inches) aperture telescope. The segmented optics experiment is to be conducted on a similarly sized telescope.

9.1 TELESCOPE REQUIREMENTS

The stellar interferometer, Comparison of Isolation Techniques, Fine Guidance and Segmented Optics telescope are combined in a single assembly which is shown in figure 9.1-1. The segmented optics telescope is independent of both the stellar interferometer, comparison of isolation techniques and the fine guidance telescope. The stellar interferometer, comparison of isolation techniques and the fine guidance experiment, while functionally independent, use the same basic telescope. The principal requirements for the fine guidance telescope are: a focal length to simulate that of a future generation orbiting large astronomical telescope, and a collecting aperture to secure adequate signal to noise ratio for a tenth magnitude star to permit pointing to 0.01 second of arc. (See computations in subsection 4.12.5.3).

A telescope of 0.6 meter (24 inch) aperture and about 75 meter focal length satisfies the requirements for the fine guidance experiment insofar as the calculations indicate that with this size collector the fine guidance system can achieve a pointing accuracy of 0.01 second of arc on stars down to magnitude 9.6, and 75 meters is representative of a maximum useful focal length to be expected of a telescope in the 4 to 5 meter aperture range.

The requirements for the stellar interferometer, although derived from entirely different premises, are in very close agreement as regards aperture. From calculations based on the 20 foot Michelson interferometer, it has been determined that a 6 inch aperture is required for each interferometer beam. The reference beams which are collected by the primary mirror must be of the same size. To accommodate two 6 inch reference apertures without obscuration by either the outer periphery of the telescope or the secondary or diagonal mirrors, an aperture for the primary of 24 inches or 0.6 meter is required. The focal length must however be shorter, as the 75 meters required for the fine pointing experiment is excessive for the precise imagery demanded of an interferometric system. Furthermore the interferometer, which collects its energy outside the confines of the primary mirror requires a secondary which is enlarged to approximately twice its normal size in order to accept these interferometer rays and transmit them to the secondary image plane which is used by the interferometer.



PRECEDING PAGE BLANK NOT FILMED.

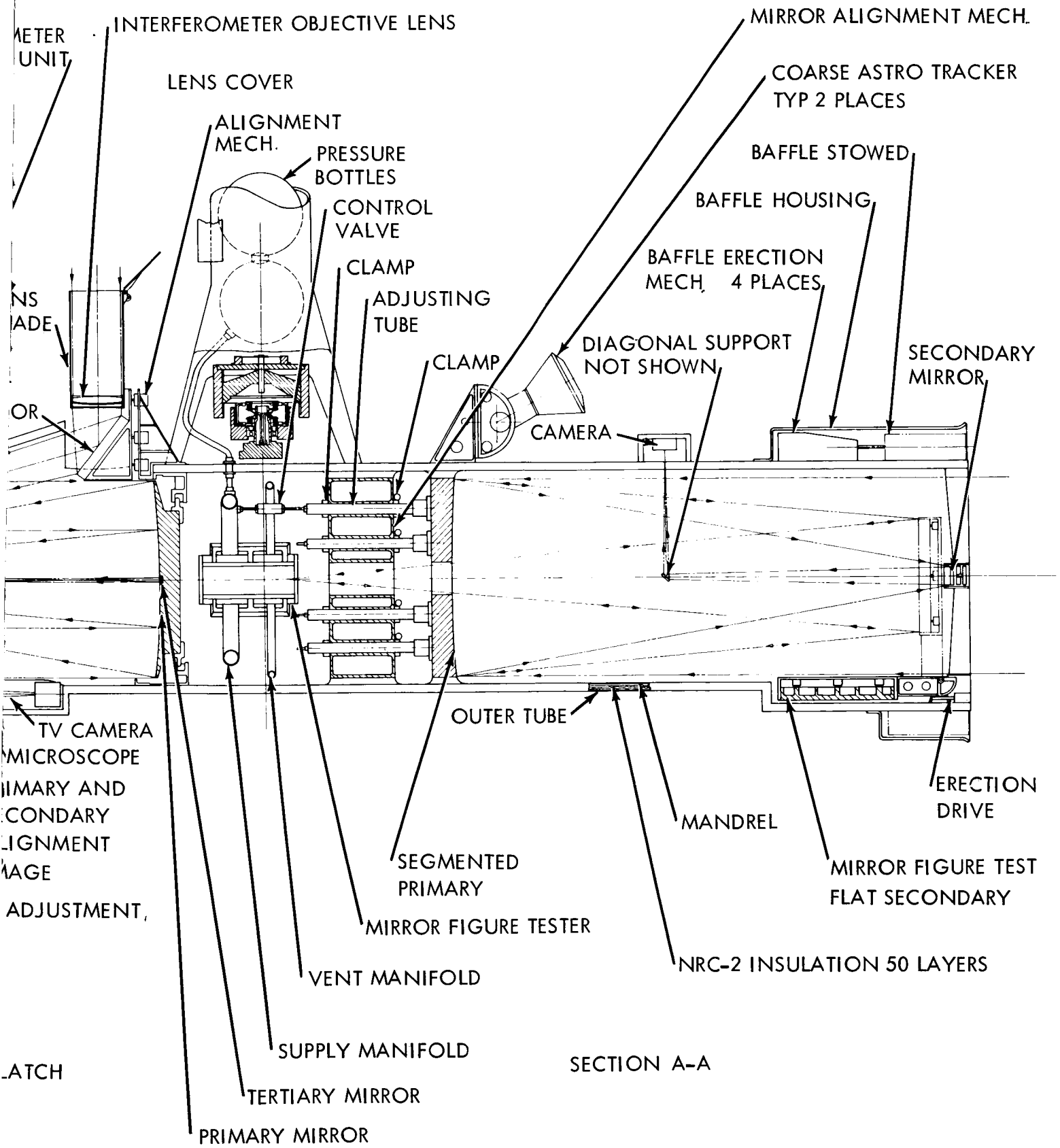


Figure 9.1-1. Fine Guidance, Segmented Optics, Isolation Comparison, and Stellar Interferometer Telescope

These requirements can be met with a Cassegrainian telescope of 0.6 meter aperture with two modifications. The secondary mirror is enlarged as described above for the interferometer, and an additional stage of magnification in the form of a tertiary mirror increases the effective focal length of the telescope to the nearly 75 meters required of the fine guidance experiment. In addition to the requirements for the major elements and the telescope there is a need for auxiliary optics such as diagonal mirrors to shift specific image planes to appropriate off-axis positions for processing in one of the experiments without interfering with the other one.

The same telescope as used for the stellar interferometer and fine guidance experiments is also used for the isolation techniques experiment. It may be argued that the fine guidance experiment should not be performed until satisfactory isolation techniques have been established. By the same token the fine guidance is needed to evaluate the effectiveness of the isolation. It is the very interdependence of the isolation and fine guidance that demands they be investigated together.

9.2 FINE GUIDANCE TELESCOPE

A telescope that meets the requirements set down in subsection 9.1 is described below. It consists of a reflecting telescope with a classical Cassegrainian secondary mirror and a Gregorian tertiary mirror, hence the name Cassegorian. This arrangement provides a focal length of 73.692 meters within an envelope no longer than 1.75 meters. Interferometer booms and optics are attached to this telescope.

9.2.1 Telescope Optics

The Cassegorian telescope consists of three major elements: A primary paraboloidal mirror of 1.678 meter focal length and with a clear aperture of 0.613 meter (24 inches); a hyperboloidal secondary mirror of -0.1766 meter focal length and 0.108 meter aperture, and a spherical tertiary mirror of 0.2434 meter focal length and 0.013 meter aperture. These mirrors are spaced 1.524 meter (60 inches) apart. In this configuration, the secondary mirror increases the effective focal length by a magnification factor of 8 and the tertiary by a factor of about 5.5. The magnification factors, while larger than conventional usage, serve to keep the overall size of the package down while maintaining a large focal length. Figure 9.2-1 is an optical schematic of this telescope configuration.

In addition to the principal mirrors described above, there are diagonal mirrors which permit the examination of each of the image planes. The first diagonal is referred to as the intermediate error diagonal. It picks off a fraction of the energy between the primary and secondary mirrors and permits it to come to a focus at the intermediate error sensor. The second diagonal is not used in the fine guidance experiment and is swung out of the way. Its function is to relay the secondary image to the interferometric sensing equipment. The third diagonal, near the tertiary focus, as shown in Figure 9.2-2, is used in conjunction with a microscope for initial

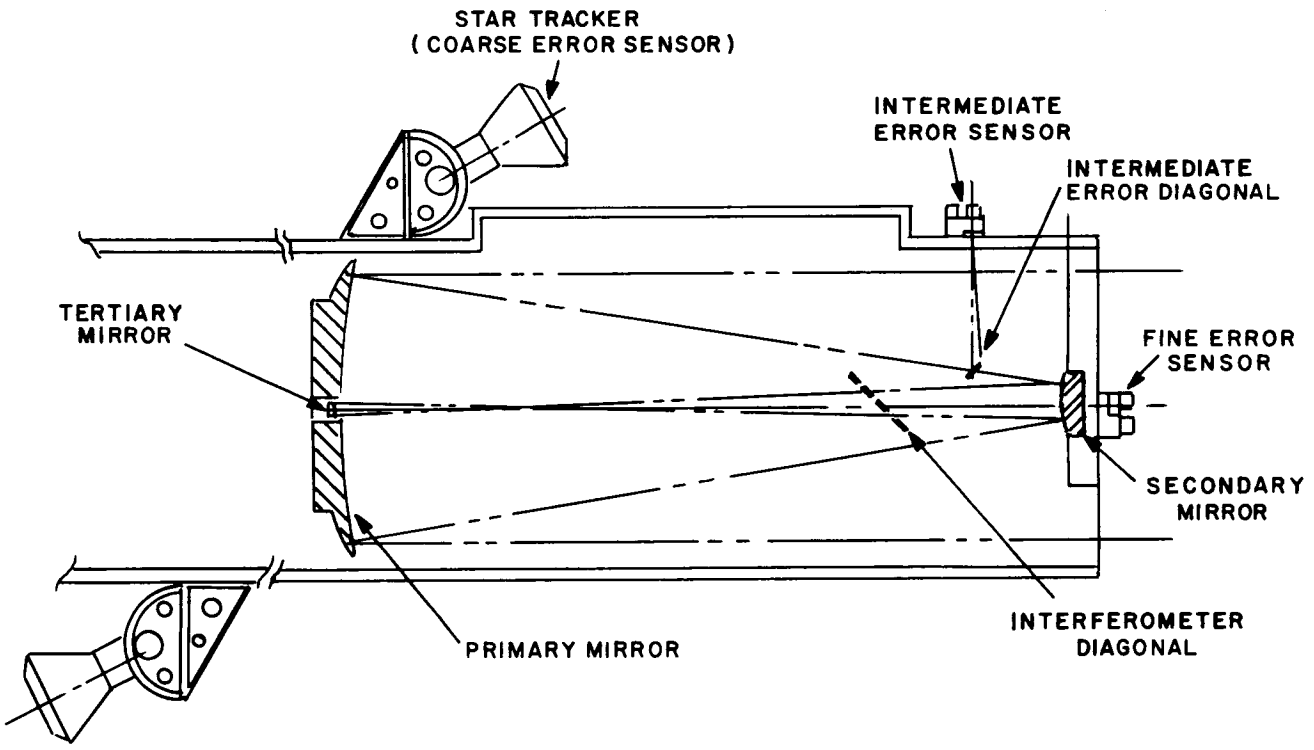


Figure 9.2-1 Fine Guidance Telescope

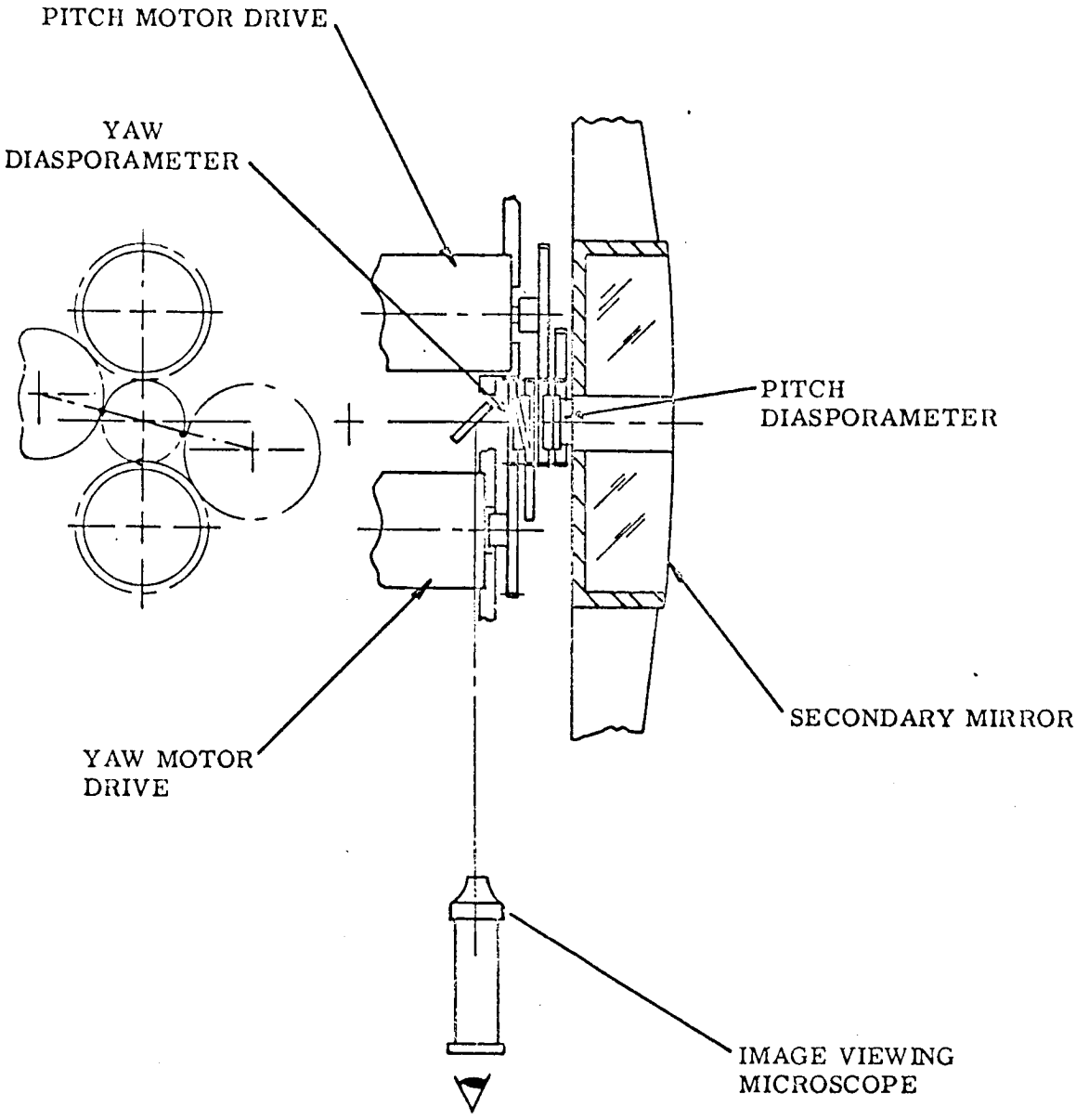


Figure 9.2-2 Fine Guidance Experiment Fine Pointing Actuator

alignment and, during fine pointing, for image position stability evaluation. Two ways of instrumentation are considered: remote television viewing, and photographic recording at predetermined time intervals. Not shown in the drawing are two large external diagonal mirrors used for off-axis fine pointing. This requirement for dim target stars and extended celestial objects needs further study. The fine guidance telescope is gimballed in roll, pitch and yaw in the coarse and intermediate modes of operation. An internal beam deflector is used for the fine pointing mode.

The coarse mode derives the telescope pointing signals from two coarse star trackers with independent telescopes and gimbals. These are aimed at two bright guide stars and derive their pointing errors with respect to the commanded guide star attitudes. In the intermediate mode the fine guidance telescope pointing correction is derived from an intermediate error sensor which is located at the focal plane of the primary mirror and views the target star. Two methods of fine pointing correction by means of beam deflection are considered applicable at the present time. They are a diasporameter and a cantilevered suspension and articulation of the tertiary mirror (Figure 9.2-3). Two methods of fine error sensing are also classified as currently applicable: crossed vibrating apertures using tuning forks (an image dissector with a square aperture is considered an alternate to the vibrating apertures) and a four sided pyramidal reflector with an alternating current image scan. Other pointing and scanning methods were considered, however, they are not applicable unless their position stability and repeatability are improved as their technology advances.

9.2.2 Interferometer Optics

The integration of an interferometer into a space telescope involves a number of serious technical problems. The ground rule was established that the interferometer experiment should not interfere with or degrade the fine guidance and isolation comparison experiments. It was therefore decided that the booms should not be erected until the fine guidance and isolation experiments were conducted at least once. It follows therefore that the booms should be mounted such that their axes pass through the telescope center of gravity. Mounted otherwise the center of gravity would shift introducing offset errors to the control system. This fact eliminated the possibility of using a conventional interferometer telescope design in which the interferometer beams are mounted at the telescope front end.

As a result four alternative optical configurations have been considered. These are:

a. A system using a focusing lens between the inboard and outboard mirrors.

b. A system in which the inboard mirrors are focusing reflectors.

c. A system in which the inboard mirrors are mounted on the front of the telescope. This necessitates changing both mirror tilt angles as the outboard mirror is moved along the beam axis.

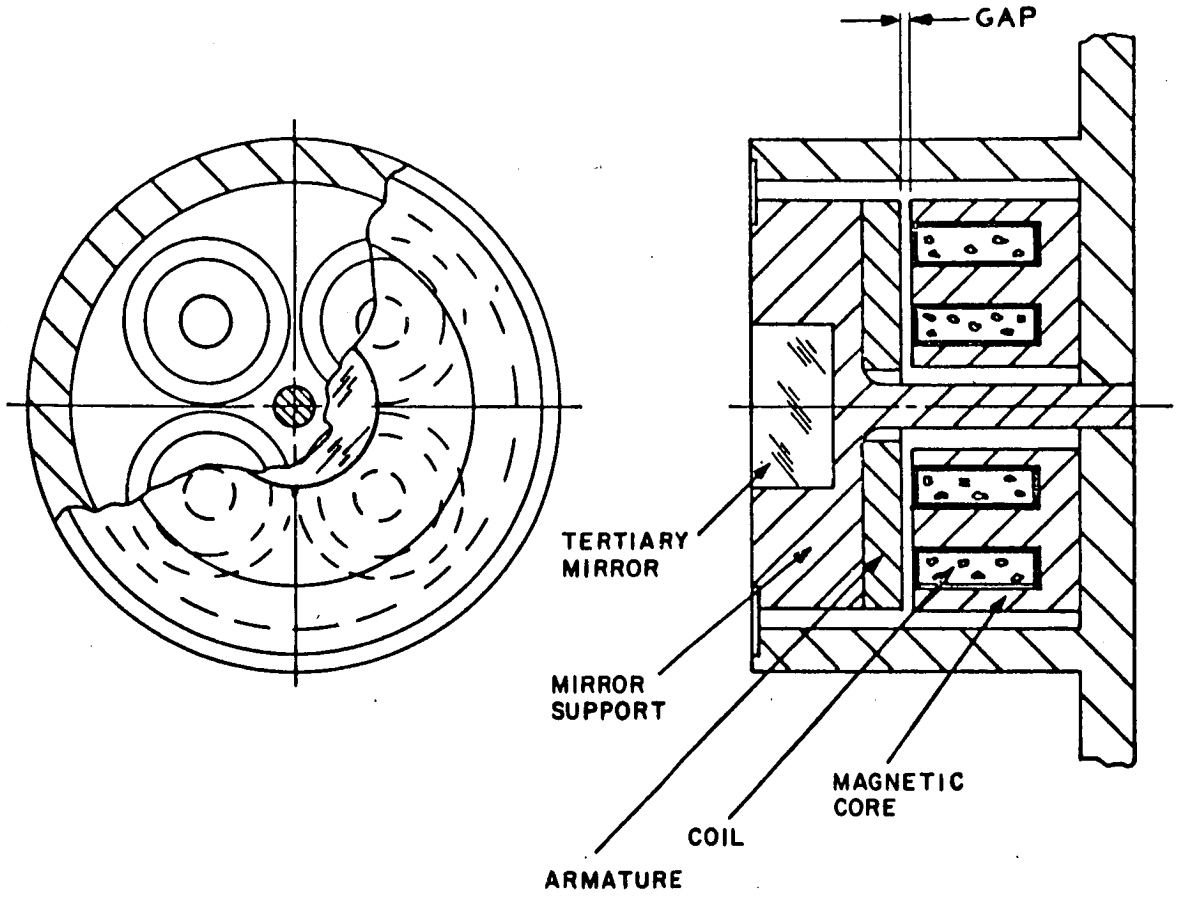


Figure 9.2-3 Fine Guidance Experiment Tertiary Mirror Cantilever Mount

d. A system using three reflections prior to the primary mirror.

The first two of these configurations were rejected. The focusing lens would absorb ultra-violet and thus was undesirable and the focusing inboard mirrors introduced excessive aberrations due to the fact that the reflecting mirrors were, by necessity, working far off axis.

The interferometer experiment requires a pointing accuracy of approximately 6 seconds. The fine guidance experiment is configured such that the fine guidance experiment will provide this accuracy in the intermediate pointing mode. Thus it is possible to detect the image prior to the fine error sensor. Therefore a removable diagonal mirror was located in front of the secondary which serves to reflect the image towards the interferometer detection equipment on the side of the telescope. This mirror is shown in figure 9.2-1.

10.0 MISSION DEVELOPMENT

The OTAES mission or missions must be able to support the individual and collective objectives of the experiment program which will evolve from the experiment development task. However, the definition of experiment objectives must be performed within the constraints imposed by the range of feasible missions. In order to provide a quick mission reference frame against which to assess this experiment feasibility, three representative orbits were defined and nine representative missions were identified as points of departure for the study.

Table 10.0-1 contains the parameters for the three orbits defined.

TABLE 10.0-1

ORBIT PARAMETERS

Parameters/Orbit	Synchronous Circular	24 Hour Elliptical	Near Earth
Inclination to the ecliptic	0° to 35°	0° to 35°	0° to 35°
Semi-major axis	42,148 km	42,148 km	7,024 km
Eccentricity	0	0.6756	0

This assumes an earth spheroid radius (R_o) equal to 6,375 km.

A comparison of the angle subtended by the earth disc and associated ground coverage circles for circular orbits is presented in figure 10.0-1. Since the radius vector varies with time for the elliptical orbit, earth coverage and subtended angle for this case are presented by figures 10.0-2 and 10.0-3. For this orbit, figure 10.0-4 presents true anomaly and figure 10.0-5 presents radius vector as a function of time from perigee passage.

The launch vehicles considered as possible OTES carriers in this study are all from the Saturn family. These vehicles are presented in table 10.0-2 with their respective stack-up or individual stages and the missions that they can accomplish.

Some of the missions are listed for more than one vehicle. A lower case (a) after the mission number indicates that this is the alternate vehicle for this mission. Each of these vehicles has the capability of performing one or more of the proposed OTES missions.

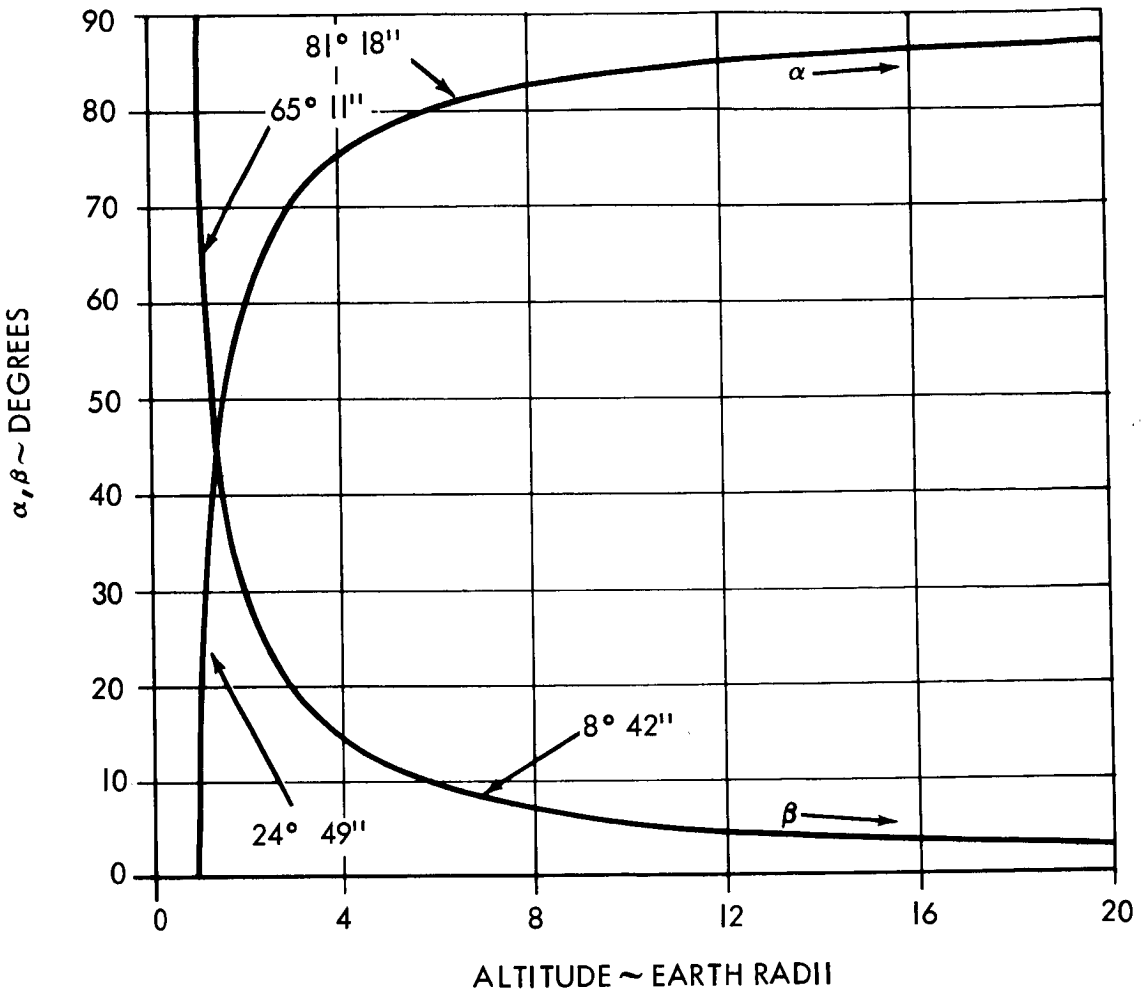


Figure 10.0-1. Geocentric Angle for Radius of Coverage, α, and Subtended Half-Angle of Earth-Disc, β, for Circular Orbits as a Function of Radius Vector.

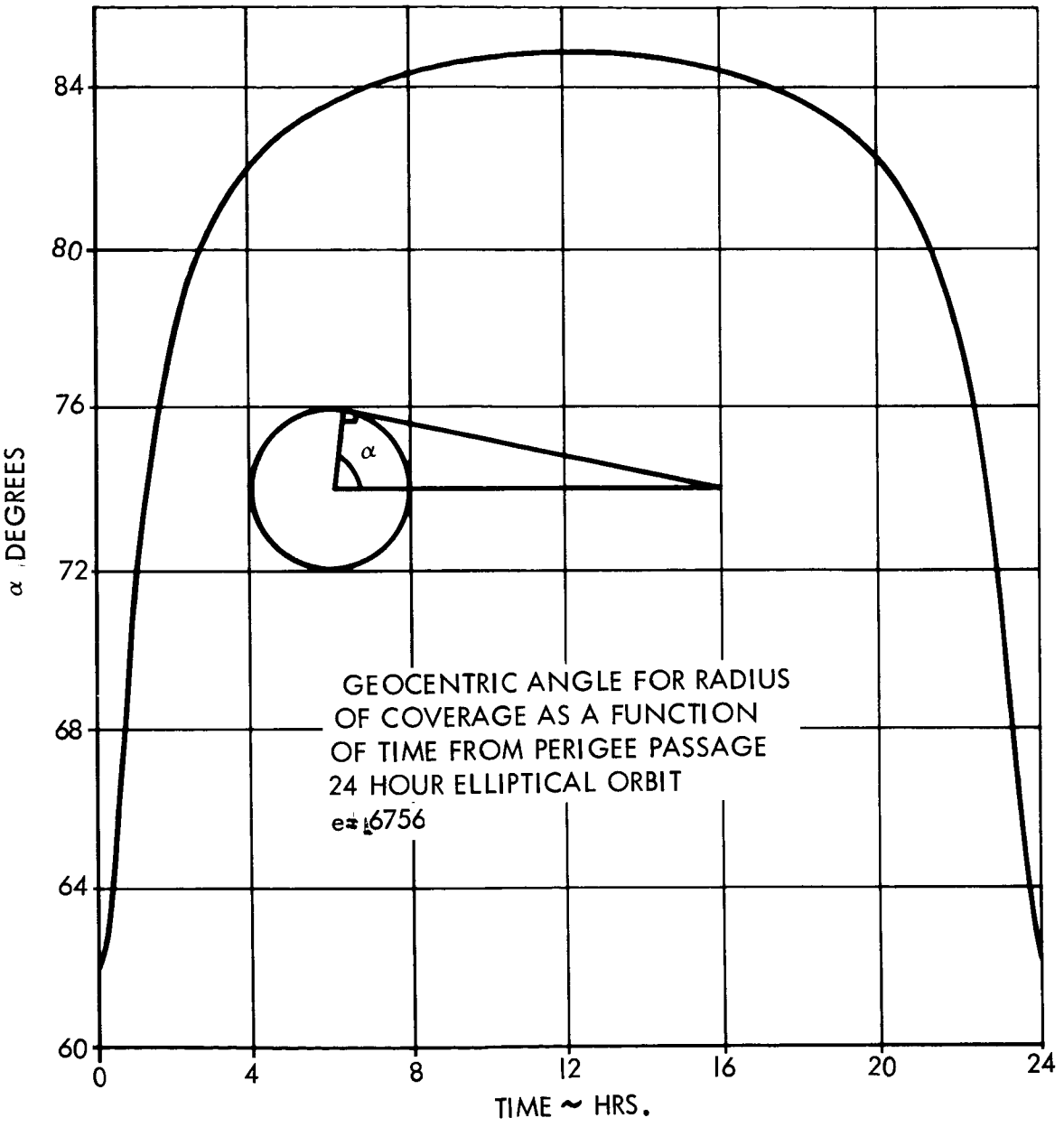


Figure 10.0-2. Geocentric Angle for Radius of Coverage as a Function of Time from Perigee Passage 24-Hr Elliptical Orbit e= .6756

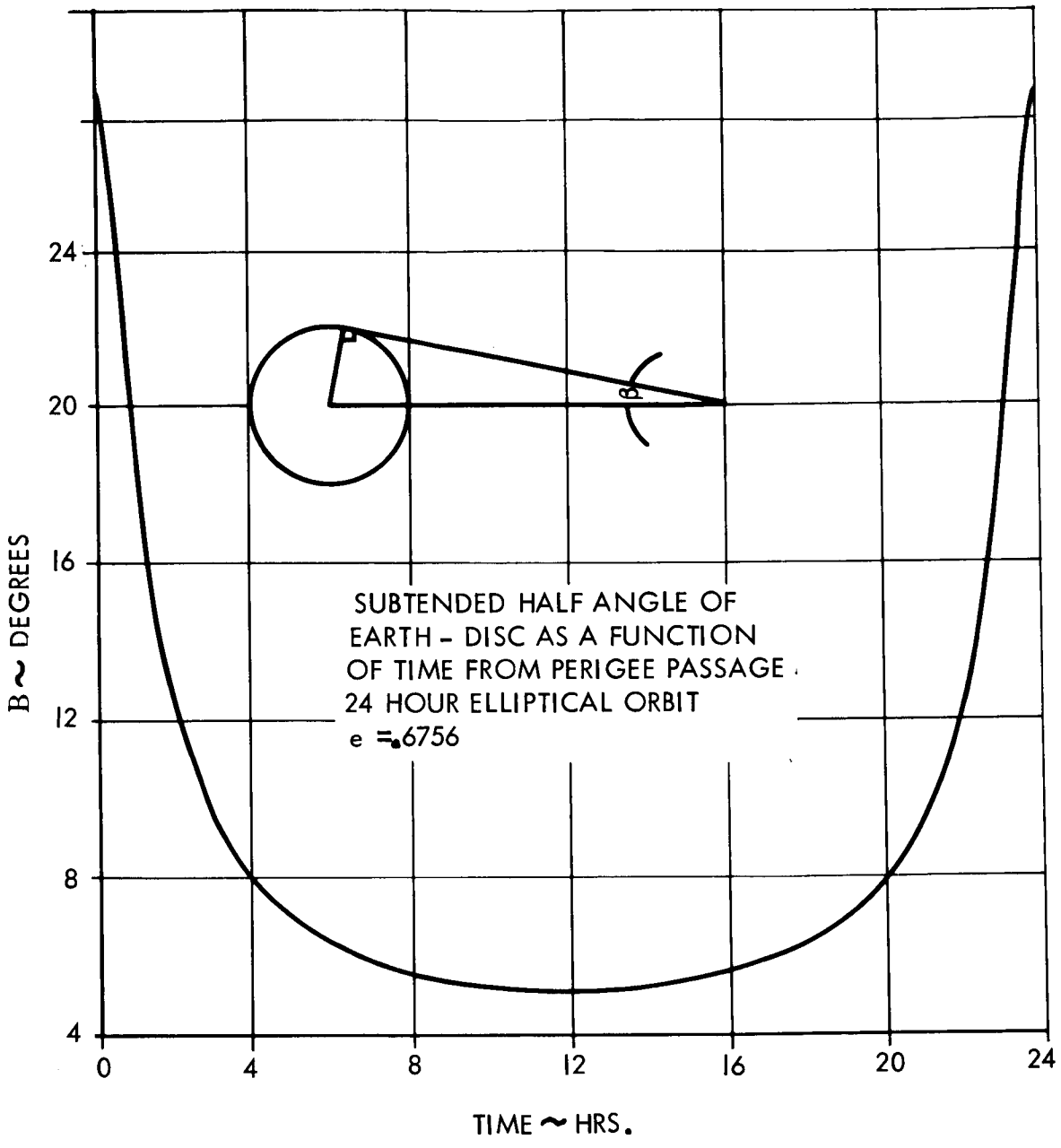


Figure 10.0-3. Subtended Half Angle of Earth-Disc as a Function of Time from Perigee Passage 24-Hr Elliptical Orbit e= .6756

3.

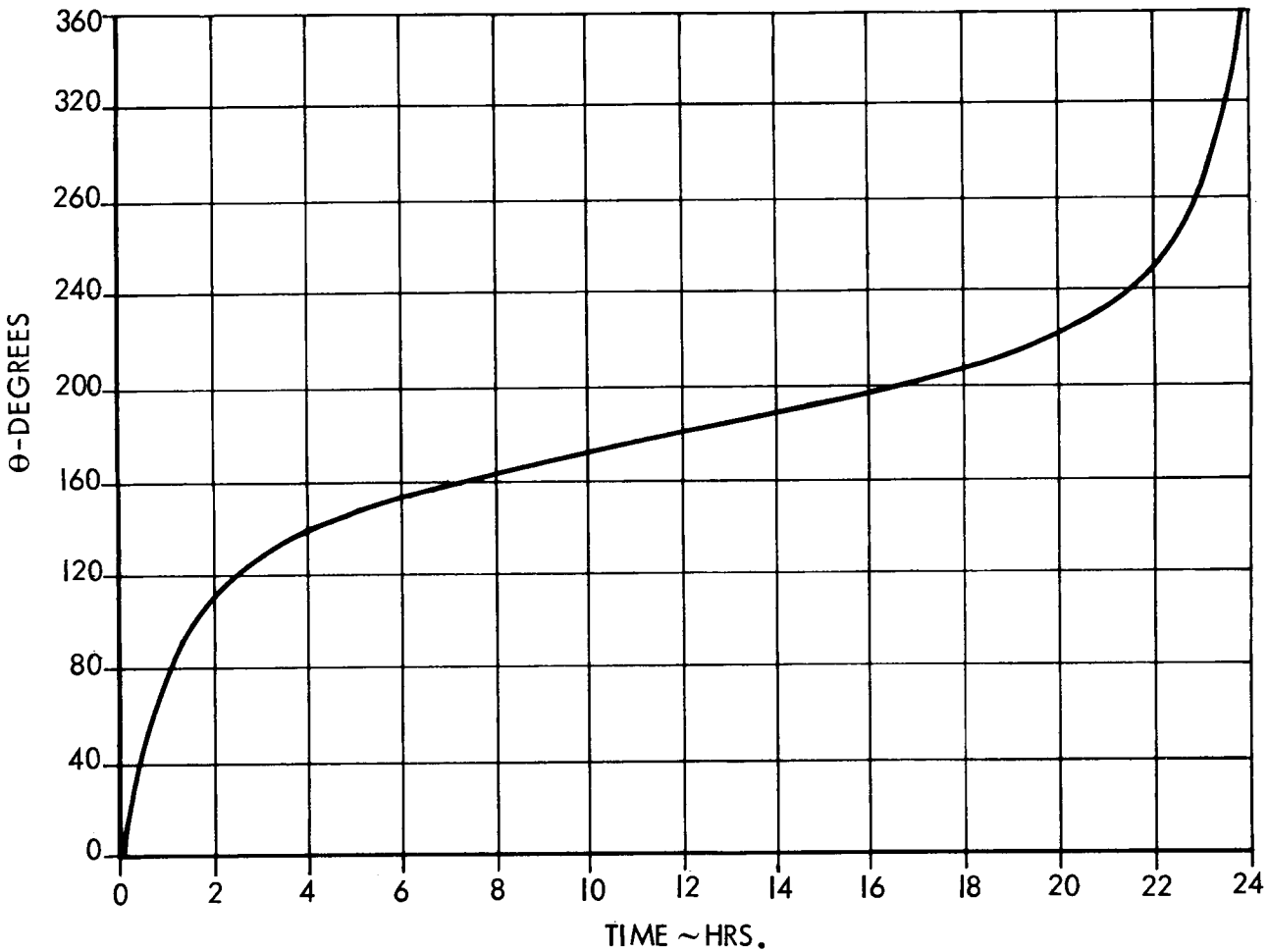


Figure 10.0-4. True Anomaly as a Function of Time from Perigee Passage - 24-Hour Elliptical Orbit. e = .6756

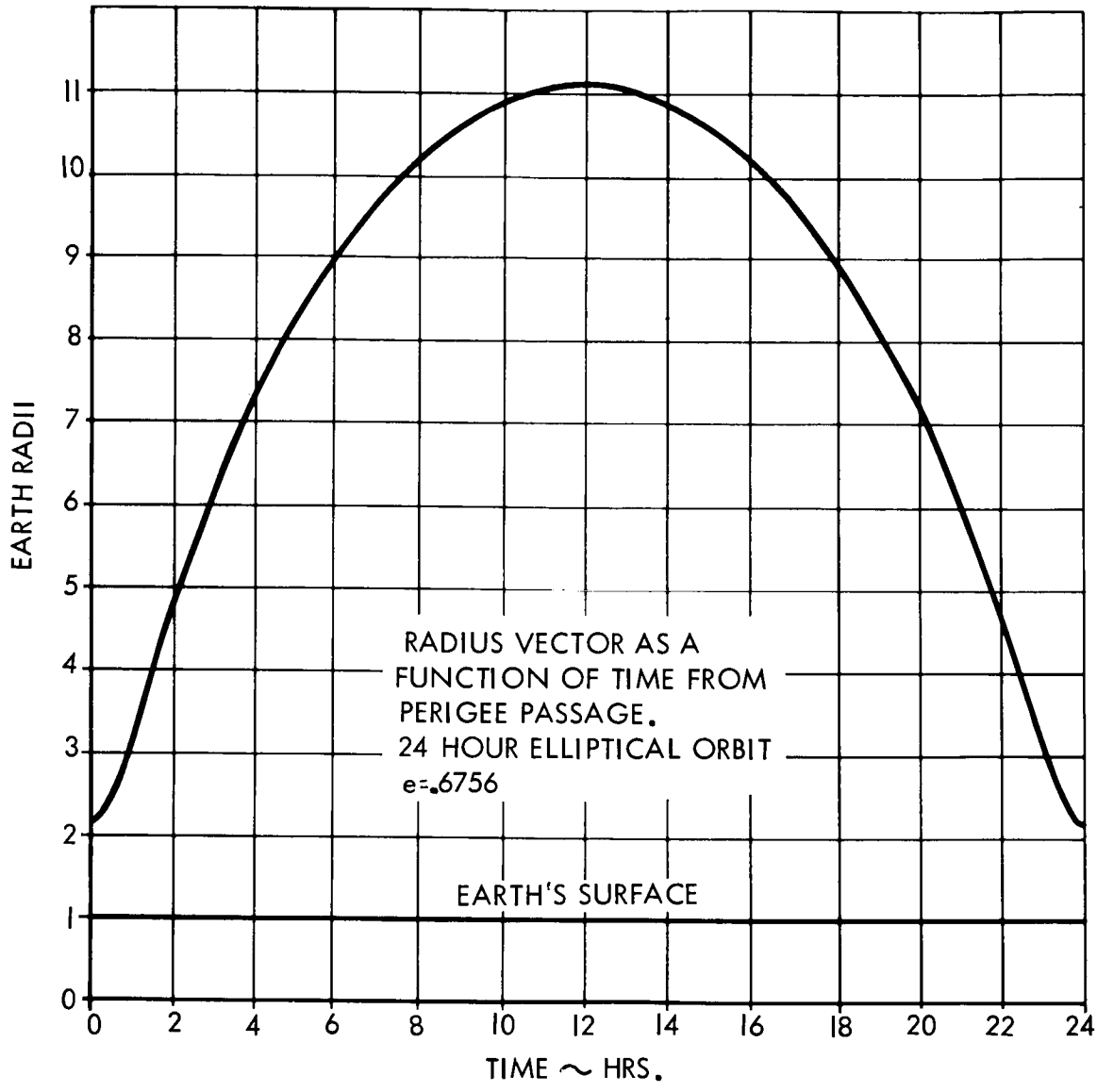


Figure 10.0-5. Radius Vector as a Function of Time from Perigee Passage 24-Hr Elliptical Orbit e= .6756

Figure 10.0-6 shows the plane change requirement to place the spacecraft in the ecliptic as a function of time of launch. A launch into the ecliptic can only be achieved with a 5 degree plane change and an instantaneous launch window or, if the vehicle has 10 degree plane change capability, the launch window is opened to 2.8 hours. This figure presents only a typical day and cannot be referenced to any particular time.

An equatorial orbit is of interest for some of the OTES missions. For this mission, a 28.5 degree plane change after orbit injection was considered in this study. The velocity requirements for this plane change is high and the payload penalty is severe.

All vehicles are launched from the ARM an azimuth of 90 degrees measured clockwise from north.

TABLE 10.0-2

POSSIBLE OTES CARRIER VEHICLES

Vehicle	Stack Up	Mission
Saturn IB	S-IB/S-IVB/OTES	V
Saturn IB/Centaur	S-IB/S-IVB/Centaur-OTES	III, IV
Saturn IB/SM*	S-IB/S-IVB/SM-OTES	IIIa, IVa
Saturn IB/Zero Stage**	Zero Stage/S-IB/S-IVB/OTES	VIIIa, IXa
Saturn IB/Zero Stage/Centaur	Zero Stage/S-IB/S-IVB/Centaur/OTES	VIIIa, IXa
Saturn IB/Zero Stage/SM	Zero Stage/S-IB/S-IVB/SM/OTES	VIII, IX
Saturn V	S-IC/S-II/S-IVB/OTES	I, II, VI, VII

* Apollo Service Module
** 4 UTC 1205 SRM

10.1 CANDIDATE MISSIONS

Nine candidate missions were identified that would be representaive of the capabilities and constraints which would obtain for the family of Saturn Class launch vehicles. These candidate missions are shown in table 10.1-1.

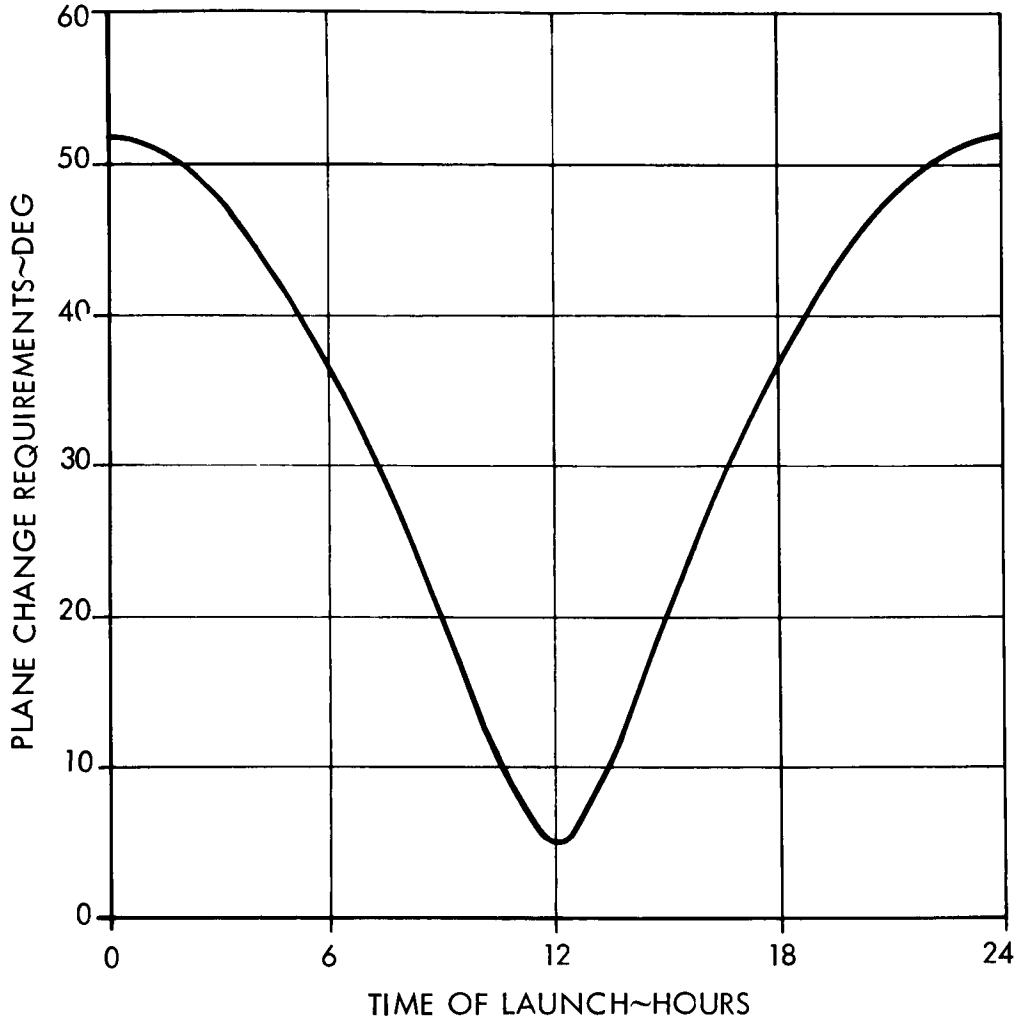


Figure 10.0-6. Plane Change Requirements for Placing Payloads in the Ecliptic Plane as a Function of Time

TABLE 10.1-1

CANDIDATE MISSIONS

Mission Number	Manned for 45 Days	Initially Unmanned But Capable of Rendezvous	Orbit	Launch Vehicle
I			Synchronous	Saturn V
II			Elliptical	Saturn V
III			Synchronous	Saturn IB/Centaur
IV			Elliptical	Saturn IB/Centaur
V			Near Earth	Saturn IB
VI	Near Earth Vehicle	High Energy Vechile	Near Earth & Synchronous	Saturn V
VII	Near Earth Vehicle	High Energy Vehicle	Near Earth & Elliptical	Saturn V
VIII			Synchronous	Saturn IB/Zero Stage
IX			Elliptical	Saturn IB/Zero Stage

Mission 1 is discussed in detail and subsequent missions are presented as developments from this basic mission to avoid unnecessary repetition.

10.1.1 Mission I Description

Mission I is manned, uses a synchronous orbit, and is sized for the Saturn V launch vehicle.

10.1.1.1 Orbit

This mission involves a 185 km parking orbit and a synchronous (35,135 km (circular)) final orbit. Minimum occultation by the earth permits great freedom in structuring astronomical observation programs. The stationary characteristics of this trajectory make it compatible with those earth oriented experiments requiring high pointing and tracking accuracies. Trajectory inclinations can be chosen to achieve ground antennae slew rates of the order of magnitude of slew rates required to track a spacecraft on a planetary trajectory. In addition, synoptic observations can be performed within the boundaries of the 160 degree earth coverage circle.

10.1.1.2 Launch Configuration

This mission is sized for the standard Saturn V launch vehicle with an extended Command Service Module (CSM) and the OTS. The launch stack-up is composed of S-IC/S-II/S-IVB/OTS/SM/CM.

The Saturn V has three propulsive stages (S-IC, S-II, and S-IVB) and an Instrument Unit (IU). Each propulsive stage has its own instrumentation and safety systems and receives guidance and control commands from the IU.

The S-IC stage is powered by five F-1 engines which burn liquid oxygen and RP-1 (kerosene) fuel to provide a nominal sea-level thrust of 33.4 million newtons (7.5 million pounds). The S-II stage is powered by five J-2 engines which burn oxygen and liquid hydrogen to provide a thrust of one million pounds in vacuum.

The S-IVB is powered by a single J-2 engine which burns liquid oxygen and liquid hydrogen to provide a thrust of 890,000 newtons (200,00 pounds) in vacuum. The S-IVB stage will have the added capability of a second burn for this mission.

The IU is a three segment, cylindrical, unpressurized structure which houses the instrumentation concerned with vehicle performance from lift-off through the second S-IVB burn, and through the spacecraft transposition phase immediately following.

The extended CSM is that developed for the Apollo lunar landing mission and modified to provide for extended duration missions. The modifications are primarily in the Service Module.

The Command Module (CM), will contain crew support systems, displays, control equipment requiring direct access by the crew, and all system needed for earth entry and landing. The CM is divided into three basic compartments: a) the crew compartment, b) the forward compartment, and c) the aft compartment.

The crew compartment, which comprises the major portion of the CM, is an oxygen pressurized [6,900 newton/meter^2 (5 psia)] , three-man cabin that maintains a habitable environment for the crew during space flights. It contains spacecraft controls and displays, observation windows, food, water, sanitation, and survival equipment.

The forward compartment is located at the apex of the conical shaped crew module. This compartment is unpressurized, and the center portion is occupied by a 0.762 meter (30 inches) diameter tunnel to permit the crew to debark from the spacecraft during flight. The major portion of the remaining area is occupied by the earth-landing system.

The aft compartment is an area located around the lower rim of the conic body. This area also is unpressurized and not accessible to the crew. It contains the reaction control motors, impact attenuation equipment, instrumentation, and consumable storage. The CM can provide pressurized space for experiments, and can return approximately 113.4 kilograms (250 pounds) of experimental payload to earth.

The Service Module (SM) is an unmanned, unpressurized vehicle that contains stores and systems which do not require direct crew accessibility. This module contains: the propulsion utilized for insertion to, and from, final orbit; fuel cells which provide spacecraft power; radiators for spacecraft cooling; and oxygen and hydrogen supplies. The SM remains attached to the CM throughout the manned portion of the mission until just prior to earth reentry when it is separated from the CM and is not recovered.

The OTAES spacecraft is one of several concepts described in section 11.2. Those concepts based on a modification of the Apollo Lunar Excursion Module (LEM) may be thought of as consisting of two joined structures: (a) a 7 meter^3 (247 ft^3) pressurized laboratory derived from the LEM ascent stage, and (b) an unpressurized rack for mounting experiments and storing subsystems externally. It contains subsystems to extend the in-orbit capability to 45 days. A 6,900 newton/meter^2 (5 psia) oxygen shirt-sleeve environment is maintained in the Ascent Stage cabin, and an air lock is provided to permit ingress or egress of the astronauts for extravehicular activity without complete depressurization of the cabin. Experiments mounted externally are limited by the payload capability of the launch vehicle and the space within the spacecraft LEM adapter, which is approximately 275 meter^3 (3,000 ft^3).

The non-LEM-derived spacecraft will support these same functions but will more optimally exploit the LEM adapter envelope.

The effects of the exhaust of the 50-50 UDMH/hydrazine and nitrogen tetroxide propellants on optical systems is not completely determined. The location of the experiments and programming of the thrusters will be accomplished so as to avoid impingement of the exhaust upon optical systems.

10.1.1.3 Mission Phases

10.1.1.3.1 Launch Phase

Launch Complex 39 and the AMR downrange instrumentation will be the facilities used for launch and checkout.

The firing of the S-IC and the S-II, and the first firing of the S-IVB inject the manned payload and the S-IVB into parking orbit. The second S-IVB firing inserts the payload into the 5-hours-plus transfer orbit. Transposition and docking are completed in this transfer trajectory and the SM fires to inject the payload into the final orbit.

The primary ground station support during manned operation will be provided by the Manned Space Flight Network (MSFN). The MSFN will be backed up by the NASA Deep Space Network (DSN). If these networks cannot meet the data requirements of the system, augmentation can be provided by NASA's STADEN network.

The central control facility for management of the manned OTAES flight operations and the manned experiment program will be located in the Manned Space Flight (MSC) Control Center, Houston.

The Mission Operation Control Rooms (MOCR), the Real-Time Computer Complex (RTCC), and the Communications Systems, and the Simulation Checkout and Training Systems (SCATS) designed for Apollo/Gemini support will be used to support OTAES during the Launch Phase, Manned Operation Phase, and the Crew Return Phase. During the Launch Phase, KSC and GOSS/DSIF stations will provide tracking information to the TRCC. The TRCC will provide ephemeris update information to the Ground Station Control Center.

10.1.1.3.2 Manned Operational Phase

A sequencer will enable spacecraft power and data handling subsystems with CSM command and ground command back-up capabilities. Limited EVA capability will be utilized in placing the spacecraft in operational condition. The spacecraft will be manned throughout this phase with ground command and CM command back-up modes. Optical collimation, alignment, and laser tuning will be performed by spacecraft crew. The manned experiment sequence will then be carried out during a period of 30 to 45 days.

All spacecraft housekeeping telemetry will be handled by the OTAES spacecraft ground station, except that life-support functions may be handled separately through a GOSS station.

10.1.1.3.3 Unmanned Operational Phase

At the end of the manned phase, an unmanned mode checkout will be performed by the OTES crew observing spacecraft operations during such unmanned operations as remote alignment, acquisition, etc.

The OTS crew will return to the command module and the CSM will de-dock and separate from the spacecraft. The CM will then separate from the SM and return to earth.

The OTAES spacecraft will go into the unmanned experiment mode. System command and control functions will be assumed by the ground station control center freeing MSC of all further spacecraft traffic.

The Ground Station Control Center will have data quick-look capability. Complete reduction and interpretation of experimental data will be performed at a data analysis center separate from the ground station.

10.1.2 Mission II Description

Mission II is manned, uses an elliptical 24-hour orbit, and uses the Saturn V launch vehicle.

10.1.2.1 Orbit

This mission involves a 185 km parking orbit and an elliptical (eccentricity = 0.6756) 24-hour orbit with an apogee altitude of 64,137 km and a perigee altitude of 7255 km. The eccentricity given above obtains from the requirement that for an equatorial orbit and a ground station on the equator, the spacecraft would be seen to traverse the sky from horizon to horizon and back, but would remain in sight of the ground station. For non-equatorial stations and/or inclined orbits, the eccentricity needed to meet the above requirements would be less.

The traverse of the apogee will yield slow slew rates and those earth-oriented experiments requiring high pointing and tracking accuracies can be programmed for this portion of the trajectory. A wide range of slew rates and range rates are achieved with this trajectory and fluctuations can be exploited in replications of experiments influenced by these variations. Geometrically, this trajectory is compatible with both astronomical experiments and earth-oriented experiments. For the high-altitude portions of the trajectory, a large earth-coverage circle results and synoptic observations can be performed. At perigee, the ground resolution is better for this trajectory (by a factor of 5) than it is for the synchronous altitude assuming comparable angular resolution limits.

10.1.2.2 Launch Configuration

This mission uses the standard Saturn V launch vehicle with an extended CSM and the OTAES spacecraft. The launch stack-up is: S-IC/S-II/S-IVB/OTS/SM/CM.

The description for these stages is identical to that given in paragraph 10.1.1.2.

10.1.2.3 Mission Phases

The phasing for this mission will be identical to that for Mission I (detailed in subsection 10.1.1.3 except that the spacecraft spends a little more than 10 hours in transfer from parking to injection at the apogee of the final orbit. A payload capability bonus is achieved by injecting at apogee rather than injecting at any other point on the trajectory.

10.1.3 Mission III Description

Mission III is initially unmanned, uses a synchronous orbit, and uses the Saturn IB/Centaur launch vehicle.

10.1.3.1 Orbit

The orbit for this mission is identical to that described for Mission I in subsection 10.1.1.1.

10.1.3.2 Launch Configurations

The launch stack-up is S-IB/S-IVB/Centaur/OTS.

The Saturn IB/Centaur launch vehicle has three propulsive stages (S-IB, S-IVB, and Centaur upper stage) and an IU. Each propulsive stage has its own instrumentation and safety systems.

The S-IB stage is powered by eight H-1 engines which burn liquid oxygen and RP-1 (kerosene) fuel to provide a nominal sea level thrust of 7.1 million newtons (1.6 million pounds).

The S-IVB stage is powered by a single J-2 engine which burns liquid oxygen and liquid hydrogen to provide a thrust of 890,000 newtons (200,000 pounds) in vacuum.

The IU is a three segment, cylindrical, unpressurized structure which houses the instrumentation concerned with vehicle performance from lift-off to the time of S-IV cutoff and separation.

The Centaur stage is powered by two Pratt and Whitney RLiDA-3-3 engines, each of which produces 66,700 newtons (15,000 pounds) of thrust in a vacuum. This upper stage will be required to restart twice to provide three burns. A self contained guidance package will provide guidance and control for the Centaur.

The payload may consist of OTAES spacecraft concepts similar to configurations shown and discussed in subsection 11.1.

10.1.3.3 Mission Phases

10.1.3.3.1 Launch Phase

The facilities used for checkout and launch will be Launch Complexes 34 or 37B and the AMR downrange instrumentation.

The firing of the S-IB, the S-IVB, and the first firing of the Centaur injects the payload into parking orbit. The second Centaur burn injects the payload into the 5-hour-plus transfer orbit. The third Centaur burn circularizes the spacecraft into final orbit.

The Centaur is then separated from the OTAES spacecraft and the solar panels and high gain antenna are deployed.

10.1.3.3.2 Operational Phase

The central control facility for management of the unmanned OTAES spacecraft flight operations and the unmanned experiment program will be located at the Space Flight Operations Facility (SFOF) at Pasadena, California. the SFOF Communications System, Data Processing System, and support systems will be used to support the OTAES spacecraft mission. The Communications System will provide internal and external transmission of information. The Data Processing Systems will provide physical recording and computer conversation of data. The support systems are comprised by the display and control consoles, the mission status board, and the Spacecraft Functional Model. Use of SFOF will make possible a much simpler ground station control center for the OTAES spacecraft ground station.

The spacecraft will be activated and controlled remotely from the ground from SFOF via the Deep Space Network augmented by one or more OTAES spacecraft ground stations.

10.1.3.3.3 Rendezvous Phase

During the lifetime of the mission, it shall be possible to rendezvous a Saturn V launched CSM with the OTAES spacecraft for intermittent manned operations. A degree of diagnosis and repair or replacement of failed components by man will improve the system reliability. Manned experiments will also be possible during this phase. All crew critical operations will be controlled by MSC as in Mission I (see subsection 10.1.1.3).

10.1.4 Mission IV Description

Mission IV is initially unmanned, uses a 24-hour elliptical orbit, and uses the Saturn IB/Centaur launch vehicle.

10.1.4.1 Orbit

The orbit for this mission is identical to that described for Mission II in subsection 10.1.2-1.

10.1.4.2 Launch Configurations

This mission is designed to employ the Saturn IB/Centaur launch vehicle. The launch stack-up is S-IB/S-IVB/Centaur/OTS.

The description for these stages is identical to that given in subsection 10.1.3.2.

10.1.4.3 Mission Phases

The phasing for this mission will be identical to that for Mission III as detailed in subsection 10.1.3.3, except that the spacecraft spends a little more than 10 hours in transfer from parking to injection at the apogee of the final orbit.

10.1.5 Mission V Description

Mission V is manned, uses a near-earth orbit, and is designed to use the Saturn IB launch vehicle.

10.1.5.1 Orbit

This mission involves a near-earth orbit of about 650 km altitude. Alternate trajectories may result in orbits much higher than this and as low as 370 km. The trade-offs leading to these alternate trajectories are discussed in subsection 10.1.5.3 for this mission.

The main attraction of this mission is the superior ground resolution achievable because of minimized slant ranges; compared to the high-energy missions. The ground resolution achievable is better by a factor of 60 for this orbit as compared to synchronous altitude, and better by an order of magnitude over the ground resolution achievable from the perigee of the elliptical orbit.

At present, this orbit has the highest crew safety factor due to the fact that all manned flights to date have been performed at near-earth orbits, and also the fact that flight altitude can be kept below regions of trapped radiation. At these altitudes, the magnetosphere affords the greatest protection from extraterrestrial radiation.

10.1.5.2 Launch Configurations

This mission is sized for the standard IB launch vehicle. The launch stack-up is S-IB/S-IVB/OTS/SM/CM.

The Saturn IB has two propulsive stages (the S-IB and the S-IV-B) and an IU. Each propulsive stage has its own instrumentation and safety systems, and receives guidance and control commands from the IU.

The description of these stages is identical to that contained in subsection 10.1.3.2.

The payload spacecraft (CM, SM and OTS) have been described in subsections 10.1.1.2 and 11.1.

10.1.5.3 Mission Phases

10.1.5.3.1 Launch Phase

The facilities used for checkout and launch for this mission will be Launch Complexes 34 and 37. Three major parameters, which influence the flight mode for this mission are: success probability of system installation, payload weight and radiation exposure of the crew. Optimizing for each of these parameters results in three different flight modes.

If the objective is to maximize the flight success probability, then the following mode (which we can call the "High Flight Reliability Mode") is the result.

Firing the S-IB and the S-IVB injects the OTS/SM/CM into final orbit. The transposition and docking produce the OTS/CM/SM stack-up. The SM can be used for maneuvering or SM fuel can be off-loaded and its engine removed to increase payload and envelope volume.

If the objective is to maximize the payload capability, then the following mode (which we can call the "Maximum Payload Mode") is the result.

Firing the S-IB and the S-IVB injects the S-IVB/OTS/SM/CM into a 185 km trajectory circular orbit. Transposition and docking effect the OTS/CM/SM stack-up and the SM first fire injects this stack-up into a transfer orbit. The SM second burn circularizes the payload into final orbit.

If the objective is to minimize the exposure of man to radiation, then the following mode (which we can call the "Low REM Mode") is the result.

Firing the S-IB and S-IVB injects the OTS/SM/CM into a 370 km orbit. Transposition and docking produce the OTS/CM/SM stack-up. The manned operational activities are performed for 45 days. At the end of this period, the SM first burn places the stack-up on a transfer orbit and the SM second burn causes insertion into the final orbit with energy comparable to a 648 km orbit or greater. Immediately after insertion, the CSM dedocks from the OTS and a third SM firing places the CSM in an entry corridor and leaves the OTS in orbit.

The ground support for this mission is as outlined in subsection 10.1.1.3.

10.1.5.3.2 Manned Operational Phase

The manned operational phase is as described in subsection 10.1.1.3.

10.1.5.3.3 Unmanned Operational Phase

The unmanned operational phase is as described in subsection 10.1.1.3.

10.1.6 Mission VI Description

Mission VI employs a manned spacecraft in a near-earth trajectory and an initially unmanned spacecraft in a synchronous orbit. This is a multiple spacecraft sized for the Saturn V launch vehicle.

10.1.6.1 Orbits

This mission involves one operational near-earth orbit similar to the one described in subsection 10.1.5.1, and another at synchronous altitude as described in subsection 10.1.1.1.

In addition to combining the experimental capabilities of Mission III and Mission V, the simultaneous operation of two spacecraft makes it possible to conduct spacecraft-to-spacecraft communications to validate techniques which demonstrate the feasibility of an earth orbiting terminus for an interplanetary optical communication link. Simultaneous earth-surface observations from the two orbits could also serve to extend ground truth available for near-earth orbits to the higher altitudes of the 24-hour elliptical orbit.

10.1.6.2 Launch Configurations

This mission is designed to use the Saturn V launch vehicle with an extended CSM and OTS configuration.

The stack-up is S-IC/S-II/S-IVB/OTS(1)/OTS(2)/SM/CM.

These stages are described in subsections 10.1.1.2 and 11.1. The spacecraft concept associated with this mission (configuration number 6) is composed of two separable vehicles seen in the stack-up as OTS(1) and OTS(2).

10.1.6.3 Mission Phases

10.1.6.3.1 Launch Phase

The facility used for checkout and launch of this mission is Launch Complex 39 and the AMR downrange instrumentation.

The firing of the S-IC, the S-II, and the first firing of the S-IVB inject the payload and the S-IVB into a 648 km circular orbit (similar to the "High Flight Reliability Mode" described in subsection 10.1.5.3) or alternately into a 370 km circular orbit (similar to the "Low REM Mode" described in subsection 10.1.5.3).

Transposition and docking produces two stack-ups: the S-IVB/OTES(1) and the SM/CM/OTS(2).

A second S-IVB burn inserts the S-IVB/OTS(1) into a 5-hours-plus transfer orbit and a third S-IVB burn place the OTS(1) unmanned in a circular synchronous orbit.

Further maneuvers for the SM/CM/OTS(2) stack-up will be as described for the "High Flight Reliability Mode" or the "Low REM Mode" described in subsection 10.1.5.3.

The primary ground station support during the first 45 days and subsequent rendezvous periods will be provided by the Manned Space Flight Network (MSFN) described in subsection 10.1.13.

10.1.6.3.2 Initial Operational Phase

The OTS(1) will be activated and controlled remotely from the ground from the Mission Control Center, Houston, via either the Manned Space Flight Network (MSFN) or the Deep Space Network (DSN).

The manned operational phase for OTS(2) is described in subsection 10.1.1.3.

10.1.6.3.3 Final Operational Phase

At the end of the manned phase (during which OTS(2) was crew controlled and OTS(1) was remotely controlled) an unmanned mode checkout will be performed by the OTS(2) crew observing spacecraft operations during such ground commanded operations as remote alignment, acquisition, etc.

The OTS(1) crew will return to the command module and the CSM will dedock and separate from the OTS(1). The CM will then separate from the SM and return to earth.

Both OTS(1) and (2) will then be in unmanned experiment modes. Systems command and control functions will be assumed by the ground station control center, thus freeing MSC of all further OTS traffic.

The ground station control center will have a data quick-look capability. Complete reduction and interpretation of experimental data will be performed at a data analysis center separate from the ground station.

During the lifetime of the mission, it shall be possible to rendezvous a Saturn V launch CSM with either OTS(1) or OTS(2) for intermittent manned operations.

10.1.7 Mission VII Description

Mission VII employs a manned spacecraft in a near-earth trajectory and an initially unmanned spacecraft in a 24-hour elliptical orbit. This is a multiple spacecraft mission using the Saturn V launch vehicle.

10.1.7.1 Orbits

This mission involves one operational orbit near earth similar to the one described in subsection 10.1.5.1 and another orbit as described for Mission II in subsection 10.1.2.1.

In addition to combining the experimental capabilities of Mission IV and Mission V, the simultaneous operation of two spacecraft make it possible to conduct spacecraft-to-spacecraft communications to validate techniques which demonstrate the feasibility of an earth orbiting terminus for an interplanetary optical communication link. Simultaneous earth surface observations from the two orbits could also serve to extend ground truth available for near-earth orbits to the higher altitudes of the 24-hour elliptical orbit.

10.1.7.2 Launch Configurations

This mission is designed to use the Saturn V launch vehicle with an extended CSM and an OTAES spacecraft.

The stack-up is S-IC/S-II/S-IVB/OTS(1)/OTS(2)/SM/CM.

These stages are described in subsections 10.1.1.2 and 11.1.6. The spacecraft concept associated with this mission is configuration number 6 which is composed of two separable vehicles that are seen in the stack-up as OTS(1) and OTS(2).

10.1.7.3 Mission Phases

The phasing for this mission is identical to that for Mission VI (described in subsection 10.1.6.3) except that the second S-IVB burn places the S-IV/OTS(1) stack-up into a 10-hour-plus transfer trajectory to the apogee of the 24-hour elliptical orbit where the third S-IV burn inserts the OTS(1) into this final orbit.

10.1.8 Mission VIII Description

Mission VIII is initially unmanned, uses a synchronous orbit, and is sized for the Saturn IB/Zero Stage launch vehicle. This mission has the same experimental capability as Mission III, but represents greater launch vehicle reliability and greater payload capability.

10.1.8.1 Orbit

The orbit for this mission is the synchronous orbit as described for Mission I in subsection 10.1.1.1.

10.1.8.2 Launch Configurations

This mission is designed to use the Saturn IB/Zero Stage launch vehicle. The launch stack-up is Zero Stage/S-IB/S-IVB/SM/OTS.

The Zero Stage consists of four multisegment solid 3.05 meters (120 inches) United Technology Center (UTC) rocket motors which impart an initial acceleration of 12.75 meter/second^2 (1.3 g) to the stack-up.

The S-IB stage, the S-IVB stage, and the IU above the S-IVB stage are described in subsection 10.1.3.2. The Apollo Service Module is employed as the upper stage and the Saturn IB/Centaur fairing/shroud of Marshall design is used. The payload spacecraft concept may be configuration numbers described in subsection 11.2.

10.1.8.3 Mission Phases

The facilities for checkout and launch will be Launch Complexes 34 or 37 and the AMR downrange instrumentation.

The Zero-Stage firing, S-IB firing, and the S-IVB firing inject the SM/OTS into parking orbit. The SM first burn injects the payload into the 5-hours-plus transfer orbit. The SM second burn circularizes the payload and then the SM is jettisoned.

After this point, the mission phasing is identical with the phasing for Mission III discussed in subsection 10.1.3.3.

10.1.9 Mission IX

Mission IX is initially unmanned, uses a 24-hour elliptical orbit, and uses the Saturn IB/Zero Stage launch vehicle. This mission has the same experimental capability as Mission IV, but represents greater launch vehicle reliability and greater payload capability.

10.1.9.1 Orbit

The orbit for this mission is the 24-hour elliptical orbit as described for Mission I in subsection 10.1.1.1.

10.1.9.2 Launch Configuration

This mission is designed to use the Saturn IB/Zero Stage launch vehicle. The stack-up is Zero Stage/S-IB/S-IVB/OTS.

These stages are described in subsections 10.1.9.2, 10.1.3.2 and 11.2.

10.1.9.3 Mission Phases

The phasing for this mission will be identical to that for Mission VIII (detailed in subsection 10.1.8.3) except that the spacecraft spends approximately 10 hours in transfer from parking to injection at the apogee of the final orbit.

10.2 RECOMMENDED MISSIONS

Of the nine candidate missions, four are recommended at this time; these are Missions I, III, V and VI. The four missions involving elliptical orbits were discarded due to the deleterious effect of the environmental radiation fluxes experienced on the lower transverses of the orbit. The recommended missions are shown in table 10.2-1.

Mission I uses a standard Saturn V stack-up and OTS configuration #1. This is initially manned and has the greatest experiment capability. It can support all of the experiments including the large interferometer boom. It utilizes a synchronous orbit and the spacecraft is initially manned for 45 days. By proper choice of the orbit inclination, the range rates can be kept within the doppler shift limits imposed by the heterodyne laser receivers. Figure 10.2-1 shows the range rates obtaining for a ground station at 35°N latitude and for different orbit inclinations. The 28.5° orbit inclination meets the orbital requirements for the laser communications experiments and provides a maximum payload capability of 27,000 Kg for a configuration #1 type spacecraft. Figure 10.2-2 depicts the High Energy Manned Mission.

Mission III uses a Saturn IB/Centaur stack-up and an OTS configuration #2. This spacecraft is initially unmanned and can support all the experiments except the Interferometer System (experiment #14) and possibly the Fine Guidance (Experiment #12), although the last mentioned experiment could be carried instead of the mirror figure experiments. This mission uses a synchronous orbit and provides the maximum payload capability of 5,200 Kg at an orbital inclination of 28.5°. The range-rate curves shown in figure 10.2-1 apply to this mission as well as to Mission I. Figure 10.2-3 depicts the High Energy S-IB/Centaur mission.

Mission V uses a standard S-IB stack-up and OTS configuration #4. This mission is characterized by frequent shadow times leading to harsh thermal conditions. This negates the Interferometer experiment with its long boom exposed to solar radiation and demanding high geometric integrity. Table 10.2-2 shows the contact profiles for two orbit inclinations and a ground station at 35°N latitude. This shows an innage rate of about 5 per cent of the orbit period. The low contact rate and high integrated shadow times (which degrade solar panel power capability) rule out the choice of laser communications experiments for this mission. However, all non-laser experiments except #14, Interferometer System, can be supported within the 12,000 Kg capability for a configuration #4 type spacecraft. Figure 10.2-4 depicts the Low Energy Manned Mission. Mission VI uses a standard Saturn V stack-up and OTS configuration #3. This is a dual spacecraft configuration with an initially manned spacecraft (OTS-2) remaining at a 649 Km, 28.5° N inclined, circular orbit and an unmanned spacecraft (OTS-1) placed in a synchronous orbit. The same

TABLE 10.2-1 RECOMMENDED MISSIONS

Mission	Launch Vehicle Stack Up	Spacecraft Configuration	Parking Orbit	Final Orbits	Payload - 1,000 Kg INC. = 28.5	Payload - 1,000 Kg INC. = 0°
I	S-IC/S-II/S-IVB	#1	185 Km	Synchronous	27.2	23.6
III	S-IB/S-IVB/CENTAUR	#2	185 Km	Synchronous	5.2	4.7
V	S-IB/S-IVB/SM	#4	185 Km	Circular 649 Km	12.2	11.2
VI	S-IC/S-II/S-IVB	#3	649 Km	One at Synchronous Altitute and One at 649 Km Circular @ 28.5° Inclinations	OTS-1 =14 *OTS-2 =14	OTS = 12 *OTS = 12

*OTES-2 remains in 649 Km circular orbit inclined at 28.5°

TABLE - 10.2-2

CONTACT PROFILE FOR A LOW EARTH ORBIT
ALTITUDE = 649 Km AND GROUND STATION LATITUDE = 35°

Inclination = 35°				Inclination = 60°			
Orbit	Contact Start (sec)	Contact End (sec)	Innage (sec)	Orbit	Contact Start (sec)	Contact End (sec)	Innage (sec)
1	No Contact			1	244	830	586
2	6200	6835	635	2	6150	6930	780
3	12300	13090	790	3	12350	12990	640
4	18500	19290	790	4	18800	18940	140
5	24700	25490	790	5	25000	25240	240
6	30910	31690	780	6	31000	31640	640
7	37150	37740	590	7	37010	37790	780
8				8	43260	43720	460
9				9			
10				10			
11	No Contact			11	No Contact		
12				12			
13				13			
14	In First 24 Hours There Is a 5.1% Contact			14	In First 24 Hours There Is a 4.9% Contact		
15				15			
16	88230	88470	240	16	88080	88810	730
17	94130	94870	740	17	94130	94870	740

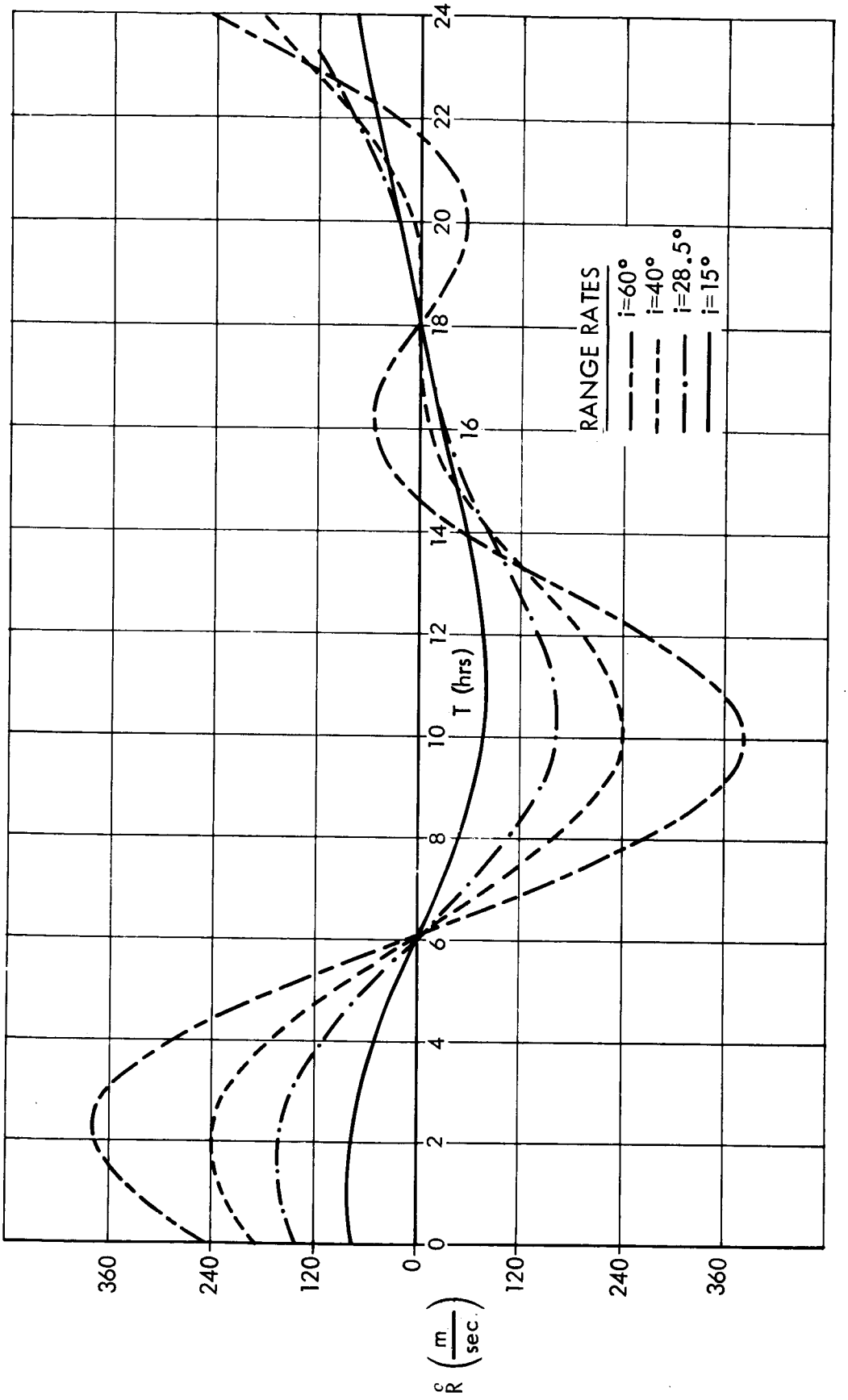
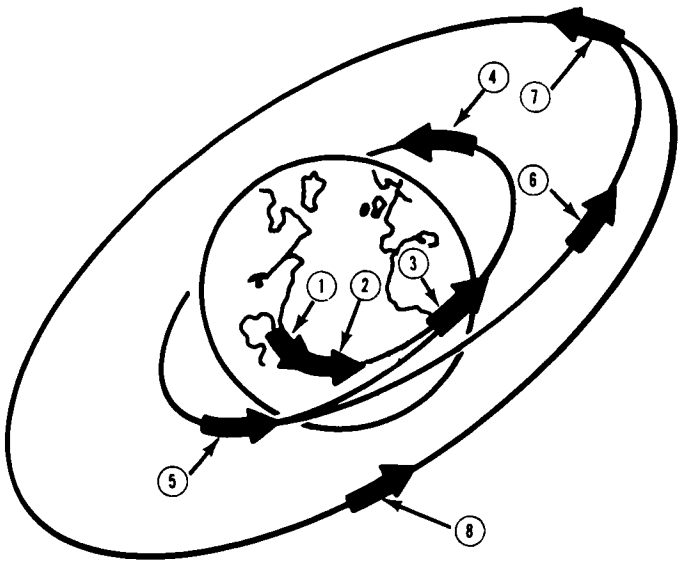
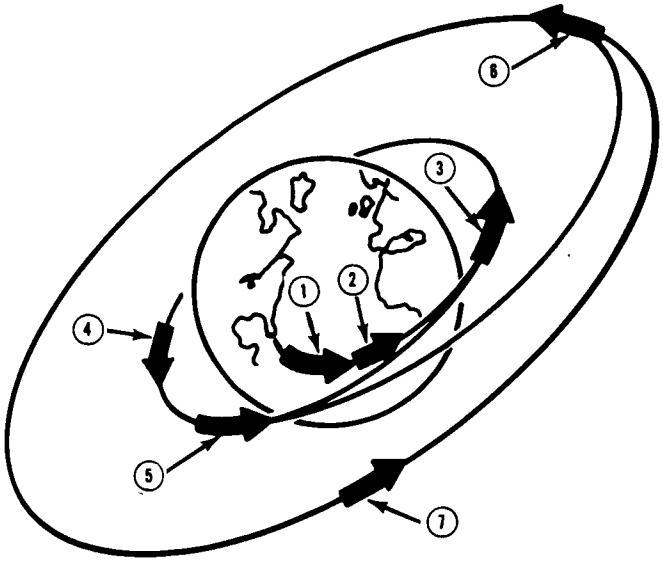


Figure 10.2-1. Range Rates as a Function of Time for Various Inclinations



① S-IC BOOST
② S- II BOOST
③ S-IVB 1ST BURN-INJECTION INTO PARKING.
④ PARKING ORBIT
⑤ S-IVB 2ND BURN-INJECTION INTO TRANSFER ORBIT.
⑥ CSM/OTES TRANSPOSITION AND DOCKING.
⑦ SM BOOST TO INJECT INTO FINAL ORBIT.
⑧ FINAL ORBIT.

Figure 10.2-2. High Energy Manned Mission - Mission I



① S-IB BOOST
② S-IVB BOOST
③ CENTAUR 1ST BURN-INJECTION INTO PARKING.
④ PARKING ORBIT
⑤ CENTAUR 2ND BURN-INJECTION INTO TRANSFER ORBIT.
⑥ CENTAUR 3RD BURN-INJECTION INTO FINAL ORBIT.
⑦ FINAL ORBIT

Figure 10.2-3. High Energy Unmanned Mission - Mission III

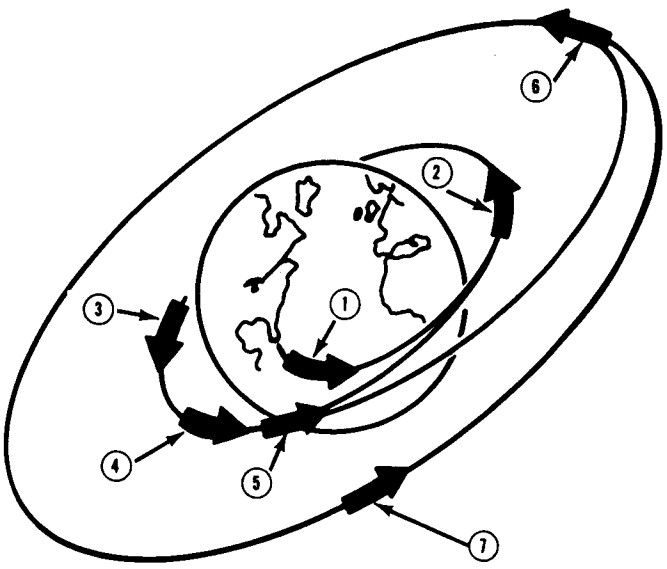
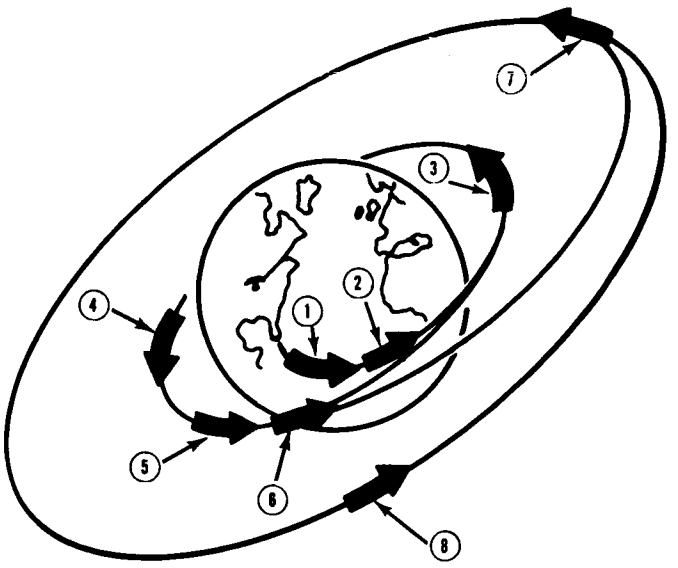


Figure 10.2-4. Low Energy Manned Mission - Mission V

orbit characteristics discussed for Mission V apply to OTS-2 and those for synchronous orbits for OTS-1. All the laser experiments can be conducted from OTS-2. An added feature for this Mission is that by converting one of the telescopes in OTS-2 into a laser receiver or transmitter, a space-to-space communications link can be established between OTS-1 and OTS-2. Weight of each OTS spacecraft can be up to 12,000 Kg for this mission. Figure 10.2-5 depicts this dual mission.



① S-IC BOOST

② S- II BOOST

③ S-IVB 1ST BURN-INJECTION INTO PARKING.

④ PARKING ORBIT

⑤ TRANSPOSITION AND DOCKING TO PRODUCE S-IVB/OTES (1) AND SM/CM/OTES (2).

⑥ S-IVB 2ND BURN INSERTS S-IVB/OTES (1) INTO TRANSFER ORBIT MANNED SM/CM/OTES (2) REMAINS IN LOW ORBIT.

⑦ S-IVB 3RD BURN INJECTS OTES(1) UNMANNED, INTO FINAL ORBIT.

⑧ FINAL ORBIT

Figure 10.2-5. Dual Mission (High Energy Unmanned & Low Energy Manned) - Mission VI

10.3 AAP MISSION CONSTRAINTS

The mission constraints imposed by Apollo vehicles have been evaluated to determine their impact on the OTAES mission. Missions for this evaluation consist of three types of earth orbits: a) synchronous, b) near earth, and c) 24-hour elliptical. The mission constraints considered for each type of orbit are: a) thermal environment, and b) data acquisition, command and control.

10.3.1 Thermal Constraints

10.3.1.1 Synchronous Orbit

The present Block II Apollo Command and Service Module (CSM) has two ECS radiators which reject the excess heat produced by the astronauts and equipment in the Command Module, and the energy from the external environment which is absorbed by the Command Module. The radiators each have an area of 50 square feet and are located 180 degrees apart on the sides of the Service Module. Both the primary and secondary coolant loops share the radiator area. The ECS radiators are capable of handling all heat loads, except at the two extremes, expected during planned Apollo missions. At the upper extreme a water boiler is used to dissipate part of the higher heat load. An electrical heater is used at the lower end to prevent the coolant from freezing during periods of minimum heat rejection. The Apollo Block II Environmental Control System has a 470 watt heater in the primary coolant loop, and a 900 watt heater in the secondary coolant loop.

Preliminary analyses indicate that the ECS radiator heat load for planned OTAES missions will be below the Apollo Block II design limits. Therefore, extensive use of the ECS heaters may be required to prevent the coolant from freezing. Use of the heaters for any period of time will impose a severe weight penalty associated with the additional hydrogen and oxygen required for the fuel cells. Another method of preventing the coolant from freezing is to use Passive Thermal Control (PTC). This method, presently planned for Apollo Lunar Missions, requires that the CSM rotate about its x-axis at a rate of from 1 to 2.5 rph. This will maintain a uniform temperature over the entire spacecraft, and prevent the coolant in the radiator from freezing. Also, possible redesign of the ECS radiators to better accommodate OTAES missions could eliminate any extensive requirement for the ECS heaters.

In a docked mode of operation (CSM/LM), the Command and Service Module ECS will be used for pressurization of the entire spacecraft. The Command and Service Module ECS will require an additional blower to insure adequate circulation throughout the entire spacecraft and to eliminate any possible "dead spots" in the Lunar Module. Also, the Command and Service Module ECS will be used to pressurize the Telescope Module if a shirtsleeve environment is required. Since many of the planned OTAES experiments require that the spacecraft maintain a fixed attitude for long periods of time, PTC rolling cannot be used to any great extent for temperature control of the ECS radiators. Therefore, the ECS heaters will be required.

If the Lunar Module operates dedocked from the Command and Service Module, the use of the CSM Environmental Control System heaters can be kept to a minimum as the CSM can conduct PTC rolling to prevent the coolant from freezing. The Lunar Module will then function in a fixed mode independent from the CSM. However, the Lunar Module ECS, presently designed for two days use, will require major modification or an entirely new system to accommodate a manned flight for 45 days.

The Service Module's Reaction Control System (RCS) provides stabilization, attitude control and docking orientation about the three axes of the spacecraft, as well as translation velocity increments, ullage accelerations and separation impulses. It consists of four identical independent units located at 90 degree intervals around the circumference of the Service Module. Each unit employs four thrusters mounted in a cluster (quad) on the external surface of the Service Module. Temperatures encountered on the shaded side of the spacecraft during a synchronous orbit will exceed the minimum temperature limits of certain RCS components. These components are the fuel, and oxidizer valves, each with a minimum temperature limit of 35°F, and the injector, with a minimum temperature limit of 20°F. A 36 watt electric heater mounted in each quad will maintain the propellant valves above 50°F for periods up to three hours and thereby prevent them from freezing.

For presently planned Apollo Lunar Missions, Passive Thermal Control (PTC) rolling of the spacecraft about its x-axis will be used to maintain the RCS quads above the minimum operating temperatures. The minimum rotation rate is 0.5 rph. For presently planned Apollo missions, electrical heater power is budgeted for a maximum three hour hold with heaters active. This hold is then followed by fifteen hours of recovery by PTC rolling with heaters inactive.

The Lunar Module (LM) Reaction Control System components are essentially the same as those located on the Service Module. There is a 48 watt heater located in each RCS quad of the Lunar Module.

In a docked mode of operation (CSM/LM), the RCS heaters will be required. PTC rolling of the spacecraft cannot be conducted for any length of time as many of the OTAES experiments require that the spacecraft operate in a fixed mode for long periods of time. Since the maximum number of quads on the shaded side of the spacecraft will be four (two each on the CSM and LM), the maximum electrical power required will be 168 watts.

In the dedocked mode of operation, the Command and Service Module can conduct PTC rolling to maintain the RCS components at operable temperatures. The RCS quads on the shaded side of the Lunar Module will require the use of the heaters.

10.3.1.2 Near Earth Orbit

The thermal constraints encountered in a near earth orbit are not as severe as those in a synchronous orbit. The Reaction Control System heaters will

not be required as there is sufficient radiant heat from the earth to maintain the RCS components above their critical temperatures.

In the docked mode of operation, the CSM Environmental Control System heaters will be required. However, if the CSM operates dedocked from the LM, PTC rolling can be used to maintain the CM Environmental Control System at operating temperatures. The LM can then operate in a fixed mode, independent of the CSM, with no requirement for RCS heaters. As previously mentioned; however, a modified or new LM Environmental Control System will be required for a manned 45-day mission.

10.3.1.3 24-Hour Elliptical Orbit

The thermal constraints discussed for a synchronous orbit also apply to a 24-hour elliptical orbit.

10.3.2 Data Acquisition, Command and Control Constraints

Methods of acquiring experimental data, and accomplishing spacecraft command and control functions will depend on the spacecraft configuration. Docked and dedocked modes of operation, and manned or unmanned operation must be considered to determine the most reliable, most economical, and easiest methods of retrieving experimental data and transmitting this information to the ground. Methods of data acquisition, and command and control will essentially be the same for all types of orbits.

10.3.2.1 Data Acquisition

In either the docked or dedocked mode of operation, experimental data may be transmitted to the ground stations from either the Lunar Module or Command Module. If the Command Module is used to transmit data to ground stations in a dedocked mode of operation, a telemetry link or hardline between the Command Module and Lunar Module will be required. EVA will be required for any data which must be gathered physically by the astronaut.

10.3.2.2 Command and Control Function

Spacecraft command and control functions will be performed in the Command Module in the docked configuration. Experiment command and control functions will be conducted in the Lunar Module. In some cases, experiment operation or sequencing may be controlled by the ground stations.

Control of the Lunar Module/Telescope Module in the dedocked mode may be accomplished by a Lunar Module guidance and control system, from the Command Module, or from the ground. If manned, the LM/TM can readily be controlled using Lunar Module equipment. The existing voice link between the Command Module and Lunar Module will be used for communications. The LM/TM could be controlled from the Command Module; however, a command link will then be required. Command and control of the LM/TM from the ground could be accomplished; however, this would not be necessary in the manned spacecraft.

10.4 GROUND STATION CONCEPTS

Although the OTAES mission studies include a number of low altitude orbits, there is much to recommend a synchronous orbit for an Optical Technology Experiment system. Thus the preliminary ground station studies have proceeded from an initial solution for the synchronous orbit mission to examine its suitability for other orbits. Within certain constraints, a synchronous orbit coupled with a judicious choice of ground-station configuration permits all of the experiments to be performed from a single ground-station complex, meaning a single set of facilities for performing all the functions associated with the experiments. This single complex, which suffices for the synchronous orbit, may also suffice for the medium altitude orbits on an intermittent basis. The additional costs of implementing a multiplicity of ground-station complexes at geographically large separations around the world, and of staffing them for this one OTAES mission, just to obtain a greater utilization factor, may be difficult to justify.

The ground-station philosophy, therefore, is that of a single set of facilities sufficient to carry out the fullest possible intent of the experimental mission. We refer to this as a one-station concept in juxtaposition to a two- or three-station globe-encircling concept; but this does not imply that all the required facilities will be collocated at a single integrated site or location. In fact, as will be amplified below, the single-station complex will most likely involve facilities at a small number of existing and new sites.

10.4.1 Mission Control

Whether the OTAES mission is viewed as an isolated experimental task or as a sequence of experiments in optical technology, a significant portion of the mission requirements are routine Apollo operations, or are operations readily programmed into existing facilities with little or no change. All the operational procedures involved with prelaunch, launch, establishment of orbit, and return-to-Earth are viewed as routine and outside the realm of experiment. Further, the experimental procedures involving command, control, telemetry, and voice communication are conceived as routine operations programmable on existing facilities. Only existing operational NASA facilities, checked out and approved for manned space missions, may be considered for any phases of the experiment involving mission safety; and these same facilities will be used for the routine functions of managing the experiment.

The mission control communications that must take place between the ground and the spacecraft can be classified under three general categories:

a. Monitoring: telemetry and/or voice monitoring of launch-vehicle and spacecraft systems (including the experiment package), the crew, and the crew systems.

b. Trajectory Measurements: including all Earth-based trajectory measurements, whether of launch vehicle or spacecraft.

c. Data Transmission to the Spacecraft: all information transmitted to the space vehicle, other than voice and the tracking interrogation.

The end product, or termination of the communication, tracking, and data acquisition systems is an information interface with human monitors, controllers, and mission directors. Generally, this means some form of visual display of the data, in most cases after several stages of processing, editing, or computing. In addition, the information to be transmitted from the ground to the spacecraft via the data up-link must originate and be processed under human monitoring and control.

Figure 10.4-1 is a block diagram of the central mission control functions.

The mission control system is comprised of five interdependent systems, which provide all the required display, control, and communication services to enable the operations staff

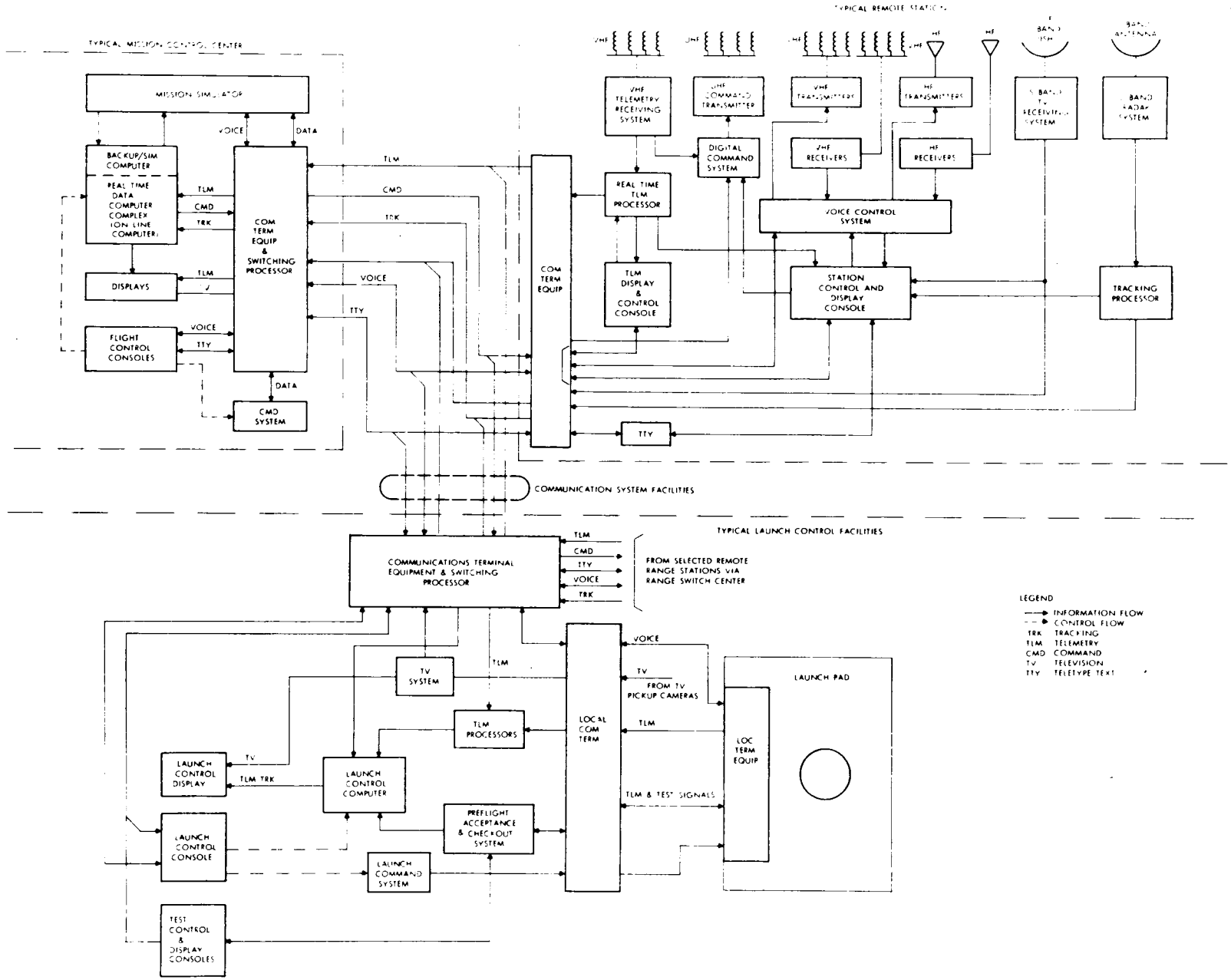


Figure 10.4-1. Simplified Block Diagram of Typical Ground Support System and Facilities

to function efficiently in performing their tasks of monitoring and directing an experiment mission. The major subsystems are discussed in the following paragraphs.

10.4.1.1 Display and Control System

The display and control system is in itself composed of five interrelated subsystems:

a. Computer Interface

b. Timing

c. Television

d. Consoles

e. Group Displays.

10.4.1.2 Real-Time Computer

The real-time computer provides the two functions of data processing and display processing. The data processing function handles the mathematical computation tasks, such as conversion of raw data to engineering units, trend prediction, limit sensing, and solution generation. A typical example of the solution generation is the recommendation of alternate maneuvers or experiments, based on the existing status of the vehicles.

10.4.1.3 Communications System

The internal communications system performs two basic functions:

a. Acts as a terminal and control point for all outgoing and incoming video voice and data to and from the network sites, the launch complex, recovery areas, and with certain restrictions, the general public.

b. Provides equipment and control facilities for routing and distributing voice, video and digital data, and hard copy within the Mission Control System.

The different types of transmission are listed to illustrate the requirements for the termination and control facilities:

a. Spacecraft-to-Ground Voice

b. Operational Voice (between remotely situated flight controllers)

c. Administrative Voice

d. Message Teletype

e. Data Teletype

f. High-Speed Telemetry Data (up to 3000 bits/second)

g. Wide-Band Telemetry Data (above 3000 bits/second)

h. Television.

To handle the digital data (i.e., telemetry, teletype, tracking, and command data) expeditiously, a communications processor should be incorporated. All digital data entering and

leaving the control center can be processed by this computer. It is capable of addressing, line switching, storing, and forwarding digital data; it also provides an error-detection capability.

The telemetry system reads out the composite FM/FM telemetry signals and the PCM bit streams, and processes them concurrently. All data is then recorded on magnetic tape, and selected parameters are simultaneously transmitted to the real-time computer via the processor for processing, storage, and display. Certain data will undergo digital-to-analog conversion, and then be transmitted directly to analog displays.

Hard-copy communication within the control center is handled by two subsystems: a teletype distribution of text to the major operational areas and a pneumatic tube subsystem between all operational areas.

The voice subsystem should consist of an intercom, a public branch exchange (PBX), and a voice switchboard to connect the external network voice trunks to the intercom. The intercom is designed on a loop concept with restricted loop access.

10.4.2 Facility for Special Experimental Operations

The optical ground terminals will be comprised partly of hardware that is strictly experimental in nature, on which mission safety will not rely, and much of which may be peculiar to this one set of experiments. The experimental equipment will be manned by research scientists rather than operations personnel. Thus, there are significant distinctions in the required psychological environment, in the required equipment reliability, in the operational procedures, and in the desired responses to unpredictable situations between the experimental components of the ground-station complex and those operational components that satisfy the requirements in the preceding paragraphs.

The physical environment desired for the optical ground facility places more severe restrictions on its siting than are imposed on radio-frequency ground facilities. Solid cloud cover or dense fog, for example, appear as opaque masks that prevent light transmission, and hence inhibit the performance of space/ground optical experiments. Even when the atmosphere is transparent, the degree of transparency is limited by haze, urban and industrial air pollution, or thin cirrus cloud, and thus may still inhibit some experiments. The turbulence of the atmosphere causes a time-varying spatial distribution of the index of refraction, scattering energy and introducing a randomness into the focus, angle of arrival, and intensity of the transmitted energy. The siting of the experimental optical equipment must be made with these considerations in mind. Such requirements tend to be incompatible with the existing radio-frequency sites.

To satisfy this wide divergence of siting criteria and operational tenor between the desired optical ground facility and existing radio-frequency installations, the concept of a separately located optical installation was developed. Because of the peculiar siting problems, the optical facility and the cooperating radio facility might well be hundreds of miles removed from one another, requiring some form of data tie-line for exchange of experimental data and for communications and control. The optical facility would also require access to the Apollo network for pointing information. Local computational facilities may be required for data handling and conversion, both for optical link experimental communications and for pointing and tracking data.

A small ground installation, considered auxiliary to the main optical facility, will be required for the point-ahead experiment. Until the relative positions of the optical and radio facilities are established with respect to the orbit, it is not possible to recommend a relative location for the point-ahead auxiliary site.

10.4.3 Location of Optical Facility

The choice of a suitable site for the optical ground facility required to support the OTAES mission is a problem beyond the scope of this study. However, a cursory review of the problem demonstrates that the site selection criteria are similar to astronomical observatory criteria except that there are more constraints and conditions imposed on the OTAES site. Not the least of these constraints is the need for minimizing the probability of poor weather conditions. A lengthy outage time on a manned mission could not only prove extremely costly, but even negate its success. A number of workers in the field have faced similar siting problems, but usually not as critical; and it is generally concluded that the southwest region of the continental U.S. holds high promise for the best available atmospheric seeing conditions. Table 10.4-1, furnished by the Smithsonian Institution Astrophysical Observatory, provides an initial insight into the fraction of time in which viewing is not possible for a representative collection of Baker-Nunn installations. Tentatively, it is assumed that an optical site will be chosen somewhere in New Mexico, Arizona, or California. Hopefully, an analysis of mission success criteria will indicate a similar choice.

10.4.4 Choice of Radio Facility

Within the confines of the single-station concept, the radio frequency and optical frequency sites are cooperating elements of a single ground-station complex. It is essential that relatively error-free data interchange and human communication be available between these remotely located installations so that they function as effectively as though they were co-located. In the case of the synchronous orbit, both locations must be within the constant communication range of the spacecraft at their respective frequencies. In the case of medium altitude orbits, the communication periods with each station (i.e., radio and optical) must overlap to a significantly large degree. These requirements mean that the radio frequency and optical frequency entities of the ground-station facility may not be separated geographically by very large distances. The two sites should be no more than a few hundred miles from one another. This means that one must look to the southwest region for an existing radio frequency supporting site.

There exist three broad categories of ground support facilities suitable for the OTAES program. These are the Manned Space Flight Network, the Deep Space Network, and the Satellite Tracking and Data Acquisition Network (STADAN). The Manned Space Flight Network began with project Mercury, and has expanded with the Gemini and Apollo projects. It provides ground support for the manned space flights of these projects, and its capabilities for communication, command and control, etc., extend to lunar distances. The Deep Space Network is maintained primarily for the support of the scientific deep space probes such as Mariner, but facilities for lunar probes and orbital vehicles also exist at these sites. The Deep Space Network provides support for space vehicles at distances that extend to the edge of the solar system. Up to the present time, the main use of the Deep Space Network has been for unmanned, scientific flights. STANDAN exists mainly for the support of unmanned, earth orbiting scientific satellites.

The capabilities of each of the three types of stations reflect the nature of the programs the stations are meant to support. The Manned Space Flight Network stations contain equipment capable of tracking at fairly high angular rates since low Earth-orbiting vehicles move relative to a fixed point on the Earth at high angular rates. The signals transmitted to Earth by such vehicles are relatively strong due to the proximity of the vehicles to Earth. These Manned Space Flight Network stations have medium gain antennas that can track at high angular rates. The Deep Space Network equipment is not required to track at such high angular rates since the distances from Earth become large. The signals received however from such deep space vehicles become very highly attenuated. Therefore, the Deep Space Network stations use very large, high gain antennas, but do not meet high speed tracking requirements.

TABLE 10.4-1

PERCENT OF VIEWING NOT ATTEMPTED DUE TO CLOUDS

Station Coordinates			Jan.	Feb.	Mar.	Apr.	May	June	July	Aug.	Sept.	Oct.	Nov.	Dec.
New Mexico		1962	36	25	27	15	5	12	49	32	48	19	26	22
253°27'(E)	+32°25'	1963	34	27	21	29	30	13	48	57	28	16	27	17
South Africa		1962	42	29	31	26	4	6	1	5	8	29	53	37
028°15'(E)	-25°58'	1963	50	23	27	28	15	21	20	2	7	30	55	49
Australia		1962	32	21	21	9	34	12	22	22	27	38	15	18
136°46'(E)	-31°06'	1963	16	22	22	22	51	35	47	21	18	17	18	22
Spain		1962	52	32	81	43	33	15	21	15	34	47	40	43
353°48'(E)	+36°28'	1963	72	49	39	39	35	32	4	19	22	19	60	45
Peru		1962	81	71	56	38	10	2	5	6	35	22	42	55
288°30'(E)	-16°28'	1963	88	95	63	56	23	2	6	15	21	26	13	52
Iran		1962	28	44	33	54	10	1	18	16	03	nil	14	38
052°31'(E)	+29°38'	1963	17	40	30	47	30	7	15	23	1	12	35	22
Curacao		1962	52	43	56	53	74	66	46	38	60	39	45	50
291°10'(E)	+12°05'	1963	70	59	51	68	70	40	64	55	63	50	65	62
Florida		1962	55	40	62	55	36	61	41	55	52	45	55	43
279°53'(E)	+27°01'	1963	57	58	47	28	50	42	44	29	49	32	49	43
Argentina		1962	53	52	38	72	51	27	39	32	22	29	35	43
294°54'(E)	-31°57'	1963	*	35	40	27	39	33	36	32	57	46	46	30
Hawaii		1962	23	41	56	39	33	5	38	18	20	16	26	33
203°45'(E)	+20°43'	1963	59	17	70	78	52	28	29	23	39	39	32	30

*No photography attempted for a 3 week period when the mirror was removed for realuminizing.

In general, the requirements of the OTAES program are most similar to those of other manned space flight programs; and, thus, the Manned Space Flight Network stations are better suited to OTAES than either of the other two types. A list of ground support facilities equipped with microwave tracking and data acquisition systems is provided in table 10.4-2. Many of the stations are provided with a dual system consisting of two transmitters and two receivers capable of providing the indicated communications service to four simultaneous manned space missions, on the assumption that no more than two missions would be in sight simultaneously. Additional storage at the site permits retention of data on the out-of-sight missions while engaged in active tracking and communication with in-sight missions.

Figure 10.4-2 is a highly simplified block diagram of the basic, nonredundant ground system capable of supporting one spacecraft. Only that circuitry that contributes to the understanding of the system function has been retained. Table 10.4-3 outlines the Unified S-Band System characteristics. Tables 10.4-4 and 10.4-5 compare OTAES requirements with Unified S-Band capabilities.

The radio frequency links with the spacecraft should be provided by existing facilities. Only two facilities that are available in the southwest area might be considered suitable; these are the NASA facilities at Goldstone Lake, California, and those at White Sands, New Mexico. Of these, White Sands may be eliminated since it will not be equipped with sufficient capability to provide RF and data processing command and telemetry functions for OTAES. The Goldstone facility, on the other hand, is particularly well suited to the OTAES support requirements. This facility is described in section 11.7, Communication and Data Handling.

TABLE 10.4-2

EXISTING GROUND SUPPORT SITES, OR SITES IN STATE OF PREPARATION FOR EARTH ORBITAL, LUNAR, AND DEEP SPACE MISSIONS

Station Location and Designation / FACILITIES	UNIFIED S-BAND SYSTEM, WITH CAPABILITIES:						
	30 foot Dish	85 foot Dish	210 foot Dish	Telemetry Reception	Voice Communication	Ringing	Updata Transmission
ANTIGUA	X			X	X	X	X
BERMUDA	X			X	X	X	X
GRAND CANARY ISLAND	X			X	X	X	X
CARNARVON, AUSTRALIA	X			X D	X D	X D	X D
HAWAII	X			X D	X D	X D	X D
GUAYMAS, MEXICO	X			X	X	X	X
GUAM	X			X D	X D	X D	X D
CAPE KENNEDY, FLA. "Spacecraft Monitoring"	X			X D	X D	X D	X D
ASCENSION ISLAND "Spacecraft Guidance & Command"	X			X D	X D	X D	X D
CANBERRA, AUSTRALIA "Tiobinbilla"		X		X D	X D	X D	X D
MADRID, SPAIN "Madrid"		X		X D	X D	X D	X D
CENTRAL TEXAS		X		X D	X D	X D	X D
JOHANNESBERG, S. AFRICA "Johannesberg"		X		X D	X D	X D	X D
ISLAND LAGOON, AUSTRALIA "Woomera"		X		X D	X D	X D	X D
GOLDSTONE, CALIF. "Pioneer"		X		X D	X D	X D	X D
GOLDSTONE, CALIF. "Echo"		X		X D	X D	X D	X D
GOLDSTONE, CALIF. "Venus"	X	X		X D	X D	X D	X D
GOLDSTONE, CALIF. "Mars"			X	X D	X D	X D	X D

X - INDICATION OF EXISTING OR PLANNED CAPABILITY PROBABLY NEAR COMPLETION - 1966.

D - DUAL SYSTEM - TWO TRANSMITTERS, TWO RECEIVERS.

TABLE 10.4-3

RF SYSTEMS CHARACTERISTICS, PRELIMINARY

Item	Characteristics	
Antenna Microwave Subsystem		
Cassegrain feed and microwave circuitry		
(1) Type	Tracking-Transmit	
(2) Gain	Receive +1.0 53 db -0.5	Transmit 51 db ± 1.0
(3) Losses	0.16 db ± 0.03	0.4 db ± 0.1
(4) Polarization	RHC	RHC
(5) Ellipticity	0.7 db ± 0.3	1 db ± 0.5
(6) Effective noise temperature	27°K ± 3 (including losses)	
(7) Beamwidth	0.36°K ± 0.03	0.45°K ± 0.03
Low-noise amplifier	Parametric	TWM
(1) Type	20 db	30 db
(2) Gain	17 Mc ± 7 (3 db) +30	11 Mc (1 db) 15 Mc (3 db)
(3) Bandwidth		
(4) Effective noise temperature	165°K -15	16°K ± 2
(5) Input signal level range	-70 dbm to threshold	-80 dbm to threshold
Receiver Subsystem		
Type	Phase-coherent double conversion superheterodyne	
Effective noise temperature (antenna at or near zenith)		
(1) SCM and reference receiver	2700°K ± 300	
(2) SCM, TWM, and reference receiver	55°K ± 10	
(3) SCM, parametric amplifier, and reference receiver	270°K ± 50	
Input signal level	-55 dbm to threshold	
Frequency		
(1) Range	2290 to 2300 Mc	
(2) Nominal	2295 Mc	
Noise bandwidth ($2B_L$)	Threshold BW	
(1) RF	12 cps +0% -20%	
	+0%	
	48 cps -20%	
	152 cps +0% -20%	
(2) Range receiver	0.8 cps +0% -20%	
	4.0 cps +0% -20%	
	12.0 cps +0% -20%	
Detected telemetry		
(1) Modulation	Phase modulation	
(2) Bandwidth (1 db)	Selectable 2.2 kc, 10 kc, 210 kc, and 0.7 Mc	
(3) Output level	0 dbm (one subcarrier at 1 rad rms modulation index under strong signal conditions)	

TABLE 10.4-3

RF SYSTEMS CHARACTERISTICS, PRELIMINARY (Continued)

Item	Characteristics
(4) Output impedance	50 Ω
10-Mc IF output for telemetry	
(1) Modulation	Amplitude, frequency, or phase
(2) Bandwidth (3 db)	6.5 Mc
(3) Output level	0 dbm (non-coherent reception) -22 dbm (coherent reception)
(4) Output impedance	50 Ω
Precision doppler	
(1) Accuracy	0.2 cps rms at carrier frequency (uncorrelated error for one-minute sample spacing)
Angle error detection	
(1) Gain tracking	Differential ± 2-db maximum
(2) Phase tracking	Differential ± 15-deg maximum
Transmitter Subsystem	
Frequency control	Phase stable, crystal-controlled oscillator: frequency synthesized from an atomic frequency standard
Stability	
(1) Frequency	1:10" for 20 min 5:10" for 10 hr
(2) Phase	5 deg rms (noise error in BW ($2B_L$) of 12 cps)
Frequency	
(1) Range	2110 to 2120 Mc
(2) Nominal	2113-5/16 Mc
Power output	10 kw
Modulation	
(1) Type	Phase
(2) Command	
(a) Bandwidth	dc to 100 kc
(b) Sensitivity	3 rad peak/v peak
(c) Input impedance	50 Ω
(3) Range	
(a) Bandwidth	dc to 2 Mc
(b) Sensitivity	5 rad peak/v peak
(c) Input impedance	50 Ω
RF Threshold Signal Levels (antenna at or near zenith)	Threshold BW 12 cps $^{+0\%}_{-20\%}$ / 48 cps $^{+0\%}_{-20\%}$ / 152 cps $^{+0\%}_{-20\%}$
SCM and reference receiver receiver	-(154 dbm ± 1.0) / -(148 dbm ± 1.0) / -(143 dbm ± 1.0)
SCM, TWM, and reference receiver	$-(170.8\ \text{dbm}^{+1.4}_{-1.2})$ / $-(164.8\ \text{dbm}^{+1.4}_{-1.2})$ / $-(159.8\ \text{dbm}^{+1.4}_{-1.2})$
SCM, parametric amplifier, and reference receiver	$-(161.9\ \text{dbm}^{+1.4}_{-1.2})$ / $-(157.9\ \text{dbm}^{+1.4}_{-1.2})$ / $-(152.9\ \text{dbm}^{+1.4}_{-1.2})$

TABLE 10.4-4

GROUND TRANSMITTER - COMPARISON OF REQUIREMENTS WITH UNIFIED S-BAND SYSTEM.

	Requirements			Available Unified S-Band	
	Narrow & Wide Band Comm. Link	Exper. Data Link	Track	DSIF	NSIF
Frequency	8,205 MC	8,220 MC	8,210 MC	2,113 5/16 MC (2110 to 2120)	2,113 5/16 (2110 to 2120)
Ampl. Power	+67.4 dbm	+ 60 dbm	+ 57 dbm	+70 dbm	+ 70 dbm
Waveg. Loss	-2.4 db	- 2.0 db	- 2 db	- 0.5 db	- 0.5 db
Transm. Power (P_t)	+ 65 dbm	+ 58 dbm	+ 55 dbm	+ 69.5 dbm	+ 69.5 dbm
Antenna Diam.	9.14 m	9.14 m	9.14 m	25.9 m	9.14 m
Antenna Gain (G_t)	+ 55 db	+ 55 db	+ 55 db	+ 51 db	+ 42 db
$P_t G_t$	+ 120 dbm	+ 113 dbm	+ 110 dbm	+ 120.5 dbm	111.5 dbm
Modulation					
Type				PM or FM	PM or FM

TABLE 10.4-5

GROUND RECEIVER - COMPARISON OF REQUIREMENTS WITH UNIFIED S-BAND SYSTEM

	Required	Available Unified S-Band DSIF	Available Unified S-Band NSIF
Polarization	--	R.H.C.	R.H.C.
Antenna Diam.	18.24 m	25.9 m	9.14 m
D^2	333 m^2	673 m^2	83.5 m^2
System Noise Temperature	440°K	100°K	100°K
D^2/T_s	0.76	6.73	0.835
Bandwidth		3 db @ 15 MC (TWM)	
Frequency & Rec. Bandwidth			
1	2,200 MC & 10 KG	2,295 MC & 6.5 MC (3 db)	
2	2,205 MC & 300 KC	-----	
3	2,208 MC & 2 MC	-----	
4	2,215 MC & 5 MC	-----	
Receiver Type	-----	Phase Coherent Double Conversion Superheterodyne	

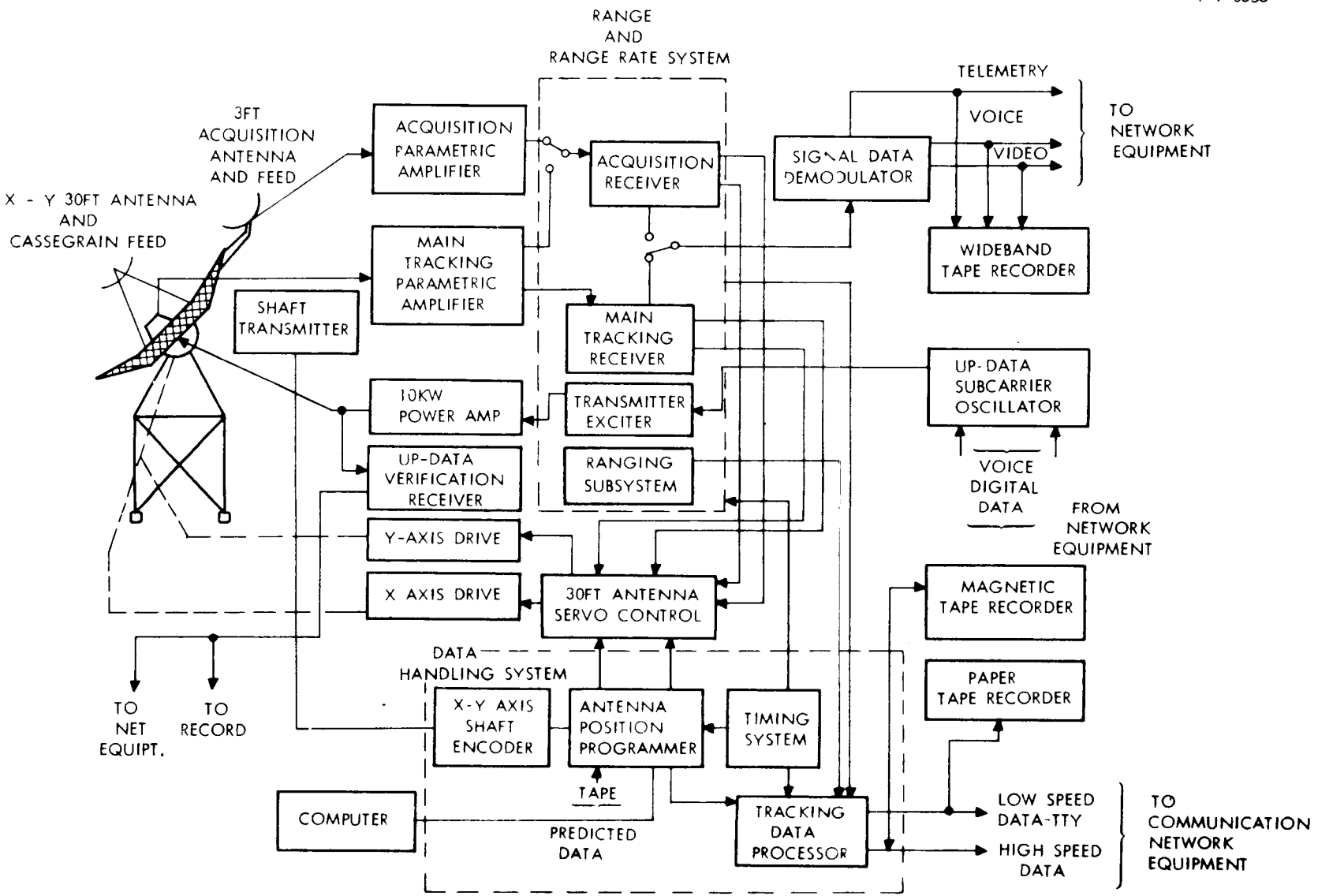


Figure 10.4-2. Basic Unified S-Band Station

11.0 SUPPORTING SPACECRAFT SUBSYSTEMS

Spacecraft subsystems were parametrically analyzed during this study for the following reasons:

a. To determine the feasibility of supporting experiment operation over the range of missions under consideration.

b. To identify alternate methods of implementing OTES missions and to bracket the more severe problem areas.

c. To identify potential trade-offs between experiment objectives, mission requirements, and spacecraft subsystems.

The information resulting from these analyses appears in this section.

11.1 CANDIDATE SPACECRAFT CONCEPTS

The philosophy of the OTAES study was to consider alternate approaches to the spacecraft design and to assess the feasibility and limitations of each approach relative to experiment and mission requirements. This approach therefore is not a preliminary design effort but rather a system analysis consistent with the level of experiment definition available.

In developing these concepts three major constraints were given. First, the spacecraft configurations had to be compatible with the LEM adapter shroud. Second, since some missions required launch with a Saturn IB, some spacecraft configurations were developed for the Centaur shroud. These, however, had to also meet the volume constraints of the LEM Adapter. Third, in order to maximize utilization of Apollo hardware, some configurations utilized the LEM ascent stage.

In a study of this nature, the requirements are necessarily broad in scope. The basic requirements established for investigating spacecraft concepts were:

a. Utilize state-of-the-art design consistent with the 1968-1971 time frame.

b. Spacecraft service life should range between one to two years.

c. The spacecraft should be capable of accomodating one to two telescopes each with aperture ranges between 75 to 155 centimeters, and two telescopes with an aperture between 25 to 40 centimeters.

d. The concepts should consider both EVA and shirt-sleeve accessibility to the telescopes.

e. The allowable weight regimes are given in table 11.1-1 for the candidate missions.

TABLE 11.1-1

ALLOWABLE PAYLOAD WEIGHTS

MISSION	STACK UP	PARKING ORBIT	FINAL ORBIT	PAYLOAD 1,000 kg	
				INC. = 28.5°	INC. = 0°
I	S-IC/S-II/S-IVB	185 km	Circular (24 hr)	27.2	23.6
II	S-IC/S-II/S-IVB	185 km	Elliptical (24 hr)	37	33
III	S-IB/S-IVB/Centaur	185 km	Circular (24 hr)	5.2	4.7
IV	S-IB/S-IVB/Centaur	185 km	Elliptical (24 hr)	6.8	6.2
V	S-IB/S-IVB/SM	185 km	Circular (350 n. mi.)	12.2	11.2
VI	S-IC/S-II/S-IVB	649 km	Circular (24 hr)	OTS-1 = 14 OTS-2 = 14	OTS-1 = 12 *OTS-2 = 12
VII	S-IC/S-II/S-IVB	649 km	Elliptical (24 hr)	OTS-1 = 18.5 OTS-2 = 18.5	OTS-1 = 16.6 *OTS-2 = 16.6
VIII	Zero Stage/S-IB/ S-IVB/SM	185 km	Circular (24 hr)	3.9	3
IX	Zero Stage/S-IB/ S-IVB/SM	185 km	Elliptical (24 hr)	6.2	5.2

*OTES (2) remaining in 649 km orbit at 28.5°

As a result of these requirements, seven basic spacecraft concepts were developed. These are discussed in the subsequent text.

11.1.1 Spacecraft Concept Number 1

Concept number 1 consists of a LEM Ascent Stage with one or more telescopes mounted below this stage such that the launch loads act through the diameter of the primary mirror. Variations of this concept are depicted in figures 11.1.1-1 through 11.1.1-3.

As can be seen from the figures, the LEM Descent Stage structure has been removed. In the launch configuration, loads are carried to the LEM adapter through a platform structure which picks up the same attachment points as the standard Apollo LEM descent stage.

Manned accessibility to the telescopes can be accomplished by an exit from the LEM ascent stage through the forward hatch, or through a new hatch in the LEM floor as shown in figure 11.1.1-4. In either case, volume constraints limit shirtsleeve accessibility to one side of the telescope structure (see figure 11.1.1-2) unless the astronaut actually enters the telescope tube.

One advantage of this configuration is that the telescope optical axis is parallel to the LEM windows. This facilitates initial acquisition by the use of manned procedures.

For a single telescope, the maximum well size would be 2.03 meters in diameter and 4.88 meters in length. The double telescopes would have a maximum well size of 2.08 meters in diameter by 4.32 meters in length without an access tube and 1.68 meters in diameter by 3.94 meters in length with an access tube.

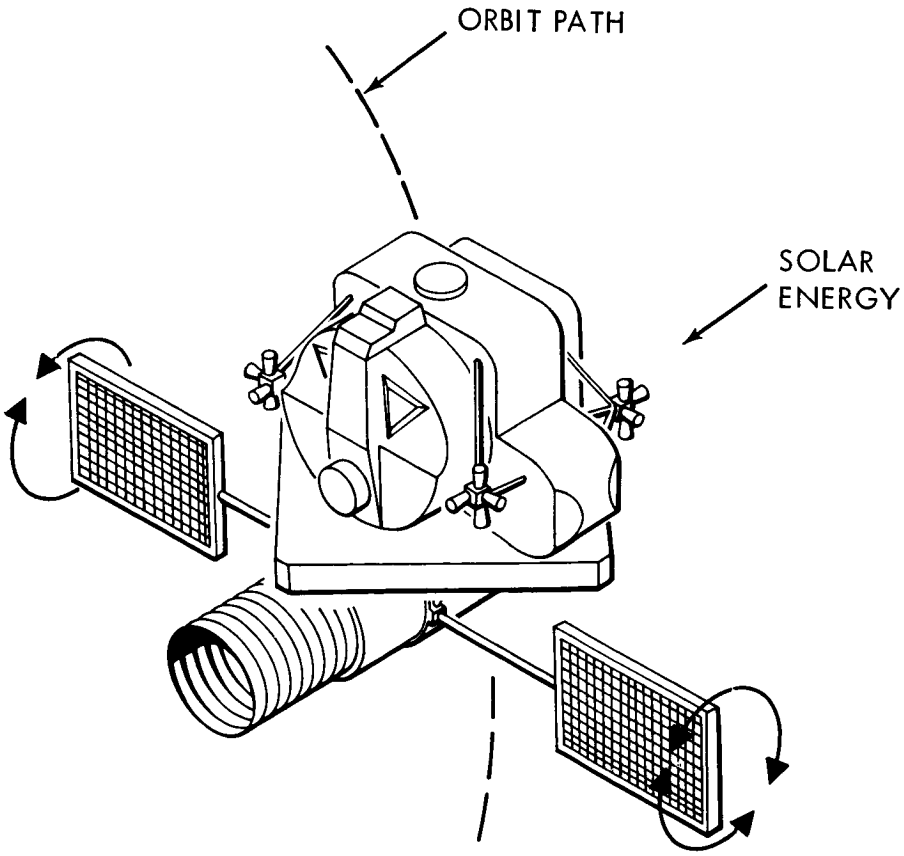
11.1.2 Spacecraft Concept Number 2

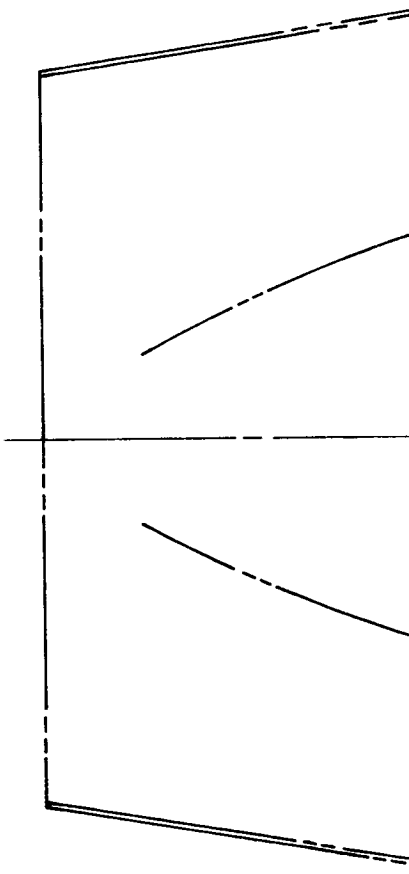
Concept number 2 consists of a LEM Ascent Stage with one or more telescopes mounted below this stage such that launch loads act along the optical axis of the primary mirror. Variations of this configuration are depicted in figures 11.1.2-1 through 11.1.2-6.

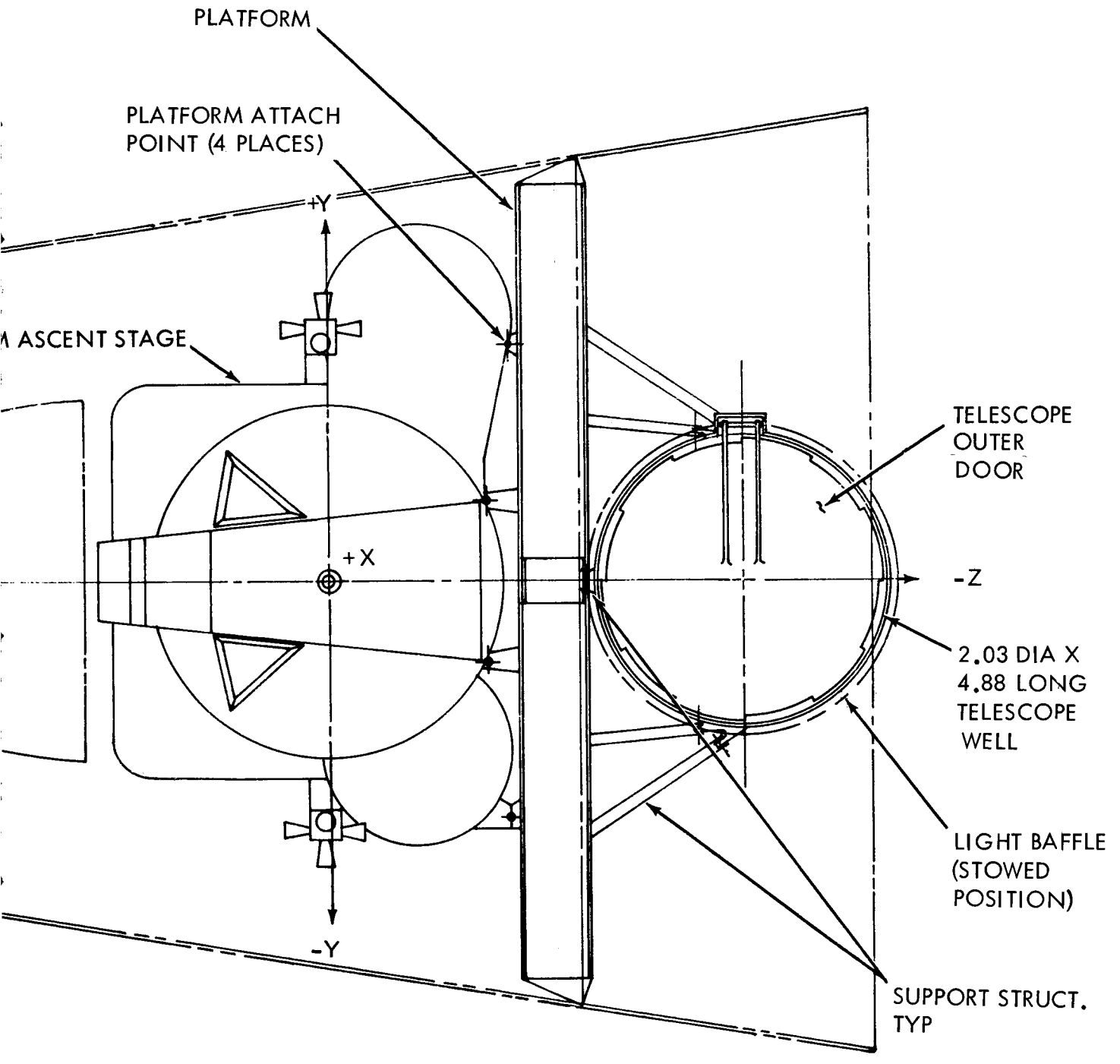
Again the LEM Descent Stage structure has been replaced with a strut structure which carries launch loads to the LEM adapter.

A major disadvantage of this concept is that it requires a smaller Service Module engine, such as the LEM Ascent engine (figures 11.1.2-1 through 11.1.2-4) or a telescope which is deployable once in orbit (figures 11.1.2-5 and 11.1.2-6.) Since a deployable telescope would be a design innovation, these concepts received a lower priority during this phase of the study.

Accessibility to the telescope would be by Extravehicular Activity (EVA) through the LEM forward hatch, or by a shirtsleeve compartment

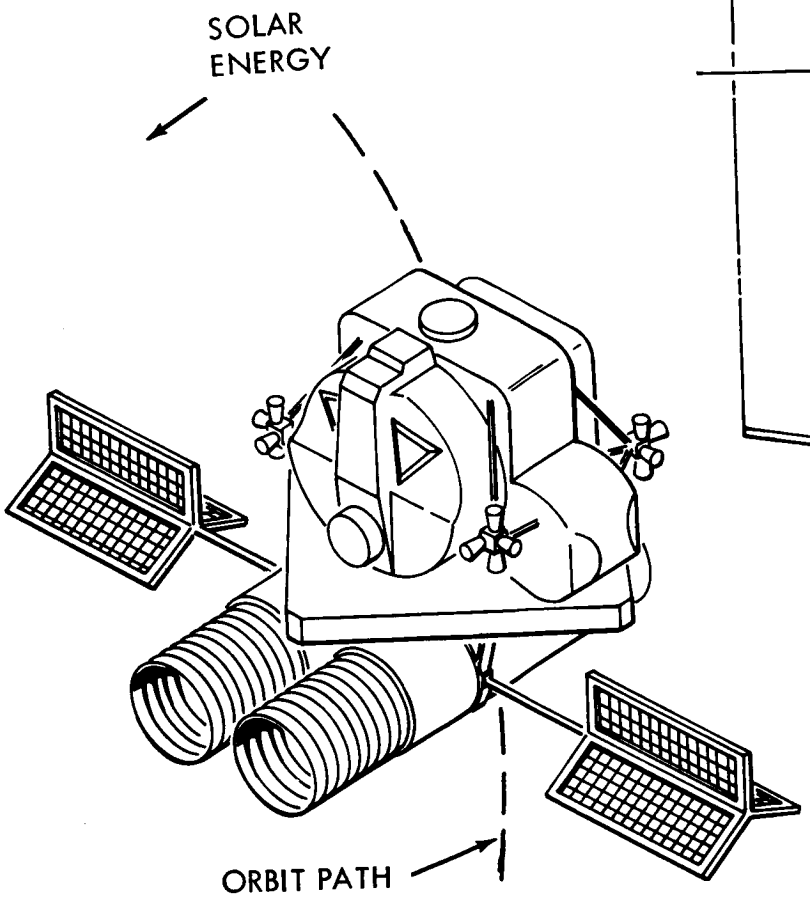

ORBIT PATH
SOLAR
ENERGY

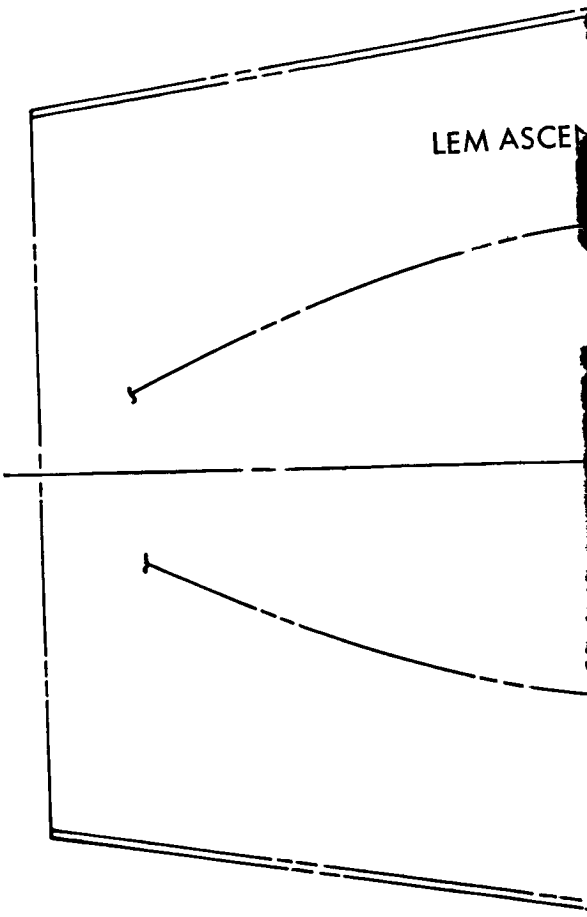


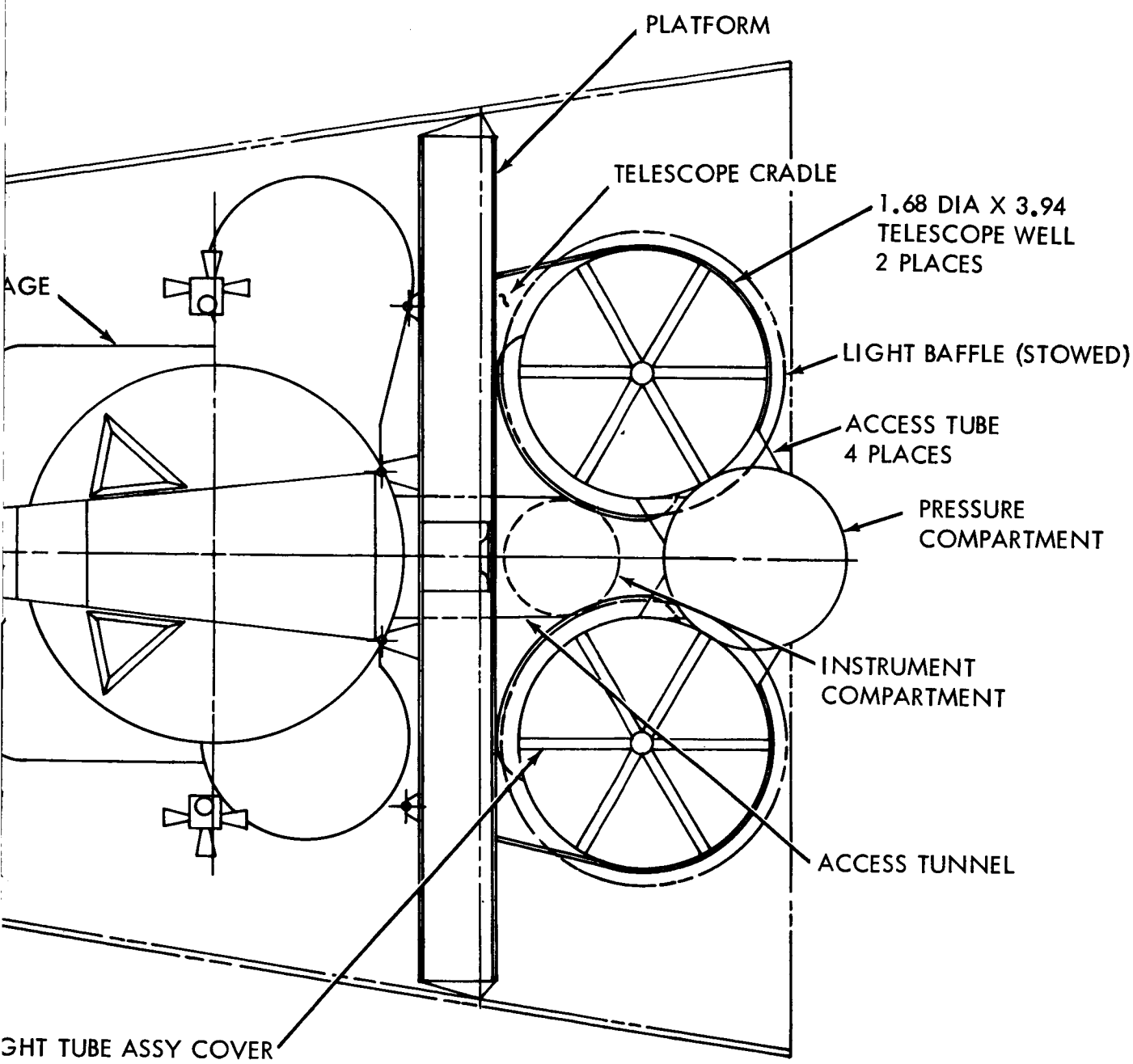


NOTE:
ALL DIMENSIONS IN METERS

Figure 11.1.1-1. Concept Number 1, Single Telescope - EVA


SOLAR
ENERGY
ORBIT PATH

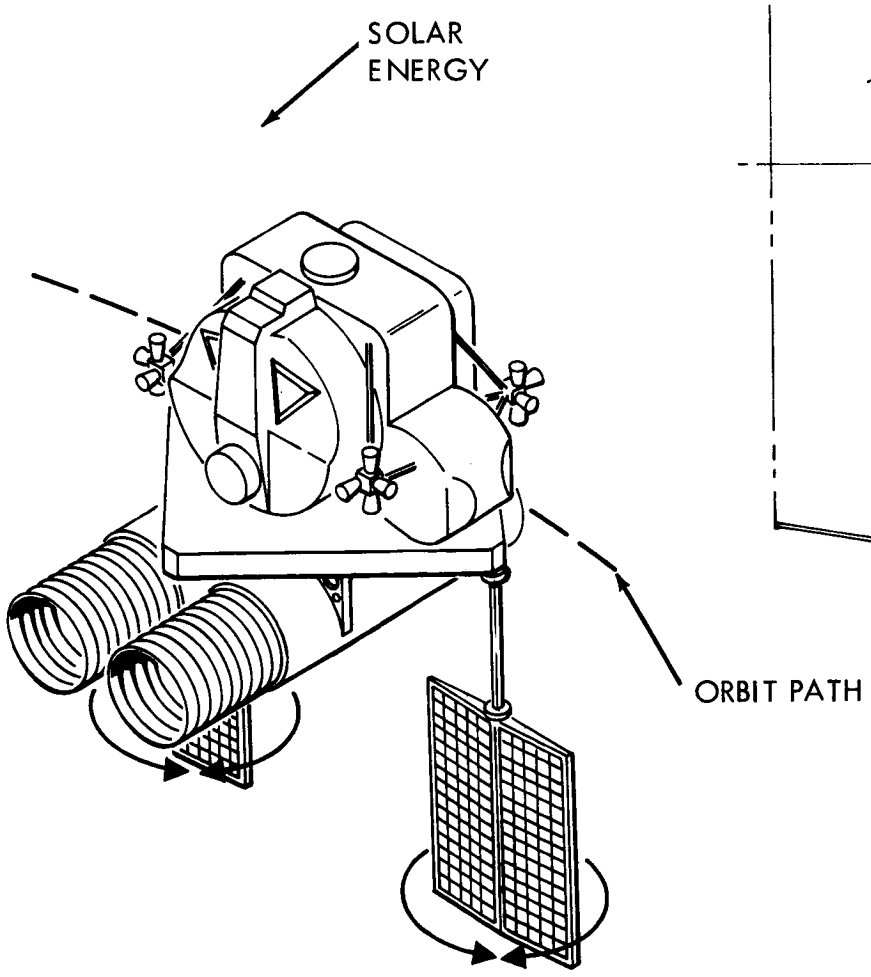

LEM ASCE

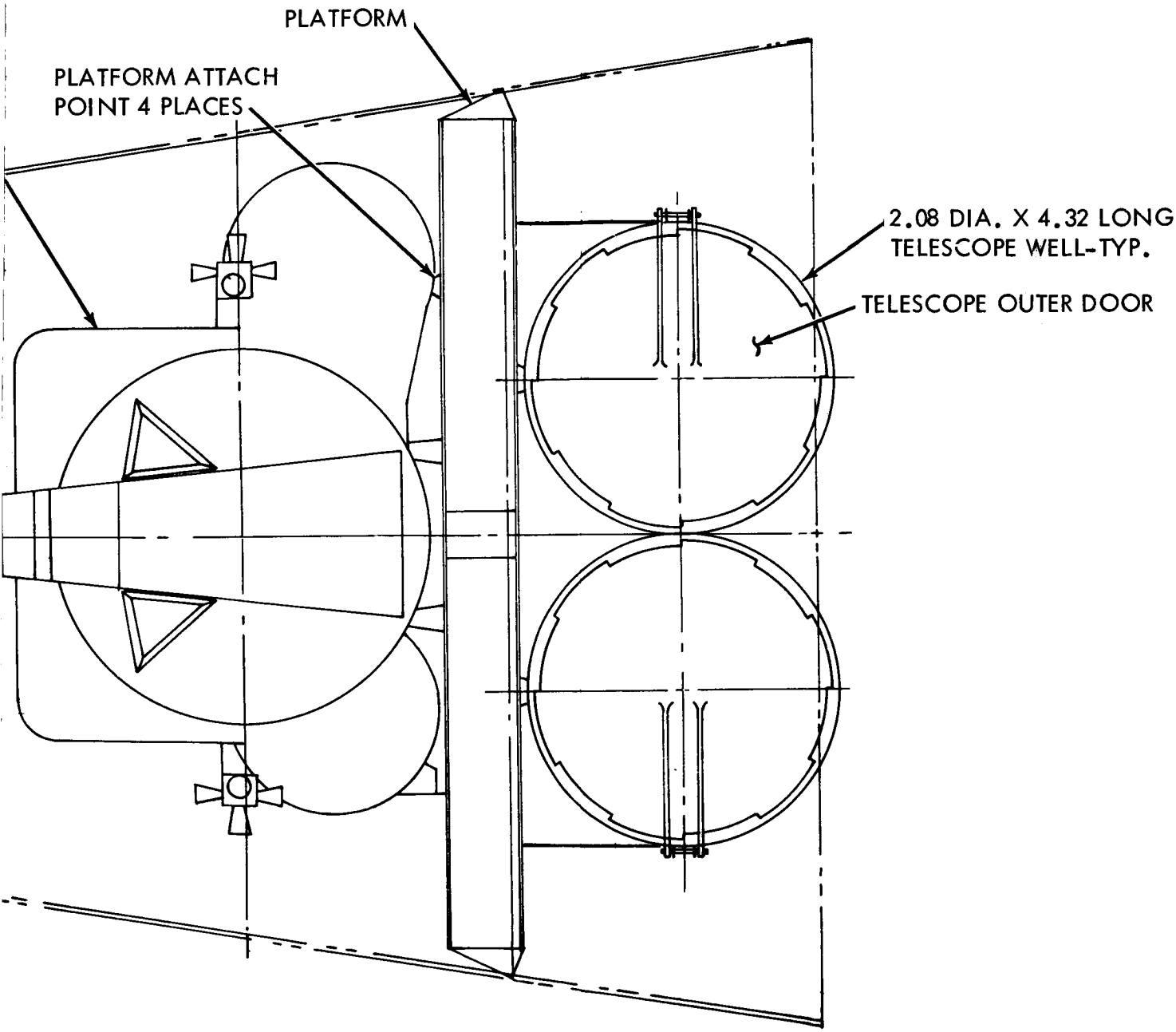


NOTE:
ALL DIMENSIONS
IN METERS

Figure 11.1.1-2. Concept No.1, Dual Telescope - Shirt Sleeve Accessibility

LEM ASCENT ST





NOTE:
ALL DIMENSIONS ARE IN METERS

Figure 11.1.1-3. Concept No.1, Dual Telescope - EVA

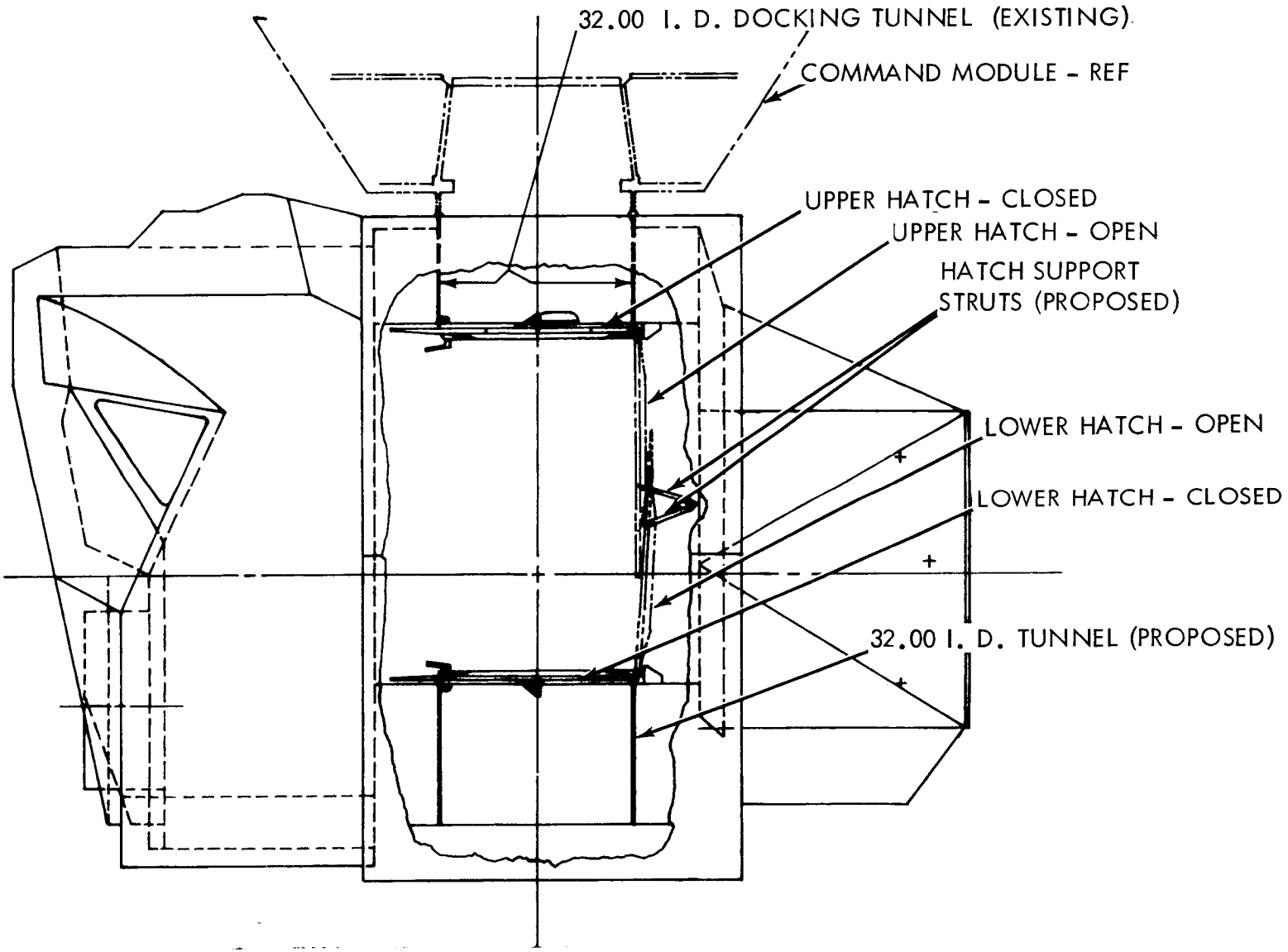
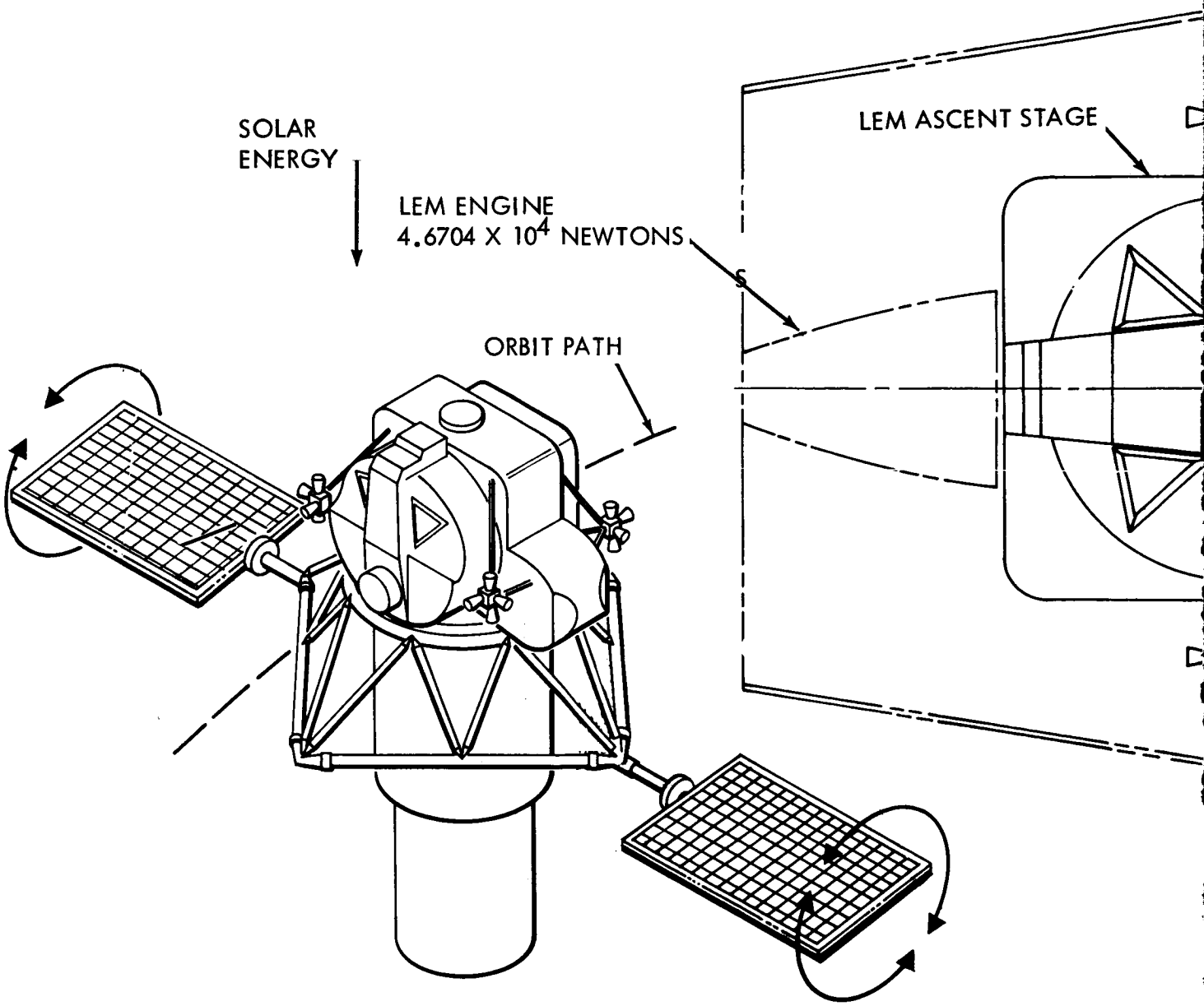


Figure 11.1.1-4. LEM Ascent Stage - Lower Hatch



PRECEDING PAGE BLANK NOT FILMED.

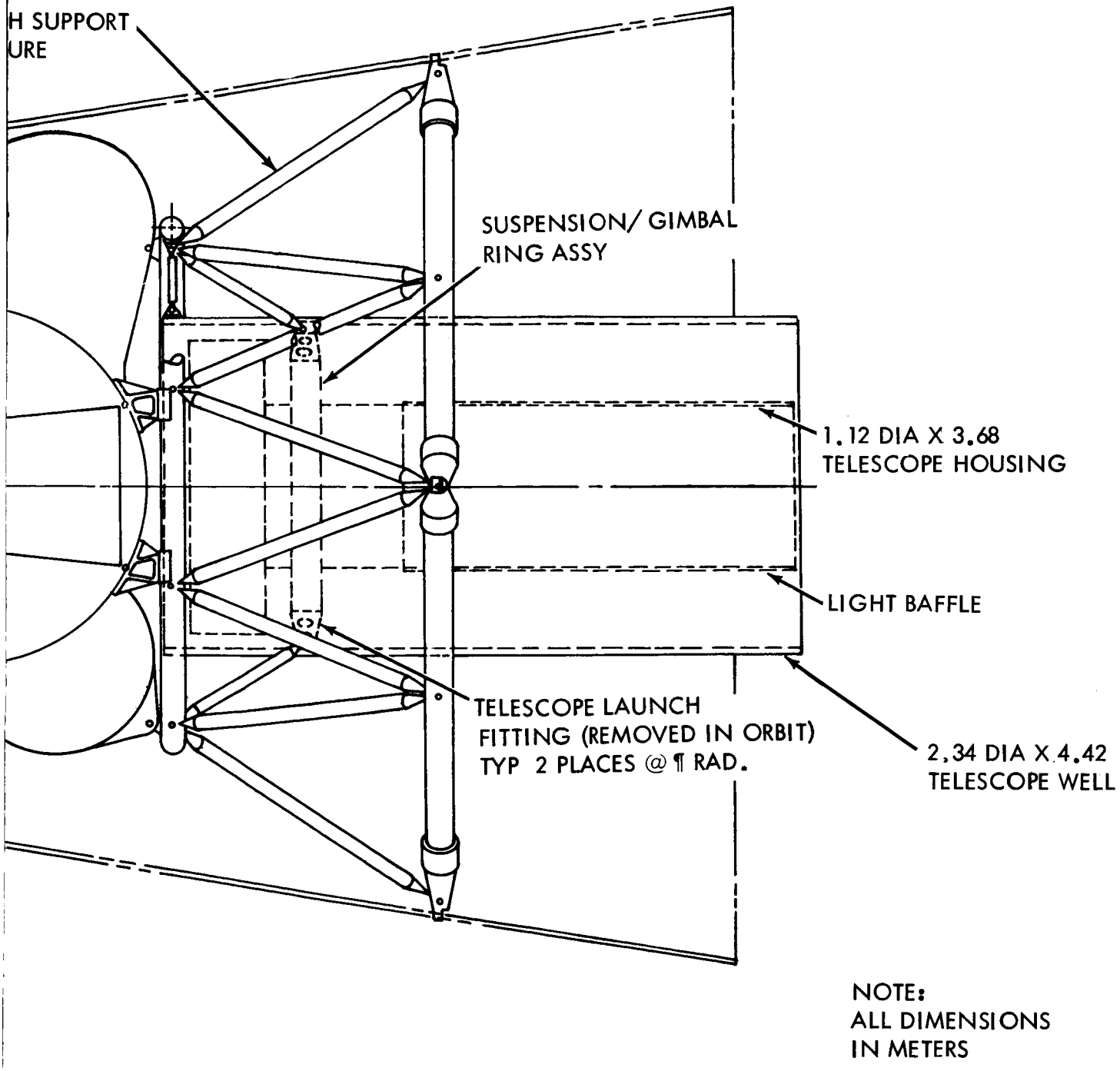
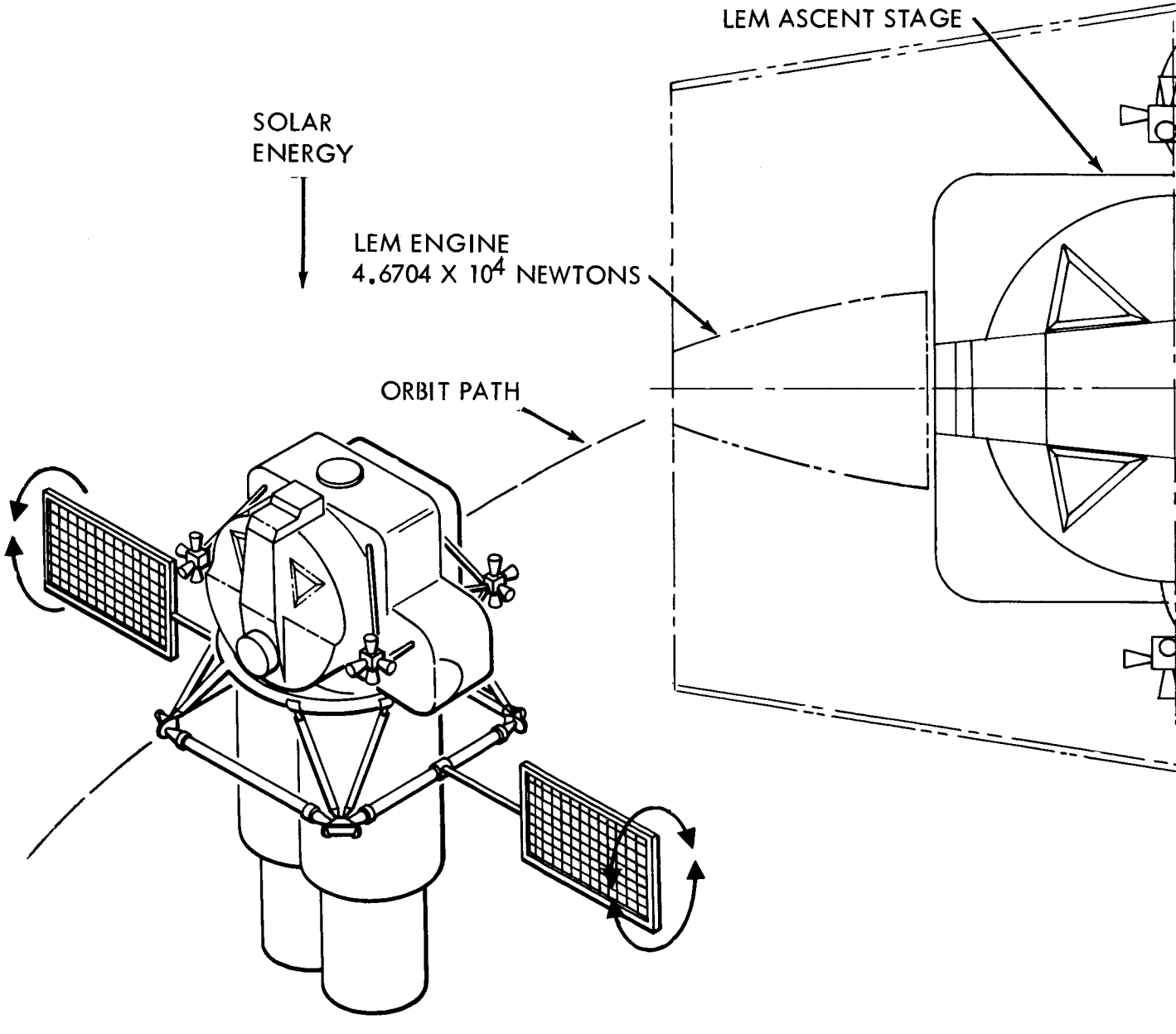


Figure 11.1.2-1. Concept No. 2, Single Telescope - EVA


LEM ASCENT STAGE
SOLAR
ENERGY
LEM ENGINE
4.6704 X 10^4 NEWTONS
ORBIT PATH

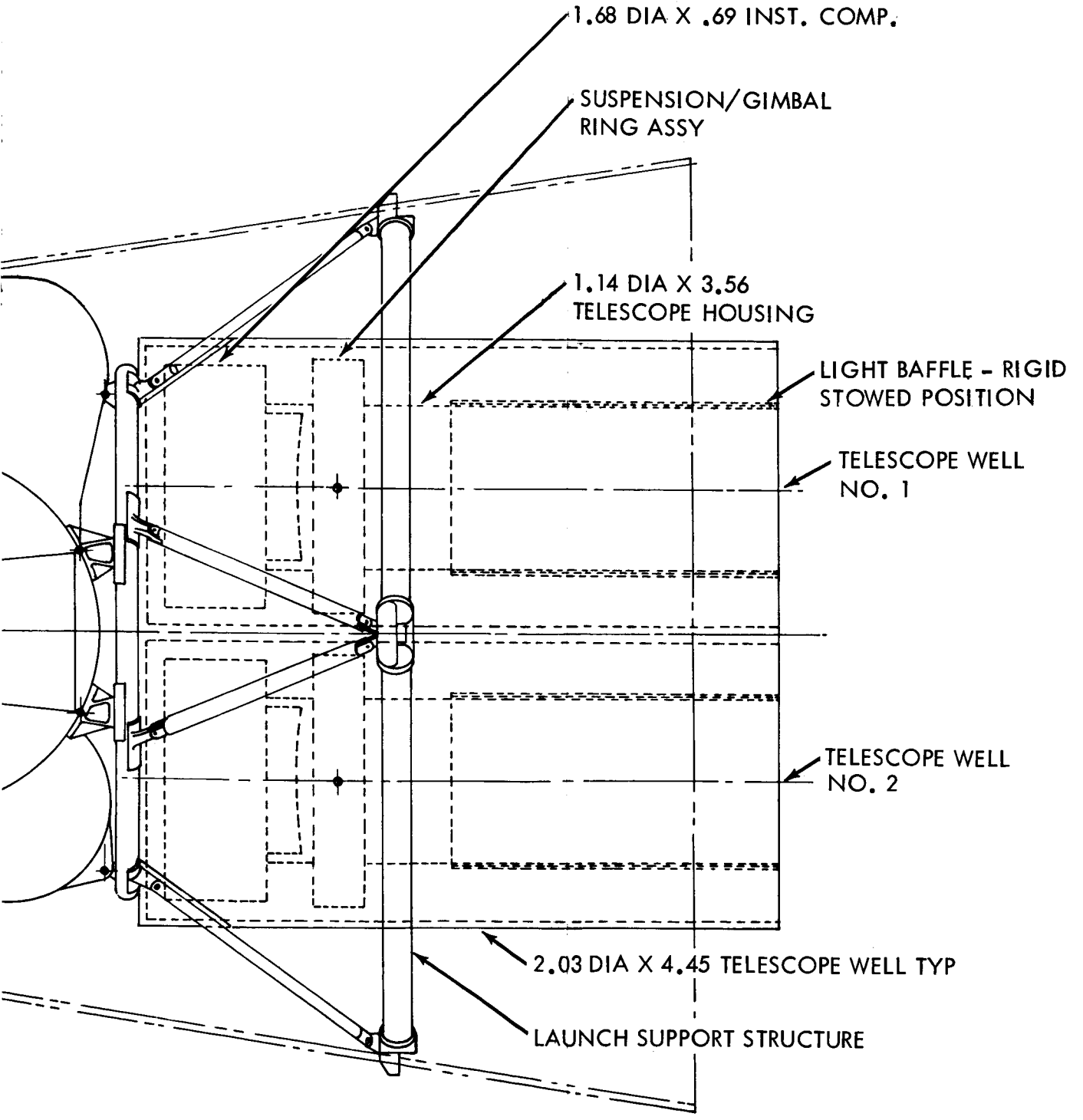
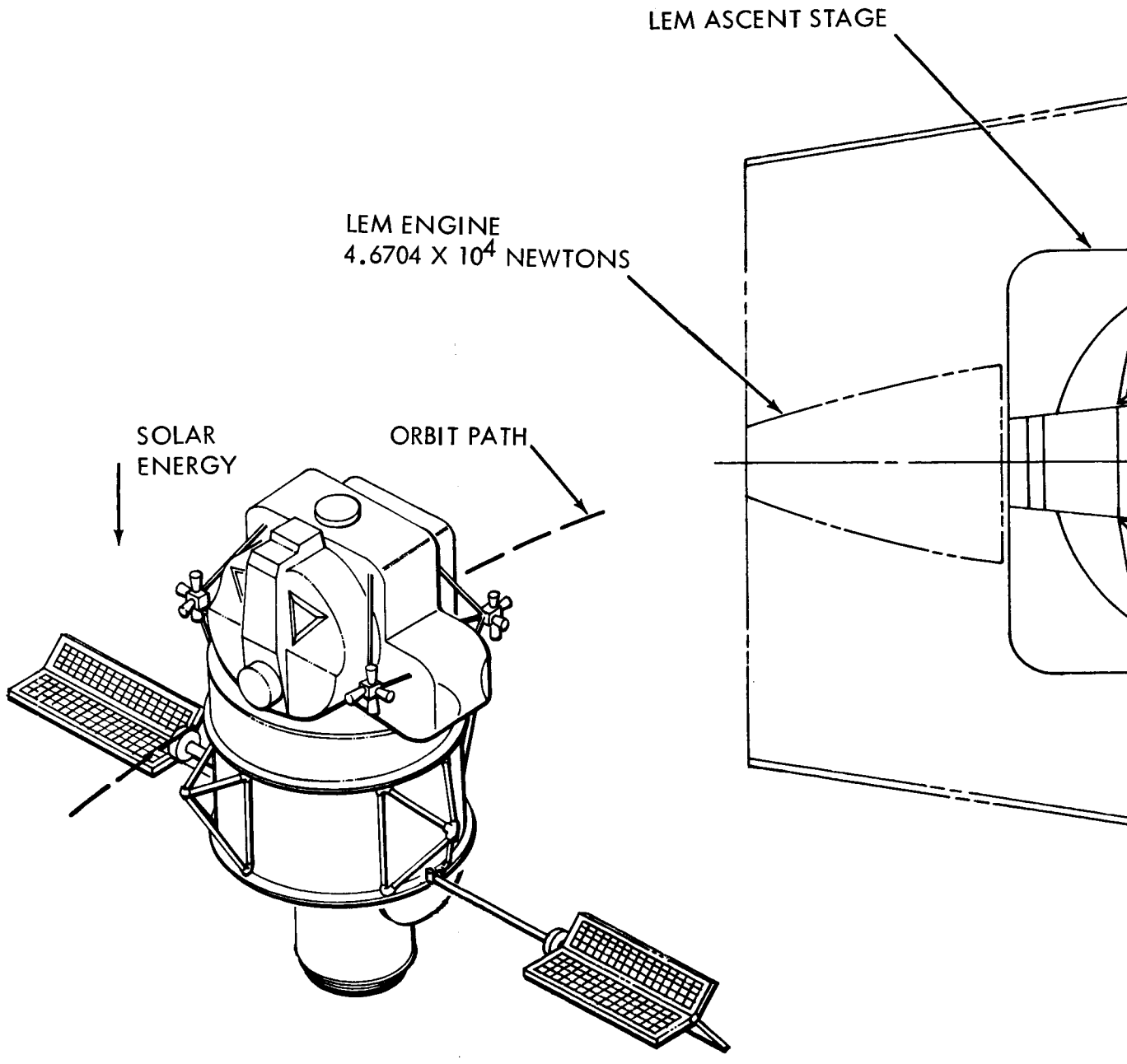


Figure 11.1.2-2. Concept No. 2, Dual Telescope - EVA


LEM ASCENT STAGE
LEM ENGINE
4.6704 X 10^4 NEWTONS
SOLAR
ENERGY
ORBIT PATH

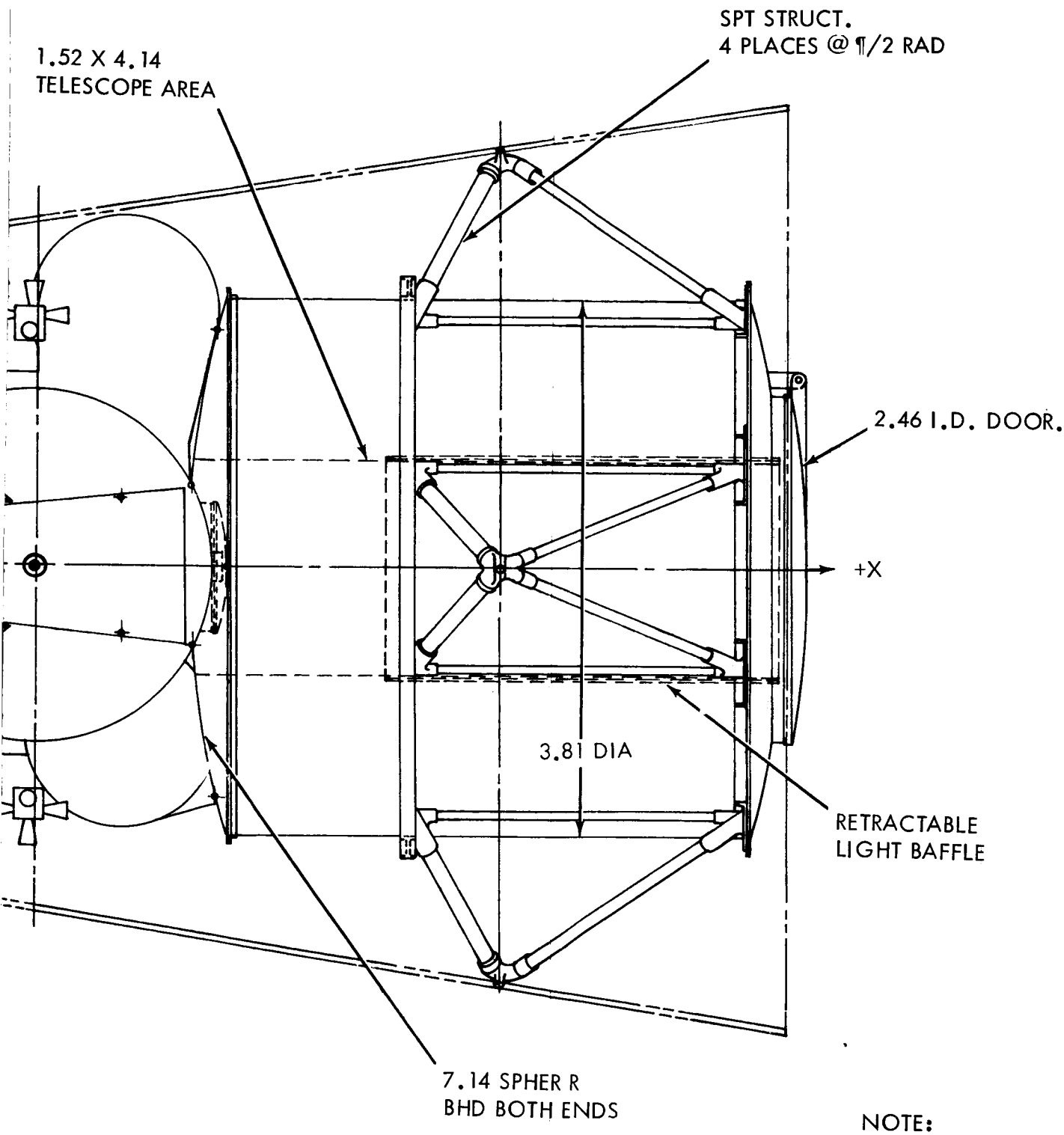
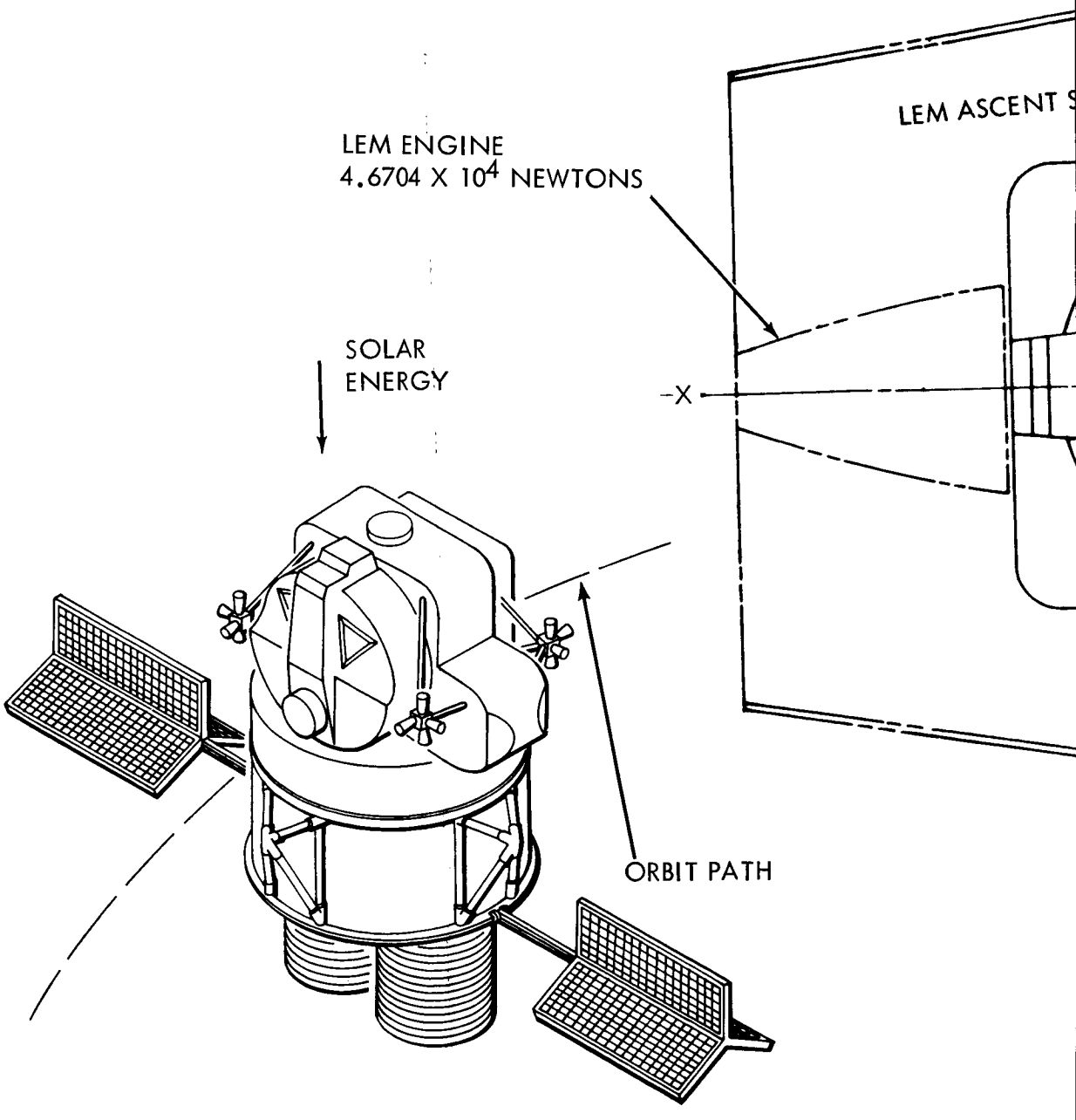


Figure 11.1.2-3. Concept No. 2, Single Telescope - Shirt Sleeve Accessibility


LEM ENGINE
4.6704 X 10^4 NEWTONS
SOLAR
ENERGY
-X
ORBIT PATH

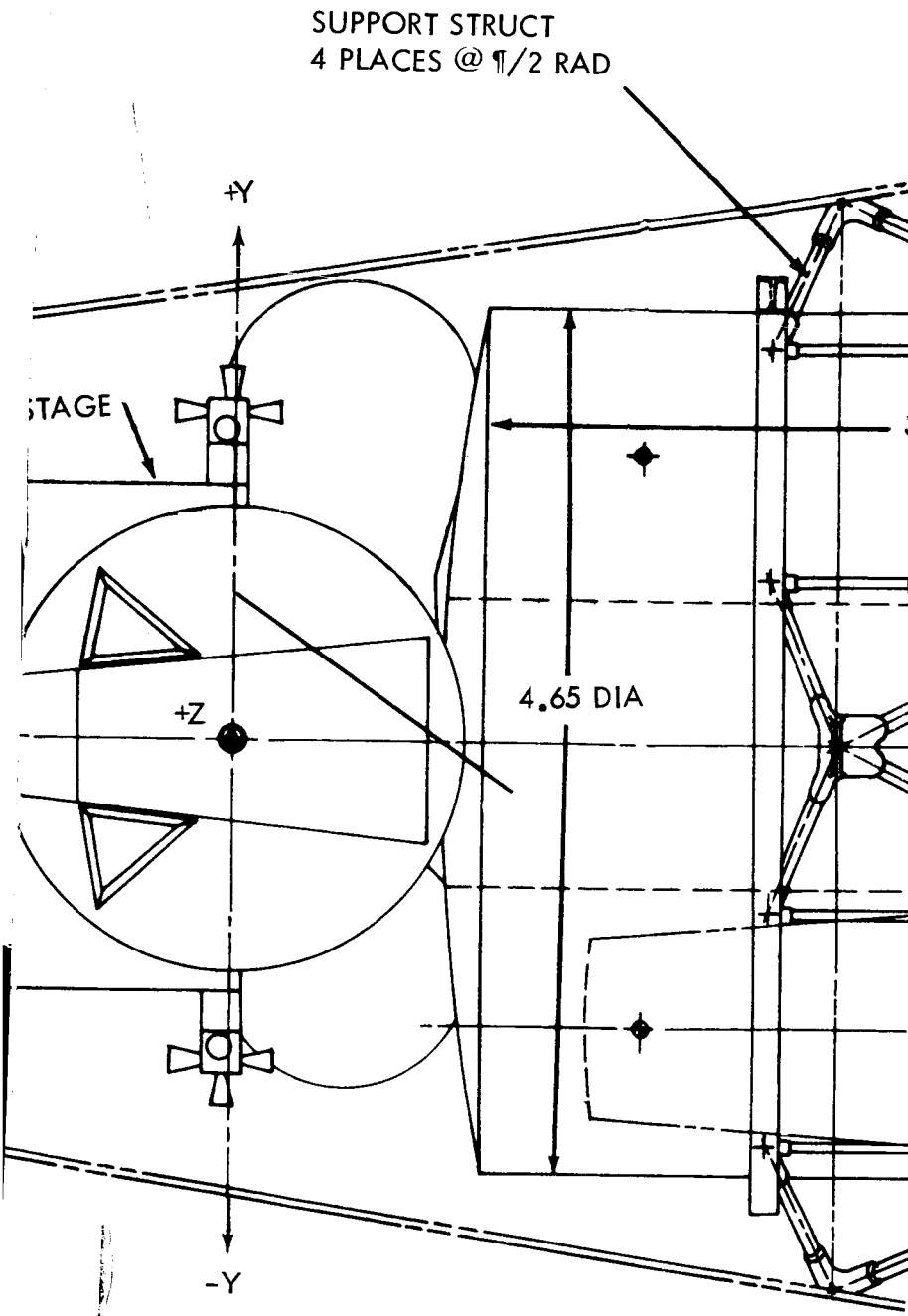
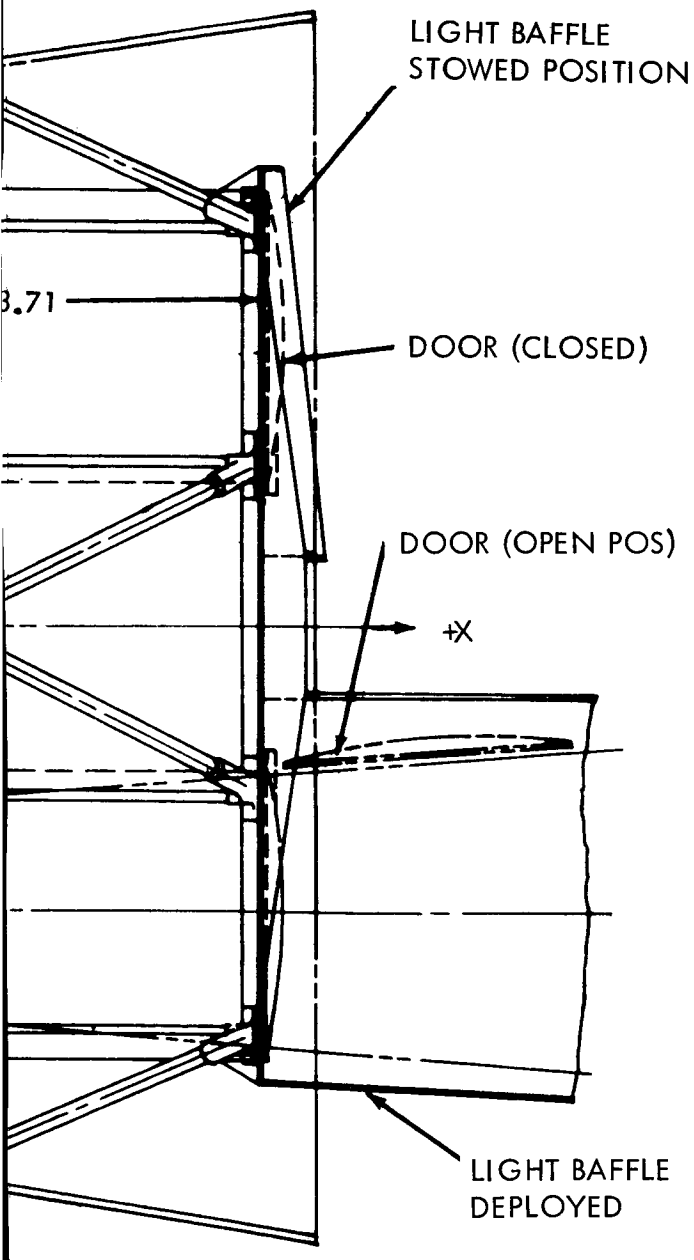


Figure 11.1.2-4. Concept No.

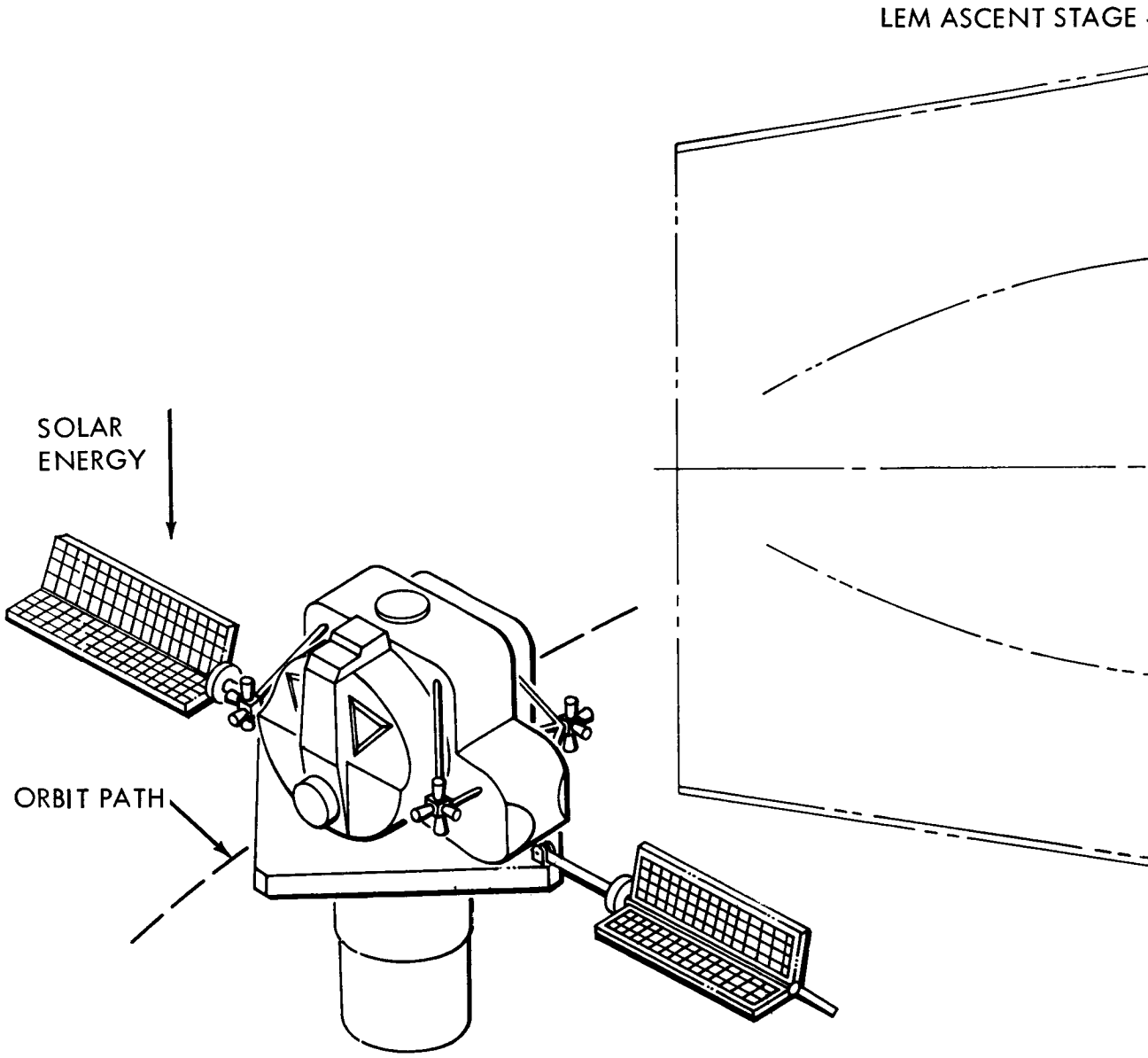


NOTE: ALL DIMENSIONS
ARE IN METERS

Dual Telescope - Shirt Sleeve Accessibility

~~2-133~~
2-134

(3)


LEM ASCENT STAGE
SOLAR
ENERGY
ORBIT PATH

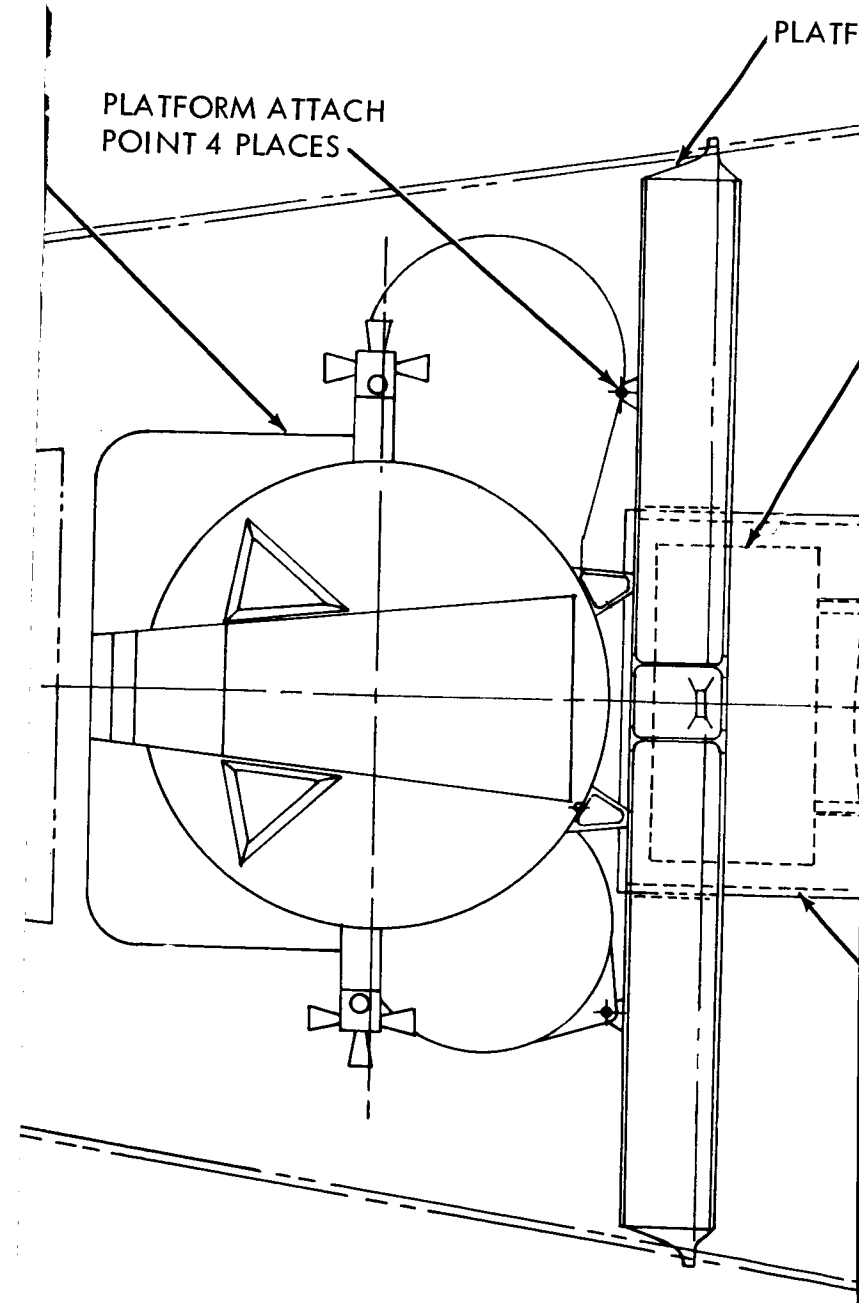
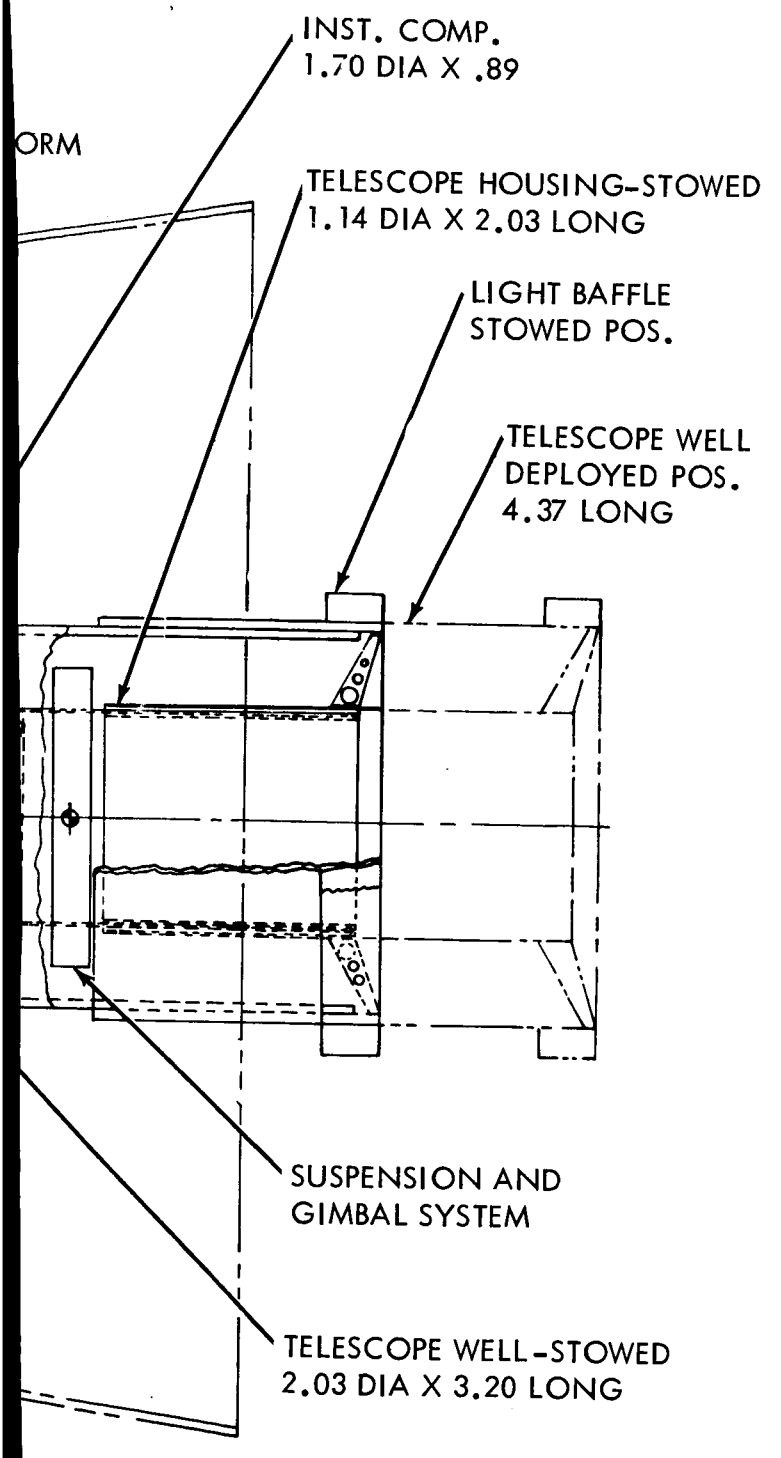
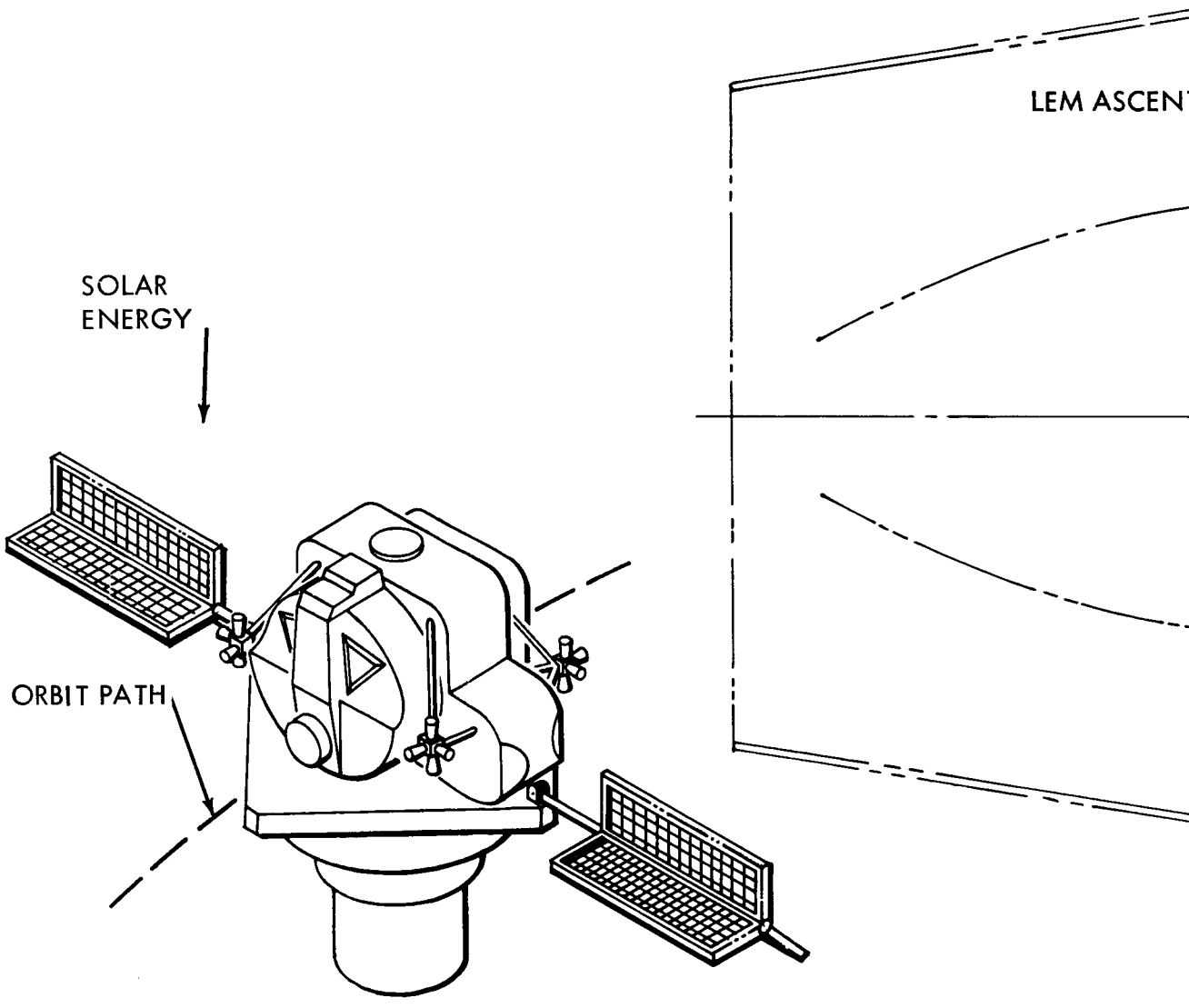


Figure 11.1.2-5



NOTE:
ALL DIMENSIONS
IN METERS

. Concept No. 2, Depoloyable Telescope - EVA


LEM ASCEN
SOLAR
ENERGY
ORBIT PATH

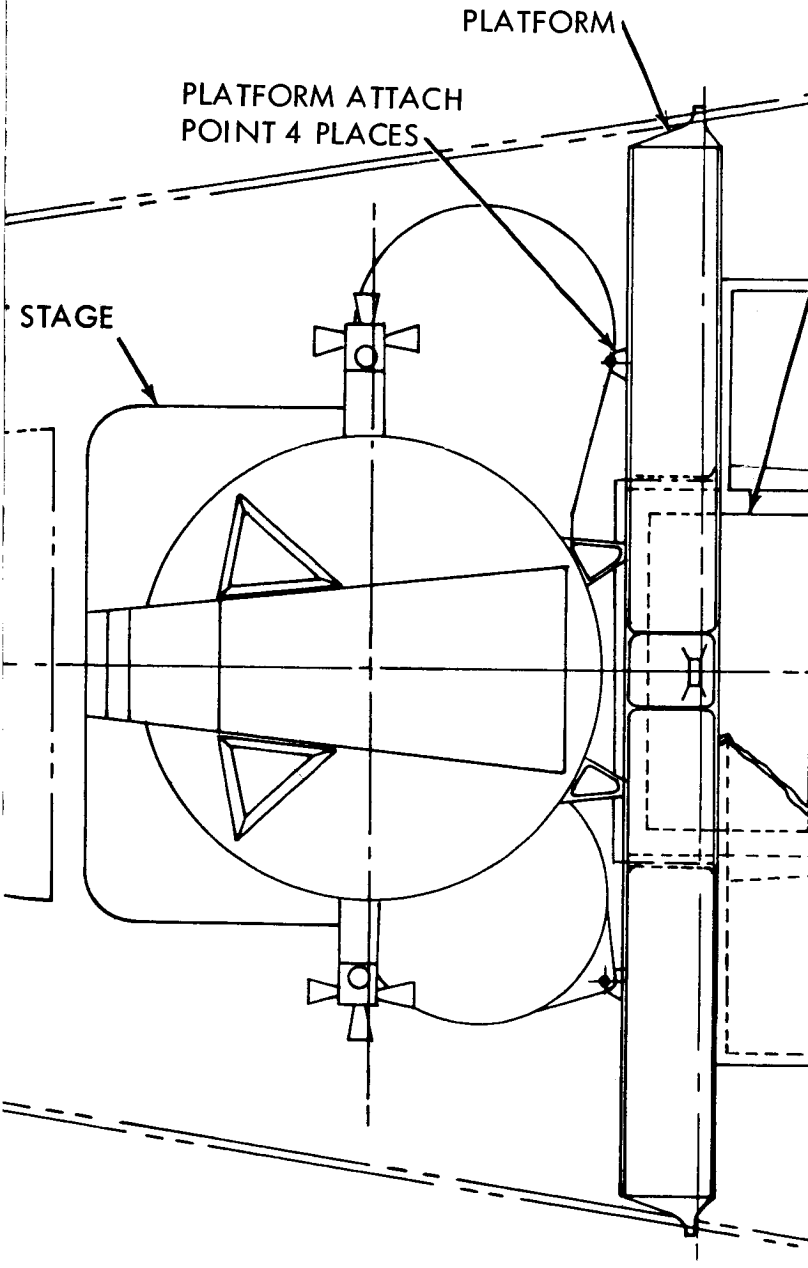
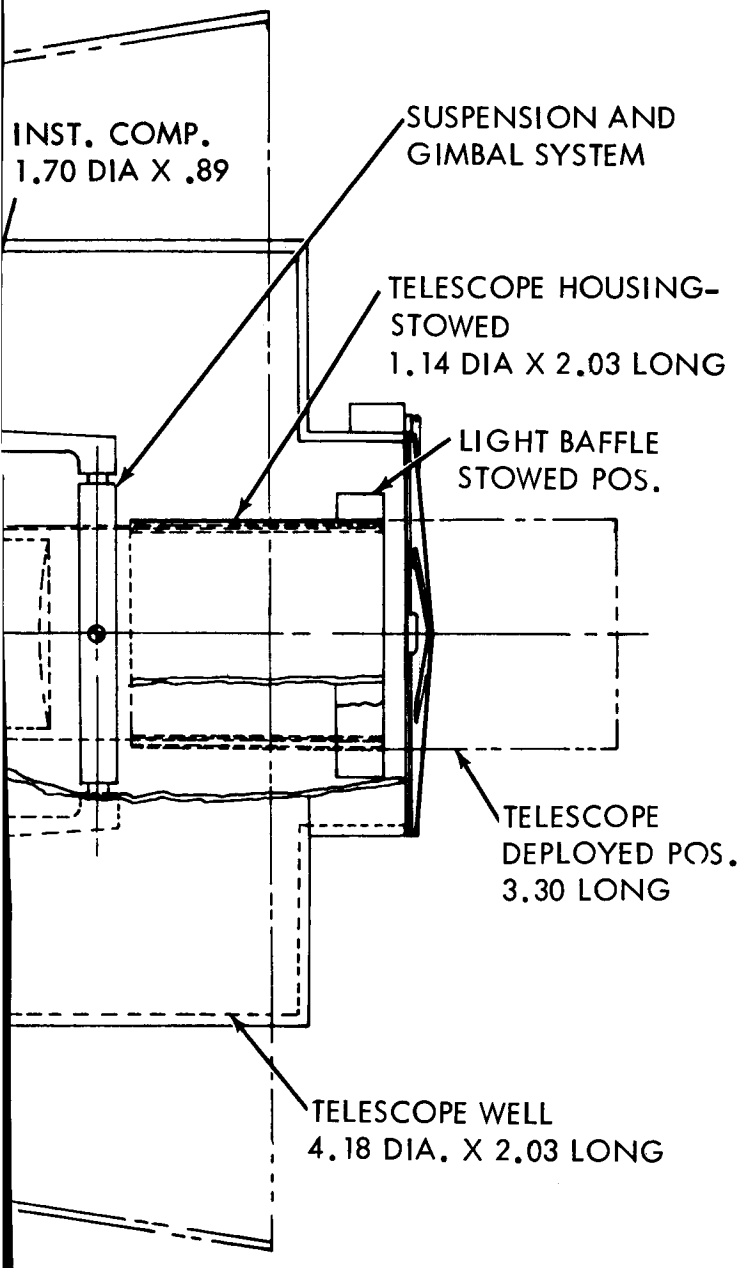


Figure 11.1.2-6. Concept No. 2, Dep



NOTE:
ALL DIMENSIONS ARE IN METERS

loyale Telescope - Shirt Sleeve Accessibility

~~2-137~~
2-138

enclosing the telescope which could be entered from the LEM forward hatch, or, in the case of the dual telescopes, from a hatch in the LEM floor. This configuration lends itself to adequate shirtsleeve accessibility around the entire telescope.

The single telescope configuration can be readily adapted to placing the experiment equipment in the area in which the LEM Ascent Stage engine is normally located for Apollo missions. In this case, crew members would have access to this equipment without leaving the LEM.

Maximum well length for this configuration ranges between 3.71 and 4.42 meters (non-deployable). Telescope well diameters on the double telescopes are limited to approximately 2.03 meters whereas the well diameter on single telescopes are for practical purposes unlimited.

11.1.3 Spacecraft Concept Number 3

Concept number 3 consists of two telescopes mounted so that launch loads act through the optical axes. This configuration basically replaces the LEM Ascent Stage in the manned mode. Figure 11.1.3-1 depicts this configuration mounted in the LEM adapter. Figure 11.1.3-2 shows the spacecraft mounted in the Centaur Shroud. In this case, the spacecraft would be launched for an unmanned mission or for rendezvous with a Command and Service Module (CSM).

In the event this configuration is used for a manned mission, accessibility is provided completely around the telescope well.

It should be noted that to perform the transposition maneuver, both the spacecraft and the CSM must rotate 180 degrees. This ensures that both launch loads and docking loads will occur in the same direction across the primary mirror.

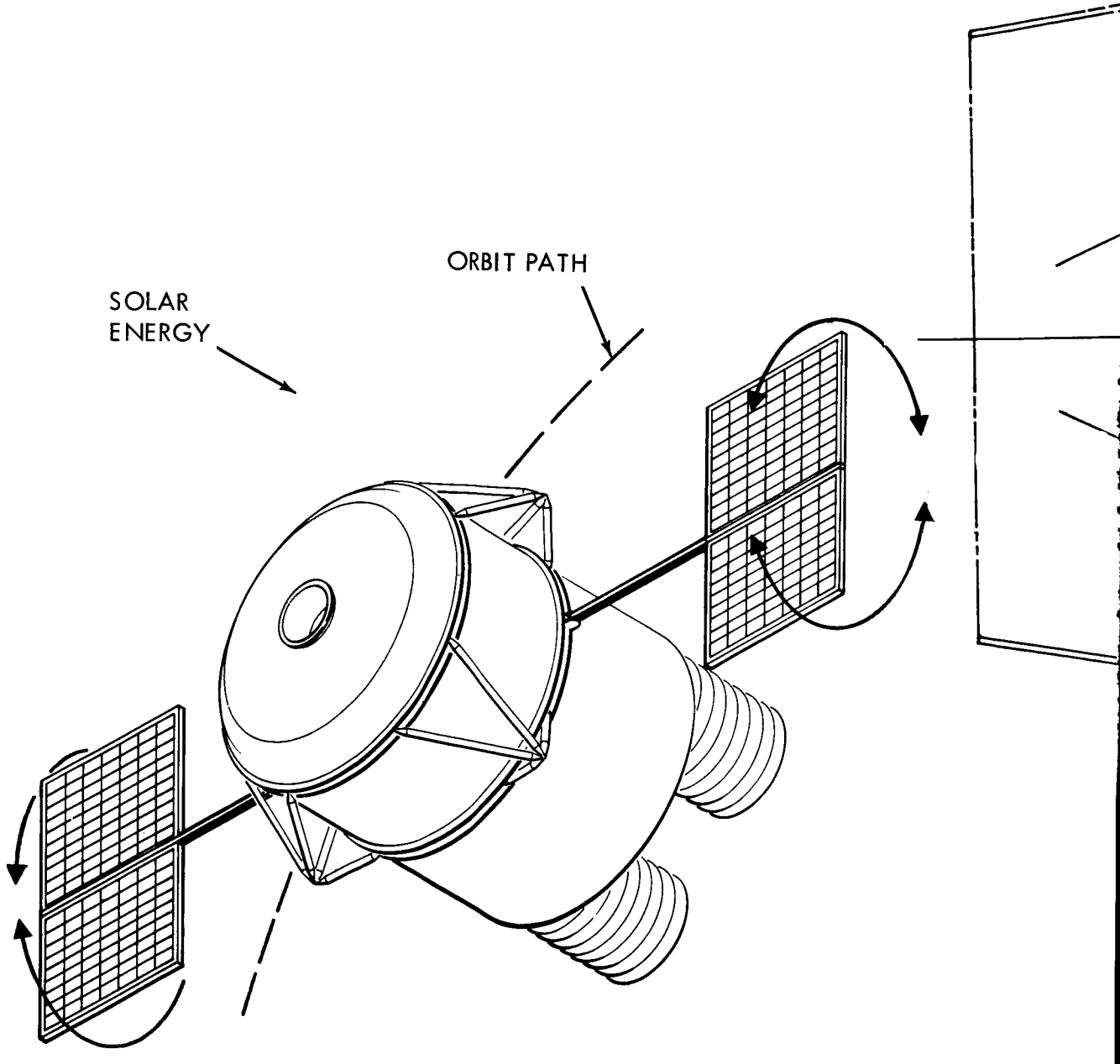
The maximum telescope well size in this configuration is 1.35 meters in diameter by 4 meters in length.

11.1.4 Spacecraft Concept Number 4

Concept number 4 consists of two telescopes mounted such that launch loads act through the diameter of the primary mirror. Figures 11.1.4-1 and 11.1.4-2 show the approach in the LEM adapter and Centaur shroud respectively. Figures 11.1.4-3 and 11.1.4-4 show a variation of the geometry again mounted in these respective shrouds.

Accessibility around the telescope well is slightly better in the former geometry. However, the second approach allows more room for packaging the solar panels, if required.

Maximum telescope well sizes for this configuration have a diameter of 1.65 meters and a length of 4.45 and 4.55 meters, respectively.



PRECEDING PAGE BLANK NOT FILMED.

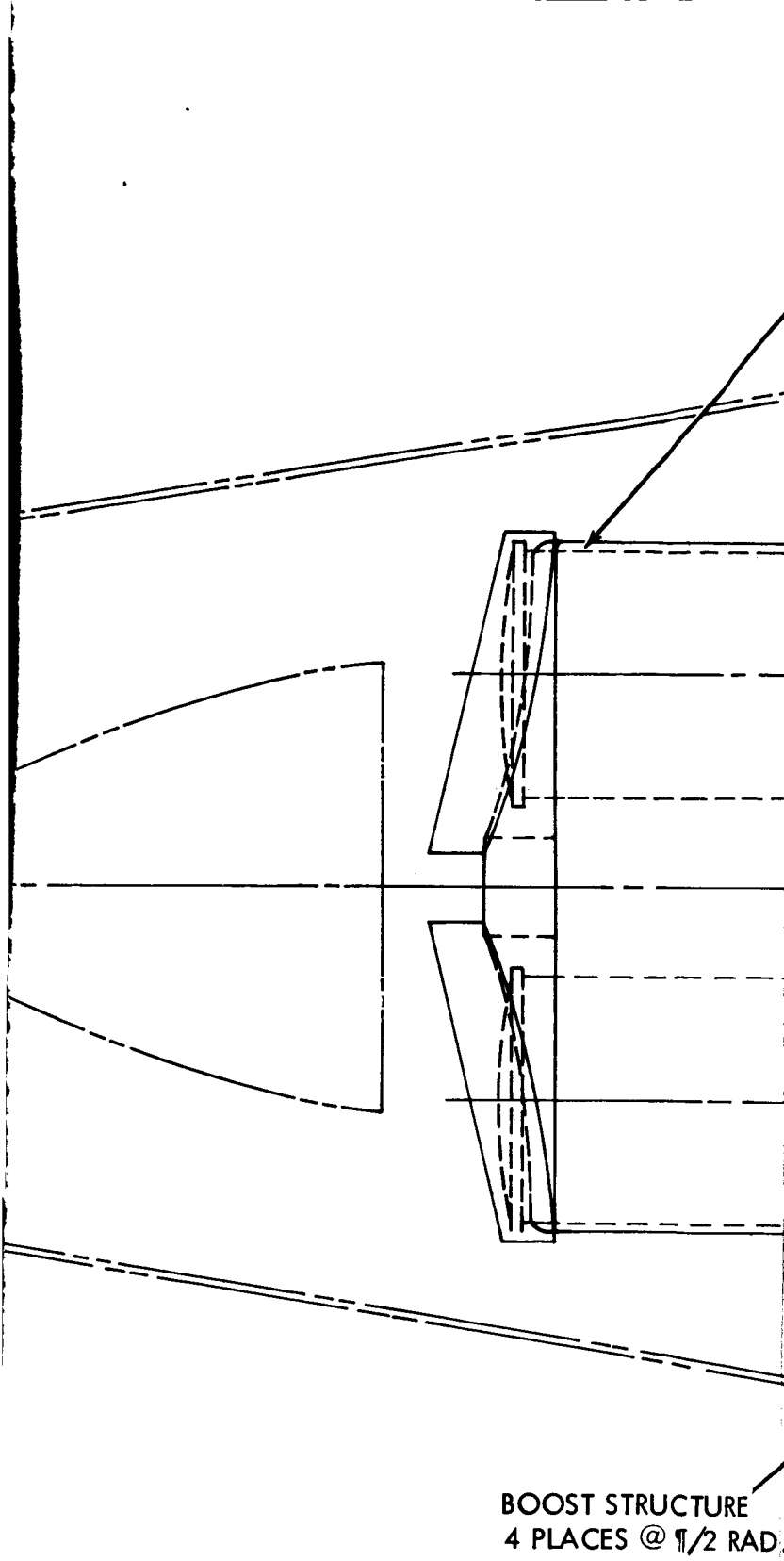
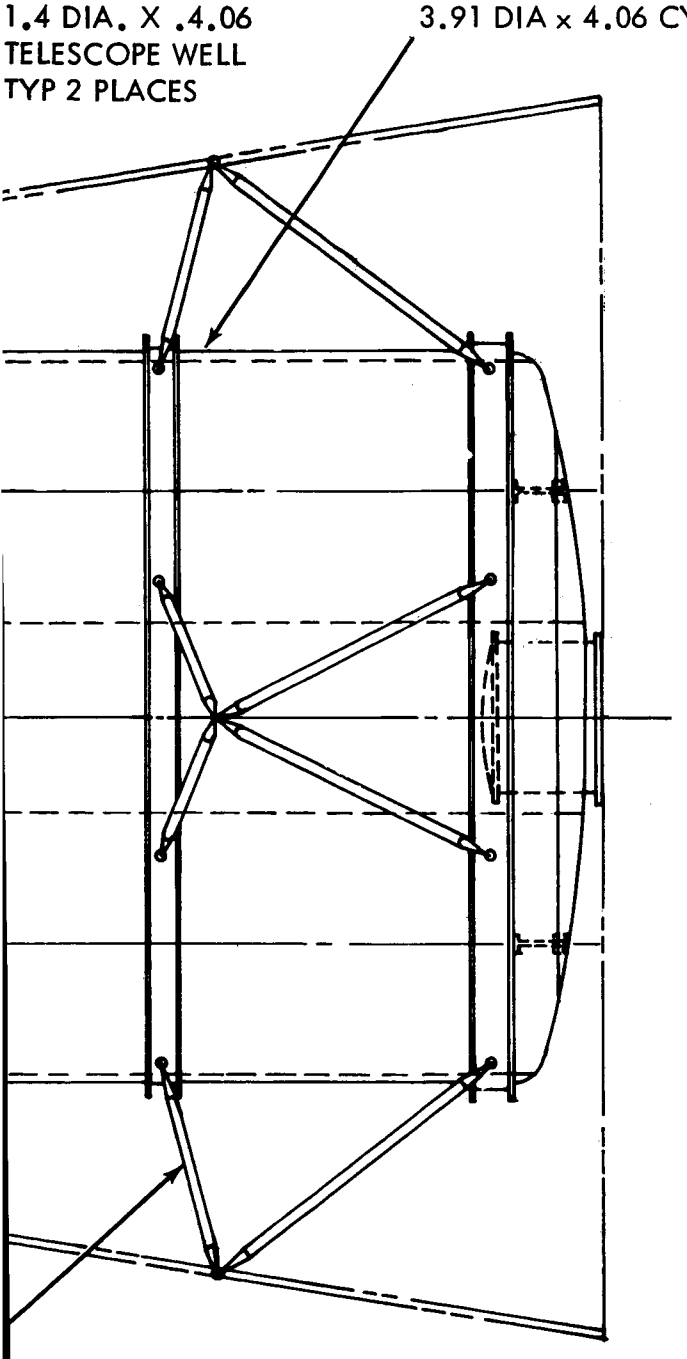


Figure 11.1.3-1.

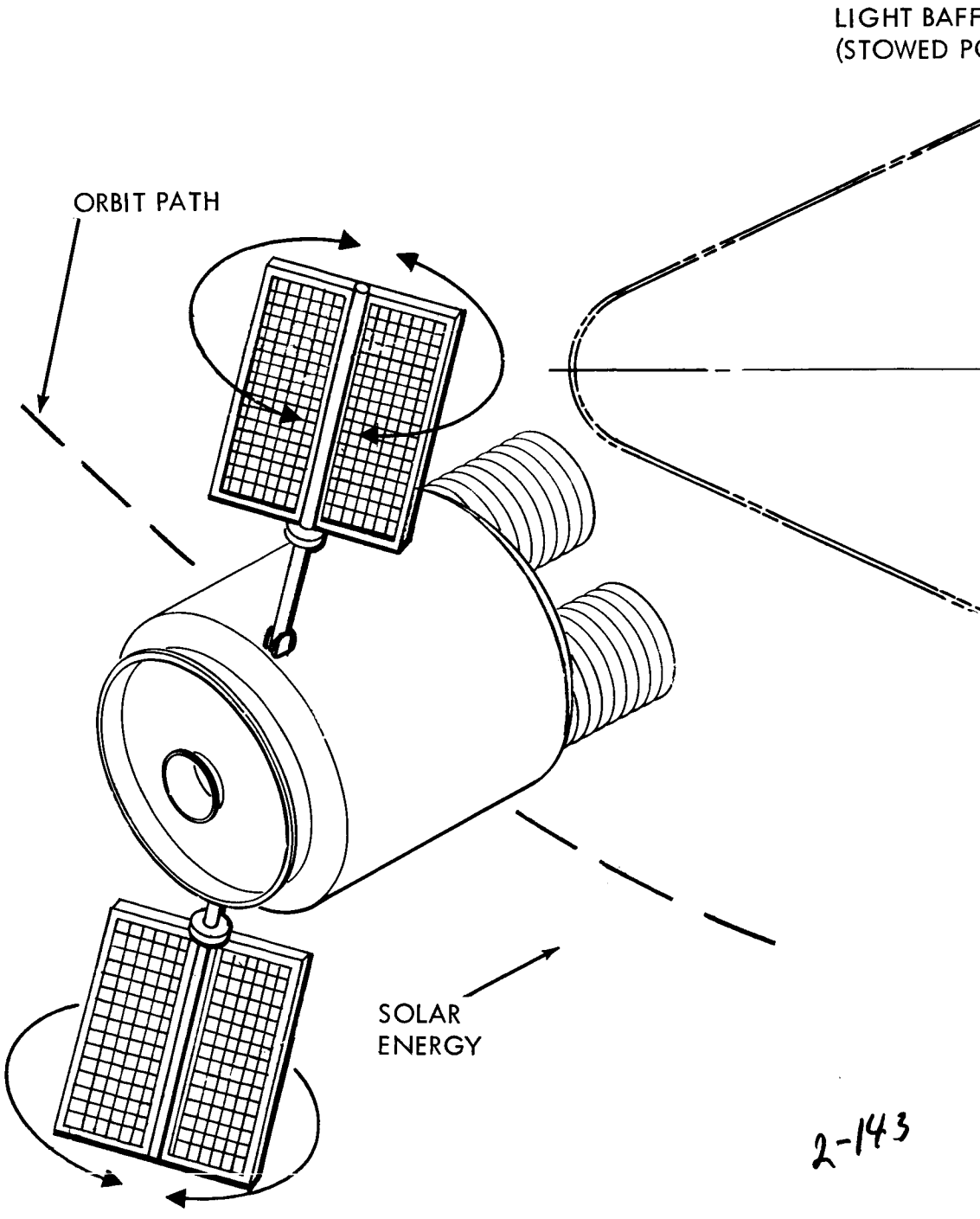


NOTE:

ALL DIMENSIONS
IN METERS

Concept No. 3, Dual Telescope in LEM Adapter

~~2-141~~
2-142


LIGHT BAFF
(STOWED PO
ORBIT PATH
SOLAR
ENERGY

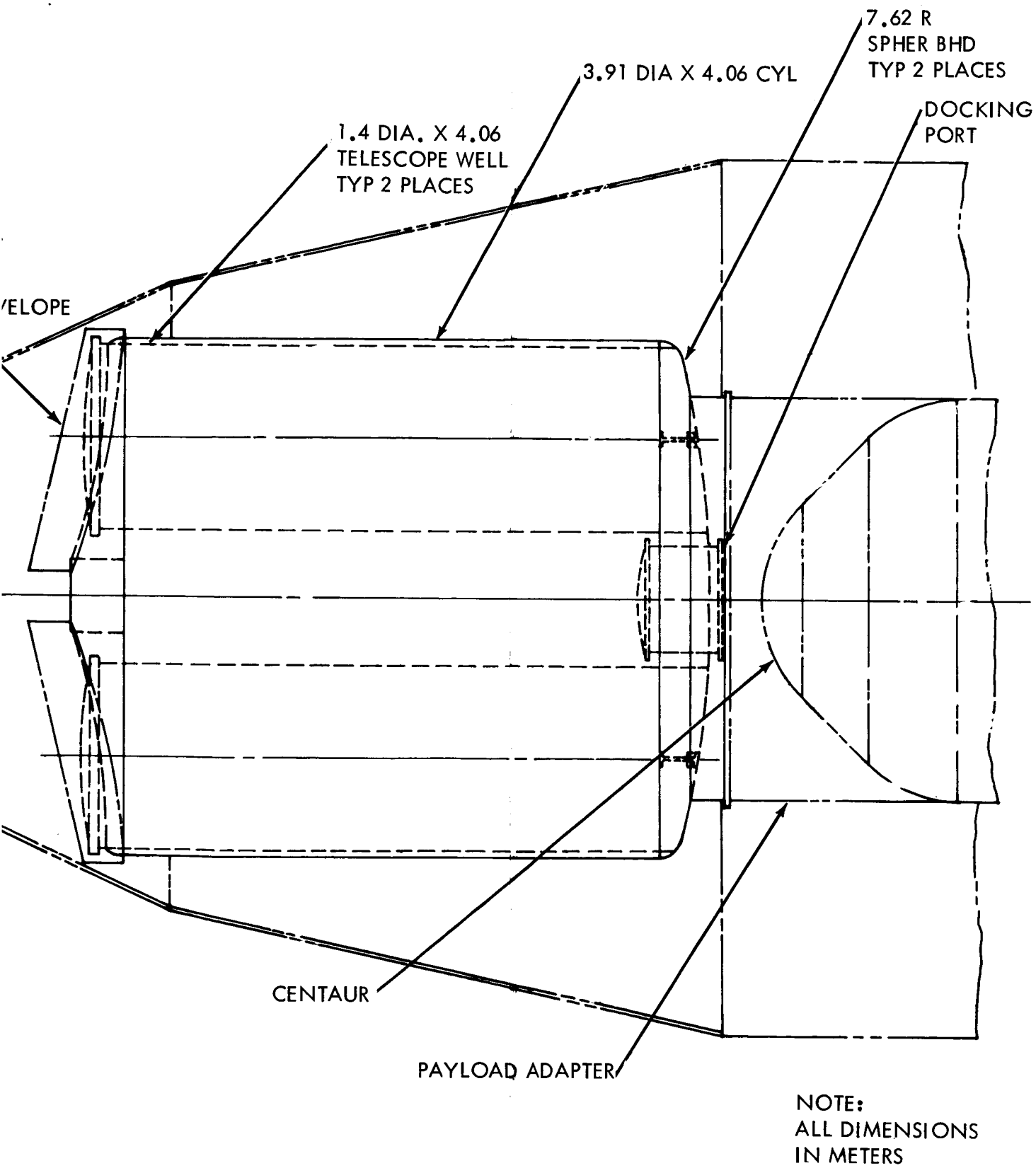


Figure 11.1.3-2. Concept No. 3, Dual Telescope in Centaur Shroud

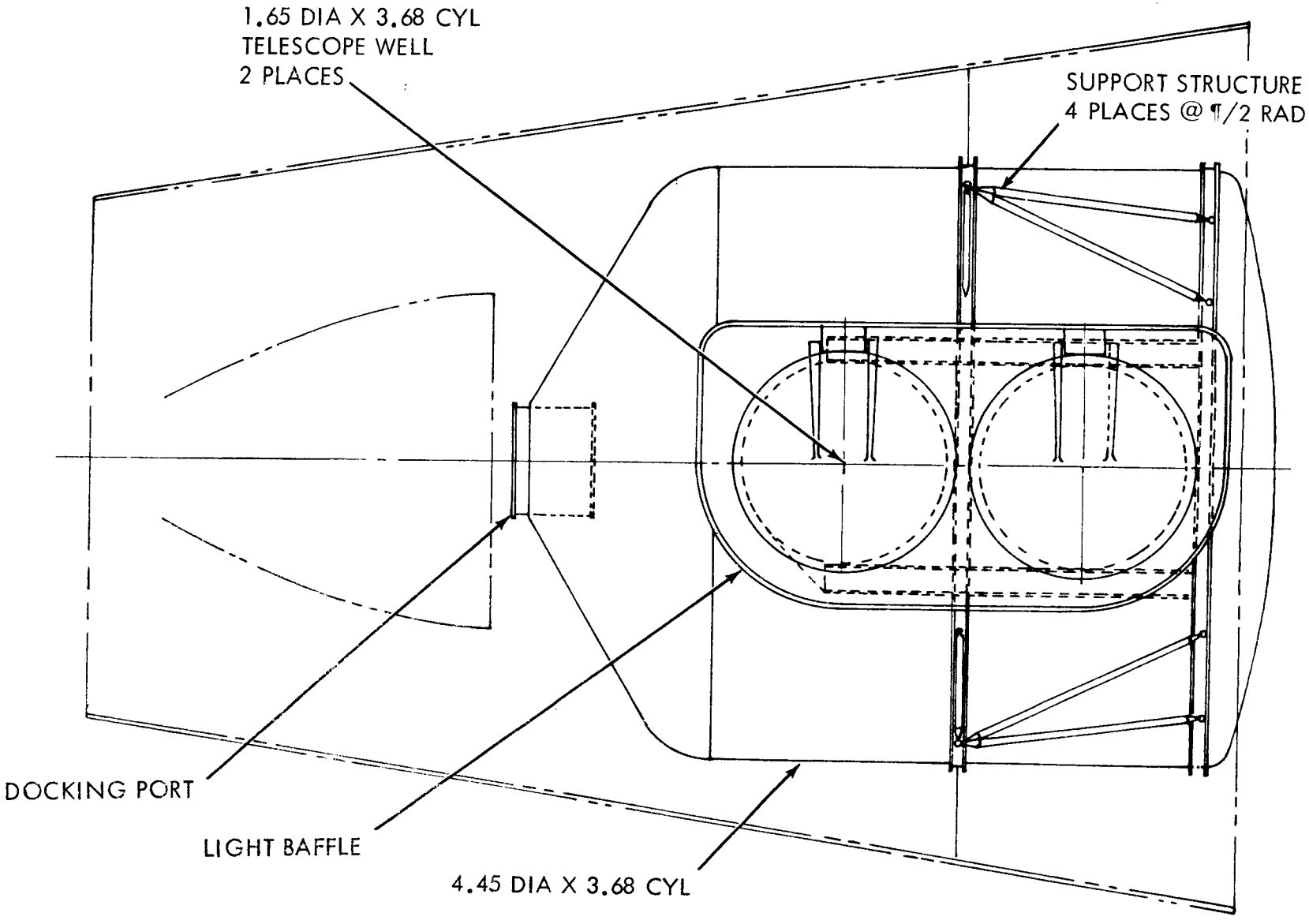
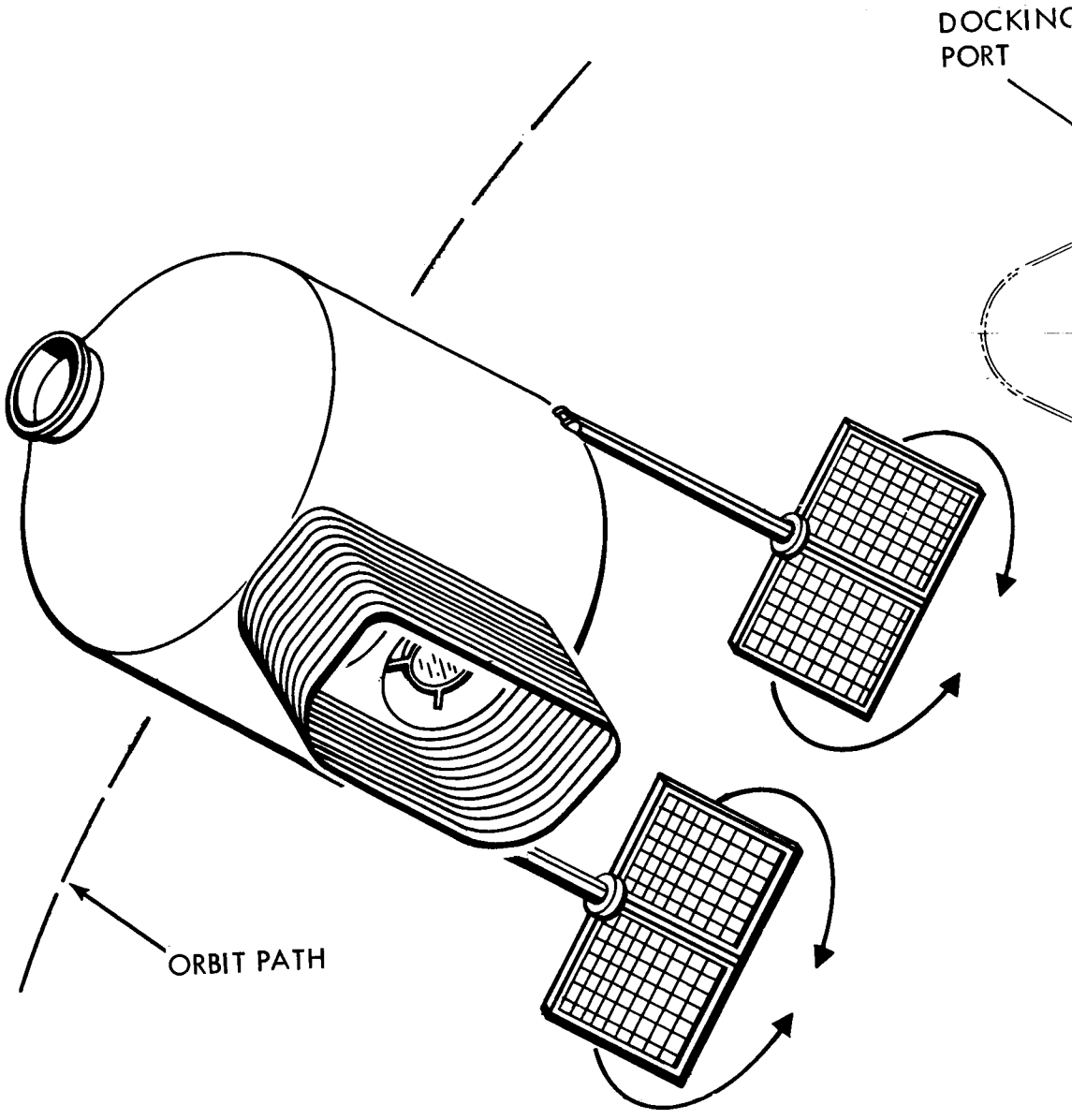


Figure 11.1.4-1. Concept No. 4, Dual Telescope in LEM Adapter



PRECEDING PAGE BLANK NOT FILMED.

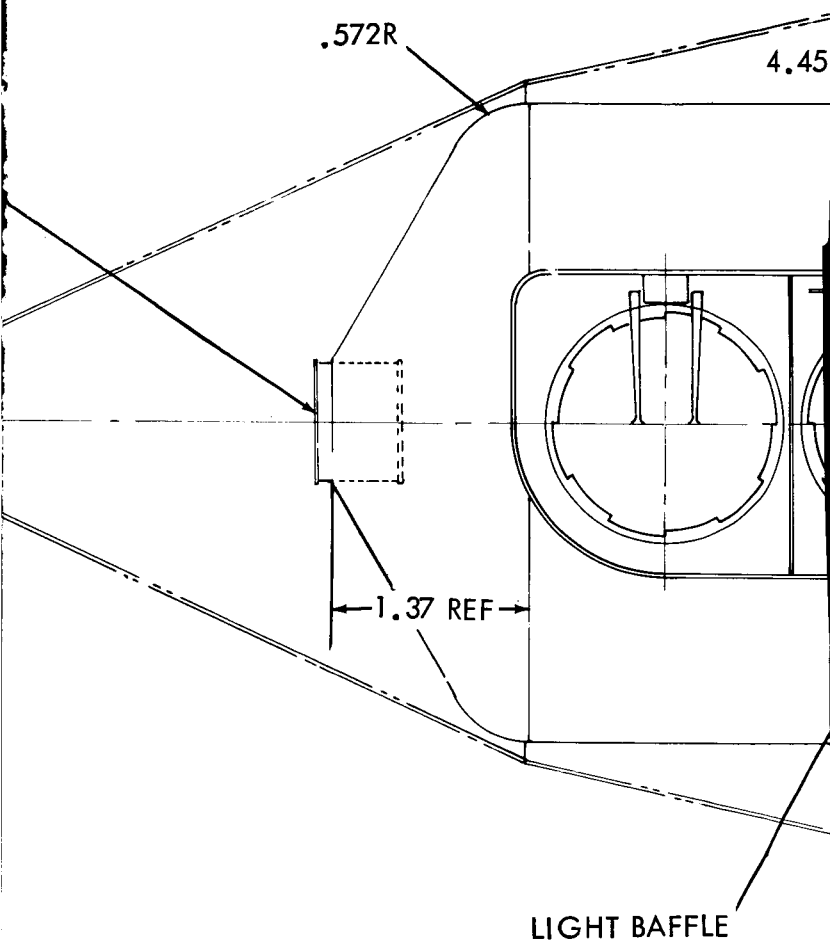
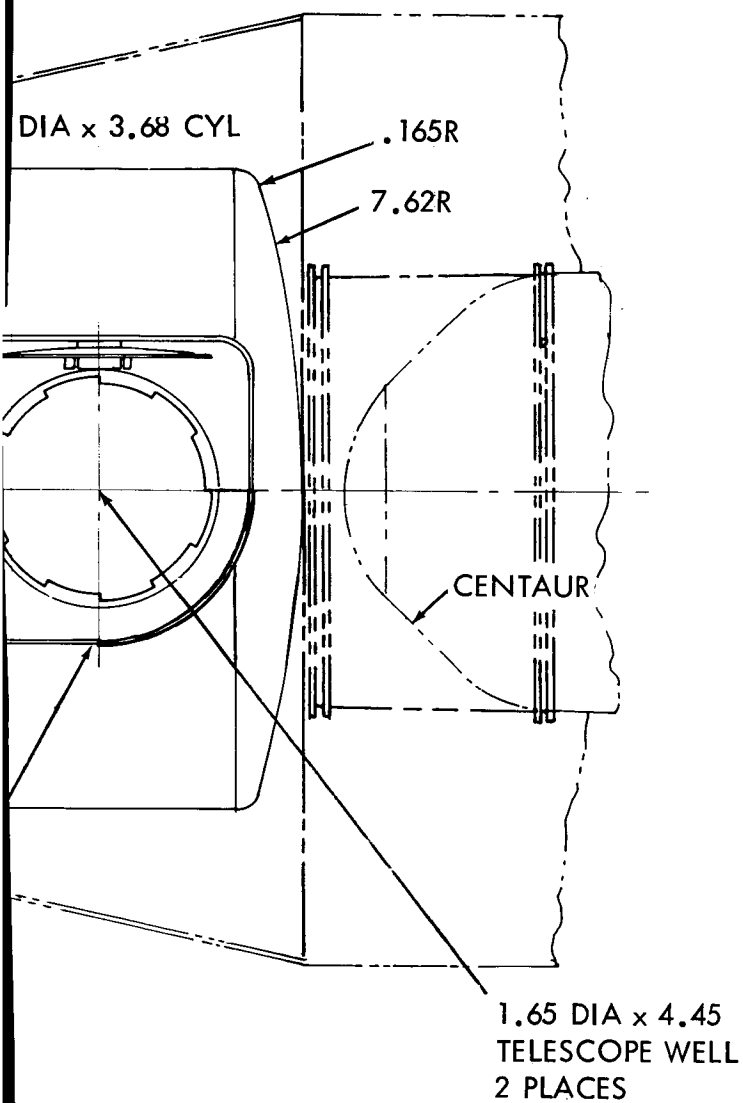


Figure 11.1.4-2. C



oncept No. 4, Dual Telescope in Centaur Shroud

2-147

(2)44

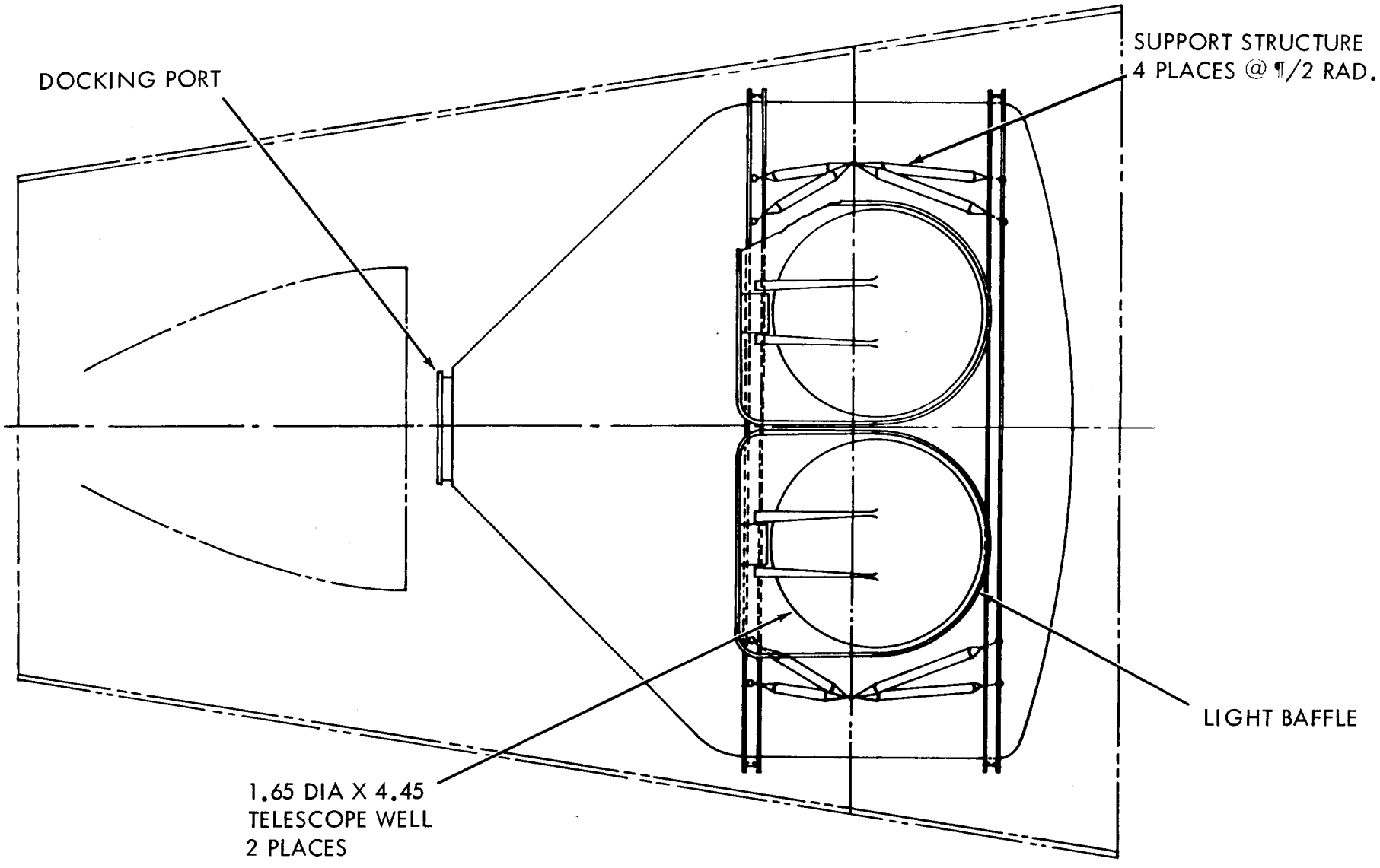


Figure 11.1.4-3. Concept No. 4, Dual Telescope in LEM Adapter

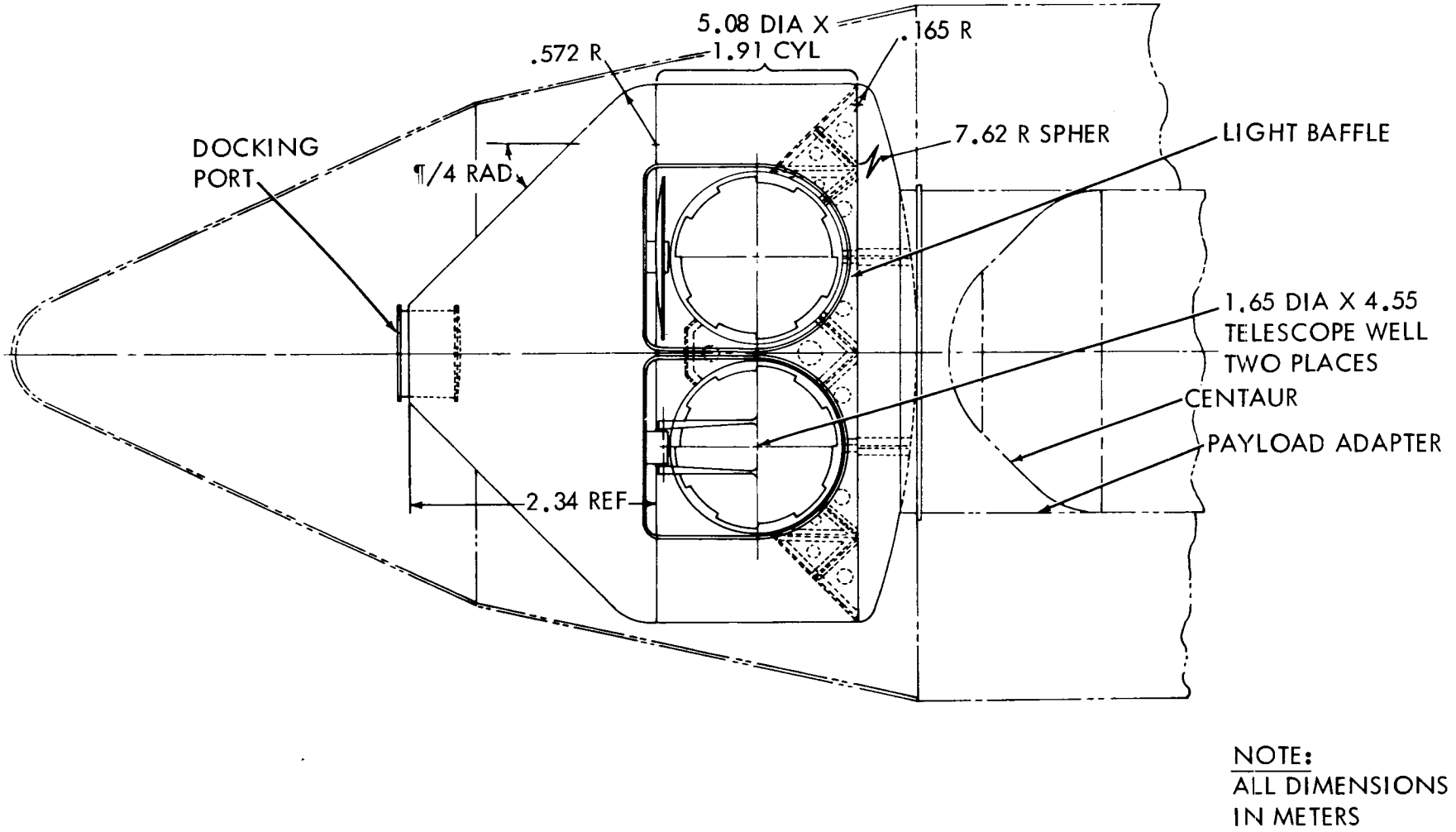


Figure 11.1.4-4. Concept No. 4, Dual Telescope in Centaur Shroud

11.1.5 Spacecraft Concept Number 5

Concept number 5 is a single telescope designed to obtain the maximum allowable length within the payload volume constraint. Figure 11.1.5-1 shows such a configuration in the LEM adapter. Figure 11.1.5-2 depicts a single telescope in the Centaur shroud. In both cases, launch loads act through the optical axis of the primary.

This telescope could be operated remotely either from a co-orbiting CSM or from the ground. By providing a docking hub in the equipment section, the telescope could be operated as an integral portion of the CSM. In this mode, shirtsleeve accessibility to the equipment bay could be obtained through the Command Module (CM) forward hatch.

The maximum telescope well size for the Centaur launch would be 1.4 meters in diameter by 5.87 meters in length. For the LEM Adapter, the maximum size would be 2.79 meters in diameter by 5.69 meters in length.

11.1.6 Spacecraft Concept Number 6

The concept was developed for the dual payload mission (Missions VI and VII). Figure 11.1.6-1 shows two spacecrafts, each containing telescopes mounted so that launch loads act through the optical axis. Figure 11.1.6-2 is similar except the telescopes are mounted so that launch loads act through the primary mirror diameter. There are numerous possible configurations for this type mission.

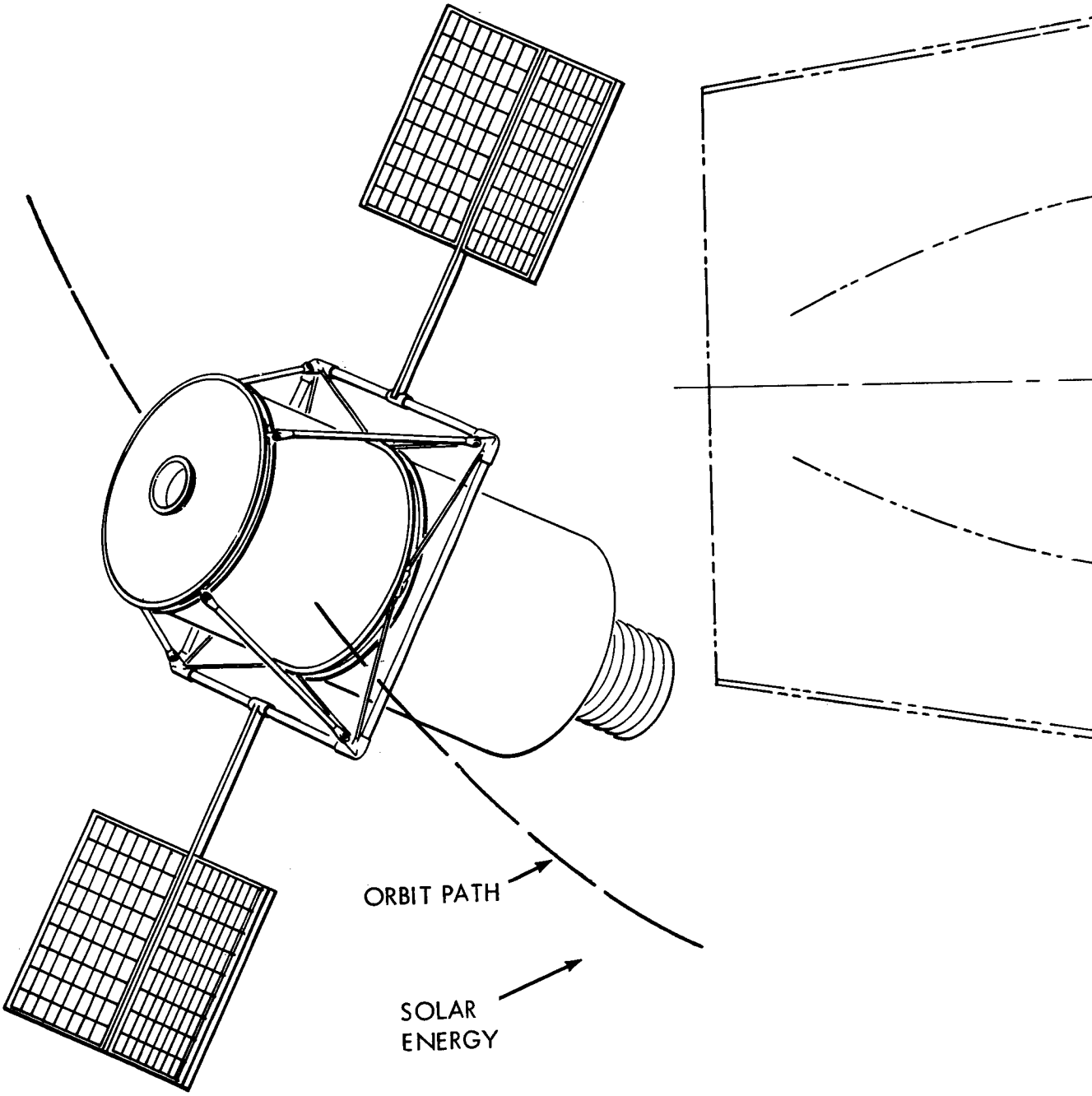
Since the Service Module (SM) engine was not required in this mission, it was assumed that this engine could be removed. This deletion will leave the entire LEM adapter section available for the payload.

For the configuration depicted in figure 11.1.6-1, the maximum telescope well size is 1.52 meters in diameter by 3.96 meters in length. For the other configuration, the maximum well size is 1.40 meters in diameter by 3.91 meters in length.

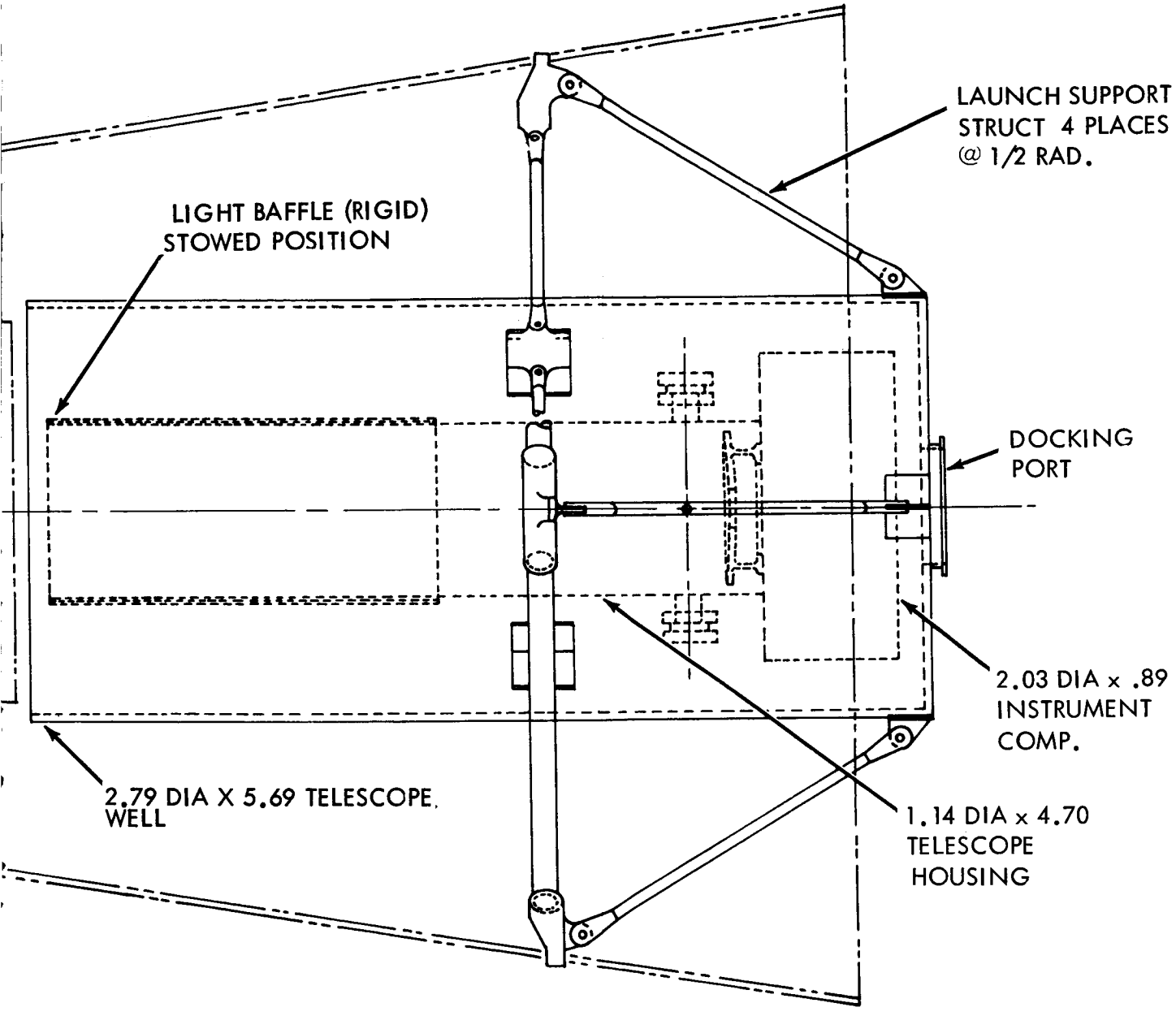
11.1.7 Spacecraft Concept Number 7

This concept was developed for the purpose of investigating problems associated with simultaneously tracking a stellar source and an earth-based laser source. Therefore, this concept consists of two telescopes which have two degrees of rotational freedom with respect to each other. Figure 11.1.7-1 depicts this configuration sized for the Centaur shroud.

In order to permit one telescope to remain fixed in inertial space (locked on a star) while the second remains fixed on an earth point, the perpendicular to the orbit plane would pass through the launch axis of the spacecraft. The two telescopes would be coupled to each other through



PRECEDING PAGE BLANK NOT FILMED.



NOTE:
ALL DIMENSIONS
IN METERS

Figure 11.1.5-1. Concept No. 5, Single Telescope in LEM Adapter

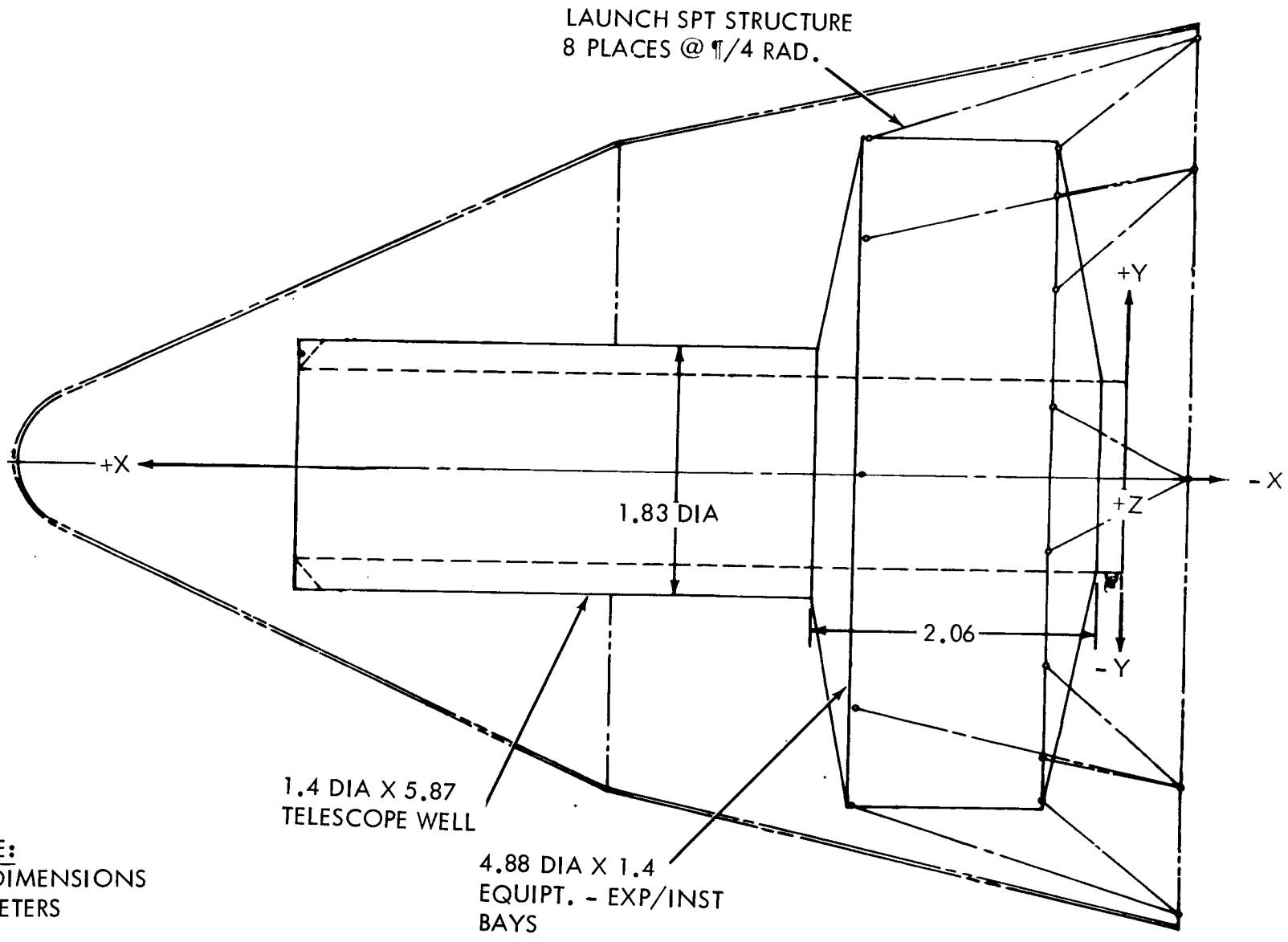
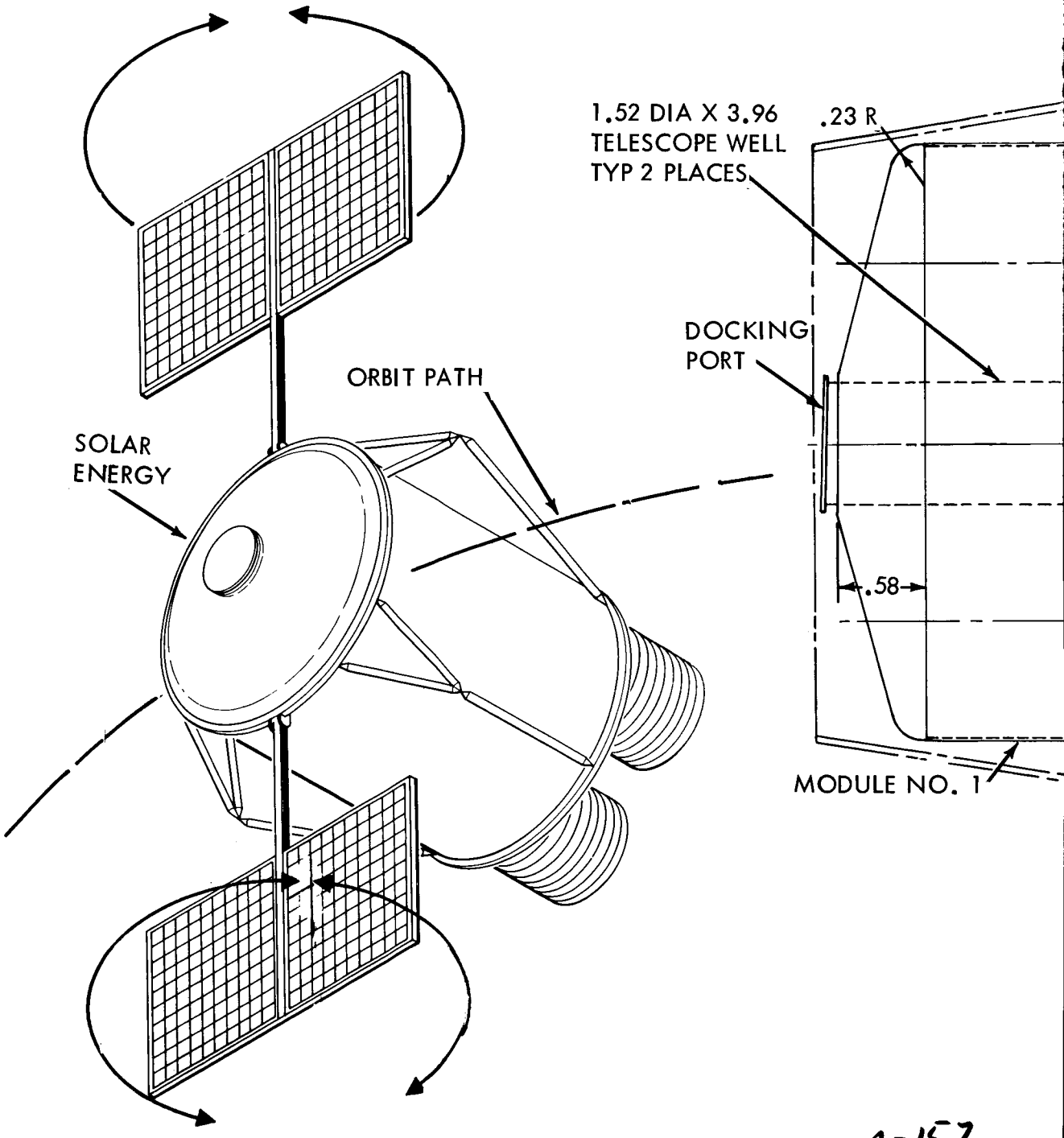


Figure 11.1.5-2. Concept No. 5, Single Telescope in Centaur Shroud


3.91 DIA X 3.66 C
1.52 DIA X 3.96
TELESCOPE WELL
TYP 2 PLACES
.23 R
DOCKING
PORT
ORBIT PATH
SOLAR
ENERGY
.58
MODULE NO. 1

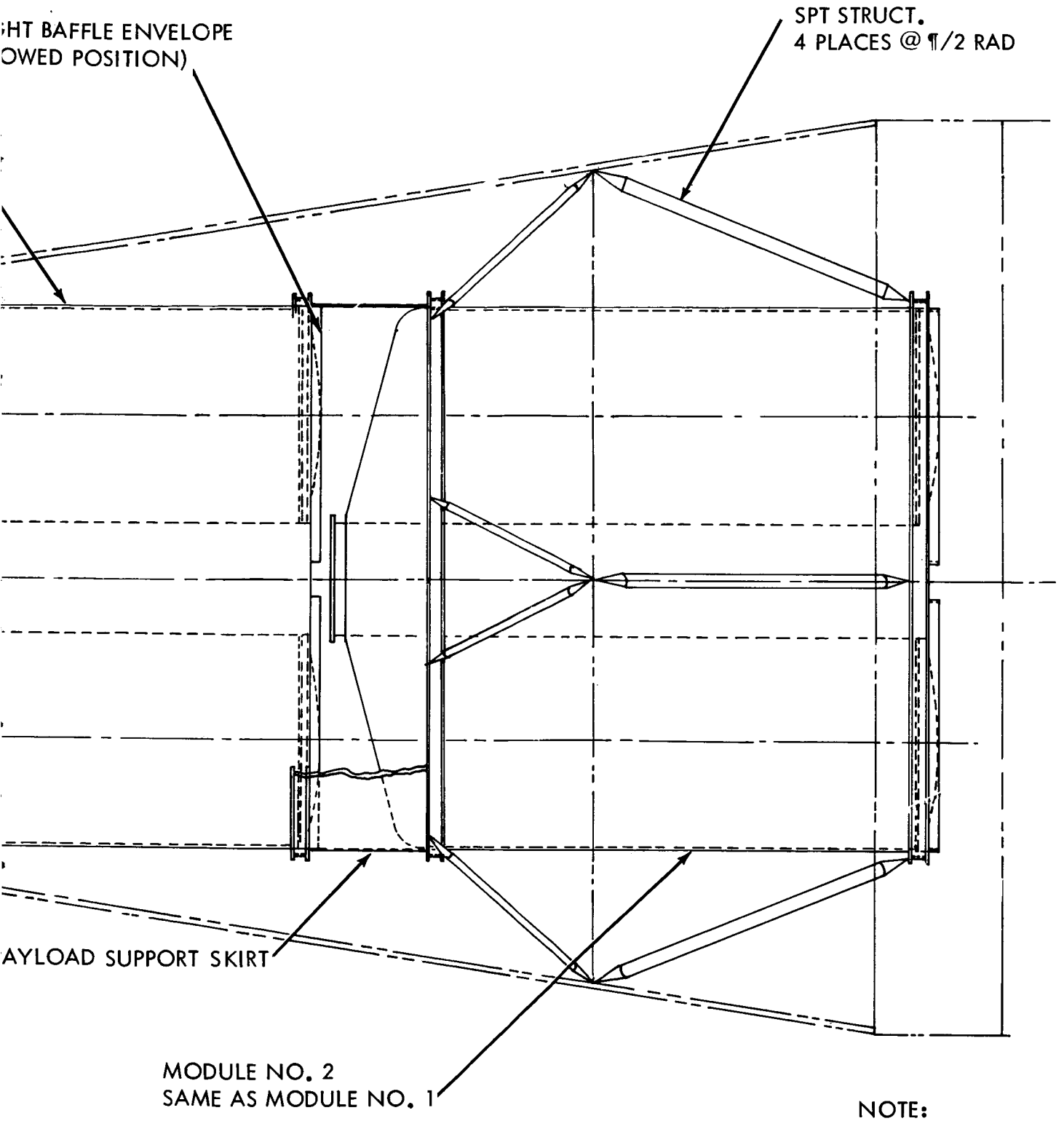


Figure 11.1.6-1. Concept No. 6, Dual Spacecraft

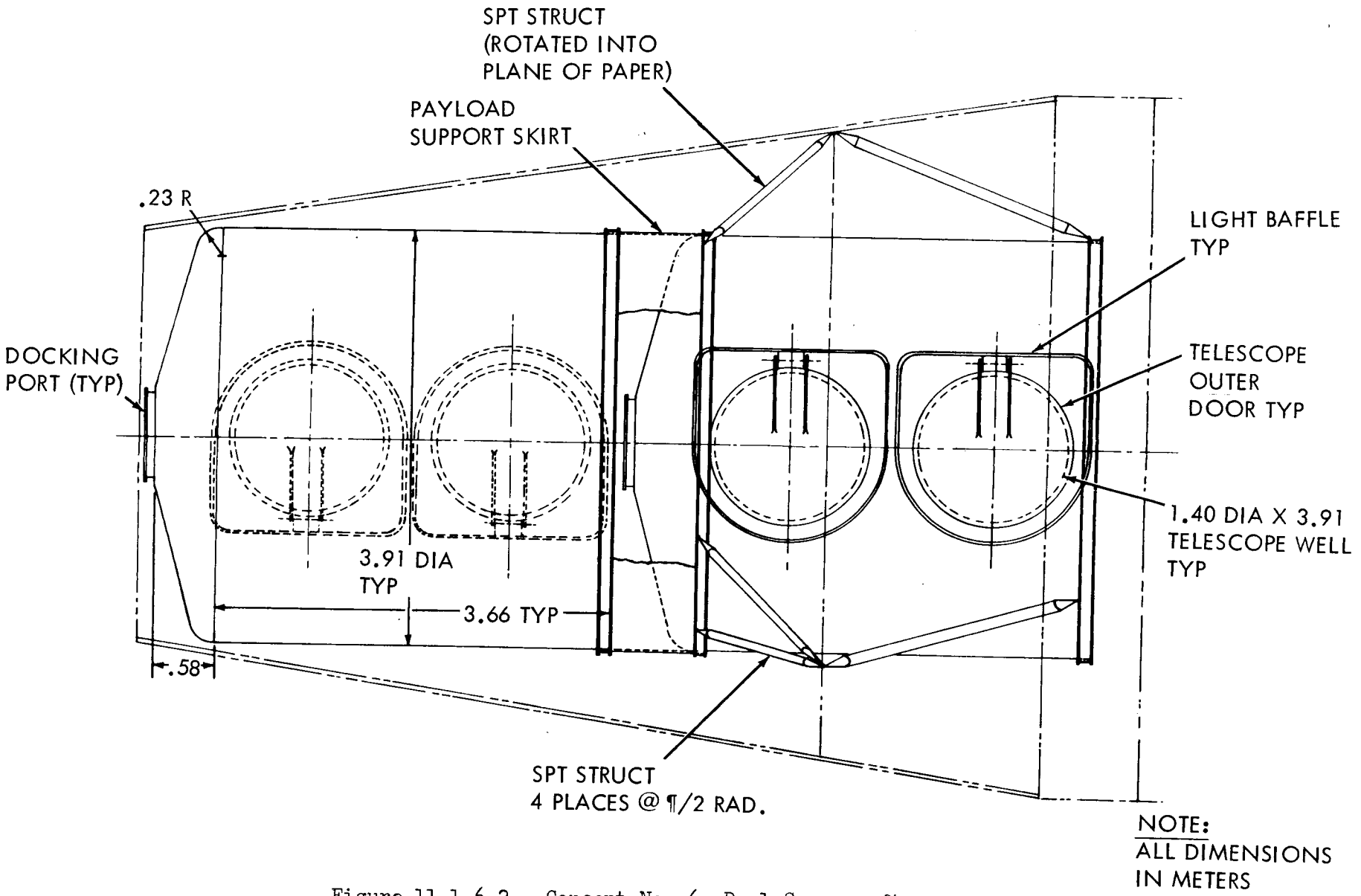
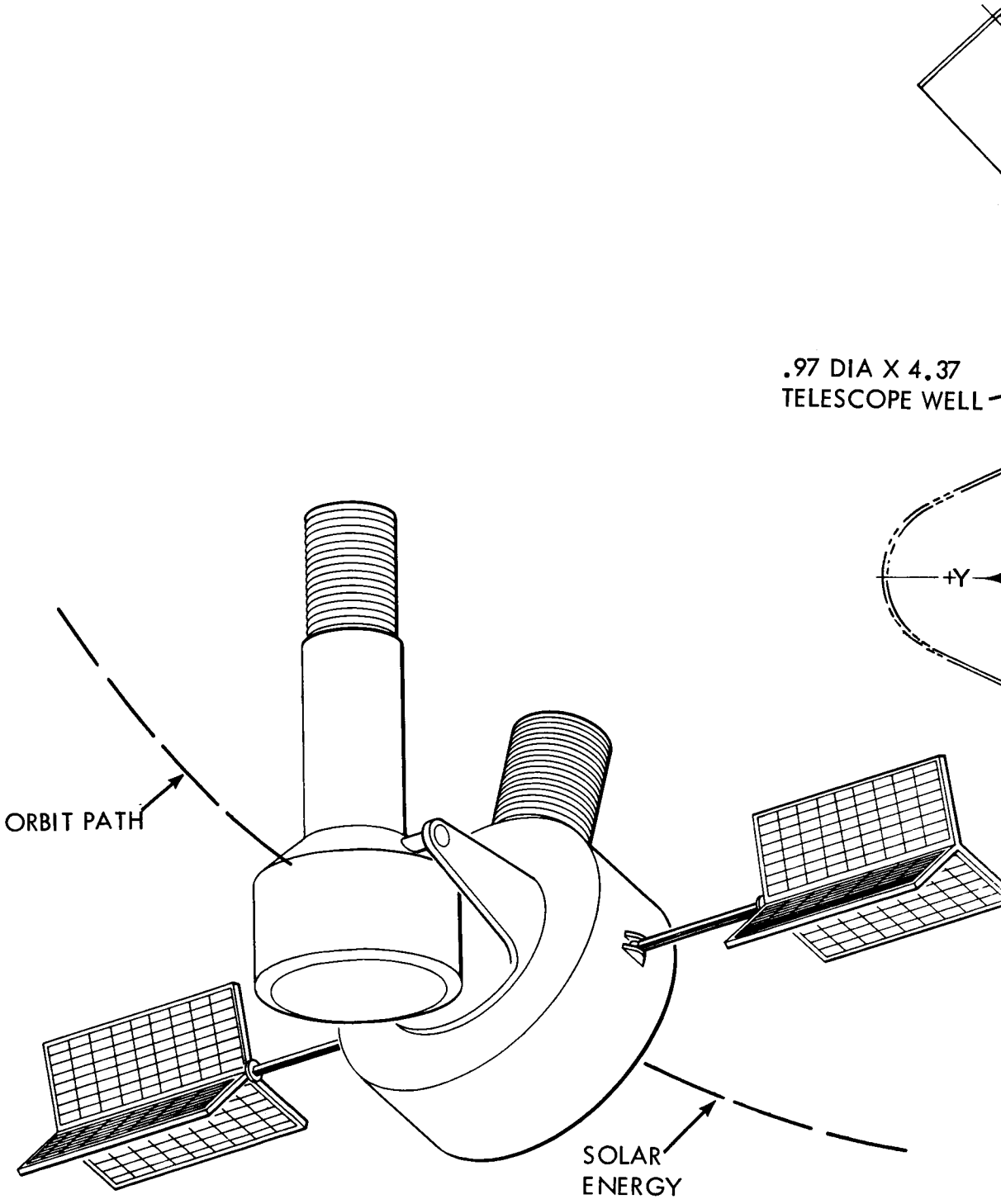
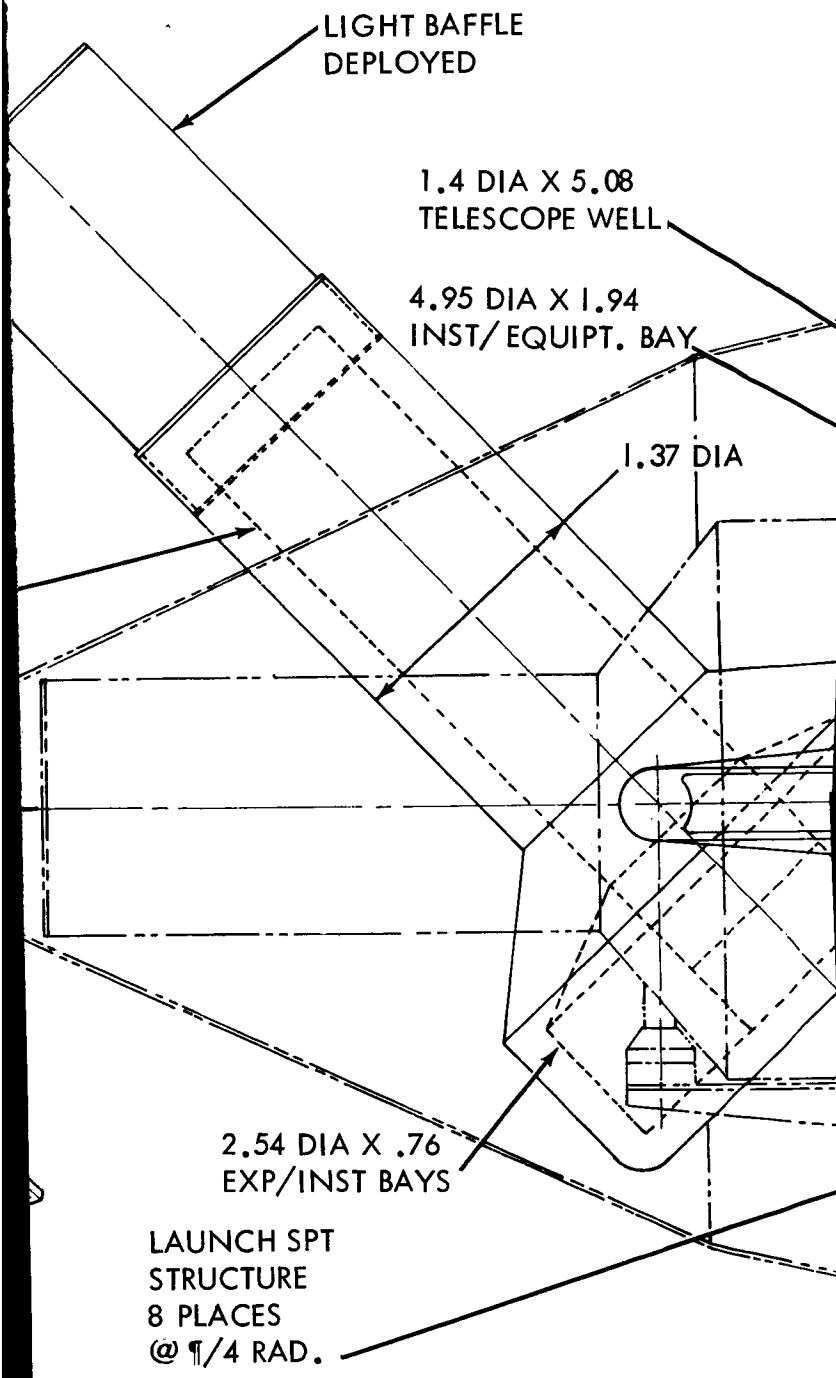
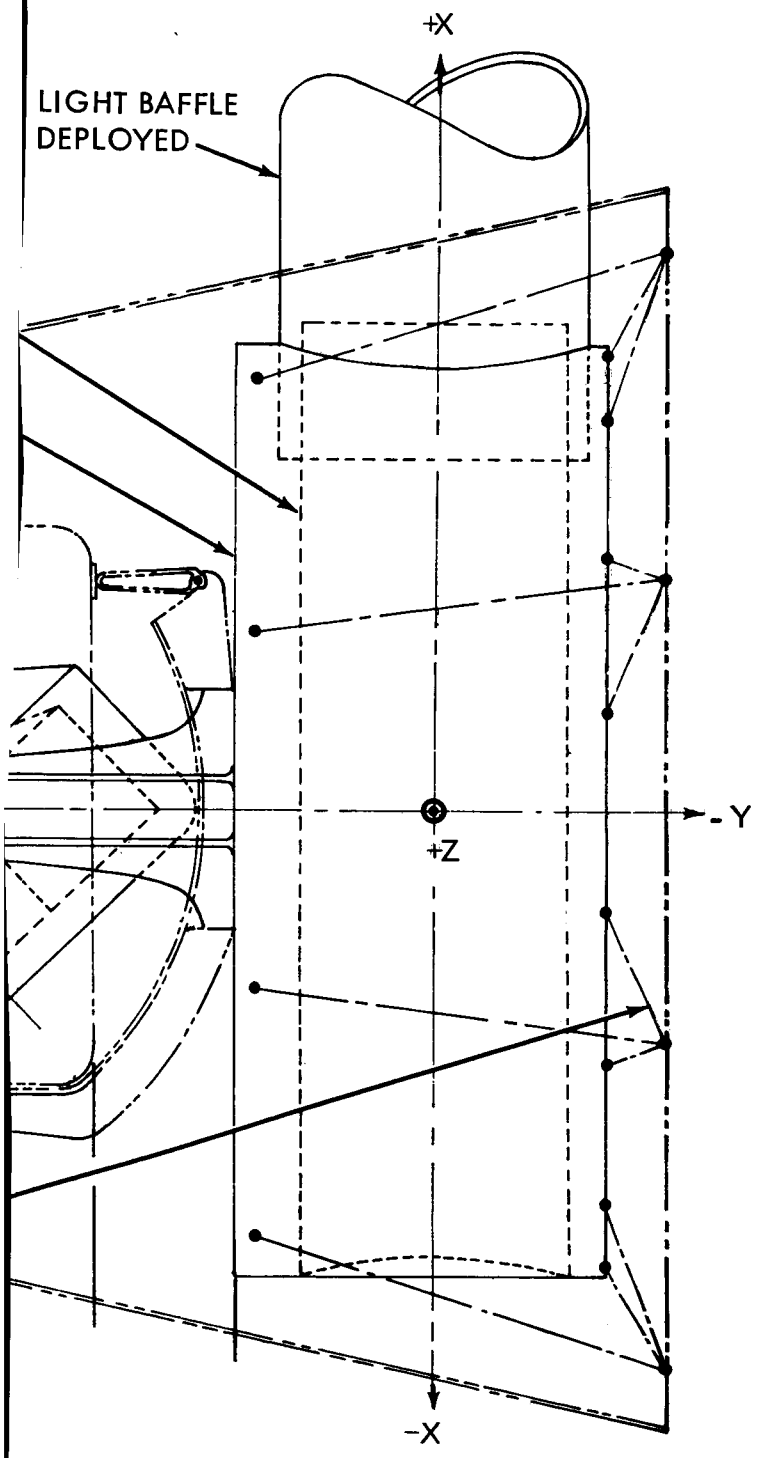


Figure 11.1.6-2. Concept No. 6, Dual Spacecraft



PRECEDING PAGE BLANK NOT FILMED.


LIGHT BAFFLE
DEPLOYED
1.4 DIA X 5.08
TELESCOPE WELL
4.95 DIA X 1.94
INST/EQUIPT. BAY
1.37 DIA
2.54 DIA X .76
EXP/INST BAYS
LAUNCH SPT
STRUCTURE
8 PLACES
@ ¶/4 RAD.



NOTE:
ALL DIMENSIONS
IN METERS

Figure 11.1.7-1. Concept No. 7, Dual Telescope

a bearing which allows 360 degrees of rotation. Furthermore, the astronomy telescope is to move in "elevation" through an angle of 90 degrees. These two movements would allow the telescope to track any star located in the hemisphere containing that telescope. This telescope could also be used to track a laser source on the earth by moving it to a coaxial position relative to the second telescope.

Although this configuration is attractive from the experimental standpoint, it represents a departure from the state-of-the-art in bearing design. A more thorough design evaluation of this approach is necessary before selection of a final spacecraft configuration.

11.2 Recommended Spacecraft Configurations

A completely integrated grouping of the OTAES experiments cannot evolve without consideration being given to the spacecraft configurations. These configurations must be compatible with each experiment group. Also, some experiments require individual attention with regard to the overall spacecraft. For these reasons the 20 different concepts presented in section 11.1 required further development. As a result of this development, 4 spacecraft configurations which include integrated experiment groups, have evolved and appear in this section. The telescope and experiment wells described in sections 4.0, 8.0 & 9.0 were developed in sufficient detail as a prerequisite to the spacecraft configuration development. The recommended spacecraft configurations contain sufficient design flexibility so as to allow for substitution of other wells or rearrangement of existing wells without degrading the overall mission concept.

11.2.1 Spacecraft Configuration Number 1

Configuration number 1 (figure 11.2.1-1 and 11.2.1-2) consists of the LEM Ascent stage with four telescope wells and one experiment well mounted below, such that the launch loads act through the diameter of the primary mirrors.

The LEM descent stage structure has been replaced with a platform structure which picks up the same attachment points as the standard Apollo LEM descent stage.

A hatch in the LEM floor, which replaces the LEM ascent engine, allows manned accessibility to the telescopes. The hatch leads to a compartment which is always pressurized. The telescope hatches can be closed and pressurized to allow access to the telescopes.

The optical axis of five telescopes is parallel to the LEM ascent stage windows which facilitates the use of man during initial telescope target

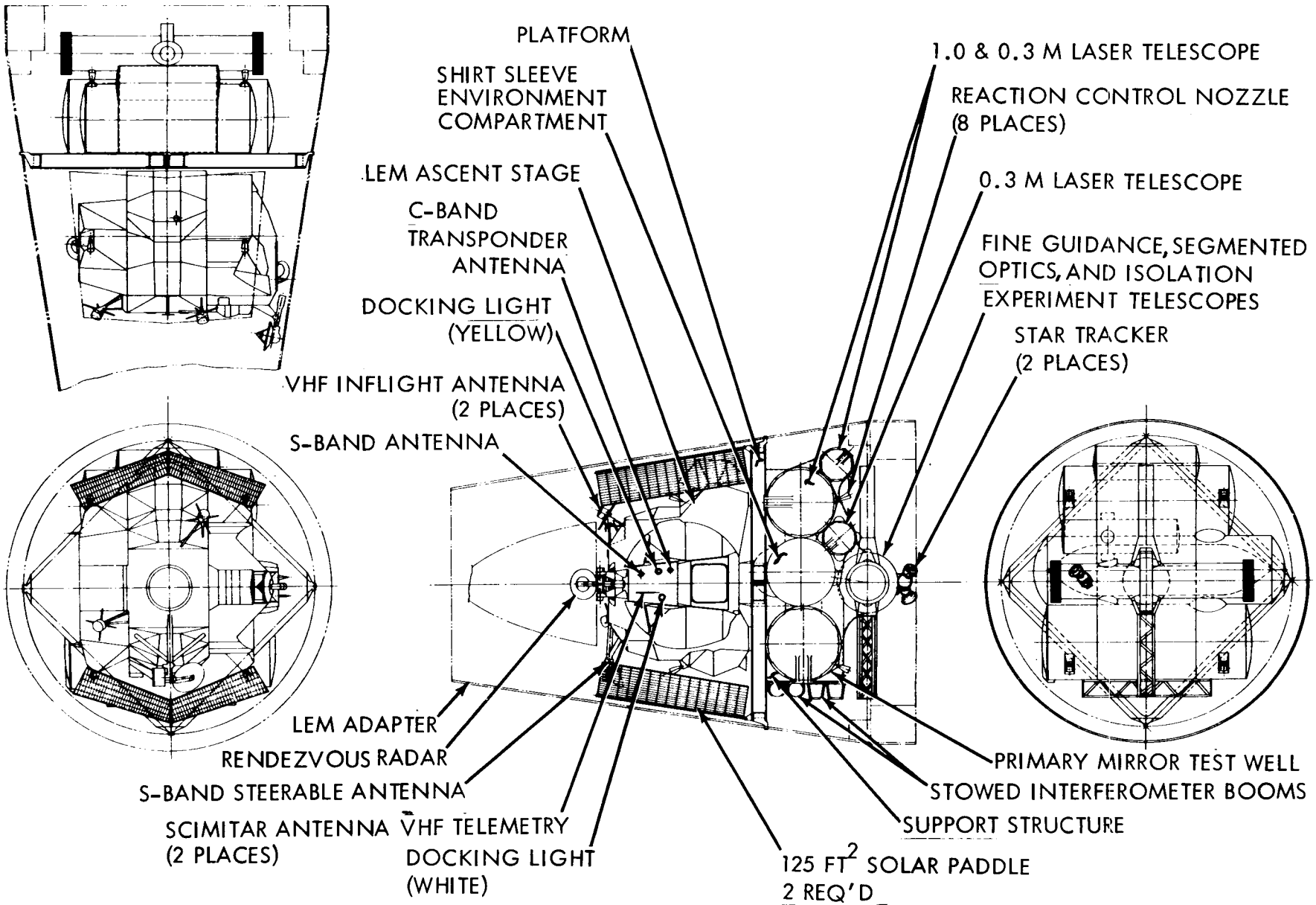


Figure 11.2.1-1. S/C Configuration Number One

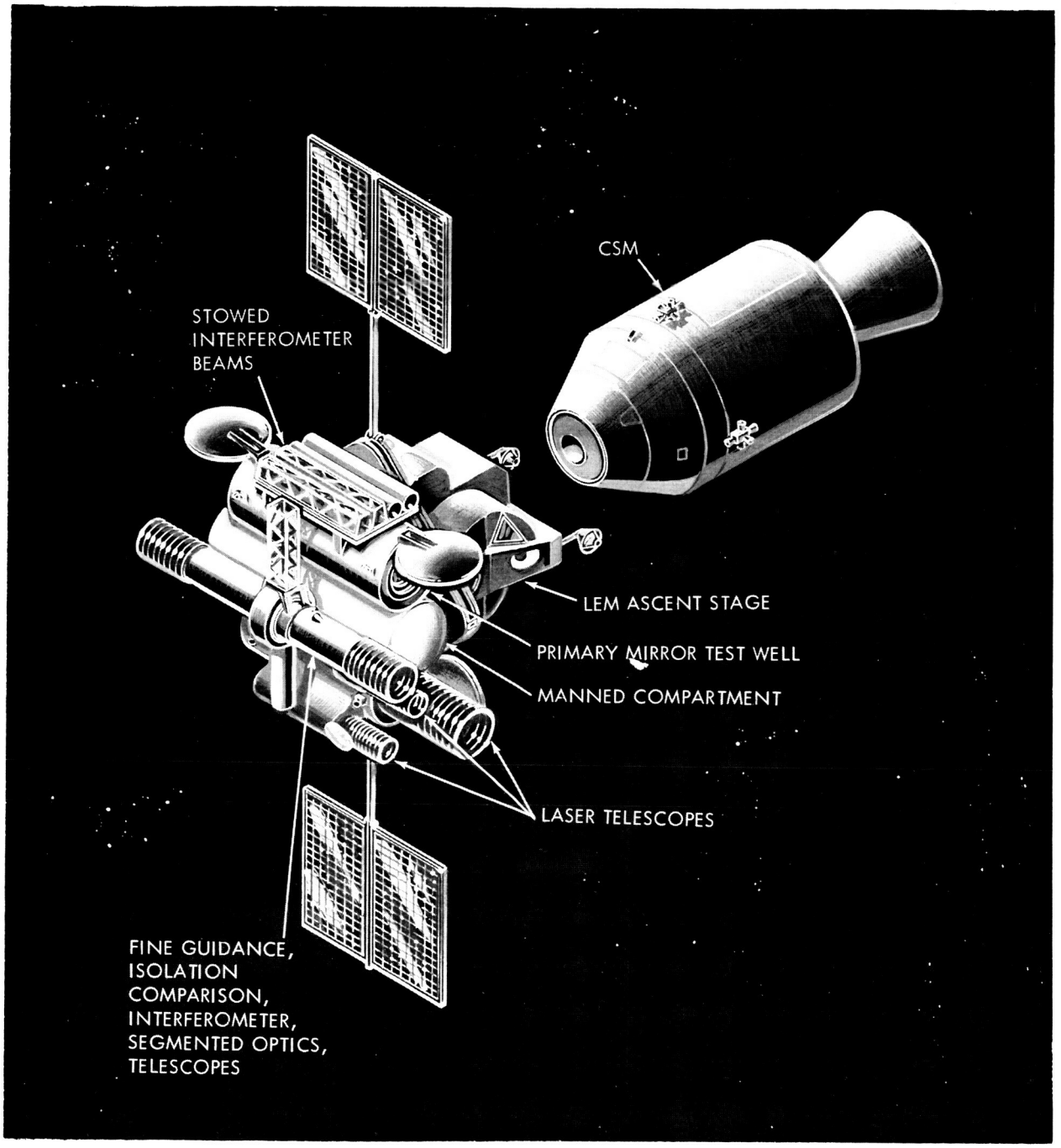


Figure 11.2.1-2. S/C Configuration Number 1

acquisition. The 0.6 meter telescope (which contains the Fine Guidance, Isolation Comparison, Segmented Optics, and Interferometer experiments) is not pressurized and if servicing is required, would be an EVA activity. Viewing ports are provided in the compartment to allow observation of all experiments in this telescope. Baffles are shown on the four experiment telescopes. Star trackers and Sun sensors have been positioned so as to permit positive acquisition in all operating spacecraft attitudes. Solar panels as shown have been configured to allow constant panel orientation to the Sun.

The stowed Interferometer booms are erected to the 0.6 meter telescope after all Fine Guidance and Isolation Comparison experiments have been conducted. This is to ensure that the 25 ft booms will not degrade the operating results of those experiments. The booms will be erected by EVA and locked in position.

The life support system for the LEM will have some modifications due to the elimination of the descent stage. The modification will primarily consist of additional storables.

The spacecraft is designed so the launch axis, which is perpendicular to the optical axis, is also perpendicular to the orbit axis. This ensures a constant spacecraft rotational angle to the Sun line enabling the RCS and spacecraft uniformity in solar heating.

Each telescope has a separate gimbal system except for the one 0.3 meter laser telescope strapped to the 1.0 meter telescope.

11.2.2 Spacecraft Configuration Number 2

Configuration number 2 (figure 11.2.2-1 and 11.2.2-2) shown in the Centaur shroud, consists of four telescope and experiment wells. The spacecraft structure and support systems basically replaces the LEM ascent stage in the manned mode. This is the only mission launched unmanned.

When this spacecraft is used in the manned mode, by rendezvous and docking, complete accessibility is provided to the telescope well. This spacecraft also contains its own environmental support system. The location of the RCS solar and Star Trackers and solar panels follow the same design philosophy used in the first configurations. Because of the large volume available this is adaptable to a large range of laboratory experiments.

11.2.3 Spacecraft Configuration Number 3

The third configuration (figures 11.2.3-1 and 11.2.3-2) contains two separate spacecrafts. This configuration was developed for the dual payload mission. It enables astronomical experiments to be conducted by one spacecraft in low earth orbit and laser experiments to be conducted in a synchronous orbit.

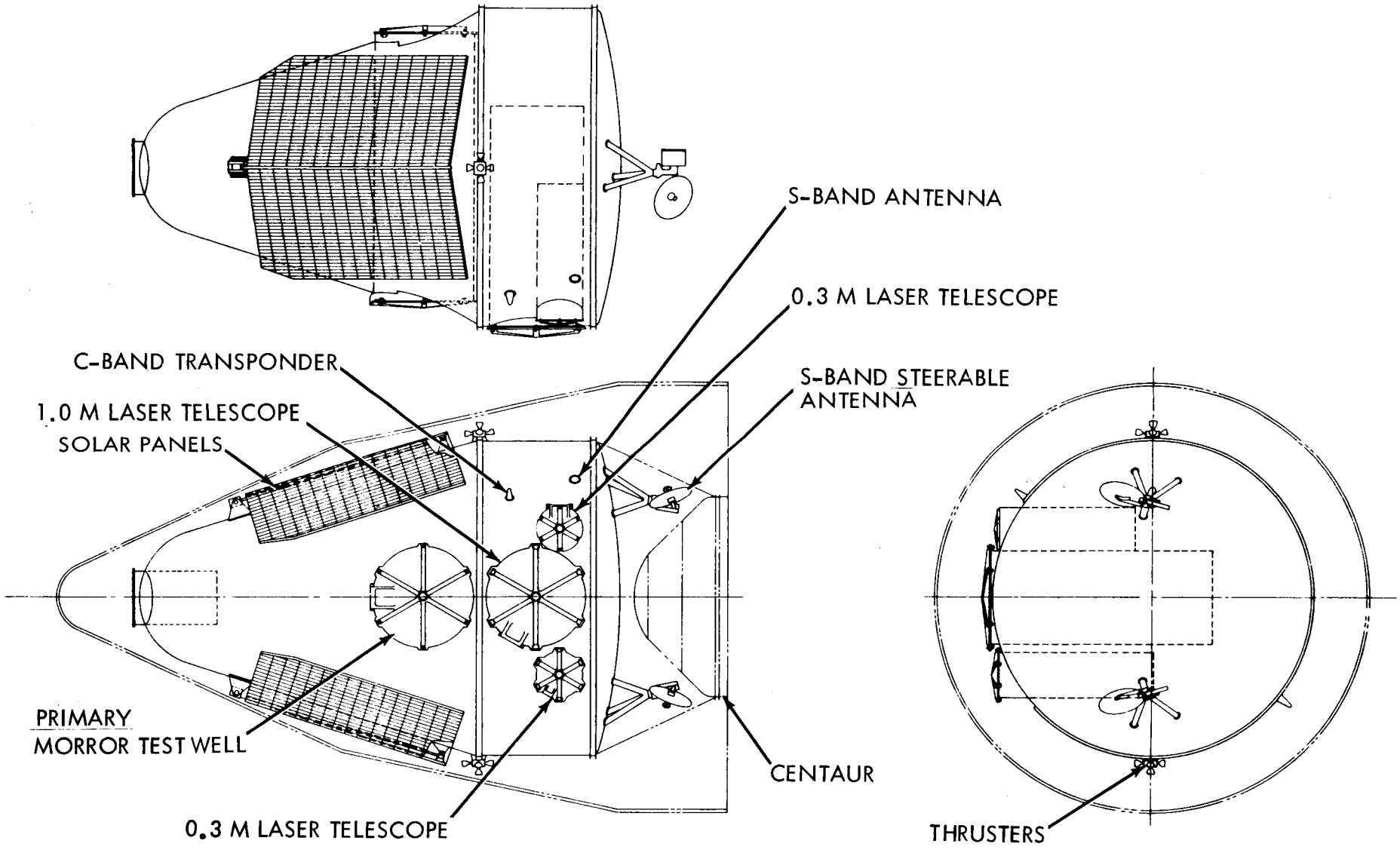


Figure 11.2.2-1. S/C Configuration Number 2

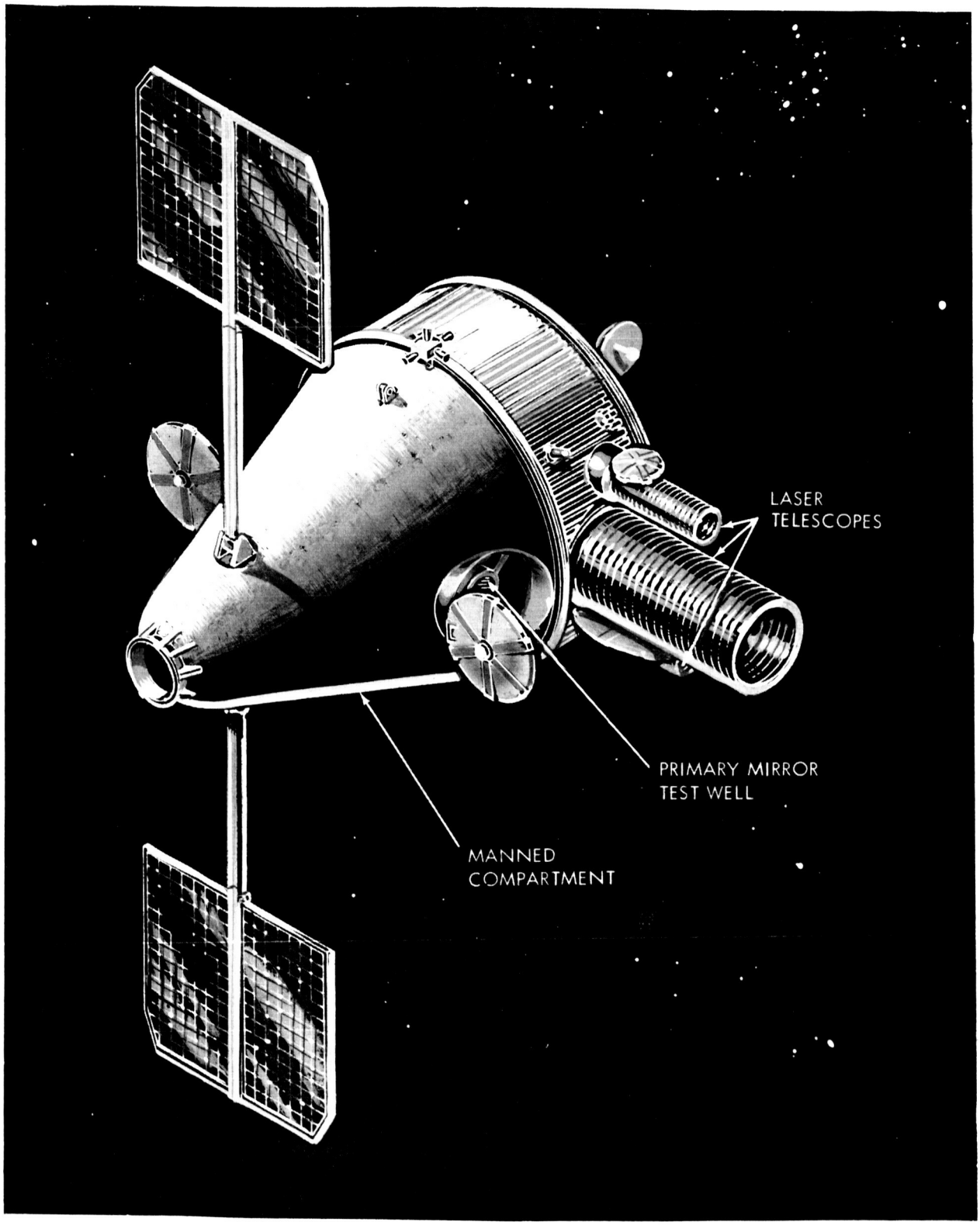


Figure 11.2.2-2. S/C Configuration Number 2

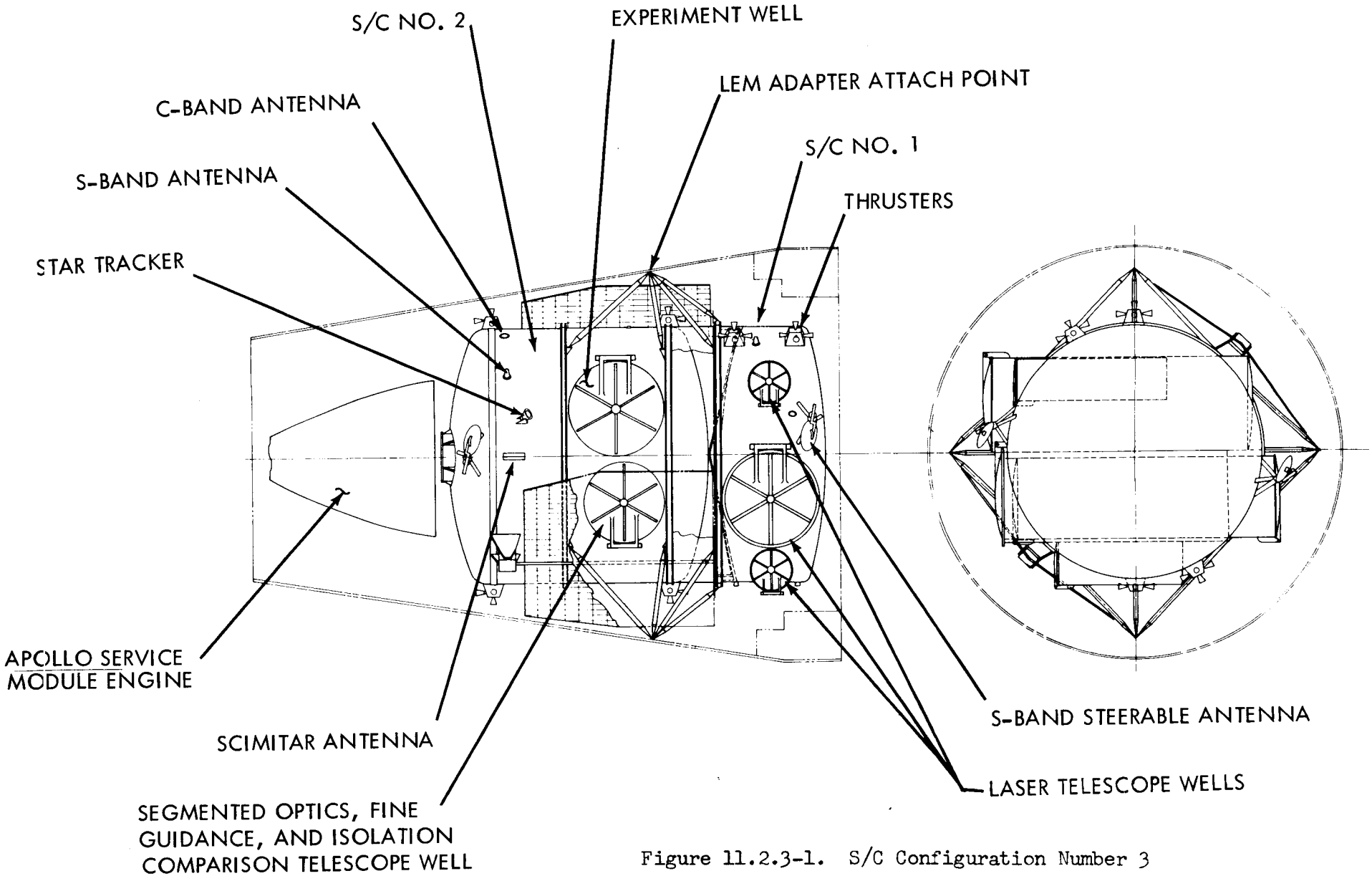


Figure 11.2.3-1. S/C Configuration Number 3

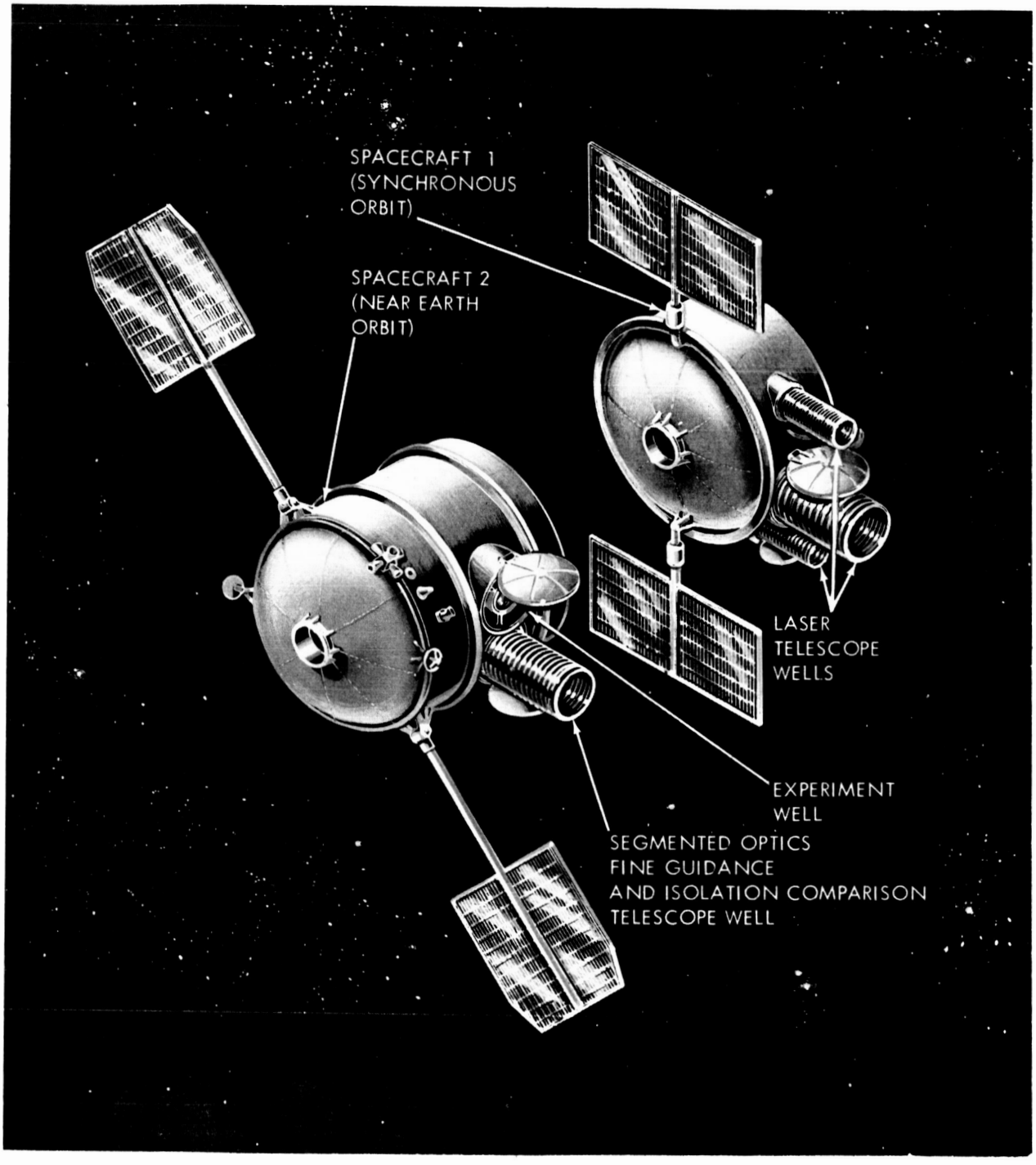


Figure 11.2.3-2. S/C Configuration Number 3

After being placed in a low earth orbit, spacecraft (2) and the CSM is separated from spacecraft (1). The S-IVB stage then places spacecraft (1) into a synchronous orbit.

The low earth orbit astronomical spacecraft has two telescopes and one experiment well. It is a manned pressurized spacecraft that will allow access to the telescopes when the telescope hatches are closed and the well pressurized. Life Support Equipment similar to that mentioned in configuration 2 will be included. The synchronous orbit spacecraft contains all three laser telescopes. This is an unmanned unpressurized spacecraft. It is separated from the S-IVB by its own RCS system and slides out on rails to prevent any interference with the stage.

11.2.4 Spacecraft Configuration Number 4

Configuration number 4 (figure 11.2.4-1 and 11.2.4-2) was developed for the astronomical experiment group. This configuration is very similar to the number one configuration. The major difference is in the elimination of the three laser experiment telescopes. It is developed for a low earth orbit whereas the number one configuration is for a synchronous orbit. Radiation protection design of the structural hull will be different from the number one configuration.

11.3 STRUCTURAL AND MECHANICAL

The experiments and spacecraft configurations under consideration posed unique structural and mechanical design problems. The structural integration of gimballed telescopes used with an existing spacecraft module which is at the same time compatible with thermal and control requirements is a substantial technical problem. This problem was approached in this phase of the study with a wide latitude of ideas and analyses which were directed primarily toward defining the important trade-off areas.

The structural and mechanical technical discussion is broken into four areas. Each area presents its own requirements, analysis, trade-offs, and recommended solutions.

A materials review was conducted to obtain a wide spectrum of mechanical and physical properties. In later studies, definite material requirements will evolve and will be based upon this review. For purposes of this feasibility study, it was advantageous to select aluminum alloys for all structural subsystems. Their advantages and wide range of application need no justification here. More definite selections will be chosen in subsequent studies.

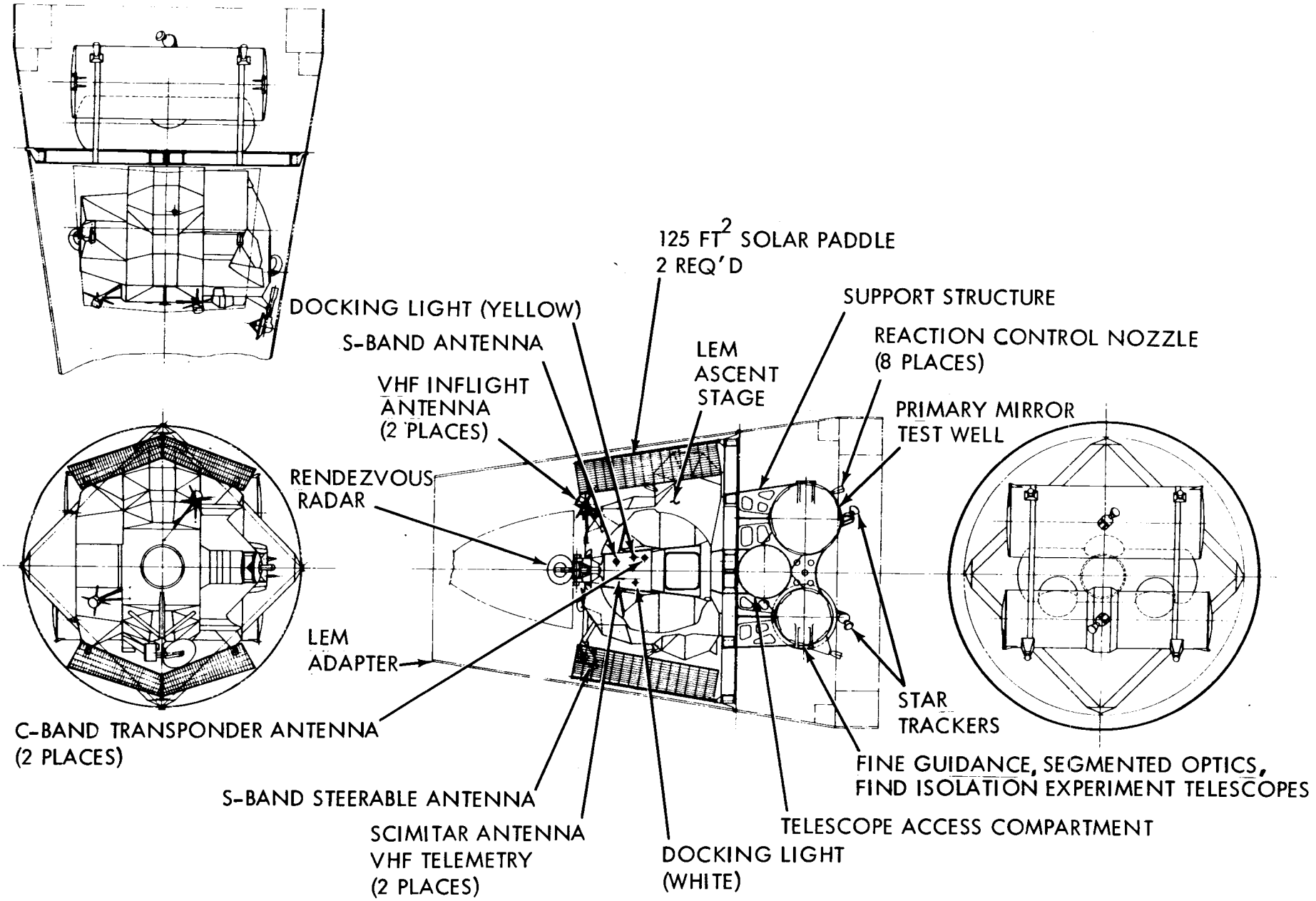


Figure 11.2.4-1. S/C Configuration Number 4

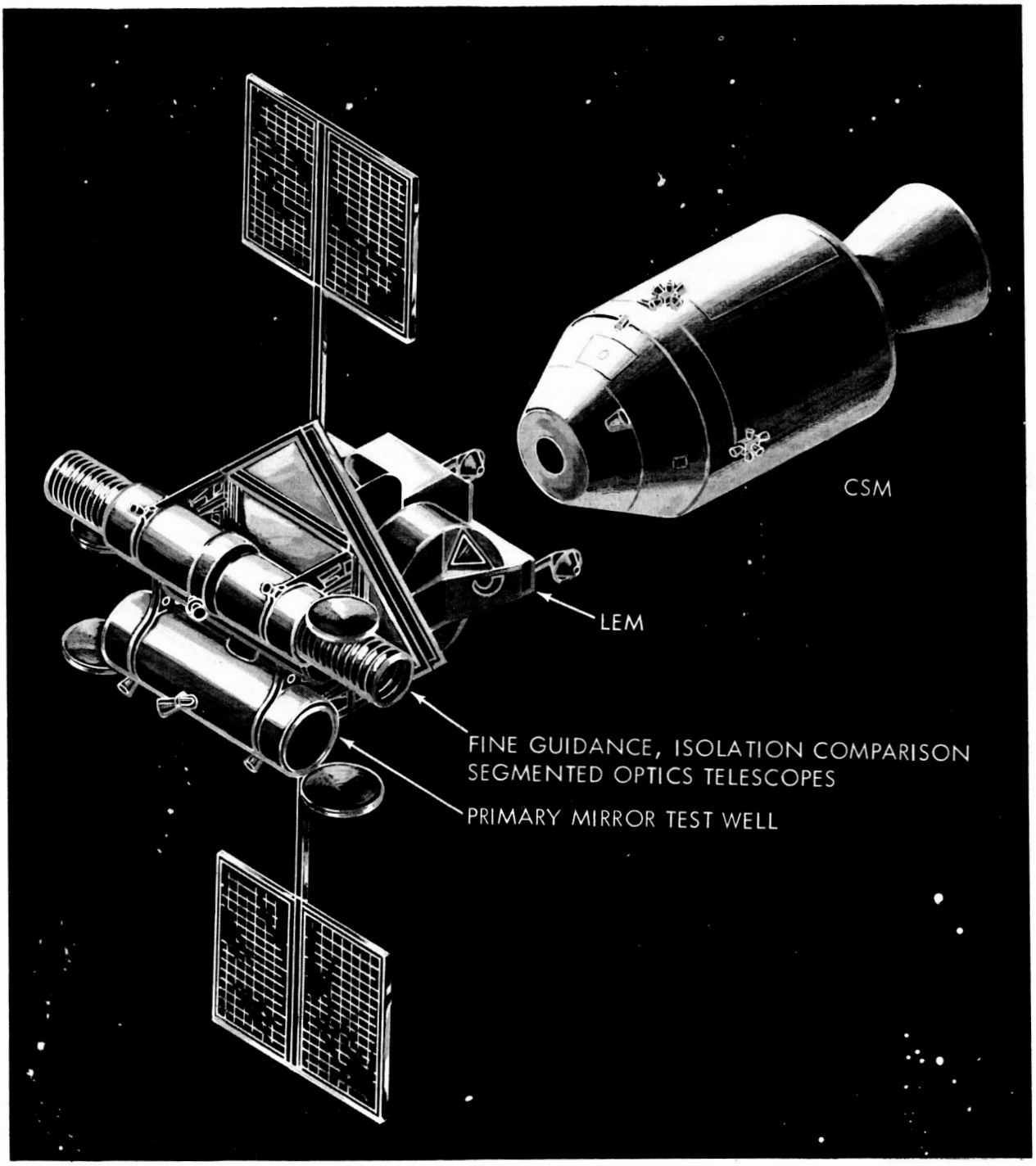


Figure 11.2.4-2. S/C Configuration Number 4

11.3.1 Spacecraft Structure

The development of the spacecraft concepts and configurations presented included a review of feasible structural concepts for each configuration. Structural integrity of the configurations were accomplished by attention to primary loadings, load paths, environmental conditions, and structural efficiency. The major effort in this study has been directed toward manned configurations because of their inherent complexity and recognized requirement to support experiments. Unmanned configurations will be mentioned only where significant trade-off areas exist with manned configurations.

11.3.1.1 Spacecraft Structural Design Criteria

Advance design conducted on the spacecraft configurations was based on the following criteria.

a. Structure designed for longitudinal launch loads of 4.0 to 5.0 g's and lateral transportation loads of 1.5 g.

b. Manned configurations using two telescopes without LEM have an initial weight of 3620 kg (8000 lb).

c. Manned configurations using telescopes with LEM have an initial weight of 7240 kg (16,000 lb).

d. Structural design and analysis is to be designed to (1.4) (Design Load) equal to the (Ultimate Load).

e. Manned cabin pressure is 0.344 bar (5 psi) and relief pressure settings at 0.413 bar (6 psi).

f. Mission duration is 1 year and manned duration is 45 days.

g. Physical size constraints are limited by the LEM adapter shroud interface and Centaur shroud.

h. Telescope wells are sized for maximum telescopes. Telescope weight is estimated at 544 kg (1200 lb).

11.3.1.2 Environmental Requirements

The space environment encountered by the spacecraft consists of radiation, vacuum, temperature, and micrometeoroid environment. Each of these areas were investigated to a degree necessary for this study.

Radiation environments for the spacecraft becomes important on manned missions. The levels of the various types of radiation have been developed in previous studies.(1) Radiation shielding for low earth-orbit spacecraft conceptual design are usually adequately provided for by the requirements of micrometeoroid shielding. Radiation shielding becomes very significant in synchronous and elliptical orbits. No attempt was made at this level of study to assess radiation levels internal to the spacecraft. This area will be investigated in subsequent phases of this study.

The vacuum environment of space does not pose any major problems to structural design. Vacuum cold welding could create minor problems when there is thermal expansion and contraction of structural joints. Surface coatings will have to be chosen to withstand a vacuum environment.

The depth of this study did not permit a comprehensive integration of thermal analysis in the design. Projected thermal gradients resulting from preliminary thermal analysis were recognized and structural hull skins and interior structure were developed within these constraints.

One of the more important design parameters to be considered is the effect of a micrometeoroid environment on the spacecraft. Hypervelocity impacts by micrometeoroid can damage the spacecraft in various ways, the more serious being penetration of the pressure hull. Large punctures causing rapid decompression must be definitely avoided. There always exists the danger of explosions or fires as the vaporized skin materials mix with the cabin atmosphere. This danger can be minimized by proper proportioning of oxygen and nitrogen in the cabin.

For purposes of this study, it will be assumed that all impacts will be caused by micrometeoroids. Surface erosion will be evaluated in subsequent studies and is not considered a significant problem here. Large meteoroids are extremely scarce and the protective measures required to stop them are prohibitive to any conceivable spacecraft design. The assumptions stated above are consistent with recognized spacecraft design.

Micrometeoroids can be grouped into two distinct classes. These classes are sporadic and shower micrometeoroids. Sporadic micrometeoroids are individual particles having a random distribution and are omnidirectional. Shower micrometeoroids exist in streams and vary in intensity and frequency. The depth of this study precludes the integration of shower micrometeoroids into the design. Only sporadic micrometeoroids will be considered in the feasibility studies of the candidate configurations.

---

(1) CCSD TN-144 Operational Environment Saturn Class Missions, Guderian, Carl, February 22, 1966.

The accepted probability of no micrometeoroid penetrations for manned spacecraft is 0.999 (1-0.999) which equals 0.001 for 1 penetration established, the required micrometeoroid flux and micrometeoroid mass for design can be calculated. Actual spacecraft conditions and sizes will be used in this analysis as a "first cut" of the required micrometeoroid protection.

The probability of no penetrations with sporadic micrometeoroids is assumed to be 0.999. Therefore,(2)

$$P_1 = e^{-np} \tag{1}$$

Where:

P_1 = probability of no penetrations of sporadic micrometeoroids.

n = number of trials or impacts.

p = probability of a single penetration in a single trial or impact.

np = expected number of penetrations.

Solving the above equation for np:

$$-0.999 = e^{-np}$$
$$np = 0.001 \tag{2}$$

The expected number of penetrations is:

$$np = N_p \tau A \delta \tag{3}$$

Where:

N_p = total micrometeoroid flux (gram impacts/ft^2/day).

A = surface area of spacecraft (ft^2).

---

(2) Purser, Faget, Smith, Manned Spacecraft Engineering Design and Operation, Fairchild Publications, Inc., N.Y., 1965.

τ = mission duration (days)

δ = earth shielding

The surface area exposed to the omnidirectional sporadic micrometeoroids is taken as the entire area. This trial will use the configuration described in subsection 11.1.3, which is the largest manned spacecraft and subsequently the most critical configuration for protection.

$$A = 2\pi r (r+h) \quad r = 6.5 \text{ ft}, \; h = 13.5 \text{ ft}. \tag{4}$$

$A = 818 \text{ ft}^2$

τ = mission duration (manned 45 days).

δ = earth shielding = $(1 + \text{Cos}\theta)/2$.

Where:

$$\text{Sin}\,\theta = \frac{R}{R + H}$$

R = radius of earth.

H = altitude of spacecraft.

A low earth orbit of 648 km (400 n.mi.) was chosen.

Therefore:

$\delta = 0.709$

Solving equation (3) for N_p

$$N_p = \frac{n \cdot p}{A \tau \delta} = 3.83 \times 10^{-8} \text{ gm/ft}^2\text{/day}$$

Micrometeoroid protection design depends on the mass of the meteoroid. Whipple gives the following relationship for an average micrometeoroid velocity of 30 km/sec as[2]

$$\log N_p = -1.34 \log m - 10.423 \tag{6}$$

This will define the primary sporadic meteoroid flux for near-earth, cislunar, and lunar operations. The minimum particle size cut-off is a 0.5 gm/cc density and a diameter of 4.1 microns, and a 7 gm/cc density with a 0.16 micron diameter.

Substituting N_p into equation (6) gives a particle mass of:

$$m = .00568 \text{ gr.} \tag{7}$$

This represents the mass of the particle that must be stopped by the spacecraft to achieve a probability of no penetrations of 0.999 for the given spacecraft.

The information presented herein will be used for the foundation of the micrometeoroid design of the hull in subsection 11.3.1.4.

11.3.1.3 Shroud Interface Structure

The candidate spacecraft concepts are housed within either a LEM adapter shroud or a Centaur payload shroud. For each configuration an attempt is made to treat both shrouds as "off-the-shelf" items. The size of the s/c will be limited by the shroud envelope volume and its load carrying capabilities.

The LEM adapter shroud has been qualified for a 14,550 kg (32,000 lb) payload over and above the Command-Service Module (CSM) weight. It has a lower section which interfaces with the IU at its bottom. The upper section attaches at the top to the Service Module (SM). This upper section will separate into quadrants that hinge outward from the bottom on command to expose the OTES for docking and separation.

The LEM Descent Stage mounts to the LEM adapter shroud at four points around the separation plane between the hinged upper section and the lower section. The use of the entire LEM (minus engines) by mounting a telescope to its Descent Stage was investigated. While this approach incurs the minimum modification, it results in a weight penalty and a maximum telescope diameter of 0.91 m (28 inches). The alternatives to the use of the Descent Stage are platforms or frames to support the LEM Ascent Stage and provide structural load paths during launch.

Each concept used with the LEM adapter shroud will be provided with interface members and hardware designed to be interchangeable with the LEM Descent Stage where it attaches to the shroud and to the Ascent Stage.

The configurations using the LEM Ascent Stage with a platform (in lieu of the Descent Stage) will weigh approximately 363 kg (800 lb) less than the Descent Stage structure.

The platform is conceived to be made up of an I-beam structure and a web skin or floor. The LEM Ascent Stage is mounted to the upper face of the platform while the platform corners mate with the LEM adapter shroud. The telescope(s) is mounted to the underside of the platform.

A truss frame configuration may also be considered as a substitution for the Descent Stage. This will produce a weight savings of 453.6 kg (1,000 lb). The truss then becomes the interface between the LEM Ascent Stage and the LEM adapter shroud. The telescope can be readily fastened either to the LEM or to the truss framework.

The interface structure for other OTES configurations consists of struts between the spacecraft structure and the four LEM adapter shroud attach points which are similar to the LEM Descent Stage struts.

There will not be any change to other interfaces such as the LEM adapter shroud, SM, or IU. Some spacecraft candidates may incorporate packaging tie rods during launch to stabilize spacecraft portions which hang down into the center of the IU. Such rods would be disconnected for spacecraft separation.

Various candidate concepts were considered as housed within the nose envelope of the Centaur Shroud. This envelope is a 6.60 m (260 inch) diameter nose fairing over the payload area of the Centaur propulsion unit or the SM propulsion unit. The payload volume here is less than for the LEM adapter shroud. The Centaur shroud separates into halves which eject outward. The shroud interfaces at the bottom with the IU and at the top of the cylindrical section with the propulsion unit. As a general case, the OTES is supported atop the propulsion unit on an adapter skirt. Spacecraft launch loads are transmitted through the adapter skirt to the propulsion unit, then into the upper end of the shroud, through the shroud, and into the IU. When the shroud is ejected, the spacecraft loads, not necessarily launch loads, are transmitted through the adapter skirt to the propulsion unit.

11.3.1.4 Spacecraft Hull Design

The configurations discussed in subsection 11.1 present a wide variety of different approaches to spacecraft design. All manned and unmanned spacecraft of the size required to house the recommended telescopes must have a large spacecraft hull structure.

The configurations mentioned above can be divided into two categories. One category utilizes the LEM Ascent Stage with the telescopes attached. The other category is a completely new spacecraft and does not utilize any previously developed major subsystems. Use of the LEM Ascent Stage eliminates the need for developing a large number of structural and mechanical subsystems. The hull design becomes limited to a pressurized access compartment. Its small size and exposed area do not pose any significant design problems.

The new spacecraft configurations become the most important area for research in this study by virtue of their inherent complexity and size. Therefore, the hull design effort was directed to new manned spacecraft configurations. The spacecraft is housed in a shroud so the hull will only be designed as a pressure hull and to transfer launch loads. All external aerodynamic and launch loads will be carried by the shroud.

All new configurations will have hull designs capable of providing a "shirtsleeve" cabin envrionment for the mission. The final cabin wall must provide the pressure container for the 0.344 bar (5 psi) atmosphere and to protect the occupant from the thermal, radiation, vacuum, and micrometeoroid environment of space. The hull must also support all spacecraft equipment during launch. Telescope launch loads, because of their size, will be directed as closely as possible to the shroud interface structure.

The hull design in this study will be based on launch loads, pressurization, and micrometeoroid protection. Radiation and thermal design considerations were not considered in this phase of the study.

Micrometeoroid shielding protection was concentrated on developing a two-layer sandwich construction. This system provides the greatest efficiency for penetration protection.

The micrometeoroids are disintegrated upon impact with the bumper or outer skin. Their kinetic energy is then dissipated in the foam layer between the skins. The inner skin, which also serves as a pressure hull, then absorbs the remainder of the meteoroid impact energy. Present penetration information deals with single plate thicknesses.

The use of multi-layer panels introduces efficiency factors. These are represented in figure 11.3.1.4-1.(3)

For a .025 m (1 inch) spacing, the efficiency factor for a foam-filled core is K - 0.34. Micrometeoroid penetration of a single sheet of aluminum is given by(2)

$$P = 2.28D \left[\frac{P_m}{P_t} \frac{V_m}{C_t} \right]^{2/3} \qquad (8)$$

It has been shown in the referenced document that the required thickness ($\bar{t}$) necessary to stop a penetration depth P is 1.5P.

$$\bar{t} = 1.5P \qquad (9)$$

Including the efficiency factor K

$$\bar{t} = 3.42K \left[\frac{6\ m}{\rho_m} \right]^{1/3} \left[\frac{\rho m}{\rho t} \frac{V_m}{C_t} \right]^{2/3} \qquad (10)$$

---

(3) ML-TDR-64-40, Space Materials Handbook, Wright-Patterson A.F.B., January, 1965 LMSC.

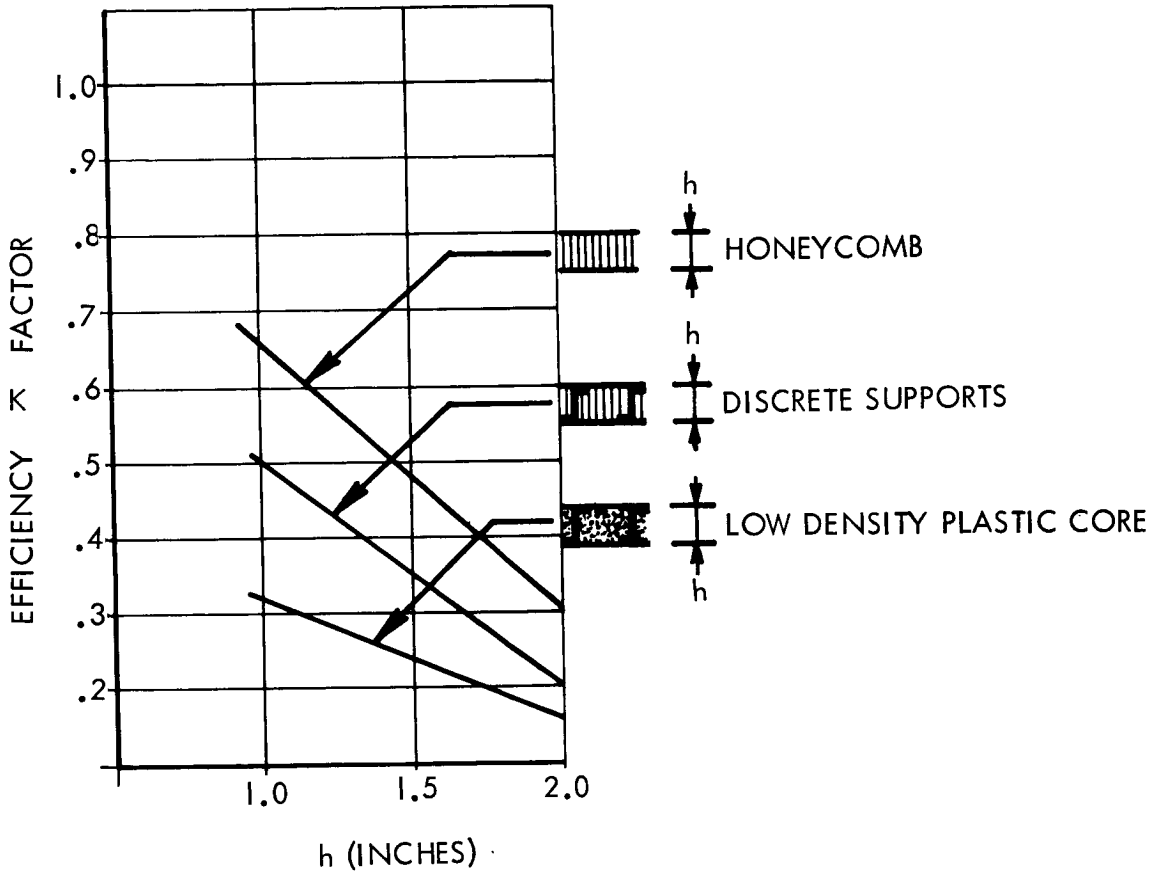


Figure 11.3.1.4-1. Efficiency Factors for Candidate Spacecraft Hulls

Where:

t = target

m = meteoroid

ρ_m = mass density of meteoroid from updated reports = 0.5 gm/cc

ρ_t = mass density of hull A_1 at 2.77 gm/cc

C_t = velocity of sound in hull A_1 at 5.104 k/sec

V = velocity of meteoroid at 30 k/sec

d = diameter of meteoroid = $\left(\frac{6m}{\rho\pi}\right)^{1/3}$; $V = m/\rho = 4/3\ (\pi d^3/8)$

$\bar{t}$ = equivalent hull thickness.

Solving for $\bar{t}$

$$\bar{t} = 1.89m^{1/3} \qquad (11)$$

(From subsection 11.3.1.2 equation number (7).

$m = 0.00568$ gm

Then $\bar{t} = 0.337$ cm (0.132 inches)

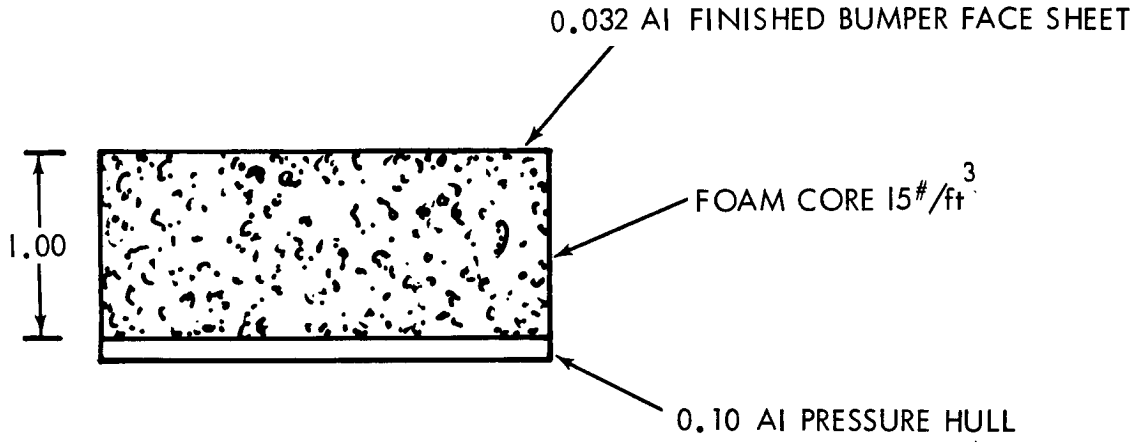
This is the required or equivalent thickness of aluminum shielding required for adequate meteoroid protection (as presented in subsection 11.3.1.2).

The aluminum sheets will be sized as follows. A 0.084 cm (0.032 inch) face sheet and a 0.254 cm (0.10 inch) inner sheet will be used for the pressure hull. A 2.54 cm (1.0 inch) space filled with foam will separate the sheets. This section is shown in figure 11.3.1.4-2. This cross section does not apply to configurations using the LEM Ascent Stage. These configurations have pressurized access compartments which are smaller in area and subsequently can be designed with less micrometeoroid protection.

The aluminum alloy chosen for the hull is Kaiser Aluminum 7039. This material has improved ballistic properties and resistance to spalling on impact by high-velocity projectiles. Also, it has good weldability, formability, corrosion resistance, and cryogenic properties.

A

MANNED SPACECRAFT HULL CROSS SECTION



B

UNMANNED SPACECRAFT HULL CROSS SECTIONS

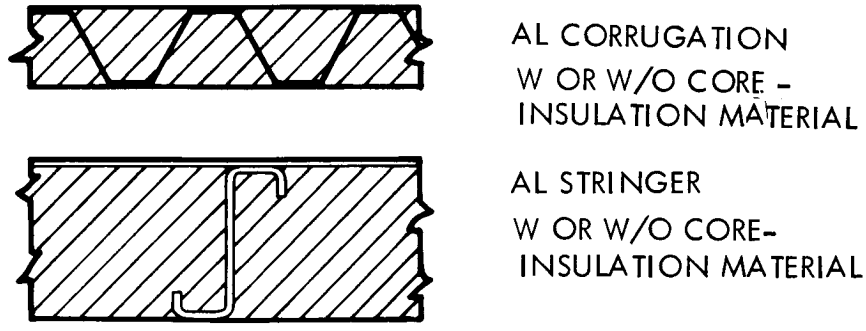


Figure 11.3.1.4-2. Spacecraft Hull Cross Sections

The most efficient foam core density cannot be accurately determined at this point. Literature on the subject shows wide variances in values.(4) However, for this study a value of 240 kg/m^3 (14.7 lbs/ft^3) will satisfy most of the research information on this subject.

The hull is also designed as a pressure vessel. Airborne pressure vessel design experience is provided almost entirely by aircraft cabin design. The criteria for operational transport cabin design is based on fracture-safe design.

Fracture-safe design is based on pressure, compartment geometry, and operating stress level. Aircraft are proof pressure designed to (limit pressure) times (1.33) being equal to (proof pressure) and an ultimate factor of 2.0 on limit pressure for the cabin. These are overshadowed by the fact that equivalent fracture factor of 4.0 is required for fracture-safe design. This factor is obtained by dividing the hoop tension stress (at limit pressure) into the ultimate tensile stress of the material.

Aircraft cabins encounter a different loading environment than a spacecraft cabin, but both must survive a large tear or a possible crack propagation. The spacecraft cabin will, therefore, be designed to the same criteria as a transport cabin with a factor of 4.0.(5)

Local areas of increased stress (like the bulkhead to cylinder interface) will be locally reinforced so as not to jeopardize the efficiency of the entire hull. The hull is designed for an operating pressure of 0.340 bar (5 psi). The limit pressure is 0.413 bar (6 psi) at which relief valves are set. Such measures as leaving the docking port open during launch will be taken to ensure that the hull will bleed the atmospheric pressure of 1.015 bar (14.7 psi) during launch.

The hoop tension stress will be limited by the fracture factor to Ftu/4 which is 4,000 bars/4 (58,000 psi/4) or 1,000 bars (14,500 psi). The thickness required for this stress level is consistent with that required for micrometeoroid penetration (see figure 11.3.1.4-2).

---

(4) NASA SP-48 Space Cabin Atmospheres, "Fire and Blast Hazards from Meteoroloid Penetration". Roth, E.M., M.D. 1964.
Rolsten, R.F. and Hunt, H.H. "Bumpers and Core Materials for Meteoroid Protection", Space/Aeronautics, September 1963, p. 105.
Pipitone, S.J., and Reynolds, B.W., Meteoroid Protection System for Space Vehicles, Goodyear Aircraft Corp., Akron, Ohio - AIAA Launch and Space Vehicle Shell Structures Conference, 4/1/63.
Hammitt, R.L., and Riedinger, L.A., The Effects of Space Environment on Optimum Multi-wall Structural Design, Lockheed Missiles and Space Company, Sunnyvale, California.

(5) NASA-SP-65 Abraham, L.H., Spacecraft Systems, Volume 1, 1965, DAC.

Efficient pressure hulls are almost entirely constructed with single skins. Pressure hulls constructed from sandwich panels tend to load the outer skin instead of both skins in amounts dependent upon the elasticity of the core material. The result is a complicated load-bearing panel.

The outer-face skin of the cross section shown in figure 11.3.1.4-2 is not continuous and is free to float on the foam core. This eliminates transferral of thermal distortions from the face skin to the pressure hull sheet. In addition, it establishes a single load path whereby all pressure loads are reacted by this inner skin.

Single skin pressure hulls greatly simplify manufacturing and fabrication. Large sandwich panel pressure hulls of this size have had limited development. Therefore, it is felt that until better techniques of sandwich construction are developed in this size, it would be quicker and more efficient to have a single skin pressure hull with a core and loose fit bumper mounted to it later.

The manufacturing sequence will be to: (a) fabricate the pressure hull, (b) install all major equipment in the hull through the telescope well openings, (c) install the assembled telescope well assembly, and (d) install minor equipment through the docking hub.

Honeycomb sandwich panels have been investigated in this report and initial research data indicates that it could be structurally efficient as a hull. However, honeycomb sandwich panels are very inefficient as micrometeoroid barriers because the core, which tends to expand upon impact, causes severe deformations on the back surface.

Self sealing hulls which have also been investigated might eventually have some application in this program. Follow-on studies will investigate these possibilities in greater depth.

Unmanned spacecraft and some configurations utilizing the LEM Ascent Stage require a simpler spacecraft structure. This structure is only required to react launch loads and to provide the proper thermal protection. No internal pressure requirements exist. Greatly reduced design requirements (as compared with manned spacecraft) exist on unmanned spacecraft for thermal, radiation, and micrometeoroid shielding.

These structural requirements have resulted in the evolution of two types of structure by the aircraft industry which need no justification here. The first type is composed of aluminum corrugations with face skins. The second is composed of aluminum skin and stringers. Both types, which are shown in figure 11.3.1.4-2 can be filled with foam material to serve either as a micrometeoroid barrier or as insulation.

Telescope well housings on most configurations using the LEM Ascent Stage will be made from one of these two hull designs. Unmmaned configurations will also employ these sections.

The differences in hull construction between manned and unmanned spacecraft point out a significant weight penalty for manned capability. This penalty, which will be determined, will become an ingredient in the man-versus-unmanned trade-off analysis.

11.3.1.5 Docking

All Candidate Spacecraft Concepts (manned and unmanned) have facilities for docking with the Apollo CSM. The philosophy is to accept the Apollo CM as a standardized vehicle and to equip the OTES spacecraft to accept it by docking operations. Those OTES configurations which use the LEM Ascent Stage are already equipped.

Docking loads result from impact during joining and from the inertial forces during maneuvers when the OTES is coupled to an Apollo CSM. Some configurations are based upon a smaller engine than that normally used on the SM. However, the intention is to design the docking structure to accommodate maneuver loads resulting from use of the higher thrust engines.

11.3.2 Light Baffle

The light baffles required by the telescopes will be designed in accordance with the latest available analytical and empirical data. An analysis of baffle systems has been completed and will be used for these designs.(6)

11.3.3 Telescope Well

The telescope well is a cylindrical housing for the telescope. The primary purpose of this well is to act as a thermal and pressure barrier.

The telescope is sensitive to thermal gradients. The telescope well may be designed to minimize these gradients. Since many of the spacecraft configurations are manned they require cabin pressurization. The telescope well allows one end of the telescope to be open for viewing while maintaining cabin pressure.

Some configurations require maintenance to the telescope or equipment within the well. To facilitate such maintenance, a hatch has been proposed for the open end to allow the telescope well to be pressurized

---

(6) Broscious, R.K., Light Baffles for Space Optics, CCSD Technical Bulletin TB-AE-66-359, July 1966.

intermittently for the convenience of the man doing the maintenance. The well shall then be treated structurally as a pressure vessel with the pressure differential of 0.344 bars (5 psi) acting externally.

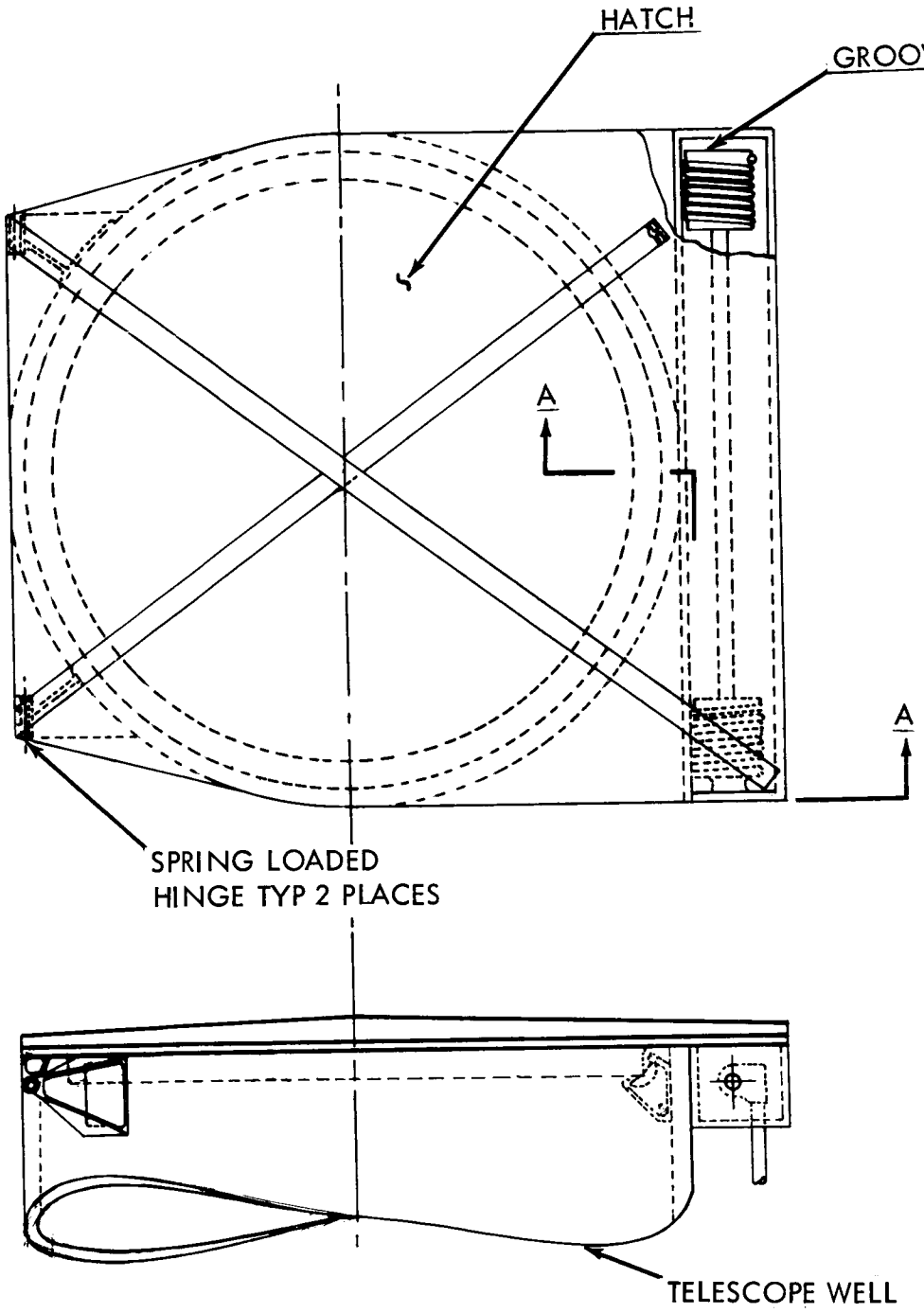
The telescope well will interface with the spacecraft at a single firm attachment. This interface will transmit launch loads as directly as possible to the shroud interface structure. Other interfaces will be flexible to prevent thermal distortions of the spacecraft from reacting upon the well. The size of the well is dependent upon the spacecraft envelope, telescope size, suspension system, and the maximum gimbal angle of the telescope. There is then a major trade-off between well size and experiment objectives.

In this phase of the study, there was no attempt to structurally design the telescope well. It is anticipated that preliminary design in this area will be performed in subsequent phases of this study. It should be pointed out, however, that there is a major trade-off in this area which must be developed. This trade-off will be between structural and thermal requirements. Thermal problems will dictate that the insulation be attached to, or sandwiched within, the wall of the well. Material selection for the structure will also be affected by thermal considerations. For example, the heat conduction advantages of beryllium may have an influence.

All configurations shown in subsection 11.1 and 11.2 (except the unmanned versions) have telescope wells with hatches at the open end. The purpose of the hatch is to enable the telescope well be be pressurized. This permits access to the telescope interior while maintaining a "shirtsleeve" environment. Hatch design requirements are dimensions of 0.76 to 1.52 m (30 to 60 in) in diameter, the capability of manned or remote operation, the ability to be opened and closed periodically during the entire mission, and the ability to withstand an internal pressure of 0.344 bars (5 psi). Pursuant to this criteria, the hatch mechanisms must be capable of operation in a space environment. Cold welding caused by vacuum and radiation effects on lubricants must be considered in preliminary design.

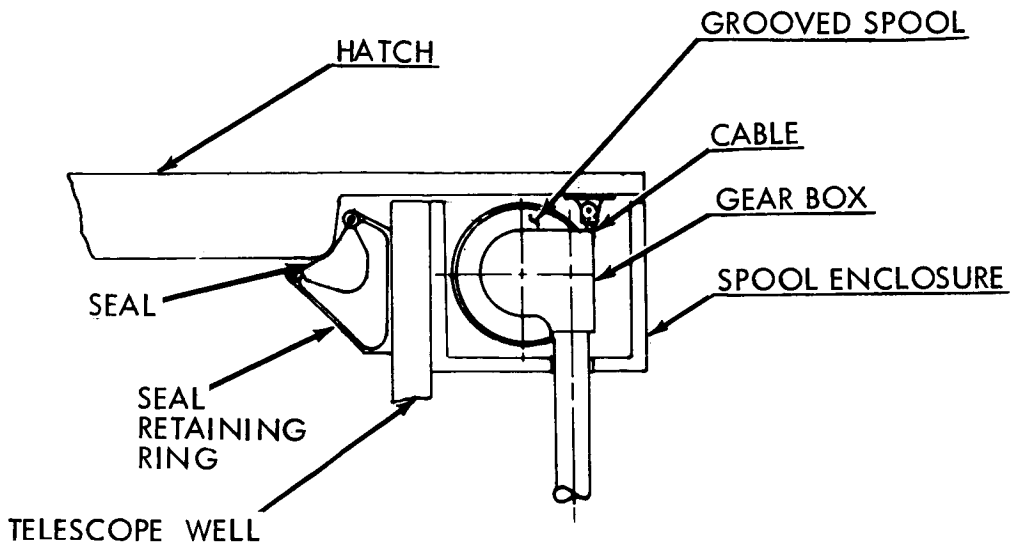
Since the hatch design has a definite impact on the well and baffle configurations, an investigation was performed on the different means of satisfying the hatch requirements. To this end, five different configurations were developed. These appear as figures 11.3.3-1 through 11.3.3-5.

The hatch depicted in figure 11.3.3-1 utilizes a cable spool method of activation. The hatch has spring-loaded hinges and is opened and retracted by the cables on the spools. The seal is a continuous neoprene type set in a special retaining ring. The hatch depresses the seal and the internal pressure energizes it.



PRECEDING PAGE BLANK NOT FILMED.

)OL



SECTION A-A

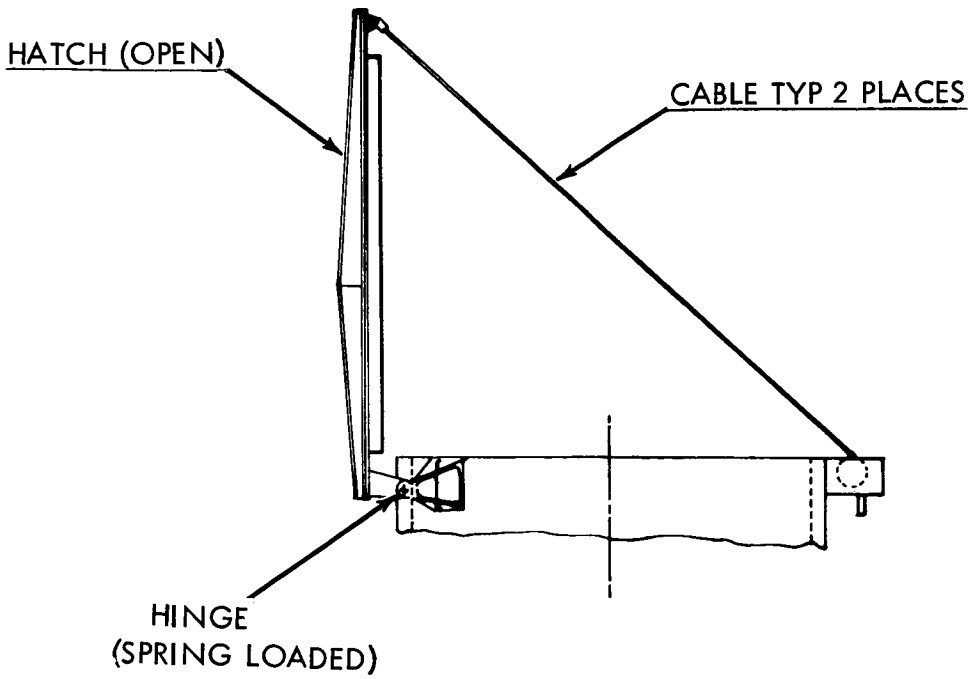
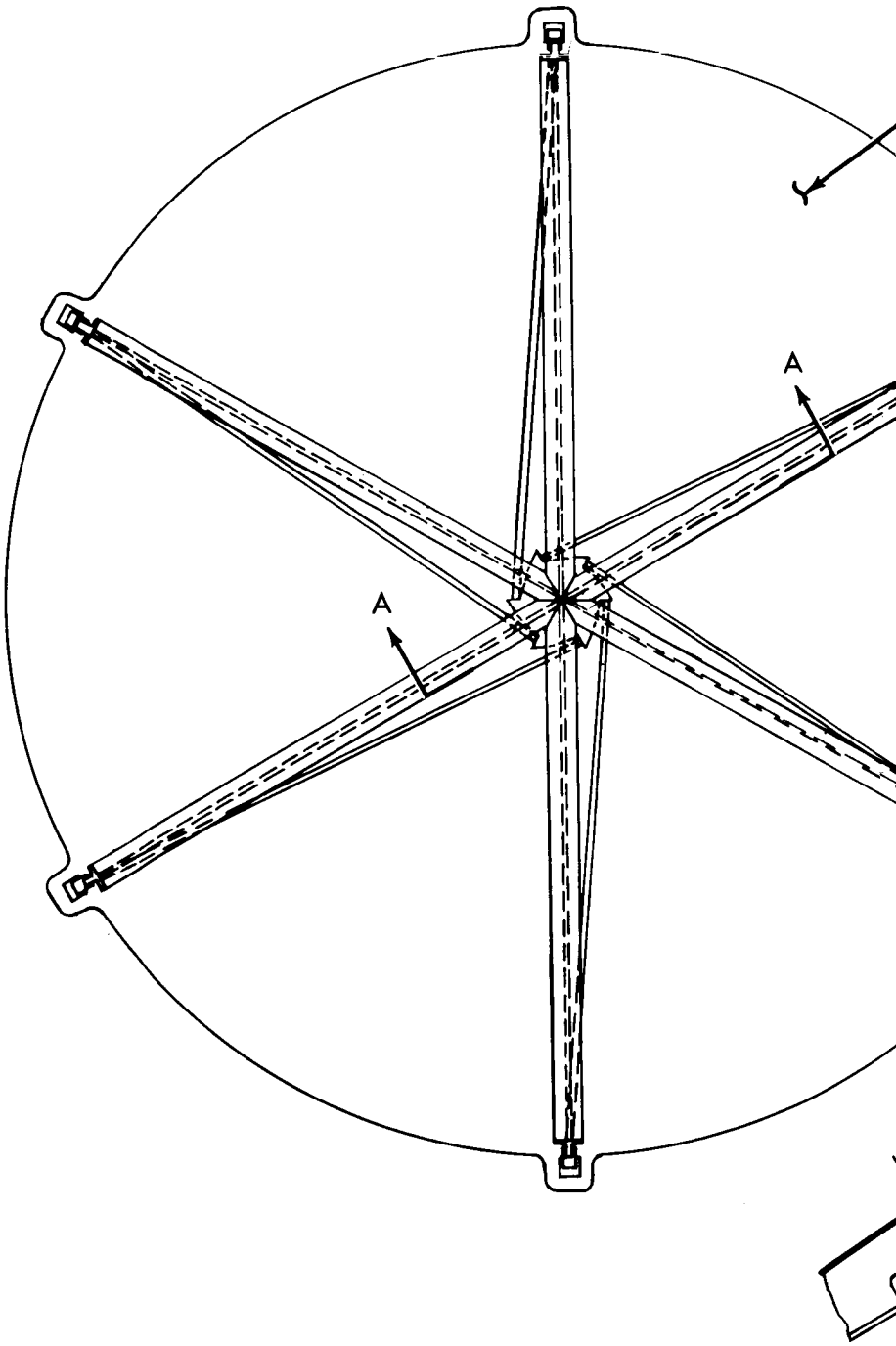


Figure 11.3.3-1. Telescope Well Hatch

~~2-189~~
2-190


A
A

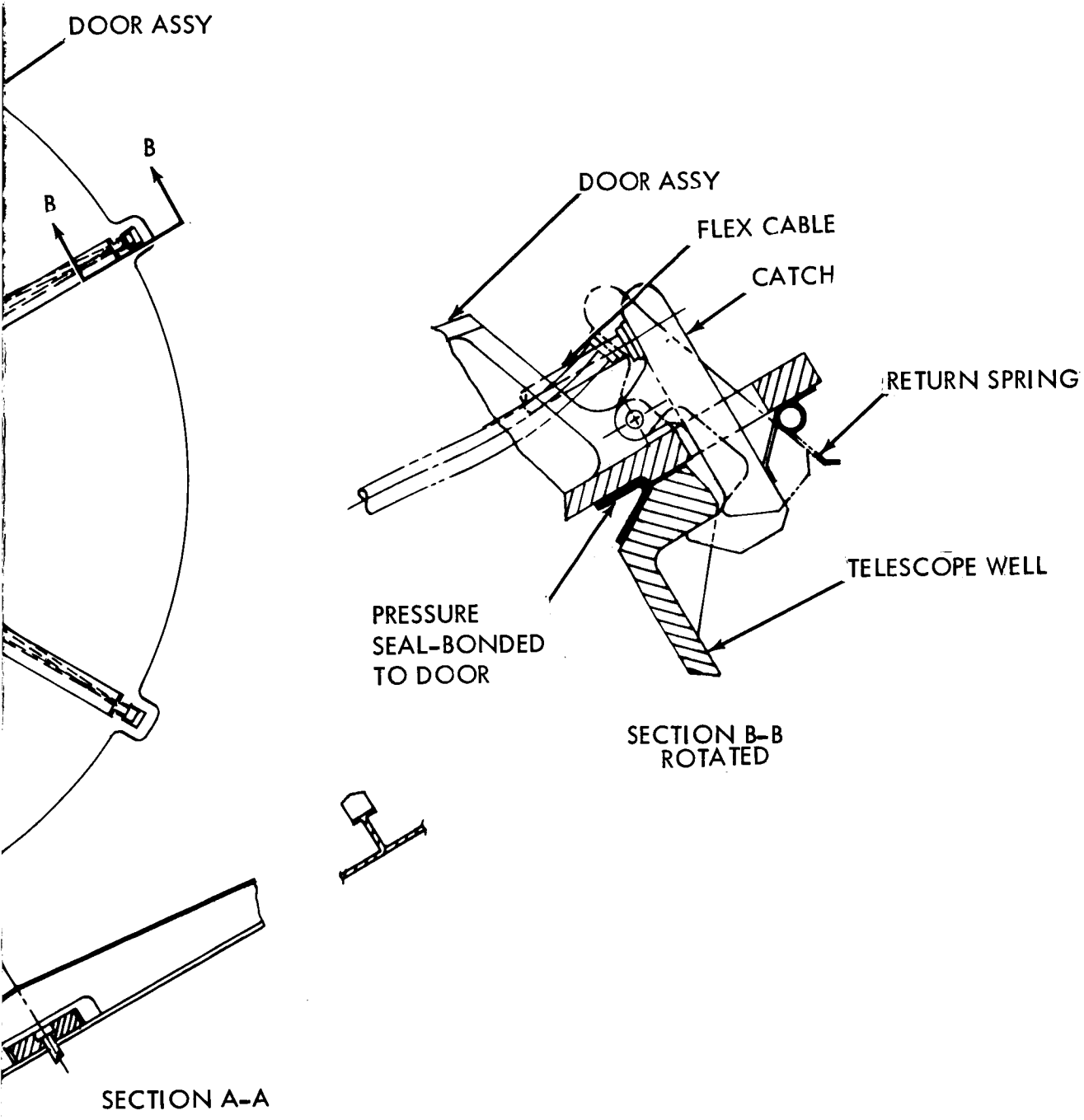
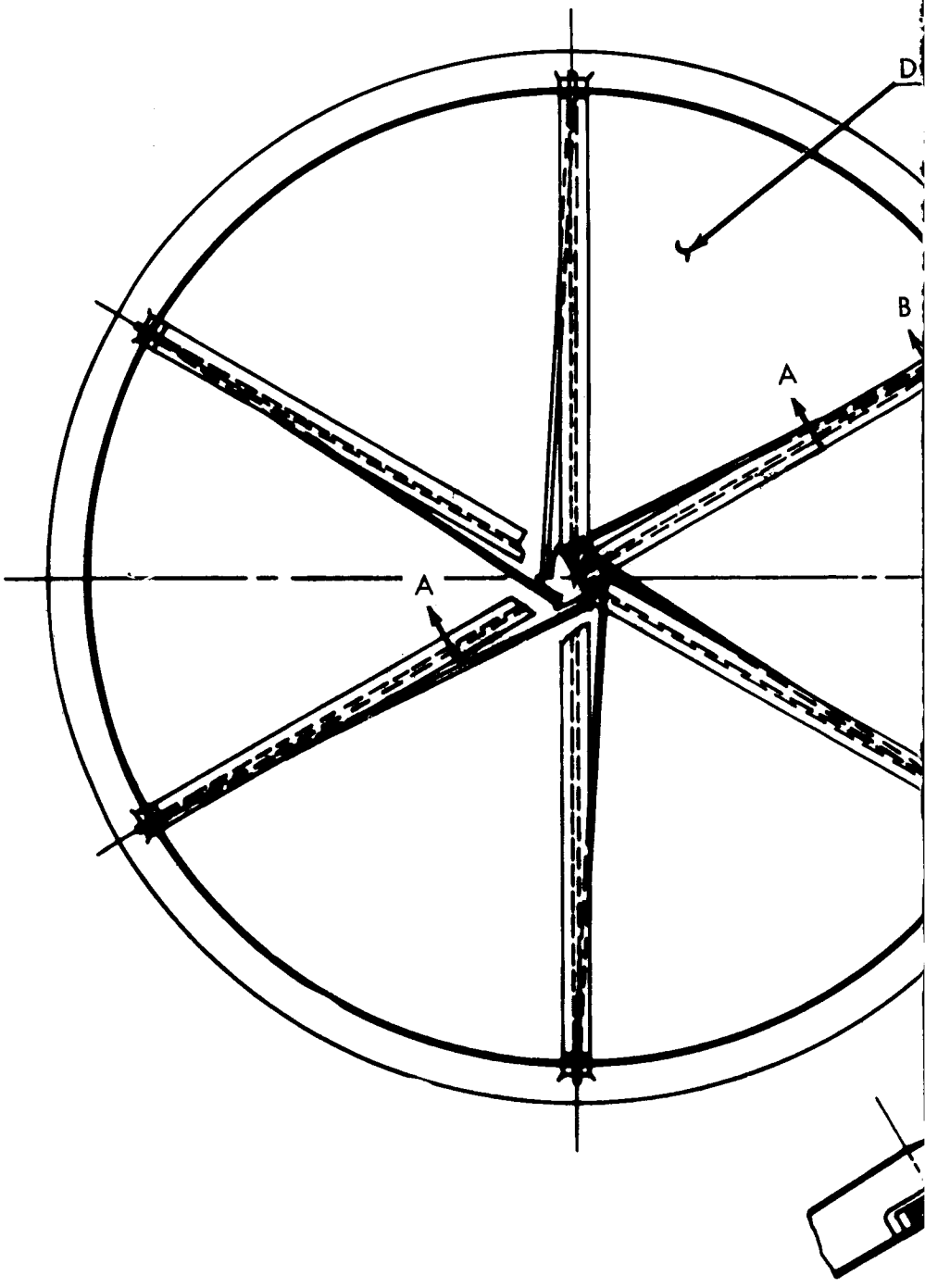


Figure 11.3.3-2. Telescope Well Hatch


D
B
A
A

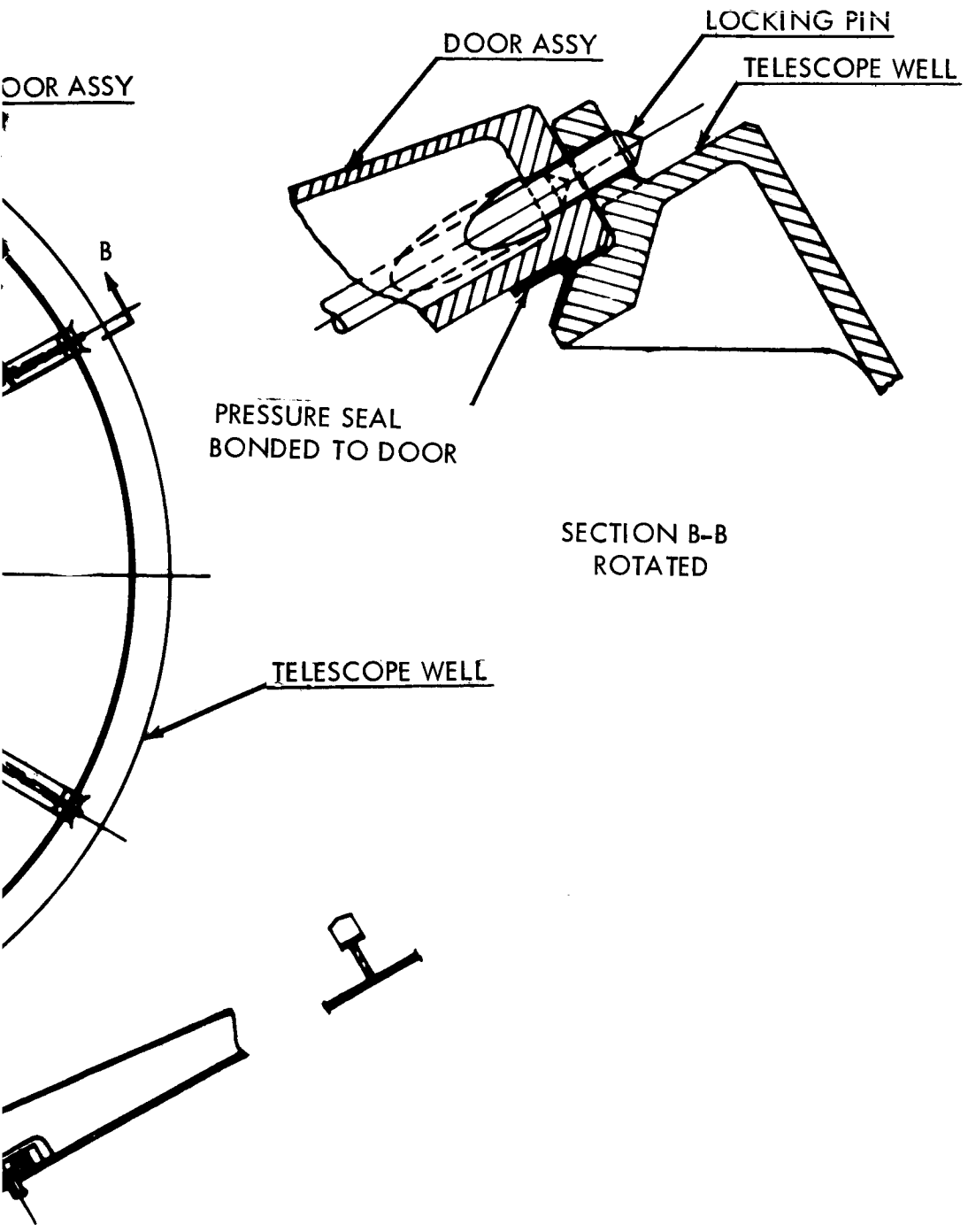
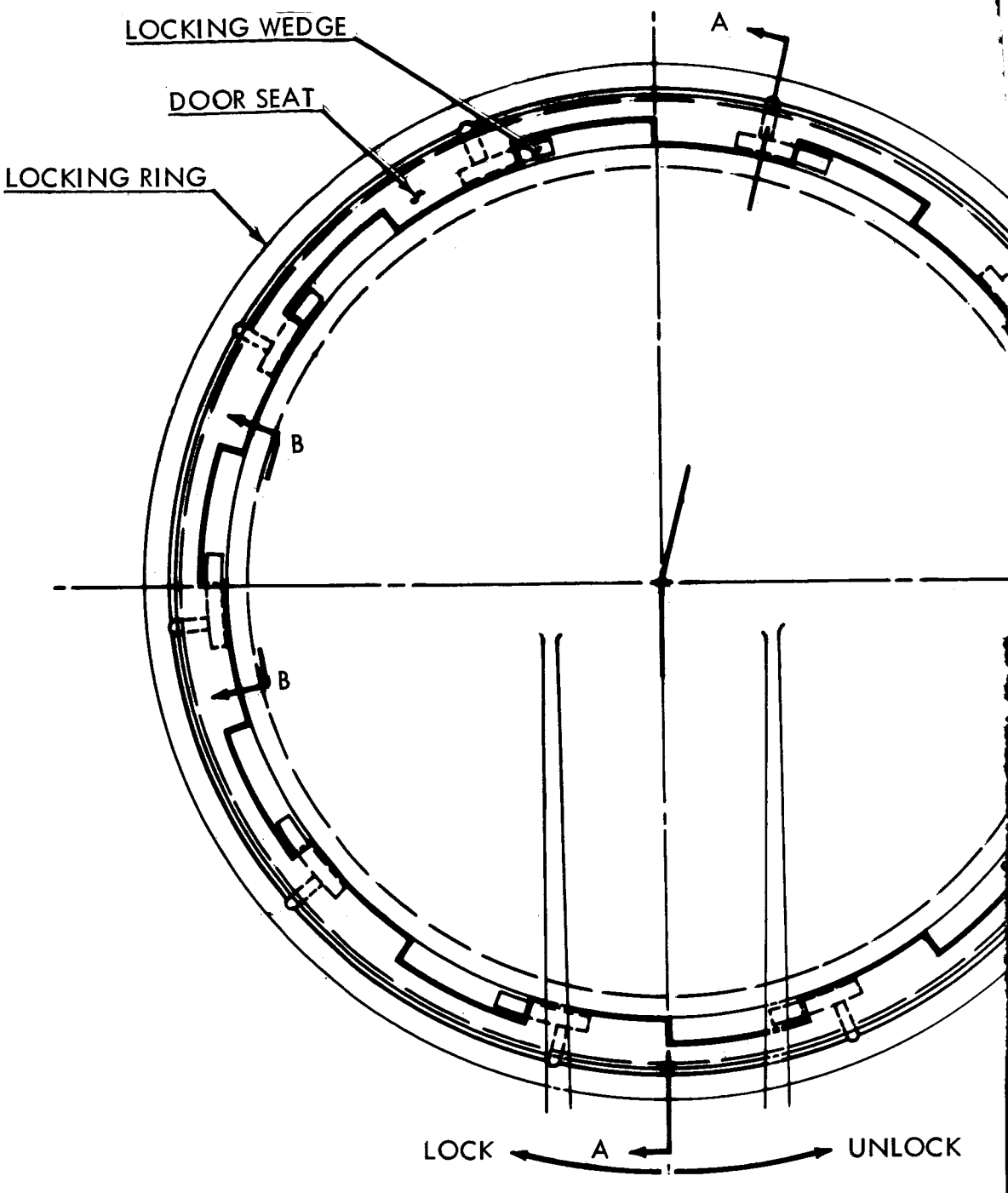


Figure 11.3.3-3. Telescope Well Hatch


LOCKING WEDGE
DOOR SEAT
LOCKING RING
A
B
B
LOCK
A
UNLOCK

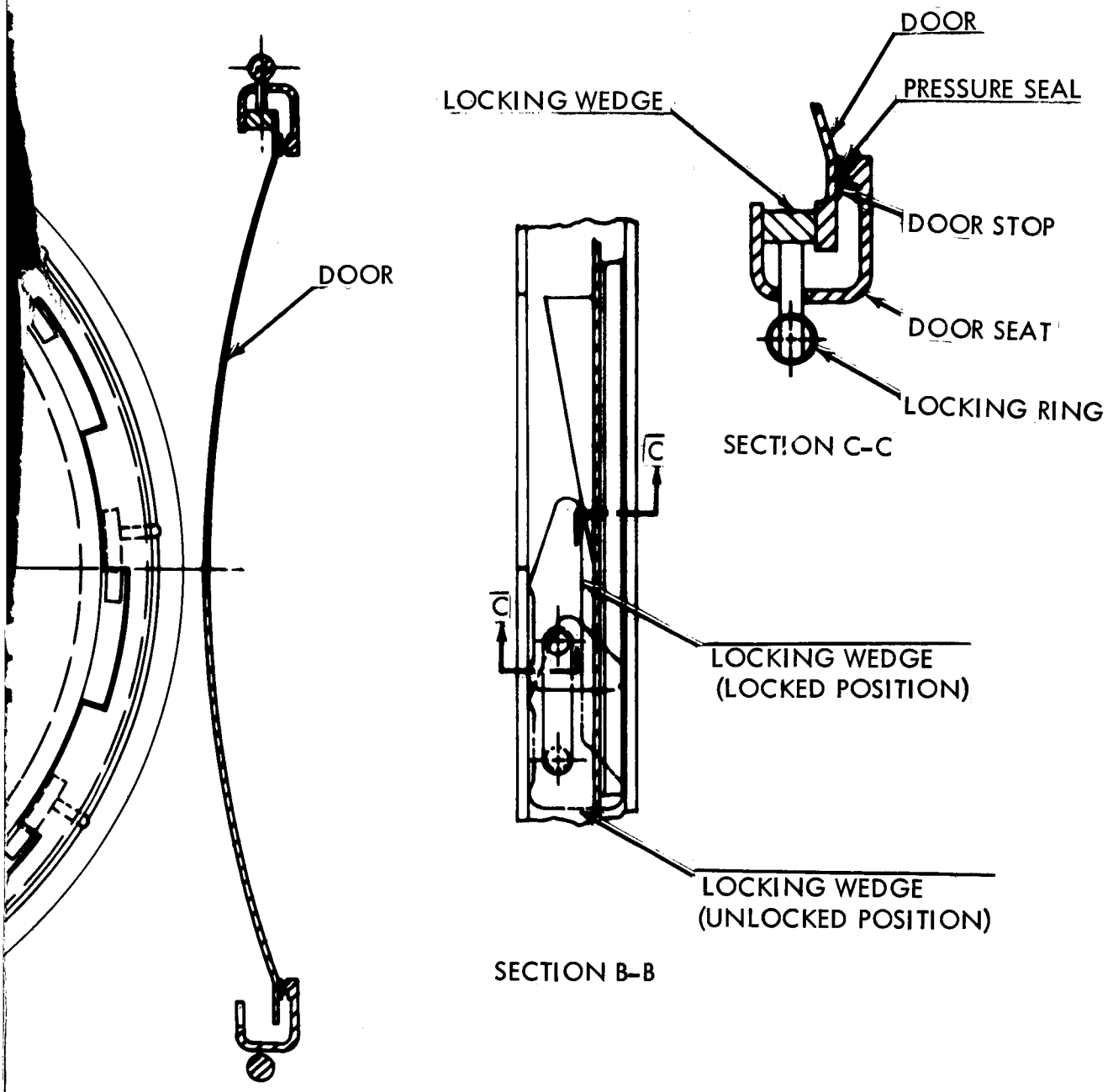
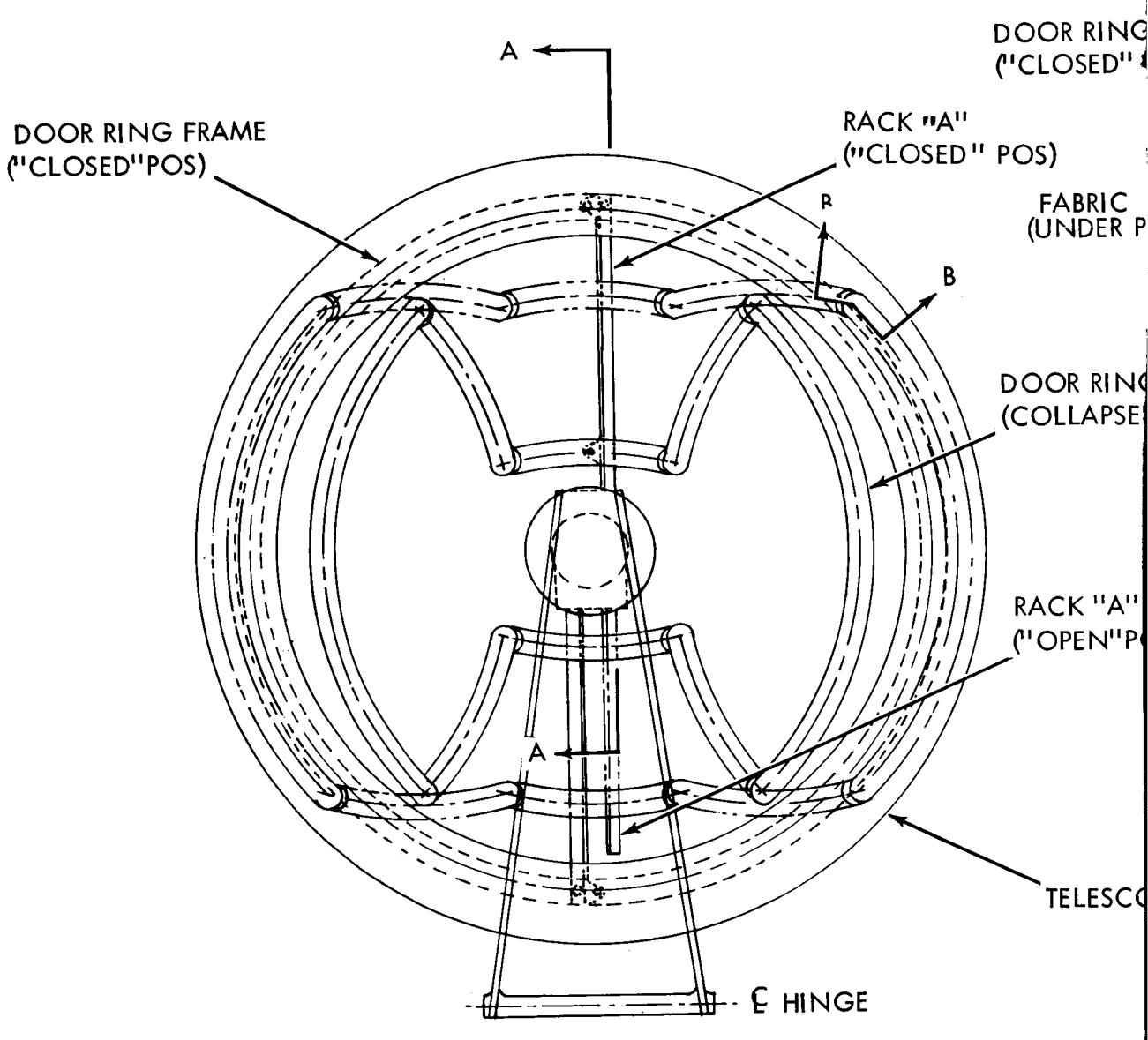
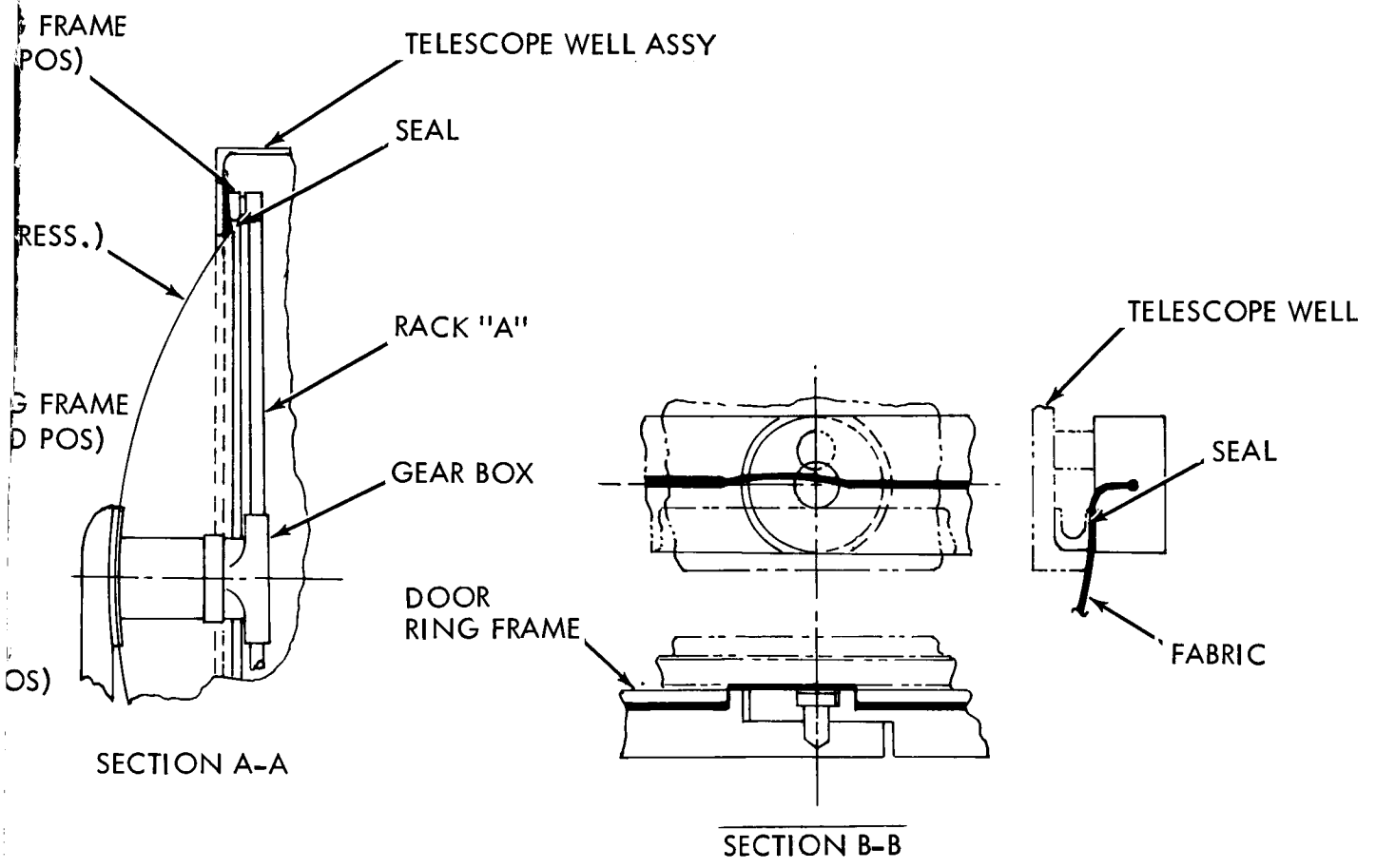


Figure 11.3.3-4. Telescope Well Hatch



FABRIC NOT SHOWN THIS VIEW



OPE WELL ASSY

Figure 11.3.3-5. Telescope Well Hatch

~~2-197~~
2-198

The hatch shown in figure 11.3.3-2 employs a series of spring-loaded catches. Opening is accomplished by rotating the center wheel. The wheel retracts flexible shafts which, in turn, retract the catches. A power-actuated hinge (not shown) then swings the hatch open. Closing reverses the procedure except that the center wheel does not have to be rotated. The spring-loaded seal is bent into position upon closing. Internal pressure then acts against it to form a pressure energized seal.

The hatch configuration shown in figure 11.3.3-1 is similar to figure 11.3.3-2 except the flexible shafts retract locking pins. The seals are as before.

The hatch shown in figure 11.3.3-4 uses a locking ring. The ring has a series of locking wedges attached to it. When the ring is rotated to lock the hatch, the locking wedges move upon an inclined surface. The incline surface is mounted on the hatch dovetails, whereas, the locking wedges are housed in the open position, under the hatch seat dovetails. The locking wedges move from their position, on to the inclined surface forcing it down and locking it. Open reverses the above procedure. The seal remains as mentioned earlier. The hatch is opened after unlocking by a power hinge (not shown).

The last hatch configuration, is shown in figure 11.3.3-5, flexible fabric. The fabric is mounted on a collapsible ring. The collapsed ring is rotated in the seat. Then the ring is opened to mate with the seat. The rotating mechanism then pulls the hatch up against the seal. Pressure in the well forces the hatch against the seat and the seal is pressure energized.

As a result of this investigation, it was concluded that the hatch design would be compatible with the baffle designs under consideration.

11.3.4 Deployable Equipment

The deployable equipment required on the OTES spacecraft are antennae, solar panels, extendable telescopes, and such auxiliary support instrumentation as interferometers.

11.3.4-1 Antennae Deployment

Antennae deployment was not considered in this phase. The level of effort in subsequent studies will be to provide mounting points and the required envelope, and to develop the structural and mechanical interface.

11.3.4-2 Deployable Solar Panels and Arrays

The solar panels and arrays are presented in subsection 11.5. Their efficiencies as power systems were discussed and the feasible combinations of solar panels were condensed to a trade-off between single blade oriented panels and three bladed fixed arrays.

The panel or array configuration when packaged or deployed is dependent on the area required, axis location, packaging envelope (which encompasses the shroud envelope and spacecraft envelope), and launch environment. Deployment will be accomplished by hinges that are spring actuated. The springs will be released in a sequenced fashion and the hinge will lock when it is fully opened. These movements, which will take place upon entering an orbit, will keep to a minimum the amount of time the arrays and panels will be packaged in a vacuum. It is anticipated that this short time element will eliminate the problem of elaborate preparations of the hinges to guard against vacuum cold welding and lubrication sublimation.

It is apparent that the reliability of the system decreases as the number of individual movements increases. This can pose significant problems where envelope constraints dictate efficient packaging volumes.

The two types of panels and arrays mentioned before present different problems. The oriented panel, with its inherent efficiency, is the smallest and therefore the simplest to pack. Its size, approximately 11.6 m^2 (125 ft^2)), and flat deployed configuration readily lends itself to all configurations utilizing the LEM ascent stage.

The continuous panel orientation requires a mechanism consisting of a motor and gear train. This mechanism has been developed, tested, and used by two manufacturers and would be suitable for application here. The manufacturers and products are: the United Shoe Machinery harmonic drive, and the Mariner Mars planetary scan drive.(7)

The three blade array is a fixed configuration. It requires approximately four times the surface area required by the oriented panels or approximately 46.6 m^2 (500 ft^2). Packaging and deployment then become more difficult as either a larger unrestricted envelope is required or more movements are necessary to fold the array into a smaller volume. The three blade array when adapted to configurations using the LEM ascent stage develop very serious packaging and deployment problems. Configurations without the LEM ascent stage have larger usable envelopes which are required to house a three blade array.

The present design is to package the three bladed array by rotating one blade 120 degrees and then folding the entire array against the spacecraft. The 120 degrees break in the packaged array improves its packaging configuration when folded back against the spacecraft. The fixed array might also require a 30 degree rotation of the entire array upon deployment. This movement can be performed by a slotted spiral hinge that would rotate the support arm upon unfolding.

---

(7) NASA SP-66 Space Technology, Volume II-Spacecraft Mechanical Engineering, Adams.

Launch loads are reacted by a mounting structure on the spacecraft. The weight of the arrays and panels (4.95 to 7.43 kg/m^2 (1 to 1.5 lb/ft^2)) indicate that launch loads should not pose a significant problem.

11.3.4.3 Extendable Telescopes

Configurations requiring extendable telescopes are presented in subsection 11.1.2. The advantage of this telescope is that the LEM Ascent Stage with a simple platform structure can be used. In addition, it permits the large SM engine to be used.

An extendable telescope is definitely an advancement of the state-of-the-art. It would require a complex mechanical system to position the lenses accurately. This problem is compounded by the design requirement dictated by a space vacuum and radiation environment. High tolerance mechanisms required for accurate positioning are degraded by vacuum cold welding. Because of these problems, the configuration received a low priority rating for this phase of the study. Continuing studies will be conducted in this area in an effort to investigate this system for future application and in particular as a possible OTAES experiment.

11.4 STABILIZATION AND CONTROL

The scope of the stabilization and control effort during Phase I has been to determine the requirements and to do the parametric analyses required before starting the preliminary design work in Phase II. Also, since the overall control system configuration chosen is fairly complex, some of the dynamics of the system was studied to determine if any particular problem areas exist.

Much of the work performed in this study which might be considered a part of the stabilization and control effort proper is reported in other sections. For example, much effort was devoted to a detailed analysis of the disturbance environment both internal and external to the spacecraft. However, since this information is required in such detail only for the Isolation Techniques Comparison experiment and the Fine Guidance experiment, all work concerned with the disturbance environment is reported in section 4.13. Some of the control system trade-off areas are discussed there also, since spacecraft control capability is an important parameter in the design of suspension systems.

11.4.1 Requirements

The primary purpose of the spacecraft attitude control system is to support the experiments. Modes of operation other than experimental, for example, acquisition, rendezvous, etc. will impose attitude control requirements. But the missions are not defined in enough detail to treat these requirements in other than a parametric fashion. Therefore, only the experimental support requirements are considered in any detail here.

At the initiation of this study, the only experiment imposing severe stabilization requirements was the LASER beam pointing experiment or 0.1 arc second beam pointing and tracking experiment, as it is now called. Both the spacecraft control and stabilization requirements and the basic overall control approach were formulated on the basis of the requirements of this one experiment. As the study has progressed, other experiments, some of which impose greater requirements, have been added. In particular, the fine guidance telescope, which incorporates several experiments, was added. Now, the requirements imposed on the spacecraft control system, by these experiments cannot be simply stated, because they are dependent on the technical approach and are subject to many trade-offs. Therefore, the discussion which follows is designed to show the trade-off areas and how the requirements were derived.

First, the basic requirement for pointing the LASER telescope is 0.1 arc seconds in both stability and accuracy and arises from the fact that for two way optical communication at narrow beam-widths the transmitting telescope must be pointed at the ground-station to an accuracy comensurate with the beam-width, namely, 0.1 arc seconds. To establish a

reference from which to effect this pointing the receiving telescope must track the upcoming beam to the same accuracy. However, because of transit times the transmitting telescope must incorporate a certain lead angle, rather than pointing in the apparent direction of the received signal. This is the basic knowledge from which the spacecraft stabilization and control requirements were initially established. The following guidelines can be immediately established on the basis of this knowledge.

a. The transmitter and receiver must share the same optics. Otherwise, the alignment requirements cannot be met.

b. The lead angle requirement for the transmitter must be met by some means other than controlling the entire telescope because of the common optics.

c. The telescope must have angular freedom relative to the spacecraft since it is inconceivable that a manned spacecraft can be stabilized to 0.1 arc seconds.

d. If the lead angle capability can be provided by some component outside the common optical train at least part of the tracking requirements can be satisfied by a similar component within the optical train.

e. Although the basic optical system is symmetrical about the optical axis (excluding polarization considerations), a roll reference for implementing the lead angle is still required.

Starting with these guidelines the stabilization requirements can be quantitatively established. The lead angle requirements can be provided by a beam deflector, and the beam deflector can also be used in a fine tracking loop to provide part of the stability. The amount of stability that can be achieved in this way depends on the fine error sensor, the signal-to-noise ratio, and the type of beam deflector that is used.* Analysis showed that for the LASER pointing application, signal-to-noise-ratio is no problem, and the shear plate beam deflector can be used at the wavelengths being considered. This type beam deflector has a wide dynamic range and a response time measured in milliseconds.

Dynamic range of the beam deflector is limited by off-axis aberrations. Therefore, a high-gain wide bandwidth inner control loop can be used, which relaxes the pointing requirements for the telescope as a whole. The fine guidance loop provides only pitch and yaw control of the received beam. Roll stability requirements depends on both the required lead angle accuracy and the magnitude of the lead angle.

---

* Most of the points briefly noted here are covered in much detail in section 4, see, for example, sections 4.13, 4.12 and 4.5.

For two-way communication from Mars (a mission which the communication and tracking experiments of the present program are designed to simulate in some respects). It is required that a roll reference be established to within less than 1 arc minute. However, from synchronous orbit where the requirements are much less severe quantitatively, the telescope pointing requirements were established to be:

a. The telescope optical axis should be directed to within ± 1 arc minute of the apparent direction of the received beam.

b. A roll reference about the optical axis must be established to within ± 1 degree.

The requirements on spacecraft stabilization and control are determined by the angular freedom given the telescope relative to the spacecraft. For a number of reasons this quantity should be minimized within practical spacecraft constraints, constraints on man's movements and spacecraft attitude control system weight. Based on initial rough order of magnitude calculations, this requirement was set at ± 1 degree in pitch and yaw. Simultaneously, because of the less severe roll requirements, it was decided to provide only pitch and yaw freedom for the telescope relative to the spacecraft. Therefore, the stability requirements for the spacecraft were established as ± 1 degree for all three axes.

Much of the analysis presented in this section is based on these requirements. But, as pointed out previously, the addition of the fine guidance telescope and associated experiments has subsequently increased these requirements. Briefly, the reason is as follows. The objective of the fine guidance experiment is to compare the effectiveness of several fine guidance loop configurations in tracking dim stars to 0.01 arc second stability. There the maximum control bandwidth is limited by noise considerations so that the use of a fast beam deflector is of little value. The order of magnitude increase in stability requirements plus the noise-limited bandwidth of the fine guidance inner loop inpose severe requirements on telescope stability. In fact, analysis showed that to meet the telescope stability requirements for a manned spacecraft, an isolation system must be provided between the spacecraft and the telescope. The net result of this decision is that the spacecraft stability requirements are now determined by the isolation system rather than by the telescope pointing requirements. Based on the trade-offs between control system weight, constraints on crew freedom and isolation system design considerations, the spacecraft stability requirements have been changed to ± 6 arc minutes in pitch and yaw and remain at ± 1 degree in roll. Again, it should be pointed out that the results summarized here are covered in much detail in the experiment write-ups, particularly in section 4.13, Comparison of Isolation Techniques experiment.

11.4.2 Technical Approach

Long term stabilization of the spacecraft to the requirements imposed by the experiments implies the need for momentum storage devices, since a momentum expulsion system would consume too much fuel. A momentum-expulsion system is still required to periodically unload the storage device. Therefore, a hybrid control system approach was adopted at the outset of this study. The overall stabilization system is summarized as follows.

a. Fine guidance loop which acts to stabilize the optical image against both angle of arrival fluctuations and telescope motion. The sensor for this loop is inside the telescope and receives the light collected by the primary mirror.

b. Coarse telescope loop which receives its error signals from the fine error sensor, another error sensor inside the telescope (one with a wider field of view, for example) or from the beam deflector. The straightforward approach is to use the position of the beam deflector as a measure of telescope error, since the overall control philosophy is for the beam deflector to follow the incoming signal, the telescope to follow the beam deflector, and the spacecraft to follow the telescope. However, this makes the telescope stabilization dependent on the fine loop. The alternate approach of using an independent error sensor for the coarse loop is therefore attractive but causes an alignment problem.

c. Spacecraft control loop which receives error signals either from the coarse telescope loop sensor or from an angle transducer which measures the relative angle between the telescope and the spacecraft. This is for pitch and yaw control. Roll control error for the spacecraft is derived from a star tracker mounted to the spacecraft.

d. The spacecraft momentum-expulsion system which is actuated by signals from the momentum device. The part of the overall system with which this section is concerned includes only the components in the spacecraft, that is, momentum storage device, the momentum expulsion system, and the roll control sensor.

The two prime candidates for the momentum storage function aboard the spacecraft are reaction-wheels and control moment gyros. The control moment gyro (CMG) was tentatively selected at the outset for analysis purposes because of the relatively low power requirements.

At the same time, to gain a more comprehensive base of knowledge from which a firm decision can be made in Phase II, once the spacecraft and mission are defined, trade-off analyses were initiated and are reported in following subsections.

Basically, then, because of differing experimental requirements two overall stabilization systems are proposed.

a. 0.1 arc second tracking experiment. The fine loop consists of a four-quadrant error sensor and a shear plate beam deflector. Errors for the coarse telescope loop are derived from the beam deflector position and the actuators are direct-current, brushless torquers acting on the mechanical gimbals in which the telescope is mounted. Error signals in pitch and yaw for the spacecraft control system are derived from angle-pickoffs on the gimbal axes and drive a two-degree-of-freedom CMG in the spacecraft.

b. Fine guidance telescope. Error signals for the fine loop are derived from a GEP type sensor and drive diasparometers. Error signals for coarse telescope control are derived from a separate error sensor which receives part of the light from the primary optical system. Control moment gyros are chosen as actuators because this telescope is supported by an isolation system which will not pass reaction torques to the spacecraft. Error signals for the spacecraft are derived from the coarse or intermediate error sensor in the telescope. Spacecraft control is the same as for a., except that all single degree of freedom CMG's are used because of the greater control torque. As mentioned earlier, the overall system for the 0.1 arc second tracking experiment was defined late in the study. Therefore, the detailed analysis is for the former only.

11.4.3 Spacecraft and Telescope Control Dynamics

As discussed previously, stability requirements on the telescope are stringent only about the pitch and yaw axes. Therefore, the telescope is given angular freedom only about these two axes, and the present analysis is concerned strictly with these two axes for both telescope and spacecraft. The actuator chosen for spacecraft control is a pair of two-axis gyros. Of interest here is the effect of actuator dynamics on telescope stability.

To determine actuator dynamics, detailed mechanization must be considered. For the gyro pair, this takes the form illustrated in figure 11.4.3-1. A control voltage applied to the torquer on the outer gimbal will produce a torque T_o. This torque acts on the spacecraft and on the gimbal to produce a gimbal rate $\dot{\alpha}$. The product of $\dot{\alpha}$ and the gyro angular momentum H gives a precession torque on the inner gimbal which produces a rate $\dot{\beta}$. But a tachometer control signal proportional to $\dot{\beta}$ is fed back to the inner gimbal torquer which produces a torque in opposition to the cross-coupled precession from the outer gimbal. Also, another effect of the inner gimbal rate is to couple a precession torque back to the outer gimbal in opposition to the torquer on that axis. Similarly, a tachometer signal is fed back to the outer gimbal to stabilize that axis.

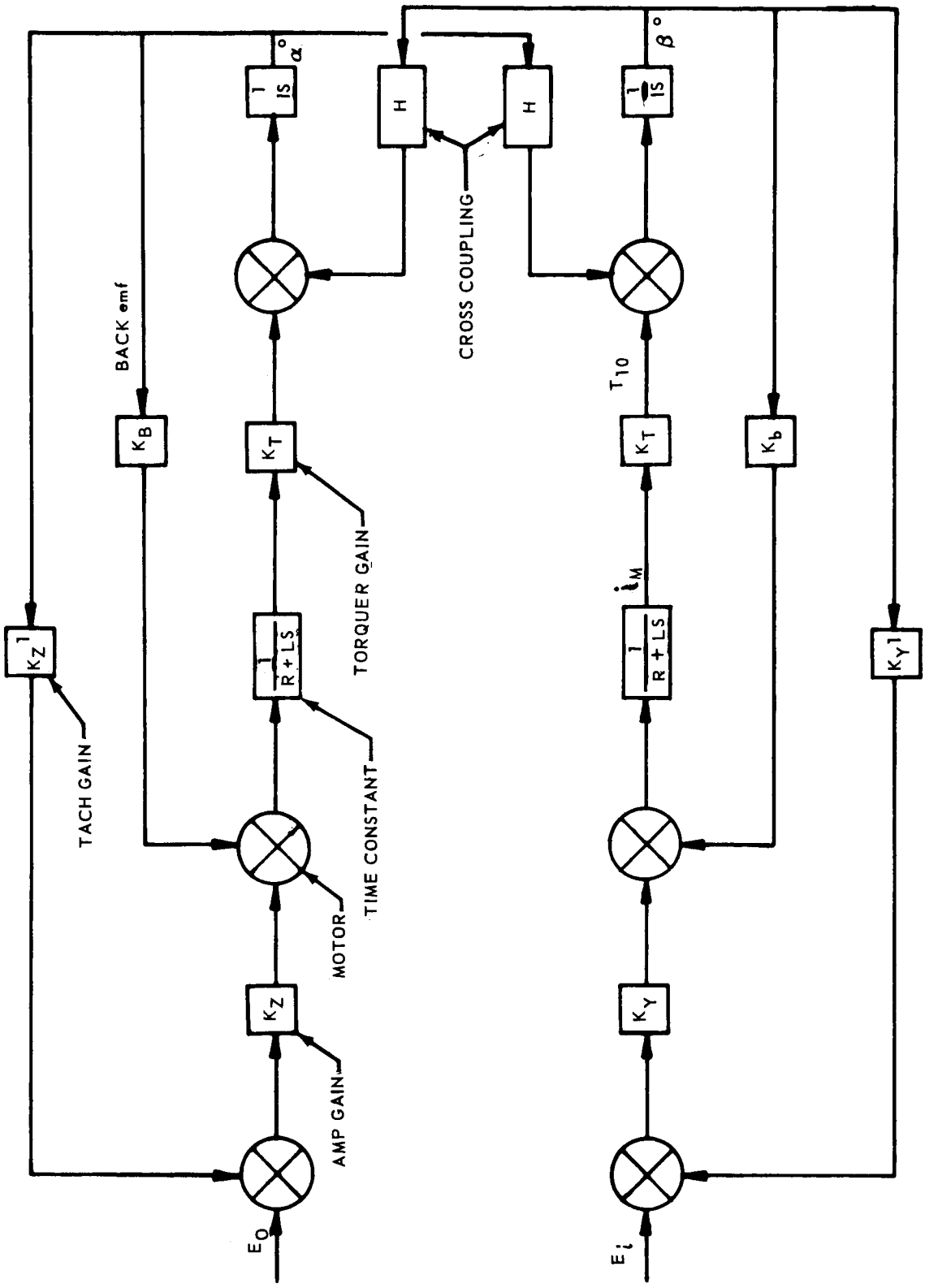


Figure 11.4.3-1. Actuator Mechanization

A control signal to either torquer produces torques on both vehicle axes. The relative values of these torques are determined by the relative control system gains. Either torque can be selected for control purposes, in which case the other torque must be considered a disturbance. For this application, the precession torque is used for control. That is, the gains are chosen so that a control signal applied to outer gimbal torquer produces a greater steady-state torque about the inner gimbal axis, and similarly for an input to the other axis.

Analysis of the configuration depicted in figure 11.4.3-1 gives the following expression for outer and inner gimbal torques in terms of the input voltages.(1)

$$T_{om} = \frac{K_m K \left(S^2 + \omega_g{}^2\right)}{\left(S^2 + 1/\tau_m\, S + {}_g{}^2\right)^2 + \omega_g{}^2/\tau^2{}_m} \qquad (1)$$

$$\left[\left(S^2 + 1/\tau_m\, S + \omega_g{}^2\right) E_o + \left(\omega_g/\tau_m\right) E_i\right]$$

$$T_{im} = \frac{K_m K \left(S^2 + \omega_g{}^2\right)}{\left(S^2 + 1/\tau_m\, S + \omega_g{}^2\right)^2 + \omega_g{}^2/\ {}_m{}^2} \qquad (2)$$

$$\left[\left(S^2 + 1/\tau_m\, S + \omega_g{}^2\right) E_i - \left(\omega_g/\tau_m\right) E_o\right]$$

where,

$K_y = K_z = K$

$K_m = K_t/R$

$\omega_g = H \cos\ \beta/I_g$

$T_m = I_g/K_m\ \ K_2$

$K_2 = KK'$

and the inductive reactance of the motor is neglected.

The steady-state values for $E_o = E_m/s$ and $E_i = 0$, are determined from application of the final value theorem:

$$T_{omss} = \text{limit}_{S \longrightarrow 0}\ S\ T_{om}(S) \qquad (3)$$

$$T_{omss} = \frac{K_m K \tau_g \omega_m}{1 + \tau_m^2 \omega_g^2} E_m \quad (4)$$

and

$$T_{imss} = \frac{K_m K \omega_g \tau_m}{1 + \omega_g^2 / \tau_m^2} E_m \quad (5)$$

The ratio which gives a measure of the cross-coupling is

$$\tau_{cc} = \frac{T_{imss}}{T_{oss}} = \frac{1}{\omega_g \tau_m} = \frac{K_m K_2}{H \cos \beta} \quad (6)$$

To use the precession torque for control purposes, this ratio should be maximized. That is, the steady-state control torque should be much greater than the steady-state disturbance transmitted to the Orthogonal axis. For a given momentum capability in the gyro, this is accomplished by increasing the gain in the rate loop. However, the initial disturbance, which acts before the rate loop can respond, is directly proportional to the amplifier and torquer gains. Therefore, to minimize both initial and final cross-coupling disturbances, the tachometer gain should be increased while the amplifier gain is held constant. However, for a given gyro angular momentum, increasing the tachometer gain reduces the effective control gain of the actuator. These considerations are illustrated in figure 11.4.3-2. The quantities plotted there are:

$$K_c = T_{imss}/E_o = \text{control gain, new-m/volt} \quad (7)$$

$$K_d = T_{omss}/E_o = \text{disturbance gain, new-m/volt} \quad (8)$$

where, in terms of the gains previously,

$$K_d = \frac{K_m K H^2}{K_m^2 K_2^2 + H^2} \quad (9)$$

$$K_c = \frac{K_m^2 K K_2 H}{K_m^2 K_2^2 + H^2} \quad (10)$$

K_2 is the total gain in the rate loop. For low rate gains, the disturbance torque approaches the control torque. Increasing the rate gain decreases the ratio but also reduces the control gain. The curves in figure 11.4.3-2 are plotted for an initial disturbance gain of $K_m K$ = 10 ft-lb/volt and H = 20 ft-lb-sec.

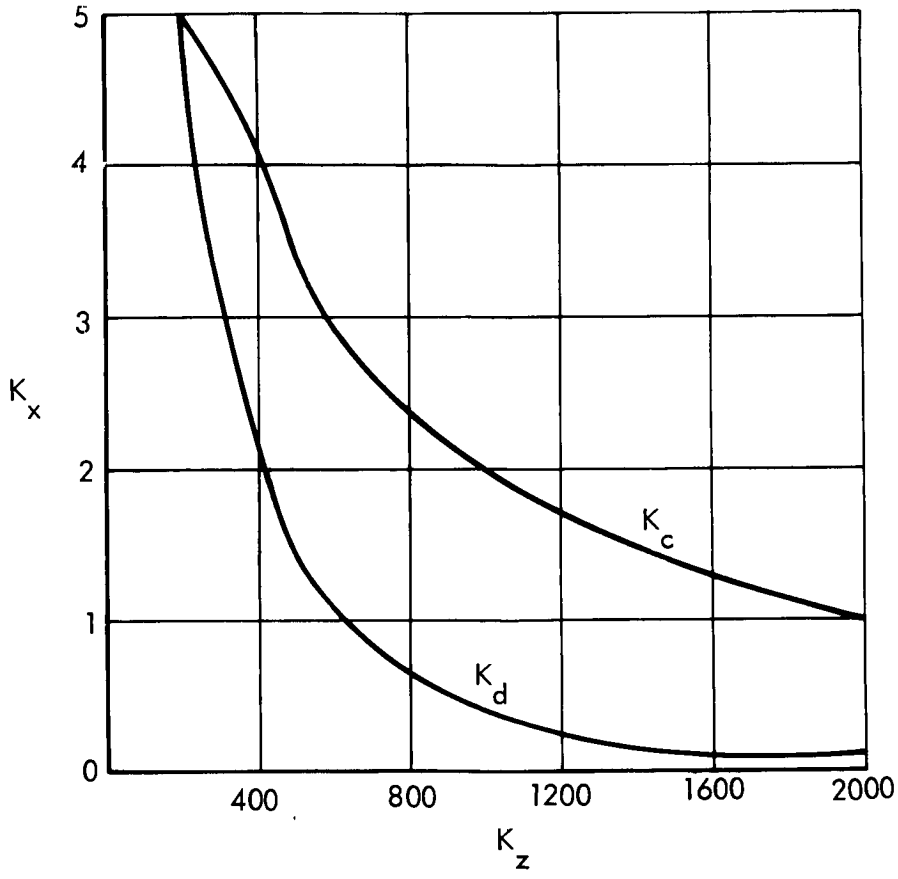


Figure 11.4.3-2. Effect of Increasing the Tachometer Gain

The fact that the initial disturbance is much larger than the steady-state control could be very undesirable if this actuator were to be used in a high control torque application; for example, stabilizing the spacecraft against peak excursions caused by man-produced disturbances. However, as discussed previously, the present concept is to operate the spacecraft practically open-loop as far as man-produced disturbances are concerned. This is feasible since the disturbance caused by the initiation of a maneuver is cancelled when the maneuver is terminated a short time later. In the meantime, the spacecraft picks up a net offset which is equivalent to an initial condition. Control system design is based on the time to recover from the initial condition.

Recovery time should be determined from a detailed analysis of experimental tasks. While awaiting such an analysis, an intuitive value of 5-minutes is being used.

To perform a general analysis of the spacecraft/telescope control system with loop dynamics is to introduce more complexity than is warranted at this stage of the study. Therefore, at the outset, engineering judgement and experience was used to generate the following set of simplifing assumptions:

a. The two telescope axes are uncoupled except through the spacecraft control system.

b. Telescope error signals are available from another source (error sensor in the fine tracking loop).

c. Spacecraft error is derived from gimbal angle pickoffs on the gimbal axes.

d. Maximum angle between telescope and spacecraft is small enough (less than one degree) to neglect trigonometric transformations.

Under these simplifications, the system is represented by the diagram shown in figure 11.4.3-3.

The coupled system is still too complex for analytic treatment (eight-order characteristic equation). Therefore, to derive numerical gains, the following additional assumptions were made:

a. The telescope and spacecraft loops are in cascade but are uncoupled. That is, torquing the telescope causes no reaction on the spacecraft, and the disturbance is independent of spacecraft loop dynamics.

b. The telescope loop is much faster than the spacecraft loops.

c. External disturbance torques are much slower than the control dynamics and may be considered constant.

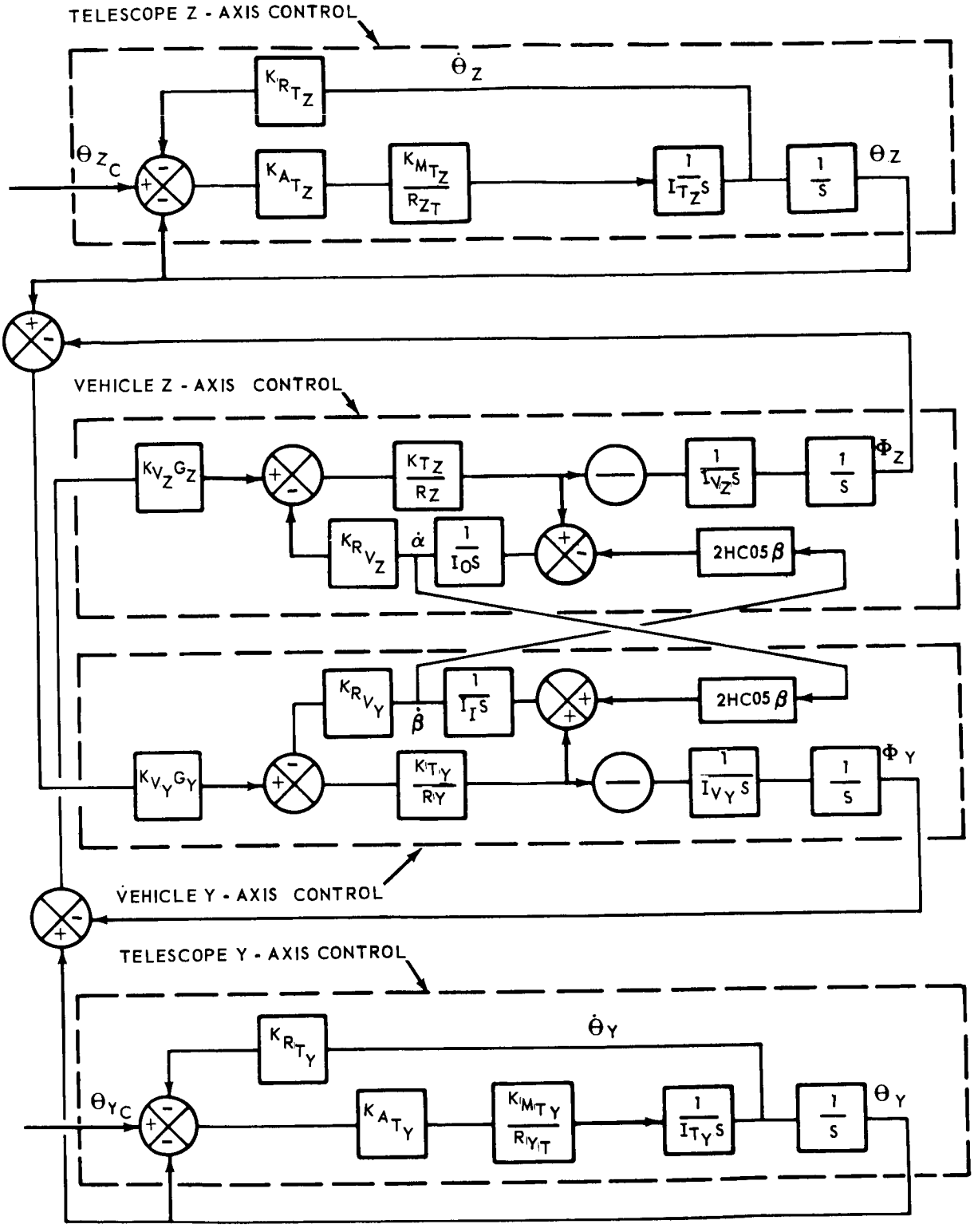


Figure 11.4.3-3. Simplified Block Diagram of the Two-Axis Control System

d. The control moment gyro is linear with no dynamics.

e. For the worst-case man-produced disturbance, the maximum instantaneous angular deflection must be less than one arc-minute.

f. For the worst-case external disturbance the maximum tolerable spacecraft steady-state error is one degree.

g. The telescope must follow the reference line of sight deviations with less than 1 arc minute error.

The results for OTES inertial data are given in table 11.4.3-1.

A stability analysis of the coupled linear system depicted in figure 11.4.3-3 was performed using root-locus techniques. Because of the large difference in the moments of inertia about the pitch (Z-axis) and yaw (Y-axis) axes of the vehicle, different control gains were required. Also, the vehicle control modes about the pitch and yaw axes are coupled together using the two-axis control concept shown in figure 11.4.3-3. Therefore, root-locus plots of the vehicle control modes about the Y and Z axes of the vehicle are presented as a function Kv_Z holding Kv_Y at its nominal value of 200 volts/rad. and as a function Kv_Y holding Kv_Z at its nominal value of 1600 volts/rad. in figure 11.4.3-4. The nominal operating points for each set of loci are, of course, the same as can be seen by comparing the closed-loop roots for $Kv_Y = 200$ in the upper plot to the closed-loop roots for $Kv_Z = 1600$ in the lower plot. As shown from these root-locus plots, further optimization of these preliminary control gains should be made in Phase II of the study.

A root locus plot of the telescope control mode in either pitch and yaw (i.e., telescope is symmetrical about the x-axis) is shown in figure 11.4.3-5. Loci of the closed-loop roots of this mode(s) are presented as a function of K_{A_T} for different values of K_{R_T}. Line of constant K_{A_T} are included to show the effect of varying K_{R_T} on the closed-loop roots of the system (i.e. the closed-loop response) as well as the normal locus of closed-loop roots as a function of K_{A_T} for a given K_{R_T}. These loci were obtained for the telescope uncoupled from the vehicle, since this is very nearly the case. Likewise, the response of the actuator is essentially independent of Kv_Y and Kv_Z.

11.4.4 System Simulation

Ultimate objective of simulating the stabilization system on the analog computer is to optimize the overall system design. However, for the three-loop system with suspension mounting, such optimization requires detailed definition of:

a. Components of each loop including dynamics and non-linearities.

TABLE 11.4.3-1

CALCULATED NOMINAL GAINS

K_{ATY} = 350 Volts/rad

K_{RTY} = 1 Volt/rad/sec

K_{ATZ} = 350 Volts/rad

K_{RTZ} = 1 Volt/rad/sec

K_{MT}/R_{ZT} = 0.1 Ft-lb/volt

K_{VZ} = 200 Volts/rad

K_{VY} = 200 Volts/rad

K_{RVZ} = 2000 Volts/rad/sec

K_{RVY} = 2000 Volts/rad/sec

$$G_Z = \frac{1 + \tau_1 S}{1 + \tau_2 S}$$

τ_1 = 20 sec

τ_2 = 2 sec

H = 100 Ft-lb/sec

I_o = 0.2

I_{VZ} = 1.3 X 10^4 Slug-ft^2

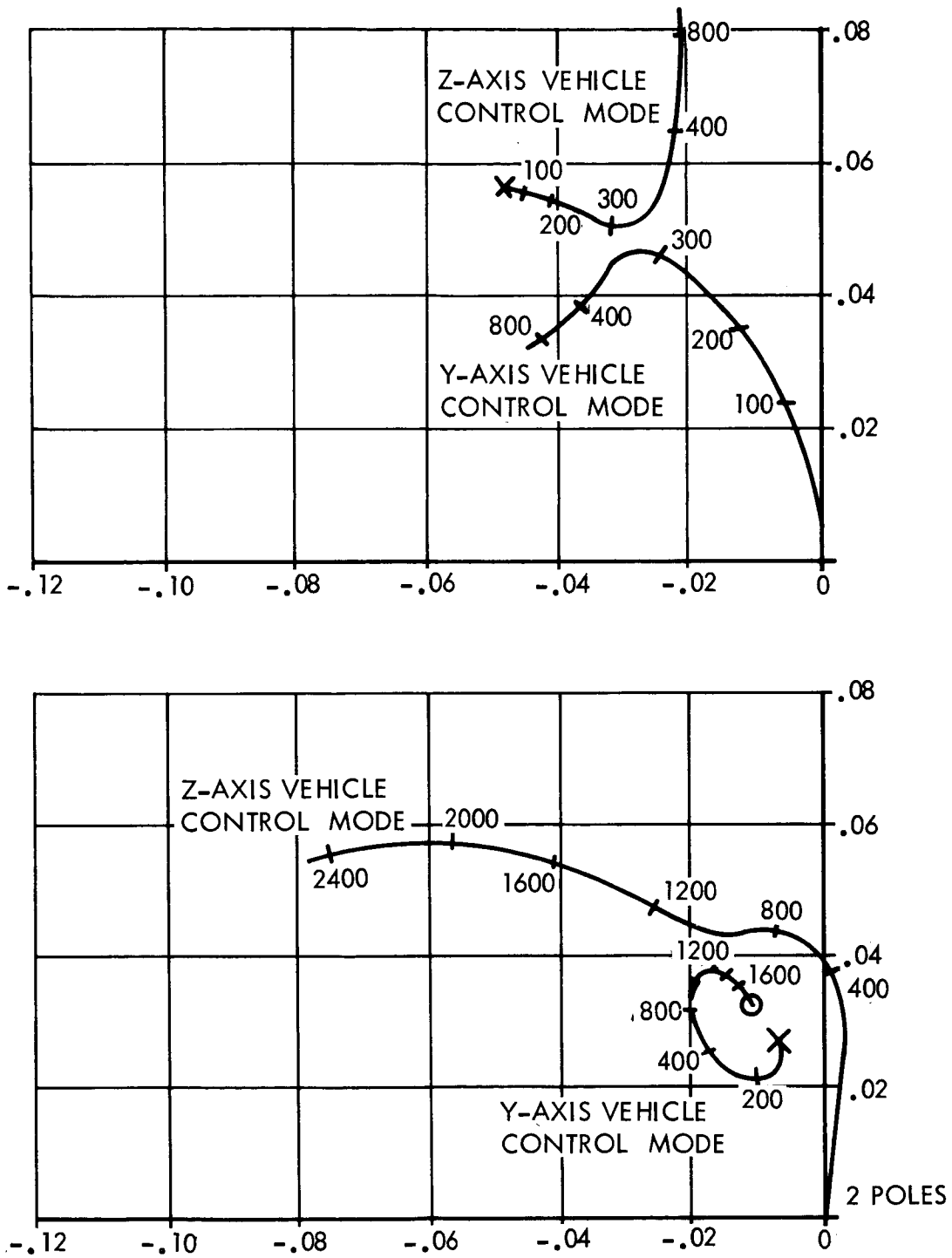


Figure 11.4.3-4. Root-Locus Plot of Vehicle Control Mode

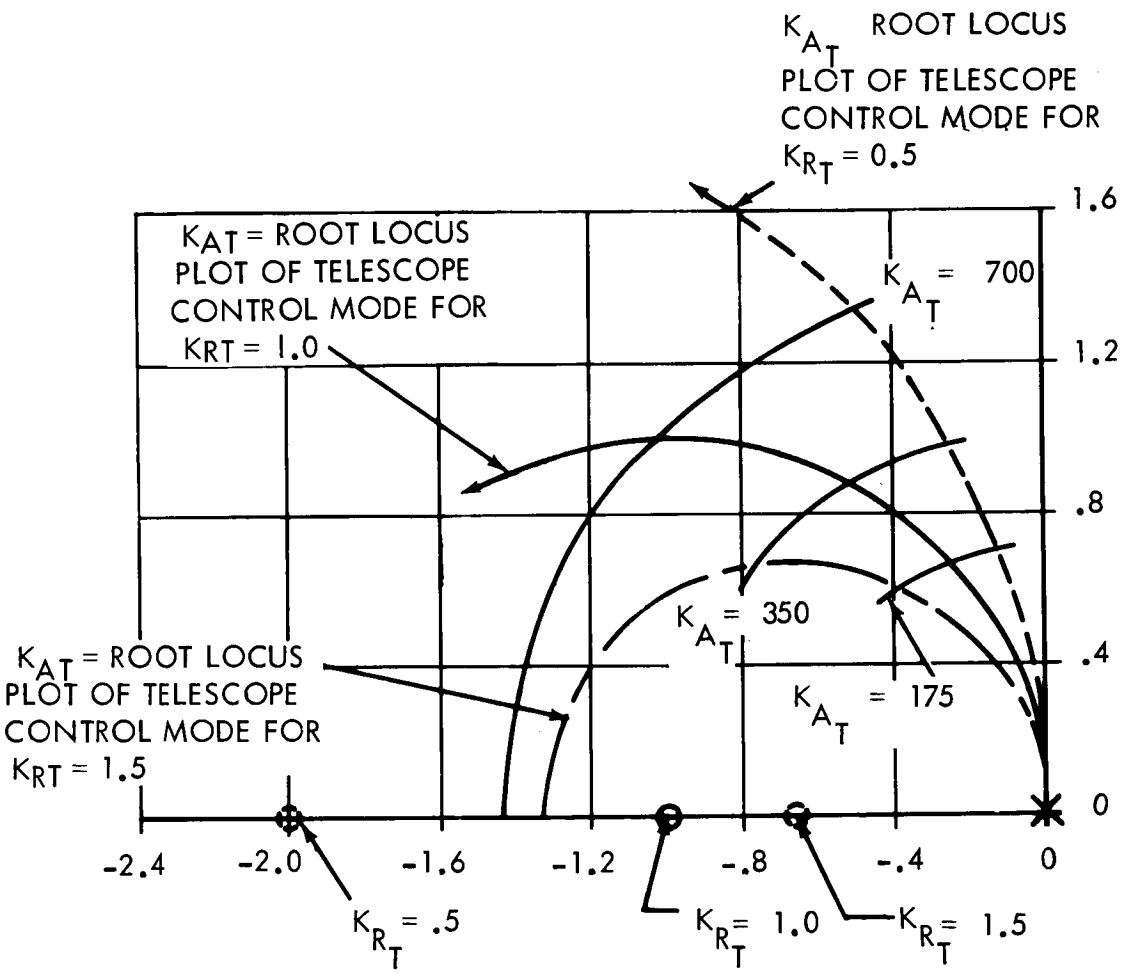


Figure 11.4.3-5. Root-Locus Plot of Telescope Control Mode

b. Detailed analysis of each suspension technique for dynamics and non-linearities.

c. Detailed definition of the disturbance environment.

d. Detailed definition of the requirements for all experiments.

This information is not available at this stage of the study. Consequently, the simulation makes no attempt to optimize the design. Rather, it proposes to accomplish two objectives: (a) determine preliminary response and error characteristics of the complex coupled system, both as a measure of basic feasibility and to indicate problem areas; and (b) lay the ground work for the detailed optimization to be performed in later phases of the study, after the required information is available.

The computer simulation setup is shown in figure 11.4.4-1. This is the control system discussed in subsection 11.4.3 with the following additions: (a) inclusion of the telescope actuator disturbance to the vehicle represented by the T_c coupling; (b) the man-produced disturbances to the vehicle represented by T_{DV} and $\ddot{x}$; and (c) the suspension system characteristics represented by the I_E coupling.

A run schedule for several production runs made are listed in table 11.4.4-1. The gains were determined by starting with the values calculated in subsection 11.4.3 and making small adjustments to improve the response but with no real attempt to optimize the design.(1)

The effect of increasing the "coast time" between initiation and termination of the disturbance is shown in figure 11.4.4-2.

The disturbance magnitude is 75 foot-pounds with 0.2 seconds duration. Although the axes were coupled for the run and the disturbance applied to both axes, only the z-axis response is shown. Notice that the general effect of increasing the coast period from 3 to 5 seconds is to increase the maximum value of the vehicle error from 13.5 arc minutes to about 25 arc minutes. This is because of the longer time period during which the velocity impulse may build up error. As discussed in subsection 11.4.3 the spacecraft control system simulated here is not designed to handle man-produced disturbances. The philosophy is to wait until man removes his own disturbance upon termination of the maneuver. The function of the control system is to bring the integrated error back to zero within a specified time period. As evident from the plots, this time is about 300 seconds, or 5 minutes.

The telescope response is fast enough to handle the disturbance. The maximum error in each case is about 0.132 arc minutes. The effect of

---

(1) Riles, J.C., Analog Computer Studies of Complex Control Systems, TN-AE-66-143, Chrysler Corporation Space Division, New Orleans, Louisiana.

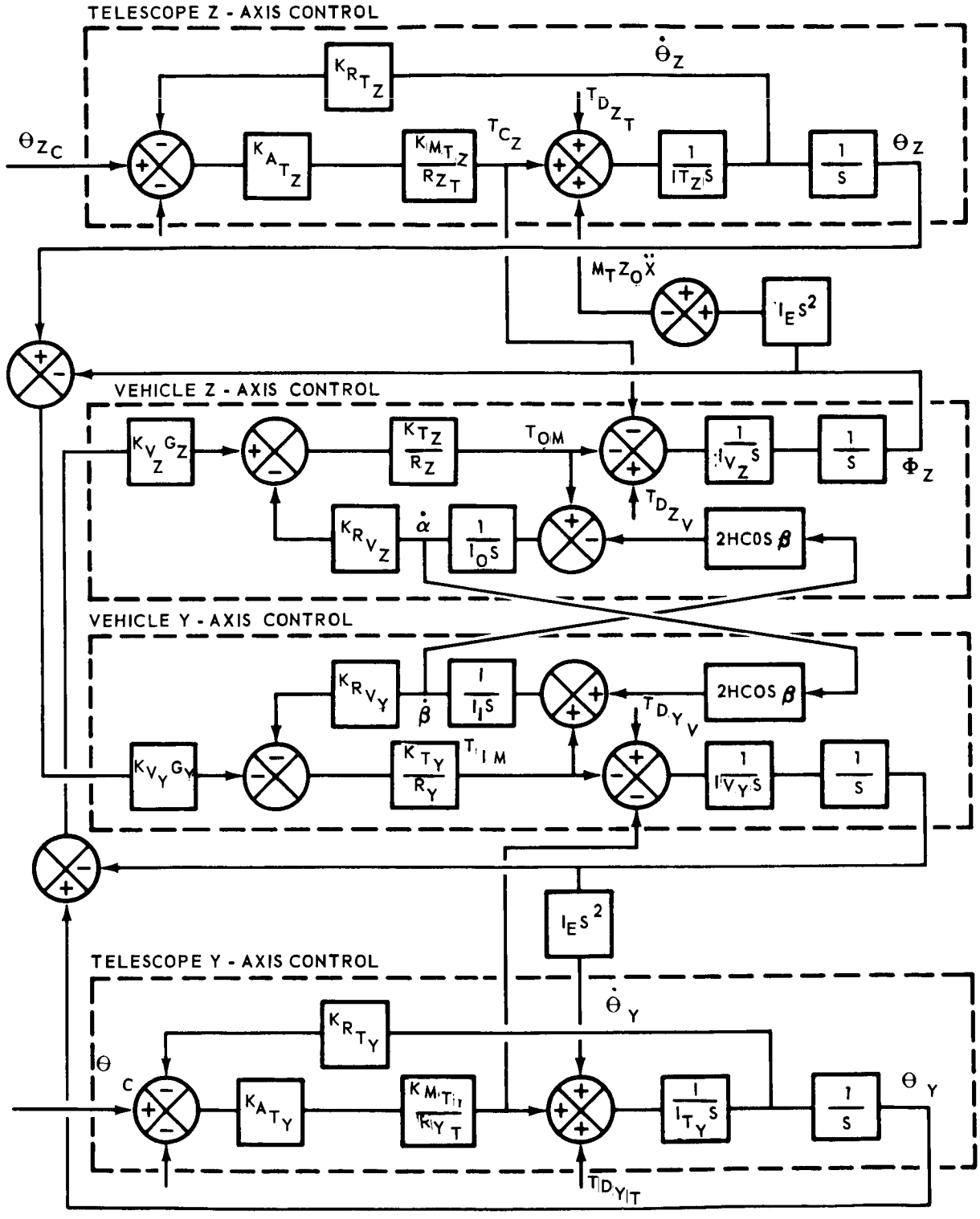


Figure 11.4.4-1. Simulation Diagram

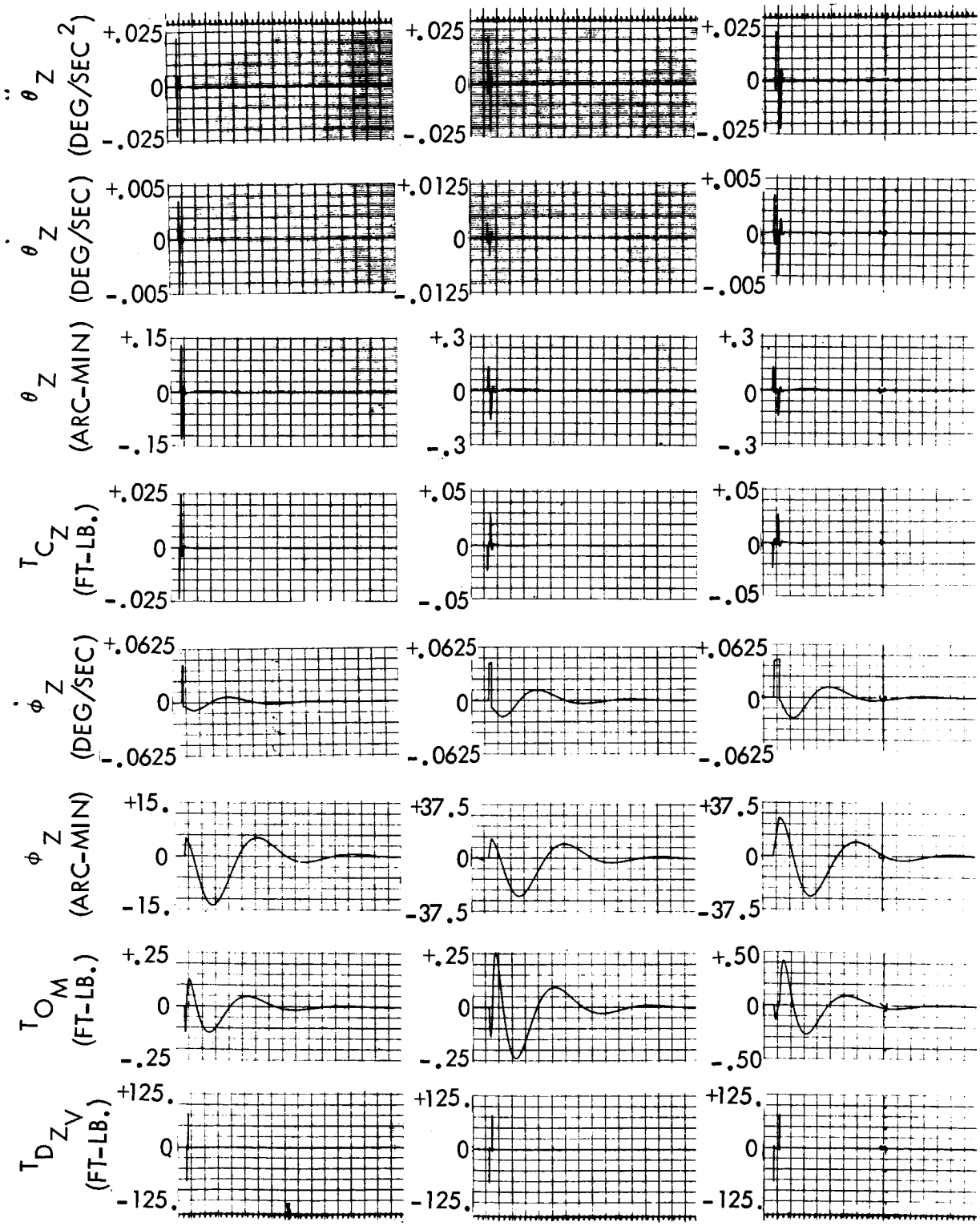


Figure 11.4.4-2. Effect of Coast Time on Response

TABLE 11.4.4-1

ANALOG COMPUTER RUN SCHEDULE

RUN	K_{VZ}	K_{VY}	K_{RVZ}	K_{RVY}	Tau_2	Tau_1	KAT_{Z+Y}	$K_{RT_{Z+Y}}$	I_e	T_D	t	T	Remarks
46	400	400	2000	2000	20	2	350	1	31.1	75	0.2	3	Coast Period
47	400	400	2000	2000	20	2	350	1	31.1	75	0.2	5	Effects
48	400	400	2000	2000	20	2	350	1	31.1	75	0.2	10	
71	400	400	2000	2000	20	2	525	1	31.1	31.1	0.1	10	
72	400	400	2000	2000	20	2	350	1	31.1	31.1	0.1	10	
100	1600	200	4000	2000	20	2	350	1	31.1	10	.5	5	
101	1600	200	4000	2000	20	2	350	1	31.1	50	.1	5	
105	1600	200	4000	2000	20	2	350	1	62.2	50	.1	5	
106	1600	200	4000	2000	20	2	350	1	93.3	50	.1	5	
107	1600	200	4000		20	2	350	1	31.1	50	.1	5	
108	1600	200	4000		20	2	350	1	62.2	50	.1	5	
109	1600	200	4000		20	2	350	1	93.3	50	.1	5	

TABLE 11.4.4-2

VEHICLE AND TELESCOPE DATA USED IN STABILITY AND CONTROL ANALYSES

SYMBOL	PARAMETER DESCRIPTION	VALUE	UNITS
I_{VZ}	Vehicle moment of inertia about the Z-axis	17300	SLUG-FT.^{2}
I_{VY}		12100	SLUG-FT.^{2}
I_{TZ}	Telescope moment of inertia about the Y-axis	343	SLUG-FT.^{2}
I_{TY}		343	SLUG-FT.^{2}
M_T	Mass of Telescope	37.3	SLUG
M_V	Mass of Vehicle		

TABLE 11.4.4-3

NOMINAL VEHICLE AND TELESCOPE CONTROL
SYSTEMS DATA USED IN STABILITY AND CONTROL ANALYSES

SYMBOL	PARAMETER DESCRIPTION	VALUE	UNITS
K_{VZ}		1600	VOLTS/RAD.
K_{VY}		200	VOLTS/RAD.
K_{RVZ}		4000	VOLTS/RAD. PER SEC.
K_{RVY}		2000	VOLTS/RAD. PER SEC.
H		100	FT-LB-SEC.
I_o		0.2	SLUG-FT^2
I_I		0.2	SLUG-FT^2
K/R_Z		0.1	FT-LB/VOLT
K/R_Y		0.1	FT-LB/VOLT
K_{ATZ}		350	VOLTS/RAD.
K_{ATY}		350	VOLTS/RAD.
K_{RTZ}		1.0	VOLTS/RAD. PER SEC.
K_{RTY}		1.0	VOLTS/RAD. PER SEC.
K/R_Z			FT-LB/VOLT
K/R_Y			FT-LB/VOLT

increasing the angular momentum of the disturbance would be of interest. However, this presents formidable scaling problems in the simulation. This fact plus the time-element involved made it impossible to obtain runs for more than two-to-one variation in the disturbance angular momentum, within the range of interest (greater than 5 foot-pound-second).

The effect of increasing the gimbal pivot offset is depicted in figure 11.4.4-3 for a disturbance into one axis only. Increasing the offset from 1 inch to 2 inches increases the maximum telescope error by the same factor, from about 0.05 arc minute to 0.1 arc minute. This is for a disturbance of 50 foot-pounds, 0.1 second duration and a 5 second coasting period. Notice that the spacecraft error remains essentially constant for increasing offsets.

The effect of increasing I_E with a disturbance on both axes simultaneously is shown in figure 11.4.4-4. The response remains exactly the same as for the single axis case for both the telescope and spacecraft. This is because the cross-coupling between axes is through the spacecraft control system, which is much slower than either the disturbance or the telescope response.

To conserve space, most of the runs were made at a slow chart speed and a 10:1 speedup in the simulation. A few runs were made with high chart speeds to show the telescope response. One such run, for nominal gains and suspension with a disturbance of 10 foot-pounds, 0.5 second duration, and a 5 second coast period, is shown in figure 11.4.4-5 for both axes. The telescope settling time is about 5 seconds and that the response is virtually the same for both axes.

The effect of increasing the telescope control loop gain is shown in figure 11.4.4-6. Increasing the gain from 350 to 525 reduces the peak telescope error from 0.37 degrees to 0.26 degrees. The disturbance shown in the lower plot, is 50 foot-pounds applied directly to the telescope with no reversal. Physically, this could represent an astronaut pushing off from the telescope while performing extra vehicular activities (EVA). Notice that the control torque called for is about 4.5 foot-pounds. A more realistic simulation would include the saturation of the torque at 0.1 foot pounds, the present design value.

Some results of the computer study are summarized in figures 11.4.4-7 and 11.4.4-8. Maximum telescope excursion and control torques are plotted as a function of gimbal pivot offset for both axes and for various telescope gains.

The conclusion from these results is that maintaining the 1 arc minute accuracy on the telescope for the disturbance environment assumed here is no problem. However, most of the effort so far has been directed toward getting a linearized version of the real system operating properly, as has been done.

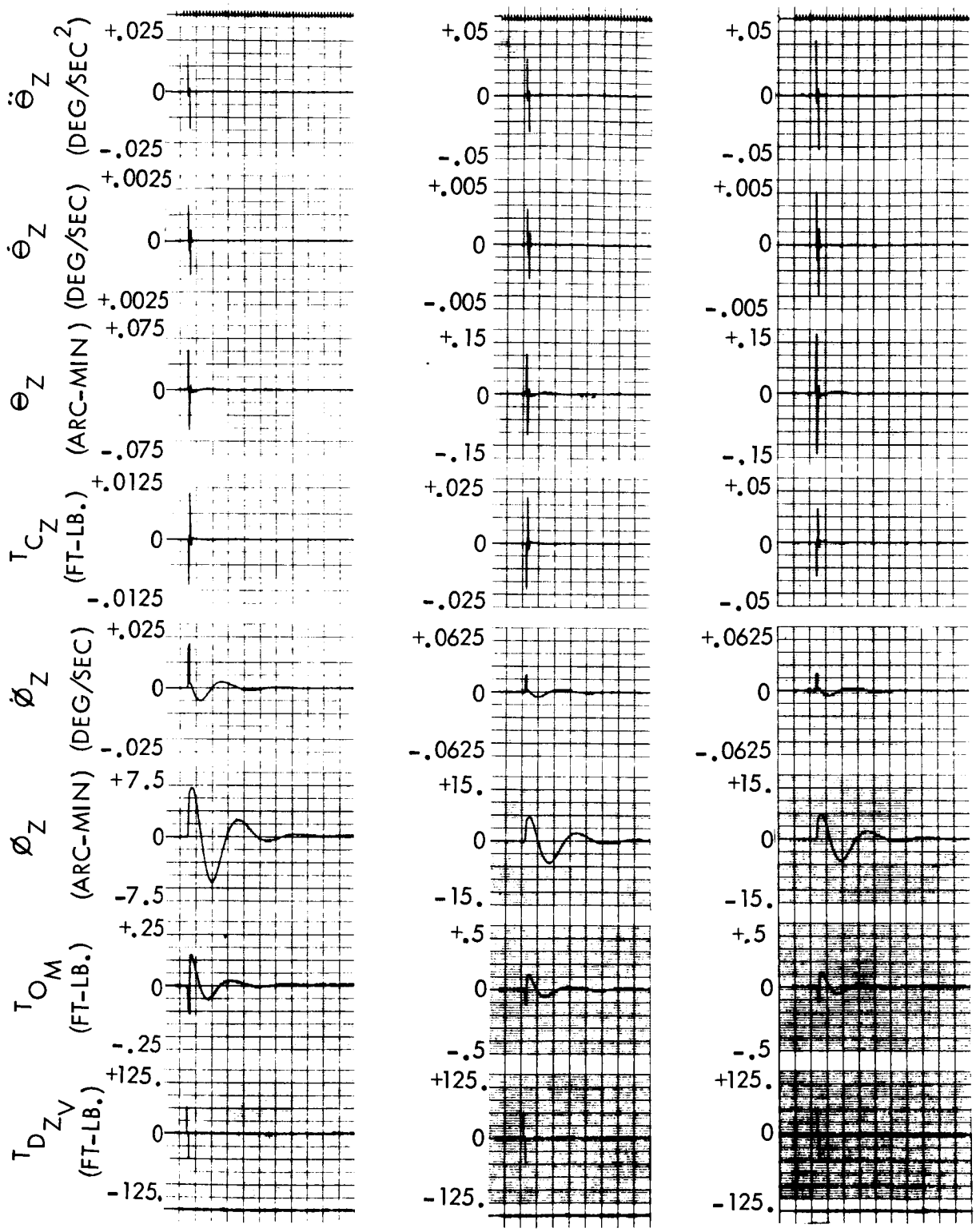


Figure 11.4.4-3. Gimbal Off-Set Effects

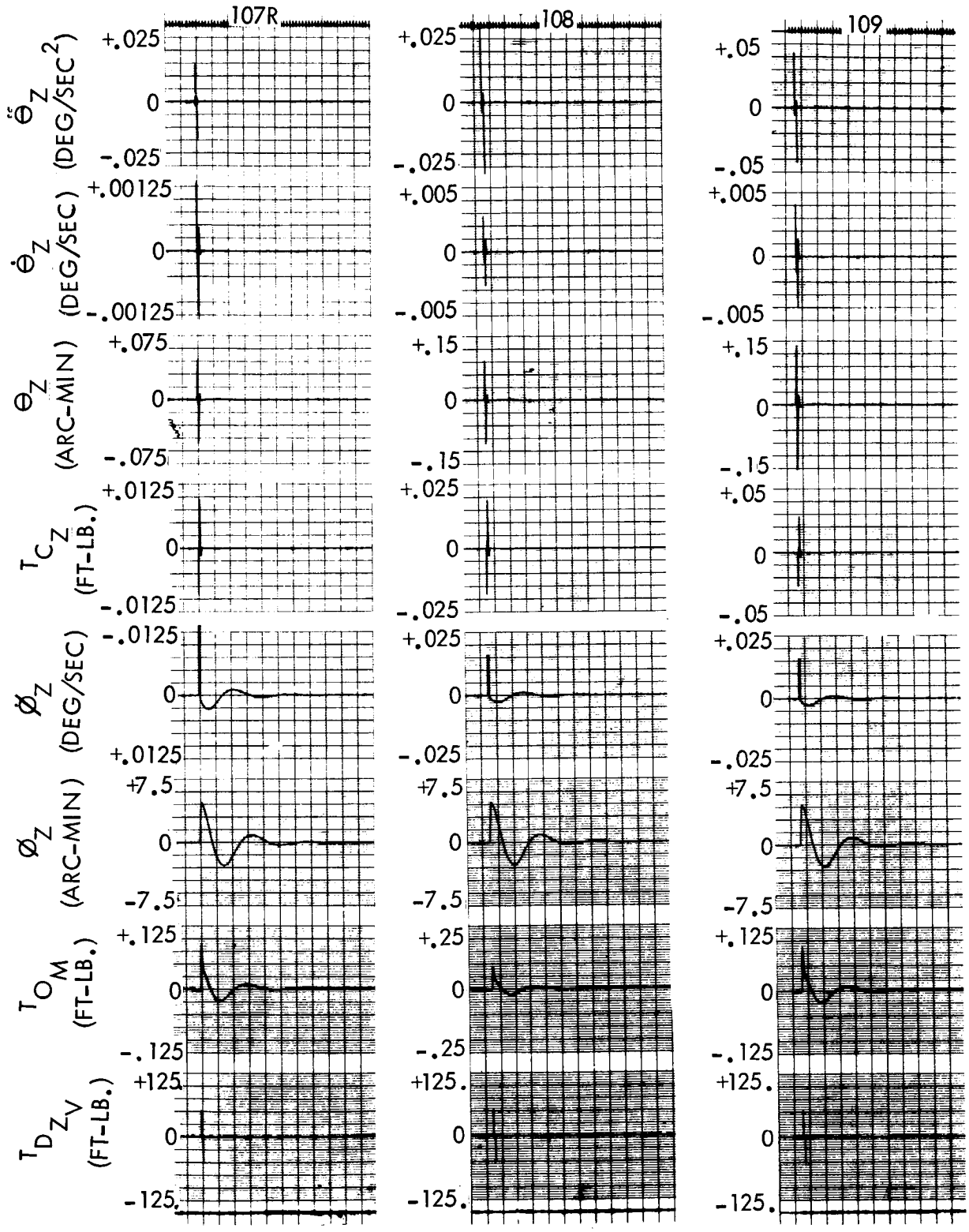


Figure 11.4.4-4. Effect of Disturbance on Both Axes

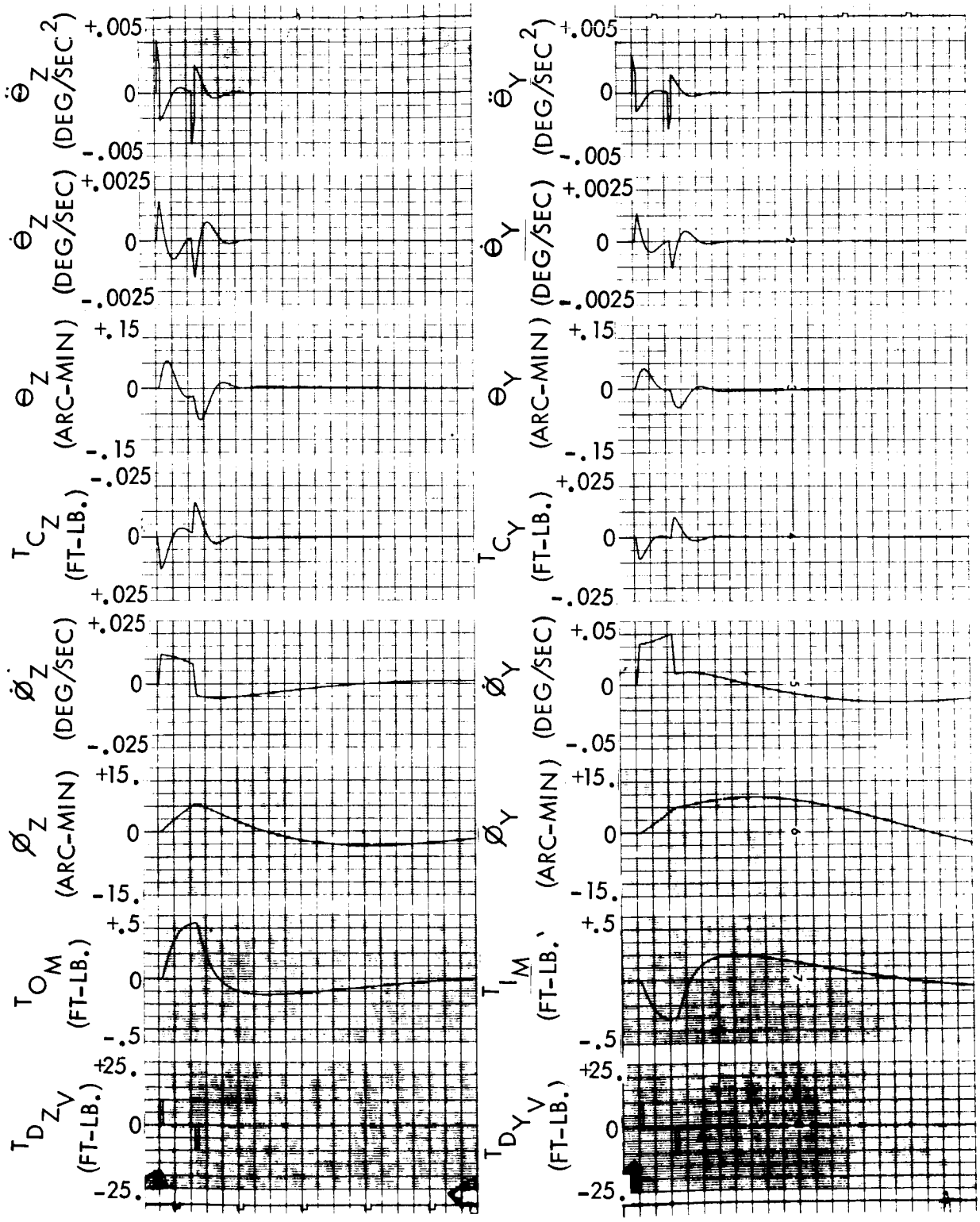


Figure 11.4.4-5. Telescope Response

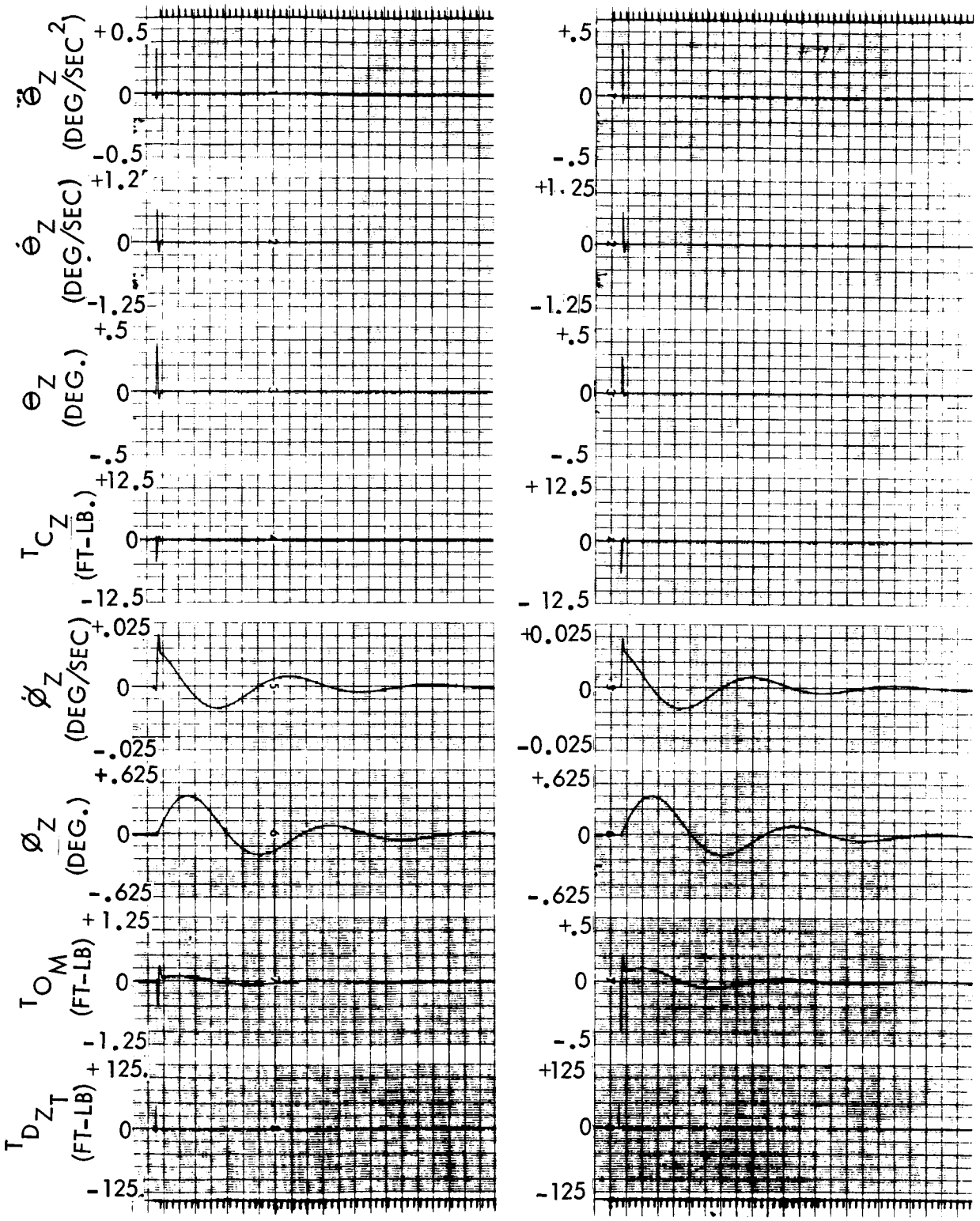


Figure 11.4.4-6. Effect of a Disturbance Applied Directly to the Telescope

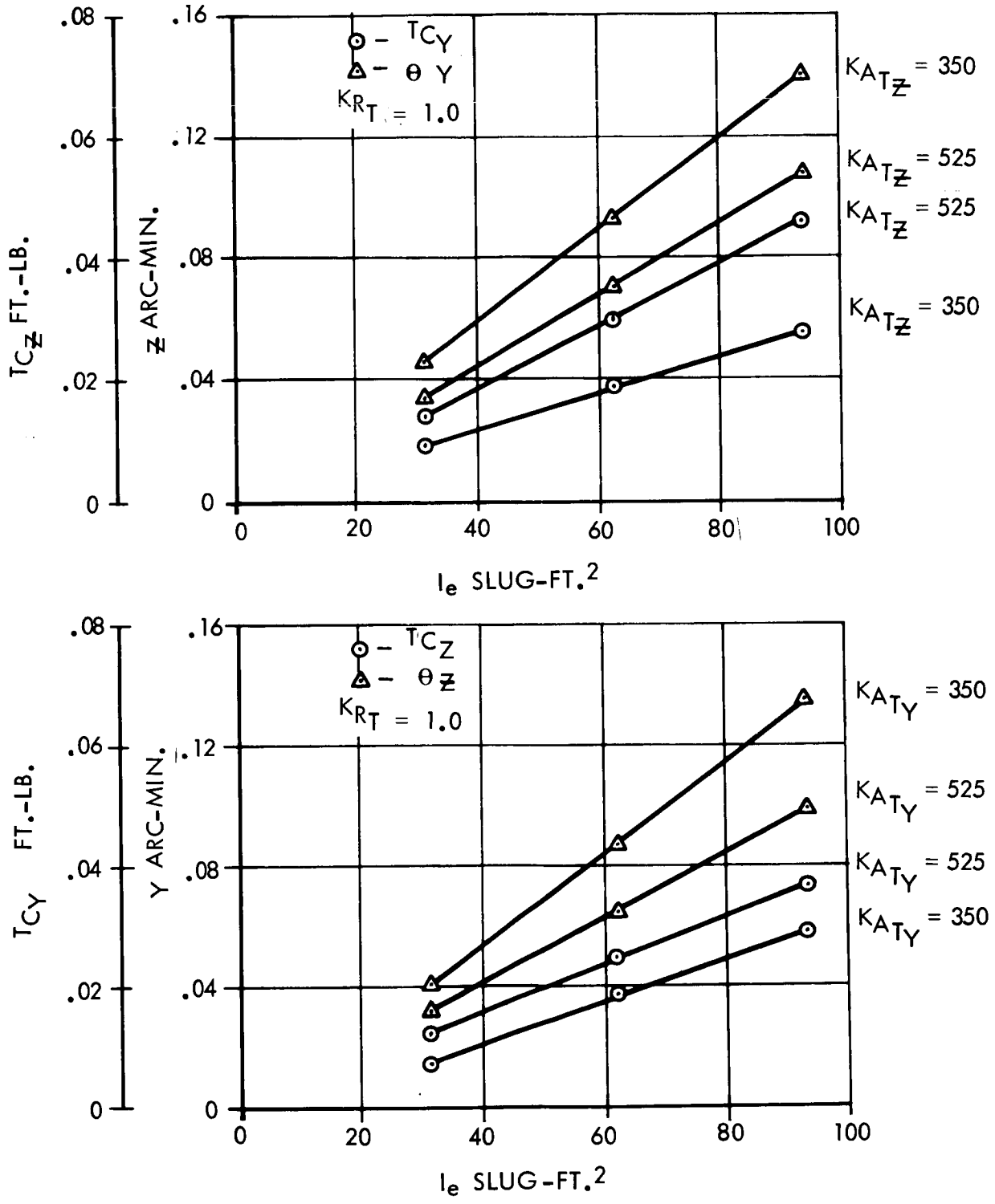


Figure 11.4.4-7. Summarization of Analog Computer Results

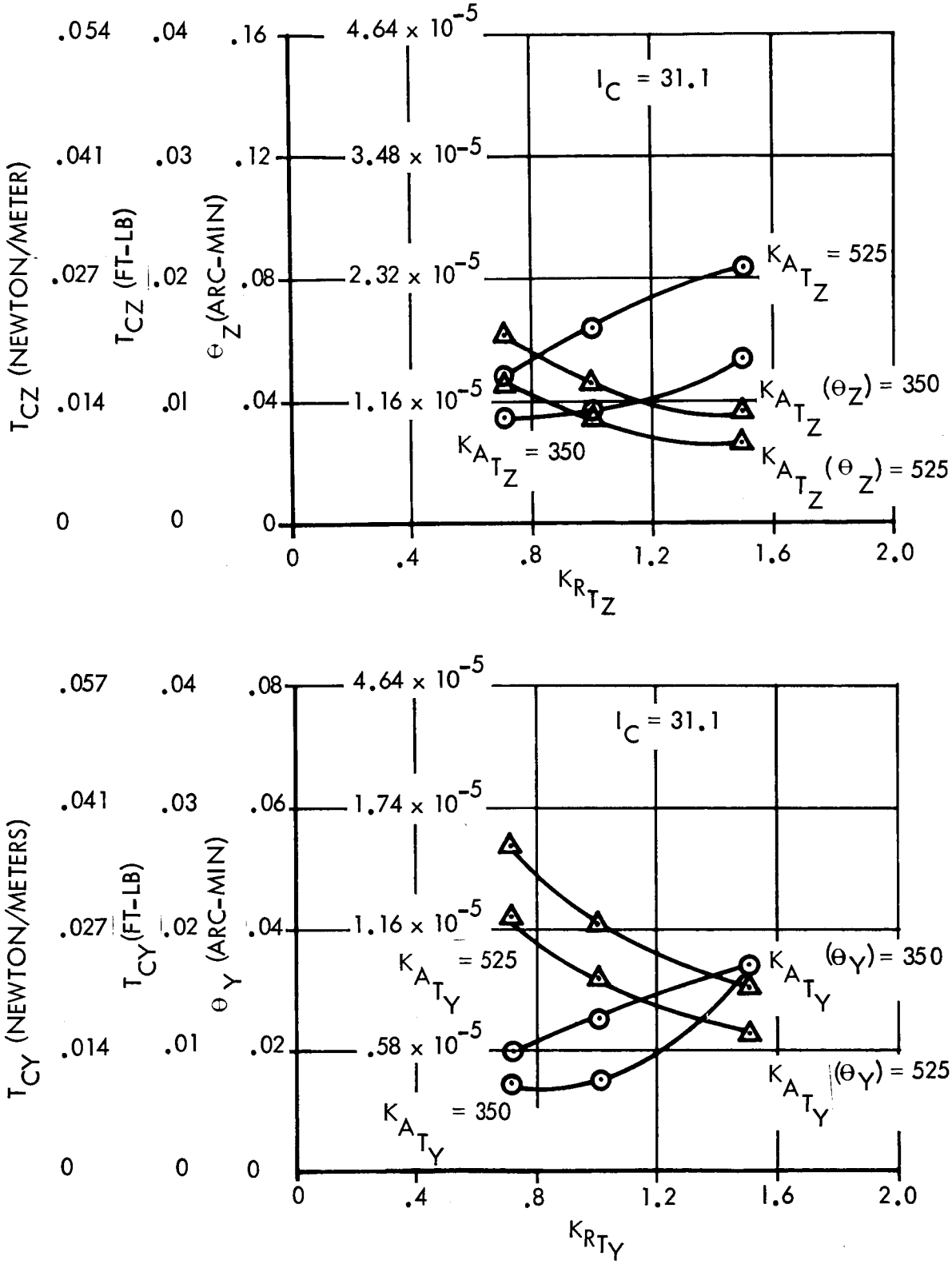


Figure 11.4.4-8. Effect of Gain and Damping on Telescope Response

During the next phase of the study, the same basic system will be used, but with the following additions:

a. The fine loop with the beam deflector characteristics and error sensor non-linearities will be included.

b. Static and running friction of the telescope torques will be simulated.

c. Non-linear characteristics of the spacecraft actuator will be included.

d. Detailed hardware characteristics of all the components such as telescope gimbal angle transducers and telescope rate feedback devices will be determined and simulated.

In addition, the spacecraft system for the fine guidance telescope operating will be simulated. As discussed previously, the fine guidance telescope was conceived and defined late in the study and no attempt was made to include this telescope in the above analysis.

11.4.5 Parametric Analysis

The objective of this analysis is to develop and show the parametric relationships between control system weight and expected disturbances for a wide range of missions. Three types of control and three types of disturbances are considered. The controls are reaction wheels, control moment gyros, and a reaction jet system. The disturbances are small impulsive, as caused by meteoroid impact, large impulsive as caused by the man-produced disturbances discussed in subsection 4.13.5-1 and slow-varying sinusoidal disturbances which may be characteristic of gravity-gradient torque, aerodynamic torque, and solar torque, depending on the attitude orientation of the spacecraft.

11.4.5.1 Impulsive Disturbance

Impulsive disturbances are caused by meteoroid impact and by movements of man in the spacecraft. These are similar in form but may differ in intensity by several orders of magnitude. The trade-off curves, shown in figure 11.4.5.1-1, are scaled for the man-produced disturbances. The results are determined for an assumed moment of inertia (I) of 23,000 Kg-meter^2 (17,000 slug-ft^2). The impulsive disturbance is assumed to produce a step change in spacecraft angular velocity (ω_o) which is proportional to the disturbance magnitude. While the control system is forcing θ_o to zero, the attitude error will reach a maximum θ_m.

The curves are presented for two types of control moment gyros, single axis (SGCMG) and double-axis (DGCMG). The weight (W) for each of these

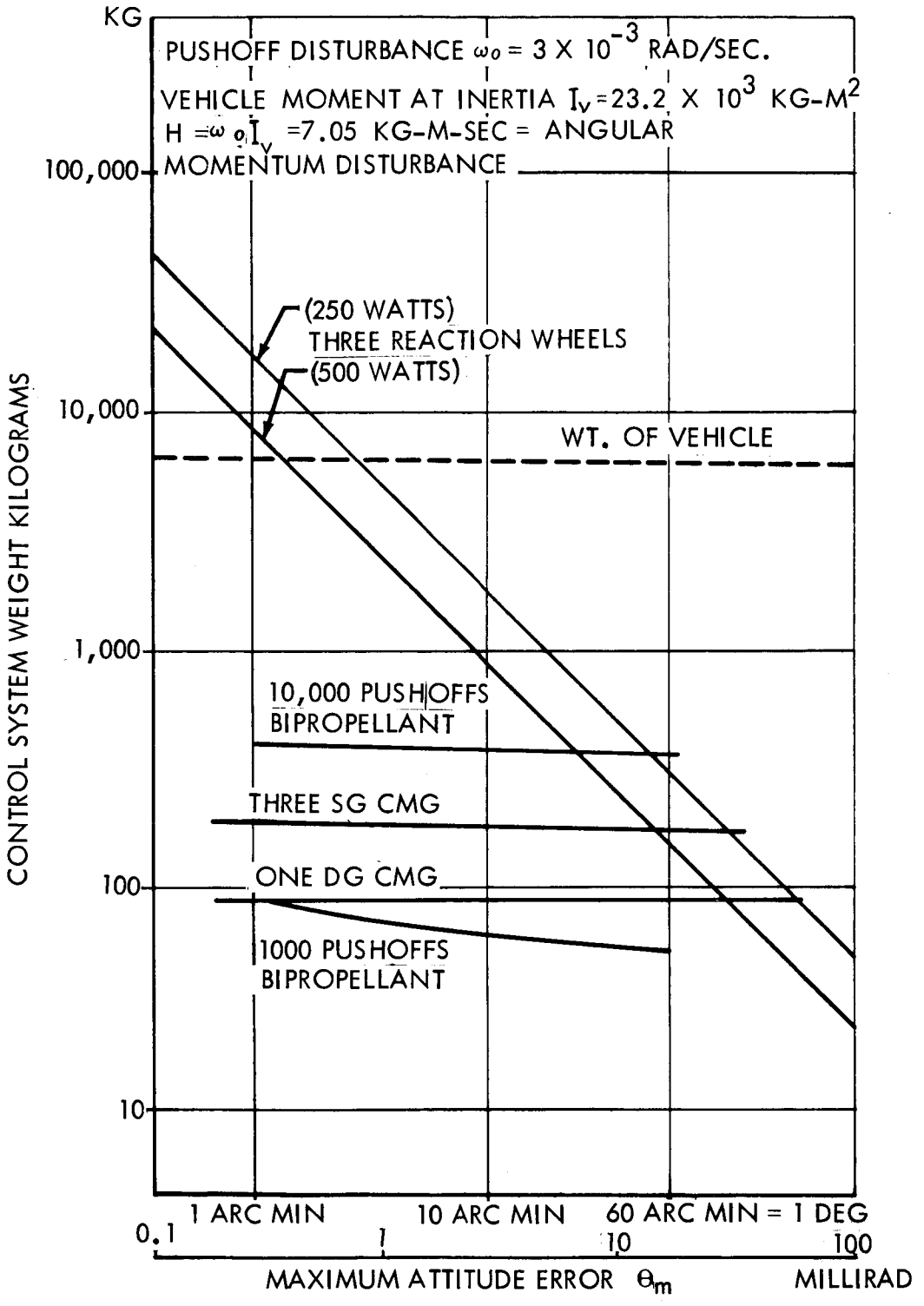


Figure 11.4.5.1-1.

is mainly dependent on the angular momentum (H) of the disturbance which, for constant I and ω_o, is fixed. The assumed gyro design is for small gimbal angles to minimize cross-coupling and for a fixed torquer size.

For reaction wheels, the curves show the trade-offs between the control system weight (W), the maximum error (θ_m), and the required power (P) for the wheel spin motor. It can be seen that the W is inversely proportional to the allowed θ_m and also inversely proportional to P.

For the mass expulsion system, observation shows that the weight of the system is relatively independent of θ_m, but unlike the momentum exchange systems (RW and CMG), W is dependent upon the number of disturbances during a mission. This is because of the propellant required for each disturbance. The curves are for 1,000 and 10,000 push-off type disturbances, and are based on an assumed biopropellant-type system that can provide a propellant with a specific impulse (I_s) of 275 seconds. Smaller values of I_s would result in larger W. This would be particularly true for the case where the number of disturbances is large (10,000). Also, since the actual I_s realized for short impulse times (the type required for control in this study) is somewhat smaller than for long duration pulses, results shown here should be considered optimistic for this type of system.

The small increase in W for the smaller values of θ_m is due mainly to the larger thrusters required. For 1 arc minute, the force (F) of the thruster is 200 Newtons (45 pounds). The required thrust is inversely proportional to the θ_m; i.e., 20 Newtons (4.5 pounds) for θ_m of 10 minutes and 3.34 Newtons (0.75 pounds) for θ_m of 1 degree. Figure 11.4.5.1-2 shows how the required F varies with θ_m and shows that hardware limitations due to the minimum impulse bit (m.i.b.) do not come into play here. Power required for this type system is about 30 watts for actuating the solenoid valve of the thruster.

From the curves, the following conclusions may be drawn:

a. For the mass expulsion system (MES)

   (1) Weight depends upon mainly the number of disturbance impulses.
   (2) Weight fairly independent of θ_m for range of interest.
   (3) Weight directly dependent on ω_o.
   (4) Control thrust is proportional to ω_o^2 and inversely proportional to θ_m.

b. For the control moment gyro, weight is mainly dependent upon ω_o (proportional to ω_o).

c. For the reaction wheel (RW), weight is inversely proportional to m, inversely proportional to available power P, and directly proportional to ω_o.

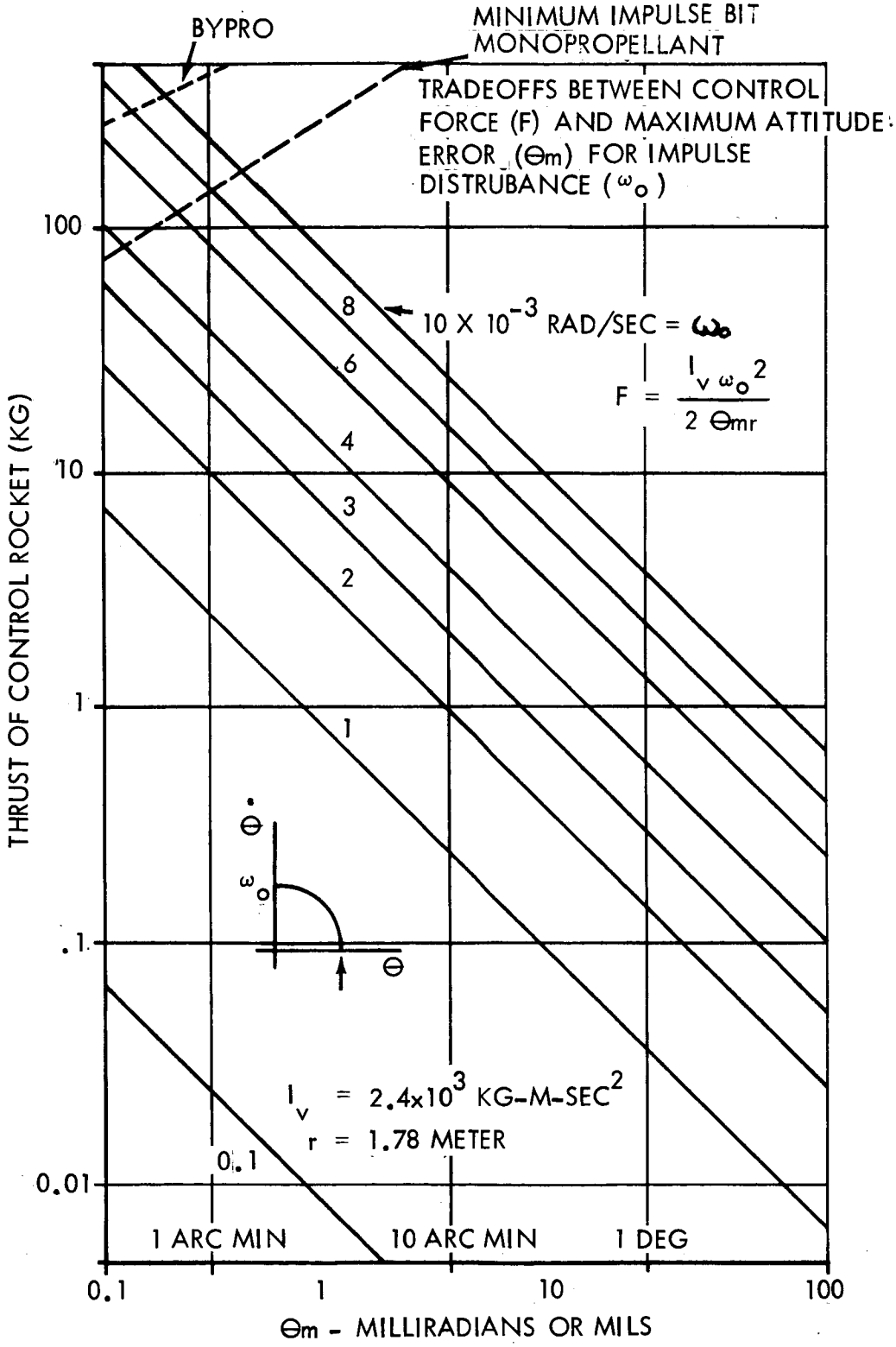


Figure 11.4.5.1-2.

d. If the disturbance has to be corrected to maintain the error to less than 1 degree, reaction wheels do not appear practical even if large amounts of power (a few hundred watts) are available. For θ_m of several degrees this system is competitive and for larger θ_m values, is superior from a weight point of view.

e. Control moment gyros are weight competitive, especially if a two-axis system is used. Their power requirements are nominal.

f. Mass expulsion system seems to be superior if the number of disturbances do not exceed three to four thousand per mission. The thruster force required is well within the state of the art even for θ_m as low as 1 arc minute.

g. Choice of the system should be based on availability and the requirements dictated by the other disturbances discussed below.

11.4.5.2 Periodic Disturbances

The results in this section are based on sinusoidal disturbances at orbital frequencies. The control system response is much faster than the disturbance so that the primary interest is in the momentum storage requirements and weight of the control system to handle these requirements. Reaction wheels and control moment gyros are each considered for the momentum storage function. The results are shown in figure 11.4.5.2-1.

Weight estimates for each of these types of control systems are given as a function of the magnitude of the disturbance torque and estimates of the maximum magnitude that can be expected are given for a 24-hour circular orbit. The weights are based on storage of the maximum vehicle angular momentum accumulated during one-half an orbit period. Unloading would occur during the other half period when vehicle torques reverse their polarity. A maximum speed of the RW was taken as 12,000 RPM and 3-degree rotation of the gimbal axis for the CMG for minimization of cross-coupling was assumed.

Maximum disturbances, taken from figure 11.4.5.2-2 are summarized below:

a. Gravity gradient. Torques due to this source were calculated for a range of altitudes from 200 nautical miles. It was assumed that the vehicle was orientated to give the largest torque, that is, a difference in the axial moment of inertias was taken as 7,230 Kg-meter^2 (5,280 slug ft^2).

b. Aerodynamic. These torques are based on preliminary estimates of the control moment coefficient (C_m) and for 1 radian angle of attack (α) of the space vehicle.

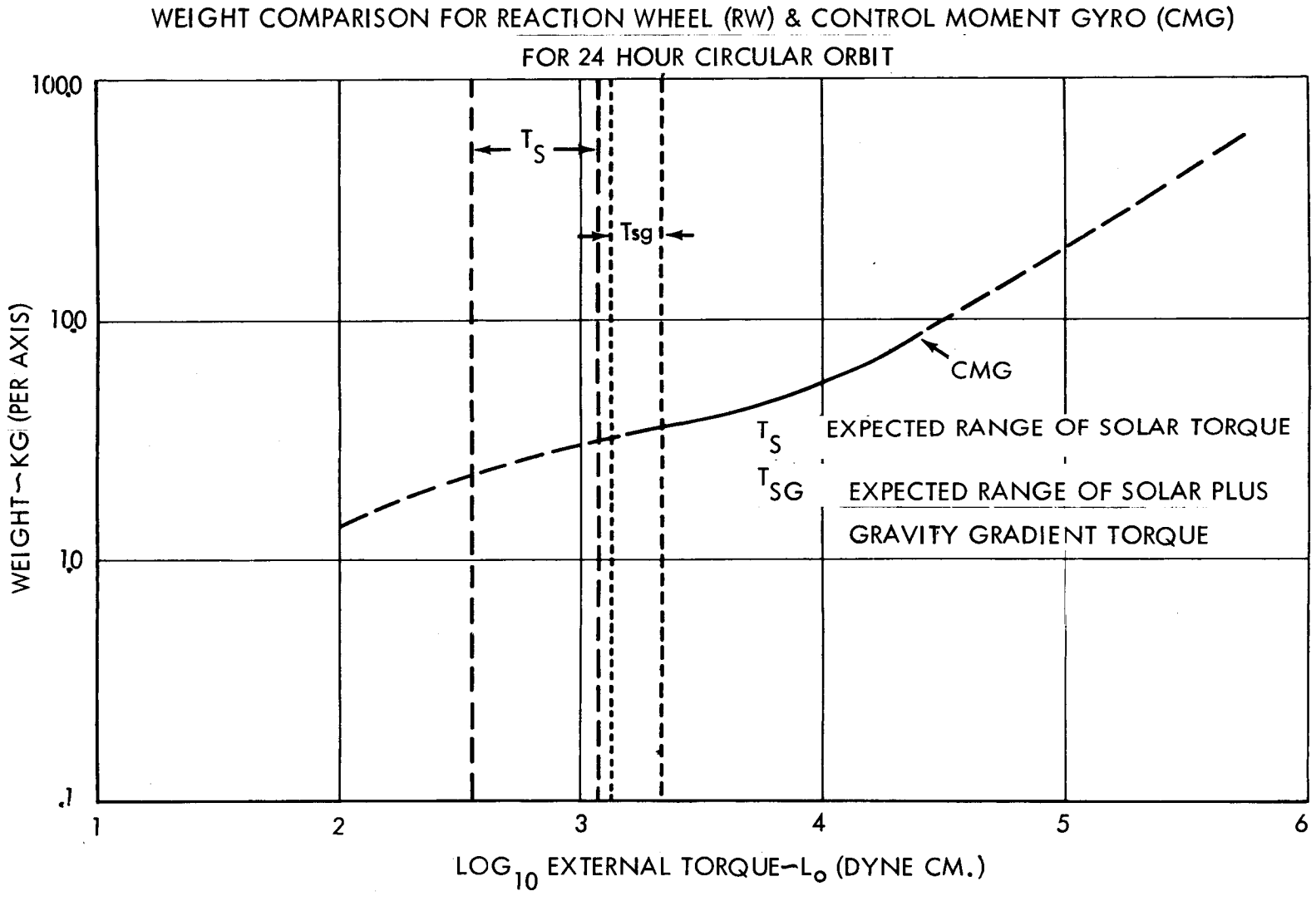


Figure 11.4.5.2-1.

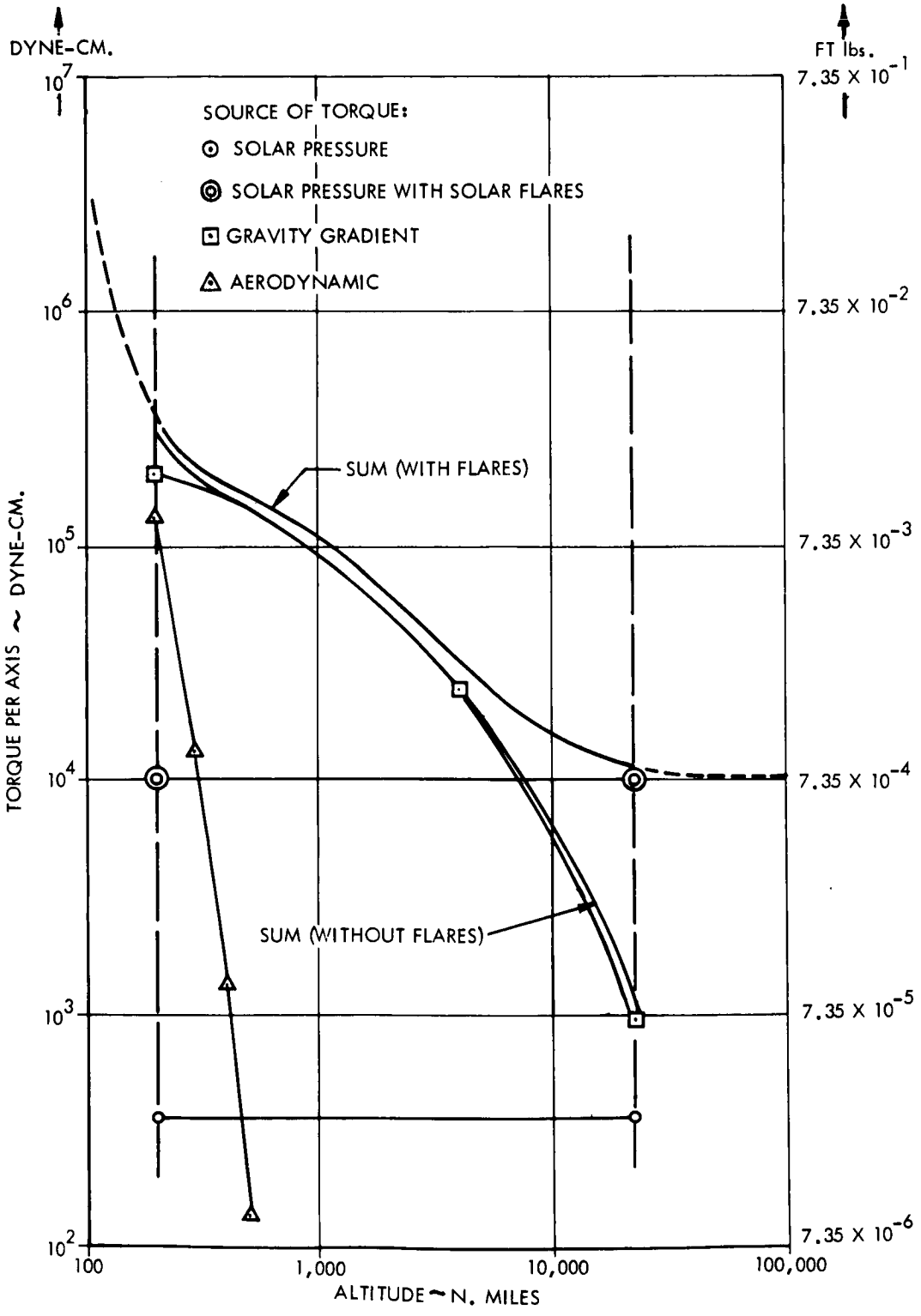


Figure 11.4.5.2-2.

c. Solar torque comes mainly from the solar panels and/or from the spacecraft structure. Estimates have been made of the disturbance due to some particular types of solar panel array. Other estimates, more crude, have been made for torques coming from the spacecraft body. Since these are based upon knowledge of the vehicle center of gravity and center of solar pressure, it is obvious that only rough estimates can be made at this time. The range of values of the estimates shown in figure 11.4.5.2-1 takes into account shifts in center of gravity due to man's displacement in the craft and a center of gravity shift with mission time as the vehicle uses it propellant for control, station keeping, rendezvous, etc.

Solar flares which can last for several orbit periods and cause a solar pressure as much as 50 to 100 times the magnitude of normal solar pressure are indicated on figure 11.4.5.2-2 but their effects are not indicated on figure 11.4.5.2-1. Sizing of the control system based on this disturbance would cause a substantial increase in the control system weight for the 24-hour circular orbit, but not for the near earth orbit where the gravity gradient and aero torques predominate. In the event that the extreme solar activity does occur, more frequent "unloading" of the RW or CMG would be required.

Figure 11.4.5.2-2 shows, in addition to the individual breakdown of the three main disturbances expected, a summary curve of the total. The latter curve is very conservative because of algebraic addition of assumed maxima.

Figure 11.4.5.2-1 shows the required CMG system weight as a function of the external torque for a 24-hour circular orbit. The range of the expected torque is determined from figure 11.4.5.2-2 and is used as a guide for approximate results. CMG weights were based on the information given in the Douglas report(2) for a single gimbal control moment gyro (SGCMG). This reference shows that a substantial weight per axis saving can be obtained by double gimbal (DGCMG) gyros which provide control about two axes. The angular momentum required for CMG weight estimates were obtained from table 11.4.5.2-1 which gives the torque and the resulting angular momentum per one-half orbit period for each of the three disturbances for the near earth and 24-hour circular orbit. If the weights as shown are considered excessive, smaller systems could be used, but propellant unloading from the RCS would then be required before the orbit half-period is reached. If the angular momentum accumulated during a half period (table 11.4.5.2-1) is used as a basis for estimating the propellant weight required for this unloading (about 150 pounds per year) it becomes apparent that not much weigh is saved from this technique for the 350 mile circular orbit discussed below.

---

(2) Douglas Aircraft Co., Report No. SM-46086, Vo. XV.

TABLE 4.2.3.3.1.2-1

TORQUE AND ANGULAR MOMENTUM

FOR THREE TYPES OF DISTURBANCE

	TORQUE (T)		ANGULAR MOMENTUM (H)					
			PER ORBIT HALF PERIOD			PER YEAR		
	NEAR EARTH CIRCULAR ORBIT - 350 N. MILES							
SOURCE	dyne-cm	lb-ft	dyne-cm-sec	$\frac{gm-cm^2}{sec}$	lb-ft-sec	dyne-cm-sec	$\frac{gm-cm^2}{sec}$	lb-ft-sec
SOLAR FL.	10,000	7.35×10^{-4}	2.75×10^{7}	2.81×10^{4}	2.02	3.17×10^{11}	3.23×10^{8}	2.33×10^{4}
SOLAR	350	2.60×10^{-5}	9.7×10^{5}	9.9×10^{2}	7.15×10^{-2}	1.11×10^{10}	1.13×10^{7}	8.25×10^{2}
GRAV. GRAD.	1.8×10^{5}	1.33×10^{-2}	4.95×10^{-8}	5.05×10^{5}	2.65×10^{1}	5.7×10^{12}	5.8×10^{9}	4.25×10^{5}
AERO	5×10^{3}	3.7×10^{-4}	1.38×10^{7}	1.41×10^{4}	1.01	1.58×10^{11}	1.61×10^{8}	1.17×10^{4}
			24 HOUR CIRCULAR ORBIT					
SOURCE								
SOLAR FL.	10,000	7.35×10^{-4}	4.33×10^{8}	4.41×10^{5}	3.18×10^{1}	3.17×10^{11}	3.23×10^{8}	2.33×10^{4}
SOLAR	350	2.60×10^{-5}	1.52×10^{7}	1.55×10^{4}	1.12	1.11×10^{10}	1.13×10^{7}	8.25×10^{2}
GRAV. GRAD.	950	7.00×10^{-5}	4.12×10^{7}	4.22×10^{4}	3.03	3.00×10^{10}	3.05×10^{7}	2.21×10^{3}
AERO	-	-	-	-	-	-	-	-

	(J) WHEEL MOMENT OF INERTIA FOR 12,000 R.P.M.				
	PER ORBIT HALF PERIOD			PER YEAR	
		$gm-cm^2$		$gm-cm^2$	lb-ft
	CIRCULAR 350 N. MILE ORBIT				
SOLAR FLARE		2.31×10^{1}		2.57×10^{5}	1.85×10^{1}
SOLAR		7.85×10^{-1}		8.98×10^{3}	6.55×10^{-1}
GRAV. GRAD.		4.02×10^{2}		4.61×10^{6}	3.38×10^{2}
AERO		1.12×10^{1}		1.28×10^{5}	9.3
	24 HOUR CIRCULAR ORBIT				
SOLAR FLARE		3.50×10^{2}		2.57×10^{5}	1.85×10^{1}
SOLAR		1.24×10^{1}		8.98×10^{3}	6.55×10^{-1}
GRAV. GRAD.		3.36×10^{1}		2.43×10^{4}	1.76
AERO		-		-	-

Table 11.4.5.2-1.

Weights for the RW were calculated, and the rotor required was found to be much less than 1 kilogram. It is expected that an RW weight of no more than 3 kilograms per axis would be sufficient.

Information similar to that in figure 11.4.5.2-1 for a 350 mile circular orbit was obtained. Here CMG weight is about twice that of the 24-hour circular orbit because of the higher angular momentum. RW weights for this orbit were about the same as those for the 24 hour circular orbit. Therefore for either orbit, the RW seems better than the CMG strictly from a weight point of view.

Power requirements for each of the two systems are small for both orbits, but are less for the RW. The reaction whell parameterization study below goes into more detail on the power and weight trade-offs.

11.4.5.3 Reaction Wheel Trade-Offs

Since reaction wheels are considered prime candidates for the control function in the OTES application, they were subjected to detailed analysis. The results are summarized in figures 11.4.5.3-1 and -2, where the relationships among moment of inertia (J), maximum wheel velocity (m), power requirements, maximum altitude error, and external disturbance (L).

A total disturbance torque of 100 dyne-cm at twice the orbital rate of synchronous altitude is assumed. Figure 11.4.5.3-1 shows that, if the maximum wheel speed is limited to 12,000 rpm because of mechanical consideration, a moment of inertia of 100 gm-cm^2 is adequate.

Figure 11.4.5.3-2 shows that for this moment of inertia and the 100 dyne-cm torque, about 10 milliwatts power is consumed (mechanical power only, assuming 100 per cent efficiency).

11.4.6 General Analysis

To optimize the control system design, an accurate estimate of the accumulated angular momentum for half an orbital period and for a full orbit must be available. Angular momentum accumulates as the time integral of external disturbances. In general, external disturbances are functions of the spacecraft angular orientation. Therefore, to determine these torques, it is necessary to know how the torques vary with orientation and the orientation of the spacecraft as a function of time for a given mission. Both these problems are straightforward applications of orbital and rotational mechanics. Numerical solutions, however, are difficult without the aid of a computer. Therefore, while waiting on a detailed mission definition, development of a general program to solve these problems was undertaken.

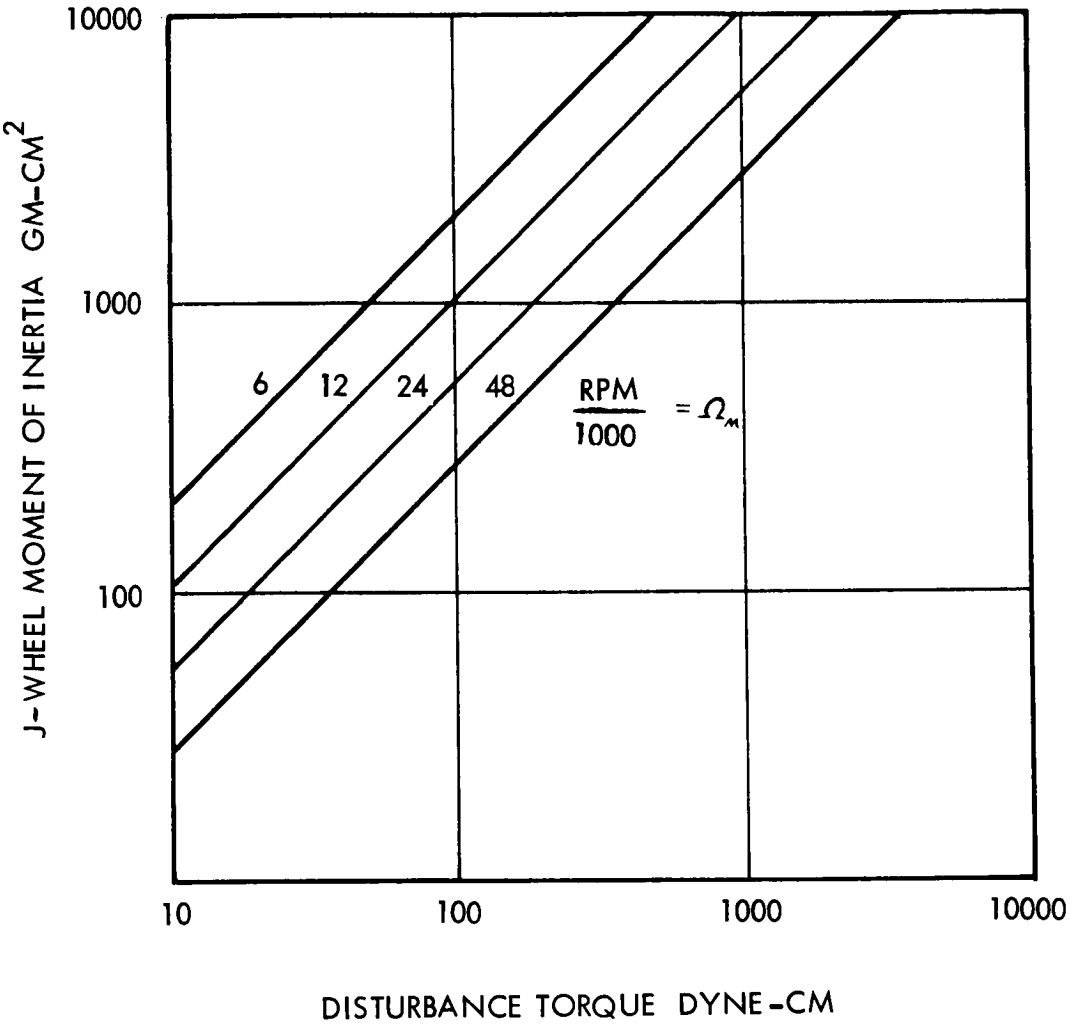


Figure 11.4.5.3-1. Reaction Wheel Moment of Inertia (J) and Maximum Angular Speed (Ω_m) Versus Spacecraft External Torque For Synchronous Orbit

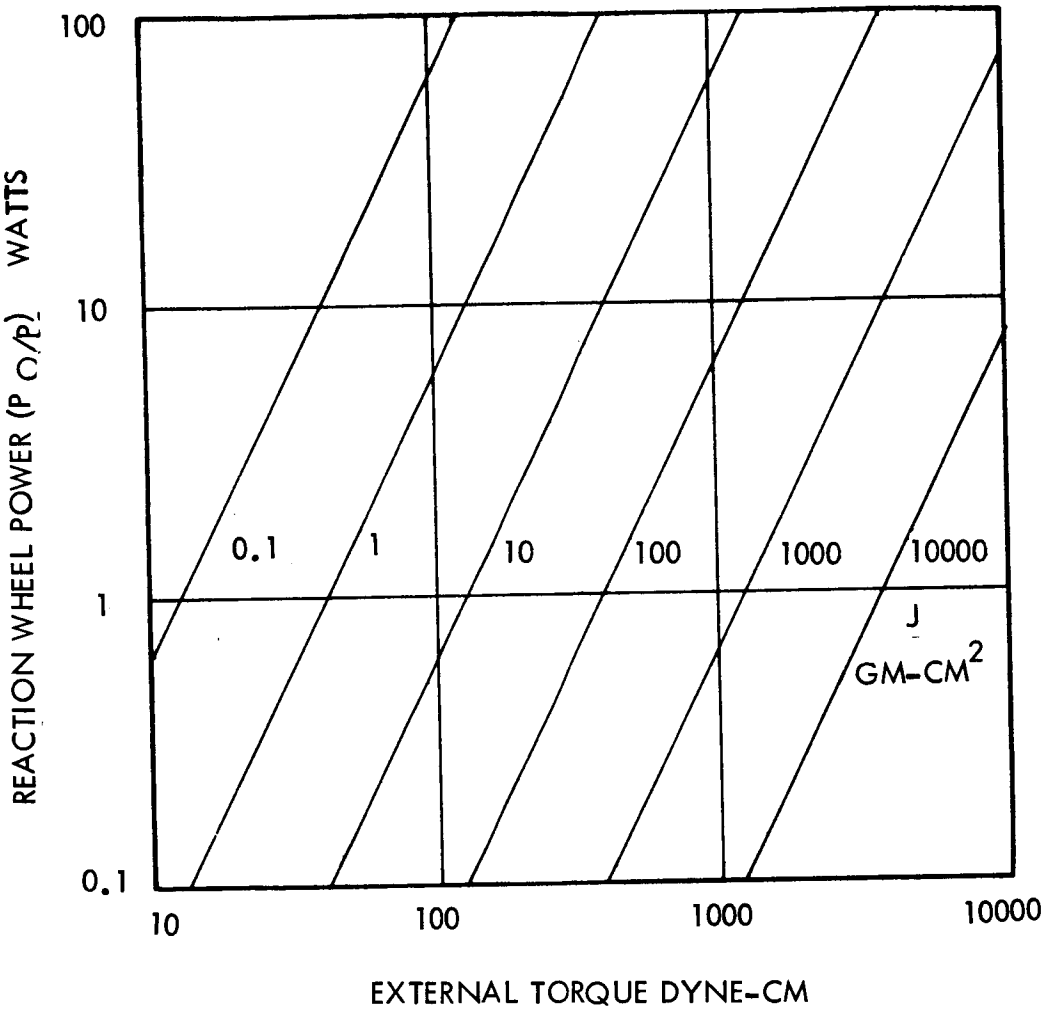


Figure 11.4.5.3-2. Reaction Wheel Power ($P_{o/p}$) And Moment of Inertia (J) Requirements Versus External Torque on Satellite For Earth Synchronous Orbit

The following approach was used: a satellite position may be described by a set of orbit parameters as illustrated in figure 11.4.6-1. If the satellite is earth-oriented (for example, with one axis directed along the local vertical, a second axis normal to the orbit plane, and the third axis completing the righthand set) the orbital parameters will also describe its orientation. If the satellite is in any other known orientation, transformations between the set of axes describing that orientation and the orbital set will describe its orientation in the latter set. Therefore, to know the satellite's orientation in any given set of fixed or rotating axes, it is only required to develop the proper transformations.

Such transformations are developed in the reference.(3) Some of the results are repeated here, as needed to develop the general time-dependent torque equations in the following section.

11.4.6.1 Torque Equations

Since the present OTES concept calls for a synchronous orbit, only the gravity-gradient and solar pressure torques are developed here. The other major source of external torque (aerodynamic forces) becomes negligible above a few hundred miles.

In general, the gravity-gradient torque is expressed as(4)

$$T = \frac{3\mu}{R_o^3}\int \frac{(\bar{P}\cdot\bar{R})\,(\bar{P}\times\bar{R})\;dm}{R_o^2} \qquad (1)$$

where

T = torque (ft-lb)

μ = earth gravitational constant (ft^3/sec^2)

R = radius vector to center of earth (ft)

dm = mass element (slugs)

P = location of dm in body axes (ft)

These quantities are illustrated in the figure 11.4.6.1-1, in which the orbital axes and body axes are defined. The dot and cross products are expanded as follows. In the body-fixed XYZ set,

---

(3) Riles, J., Some Useful Coordinate Transformations for Space Dynamics Problems, TB-AE-66-349, Chrysler Corp. Space Div., New Orleans, La.

(4) Thomson, W.T., Passive Altitude Control of Satellite Vehicle in Guidance and Control of Aerospace Vehicles, McGraw Hill, 1963.

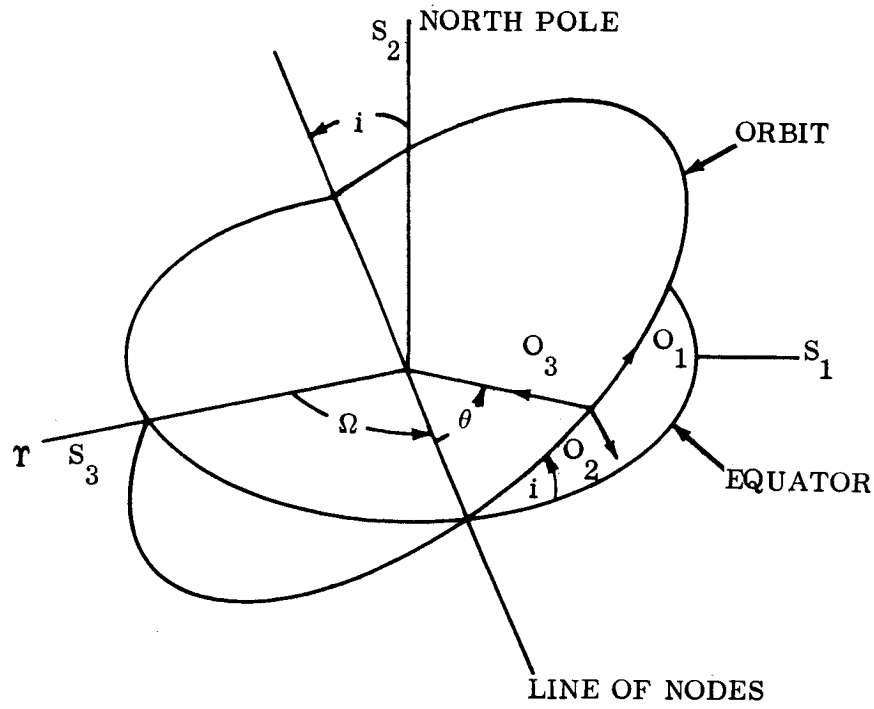


Figure 11.4.6-1. Angular Orientation of Orbit Axes Relative to Earth-Centered Inertial Axes

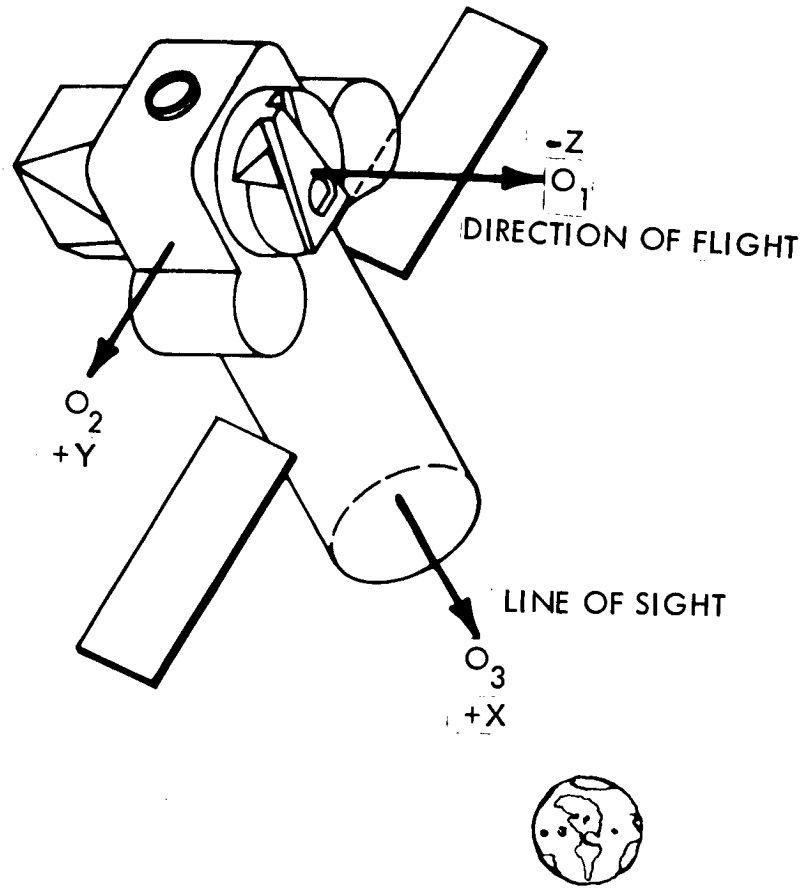


Figure 11.4.6.1-1. Sketch of Spacecraft and Orbital Axes For Zero Slew Angles

$$\bar{P} = X\,\bar{i} + Y\,\bar{j} + Z\,\bar{k} \tag{2}$$

and in the orbital set

$$\bar{R}_o = R_o\,\bar{O}_3 \tag{3}$$

where $\bar{i}$, $\bar{j}$, $\bar{k}$ are unit vectors in the body set and $\bar{O}_3$ is a unit vector in the orbital set.

$$\begin{aligned} D_3 = {} & \bar{i}\,\mathrm{Cos}\,\phi\,p\;\;\mathrm{Cos}\,\phi\,y + \bar{j}\,(\mathrm{Sin}\,\phi\,r\;\;\mathrm{Sin}\,\phi\,p\;\;\mathrm{Cos}\,\phi\,y \\ & - \mathrm{Cos}\,\phi\,R\;\;\mathrm{Sin}\,\phi\,y) + \bar{k}\,(\mathrm{Cos}\,\phi\,r\;\;\mathrm{Sin}\,\phi\,p\;\;\mathrm{Cos}\,\phi\,y \\ & + \mathrm{Sin}\,\phi\,R\;\;\mathrm{Sin}\,\phi\,y) \end{aligned} \tag{4}$$

Substitution of equations (2), (3) and (4) into (1) and carrying the indicated operations yields the following types of terms

(a) $$\int (y^2 - z^2)\, f_1(\phi)\, dm \tag{5}$$

(b) $$\int xy\, f_2(\phi)\, dm \tag{6}$$

where

f_1 and f_2 are functions of the ϕ angles.

If we assume that the body axes are principal axes, all the product terms of type (b) vanish, and the type (a) terms yield moment of inertia differences. That is

$$\int (y^2 - z^2)\, f_1(\phi)\, dm = (I_z - I_y)\, f_1(\phi) \tag{7}$$

and

$$\int xy\, f_2(\phi)\, dm = 0 \tag{8}$$

Performing the integration gives the torque equations in terms of the spacecraft orientation in the orbital set of coordinates.

$$T_X = \frac{3\mu}{R_o^3} (I_z - I_y) (\sin\phi R \sin\phi P \cos\phi Y - \cos\phi R \sin\phi Y)$$

$$(\sin\phi R \sin\phi Y + \cos\phi R \sin\phi P \cos\phi Y) \quad (9)$$

$$T_Y = \frac{3\mu}{R_o^3} (I_X - I_Z) (\cos\phi P \cos\phi Y) (\sin\phi R \sin\phi Y + \cos\phi P \cos\phi Y \sin\phi P) \quad (10)$$

$$T_Z = \frac{3\mu}{R_o^3} (I_Y - I_X) (\cos\phi P \cos\phi Y) (\sin\phi R \sin\phi P \cos\phi Y - \cos\phi P \sin\phi Y) \quad (11)$$

where,

μ = gravitational constant of the earth

R_o = radius of orbit (ft)

I_X, I_Y, I_Z = moments of inertia (slug-ft^2)

X,Y,Z = pitch, yaw, and roll angles.

If the time-variation of these angles is known, the time-variation of the torque is also known.

The slew angles depend on the mission. For experiments which require a ground station to be tracked, the time-variation of the angles is determined as follows:

a. The position of the tracking station relative to the stars is known since it depends only on the earth's motion.

b. The position of the satellite relative to the stars is also known because it depends only on the orbital parameters.

c. Therefore, the direction of a line joining the two is also known relative to the stars.

d. This direction, relative to the orbital set, is determined by transforming the orbital set of coordinates into an inertial set.

The details of the derivation are given by Riles(5). The results are given below.

$$P = \sin^{-1} \left\{ \frac{1}{R} \left[- C_1 \operatorname{Sin} \wedge_T \operatorname{Sin}\theta + C_2 \cos i \sin \wedge_T \cos\theta - C_4 \cos\theta - C_2 \cos \wedge_T \sin\theta \right] \right\} \quad (12)$$

$$Y = \sin^{-1} \left\{ \frac{1}{R \cos\phi P} \left[C_2 \sin i \sin \wedge_T + C_3 + C_1 \sin i \operatorname{Cos}_T \right] \right\} \quad (13)$$

$$R = \left\{ R_e^2 - R_o^2 + 2 R_o \left[- C_1 \sin\wedge_T \cos\theta - C_2 \cos i \sin\wedge_T \sin\theta + C_1 \cos i \cos\wedge_T \sin\theta + R_o \right] \right\}^{\frac{1}{2}} \quad (14)$$

Where

$$C_1 = R_e \cos\lambda_T \sin\Omega$$

$$C_2 = R_e \cos\lambda_T \cos\Omega$$

$$C_3 = R_e \sin\lambda_T \cos i$$

$$C_4 = R_e \sin\lambda_T \sin i$$

and

$$\wedge_T = \quad _{To} + \omega_e t$$

$\wedge_{To}$= logitude of tracking station.

ω_e = earth's rate.

t = local sideral time for the tracking station.

λ_T = latitude of the tracking station measured positive in the southern hemisphere.

$\theta = \omega + \theta'$

---

(5) J. C. Riles, Development of a Computer Program to Solve Rotational Dynamics Problems. TN-AE-66-144, Chrysler Corp., Space Div., New Orleans.

ω = arguement perigee

θ^1 = true anomaly

Ω = right ascension

i = orbit inclination.

A program to solve the above equations on the 7094 computer has been developed.

Notice that range, range rate, and slew rates are also given as by-products of the calculations.

It should be pointed out that the roll angle doesn't appear because, with the yaw-pitch-roll sequence, it is completely arbitrary. A modification of this program uses this fact to null the body rates about the roll axis.

The details are given in the reference

11.4.6.2 Solar Radiation Pressure Torque

At synchronous altitude, solar radiation pressure torque will be a major contribution to accumulated satellite angular momentum. Solar torque is a function of satellite projected area normal to the sun line, offset of the centroid of this area from the satellite center of mass, and reflection characteristics of the surface. In general, all of these are functions of satellite orientation relative to the sun line, which in turn is a function of time that depends on the particular mission.

In general, and especially for the OTES, the orientation of the spacecraft satellite relative to the sun is a function of orbital position. Therefore, to determine the direction of the sun vector in body-fixed coordinates, it is necessary first to determine its direction relative to inertial cooridnates, then transform to orbital parameters, and finally transform to body-fixed coordinates in accordance with the particular mission. The illustration in figure 11.4.6.2-1 shows earth-centered inertial coordinates related to earth-centered ecliptic coordinates by the ecliptic angle i_c. The position of the sun is measured from the vernal equinox by the angle m in the ecliptic plane. The direction of the sun line is

$$\frac{\bar{S}}{S} = \bar{S}_3 \cos m + \bar{S}_1 \sin m \qquad (15)$$

where $\bar{S}/S$ is a unit vector directed toward the sun.

Transforming $\bar{S}_3$ and $\bar{S}_1$ into the orbital set of coordinates also illustrated in figure 11.4.6.2-1.

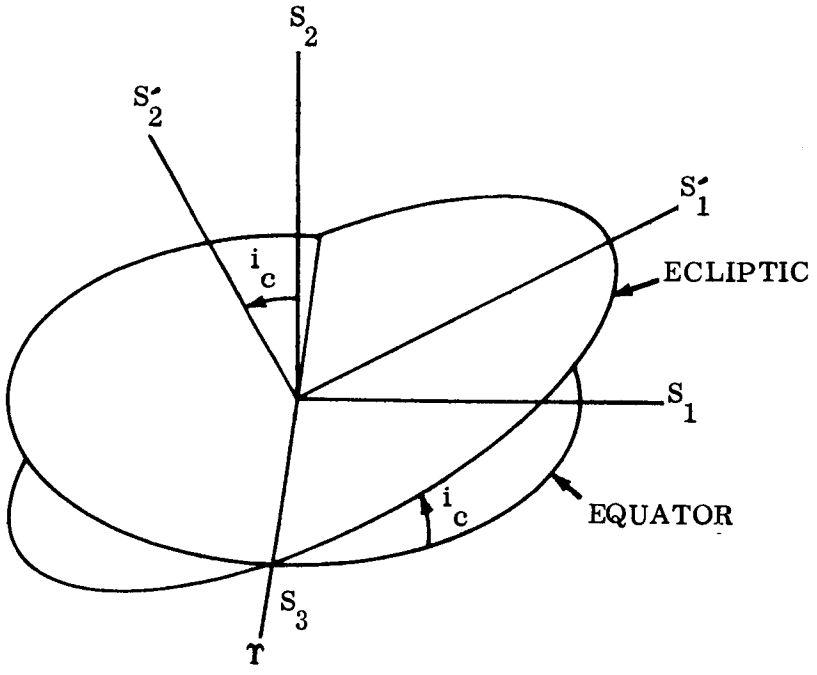


Figure 11.4.6.2-1. Angular Orientation of Ecliptic Axes to Earth-Centered Inertial Axes

$$\bar{S}_S = \cos m\,(-\sin\theta\cos\Omega - \cos i\sin\Omega\cos\theta)\,\bar{O}_1 + \cos m\,(-\sin i\sin\Omega)\,\bar{O}_2 + \cos m\,(-\cos\theta\cos\Omega + \cos i\sin\Omega\sin\theta)\,\bar{O}_3 + \sin m\,(-\sin\theta\sin\Omega\cos i_c + \cos i\cos\Omega\cos\theta\cos i_c + \cos\theta\sin i\sin i_c)\,\bar{O}_1 + \sin m\,(\sin i\cos\Omega\cos i_c - \cos i\sin i_c)\,\bar{O}_2 + \sin m\,(-\cos\theta\sin\Omega\cos i_c - \cos i\cos\Omega\sin\theta\cos i_c - \sin\theta\sin i\sin i_c)\,\bar{O}_3 \quad (16)$$

$$\bar{S}_S = \eta_1\,\bar{O}_1 + \eta_2\,\bar{O}_2 + \eta_3\,\bar{O}_3 \quad (17)$$

where

$$\eta_1 = \cos m\,(-\sin\theta\cos\Omega - \cos i\sin\Omega\cos\theta) + \sin m\,(-\sin\theta\sin\Omega\cos i_c + \cos i\cos\theta\cos i_c + \cos\theta\sin i\sin i_c) \quad (18)$$

$$\eta_2 = \cos m\,(-\sin i\sin\Omega) + \sin m\,(\sin i\cos\Omega\cos i_c - \cos i\sin i_c) \quad (19)$$

$$\eta_3 = \cos m\,(-\cos\theta\cos\Omega + \cos i\sin\Omega\sin\theta) + \sin m\,(-\cos\theta\sin\Omega\cos i_c - \cos i\cos\Omega\sin\theta\cos i_c - \sin\theta\sin i\sin i_c) \quad (20)$$

These are the direction cosines of the sun line in the orbital set of coordinates. Since it is principally at synchronous altitude that solar radiation pressure is relatively important, and because at this altitude a satellite directed to any geographical point on the earth is directed to within a few degrees of the center of the earth, a reasonable approximation for all earth-oriented satellites is that body-fixed axes coincide with the orbital axes. For this condition the 's are the direction cosines of the solar vector in the body-fixed set, and the solar torque is determined as follows.

Let:

A_1 = projected area normal to 0,

l_{12} = O_2 component of A_1 centroid offset

l_{13} = O_3 component of A_1 centroid offset and similarly for the other axes.

The solar torques are:

$$T_1 = -S\mu_3 A_3 \eta_3 l_{32} + S\mu_2 A_2 \eta_2 l_{23} \quad (21)$$

$$T_2 = -S\mu_1 A_1 \eta_1 l_{13} + S\mu_3 A_3 \eta_3 l_{31} \quad (22)$$

$$T_3 = S\mu_1 A_2 \eta_1 l_{12} - S\mu_2 A_2 \eta_2 l_{21} \quad (23)$$

where:

S = solar constant (lb/ft^2)

μ = reflection coefficient.

The A's and l's are highly dependent on the particular satellite under consideration. The reflection coefficient varies from unity for complete absorption to two for complete reflection.

Equations (18) through (20) and (21) through (23) are being incorporated in the general program described above. Of course, the direction cosines of the seen vector are of interest in other areas such as power, thermal control, and mission analysis.

11.4.7 Reaction Control System

The Reaction Control System (RCS) is used for ΔV correction, for station keeping, for attitude control during maneuvering, and for desaturation of momentum storage devices.

Preliminary analyses indicate that the lightest Reaction Control System would be a storable, hypergolic bipropellant, pressure fed system. This system will utilize components which will have been developed and flight qualified in pre-OTES programs. This would tend to minimize development and qualification cost, and lead times.

The use of cold gas (nitrogen), monopropellants (90 per cent hydrogen peroxide and hydrazine), and bipropellant (nitrogen tetroxide/50-50 dydrazine-UDMH) systems were investigated for providing the ΔV (457 m/sec) and angular impulse (5016 N-m-sec) requirements developed previously. Figure 11.4.7-1 shows the estimated system weights for various combinations of these propellants.

Figure 11.4.7-1. Estimated OTES Reaction Control System Weights* For Various Propellants

		VELOCITY INCREMENT REQUIREMENTS			
		COLD GAS	MONOPROPELLANT		BI PROPELLANT
		N_2 I_{sp} = 65 sec	H_2O_2 I_{sp} = 150 sec	N_2H_4 I_{sp} = 220 sec	I_{sp} = 280 sec
ANGULAR MOMENTUM REQUIREMENTS	COLD GAS N_2 I_{sp} = 65 sec	4000+	1420	1135	1000
	MONOPROPELLANT H_2O_2 I_{sp} = 150 sec		1360	1045	905
	MONOPROPELLANT N_2H_4 I_{sp} = 220 sec			1000	860
	BI PROPELLANT I_{sp} = 280 sec				816

* In Kilograms

Basically, the selected Reaction Control System consists of 16 thrusters supplied by two separate propellant supply sections. The thrust chambers and the dual propellant supply sections make up two parallel, independent subsystems. Table 11.4.7-1 and figure 11.4.7-2 show the perliminary equipment list and schematic diagram, respectively, for the Reaction Control System.

The RCS uses hypergolic propellants that consist of a 50-50 fuel mixture of hydrazine (N_2H_4) and unsymmetrical dimethylhydrazine (UDMH) with nitrogen tetroxide (N_2O_4) as the oxidizer. The weight mixture ratio of oxidizer to fuel is 2.0.

The propellant supply subsystems include all the propellant storage, pressurization, and feed components necessary for the delivery of fuel and oxidizer to the thrusters. Each subsystem has six cylindrical propellant tanks, three titanium fuel tanks, and three aluminum tanks for the oxidizer. In this phase of the study, existing tank sizes were utilized and no attempt was made to optimize the tankage. The liquid propellants are contained in positive expulsion metallic bellows. Although weighing more than teflon bladders, metal bellows were chosen because the long terms space storage requirement (2 years) makes them more realistic than the more permeable teflon bladders.

The six tanks in each subsystem are pressurized by a 27.58 million newtons/square meter (4000 psi) nitrogen supply acting on the bellows to force the propellants into the manifolds which supply the eight thrusters in that subsystem. Each nitrogen supply consists of three spherical titanium tanks. For this phase of the study, nitrogen was selected rather than helium as a pressurant because of its lower leakage rate.

Standardized 444.8 newtons (100 lb) thrusters, capable of either pulse-mode or steady-state operation, were selected in this phase of the study. Although this thrust level is high for the type of performance required, the minimum angular impulse produced by the thrusters about a single axis is approximately an order to magnitude less than that accumulated by the momentum exchange system each orbit. Therefore, even thrusters having a large degradation of minimum impulse would still be capable of desaturating the momentum storage devices and could also provide the large velocity increments needed.

Location of the RCS thrusters presents a heating problem on several of the configurations under consideration, especially with configurations 1 and 2. On these configurations, the present location of the thrusters on the Lunar Excursion Module is unsatisfactory because the exhaust from the downward firing thrusters impinge on the Telescope Module. This would undoubtedly cause a severe heating problem. Depending upon the particular configuration (1 or 2), the sideward firing thrusters would also effect the solar panels to varying degrees. A detailed analysis of these problems is scheduled for subsequent phases of this study. Except for 1, 2 and 7 configurations, it is possible to locate the thrusters in such a manner that the

TABLE 11.4.7-1

REACTION CONTROL SYSTEM EQUIPMENT LIST

QUANTITY	ITEM	INDIVIDUAL DIMENSIONS (m)	TOTAL MASS (Kg)
	RCS (Total)		(949.18)
6	Fuel Tanks	dia. - 0.318 length - 0.813	34.02
6	Oxidizer Tanks	dia. - 0.318 length - 0.982	42.40
8	Nitrogen Tanks	dia. - 0.231	20.68
16	Thrusters	dia. - 0.076 length - 0.254	64.59
	Lines, Valves, Etc.		91.71
	Filters		
2	Fuel		
2	Oxidizer		
2	Pressurant		
	Fill and Ground Test Connectors		
8	Fuel		
8	Oxidizer		
14	Pressurant		
	Valves		
8	Oxidizer		
8	Fuel		
2	Pressurant		
4	Relief		
8	Check		
2	Regulators		
4	Burst Diaphragm		
	Fuel		226.80
	Oxidizer		453.60
	Nitrogen		15.38

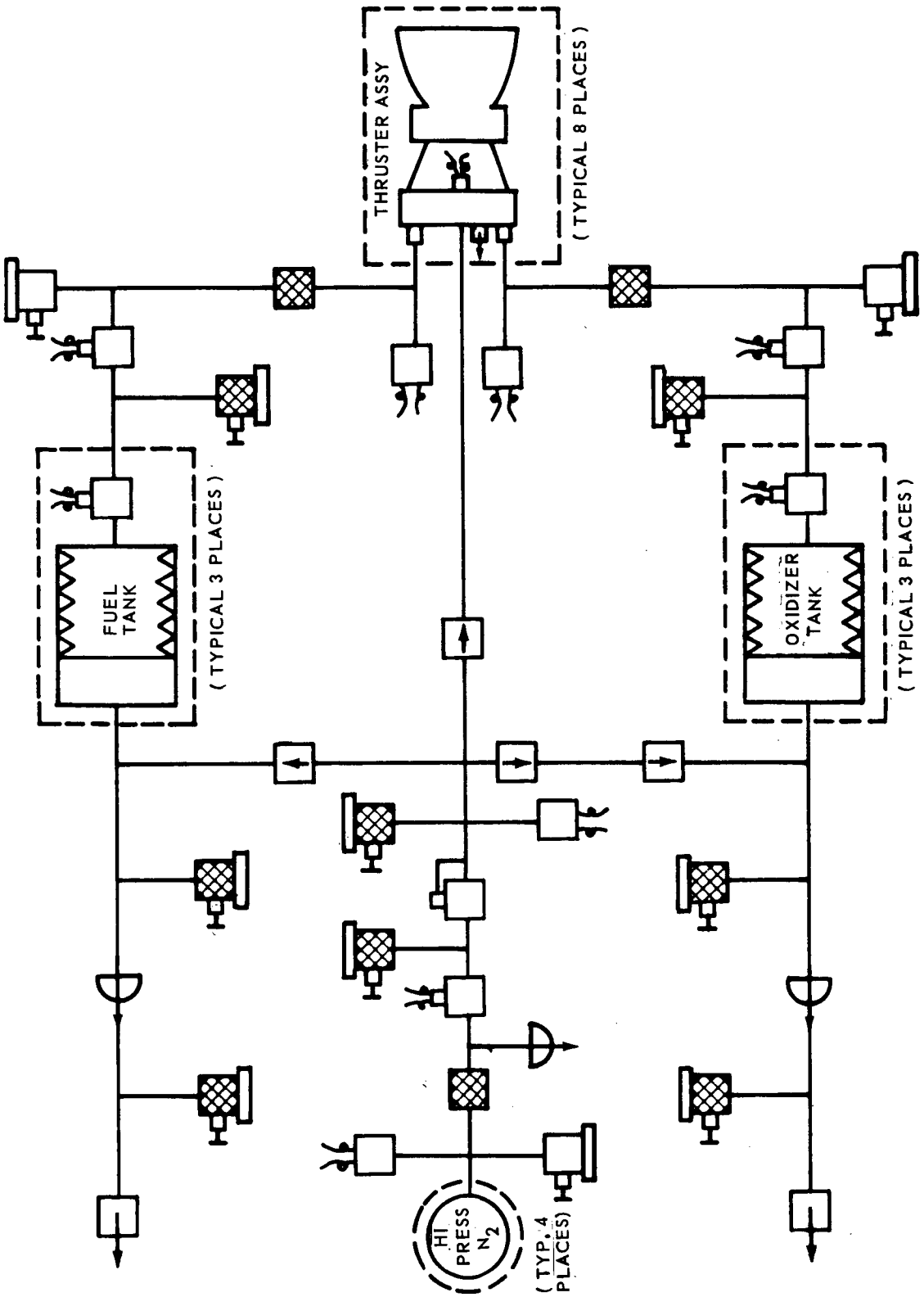


Figure 11.4.7-2. Reaction Control System Schematic

exhaust plume does not pass through the telescope's line of sight and/or impinge on the spacecraft and solar panels. However, this is accomplished only at the expense of thruster moment arms.

On configuration 7, it would be virtually impossible to locate the thrusters to eliminate exhaust gas impingement on the movable telescope. In addition, if reorientation of the movable telescope on this configuration causes a large displacement of the spacecraft's center of gravity, then it would be impossible to keep the RCS thrusters from producing an undesirable translation motion.

After definition of the mission and configuration, the reaction control system will be optimized in terms of propellants, types of engines, engine location, engine performance, engine life, pressurant, and tankage. The purpose of these efforts was to indicate the existence of potential problems.

11.5 POWER

11.5.1 Load Profile Analysis

Before more than the most cursory of analysis of the candidate power systems can be initiated, it is necessary to determine the magnitude of the electrical power requirements and the duration of the requirements. Not only is the load profile important to the power system selection but of equal importance is the existance of possible constraints on the experiments.

11.5.1.1 Inputs and Assumptions

The following ground rules were considered and adhered to in constructing the load profile.

a. The load profile is based on the average steady state power variations of each particular subsystem and/or experiment. Intermittent loads with relatively low duty cycle are averaged with the steady state power variations of that particular subsystem or experiment causing the intermittent load.

b. The power losses resulting from conversion subsystems are included in the power profiles.

c. The time phasing of experiments is compatible with the flight plan specified in section 12.0 Experiment/Mission Time Phasing, Vol. II.

d. The maximum peak load is a worst case condition obtained by evaluating the time phasing of experiments causing intermittent loads and summing those that could occur simultaneously.

e. In cases where the power requirements were not defined, comparable S-IB equipment requirements were used where applicable.

In addition to these groundrules, it was necessary to make several assumptions in order to determine the electrical load profile. These assumptions are:

a. Class A power (see section 11.5.1.2) will be supplied from a separate source.

b. Electrical power requirements during checkout do not exceed the maximum during any other time.

c. An average of approximately 200 measurements will be required throughout the mission and the power required per measurement is comparable to that of the S-IB Stage.

d. That the experiments requiring lasers will be repeated every 10 days during the unmanned portion of the mission.

e. All data receivers are on at all times.

f. The beacon transmitter is on when other transmitters are off.

11.5.1.2 Load Profiles

A preliminary power profile was generated to provide a basis for the power system investigation. The power load requirements are classified into three categories or classes.

Class A power, which encompasses all loads necessary for manned operation, includes such equipment as the environmental control system and cabin lighting. Class A power is required only for the manned portion of any OTAES mission. The hardware for OTAES is based on existing hardware and, as a consequence, the power requirements and power source for Class A power will be similar to those for Apollo and the LEM. Class A power requirements are, therefore, not included in the power profile.

Class B power includes those loads necessary to maintain the spacecraft. Among the equipment in this class are the command and control, information gathering and processing, and information display and transmission. Class B power is required for the entire duration of the mission (i.e., manned and unmanned).

Class C power includes those loads necessary to operate the experiments. Figure 11.5.1.2-1, OTAES Power Profile, presents the load profile for the OTAES power system. The power levels are based on the Electrical Load Summaries of table 11.5.1.2-1, OTAES Spacecraft Equipment, table 11.5.1.2-2, OTAES Experiments Requiring Lasers, and table 11.5.1.2-3 OTAES Experiments Not Requiring Lasers. From figure 11.5.1.2-1, the maximum steady state power required is 2445 watts. The average power required during the manned portion of the mission is 1565 watts and during the unmanned portion of the mission the average power is 1414 watts.

The times during the mission that power is required by the various subsystem and experiment equipment is also shown in figure 11.5.1.2-1.

The average power required during the unmanned portion of the mission is lower than during the manned portion of the mission because of the reduced duty cycle for experiments requiring lasers.

The maximum transient power which can be expected to be superimposed on the steady state requirements is approximately 650 watts, of which 450 watts is due to the operation of the Spacecraft Reaction Control System. The duration of this transient is not expected to last for more than 30 seconds.

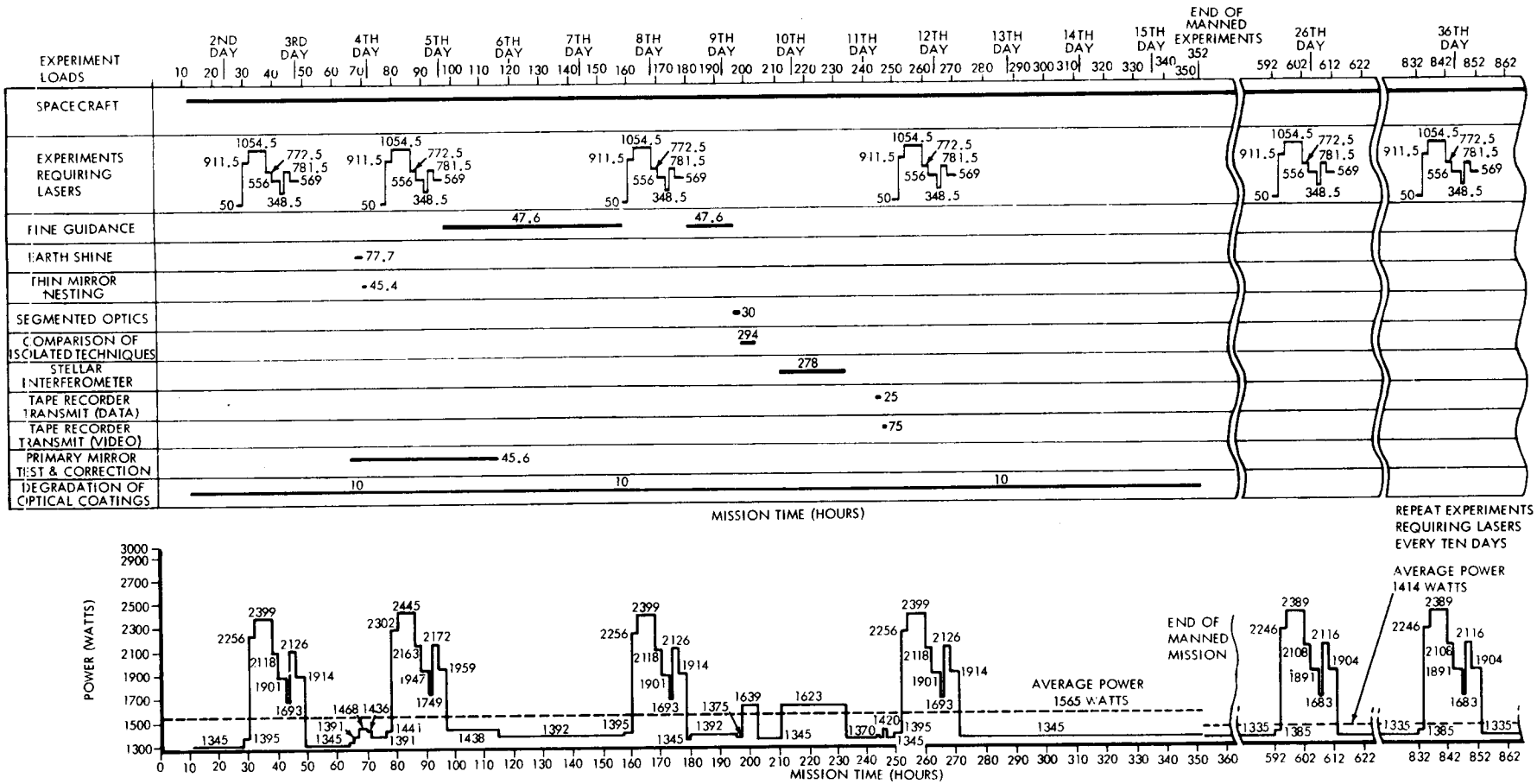


Figure 11.5.1.2-1. OTAES Power Profile

TABLE 11.5.1.2-1

ELECTRICAL LOAD SUMMARY,

OTAES SPACECRAFT EQUIPMENT

EQUIPMENT	AVERAGE POWER (WATTS)
Command Rcvr #1 & #2	15
Command Decoder #1	5
Command Decoder #2	5
Spacecraft Stabilization	268
Reaction Control System	75
High Gain Antenna Pointing	11
1.0 Meter Mirror Htrs.	100
Info Process & Control Unit	60
N.B. & W.B. T/M Encoders	6
Sensors & Signal Conditioning	440
On Board Programmer	100
Exper Data Rcve & De Mox #3	35
Tracking Rcvr #4	85
Exper Dat Xmttr & MOD #4	50
N.B. Data Xmttr & MOD #2	30
N.B. Data Xmttr & MOD #3	50
TOTAL AVG. PWR.	1,335

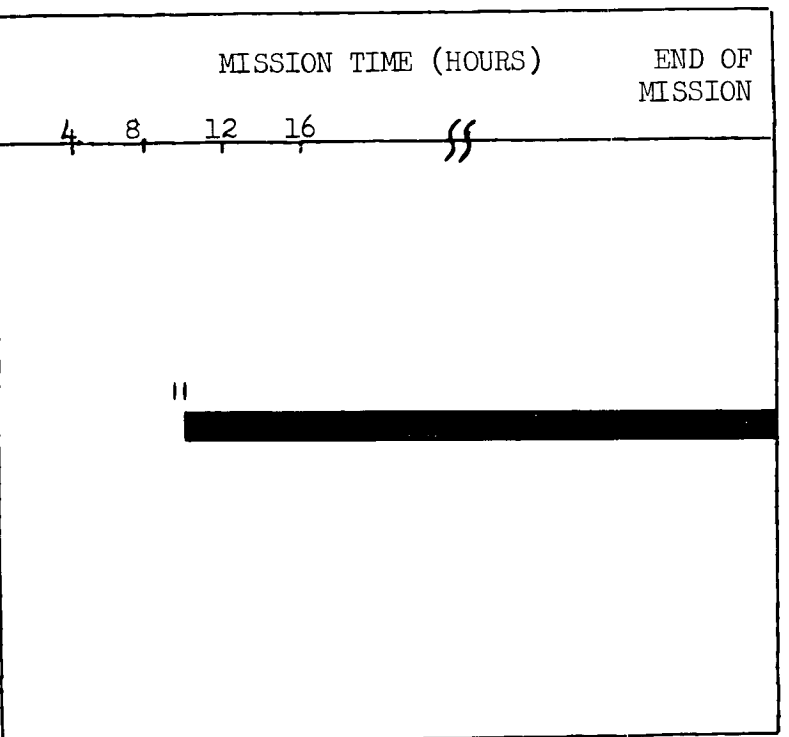
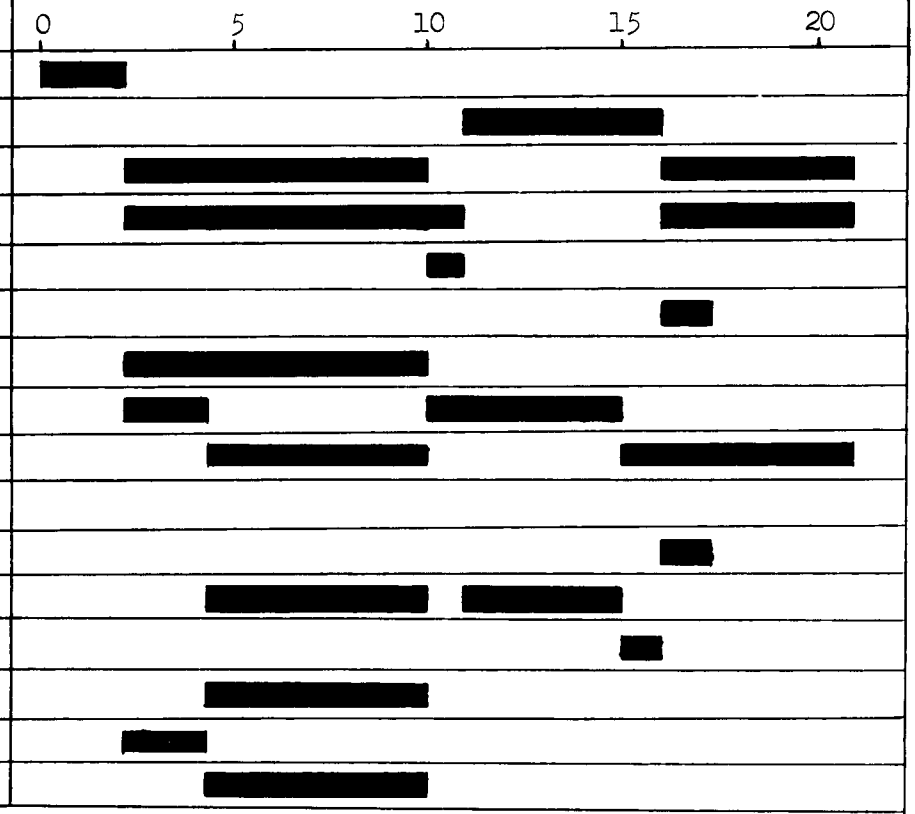


TABLE 11.5.1.2-2
ELECTRICAL LOAD SUMMARY
OTAES EXPERIMENTS REQUIRING LASERS

EXPERIMENT	AVERAGE POWER (WATTS)
Standby	50
	25
Opt. Heterodyne on Earth	197.5
Opt. Heterodyne on S/C	248.5
Comm. with 10 MHz Bandwidth	254.5
	135
Direct Detection	51
0.1 Arc Sec Tracking of Ground Beacon	279.5
	72
Earth Shine	77.5
Point Ahead	251.5
Tracking Transfer	251.5
Pulse Distortion	49.5
Atmospheric Measurement	135
	184.5



NOTE: The 21 hour cycle of experiments requiring lasers is repeated during the following Manned Mission times: 28 to 49 hrs.; 76 to 97 hrs.; 158 to 179 hrs.; 250 to 271 hrs.

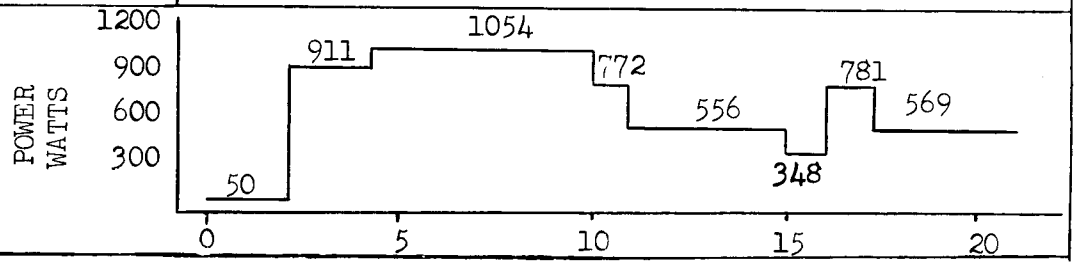


TABLE 11.5.1.2-3

ELECTRICAL LOAD SUMMARY

OTAES EXPERIMENT NOT REQUIRING LASERS

EXPERIMENT	AVERAGE POWER (WATTS)	EXPERIMENT TIME (HOURS) * SEE NOTE BELOW 0 1 2 3 4 5 22 50 99 341 END OF MISSION
Fine Guidance	48.0	
Stellar Interferometer	278.0	
Comparison of Isolation Techniques	294.0	
Segmented Optics	30.0	
Degradation of Optical Coatings	10.0	
Thin Mirror Nesting	45.4	
Primary Mirror Test & Correction	45.4	

NOTE: See Figure 2 for Mission Times When the Above Experiments Require Power.

11.5.1.3 Power Constraints on Experiments

Although several load equipments have a requirement for relatively large amounts of power, the time phasing of the experiments is such that large peaks occur only for those periods of time when the lasers are operating.

Since the peak loads are supplied from secondary batteries and batteries are energy related, it is recommended that the lasers not be operated during the shadow portion of the orbit if solar cells are the primary power source. If RTG's are used, this restriction will not occur since the power source is unaffected by shadow operation.

11.5.2 Radioisotope Thermoelectric Generator

Radioisotope thermoelectric generators (RTG) have some degree of space usage behind them. In addition, a number of programs are currently underway which will add significantly to the technology.

The design of an RTG is relatively straight-forward, but the various components that comprise the RTG must be considered as an integral unit. The three topics to be discussed in this section are: isotope selection, design of the generator, and the performance and integration of the entire subsystem.

11.5.2.1 Isotope Selection

Although there are approximately 1300 isotopes known, relatively few have the necessary characteristics to make them attractive as space energy sources. Among the properties that must be considered are the half-life, power density, thermal characteristics type of radiation emitted, cost and availability.

Consideration of the half-life (the time required for the isotope to decay to one-half of its original power density) reduces the number of candidates to somewhere around one hundred isotopes. After considering the other factors, only nine isotopes can be considered as candidates for space operation. These isotopes and their properties are summarized in table 11.5.2.1-1.

Although the isotopes presented in table 11.5.2.1-1 have been considered for space power applications, all save the alpha emitters have radiations that would require very heavy shields for the OTAES. Discussions with the Atomic Energy Commission indicate that the two curium isotopes will not be produced in quantities of sufficient magnitude for large power applications. As a consequence, only polonium 210 and plutonium 238 can be considered for the OTAES.

Plutonium 238 has a projected availability of fifteen thermal kilowatts a year. Since each of the four modules requires ten thermal kilowatts, it is evident that several years total production will be required. Since other space missions of a higher priority than OTAES will require plutonium 238, polonium 210 is left as the only logical candidate.

Table 11.5.2.1-1.

ISOTOPE HEAT SOURCE SUMMARY

Isotope	Typical Compound Form	Half Life (year)	Radiation Emitted	Density (gm/cc)	Power Density (watt/cc)	Thermal Conductivity (cal/sec-cm - °C)	Melting Point (°C)	Shielding Req'm'ts.	Thermal & Radiation Stability	Capsule Compatibility
Polonium 210	Polonides	.38	α	9.3	12.10	$1.55(10)^{-2}$	72000	Very Light	Good	Good
Plutonium 238	PuO_2	86.4	α	10.0	3.9	$1.55(10)^{-2}$	2240	Very Light	Good	Good
Curium 242	Cm_2O_3	0.45	α, n	9.0	397.0	$1.67(10)^{-2}$	1950	Light	Good	Good
Curium 244	Cm_2O_3	18.0	α, n	9.0	22.5	1.67(10)-2	1950	Light	Good	Good
Cerium 144	CeO_2	0.78	β,γ,x	7.13	149.9	.0245	2600	Moderate to heavy	Thermal Decomp. & Phase Change	Reacts with Mo, Ta, W, Ir at 7140°C
Strontium 90	$SrTiO_3$	27.7	β,x	5.11	2.30	.0132	1910	Moderate to heavy	Good	Excellent
Cesium 137	Cesium Borosilicate Glass	$30 \pm .3$	β,γ,x	3.1	0.24	1-2(10)-3	1100*	Moderate to heavy	Glass Devitrifies 1000°C	Excellent
Promethium 147	Pm_2O_3	2.67	β	6.6	2.03	6(10)-3	2350	Light	Good	Excellent
Cobalt 60	Metal	5.24	β,γ	8.7	48.0	0.13-0.17	1480	Heavy	Excellent	Excellent

*Softening Point

α - Alpha
β - Beta
γ - Gamma
x - Penetrating Bremstrahling
n - Neutron

11.5.2.2 Generator Design

The generator is made up of a number of components. Although these components can be arranged in any of several different ways, the configuration chosen for the OTAES is cylindrical in nature. This configuration was chosen because of the design experience that has been obtained in making RTG's for space applications. Figure 11.5.2.2-1 shows a schematic for a typical generator.

Since it is not practical to build a single unit, several 500 watt modular RTG's will be electrically interconnected to provide the OTAES with the power required.

Isotope energy sources are not constant power devices. Due to their very nature, the power density decreases with time. Equation (1) expresses this power decay.

$$P = P_o e^{-\lambda t} \qquad (1)$$

where,

P_o = Initial power density.

P = Power density at time t.

t = Time.

λ = Decay constant.

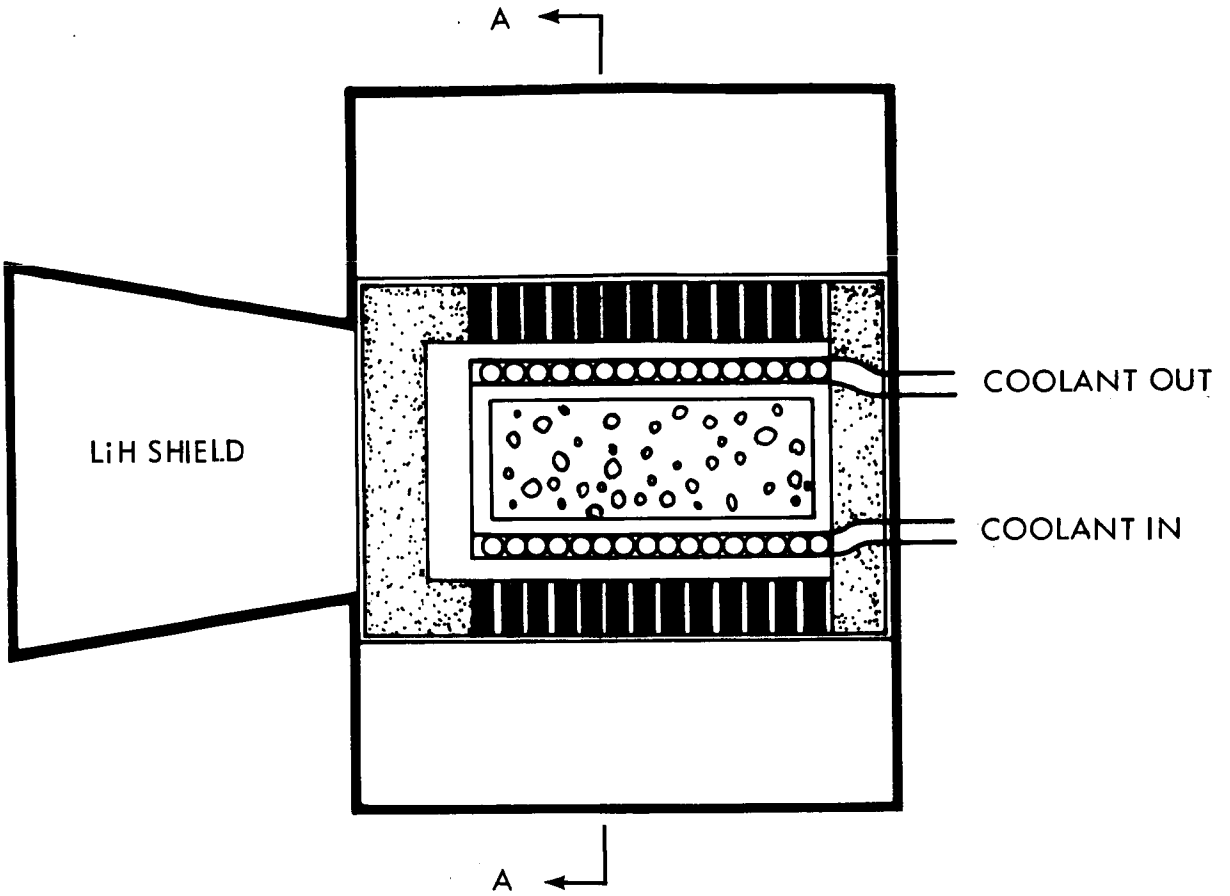
The generator under consideration has a requirement for an isotope power of 10,000 thermal watts at the end of the mission. Since the isotope is polonium 210 (half-life is 138 days) and the mission duration is 400 days, it is evident that considerably more energy will be available at the start of the mission than can be used by the thermoelectric generator.

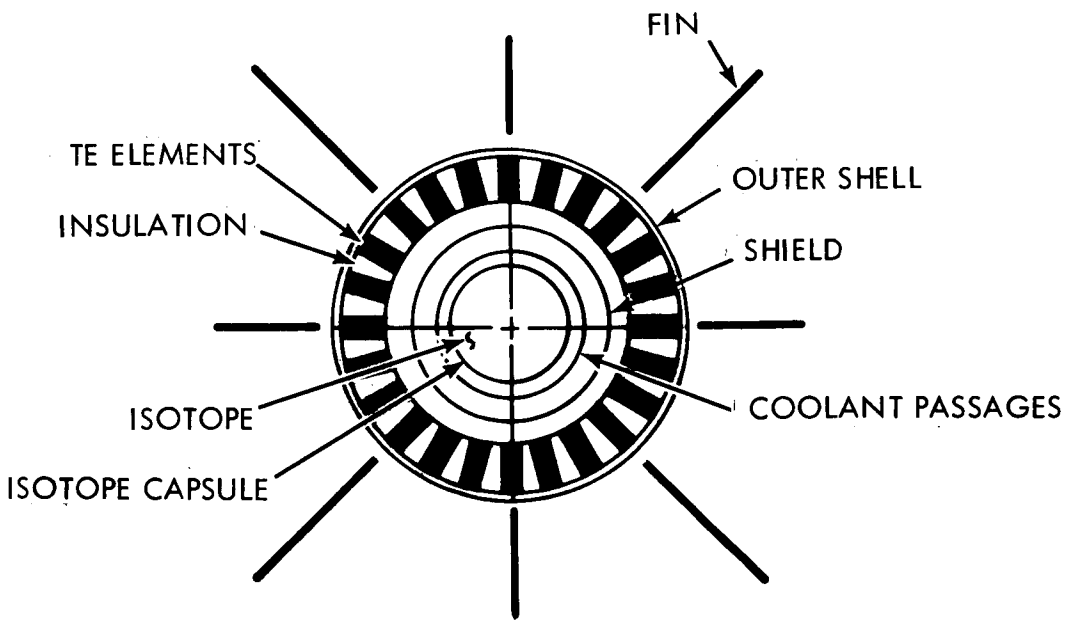
At the start of the mission 74,000 thermal watts of isotope must be contained. For polonium 210, this will require 1.510 Kg of source material.

The primary design criteria for the isotope container is that the isotope must be contained under any possible condition. Thus, the design of the capsule must consider impact on a solid media, thermal excursions, internal pressure build-up, and submersion in sea water. Prior studies have indicated that by having voids inside the capsule to eliminate the internal pressure problem a capsule designed to withstand impact will also withstand the other rigors to which it will be subjected.

The ratio of outer to inner diameter for the capsule can be found by the equation

$$\frac{b}{a} = \left[\frac{1}{1-2\,(P_B V/\sigma)}\right]^{\frac{1}{2}} \qquad (2)$$





SECTION A-A

Figure 11.5.2.2-1. Typcial Isotope Thermoelectric Generator

where,

P_B = bulk density of capsule.

V = impact velocity.

σ = allowable stress in material.

Using stainless steel as a capsule material and a safety factor of two for the allowable stress yields a diameter ratio of 1.1 for the capsule.

The allowable internal pressure for this value of b/a is

$$P = \frac{\sigma_P}{\left[\frac{(b/a)^2 + 1}{(b/a)^2 - 1}\right]} = 5590 \text{ psia} \qquad (3)$$

The void volume ratio yielding this pressure is 0.125.

Since the polonides have a density of ten grams per cubic centimeter, the volume of the isotope is 151.0 cubic centimeters. Allowing for the void volume the total volume contained is 1209 cubic centimeters.

The thermoelectric elements will be mated to the outer surface of the capsule so the surface area of the generator is important. With the interior volume of the capsule fixed, it is possible to vary the surface area by varying the capsule length to outer diameter ratio.

In order to effectively utilize an isotope heat source for space electric power generation the thermal energy available from the isotope must be converted to electrical energy. For this study, thermoelectric energy conversion will be used. A thermoelectric conversion device is basically a heat engine which takes energy in the form of heat, converts a portion of the heat to useful electric power, and then rejects the waste heat energy.

The fundamental physical properties of a thermoelectric material are:

S = Seebeck coefficient (μv/°K)

ρ = Electrical resistivity (μohm - cm)

k = Thermal conductivity (watt/cm-°K)

These properties are combined to yield a derived parameter called the figure of merit, Z. For a single element,

$$Z = \frac{S^2}{\rho k} \qquad (4)$$

Usually an n- type and a p- type element are combined to form a thermoelectric couple. The figure of merit for a couple is

$$Z_c = \frac{(Sn + Sp)^2}{[(k_n \rho_n)^{\frac{1}{2}} + (k_P \rho_P)^{\frac{1}{2}}]^2} \tag{5}$$

An efficiency term, usually referred to as the materials efficiency (η_M) is a function of the hot and cold junction temperatures, and the figure of merit.

$$\eta_M = \frac{M-1}{M+T_c/T_n} \tag{6}$$

where: $$M = \left[1 + \frac{Z(T_n+T_c)}{2} \right]^{\frac{1}{2}}$$

The ideal generator efficiency (η_g) is the carnot efficiency (η_c) times the materials efficiency.

$$\eta_g = \eta_M \eta_c = \frac{T_n-T_c}{T_n} \eta_M \tag{7}$$

When optimizing a thermoelectric generator, all parameters are usually adjusted to obtain maximum efficiency. The only parameter which are under the direct control of the designer are the thermoelement dimensions. For optimum operation, the relationship between the variables should be

$$\frac{A_n L_P}{A_P L_n} = \left[\frac{\rho_n k_P}{\rho_P k_n} \right]^{\frac{1}{2}} \tag{8}$$

From a practical design point, the lengths should be nearly equal so that the areas of the thermoelements become directly controlled by the physical properties of the elements. Table 11.5.2.2-1 summarizes the properties of importance for the thermoelectric elements that will be considered in this analysis.

TABLE 11.5.2.2-1

Material	Lead Telluride
Hot Junction Temperature (°K)	800°K
Cold Junction Temperature (°K)	400°K
Electrical Resistivity (ohm-cm)	
N - Type Material	$2.50\ (10)^{-3}$
P - Type Material	$3.20\ (10)^{-3}$
Thermal Conductivity (watt/cm - °K)	
N - Type Material	$1.39\ (10)^{-2}$
P - Type Material	$1.63\ (10)^{-2}$
Seebeck Voltage (Volt/°K)	
N - Type Material	$2.15\ (10)^{-4}$
P - Type Material	$2.30\ (10)^{-4}$

It is possible to vary the individual couple performance by varying the generator output voltage but when one considers the total hot junction area required by the thermoelectric elements, the performance is relatively independent of the voltage. Consequently, the voltage will be 28 volt d.c. since it is compatible with most utilization equipment requirements.

From the discussion of the isotope and its container, it was evident that the surface area of the capsule should correspond to the area at the hot junction of the thermoelectric elements. The hot junction that can be determined from theoretical considerations is not realistic since there is more to a couple than just the thermoelectric material. Figure 11.5.2.2-2 shows a typical couple.

A gap must be left between the capsule surface and the hot junction surface to provide space for the coolant passage and the shielding.

Figure 11.5.2.2-3 shows the results of the comparing the thermoelement length and isotope container L/b ratio with the surface area as the parameter of comparison. The dashed lines show the effect of the area utilization factor on surface area required and the solid lines show the effect of gap width on surface area available. Although polonium 210 is the isotope of interest, a single curve is included showing the available surface area when plutonium 238 is used as the isotope.

To illustrate the use of the figure, let us consider the particular case when $f_a = 1.00$ and the gap is zero. First selecting the element length (1 cm) read the surface area required. With this surface area read the capsule L/b ratio that will provide the required area (2.5:1). It is also possible to select a capsule L/b ratio and determine the thermoelement length.

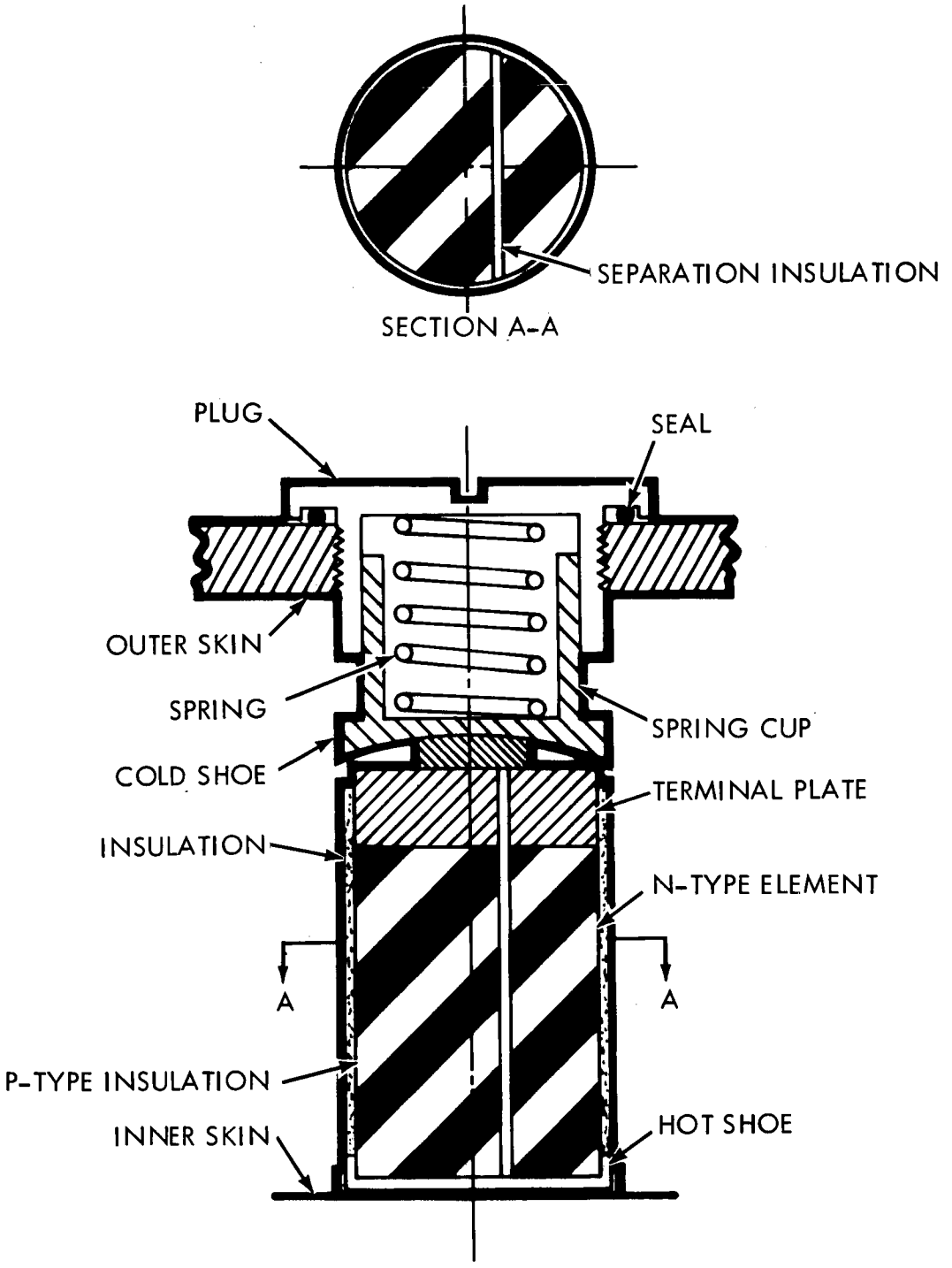


Figure 11.5.2.2-2. Typical Thermoelectric Couple

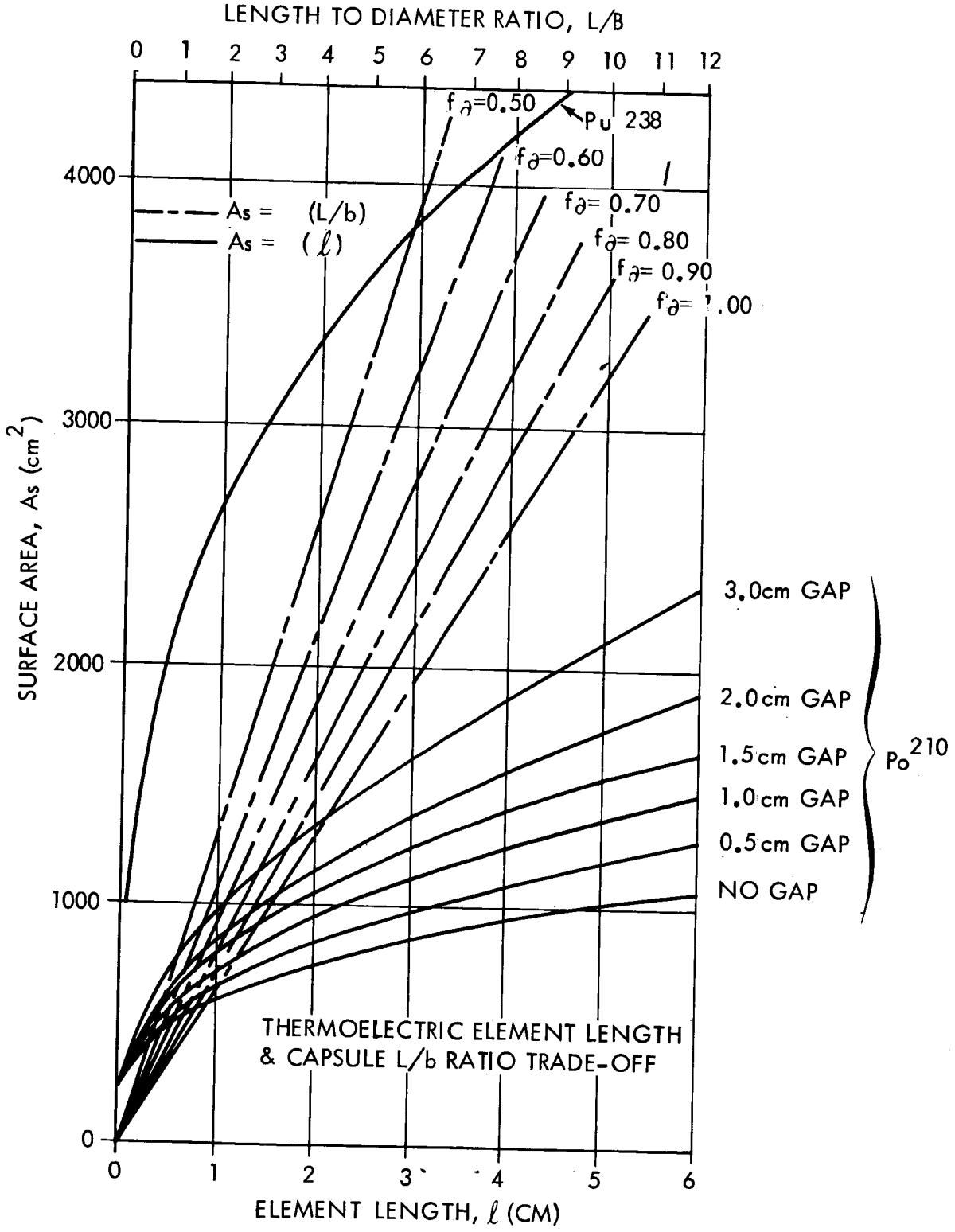


Figure 11.5.2.2-3. Thermoelectric Element Link & Capule L/B Ratio Tradeoff

Several facts are evident from inspection of the figure. First, selecting a specific value of L/b, it is possible to obtain increasing smaller element lengths (hence TEG weight) by decreasing the gap between the isotope container surface and the thermoelectric hot junction area. Decreasing the area utilization factor will further decrease element length but there will be a deleterious effect since the surface area through which heat can be lost will increase (hence a decrease in generator efficiency).

Second, there is a maximum element length which can be utilized if a reasonable value of L/b is to be used. This maximum length tends to increase as the gap is increased.

Third, there is a decided weight penalty associated with using plutonium 238 as a heat source since relatively long thermoelectric elements must be utilized.

Two of the variables in figure 11.5.2.2-3, the area utilization factor and the gap between the isotope capsule and the hot junction, can be determined by further analysis.

If the shape of the thermoelements is assumed to be a right circular cylinder, which is the usual practice, it is possible to estimate the area utilization factor to some degree of accuracy. With the T.E. elements aligned such that a single line will pass through the centers of each line and another line can be passed through each row, the area utilization factor is 0.785. This assumes, of course, that each element is in contact with its neighboring elements. Since some allowance must be made for encapsulation and to prevent electrical shorting a value of $f_a = 0.60$ will be utilized in this study.

Figure 11.5.2.2-4 shows the power of polonium 210 as a function of time. As can be seen there are two heat dissipation requirements which must be met by the subsystem. First the subsystem must dissipate 64,000 thermal watts at the start of the mission (74,000 watts on the pad) and second the subsystem must be capable of dumping a total of $2.44\ (10)^7$ watt-hours of thermal energy over the 400 day mission.

The heat dissipation system has two operational modes. The modes are:

a. Launch Pad Cooling - All heat generated by the isotope must be carried away from the generator and dissipated external to the vehicle. Since the shroud must be in place, it is necessary to keep the RTG at a relatively low temperature so as to preclude weakening the structural materials of the spacecraft and launch vehicle and to allow launch site personnel to work in the vicinity of the generator.

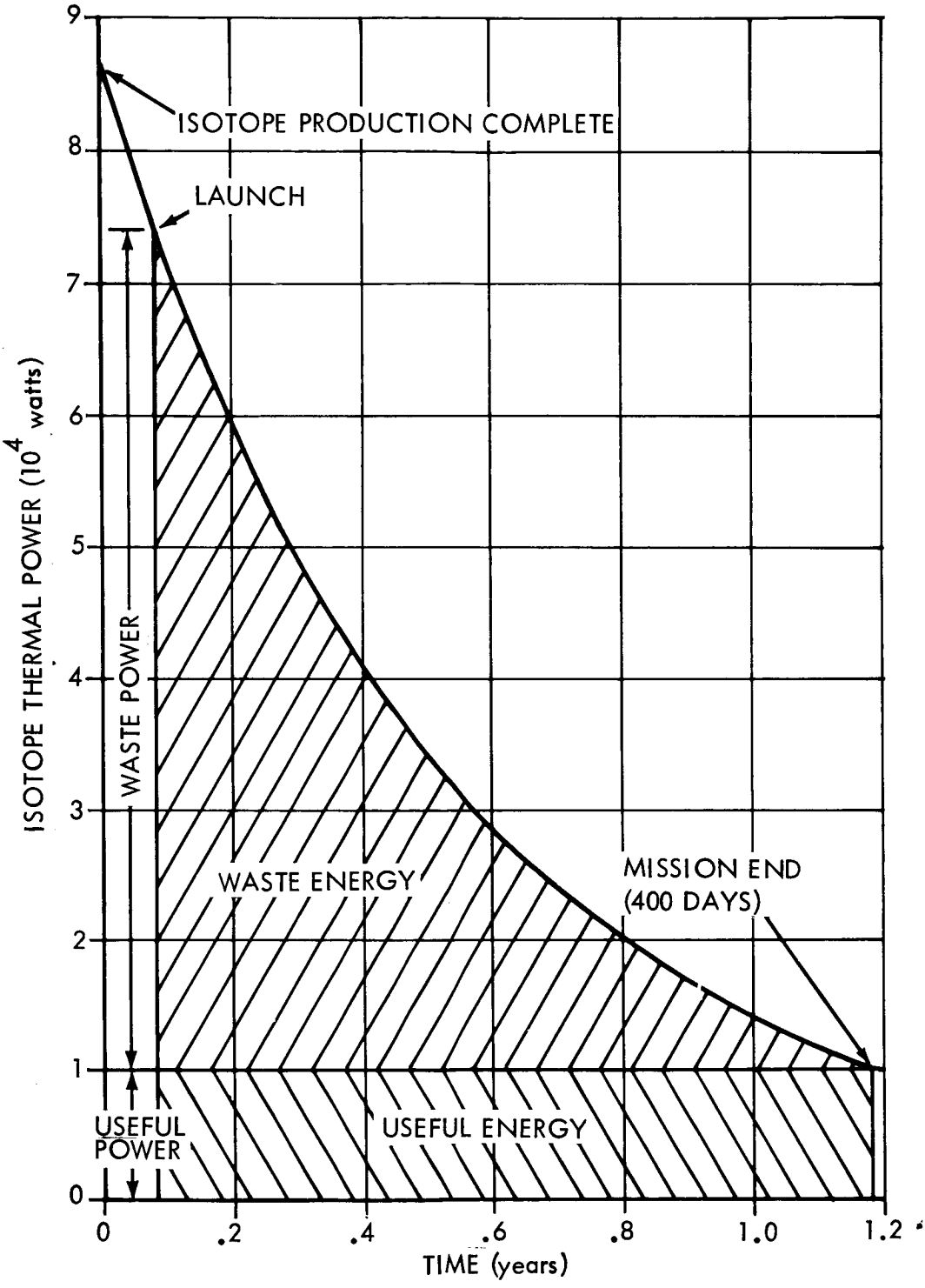


Figure 11.5.2.2-4. Polonium 210 Power Variation With Time

b. Operational Cooling - Once the power system begins to operate, the heat dissipation subsystem must handle the thermal energy of the isotope in excess of that required by the generator. The subsystem must be high temperature in nature since radiation will necessarily be a part of the heat rejection scheme and since the generator must operate at a relatively high temperature.

Since the requirements for the two operational modes are quite diverse, it is necessary to consider two separate subsystems, one for each of the operational mode.

Let us first consider the operational mode since it is the most stringent of the two modes. Although it would be desirable to use a passive heat dissipation technique for the capsule, the high initial waste power level and the large amount of energy which must be dumped, preclude using anything but an active subsystem for both the launch pad and space modes of operation.

The selection of a working fluid is of paramount importance. There are three primary candidates of interest for the fluid and they are water, mercury, and a eutectic mixture of sodium and potassium called NaK (78% potassium). Table 11.5.2.2-2 is a summary of the properties of interest for the temperature range of interest (1500-1600°R).

TABLE 11.5.2.2-2

Property	Water	Mercury	NaK
Melting point (°K)	273.	234.	262.
Boiling point (°K)	373.	630.	1064.
Density of liquid (gm/cc)	1.0	12.7	0.720
Thermal conductivity $\left(\frac{\text{watt}}{\text{cm-°K}}\right)$	0.579	12.29	25.9
Specific heat $\left(\frac{\text{watt-hr}}{\text{lb-°K}}\right)$	1.23	.039.	0.258
Compatibility with stainless steel	Good	Good to 1600°R	Good to 2200°R

The fluid selected for this application is NaK since it offers good heat transfer properties and can operate at reasonable system pressures.

The first component to be considered in the analysis of the active heat dissipation is the radiator. The radiator will consist of a number of parallel tubes containing NaK. As the liquid flows through the tubes, it gives heat up to the walls which in turn transfer the heat by conduction, to fins from which the heat is radiated.

Since this study is preliminary in nature, several simplifying assumptions will be made. These assumptions are:

a. All heat rejected will occur from the extended surfaces.

b. The radiator will consist of a number of tubes, each of which has the same mass flow rate and the same temperature drop.

c. Headers and manifolds will be considered to be perfectly insulated.

Thermodynamic analysis of the radiator indicates that the weight of the fins is only dependent upon the fin root thickness which would indicate that it is desirable to use a very thin fin. As the fin thickness decreases, however, the tube length must increase to maintain the necessary surface area. Since the tube walls are sized to prevent meteoroid puncture and increasing tube length increases vulnerable area, it is evident that a trade-off exists between fin root thickness and radiator weight.

Figure 11.5.2.2-5 shows the total weight of the radiator as a function of fin root thickness. The dashed lines represent the weight of the fins and the tubes for the particular case when ten tubes are used. As can be seen from the figure, a minimum weight does occur and that increasing the number of tubes tends to decrease the point of minimum weight.

By using the values of minimum weight and the corresponding optimum fin root thickness it is possible to determine the other radiator parameters. Figure 11.5.2.2-6 shows the tube inner diameter, the tube wall thickness, and optimum fin root thickness as a function of the number of tubes. Figure 11.5.2.2-7 shows the overall radiator performance in terms of total weight, radiator length and radiator width.

From figure 11.5.2.2-7 it is evident that although the weight of the radiator is low, the length and width can be undesirable even for a large number of tubes. A flat panel is not the only configuration that can be used for the radiator. It is possible to segment the radiator so that three, four, or more individual panels can be used.

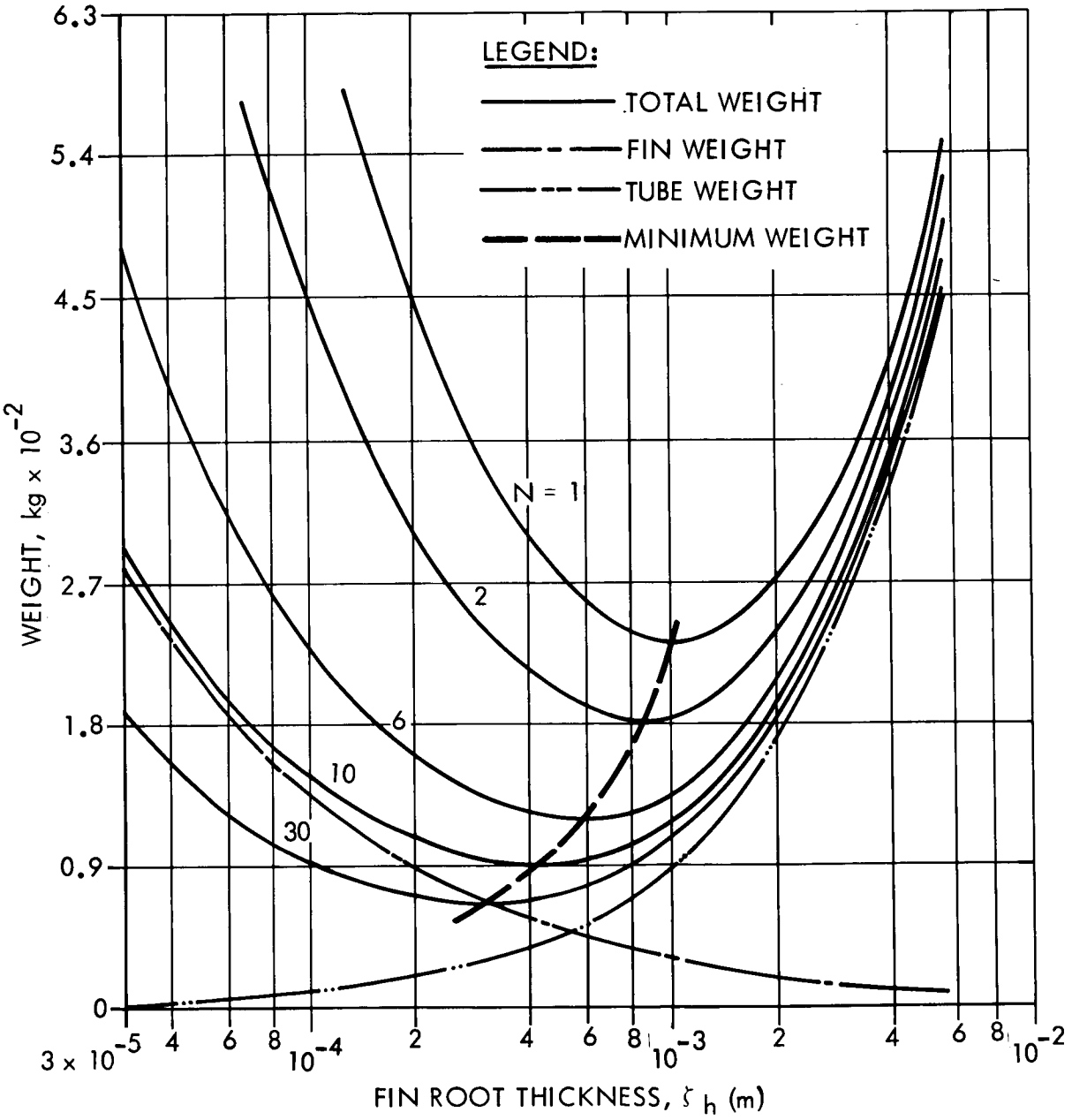


Figure 11.5.2.2-5. Radiator Weight Variation With Fin Root Thickness

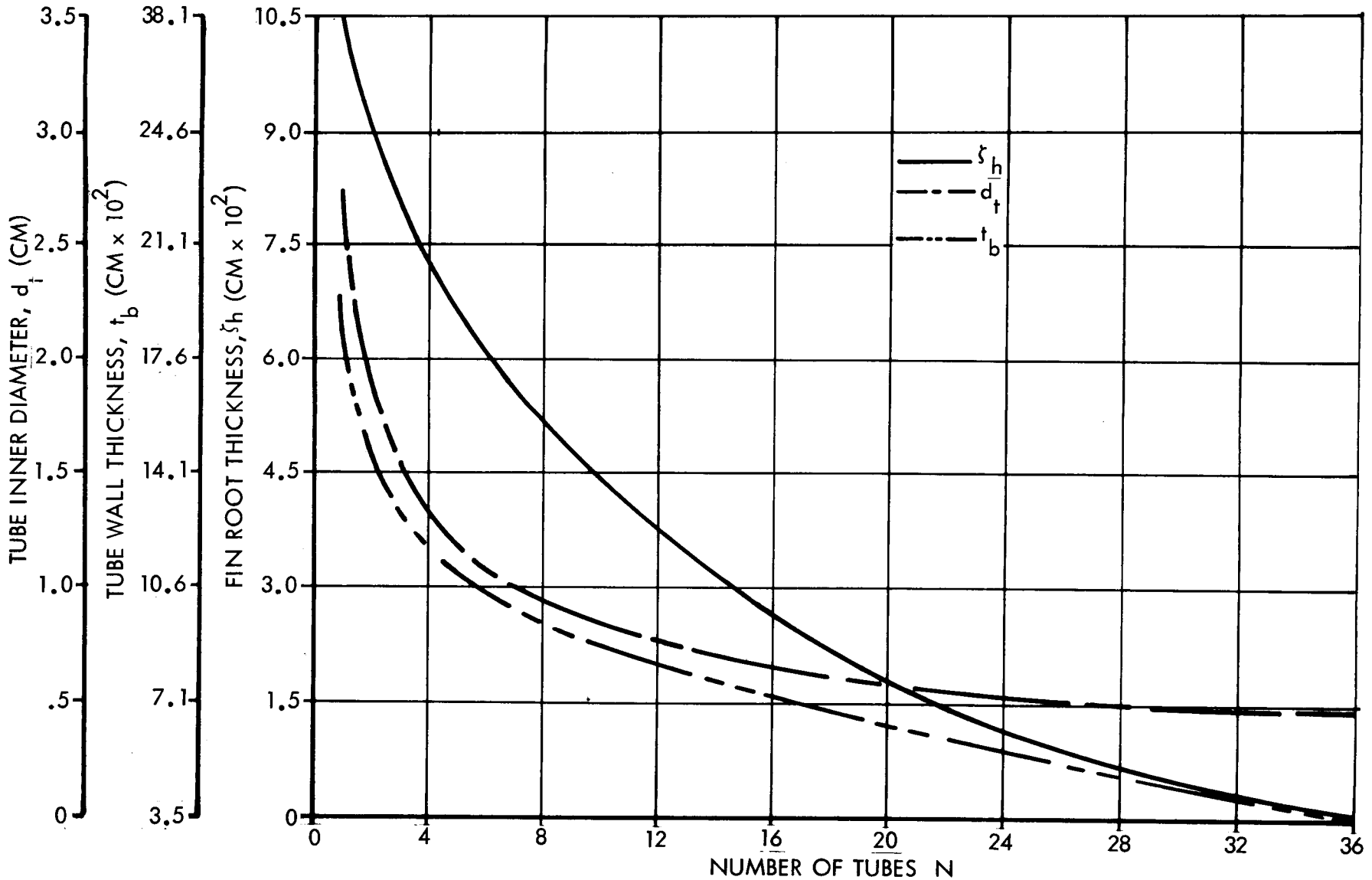


Figure 11.5.2.2-6. Radiator Design Parameter

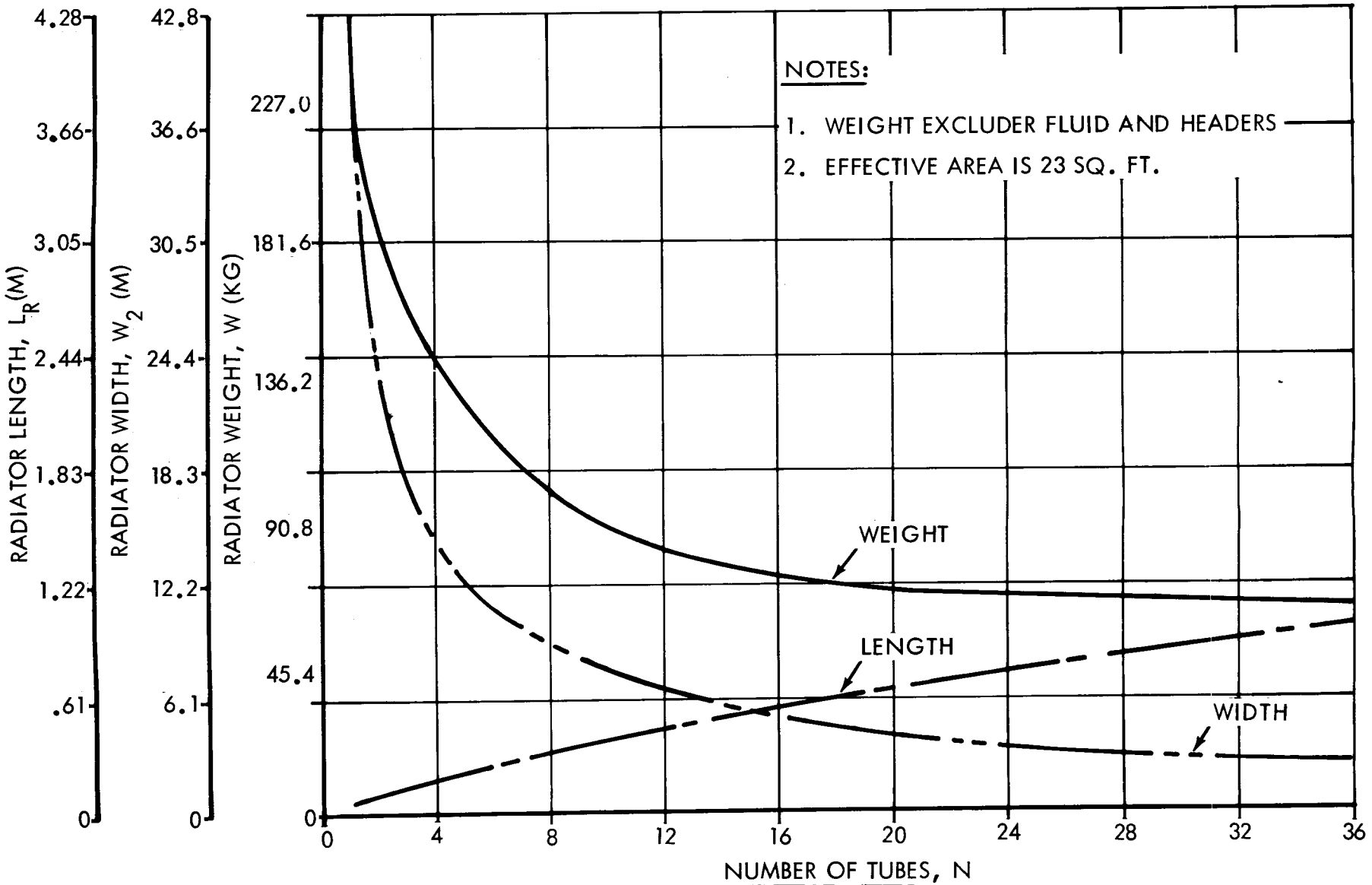


Figure 11.5.2.2-7. Radiator Performance Variation

Since the fin length is independent of the amount of heat to be radiated, increasing the number of panels will decrease the individual tube length required (the total tube length will remain the same). Increasing the number of panels, will, however have the deleterious effect of increasing radiator area to overcome interradiation between panels. Calculation of the weight and height as a function of the number of panels shows that above four panels there is not only a weight penalty but also an increase in the platform height to compensate for thermal radiation between the panels.

The choice between a three or four panel radiator configuration must be based upon the ease of integration since the weight of either is relatively close. Since there is a slight advantage in favor of the four panel radiator in terms of minimum platform height, a four panel radiator will be used.

The number of tubes will be determined by the constraints arising from packaging the system for launch. For this study the packaging space will be dictated by considering a circle with a radius of 3.02 m and a maximum platform height of 0.915 m. Sixteen tubes is the maximum number that can be accomodated. Using fewer than sixteen tubes, the radiator could be packaged but only with a weight penalty. As a consequence, sixteen tubes will be used. Table 11.5.2.2-3 summarizes the characteristics of the radiator for a four panel radiator with sixteen tubes (4 per panel).

As mentioned previously, two modes of operation must be considered for the auxiliary heat dissipation subsystem. The previous analysis has been concerned only with the radiator for the operational mode but this plus the launch mode must be considered in determing the parameters of the subsystem where it is in contact with the isotope capsule.

In order to remove the heat from the isotope capsule, the coolant tube spirals around the capsule. The tube is so coiled about the capsule that it doubles back upon itself. The fluid picks up half of the heat load on each pass. In this way, a relatively constant hot junction temperature can be maintained.

To provide cooling on the launch pad, a second loop is coiled about the capsule. This coolant passage will be the same size as the NaK tube but will contain water.

The case where the operational mode is used will be considered as the point of departure for analysis. Since the mass flow rate at the capsule is the same as in the radiator heater ($0.105 \frac{m^3}{min}$) and the same fluid velocity is used, the diameter of the tube will be one inch.

The luanch pad cooling loop must be capable of carrying off all of the power generated on 74,000 watts at the time of isotope fueling of the

TABLE 11.5.2.2-3

RADIATOR CHARACTERISTICS

Material	Stainless Steel
Working Fluid	NaK
Number of Panels	4
Fluid Tubes Per Panel	4
Panel Length (Along Tube) (m)	1,748
Panel Height (m))	0.564
Minimum Radiator Height (m)	0.786
Radiator Total Area (m^2)	3.94
Radiator Effective Area (m^2)	2.90
Radiator Weight (Kg)	14.15
Tube Inner Diameter (cm)	0.680
Tube Wall Thickness (cm)	0.0384
Fluid Flow Velocity (m/sec))	3.05
Fin Root Thickness (cm)	0.0266
Fin Root to Tip Length (cm)	38.1
Pressure Loss in Radiation (newton/m^2)	$1.13(10)^5$
Probability of No Penetrations or Radiator Tubes in 400 Days	0.900

generator. Since the temperature must be kept low to prevent injury to the launch crew and weakening of the spacecraft structure, the maximum temperature will be set at 339° K. The temperature rise in the fluid as it passes through the generator will be 55.9°C. The mass flow rate for the water is 0.443 kg/sec or .0191 m^3/min. The tube inner diameter is two centimeters which means that the fluid velocity will be 0.525 meter/second.

Once the water has collected the energy of the isotope it passes out of the vehicle and is colled and then recirculated through the capsule. Upon launch, the water lines are broken. Once orbit has been achieved, the shroud over the RTG would be rejected and the NaK subsystem would be used to carry off the isotope waste energy. The thermal lag inherent in the system will prevent excessive heat in the time interval between launch and shroud ejection.

Although no analysis of the pump for the NaK subsystem will be included in this study, the pump must be able to inpart a head of 1.73×10^5 newton/m^2 the working fluid. The type of pump which will be used will be an electromagnetic pump. The energy is imparted to the fluid by crossed electrical and magnetic fields which interact and do work on the fluid. A pump of this type will weigh approximately fifteen pounds. Figure 11.5.2.2-8 shows the complete auxiliary heat dissipation subsystem.

The shielding for the generator will be a critical component due to the heavy weight of the materials used and the necessity to protect sensitive electronic components and man from the radiation of the isotope. Polonium 210 alpha decays to lead 206 and will not, therefore, have any problem due to radiation. from the daughter. Although polonium is usually considered to be a pure alpha emitter, there is a very small amount of gammas and neutrons emitted. It is these gammas and neutrons which must be shielded against.

The dose rate at the target can be reduced by two methods -- increasing the separation distance between the source and the target or mass between the source and the target. The radiation dosage that man can tolerate has been the subject of a great many studies and test programs but the results vary over a wide range because of the unpredictability of the radiation interplay with the various cell types. For this study, a dose rate of 1.4 millirad per hour will be used.

Electronic components are also susceptable to radiation but the allowable dosages can be predicted with far more accuracy. Assuming a total allowable dosage for the electronics of 10^7 RAD, it is evident that adequate shielding for the electronics for a 400 day mission would be present if shielded for man.

The shielding philosophy that will be used in this study will be to provide a shadow shield on the end of the generator facing the spacecraft sufficient for the 1.4 millirad per hour dose rate and circumferential shielding around the generator sufficient to reduce the

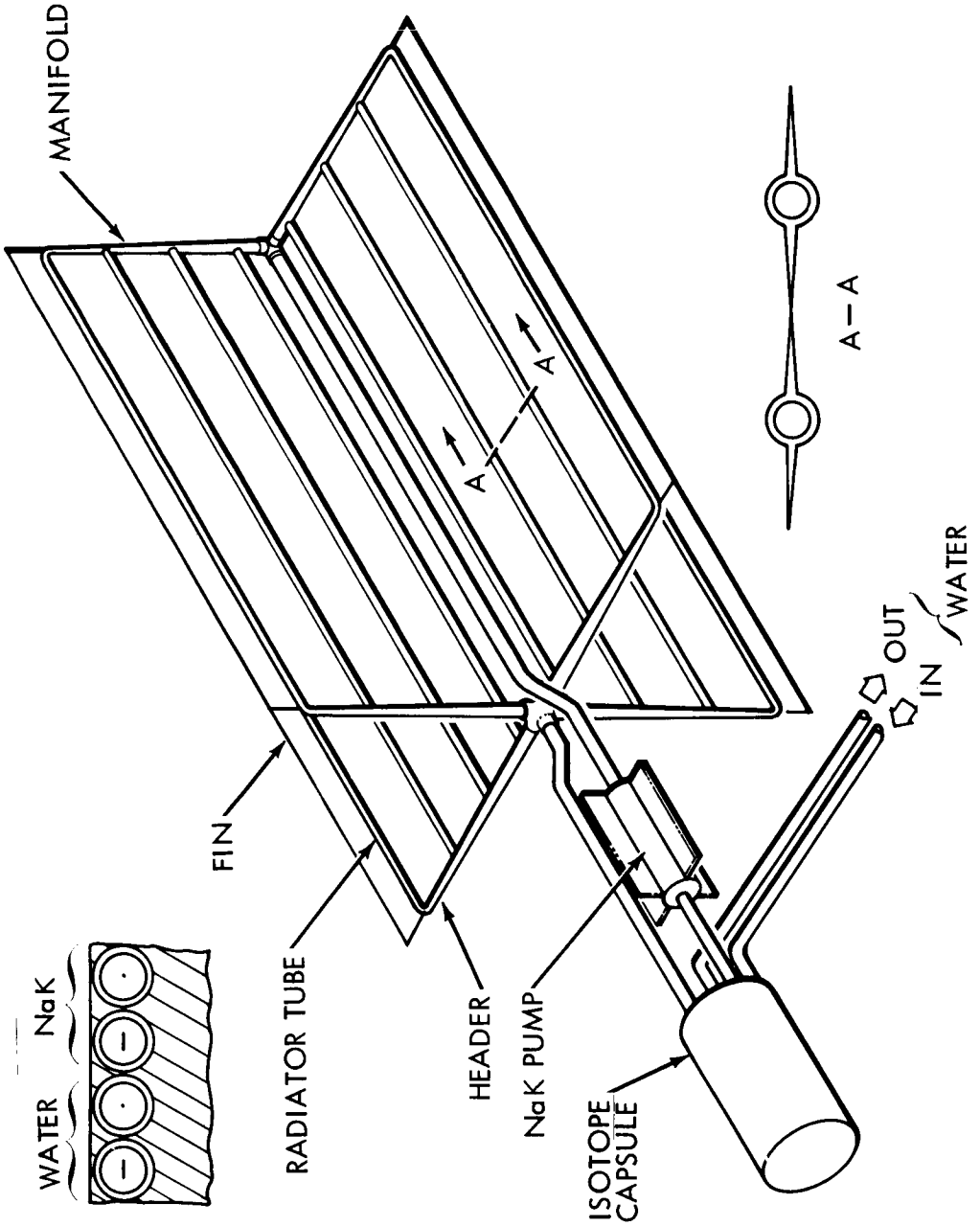


Figure 11.5.2.2-8. Auxiliary Heat Dissipation Subsystem

dose rate to 28 milliard per hour. The higher dose rate is permissible since the astronaut will only be within this region for short periods of time.

The shielding of the gammas will be accomplished by depleted uranium and the neutrons will be shielded by lithium hydride. Previous analy- shows that three centimeters of depleted uranium will be required for the end shield and 1.3 centimeters for the circumferential shield. The lithium hydride shield for neutrons will be 32.5 centimeters on the end of the generator.

As was mentioned previously, a decrease in the area utilization factor will tend to increase the heat lost through the insulation. The heat lost through the insulation is expressed by the equation

$$\dot{Q}_{LR} = \frac{\pi k_i L (T_n - T_c)(1 - f_a)}{6 \ell_n (d + 2\ell/d)} \qquad (9)$$

where,

$$d = b + 2 (GAP)$$

Using diatomaceous silica powder as the insulation material (k_i = 1.730 (10)$^{-3}$ watts/cm - °K in vacuum) it is possible to evaluate the equation in terms of the parameters shown in figure 11.5.2.2-3. The equation now reduces to:

$$\dot{Q}_{LR} = \frac{0.362 L (1 - f_a)}{\ell n (d + 2\ell/d)} \qquad (10)$$

The generator will also lose heat through the end where no thermoelements are located

$$\dot{Q}_E = \frac{0.543 (d + 2\ell)^2}{t_i} \qquad (11)$$

The equation for the total heat lost through the insulation now reduces to

$$\dot{Q}_L = \frac{0.1449 L}{\ell n (d + 2\ell/d)} + \frac{0.543 (d + 2\ell)^2}{t_i} \qquad (12)$$

By using this equation, it is possible to determine the power lost through the insulation as a function of the L/b ratio and the insulation thick- ness. Figure 11.5.2.2-9 shows this relationship.

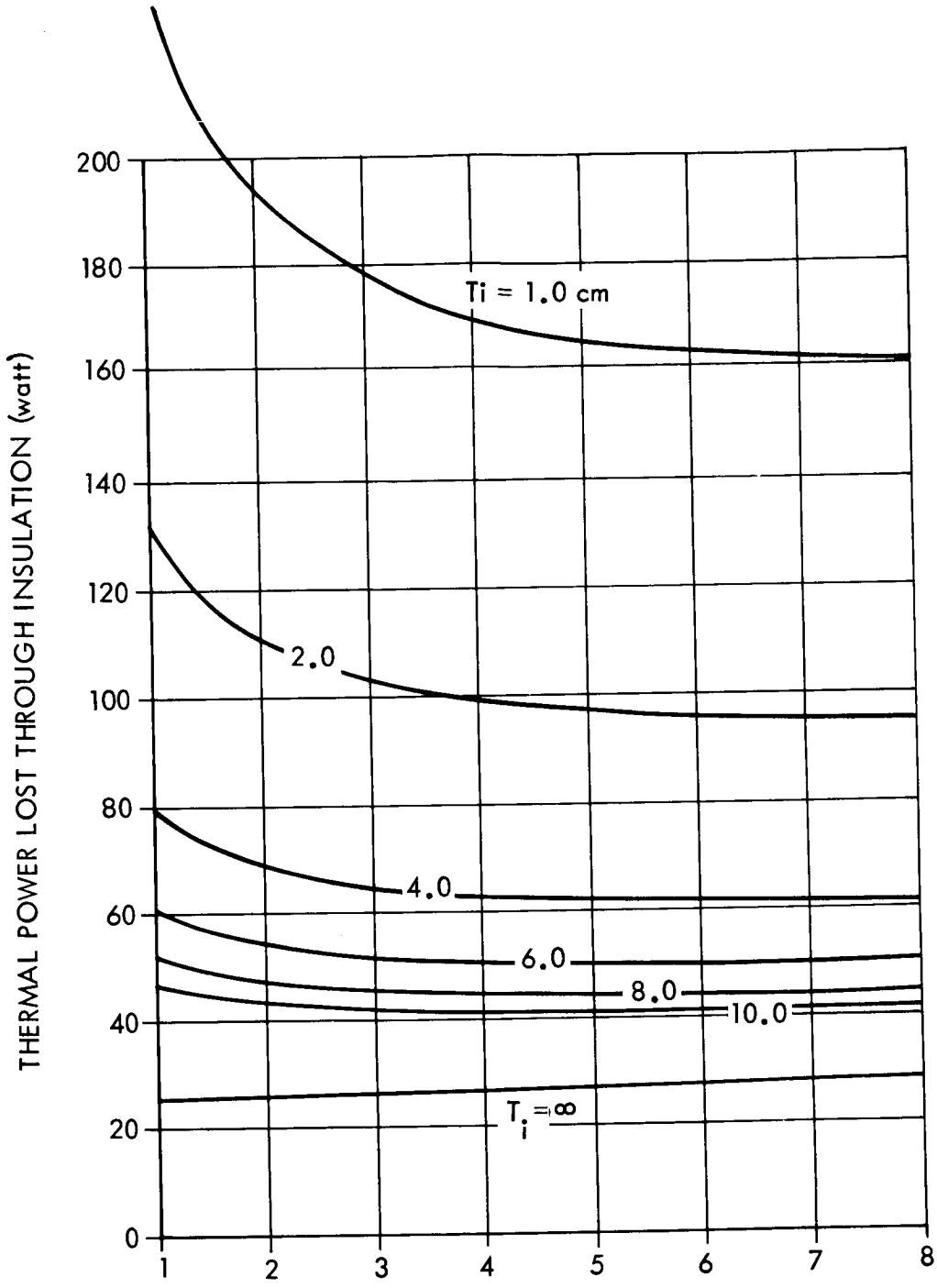


Figure 11.5.2.2-9. Thermal Losses Through Insulation

As can be seen from figure 11.5.2.2-2 there is a lower bound to the heat lost through the insulation. This bound is, of course, set by the case where the end insulation is infinitely thick. Since the insulating qualities of the generator ends are not materially increased by using more than six centimeters of insulation, this amount will be used.

It is also interesting to note that the heat lost with six centimeters of insulation is relatively independent of the L/b ratio.

The outer shell of the generator serves to encapsulate the entire generator and to provide a point of contact for the fins. As a consequence, the shell can be very thin. For this study a shell thickness of 0.2 centimeters will be used.

The fins are sized to radiate the excess generator energy and for this study will be 6 centimeters from root to base and 0.5 centimeters thick. There will be eight fins and each will run the length of the generator.

Now that the various components of the radioisotope thermoelectric generator have been analyzed, the generator must be considered as an integrated unit. Figure 11.5.2.2-9 shows the weights of the various components as a function of the L/b ratio. As can be seen from this figure, the minimum weight occurs at L/b = 2. Table 11.5.2.2-4 summarizes the design of a 500 thermoelectric generator module.

11.5.2.3 Integration and Performance

Not only is it important to consider a single RTG module but also the relationship between the modules and the OTAES. The modules produce 500 watts per module so several will be required. In addition, there will be periods of time when power in excess of the RTG capabilities will be required. The power generation equipment must also be mounted to a spacecraft of some type. As a consequence, the integration of the power system must also be investigated.

From the discussion of the load profile for the OTAES (section 11.5.1) it was seen that the average power required is 1565 watts and the peak energy requirements during laser operation of 10,800 watt-hours. The peak energy requirements will be met by secondary batteries and the additional power for recharging the batteries will come from adding additional RTG modules.

The batteries selected for this application are of the silver cadmium type. Since only forty charge/discharge cycles will be required for the entire 400 day mission, the batteries can be discharged to 75 per cent of their capacity. The energy density of 59.9 watt-hours per kilogram.

In order to recharge the batteries in a reasonable length of time, the total output of the RTG's must be 2200 watts. Since the specific weight of the RTG's is less than the specific weight of the batteries a trade-off exists between weight and primary power source output

TABLE 11.5.2.2-4

500 WATT ISOTOPE THERMOELECTRIC GENERATOR

SUMMARY

HEAT SOURCE	
ISOTOPE	Po^{210}
THERMAL POWER LAUNCH (WATT)	74,000
WEIGHT OF ISOTOPE (Kg)	1.510
VOID VOLUME RATIO	0.125
CAPSULE MATERIAL	STAINLESS STEEL
CAPSULE WEIGHT(Kg)	3.55
CAPSULE L/b	2:1
AUXILIARY HEAT DISSIPATION	
WORKING FLUID (OPERATIONAL	NaK
WORKING FLUID (PRE-LAUNCH)	WATER
RADIATOR	
NUMBER OF PANELS	4
TUBES PER PANEL	4
WEIGHT (Kg)	14.18
AREA (m^2)	3.94
INLET TEMPERATURE (°K)	890.
OUTLET TEMPERATURE (°K)	834.
PUMP WEIGHT (Kg)	6.81
PLUMBING & FLUID WEIGHT (Kg)	5.00
SHIELDING	
CIRCUMFERENTIAL SHIELD	URANIUM
MATERIAL	1.00
THICKNESS (cm)	22.00

TABLE 11.5.2.2-4 (CONTINUED)

SHIELDING	
WEIGHT (Kg)	18.36
END SHIELD	
MATERIAL	URANIUM
THICKNESS (cm)	3.00
WEIGHT (Kg)	17.64
END SHIELD	
MATERIAL	LiH
THICKNESS (cm)	32.5
WEIGHT (Kg)	5.71
THERMOELECTRIC GENERATOR	
MATERIAL	PbTE
NUMBER OF COUPLES	280.
COUPLE LENGTH (cm)	.92
COUPLE DIAMETER (cm)	1.59
THERMOELECTRIC WEIGHT (Kg)	9.05
HOT JUNCTION TEMPERATURE (°K)	800.
COLD JUNCTION TEMPERATURE (°K)	400.
INSULATION MATERIAL	DIATOMACEOUS SILICA
INSULATION WEIGHT (Kg)	1. 97
OUTER SHELL & MISC.	
MATERIAL	COPPER
SHELL THICKNESS (cm)	2.00
SHELL WEIGHT	3.65

TABLE 11.5.2.2-4 (CONTINUED)

OUTER SHELL & MISC.	
NUMBER OF FINS	5.93
FIN WEIGHT (Kg)	9.24
MISCELLANEOUS WEIGHT (Kg)	27.00
STRUCTURAL WEIGHT (Kg)	10.00
MODULE PERFORMANCE	
GENERATOR LENGTH (cm) (WITHOUT NEUTRON SHIELD)	34.16
GENERATOR DIAMETER (cm) (WITHOUT FINS)	19.43
GENERATOR VOLUME(cm^3)	12,000.
GENERATOR WEIGHT (Kg)	133.65
DEPLOYED AREA (m^2)	3.94

level. As the nominal power level is increased above the 1565 watt value, less power must be supplied from the batteries. Figure 11.5.2.3-1 shows the weight-power level trade-off.

As can be seen from figure 11.5.2.3-1 there are two minimums involved. For this study, however, the minimum weight point is of the most interest.

The minimum weight occurs at power level of 1900 watts. To allow for contingencies, a power level of 2000 watts will be used. This will require four 500 watt generators.

The four generators must be attached to the spacecraft if they are to be effective but they must be located where the radiator will create the least interference with the spacecraft and where the isotope source is a maximum distance from the sensitive components. Figure 11.5.2.3-2 a typical spacecraft configuration with the four isotope thermoelectric generators.

Since the RTG's are unaffected by orbits where the system is in the shadow of the earth, a single design applicable to any of the missions under consideration with very minor variation in performance.

11.5.3 Photovoltaic Power System Design

Of all the power system concepts that have been used in space, none has been used more frequently than solar cells. The ready availability of solar energy makes this energy conversion concept attractive not only for present day systems but also for missions that may be flown in the future.

Unlike an isotope thermoelectric generator, a solar cell cannot operate in the shadow of the earth since the sun is its source of energy. Consequently, secondary batteries are an integral part of the system. This portion of the report will discuss the photovoltaic and the energy storage subsystems as well as the integrated system.

11.5.3.1 Photovoltaic Subsystem

Although solar cells are an attractive power subsystem, the space environment will degrade their performance with time. The most critical environmental effects on solar cells are temperature, radiation, and meteoroid impact.

The standard test temperature for solar cell performance is 28°C. Above this temperature, there is a decrease in power production capability while below 28°C there is an increase. Figure 11.5.3.1-1 shows the effect of temperature on the power output of a typical cell. It should be noted that the current remains relatively constant over the temperature range, but the voltage is nearly parallel with the power curve.

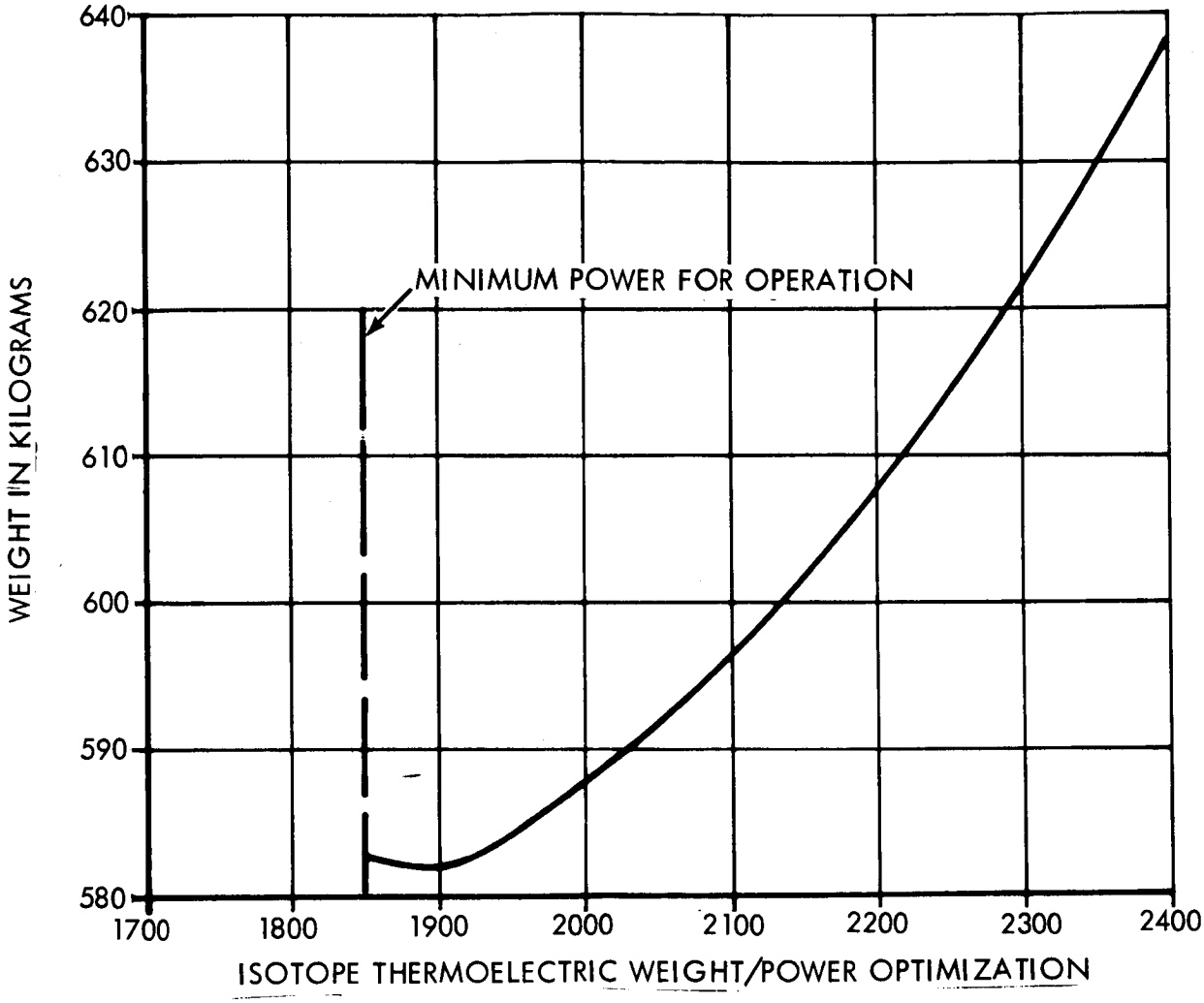


Figure 11.5.2.3-1. Isotope Thermoelectric Weight/Power Optimization

INTEGRATED RTG CONFIGURATION

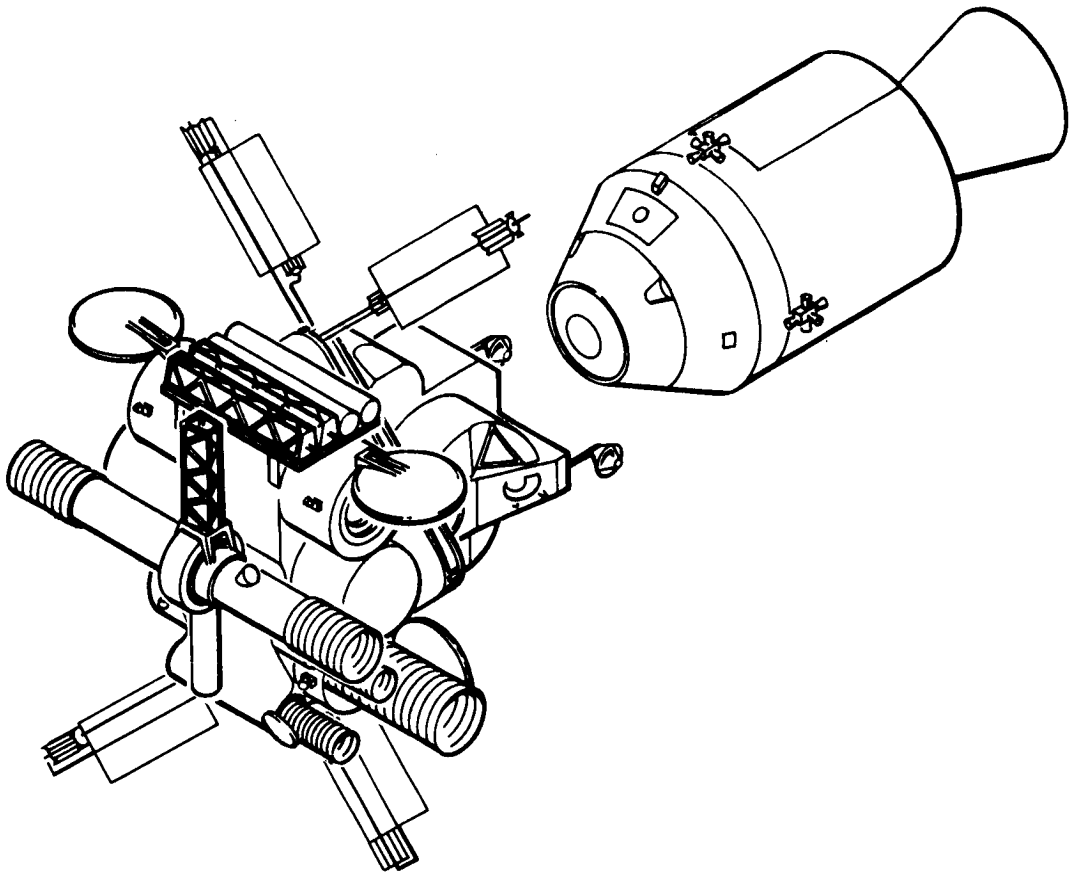


Figure 11.5.2.3-2. Integrated RTG Configuration

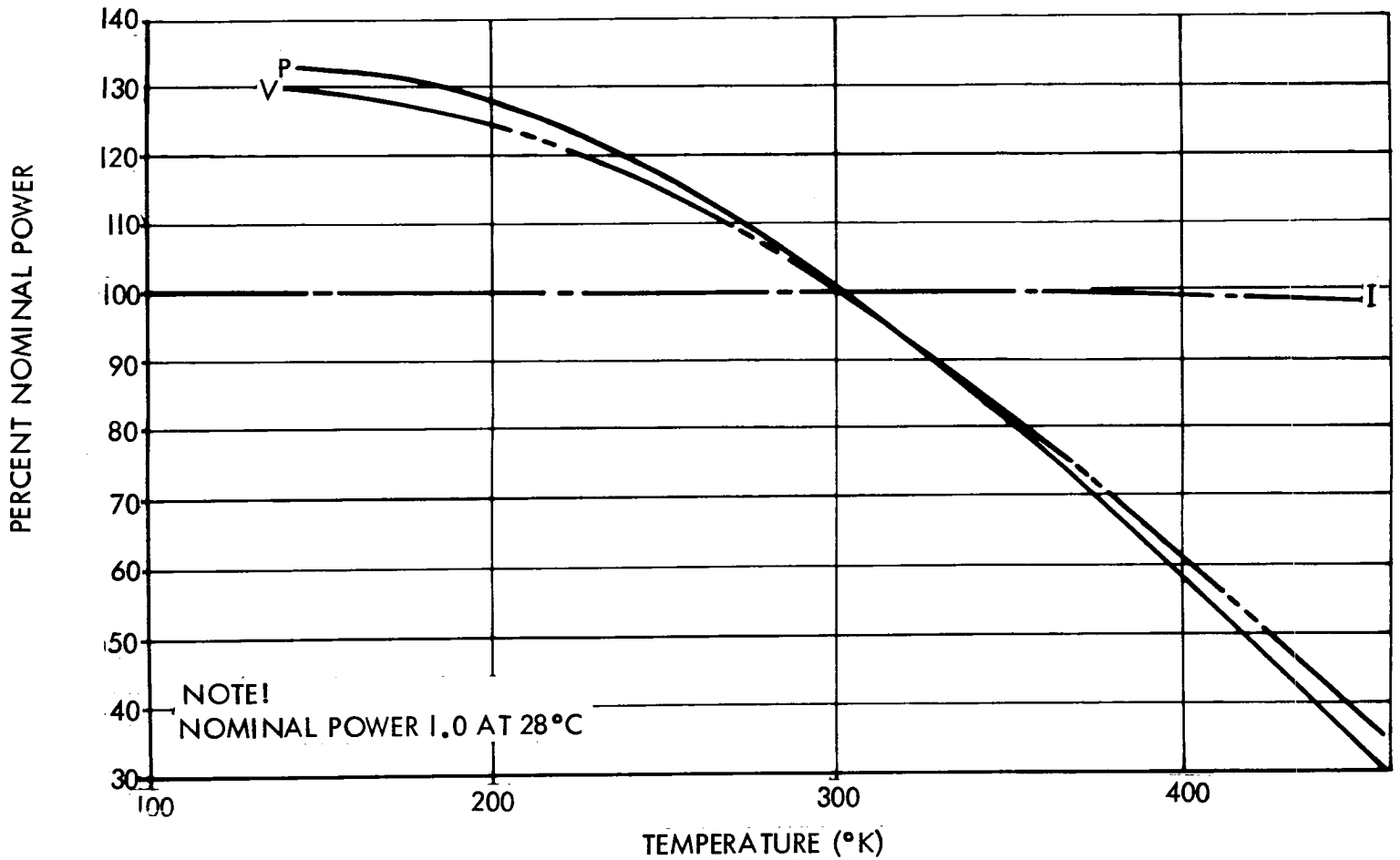


Figure 11.5.3.1-1. Effect of Temperature on Solar Cell Performance at the Maximum Power Point

INTEGRATED RTG CONFIGURATION

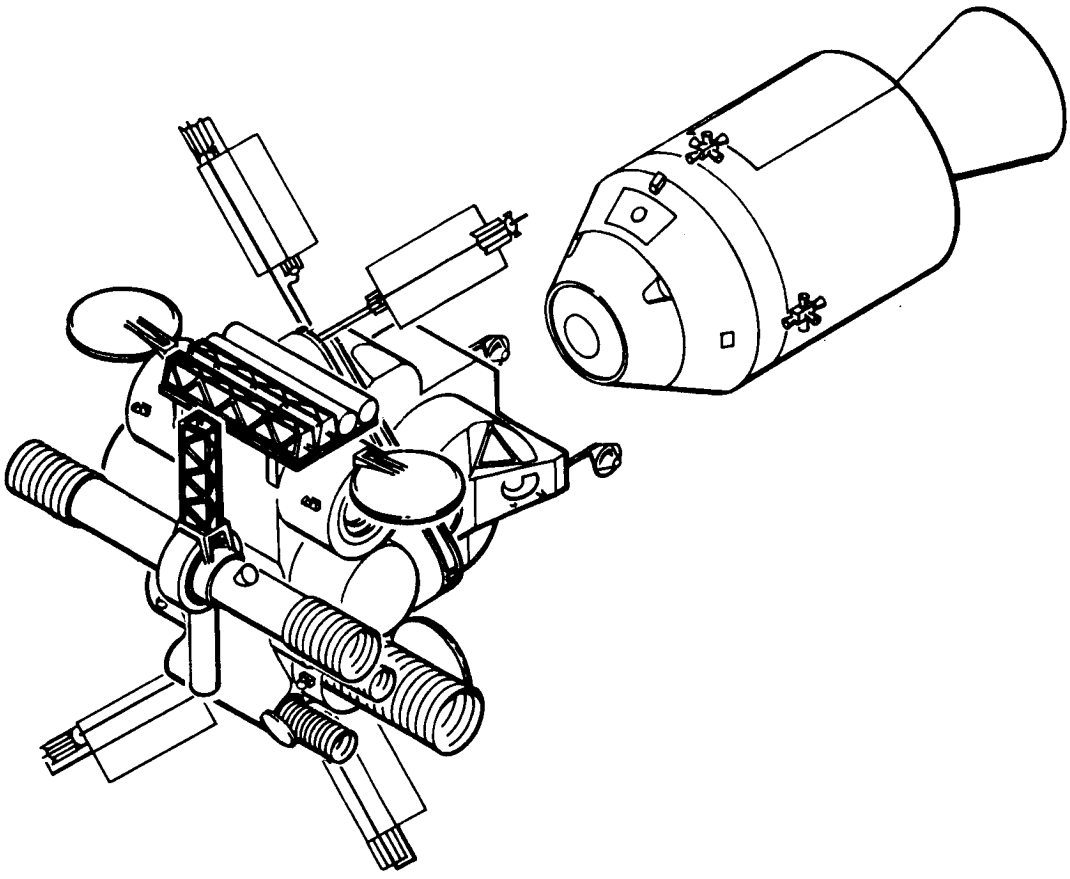


Figure 11.5.2.3-2. Integrated RTG Configuration

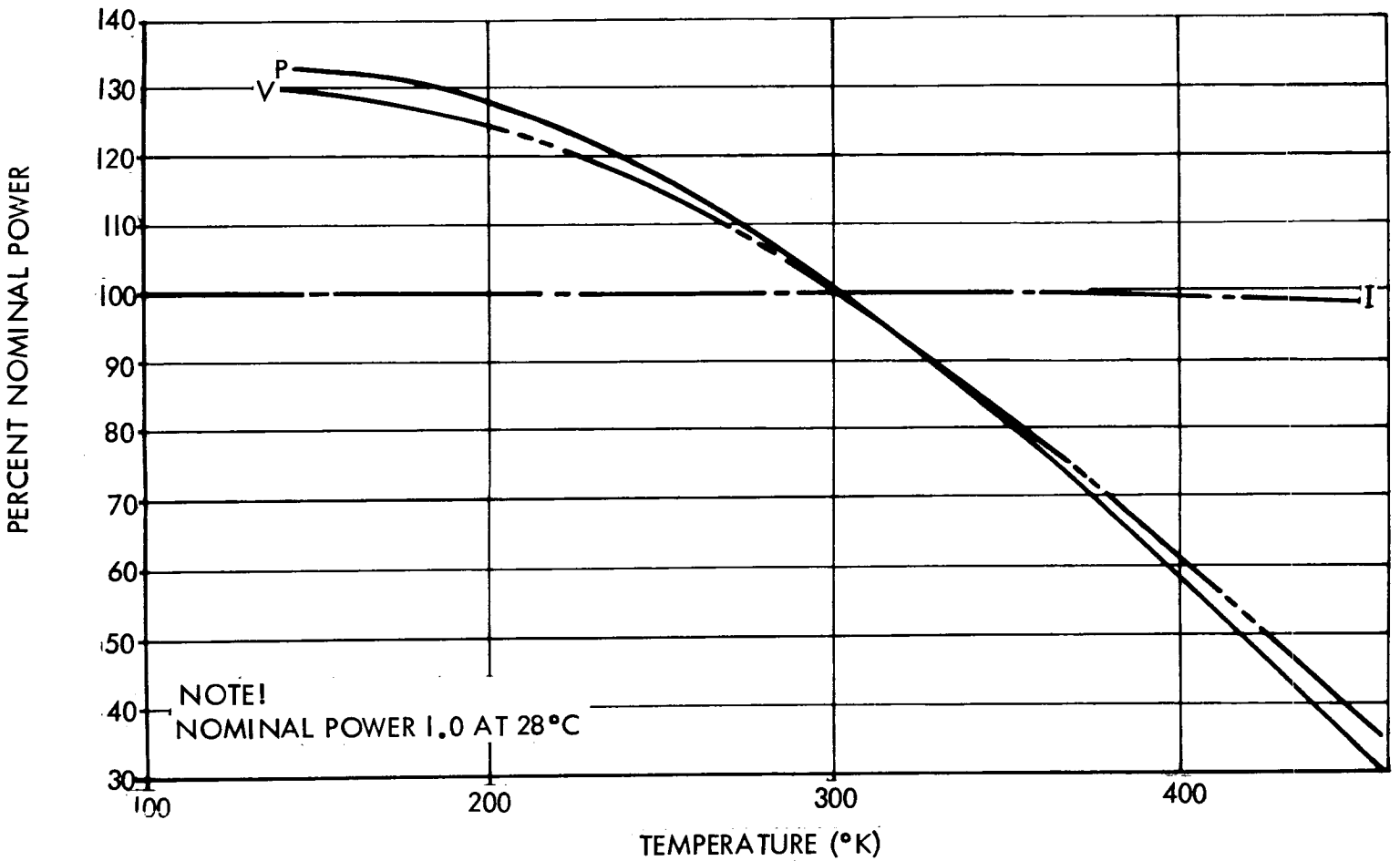


Figure 11.5.3.1-1. Effect of Temperature on Solar Cell Performance at the Maximum Power Point

The deleterious effect of radiation on solar cells is due to the formation of defect centers throughout the crystal. In essence, the radiation reduces the chance of a photon produced electron-hole pair reaching the N/P junction region. The pair production decreases as the radiation increases.

The primary sources of radiation in space are the Van Allen belts and solar flares. For low earth orbits neither of these sources are of sufficient magnitude to effect solar panel operation and for high circular orbits only the solar flares are a hazard. The elliptical orbit, on the other hand, must consider both Van Allen and solar flare radiation. A spacecraft in the 24 hour-elliptical orbit makes one pass through the Van Allen belts each day and will be under the influence of the solar protons. In actual practice, cover slides are placed on the solar cells to afford some degree of protection.

The radiation damage to the photovoltaic array can be offset by increasing the array area, increasing the cover slide thickness or a combination of the two. Since either of the methods can increase array weight, it is desirable to determine the most nearly optimum combination of area and cover slide thickness increase. Figure 11.5.3.1-2 presents the relative array weight as a function of cover slide thickness. Also shown in this figure is the decrease in array area that occurs with increased cover slide thickness.

Figure 11.5.3.1-2 is based on the 400 day elliptical orbit and considers Van Allen radiation and protons resulting from solar flares. As can be seen, a 14 mil cover slide offers minimum weight. It should be pointed out that the data used to produce figure 11.5.3.1-2 is a "worst case" condition and other orbits will require less than this amount of shielding. Even for orbits where radiation is not a problem, some shielding will be required to protect against meteoroids. Studies will be required to protect against meteoroids. Studies indicate that the penetration depth of meteoroids in cover slides is approximately seven times the diameter of the incombing particle. Based on this assumption that a relationship exists between particle size and penetration depth, it is possible to obtain an estimate of panel degradation due to meteoroids.

Just as it was possible to obtain a nearly optimum cover slide thickness for protection against radiation, it is also possible to perform a similar trade-off for meteoroid protection. Figure 11.5.3.1-3 presents the relative weight and area of a solar panel versus the shield thickness. From figure 11.5.3.1-3, it is evident that minimum weight is obtained when a 7 mil slide is utilized.

In addition to penetration of the cover slides, consideration must also be given to crazing of the surface. Results of tests in which 220 gril silicon carbide was used to sandblast cells with cover slides

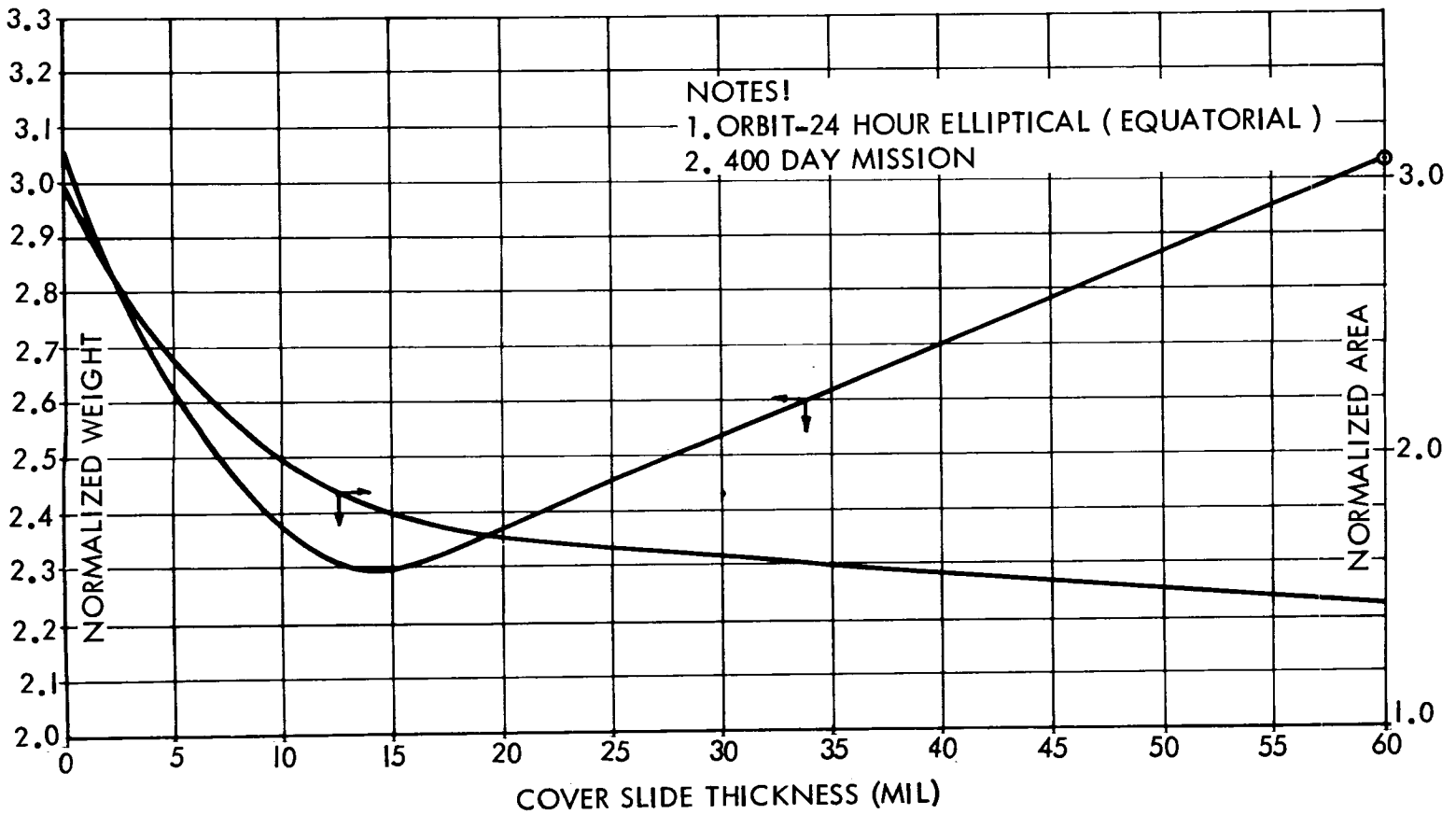


Figure 11.5.3.1-2. Photovoltaic Weight and Area as a Function of Radiation Protection Thickness.

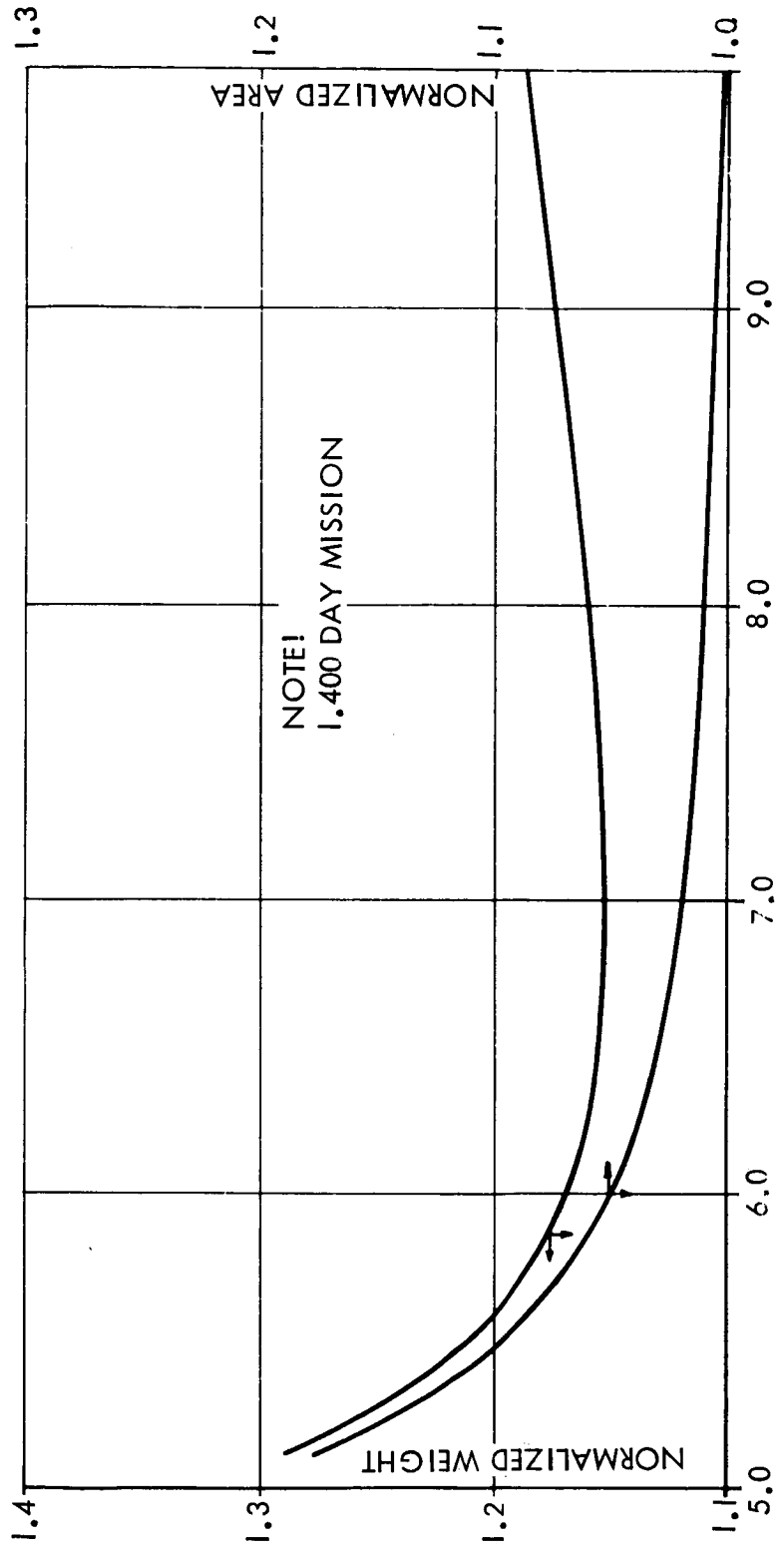


Figure 11.5.3.1-3. Photovoltaic Weight and Area as a Function of Meteoroid Protection Thickness.

resulted in a power decay of 11 per cent at 1000 craters per cm^2, increasing to 60 per cent at 10^6 craters per cm^2. For this study, a degradation of 11 per cent will be assumed to account for surface crazing.

The curves in figures 11.5.3.1-2 and 11.5.3.1-3 cannot be considered as absolute. They do indicate, however, that a trade-off does exist between the degree of protection and the cover slide thickness. When both figures are considered, the approximate upper and lower bounds on the shield thickness can be determined. The range, which includes all orbits under consideration, is 6-7 mil minimum allowable and 14-15 mil maximum required thickness.

The solar cell by itself is a very small device capable of producing only tens of milliwatts of power. In order to provide the power requirements of the OTAES, a large number of solar cells must be electrically interconnected. Typically, six or eight cells would be connected in parallel to form a module. Connection of the cells in this manner means that the module output voltage is the same as an individual cell and the current the sum of the component cells. Failure of a single cell will decrease the power producing capability of the module only by the power output of that one cell. The modules are electrically connected in series to form a string. The number of cells in a string is dependent upon the output voltage desired since the module voltages are additive. The total power output of an array is provided by connecting the various strings in parallel.

The cells can be mounted to the array in either of two ways. They can be shingled or flat mounted. With front contact cells, the shingled approach allows a higher packing factor to be obtained (0.88 for shingled as opposed to 0.85 for flat mounted). For wrap-around cells, however, the packing factor for the flat mounted cells is somewhat higher (approximately 0.90). Since a number of possible array configurations are possible, let us consider the relative merits of various configurations.

Table 11.5.3.1-1 summarizes the results of analyzing the various panel configurations. The table is based on a nominal power level of two kilowatts. Configuration A (2-1 blade arrays at $\pi/2$ radians) is simple to package and deploy. The total aspect ratio for both arrays varies over a wide range which also means a wide variation in power output. The aspect ratio for each blade varies from zero to one-half and thus extreme solar torques are to be expected. Configuration B (2-4 blade arrays at $\pi/2$ radians) has the same problem with aspect ratio variations as configuration 1, although to a lesser degree. The solar torque developed are relatively minor but deployment and storage is complex.

Configuration C (2-3 blade arrays at π/radians) has minor variation in aspect ratio and very small solar torques. Although deployment is complex, there does not appear to be a problem with storage. Configuration

TABLE 11.5.3.1-1

SOLAR PANEL CONFIGURATION SUMMARY

CONFIGURATION		ASPECT RATIO MAX	MIN	AVG	ARRAY WEIGHT (lb)	ARRAY AREA (ft^2)
A	2 single blade arrays @ $\pi/2$ radians	0.354	0.250	0.318	375	1000
B	2 four blade arrays @ $\pi/2$ radians	0.280	0.250	0.272	375	1000
C	2 tri-blade arrays @ $\pi/2$ radians	0.279	0.269	0.274	338	904
D	2 single blade arrays @ $\pi/3$ radians	0.289	0.250	0.276	375	1000
E	4 single blade arrays @ $\pi/2$ radians	0.354	0.250	0.318	375	1000
F	ORIENTED	1.00	1.00	1.00	250	250

Configurations A-E have cells on both sides of blades.

D (3-1 blade arrays at $2\pi/3$ radians) has a relatively minor variation in aspect ratio. The solar torques are also small and the packaging and deployment are straight forward, the configuration may, however, be limited in application to only a few spacecraft configurations.

Configuration E (4-1 blade arrays at $\pi/2$ radians) is attractive from the standpoint of packaging and deployment but the variation in aspect ratio is the same as configuration 1. Solar torque is a problem although not as severe as configuration 1.

Configuration F (2-1 arrays at 0 radians) is oriented with respect to the sun. Not only is there a definite performance advantage with the concept, but there is no variation in aspect ratio. Solar torques are negligible and the concept is simple to deploy and store.

From table 11.5.3.1-1 it is evident that performance alone is not an adequate criteria for selecting the most promising fixed orientation array. Although there is a slight advantage for configuration 3, there is no difference in the specific weight and area between the other unoriented array concepts. Thus, the qualitative parameters must be the deciding factor. Due to the rather constant power output and the small solar torques developed with configuration 3, this type of unoriented array will be considered in the analysis that follows. Although the deployment is more complex than the other unoriented concepts, this one factor is not of sufficient magnitude to outweigh the advantages of this concept.

The choice between an oriented and unoriented array would be relatively straightforward if the selection could be entirely contained within the power subsystem. Unfortunately, this is not the case. The clearly superior performance of an oriented array in terms of weight, area, cost and quality of power produced must be weighed against the lack of interference with the mission functions offered by an unoriented array.

Since the final selection must be determined exterior to the power generation subsystem both the two-3 blade unoriented and oriented arrays will be considered for the remainder of the study.

One important question which must be answered in considering the fixed configuration is what the actual power variation will be. Variation in power output arises from the change in the angle of solar incidence, and the change in panel temperature as the spacecraft moves through its orbit.

In order to develop a general model for the power variation it is necessary to make three qualifying assumptions. These are:

a. The orbit considered is a 24-hour orbit in the elliptical plane.

b. The solar panel is sized to deliver the nominal power level at maximum temperature.

c. The solar panel output varies as the cosine of the angle of incidence.

By combining the temperature variation with the aspect ratio variation, it is possible to determine the normalized power output for the three blade arrays as a function of orbit position. Figure 11.5.3.1-4 shows this variation.

An oriented array does not suffer from the aspect ratio and temperature variations that have just been described. Since the panels are oriented toward the sun the aspect ratio is essentially constant and equal to unit, the temperature of the panel will also be constant. Wide variations will occur only when the panels are in the shadow of the earth. With the same assumptions as with the fixed array, the maximum temperature will be 325°K and the minimum 167°K.

Although the preceding discussion is based on orbits in the ecliptic plane, it must be remembered that several missions under consideration have orbits which are out of this plane. This being the case, the power output curves shown in figure 11.5.3.1-4 must be multiplied by the cosine of the angle of inclination. The power output variation obtained in this manner can only be considered an approximation since different shadings of the solar panels are likely to occur. This will, in turn, affect the temperature profile of the panels. Another factor which must be considered is the fact that the time spent in the earth's shadow for other orbits will change.

Operation in a low earth orbit will also make a difference in the previeus analysis. The orbit period, will, of course, be shorter, thus decreasing the maximum temperature and increasing the minimum temperature. The increase in the minimum temperature will be aided by the increased heat input from the earth.

Using the solar cell data and the missions discussed in section 10.2, it is possible to set forth the parameters of importance for the two photovoltaic array configurations. Since the total weight, volume, and deployment area of the arrays are scaleable with power level, these specific values of these parameters will be used. See table 11.5.3.1-2.

11.5.3.2 Energy Storage Subsystem

Although either of the photovoltaic subsystems is capable of producing the nominal power level, any real application will have periods

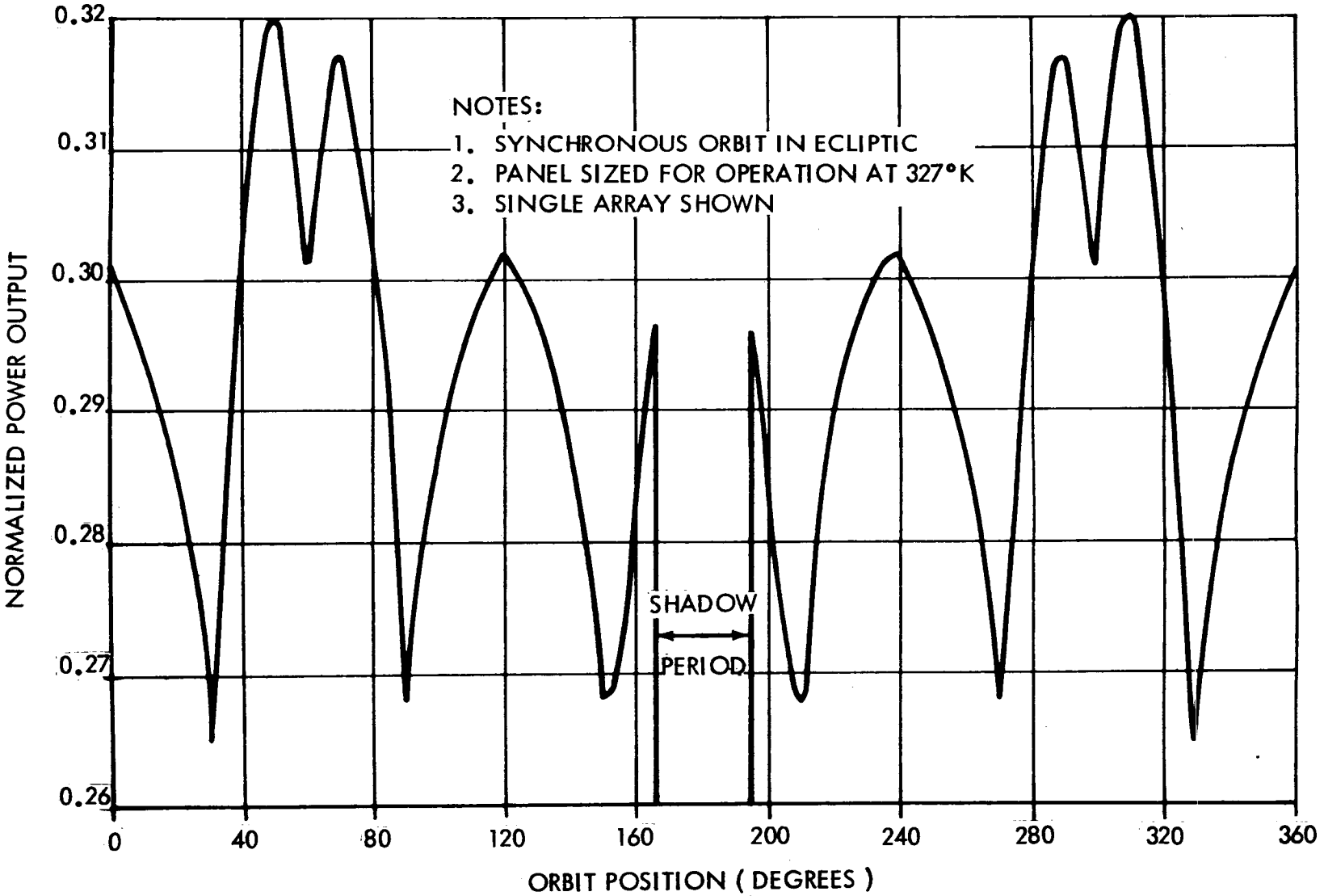


Figure 11.5.3.1-4. Unoriented Array Power Production Capability as a Function of Orbit Position

TABLE 11.5.3.1-2

PHOTOVOLTAIC SUBSYSTEM PERFORMANCE SUMMARY

PARAMETER	VALUE					
Cell Type	2 CMX2CM, Silicon, Wrap-Around					
Cell Thickness (mm)	0.254					
Cell Efficiency	12.0					
Packing Factor	0.90					
Surface Crazing	0.90					
Arraying Technique	2 Oriented Panels			2 Three-Blade Arrays		
Cell Weight (Kg/M^2)	.654			1.308		
Substrate Weight (Kg/M^2)	2.44			2.44		
Miscellaneous Weight (Kg/M^2)	.488			0.946		
Aspect Ratio	1.00			0.269		
Mission*	1	2	3	1	2	3
Cover Slide Thickness (mm)	0.152	0.254	0.254	0.152	0.254	0.254
Cover Slide Weight (Kg/M^2)	0.400	0.663	0.663	.800	1.338	1.338
Total Weight (Kg/M^2)	3.96	4.23	4.23	5.49	6.01	6.01
Meteoroid Degradation Factor	0.952	0.998	0.998	0.952	0.998	0.998
Radiation Degradation Factor	0.950	0.792	0.792	0.950	0.792	0.792
Thermal Degradation Factor	0.900	0.900	0.825***	0.900	0.900	0.825***
Array Specific Weight (Kg/KW)						
Array Specific Area (M^2/KW)**						
Array Specific Volume (M^3/KW)						

* Mission 1 - Low Earth Orbit.
Mission 2 - 24 Hr. in Ecliptic Plane.
Mission 3 - 24 Hr. in Equatorial Plane.

** Based on one side of blades.

*** Includes degradation due to orbit inclination.

where power in excess of the nominal will be required. In addition, solar cell arrays can produce power only when they receive solar energy and will require another source of energy in the shadow of the earth. For both of these conditions, energy storage (namely, secondary batteries) will be required.

It is extremely important to know the discharge and the charge items required by the batteries. The worst case occurs, of course, when the spacecraft is in the ecliptic plane. Here, there is one period of darkness for each orbit. If the spacecraft does not operate in the plane of the ecliptic, the shadow periods may occur less frequently.

The energy output and life of a secondary battery is highly dependent upon a number of parameters. Under continuous cycling, the interacting effects of the duration, operating level, the ratios of various operating parameters for the charge and discharge portions of the cycle, temperature, depth of discharge, overcharge, and the states of charge at various points in the cycle must be considered.

The performance of the batteries in terms of energy density, i.e., watt hours per kilogram or watt hours per cubic centimeter, can be related to these curves by considering that they represent the energy density at 100 per cent depth of discharge. Table 11.5.3.2-1 presents the important parameters for the two types of batteries under consideration

TABLE 11.5.3.2-1

SECONDARY BATTERY PERFORMANCE SUMMARY

PARAMETER	NiCad	SilCad
Theoretical		
Coulombic Capacity (2-hr/Kg)	181.	212.
Energy Density (w-hr/Kg)	236.	264.
Energy Density of Batteries (100% DOD)		
@Rated Capacity (w-hr/Kg)	29.8	48.5
Packaged Cells (w-hr/Kg)	19.52	38.8
Rated Capacity (w-hr/cc)	.0549	.1340
Packaged Cells (w-hr/cc)	.0366	.1072
Cell Voltage	1.22	1.08
Operating Temperature		
Upper (°C)	+40	+40
Lower (°C)		

Since the batteries are discharged to some degree whenever they supply power to the spacecraft loads, they must be returned to full charge. This charging is accomplished by draining power from the solar cell panels when they are receiving the energy of the sun.

11.5.3.3 Integration and Performance

Just as it is necessary to consider the integrated performance of the RTGs, so it is necessary to consider the performance of the photovoltaic power system. Unlike the RTG, however, the solar cell system is very dependent upon the orbit selection.

The synchronous orbits imposes no major problems on the integrated system since the shadow portion of the orbit is relatively short in comparison to the charge time available. Figure 11.5.3.3-1 shows the trade-off between solar panel total power level and panel plus battery weight for both types of arrays. The orbit considered is a 24-hour synchronous orbit in the plane of the ecliptic.

As can be seen from figure 11.5.3.3-1, the minimum weight occurs at a power level of 1965 watts. This power includes the power to spacecraft loads, to recharge the secondary batteries, and the excess power that must be dissipated by resistive loads.

For low earth orbits, the picture changes drastically. Using the same load profile for the experiments two problems arise. First, the orbit period is ninety minutes of which 55 minutes is spent in the light and 35 minutes is spent in the dark. The batteries to supply the dark time power, therefore, must be charged rapidly. The second problem arises since the peak loads must still be met.

Since the cycle life requirements for the two battery loads are quite divergent, separate battery packs will be provided for the dark time and peak load conditions. Nickel cadmium secondary batteries will be used to provide power during dark portions of the orbit and silver cadmium batteries will be used for peak loads.

The nickel cadmium batteries must be capable of 6400 cycles which means a relatively low depth of discharge (40 per cent). For this depth of discharge, an energy density of 7.35 watt-hour per kilogram is applicable. The silver cadmium batteries, on the other hand, must be capable of only 40-50 cycles and can operate at a 75 per cent depth-of-discharge. An energy density of 29 watt-hours per kilogram corresponds to this depth of discharge.

A trade-off analysis between solar panel power level and array plus battery weight was performed for the low earth orbit. The results of this analysis shows that the minimum weight power system occurs at a power level of 4370 watts. At this power level the combined weight of the oriented array is 365 kilograms. The power level includes

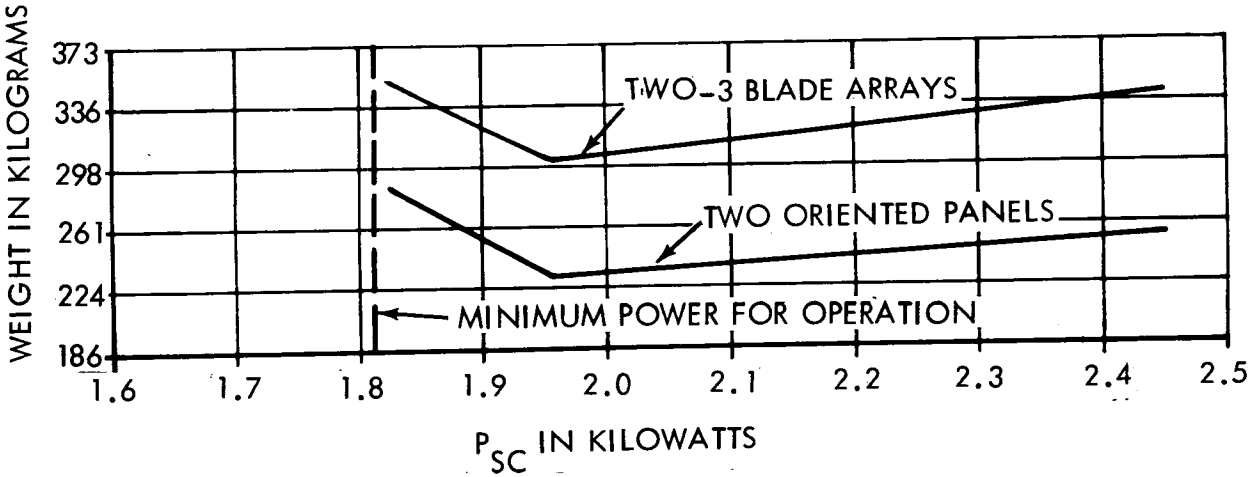


Figure 11.5.3.3-1. Photovoltaic Weight/Power Optimization

battery charging power and power for all loads equipments. It is interesting to note that the minimum weight point occurs at a power level such that there is no requirement for peak load batteries. The panels are sized to provide the full 2400 watts plus the dark time battery charging power.

Since including the laser experiments for the low earth orbit missions dictates high power levels and hence a heavy system, it is recommended that lasers be eliminated for the low earth orbit missions. If the lasers are eliminated, the total power producing capability required decreases to 2551 watts and the weight reduces to 202 kilograms.

The photovoltaic power system must also be integrated with the spacecraft. Section 11.2 discusses the various spacecraft configurations and the figures shown in that section show the panel configurations and the method of attachment to the spacecraft. The methods for deploying the panels in orbit is similar to the methods used on previous satellites and will consequently introduce no significant problems.

11.5.4 System Comparison and Selection

In order to select the power system approach best suited to the range of possible OTAES configurations it is necessary to compare the photovoltaic and the isotope thermoelectric system from a performance and an integration standpoint.

11.5.4.1 Performance

Table 11.5.4.1-1 summarizes the performance of the three candidate power systems. The table includes data for each of the orbits considered. The data in the table represents the performance of the integrated power systems.

As can be seen from the table, the oriented photovoltaic system offers clearly superior performance for all the missions considered. The unoriented photovoltaic system has better performance than the isotope thermoelectric generator for the synchronous orbits, but for the low orbits, there is a slight performance advantage for the RTG.

Based upon performance, the power system for the OTAES should be an oriented photovoltaic system for all of the missions considered.

11.5.4.2 Integration

Performance is not the only factor to consider. The integration of the power systems into the entire system is of paramount importance.

TABLE 11.5.4.1-1
POWER SYSTEM PERFORMANCE COMPARISON

MISSION	PARAMETER	CONCEPT		
		ORIENTED SOLAR CELL	UNORIENTED SOLAR CELL	ISOTOPE TE GENERATOR
1	Primary Power Source Power Level (watt)	4370	4370	2000
	Primary Power Source Weight (Kg)	157	404	536
	Energy Storage Subsystem Weight (Kg)	207	207	46
	Power Conditioning Weight (Kg)	24.6	24.6	19.9
	Miscellaneous Weight (Kg)	34.6	34.6	16.3
	Total Weight (Kg)	423.2	669.2	618.2
	Primary Power Source Volume (M^3)	3.03	5.63	4.80
	Energy Storage Subsystem Volume (M^3)	.0735	.0747	.0166
	Miscellaneous Volume (M^3)	.0198	.0198	.0200
	Total Volume (M^3)	3.1233	5.7245	4.8366
	Total Deployed Area (M^2)	39.6	73.6	15.6
2	Primary Power Source Power Level (watt)	1965	1965	2000
	Primary Power Source Weight (Kg)	86.8	228	536
	Energy Storage Subsystem Weight (Kg)	194.2	194.2	46
	Power Conditioning Weight (Kg)	19.9	19.9	19.9
	Miscellaneous Weight (Kg)	26.8	30.0	16.3
	Total Weight (Kg)	327.7	472.1	618.2
	Primary Power Source Volume (M^3)	1.555	3.88	4.80
	Energy Storage Subsystem Volume (M^3)	.0690	.0701	.0166

TABLE 11.5.4.1-1 - POWER SYSTEM PERFORMANCE COMPARISON (cont'd)

MISSION	PARAMETER	CONCEPT		
		ORIENTED SOLAR CELL	UNORIENTED SOLAR CELL	ISOTOPE TE GENERATOR
	Miscellaneous Volume (M^3)	.0162	.0162	.0200
	Total Volume (M^3)	1.6402	3.9663	4.8366
	Total Deployed Area (M^2)	20.3	37.7	15.6
3	Primary Power Source Power Level (watt)	1960	1960	2000
	Primary Power Source Weight (Kg)	98.5	247	536
	Energy Storage Subsystem Weight (Kg)	76.3	76.3	46
	Power Conditioning Weight (Kg)	19.9	19.9	19.9
	Miscellaneous Weight (Kg)	26.8	30.0	16.3
	Total Weight (Kg)	221.5	373.2	618.2
	Primary Power Source Volume (M^3)	1.685	3.14	4.80
	Energy Storage Subsystem Volume (M^3)	.0270	.0276	.0166
	Miscellaneous Volume (M^3)	.0162	.0162	.0200
	Total Volume (M^3)	1.7282	3.1838	4.8366
	Total Deployed Area (M^2)	22.0	41.0	15.6

Since the final spacecraft configuration has not been selected at this time, the choice between the oriented and unoriented arrays should be delayed pending continued analysis of the integration problems.

Both concepts can be easily integrated with any of the spacecraft configurations under consideration but the performance advantage of the oriented array must be weighed more carefully against the simplicity of the unoriented array.

The radioisotope thermoelectric generator can be eliminated from further contention because of the integration problems. The high temperature of the radiator is such that the structural integrity of the spacecraft might be compromised. The high temperature of the radiator may also preclude EVA activities in the vicinity of the RTG's

11.6 ENVIRONMENTAL CONTROL SYSTEM

Manned missions were given primary consideration during this phase of the OTAES study and therefore further investigations of the Environmental Control System were conducted. The purpose was twofold:

a. To insure compatibility between OTES manned missions and current Apollo Application Program (AAP) plans; and

b. To determine the effects of and means of reducing contamination of the optical surfaces in the telescope compartment.

11.6.1 Apollo Applications Program Criterion

Under the study's ground rules, all manned OTES configurations were considered part of the Apollo Applications Program (AAP), hence the criteria developed for the OTES Environmental Control System (see table 11.6.1-1) were based on the environment presently being emphasized in the AAP. The criteria established in this phase were identical to those developed during Phase I.

11.6.2 Contamination Control of Optical Surfaces

Contaminants could present a serious problem by causing degradation in the performance (resolution, transmissivity, reflectivity, etc.) of optical surfaces. Exhaust products from the Reaction Control System's thrusters, vented substances, and dust and moisture from the spacecraft's cabin provide potential sources of contamination. While dust and moisture from the cabin would be the major source of contamination within the telescope well, the external surfaces (view ports) would be primarily influenced by impingement of thruster exhaust gases. Contamination can be minimized by properly locating the thrusters and vents, and by isolating the telescope's components from the astronauts.

TABLE 11.6.1-1

ENVIRONMENTAL CONTROL SYSTEM CRITERION

Mission duration (minimum)	45 days
Number of crew (maximum)	2 or 3
Atmosphere (by partial pressure)	O_2-N_2/70%-30%
Total pressures (absolute)*	
Normal	34,473.8 $\pm$ 1,378.9 N/m^2
Emergency (for 2 minutes with 0.0127 m dia. hold)	24,131.7 N/m^2
Relief setting	41,368.5 $\pm$ 1,378.9 N/m^2
Partial pressures (absolute)	
Oxygen	24,131.7 N/m^2
Nitrogen	10,342.1 N/m^2
Carbon dioxide (nominal)	3.5 mm Hg
Carbon dioxide (maximum for short periods of time)	5.0 mm Hg
Temperatures	
Cabin	297.1 $\pm$ 2.8°K
Suit	292.1 - 293.4°K
Relative humidity	40 - 70%
Volume to be pressurized (maximum)	70.8 m^3
Number of repressurizations	To be determined by mission

* Suit pressures will be slightly higher.

11.6.2.1 Sources of Contamination

The three major sources of possible optical contamination are:

a. Material vented overboard.

b. RCS thruster exhaust products.

c. Solids and moisture from within the spacecraft.

The degree of seriousness to which optical surfaces are effected by each of these depends upon the relative location of surface and the source of contamination.

Contamination resulting from vented substances, such as water, will present a problem to the external surfaces which are in the immediate vicinity of the discharge port. Formation of frost or ice on nearby functional surfaces could easily render them inoperative.(1)

Impingement of exhaust products from the RCS thrusters could cause a degradation in the performance spacecraft's external functional surfaces. Although a cold gas system would not present a problem, a hot gas system would produce contaminants in the form of condensed phase products of combustion, partially combusted products and erosion products from the engines.

Experimental evidence(2) indicates a 45 per cent degradation can be obtained in the performance of a solar reflector due to direct impingement of a rocket's exhaust. Results of the same study also indicate losses of up to 7 per cent in solar cells performance because of exhaust impingement. Although decrease in the normal (perpendicular) transmittivity of optical windows was also observed after exhaust gas impingement, the same parts were almost opaque when viewed through at non-normal directions.

Exhaust gas contamination of internal surfaces could be a potential problem, especially during translation maneuvers where several thrusters would be fired simultaneously. Recirculation of exhaust gases (similar to that in the base region of a launch vehicle) in the region of telescope's aperture, or expansion of the thrusters exhaust plume around the lip of the light baffle could cause migration of exhaust products intothe interior, where deposits could accumulate on the optical surfaces.

---

(1) Lehrer, S. and Upper, C.E., "Space Propulsion System Installation Technology", Seventh Liquid Propulsion Symposium, June 1965.

(2) Program to Study and Resolve Rocket Engine Installation Problems Related to Maneuvering Satellite Vehicles", AFRPL-TR-65-42, Astrosystems International, Incorporated, February 1965.

This problem will have to be examined in depth once the type, size and location of the RCS thrusters, and the exceptable contamination levels for the optics have been established.

Solid particles and moisture from the manned compartments seem to be a primary source of contamination in a pressurized telescope well to which the astronauts have access. The astronauts insensible water losses and perspiration (1.5 to 4.0 liters per man per day)(3) constitute the major source of moisture in the spacecraft. Solid particles from the cabin and the astronauts' skin, hair, etc. could form the nuclei about which condensation would occur.

If the pressurizing gas contains moisture and solids, which it would if an opening between the well and the manned compartment exists there is a possibility of moisture condensing/freezing on surfaces. Figure 11.6.2.1-1 delineates the surface temperature at which condensation would occur in the operating range of the Apollo's ECS. The figure indicates that for the Apollo environmental conditions, condensation would be a problem on any surface below 21°C. Freezing would occur on any surface which is below 0°C. Although the moisture would return to the vapor state when the telescope compartment is depressurized, the solids might adhere to the surface due to electrostatic forces. And the accumulation of particles due to numerous repressurizations might render functional optical surfaces inoperative.

11.6.2.2 Contamination Control

Contamination of external functional surfaces by vented substances and RCS thruster exhaust gases can be eliminated, for the most part, by locating the surfaces, thrusters and discharge ports so as to minimize impingement.

Should contaminants from these sources impose a problem to surfaces within the telescope compartment, the telescopes' aperture could be closed during venting and RCS operations.

There are several methods of preventing cabin moisture/dust contamination of optics within the telescope compartment which should be tested. Minimizing contamination during adjustment of the optics could be accomplished through the use of pressure suits, glove box techniques, remote control, or maintaining optical surfaces above the atmosphere's dewpoint temperature.

Remote control would be the best method of preventing contamination when only adjustments are needed. Other techniques would be necessary if direct excess is required to make modifications within the telescope compartment, such as to the telescopes' isolation system.

---

(3) "Bioastronautics Data Book" NASA SP-3006, NASA, 1964, p. 12-2.

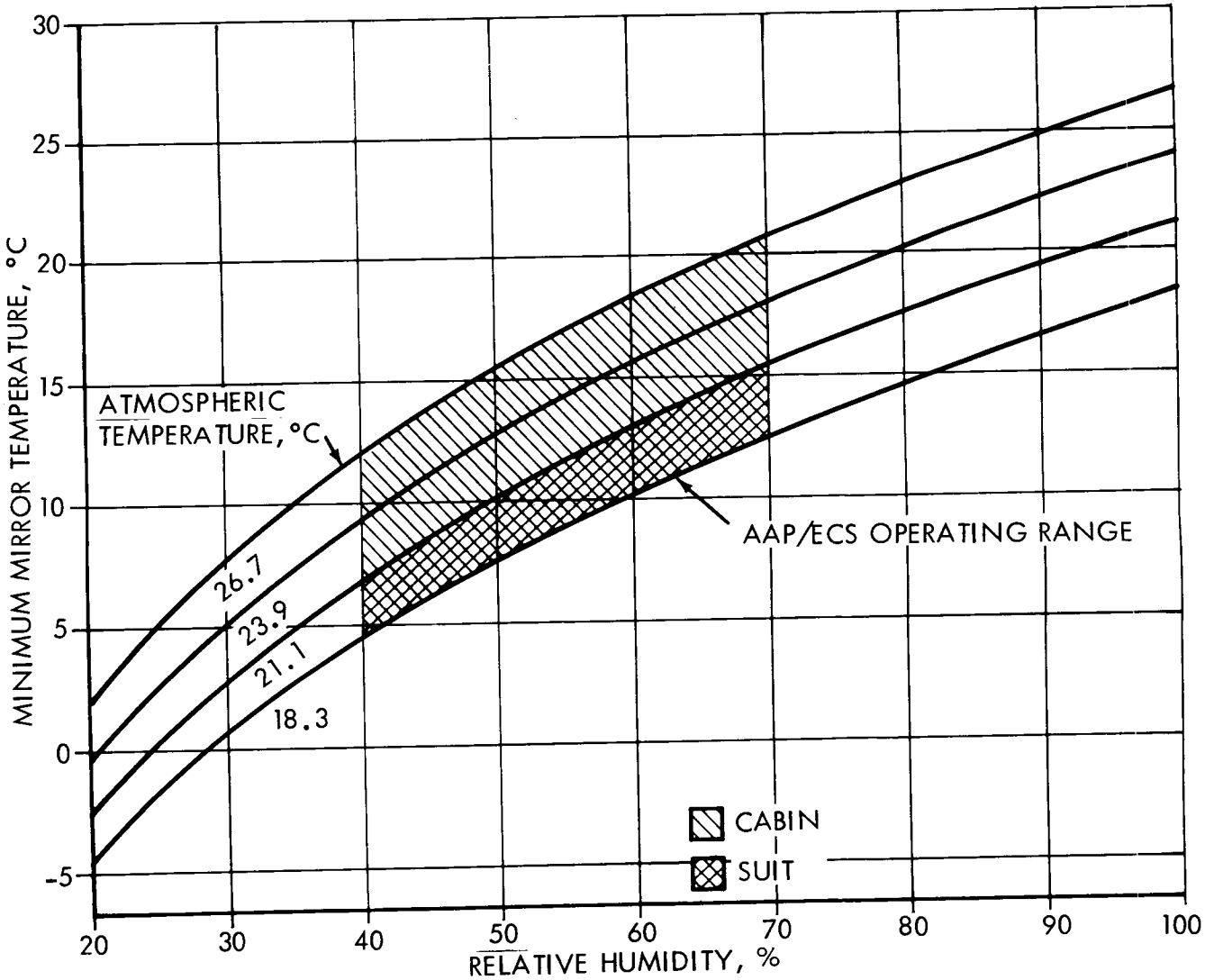


Figure 11.6.2.1-1. Minimum Mirror Temperature Required to Prevent Condensation

One method of minimizing contamination while still providing access to the telescope compartment would be to depressurize the entire module and have the astronauts perform the adjustments while in a fully-pressurized spacesuit. The water lost by the astronaut would be removed by the ECS through an umbilical. Portable life support systems or back packs could not be used since they would consitute a source of moisture (from the water boilers in the pack's heat rejection systems).

If the fully pressurized suit proves too awkward to allow intricate operations to be performed, then a suit operating at a lower pressure differential could provide a second method whereby the effects of moisture and dust are minimized. Contaminants initially in the cabin's atmosphere could be removed by depressurizing the cabin and repressurizing both the cabin and well with a dry atmosphere prior to venting the spacesuit. The ECS would remove the water vapor from the suit through an umbilical.

Both methods discussed above would have weight penalties associated with the repressurizations. A third method which would also incur a weight penalty, but to a lesser degree, would use the glove box technique. Even though the manned compartment would not require depressurizing, the telescope well would have to be pressurized with an inert atmosphere. Although this method eliminates the possibility of atmospheric contamination without depressurizing the entire module cabin, nothing could be transferred from the cabin into the well. Also the types of operations performed by the astronauts might be limited by their inability to reach certain areas within the well.

Finally, if some contamination could be tolerated, the problem of condensation could be eliminated by designing the thermal control system to maintain the internal functional surfaces above 21°C. This technique would preclude any accumulation of particles contained in the condensate and particles smaller than 40 microns (approximate filtering capability of the Gemini and Apollo's ECS) would be of primary concern. Further reduction in the contamination levels could possibly be achieved by designing smaller filters or by forcing a warm dry gas across the surfaces. Adjustments inside the telescope compartment could be carried out after simply pressurizing the telescope well with the cabin's atmosphere.

Although each of the techniques discussed above have advantages and disadvantages, the selection of a method to prevent optical contamination from the cabin's atmosphere will have to be based on the number and types of adjustments needed, and the modifications required within the telescope compartment.

11.7 COMMUNICATION AND DATA HANDLING

There are at present three broad categories of ground support facilities in existence which are suitable for the support of the OTAES program: the Manned Space Flight Network, the Deep Space Network, and the Satellite Tracking and Data Acquisition Network (STANDAN). The capabilities of each of the three types of stations reflect the nature of the programs the stations are meant to support. In general, the requirements of the OTAES program are most similar to those of other manned space flight programs, and thus the Manned Space Flight stations are better suited to OTAES than either of the other two types. The siting studies described in section 10.4 suggest the use of the Goldstone facility. Fortunately, it contains what appear to be ample facilities since it supports all three networks.

The station best suited for the OTAES ground support task is the Apollo station presently under construction as part of the Manned Space Flight Network. This station utilizes the Unified S-Band equipment specified by NASA as standard for the non-Earth orbiting phases of the Apollo moon mission. However, the 85-foot antenna at Goldstone, unlike the other DSN antennas, will be able to track at the 5 degrees per second rate required for Earth-orbiting vehicles. Thus, it will be possible to use the Goldstone station for support of Apollo during the Earth-orbital phases of the mission, despite the fact that the Unified S-Band system was designed primarily for communications with the Command/Service Module (CSM) and Lunar Excursion Module (LEM) during lunar and trans-lunar phases of the mission.

There will be several communications links with the Mission Control Center (MCC) at Houston allowing for real-time processing of telemetry and tracking data at MCC. The links include voice, television, a full duplex teletype line, a high-speed line (up to 2400 bits per second), and a microwave link capable of handling up to 50 kilobits per second. The equipment being installed at Goldstone for Apollo will allow OTAES to transmit and receive the normal command and control signals, systems telemetry, and biomedical information simultaneously with the experimental data, with some exceptions.

The equipment being installed at Goldstone (not including the back-up equipment being installed at the nearby JPL facility) consists of the following:

1 analog recorder
2 wide-band recorders
1 narrow band recorder
1 voice recorder
2 remote site data processors
1 facility intercom
3 PCM decommutation systems
1 PCM simulator
1 TV monitor
1 85-foot antenna system.

11.7.1 Command and Telemetry

The Unified S-Band System combines all tracking and communications between the spacecraft and the ground stations into a single frequency band. Up-link transmission takes place on two signals which are modulated on carriers located at 2101.8 MHz and 2106.4 MHz, respectively. Down-link reception takes place at any two of four carrier frequencies: 2272 MHz, 2277.5 MHz, 2282.5 MHz, and 2287.5 MHz. The voice and update data are modulated onto subcarriers and combined with the ranging data to form a composite signal which phase-modulates a carrier in the up-link system. Likewise, the voice and telemetry data to be transmitted from the spacecraft are modulated onto subcarriers, combined with the video ranging signals, and used to phase-modulate the down-link carrier frequency. The transponder transmitter can also be frequency-modulated for the transmission of television information or recorded data instead of ranging signals.

The different combinations of signals to be transmitted in the Apollo program are summarized in tabular form in figure 11.7-1 (the primary LEM down link modes are 1, 7, and 10), figure 11.7-2 (mode 2 is the primary PM high data mode), and figure 11.7-3. The main reason for the use of the wide-band FM mode is to allow the transmission of TV or high-speed playback of taped data. Figures 11.7-4 and 11.7-5 summarize the transmission modes used in up-link communications with both LEM and CSM. In the high data modes, up-data, voice, and the pseudo-random noise (PRN) range code are all transmitted simultaneously. The up-data channel is capable of PCM transmission in the order of 5 kilo bits per second. Thus, during the noncritical maneuvering phases of the OTAES mission, some or all of the up-data band within the 5-MHz channel could be used for up-link scientific command data.

The Goldstone system contains two sets of receivers: one for the CSM and the other for the LEM. If there is only a single OTAES vehicle in orbit as part of the OTAES experiment, two of the four 5-MHz channels are available in their entirety for use in down-link telemetering of the experimental data. The same argument applies to the up-link requirement. The entire capability of the 5-MHz channel reserved for LEM is available for use on OTAES if required.

As the system is presently designed, it is possible to receive at a single dual Unified S-Band site, up to four 5-MHz channels of information simultaneously. Any one channel may contain up to 51.2 kilobits of PCM data as well as voice, and about 10 kHz of analog data on three separate subcarriers. As an alternate, a single channel may be used to transmit television video, although such use of a channel precludes transmission of any additional information on the channel. It should be noted that the analog information is sent as a FM signal on a subcarrier or main carrier; thus, the information bandwidth is much smaller than the actual transmission channel bandwidth.

Telemetry data received in the S-Band system is demodulated in the various subcarrier demodulators and is decommutated and distributed by the PCM system. Selected telemetry parameters are then transferred to the telemetry data processor and to the command data processor. The telemetry data processor may then send signals to a magnetic tape recording unit for storage and/or to display consoles for display. Data will also be processed by the TM data processor for transmission in real time to control center over high-speed lines.

The data is transmitted serially from the spacecraft in a synchronized major frame consisting of 192 minor frames. Each minor frame consists of 80 eight-bit words. The major frame is read into the ground system at 51.2 kilobits/second and requires 2.4 seconds for a complete major frame transmission. The PCM ground station strips out those parameters associated with spacecraft subsystem status and engineering factors, which are contained for the most part in the prime subframe, and transfers them to the computer in parallel at 1728 eight-bit words per 2.4 seconds.

11.7.2 Data Processing

Each Apollo Unified S-Band site will have two identical computing systems: one will handle the processing of telemetry data, and the other will process command and control data. The computers used are modified versions of the Univac 642B. The 642B is a general-purpose, medium scale, solid state, parallel, binary machine. Its memory is a random access magnetic core tape with overlap capability. The memory has a cycle time of 2.0 microseconds and a capacity of 32 K 30-bit words, expandable to 131 K, all directly addressable. Real-time input/output is facilitated via the 16 input and 16 output channels, all fully buffered, under the control of 81 interrupts.

The peripheral equipment associated with the computers consists of the following:

a. UNIVAC 1540 magnetic tape units

b. UNIVAC 1259 teletype adaptor

c. UNIVAC 2008/10 data transmission units (DTV)

2282.5 Mc Carrier Combination	Information	Modulation Techniques	Subcarrier Frequency	Carrier Phase Deviation
1	Carrier			
	Voice	FM/PM	1.25 Mc	0.7 Radians
	51.2 kbps TM	PCM/PM/PM	1.024 Mc	1.3 Radians
2	Carrier			
	PRN	PM on Carrier		0.2 Radians*
	Voice	FM/PM	1.25 Mc	0.7 Radians
	51.2 kbps TM	PCM/PM/PM	1.024 Mc	1.3 Radians
3	Carrier			
	1.6 kbps TM	PCM/PM/PM	1.024 Mc	1.3 Radians
4	Carrier			
	BU Voice	PM on Carrier		0.8 Radians
	1.6 kbps TM	PCM/PM/PM	1.024 Mc	1.3 Radians
5	Carrier			
	Backup Voice	PM (24 db clipping)		0.8 Radians
6	Carrier			
	Key	AM/PM	512 kc	1.4 Radians
7	Carrier			
(Lunar Stay Mode)	Voice/Biomed	FM/PM	1.25 Mc	1.3 Radians
	1.6 kbps TM	PCM/PM/PM	1.024 Mc	.7 Radians
8	Carrier			
	Voice/EMU/ Biomed	PM on Carrier (no clipping)		TBD
	51.2 kbps TM	PCM/PM/PM		
				Carrier Deviation Ratio
9	Voice/EMU/ Biomed	FM/FM	1.25 Mc	0.17
	TM	PCM/PM/FM	1.024 Mc	0.37
10	TV	FM at Baseband		2.0
	Voice/EMU/ Biomed	FM/FM/FM	1.25 Mc	0.17
	1.6 or 51.2	PCM/PM/FM	1.024 Mc	0.37

*Down PRN ranging phase deviation is to be set with up-voice and up ranging modulation (Table I Comb 3) and with a high signal-to-noise ratio in the turn around channel.

Figure 11.7-1. LEM Down-Link MSFN S-Band Transmission Combination Summary

2287.5 Mc Carrier Combination	Information	Modulation Technique	Subcarrier Frequency
1	Carrier		
	Voice	FM/PM	1.25 Mc
	51.2 KBPS TM	PCM/PM/PM	1.024 Mc
2	Carrier		
	PRN	PM On Carrier	
	Voice	FM/PM	1.25 Mc
	51.2 KBPS	PCM/PM/PM	1.024 Mc
3	Carrier		
	PRN	PM On Carrier	
	Voice	FM/PM	1.25 Mc
	1.6 KBPS	PCM/PM/PM	1.024 Mc
4	Carrier		
	Voice	FM/PM	1.25 Mc
	1.6 KBPS	PCM/PM/PM	1.024 Mc
5	Carrier		
	1.6 KBPS	PCM/PM/PM	1.024 Mc
6	Carrier		
	Key	AM/PM	512 kc
7	Carrier		
	PRN	PM On Carrier	
8	Carrier		
	Backup Voice	PM On Carrier	
	1.6 KBPS TM	PCM/PM/PM	1.024 Mc
9	Carrier		
	PRN	PM On Carrier	
	1.6 KBPS TM	PCM/PM/PM	1.024 Mc

Figure 11.7-2. CSM To MSFN S-Band Transmission Combination Summary (PM Mode)

2272.5 Mc Carrier Combination	Information	Modulation Technique	Subcarrier Frequency
1	Playback Voice at 1:1	FM at Baseband	
	Playback CSM 51.2 KBPS TM at 1:1	PCM/PM/FM	1024 kc
	Scientific Data Playback at 1:1	FM/FM	95 kc
		FM/FM	125 kc
		FM/FM	165 kc
2	Playback Voice at 32:1	FM at Baseband	
	Playback CSM 1.6 KBPS TM at 32:1	PCM/PM/FM	1024 kc
	Scientific Data Playback at 32:1	FM/FM	95 kc
		FM/FM	125 kc
		FM/FM	165 kc
3	Playback LEM 1.6 KBPS Split Phase TM at 32:1	FM at Baseband	
4	Television	FM at Baseband	
5	Real-Time Scientific Data	FM/FM	95 kc
		FM/FM	125 kc
		FM/FM	165 kc

Figure 11.7-3. CSM to MSFN S-Band Transmission Combination Summary (FM Modes)

Combination	Information	Modulation Technique	Subcarrier Frequency	Carrier Phase Deviation
1	Carrier, PRN	PM on Carrier	-	0.37 Radians
2	Carrier, Voice	FM/PM	30 kc	1.4 Radians
3	Carrier			
	PRN	PM on Carrier	-	0.37 Radians
	Voice	FM/PM	30 kc	1.4 Radians

Figure 11.7-4. LEM Up-Link S-Band Transmission Combination Summary

2106.4 Mc Carrier Combinations	Information	Modulation Technique	Subcarrier Frequency
1	Carrier, PRN	PM On Carrier	-
2	Carrier, Voice	FM/PM	30 kc
3	Carrier, Up-Data	FM/PM	70 kc
4	Carrier		
	PRN	PM On Carrier	-
	Voice	FM/PM	30 kc
5	Carrier		
	PRN	PM On Carrier	-
	Up-Data	FM/PM	70 kc
6	Carrier		
	PRN	PM On Carrier	-
	Voice	FM/PM	30 kc
	Up-Data	FM/PM	70 kc
7	Carrier		
	Voice	FM/PM	30 kc
	Up-Data	FM/PM	70 kc
8	Carrier		
	Voice Backup	FM/PM	70 kc

Figure 11.7-5. MSFN to CSM S-Band Transmission Combination Summary (PM Modes)

d. UNIVAC Model 1000 computer address matrix (CAM) adaptor and Greenwich mean time (GMT) buffer

e. Motorola TP-4000 3000-word per minute line printer

f. UNIVAC 1299 distribution switchload

g. Console computer interface adaptor (CCIA)

A block diagram of the entire data processing system is shown in figure 11.7-6. Under normal conditions, each computer will serve only that function indicated by its name. However, if either computer fails, its functions may be taken over by the other by means of a third program which must be loaded into the remaining computer. In this event, the peripheral devices formerly associated with the failed computer are also switched over to the other computer manually at the 1299 switchboard. Units which do not require switching are the input/output (I/O) console, the 1259 TTY adaptor, the GMT buffer, and the 1540 magnetic tape unit. These units are connected directly to the computer.

Figure 11.7-7 indicates telemetry data flow. Data received from the pulse-code modulation (PCM) station will be processed by the telemetry computer and formatted for transfer to the memory character vector generator (MCVG). Data displayed on the cathode ray tube (CRT) will be refreshed from the MCVG. Selection of data to be displayed on the CRT will be made from the data request keyboard (DRK). Parameters in the various display formats will be limit-sensed by the computer. Indications will be given on the DRK of formats which contain out-of-limit parameters. Analog functions from the telemetry data to be displayed on recorders associated with the systems consoles will be stripped from the telemetry data by the computer and routed to digital/analog (D/A) converters in the CCIA. The D/A converters will be hard-wired to the recorders. Selection of one of six groups of parameters can be made by a switch on the recorder.

11.7.3 Possible Modifications

It may be desired to send analog signals of a bandwidth appreciably greater than 10 kHz during certain of the experiments. As long as the total bandwidth of these signals does not exceed about 500 kHz, it may be possible to provide transmission of such signals by means of minor modifications in the ground support equipment, and by redesign in the transmitter if the need for such modifications is justified. Such modifications would involve augmentation of the present system by the addition of several subcarriers to the normal FM carrier signal. These subcarriers would have to be separated by sufficient bandwidth to insure the ability to modulate with a high frequency signal without interfering with adjacent signals. In addition, new modulators would have to be added to the space vehicle electronics. Furthermore, new subcarrier discriminators would have to be added on the ground to recover the wide-band signals.

If it is considered essential to transmit signals of bandwidths greater than about 500 kHz, it may be possible by further modification of the equipment on both transmitting and receiving ends to amplitude, rather than frequency modulate the main carrier on a particular channel. The resulting signal would be, needless to say, of inferior quality compared to that of the FM signal presently used. However, up to 2.5 MHz of bandwidth may be procured in this fashion.

If bandwidths greater than 2.5 MHz are required, however, the modifications to the equipment become so large that they must be considered major engineering development programs.

As far as the up-link requirements are concerned, there appears to be more than enough capability already available in a single 5-MHz channel. If need be, the other channel may also be utilized, making available an additional 5 kilobits of data handling capacity.

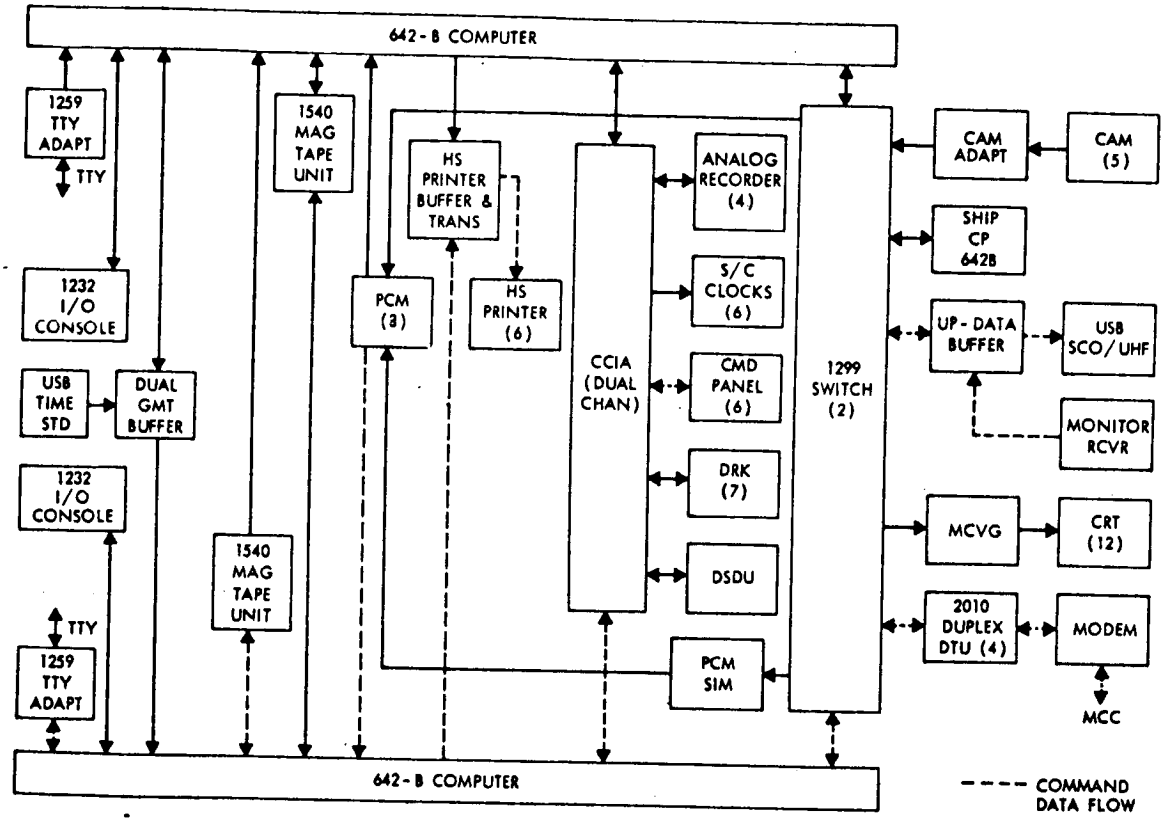


Figure 11.7-6. Block Diagram of USB Data Processing System

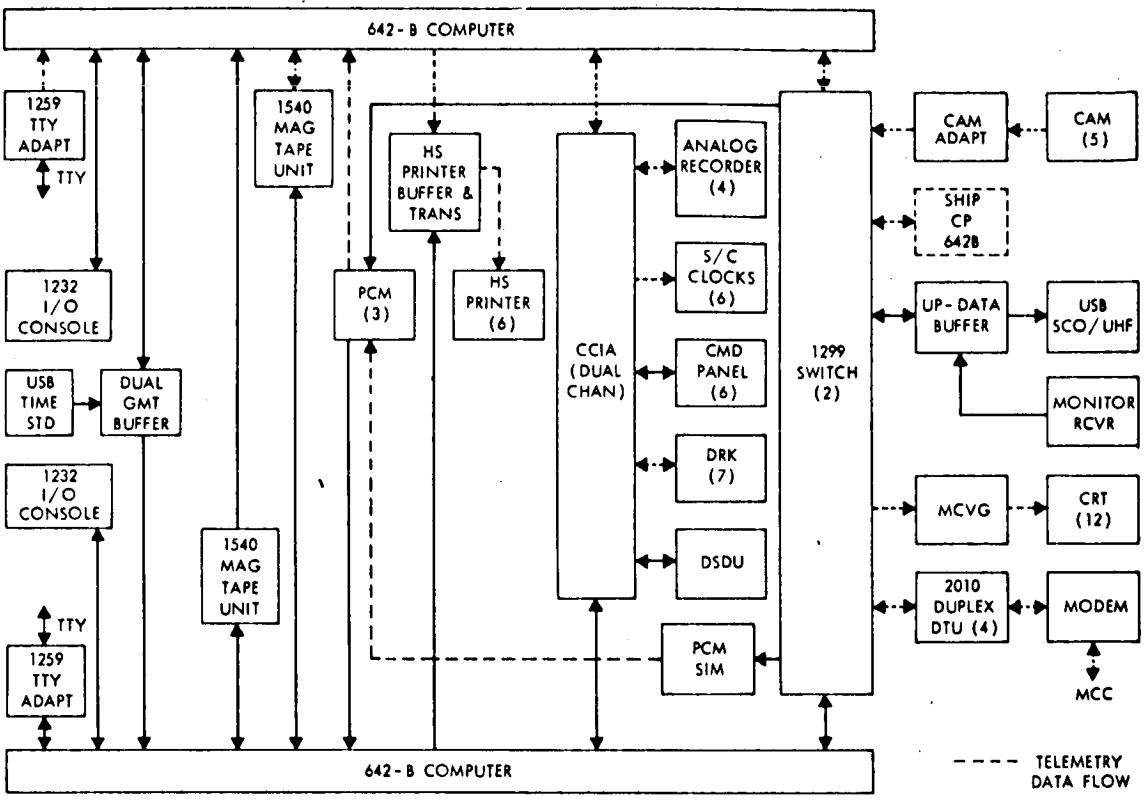


Figure 11.7-7. Telemetry Data Flow

In summary, the Goldstone facility may be adequate as a ground support station for the OTAES program. The existing equipment may be used without any appreciable modification if the requirements are so tailored.

11.7.4 Required Technology Development for OTAES Telemetry

New techniques must be developed for the measurement of the transmitted and received signals required in the 10 MHz experiment because the telemetry link can not measure or transmit the 10 MHz or even the 1 MHz information that is being transmitted over the optical communications link. For monitoring the video transmission to the spacecraft it may be possible to take pictures of the received test pattern, and then scan it at a slow rate for transmission to the ground. For digital communication tests, a fixed message may be sent at high data rates and compared with a similar message in the satellite so that the errors could be tabulated in the satellite and sent back as a number over the telemetry link. Each experiment should be reviewed and measurement techniques developed to collect the high rate data in a form that will summarize the information received so it may be transmitted over the lower capacity RF link.

REFERENCES

1. "Proceedings of the Apollo Unified S-Band Technical Conference," Goddard Space Flight Center, July 14-15, 1965, NASA SP-87.

2. "Telemetry On-Line Monitoring, Compression, and Transmission System for the Manned Space Flight Network (TOMCAT)," Volume I, Systems Description, Goddard Space Flight Center, September 1964, N64-33567.

3. "Estimated 1963-170 Capability of the Deep Space Instrumentation Facility for Apollo Project," Jet Propulsion Laboratory, EPD-29, Rev. I, 2-1-62.

4. R. L. Schroeder and John Zvara, "Design Considerations for the NASA Ground Operational Support System," Raytheon & Company, July 1962, N63-17968.

5. Manfred Eimer and Robertson Stevens, "Tracking and Data Handling for the Pioneer III and Pioneer IV Firings," Jet Propulsion Laboratory, External Publications No. 701, August 14, 1959.

6. G. Truszynski, "Satellite Data Recovery and Tracking System," from the Proceeding of the Conference on Artificial Satellites, Virginia Polytechnic Institute, August 1963.

7. H. Stiltz, "Aerospace Telemetry," Prentice-Hall, Inc. Englewood Cliffs, New Jersey, July 1964.

12.0 EXPERIMENT/MISSION TIME PHASING

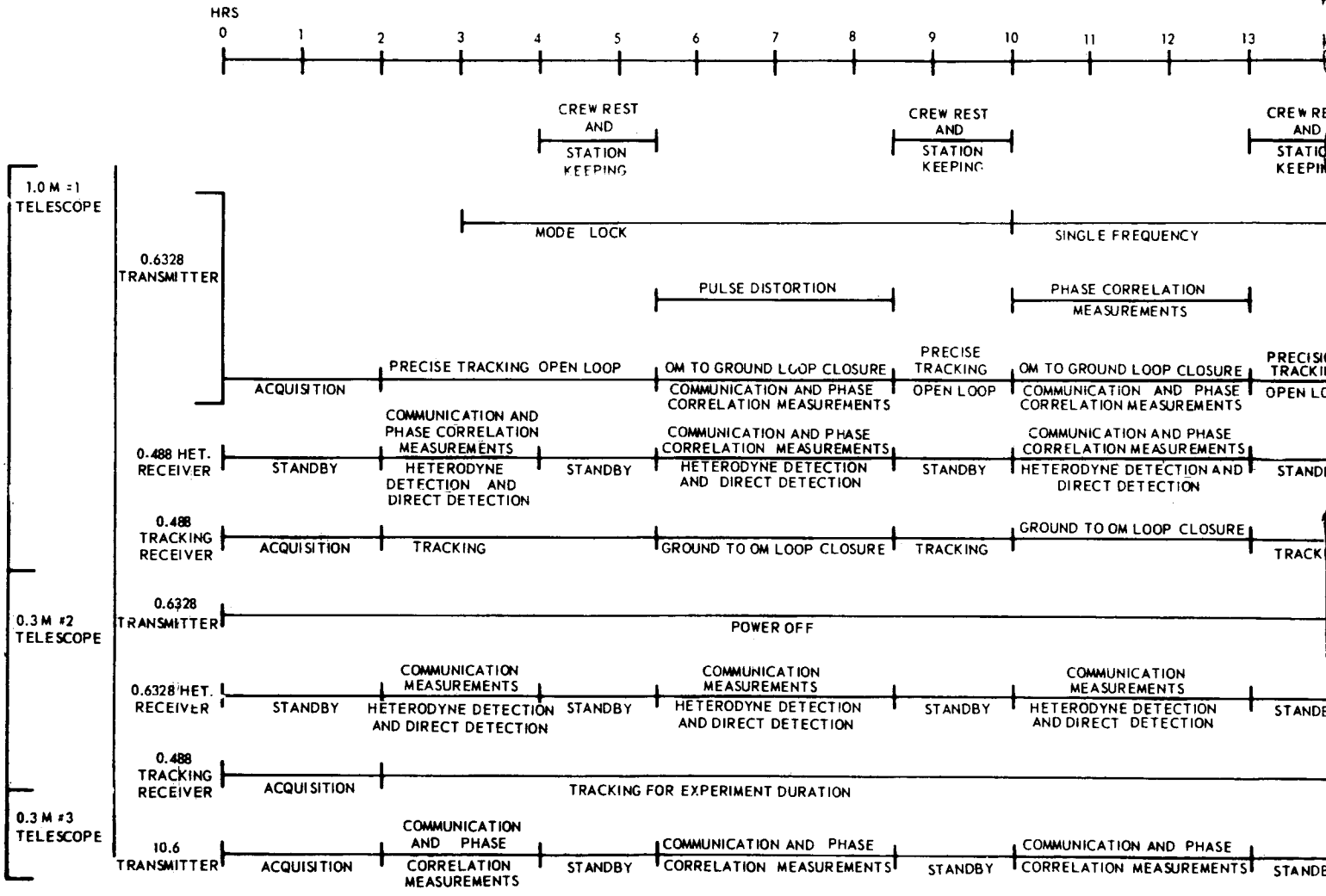
As part of the optical technology experiment analysis and integration efforts, candidate combinations of several launch vehicle stackups, flight missions, spacecraft configurations and optical technology experiments were evaluated. A discussion of these candidate combinations appear in section 10.2, Volume II.

From among the alternative considerations, one of the preferred considerations includes a S-IC/S-II/S-IVB/OM/CSM launch stackup for a synchronous orbit mission with a manned portion followed by an unmanned portion; and spacecraft configuration No. 1 in a LEM adapter housing sixteen optical technology experiments.

A mission flight plan has been developed for an approximate 373 hour manned synchronous orbit mission. The flight plan (table 12.2-1) presents mission phases, events and necessary CSM/OM spacecraft system sequences which will be compatible with flight crew capabilities, work/rest cycles and man/machine performance time constraints. A portion of table 12.2-1 is illustrated in time-line form as figure 12.0-1.

Several abbreviations were also employed in the mission groundrules and as flight plan entries. These abbreviations consist of the following:

AGC	Apollo Guidance Computer
CES	Crew Equipment System
C&I	Communication and Instrumentation System
CM	Command Module
CSM	Command and Service Modules
C&W	Caution and Warning System
ECS	Environmental Control System
EMS	Entry Monitor System
EPS	Electrical Power System
EVA	Extravehicular Activities
G&N	Guidance and Navigation System
IMU	Inertial Measurement Unit
IVA	Intravehicular Activities
LES	Launch Escape System
MHz	Megahertz
MSFN	Manned Space Flight Network
NAV	Navigation
OM	OTAES Module
PU	Propellant Utilization System
RCS	Reaction Control System
SCS	Stabilization and Control System


HRS
0
1
2
3
4
5
6
7
8
9
10
11
12
13
CREW REST AND STATION KEEPING
CREW REST AND STATION KEEPING
1.0 M #1 TELESCOPE
0.6328 TRANSMITTER
MODE LOCK
SINGLE FREQUENCY
PULSE DISTORTION
PHASE CORRELATION MEASUREMENTS
ACQUISITION
PRECISE TRACKING OPEN LOOP
OM TO GROUND LOOP CLOSURE
COMMUNICATION AND PHASE CORRELATION MEASUREMENTS
PRECISE TRACKING
OPEN LOOP
OM TO GROUND LOOP CLOSURE
COMMUNICATION AND PHASE CORRELATION MEASUREMENTS
0.488 HET. RECEIVER
STANDBY
COMMUNICATION AND PHASE CORRELATION MEASUREMENTS
HETERODYNE DETECTION AND DIRECT DETECTION
STANDBY
COMMUNICATION AND PHASE CORRELATION MEASUREMENTS
HETERODYNE DETECTION AND DIRECT DETECTION
STANDBY
COMMUNICATION AND PHASE CORRELATION MEASUREMENTS
HETERODYNE DETECTION AND DIRECT DETECTION
0.488 TRACKING RECEIVER
ACQUISITION
TRACKING
GROUND TO OM LOOP CLOSURE
TRACKING
GROUND TO OM LOOP CLOSURE
0.3 M #2 TELESCOPE
0.6328 TRANSMITTER
POWER OFF
0.6328 HET. RECEIVER
STANDBY
COMMUNICATION MEASUREMENTS
HETERODYNE DETECTION AND DIRECT DETECTION
STANDBY
COMMUNICATION MEASUREMENTS
HETERODYNE DETECTION AND DIRECT DETECTION
STANDBY
COMMUNICATION MEASUREMENTS
HETERODYNE DETECTION AND DIRECT DETECTION
0.488 TRACKING RECEIVER
ACQUISITION
TRACKING FOR EXPERIMENT DURATION
0.3 M #3 TELESCOPE
10.6 TRANSMITTER
ACQUISITION
COMMUNICATION AND PHASE CORRELATION MEASUREMENTS
STANDBY
COMMUNICATION AND PHASE CORRELATION MEASUREMENTS
STANDBY
COMMUNICATION AND PHASE CORRELATION MEASUREMENTS

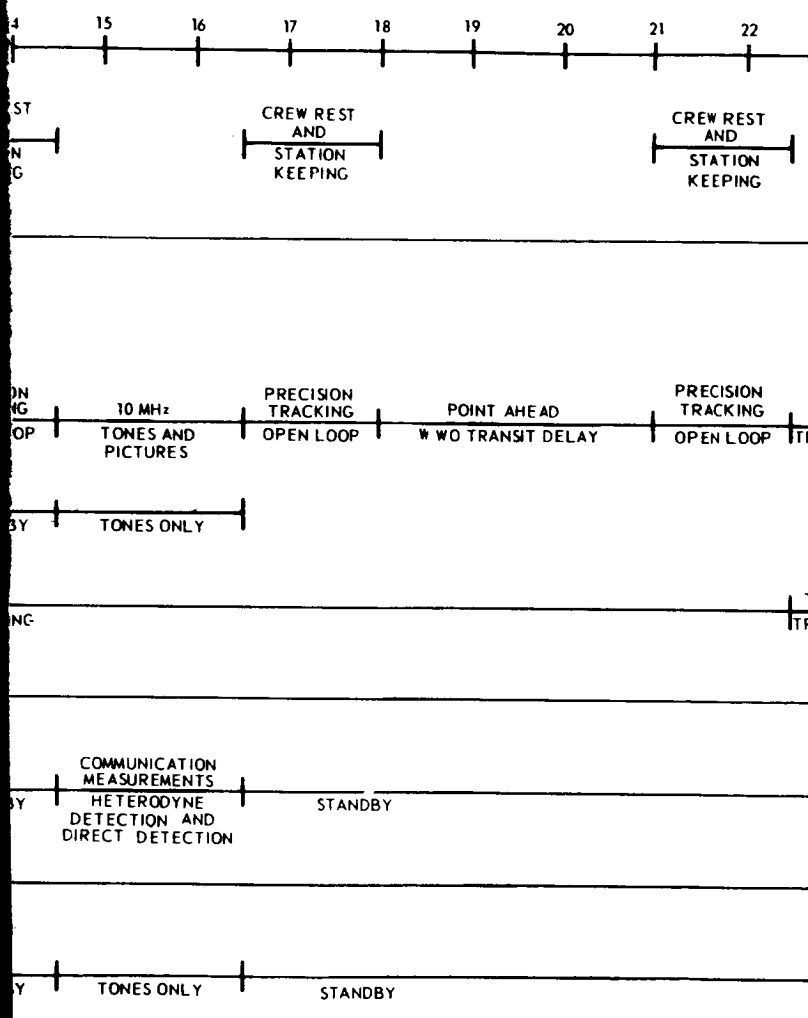
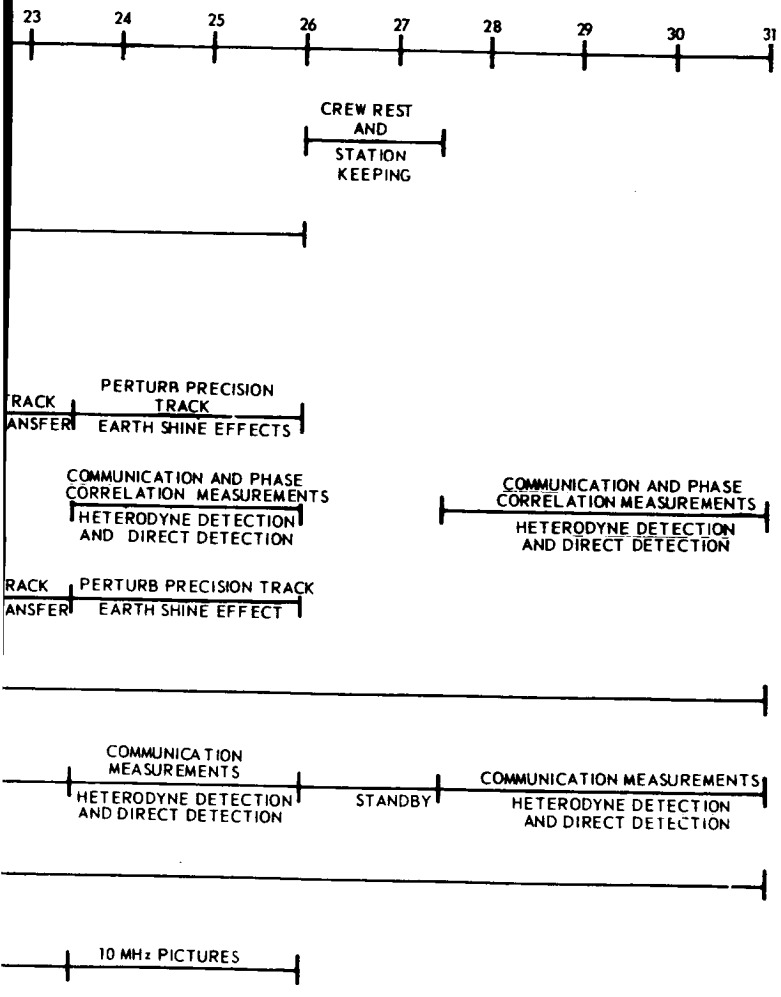

15
16
17
18
19
20
21
22
CREW REST AND STATION KEEPING
CREW REST AND STATION KEEPING
10 MHz
TONES AND PICTURES
PRECISION TRACKING
OPEN LOOP
POINT AHEAD
W WO TRANSIT DELAY
PRECISION TRACKING
OPEN LOOP
TONES ONLY
COMMUNICATION MEASUREMENTS
HETERODYNE DETECTION AND DIRECT DETECTION
STANDBY
TONES ONLY
STANDBY

Figure 12.0-1.



Portion of Mission Flight Plan in Time-Line Form

S/A Switching Action
SM Service Module
SPS Service Propulsion System

12.1 MISSION GROUNDRULES

In developing the flight plan, several groundrules were stipulated and incorporated into the formulation of this representative OTES mission.

The mission flight plan groundrules include the following:

1. The CSM/OM spacecraft will be designed with the capability to be launched on any day of the month (consistent with natural environment considerations) during the single daily launch window that provide optimum performance.

2. The CSM/OM vehicle will be launched due east from the Merritt Island Launch Area, Cape Kennedy, into a 100 n. mile earth parking orbit inclined at 28.5° to equator.

3. Injection into transfer ellipse will be performed with perigee and subsequent apogee over equator.

4. The S-IVB booster guidance and control system will be used to guide the CSM/OM vehicle until the termination of transfer ellipse injection.

5. The CSM G&N system will be used to guide the CSM vehicle until the termination of synchronous orbit and transearth transfer injection.

6. At apogee, a 28.5° plane change and synchronous orbit circularization maneuver will be performed simultaneously. This will result in a synchronous orbit situated over the equator.

7. All three crewman will be in space suits during launch, delta V, EVA and entry functions.

8. At least one astronaut will be wearing a vented or pressurized space suit at all times during flight. In the vented condition, the faceplate may be either open or closed.

9. All three crewmen will be restrained in the CM crew couch system during the boost, delta V, transposition and docking, dedocking and separation, re-entry, parachute deployment and touchdown phases of the mission.

10. The crew will be awakened four hours prior to earth lift-off and eat a low-residue meal.

11. Under nominal conditions, a crewman will stay awake not more than eighteen hours.

12. During delta V and EVA functions, all three crewman will be awake.

13. During the last two days of preflight preparation, the crew will utilize oral and suppository Dulocolax.

14. Each crewman will be occupied with inflight life sustenance functions twelve or less hours each day. These mission hours for life sustenance will consist of: one or two periods of rest and sleep totalling six to eight hours (normally eight hours except when body movements, involved in crew work rotation and changeover or alteration in work and rest periods, will degrade a programmed optical technology experiment); three one hour meal periods of food and water preparation, consumption, and leftover disposal; four ten minute periods for isometric exercises; two ten minute periods for medical monitoring; and one hour for personal hygiene.

15. Inflight time frames, not programmed for spacecraft control, station-keeping and optical technology experiments, will be allocated for crew life sustenance functions.

16. The total daily metabolic load for each crewman will be 11,200 BTU's for a pressurized vehicle and 12,00 BTU's for a depressurized vehicle.

17. The daily water production for each crewman will be 4.0 lbs for a pressurized vehicle and 9.8 lbs for a depressurized vehicle.

18. The daily carbon diodide production for each crewman will be 2.12 lbs for a pressurized vehicle and 2.27 lbs for a depressurized vehicle.

19. The daily oxygen production for each crewman will be 1.84 lbs for a pressurized vehicle and 1.97 lbs for a depressurized vehicle.

20. The daily water consumption for each crewman will be 6.6 lbs for a pressurized vehicle and 12.4 lbs for a depressurized vehicle.

21. The daily urine production for each crewman will be 2.6 lbs for both pressurized and depressurized vehicle.

22. The CSM IMU and AGC will be operating during the entire manned synchronous orbit to maintain CSM/OM attitudes and provides capability for continuous MSFN communications.

23. During a period when optical technology experiments are being conducted, which require a stably oriented OM, the flight crew will be physically restrained in a containment system and their body motions will be minimized.

24. Body motions may occur under the #1 telescope precision-tracking/open-loop-mode during crew work rotation and changeover and alteration in work and rest periods. However, these motions will be performed carefully by the crew, so as not to disturb a line of sight exceeding 30 arc-seconds, which is the field of view of the telescope.

25. The CSM/OM spacecraft design will be such that, in synchronous orbit during optical technology experiment functions, periodic stationkeeping will be performed in the CM and OM. This periodic stationkeeping will consist of: CM and OM ECS status checks every two hours; CM and OM C&I and CES status test every four hours; CSM RCS, SPS Parameter and Propellant System status checks every four hours; CM and OM EPS status tests every six hours; and ECS CO_2 absorber filter replacement every twelve hours.

26. The CSM will supply the OM with all oxygen requirements when both vehicles are docked and when man is performing optical technology experiment setup and operation functions.

27. The CSM will provide primary G&N, SCS and RCS capabilities for CSM/OM attitude reorientations during the manned synchronous orbit mission.

28. During rest and sleep periods, the CM couch restraint system will be designed to prevent a crewman from performing body motions which will induce CSM/OM perturbations.

29. Under nominal conditions, a crewman will egress from the CM main hatch during EVA, though backup egressing can occur through the OM side hatch.

30. Prior to EVA preparation under nominal conditions, the OM will be sealed from the CM by reinstalling and securing the OM pressure hatch.

31. EVA preparation will extend for thirty minutes with a minimal five minutes from CM repressurization from 0.0 to 5.0 psia.

32. Post EVA will extend for sixty-two minutes with a minimal fifty-three minutes for CM repressurization from 0.0 to 5.0 psia.

12.2 MISSION FLIGHT PLAN VARIABLES

This flight plan of man-machine functions during synchronous orbit has been developed conservatively to minimize the overall mission time duration. However, a number of flight-related extenuating conditions may realistically extend the duration of the mission.

The optical technology communications and atmospheric physics experiments should occur during periods of opportune weather and atmospheric conditions. Inopportune conditions may delay the operation of the experiments to later mission time frames.

A flight crewman may inadvertently initiate unprogrammed motions of a magnitude and direction to cause OM perturbations. The perturbations, in turn, may disrupt fine tracking during such experiment as phase correlation measurements, communication with megahertz bandwidth, and optical heterodyne detection on the spacecraft and earth. If fine tracking is disrupted and the OM has reverted to an intermediate or coarse tracking mode, then the statistical purposes in the experiments would be compromised. To avoid this condition, a contingency procedure will have to be implemented to re-achieve fine tracking before the nominal fine tracking operations can be resumed.

Instrumentation associated with CSM and OM stationkeeping and optical technology experiments may malfunction during flight and such degraded modes may require the crew to perform diagnostic troubleshooting and remedial maintenance functions.

Another extenuating condition, involving potential sunlight impingement upon telescope sensors, may occur as the earth, sun and CSM/OM geometry changes. In order to avoid this condition, the operation of optical technology experiments will have to be postponed or interrupted for periods of two-and-a-half hours.

For these salient reasons, the flight plan for the manned synchronous orbit mission (table 12.2-1) is extended an additional thirty per cent or 77.25 mission hours. This time frame extension is placed in a section of the flight plan preceding CSM/OM preparation for dedocking and unmanned OM experiment operations.

After post-CSM separation from the OM and during flight crew return to the earth, the unmanned portion of the synchronous orbit mission will commence. The flight crew, prior to their OM departure, will checkout and place the OM guidance, stabilization control and other stationkeeping systems, as well as the optical technology communications and atmospheric physics experiments, into the proper operating modes. This checkout and setup will enable ground-based control of the unmanned OM spacecraft during synchronous orbit stay time. The ground will also be able to conduct all the optical technology communications and atmospheric physics experiments, e.g., pulse distortion measurements, phase correlation measurements, communication with megahertz bandwidth, optical heterodyne detection on earth and on the OM, and direct detection optical communication from space to ground. The objectives in running these experiments are twofold in nature: (a) to obtain long-term statistical data; and (b) to obtain measurements during the widest possible variety of atmospheric conditions.

For the first of these two objectives, a synchronous orbit mission running periods of many hours or days will be desirable. The initial unmanned tests should be conducted during a period of relatively static air mass behavior to avoid interruptions due to the statistical nature of the first experiment objective.

For the second objective, the period of operation will be determined by temporal characteristics of the atmospheric condition being explored. For example, it will be interesting to conduct all six communications and atmospheric physics experiments during an orderly air mass frontal passage, such as a warm front. This type of exploration, however, in subject to the hazard of an increasing cloud cover, resulting in intermittent establishment of the propagation link.

TABLE 12.2-1

MANNED SYNCHRONOUS ORBIT MISSION FLIGHT PLAN

Mission Time	Mission Event
Hr/Min/Sec	
Launch Phase	
Start	
00.00.00	S-IC ignition and liftoff.
00.02.31	S-IC engine cutoff and separation.
00.02.34	S-II ignition.
00.02.54	LES tower jettison.
00.09.02	S-II engine cutoff and separation.
00.09.03	S-IVB engine ignition sequence.
00.11.52	S-IVB engine cutoff and start earth orbit coast.
Earth Orbit Phase	
00.20	Perform G & N and ECS status checks.
00.26	Perform EPS status check.
00.30	Perform SM-RCS and EMS status checks.
00.34	Perform CM-RCS status check.
00.38	Perform C&W lights check.
00.42	S-IVB ullage vent 1.
01.11	S-IVB ullage vent 2.

TABLE 12.2-1 (CONTINUED)

Mission Time	Mission Event
Start	
01.12	Perform IMU fine alignment and checks.
01.28	Perform landmark NAV sightings.
01.42	S-IVB ullage vent 3.
01.49	Perform landmark NAV sightings.
01.54	Perform SM-RCS, ECS and EPS status checks.
02.11	S-IVB ullage vent 4.
02.12	Perform trajectory and ephemeris computation.
02.30	Obtain transfer ellipse injection parameter data.
02.33	Perform IMU coarse alignment.
02.38	Perform IMU fine alignment.
02.41	S-IVB ullage vent 5.
02.45	Perform IMU fine alignment check
02.48	Perform SCS attitude alignment.
02.50	Prepare AGC for transfer ellipse injection.
03.01	S-IVB Propulsion System ignition and transfer ellipse injection.
Transfer Ellipse Phase	
03.06	Compute and check delta V parameters with programmed parameters and MSFN data.
03.09	Perform SM-RCS check.
03.10	Perform delta V SPS gimbal securing.
03.11	Orient vehicle to specified attitude for transposition and docking.
03.14	Perform ECS status check.
03.15	Obtain and insert IMU alignment data in AGC.
03.16	Place G & N in attitude control mode.
03.21	Initiate CSM/OM/S-IVB separation and transposition.
03.41	Pressurize OM and transit tunnel and perform CSM/OM hard docking.

TABLE 12.2-1 (CONTINUED)

Mission Time	Mission Event
Start	
03.49	Initiate CSM/OM separation from S-IVB.
03.53	Perform ECS, SM-RCS, SPS Parameter and Propellant, EPS, CM-RCS and SPS status checks.
04.04	Perform transfer ellipse NAV sightings 1 through 6.
05.00	Perform ECS and EPS status checks.
06.00	Perform ECS and EPS status checks.
06.52	Perform ECS and EPS status checks.
06.54	Perform transfer ellipse NAV sightings 7 through 12.
07.41	Perform IMU coarse alignment.
07.43	Maneuver CSM/OM to bisect two reference stars with CM optics.
07.46	Maintain bisector attitude with SCS attitude control mode.
07.52	Perform IMU fine alignment and check.
08.01	Perform SCS attitude alignment.
08.02	Obtain synchronous orbit injection parameter data.
08.10	Perform EPS, ECS, CES, SPS, SM-RCS, and G & N status checks and preparation for injection.
08.17	Turn on SPS propellant gauging subsystem.
08.20	SM-RCS ullage ignition and ullage acceleration monitoring.
08.21	SPS ignition and synchronous orbit injection.
Synchronous Orbit Phase Manned Pre-Experiment Period	
08.25	Confirm synchronous orbit acquisition.
08.25	Set G & N and PU controls.
08.30	Perform ECS, SPS Parameter and Propellant, SM-RCS, and EPS status checks.
08.48	Activate S-band and align high gain antenna with MSFN.
08.50	Perform IMU coarse alignment.
08.56	Perform IMU fine alignment.

TABLE 12.2-1 (CONTINUED)

Mission Time		Mission Event
Start		
08.59		Place high gain antenna in automatic track mode.
09.02		Perform IMU fine alignment check.
09.03		Maneuver CSM/OM to desired synchronous orbit attitude.
09.10		Perform orbital NAV sightings 1 through 6.
09.48		Check OM cabin pressure for leakage.
09.49		Equalize CM and interlock pressure.
09.51		Remove and stow CM pressure hatch.
09.53		Remove and stow CM thermal hatch.
09.54		Perform CM EPS status check.
09.55		Disconnect and stow probe in CM.
09.57		Perform ECS status check.
09.58		Disconnect and stow drogue in CM.
10.02		Set OM cabin pressure equalization.
10.04		Open OM hatch.
10.06		One man transfer to OM.
10.08		CM/OM communication check.
10.11		Activate and checkout OM stationkeeping subsystems.
10.25		Erect solar panels.
Synchronous Orbit Phase/Manned Experiment Period		
Note: CM and OM stationkeeping events will be performed over the duration of this period as specified in Flight Plan Groundrule 25.		
Start	End	
11.00	14.00	Turn on and stabilize #1, #2 and #3 telescope lasers and associated electronics.
11.00	359.15	Switch on timer for cumulative exposure experiment box. Degradation of optical materials and coating experiment.
11.10	14.00	Align #1 telescope secondary and primary mirrors.
16.00	17.00	Align #3 telescope 10.6 transmitter.
17.00	20.00	Align #2 telescope 0.6328 transmitter.

TABLE 12.2-1 (CONTINUED)

Mission Time		Mission Event
Start	End	
22.00	26.00	Conduct tests on laser transmitter performance and perform optical and electrical adjustments.
28.00	30.00	Resume test and adjustment activity.
30.00	32.00	Verify #1, #2 and #3 telescope alignment and associated equipment operation.
34.00	35.00	Perform IMU fine alignment, NAV sightings and trajectory determination.
NOTE: The #1, #3 and #3 telescopes are earth oriented.		
35.00	66.00	Perform #1, #2 and #3 telescope laser experiments including: Pulse distortion measurements; phase correlation measurements; communication with megahertz bandwidth; optical heterodyne detection on earth; optical heterodyne detection on the spacecraft; direct detection optical communication from space to ground; precision tracking of a ground beacon; transfer tracking from one ground station to another; and point-ahead and space to ground loop closure.
NOTE: An activity time-line of these laser experiments are illustrated in figure 12.0-1.		
74.00	74.30	Prepare for EVA.
74.30	74.40	Deflate and stow pneumatic suspension system in 1.25 meter experiment well (EVA). Alignment of large optics in space experiment.
74.40	75.40	Deploy primary and secondary mirror (EVA).
75.40	76.42	Perform post-EVA functions.
76.42	77.42	Perform IMU fine alignment, NAV sightings and trajectory determination.
79.42	80.32	Install autocollimator and align secondary mirror to autocollimator. Verification of thin mirror nesting principle experiment.
80.32	81.32	Align secondary to primary mirror.
81.32	81.52	Check image plane.

TABLE 12.2-1 (CONTINUED)

Mission Time		Mission Event
Start	End	
81.52	82.52	Align and evaluate primary mirror.
84.52	86.37	Setup and align mirror, evaluate smoothness, and observe surface. Primary mirror figure test and correction experiment.
86.37	87.07	Apply heat to mirror and record surface changes.
89.07	91.37	Perform precision tracking with changed earthshine effects. Precision tracking of ground beacon experiment.
91.37	92.37	Re-evaluate primary mirror. Verification of thin mirror nesting principle experiment.
92.37	93.37	Perform IMU fine alignment, NAV sightings and trajectory determination.
95.30	112.00	Perform #1, #2 and #3 telescope laser experiments including: all communications and atmospheric physics experiments; precision tracking experiment.

Note: The ordering of these experiments are similar to the experiments illustrated in figure 12.0-1.

114.00	115.00	Perform SCS attitude maneuver with OM #4 telescope reoriented to space.
115.00	115.30	Apply heat to mirror and record surface changes. Primary mirror figure test and correction experiment.
115.30	116.30	Perform IMU fine alignment, NAV sightings and trajectory determination.
116.30	116.45	Evaluate primary mirror sensitivity and response time to thermal corrections. Primary mirror figure test and correction experiment.
118.45	142.45	Alignment of #4 telescope fine guidance, electrical checkout and tracking of simulated star. Fine guidance experiment.

TABLE 12.2-1 (CONTINUED)

Mission Time		Mission Event
Start	End	
124.00	124.15	Evaluate primary mirror sensitivity and response time to thermal corrections. Primary mirror figure test and correction experiment.
142.45	143.00	Evaluate primary mirror sensitivity and response time to thermal corrections.
143.00	144.00	Perform IMU fine alignment, NAV sightings and trajectory determination.
146.00	146.30	Perform star acquisition and refinement to fine pointing. Fine guidance experiment.
146.30	151.30	Perform pointing stability tests with fine sensor and attitude control system #1.
154.00	159.00	Perform pointing stability tests with fine sensor and attitude control system #2.
161.00	162.00	Perform SCS attitude maneuver with OM #1, #2 and #3 telescopes reoriented to earth.
162.00	163.00	Perform IMU fine alignment, NAV sightings and trajectory determination.
165.00	181.30	Perform all laser communications and atmospheric physics experiments with the #1, #2 and #3 telescopes.

Note: The ordering of these experiments are similar to the experiments illustrated in figure 12.0-1.

183.00	184.00	Perform SCS attitude maneuver with OM #4 telescope reoriented to space.
184.00	185.00	Perform IMU fine alignment, NAV sightings and trajectory determination.
187.00	187.30	Perform star acquisition and refinement to fine pointing. Fine guidance experiment.

TABLE 12.2-1 (CONTINUED)

Mission Time		Mission Event
Start	End	
187.30	193.30	Perform pointing stability tests with fine sensor and attitude control system #3.
194.30	199.30	Perform pointing stability tests with fine sensor and attitude control system #4.
201.30	206.30	Perform pointing stability tests with fine sensor and attitude control system #5.
208.30	208.50	Evaluate all five fine sensor and attitude control systems.
208.50	210.20	Perform Ronchi test pattern line adjustments and expose film to the #5 telescope 24 inch segmented mirror. Segmented optics experiment.
210.20	211.20	Perform SCS attitude maneuver with OM #4 telescope boresighted to same target as #5 telescope.
211.20	211.50	Photograph target image in #4 telescope.
213.50	217.00	Acquire guide star, stabilize the #4 telescope mount with gimbals unlocked and fine loop disabled, switch to fine tracking mode, and perform unprogrammed and programmed body motions. Comparison of isolation techniques experiment.
225.00	225.30	Prepare for EVA.
225.30	226.10	Erect interferometer short beam (EVA). Interferometer system experiment.
226.10	227.12	Perform post-EVA functions.
227.12	223.00	Monitor short beam stability vibration and image quality during unprogrammed body motions and CSM/OM attitude maneuvers.
233.00	233.30	Prepare for EVA.
233.30	234.10	Erect interferometer long beam (EVA).
234.10	235.12	Perform post-EVA functions.

TABLE 12.2-1 (CONTINUED)

Mission Time		Mission Event
Start	End	
239.00	243.00	Monitor long beam stability vibration and image quality during unprogrammed and programmed body motions and CSM/OM attitude maneuvers.
245.00	256.00	Conduct short beam, long beam, and ultraviolet interferometer operations.
258.00	259.00	Perform SCS attitude maneuver with OM #1, #2 and #3 telescopes reoriented to earth.
259.00	260.00	Perform IMU fine alignment, NAV sightings and trajectory determination.
262.00	278.30	Perform all laser communications and atmospheric physics experiments with the #1, #2 and #3 telescopes.

Note: The ordering of these experiments are similar to the experiments illustrated in figure 12.0-1.

Note: The flight plan for the manned synchronous orbit experiment period constitutes an additional thirty per cent or 80.25 mission hours. The rationale for this time frame extension is discussed in section 12.2, mission flight plan variables.

358.45	359.15	Prepare for EVA.
359.15	359.28	Remove test panel from cumulative exposure experiment box and stow in CM. Install new test panel into experiment box (EVA). Degradation of optical materials and coating experiment.
359.28	360.30	Perform post-EVA functions.

Synchronous Orbit Phase/Manned Post-Experiment Period

Start		
362.30		Perform OM G & N, SCS, RCS, EPS and C & I checkout and place into ground control operational modes.
363.30		Perform OM #1, #2 and #3 telescope instrumentation status checks and place into ground control operational modes.

TABLE 12.2-1 (CONTINUED)

Mission Time	Mission Event
Start	
364.00	Retrieve and install OM pressure and thermal hatches.
364.10	Retrieve and install drogue in OM.
364.20	Retrieve and install CM pressure and thermal hatches.
364.30	Communicate OM jettison countdown operations to MSFN.
364.32	Ignite sharped changes to separate CSM from OM.
364.33	Translate CSM away from OM.

Note: OM commences synchronous orbit phase/unmanned experiment period. The period is discussed in the later part of section 12.2 Mission Flight plan variables.

364.36	Perform IMU fine alignment.
364.37	Perform ECS and EPS status checks.
364.42	Perform IMU fine alignment.
364.45	Perform NAV sightings.
365.05	Perform G & N status checks.
365.20	Perform SM-RCS and SPS status checks.
365.50	Perform ECS status checks.
365.59	Perform IMU fine alignment and check.
366.19	Perform NAV sightings.
366.44	Determine CSM trajectory.
366.45	Perform ECS and EPS status checks.
366.51	Acquire transearth coast injection parameter data and compare with MSFN data.
366.54	Perform IMU coarse alignment.
367.05	Perform IMU fine alignment and check.
367.12	Maneuver CSM to desired transearth coast injection attitude.
367.14	Perform SCS alignment.
367.18	Perform SCS, G & N, CES, SPS, SM-RCS and EPS preparation for transearth coast injection.
367.28	Initiate SM-RCS ullage and SPS ignition and cutoff for transearth coast injection.

TABLE 12.2-1 (CONTINUED)

Mission Time	Mission Event
Transearth Coast and Re-Entry Phase	
Start	
367.30	Perform post delta V gimbal motor shutoff, EPS, SPS Parameter and Propellant, and ECS status checks.
367.45	Perform G & N operation check.
368.05	Determine CSM trajectory.
368.08	Perform IMU coarse alignment.
368.23	Perform IMU fine alignment and check.
368.32	Perform SCS attitude alignment.
368.36	Perform SCS, G & N, CES, SPS, SM-RCS and EPS preparation for delta V.
368.46	Initiate SM-RCS ullage and SPS ignition and cutoff for midcourse correction.
368.48	Perform post delta V gimbal motor shutoff, EPS, SPS Parameter and Propellant, and ECS status checks.
369.35	Perform ECS and EPS status checks.
369.48	Perform G & N operation check.
370.08	Obtain trajectory parameters for delta V from MSFN.
370.13	Perform IMU coarse alignment.
370.28	Perform IMU fine alignment and check.
370.42	Maneuver CSM to desired delta V attitude.
370.48	Perform SCS attitude alignment.
370.52	Perform SCS, G & N, CES, SPS, SM-RCS and EPS preparation for delta V.
371.02	Initiate SM-RCS ullage and SPS ignition and cutoff midcourse correction.
371.04	Confirm delta V acquisition with MSFN.
371.06	Perform post delta V gimbal motor shutoff, EPS, SPS Parameter and Propellant, SM-RCS, CM-RCS, and EPS status checks.
371.16	Perform IMU coarse alignment
371.33	Perform IMU fine alignment and check.
371.34	Perform EMS status check and ECS preseparation check.
371.37	Perform SCS alignment.
371.40	Maneuver CSM to MSFN confirmed CM-SM separation attitude.

TABLE 12.2-1 (CONTINUED)

Mission Time	Mission Event
Start	
371.50	Perform EPS separation operations.
371.51	Activate mission sequence logic and pyrotechnic CM-SM separation.
371.56	Perform CM-RCS, mission sequences, and EPS post-separation checks.
372.30	Perform CM-RCS, ECS, G & N and SCS entry checks.
372.33	Maneuver CM to MSFN confirmed entry attitude.
372.44	Initiate CM entry operations.
373.02	Perform CM touchdown operations.

13.0 TYPICAL OTAES SUBSYSTEM/COMPONENT SUMMARY

13.1 GENERAL

Previous sections of this report have described means by which data may be obtained for the development of optical technology. Certain experiments have been identified by which desired data may be collected. Because of the similarity and commonality of many functional components in various experiments, integrated experimental packages are conceived. The integrated package permits one experimental package to fulfill the functional requirements of several experiments.

Chrysler's past participation in major launch vehicle and spacecraft programs have revealed the necessity for investigating conceptual applications of hardware at the earliest opportunity in a program. This approach provides assurance that conceptual techniques are within the anticipated state-of-the-art at the projected time of systems development.

During the conceptual/feasibility phase of this program, acceptable systems approaches and equipment concepts were considered in conjunction with the assessment of engineering and technological requirements. The result of this approach provides the definition of limits for conceptual and theoretical technological development. These limits were then used in the development of the program plan followed during this phase of the study.

The individual experiment functional requirements were integrated into conceptual experiment packages. An equipment list for each experiment package and a systems part list for each proposed spacecraft configuration were developed. These are summarized in tables 13.2-1 and 13.3-1. The development of the equipment list and systems part list, utilizing existing state-of-the-art components and Apollo subsystems, provides preliminary design criteria for the next phase of this program. In addition, these lists represent a point of origin for conceptual design refinements in later phases of the program.

13.2 INTEGRATED EXPERIMENT PARTS LIST

A parts list of the major components required in each of the proposed telescopes and experiment wells is presented as table 13.2-1. Pictorial **presentations of these experiment packages are presented here as well as in preceeding sections of this report:**

Experiment Package Title	Figure Number
a. OTAES 1.0M & 0.3M Laser Telescope Gimbaled Assembly	8.2-1
b. 0.3M Telescope Gimbaled Assembly	8.4-1
c. Interferometer Fine Guidance Segmented Optics Assembly	9.1-1

d. Primary Mirror Test Well Assembly	4.10-1b and 4.11-6
e. Fine Guidance Test Well Assembly	Not presented; equip. requirements similar to c. above minus Interferometer components.

13.3 SPACECRAFT SYSTEMS PART LIST

A parts list of required major systems in each of the proposed spacecraft configurations is presented as table 13.3-1. This considers major systems presently utilized in the Apollo program wherever possible. Modifications of these systems, that are required to adapt them to use in the OTAES, have not been reflected in this parts list. Such modification shall be considered in later phases of this study.

Pictorial presentations of the four proposed configurations are presented in the following figures of this report:

Configuration Number	Figure Number
1	11.2.1-1 & -2
2	11.2.2-1 & -2
3	11.2.3-1 & -2
4	11.2.4-1 & -2

13.4 SPACECRAFT SYSTEMS COMPONENTS LIST

A parts list of typical major components in several spacecraft systems is presented as table 13.4-1. Each spacecraft system has been analyzed as to its required function; however, each system has not been analyzed as to component requirements. During the design phase of this study each system will be analyzed and designed to meet the desired functional requirements dictated by mission objectives.

INTEGRATED EXPERIMENT PARTS LIST
TABLE 13.2-1

A. OTAES 1.0M AND 0.3M LASER TELESCOPE GIMBALED ASSEMBLY

1. Outer Tube Assembly

2. 1.0M Laser Telescope Assembly
   a. Inner Tube Assembly
   b. Baffle System Subassembly
   c. Optical Bench
   d. Gimbal System
   e. Pressurized Hatch Subassembly
   f. Insulation Barrier
   g. Secondary Mirror Adjustment Subassembly
   h. Secondary Mirror
   i. Primary Mirror
   j. Primary Mirror Support
   k. Galilean Ocular
   l. Fine Beam Deflector
   m. Beam Deflection Circuit
   n. Point Ahead Diasporometer
   o. Pupil Matching Telescope, Typ 5 places
   p. 6238 Å Modulator
   q. 6238 Å Laser Transmitter
   r. 6238 Å Beam Splitter
   s. 6238 Å Transmission Monitor
   t. Shutter and Mirror Subassembly
   u. 4880 Å Beam Splitter, Typ 6 places
   v. 4880 Å Pyramid Prism Reflector Tracker
   w. 4880 Å Modulator
   x. 4880 Å Oscillator/Receiver
   y. $\lambda/4$ plate
   z. $\lambda/4$ filter
   aa. Polarization Analyzer
   bb. 4880 Å Detector, Typ 4 places

3. 0.3M Laser Telescope Assembly
   a. Inner Tube Subassembly
   b. Inner Tube Interconnect Structure
   c. Baffle System Subassembly
   d. Optical Bench
   e. Pressurized Hatch Subassembly
   f. Insulation Barrier
   g. Secondary Mirror Adjustment Subassembly
   h. Secondary Mirror
   i. Primary Mirror
   j. Primary Mirror Support

INTEGRATED EXPERIMENT PARTS LIST
TABLE 13.2-1
(CONTINUED)

k. Galilean Ocular
l. Point Ahead Diasporometer
m. Beam Splitter
n. Transmission Monitor
o. Pupil Matching Telescope, Typ 2 places
p. Modulator
q. 10.6μ Laser Transmitter

B. 0.3M TELESCOPE - GIMBALED ASSEMBLY

1. Outer Tube Assembly
2. Pressure Hatch Assembly
3. Baffle
4. Baffle Ejection Mechanism, Typ 4 places
5. Gimbal System, Single
6. Inner Tube Assembly
7. Optical Bench
8. Primary Mirror
9. Primary Mirror Support
10. Secondary Mirror
11. Secondary Mirror Support
12. Insulation Barrier
13. Galilean Ocular
14. Fine Beam Deflector
15. 6238 Å Laser Oscillator/Receiver
16. Detector, Typ 4 places
17. λ/2 Plate
18. λ/4 Plate
19. λ/4 Plate Filter
20. Polarization Analyzer
21. Pupil Matching Telescope, Typ 2 places
22. Beam Splitter, Typ 4 places
23. 4880 Å Pyramid Prism Reflector Tracker
24. Modulator, 4880 Å
25. Mirror, Typ 2 places
26. Transmission Monitor
27. Flip Mirror
28. Point Ahead Diasporometer
29. Pupil Matching Telescope, Typ 2 places
30. Modulator, 6238 Å
31. 6238 Å Laser Transmitter

C. INTERFEROMETER FINE GUIDANCE SEGMENTED OPTICS ASSEMBLY

1. Outer Tube Assembly
2. Baffle System Subassembly, Typ 2 places

INTEGRATED EXPERIMENT PARTS LIST
TABLE 13.2-1
(CONTINUED)

3. Baffle Erection Subassembly, Typ 4 places
4. Secondary Mirror
5. Secondary Mirror Support
6. Segmented Optics Camera
7. Segmented Optics Camera Mirror
8. Segmented Optics Camera Mirror Support
9. Coarse Astro Tracker
10. Coarse Astro Tracker Support
11. Mirror Figure Test Flat Secondary Subassembly
12. Mirror Figure Test Flat Secondary Drive Subassembly
13. Segmented Mirror, Primary
14. Segmented Mirror Support and Control Subsystem
15. Segmented Mirror Control Pressure Bottles
16. Segmented Mirror Figure Tester
17. Interferometer Boom Tubular Subassembly
18. Interferometer Boom Truss Subassembly
19. Interferometer Lens Shade Subassembly
20. Interferometer Objective Lens
21. Interferometer Flat Mirror
22. Interferometer Flat Mirror Support
23. Interferometer Flat Mirror Support Control
24. Interferometer Diagonal Flat Mirror
25. Interferometer Diagonal Flat Mirror Support
26. Interferometer Diagonal Flat Mirror Fine Adjustment
27. Interferometer Diagonal Flat Mirror Erection Mechanism
28. Interferometer Intermediate Error Sensor
29. Interferometer Intermediate Error Diagonal Mirror
30. Interferometer Intermediate Error Diagonal Mirror Support
31. Interferometer Corrector Primary Diagonal Mirror
32. Interferometer Corrector Secondary Diagonal Mirror
33. Interferometer Corrector Unit
34. Interferometer Alignment Image Unit
35. Microscope
36. TV Camera
37. Primary Mirror
38. Primary Mirror Support
39. Secondary Mirror
40. Secondary Mirror Support
41. Tertiary Mirror
42. Fine Pointing Diasporometer, Typ 2 places
43. Fine Pointing Diagonal Mirror
44. Fine Pointing Diagonal Mirror Support
45. Fine Error Sensor
46. Reference Image Aperature Subassembly

INTEGRATED EXPERIMENT PARTS LIST
TABLE 13.2-1
(CONTINUED)

D. PRIMARY MIRROR TEST WELL ASSEMBLY

1. Outer Tube Assembly
2. Hatch Assembly, Typ 2 places
3. Pressure Relief Valve, Typ 4 places
4. Optical/Alignment Instrumentation Assembly
5. Secondary Mirror
6. Secondary Mirror Support Assembly
7. Primary Mirror, Thin Wall
8. Primary Mirror Support Assembly
9. Rotating Mirror
10. Rotating Mirror Support
11. Porthole Assembly
12. Primary Mirror
13. Primary Mirror Support
14. Secondary Mirror
15. Secondary Mirror Support
16. Secondary Mirror Alignment Mechanism

E. FINE GUIDANCE SEGMENTED OPTICS ASSEMBLY

1. Outer Tube Assembly
2. Baffle System Subassembly, Typ 2 places
3. Baffle Erection Subassembly, Typ 4 places
4. Secondary Mirror
5. Secondary Mirror Support
6. Segmented Optics Camera
7. Segmented Optics Camera Mirror
8. Segmented Optics Camera Mirror Support
9. Coarse Astro Tracker
10. Coarse Astro Tracker Support
11. Mirror Figure Test Flat Secondary Subassembly
12. Mirror Figure Test Flat Secondary Drive Subassembly
13. Segmented Mirror, Primary
14. Segmented Mirror Support and Control Subsystem
15. Segmented Mirror Control Pressure Bottles
16. Segmented Mirror Figure Tester
17. Primary Mirror
18. Primary Mirror Support
19. Secondary Mirror
20. Secondary Mirror Support
21. Tertiary Mirror
22. Fine Pointing Diasporometer, Typ 2 places
23. Fine Pointing Diagonal Mirror

INTEGRATED EXPERIMENT PARTS LIST
TABLE 13.2-1
(CONTINUED)

24. Fine Pointing Diagonal Mirror Support
25. Fine Error Sensor
26. Reference Image Aperature Subassembly

ITEM NO.	PARTS LIST	SPACECRAFT CONFIGURATION				
		1	2	3		4
				"A"	"B"	
1	OTAES 1.0M & 0.3M Laser Telescope - Gimbaled Assembly	X	X	X		
2	0.3M Telescope Gimbaled Assembly	X	X	X		
3	Interferometer Fine Guidance Segmented Optics Assembly	X				
4	Primary Mirror Test Well Assembly	X			X	X
5	Fine Guidance Segmented Optics Assembly		X		X	X
6	LEM Ascent Stage	X				X
7	LEM/Experiment Module Adapter	X				X
8	Experiment Module Structure Assembly	X	X	X	X	X
9	Experiment Module Adapter		X	X	X	
10	Docking Part Assembly		X		X	
11	Solar Panel/Support Assembly	X	X	X	X	X
12	Electrical Power Distribution System	X	X	X	X	X
13	Data Acquisition and Conditioning System	X	X	X	X	X
14	Data Transfer System	X			X	X

SPACECRAFT SYSTEMS PART LIST

TABLE 13.3-1

ITEM NO.	PARTS LIST	SPACECRAFT CONFIGURATION				
		1	2	3		4
				"A"	"B"	
15	Data Transmission System		X	X		
16	Spacecraft Control System		X	X		
17	RF Tracking System		X	X		
18	Experiment/Ground Control System		X	X		
19	Experiment/Spacecraft Control System	X	X		X	X
20	Interferometer Storage Rack Assembly	X				
21	LEM/CSM Communication System	X				X
22	LEM/Experiment Module Intercom System	X				X
23	Reaction Control System	X	X		X	X
24	Environmental Control System	X	X		X	X
25	CSM/Experiment Module Intercom System		X		X	

SPACECRAFT SYSTEMS PART LIST
TABLE 13.3-1 (Continued)

A. Attitude Control System

1. Command Receiver
2. Command Decoder
3. Control Moment Gyro
4. Control Gyro
5. Spin Motors
6. Torque Motors
7. Sensors
8. Amplifiers
9. Transponder Receiver
10. Command Detector
11. Command Decoder
12. Guidance Computer
13. Inertial Measuring Unit

B. Solar Panel/Support Assembly

1. Panel Frame
2. Panel Arms
3. Drive Mechanism
4. Sun Sensor
5. Position Indicator
6. Solar Panels

C. Data Acquisition and Conditioning System

1. Transducers
2. Digital Multiplexer
3. Converter
4. Programmer
5. Analog Multiplexes
6. Calibrator
7. Signal Conditioner
8. Power Amplifier
9. Transceivers
10. Pre-Mod Processor
11. Signal Conditioner
12. Recorder
13. Vidio Amplifier

D. Data Transmission System

1. Low Gain Antenna
2. High Gain Antenna
3. RF Switches
4. Transponder Receiver
5. Command Detector
6. Command Decoder
7. Vidio Tape Recorder

Spacecraft System's Components List
Table 13.4-1

D. Data Transmission System (cont)

8. Synd Generator
9. Transponder Transmitter
10. Telemetry Modulator
11. Telemetry Data Handling
12. Mode Controller
13. Transmission Rate Controller
14. Power Amplifier
15. Power Divider

E. RF Tracking System

1. Signal Generator
2. Modulation Filter
3. Transmitter
4. Antennas

F. Experiment/Ground Control System

1. High Gain Antenna
2. Low Gain Antenna
3. Command Receiver
4. Command Decoder
5. Control Gyro
6. Sensor
7. Amplifier
8. Guidance Computer
9. Inertial Measuring Unit
10. Transponder Receiver
11. Command Detector
12. Command Decoder
13. Signal Generator

G. Reaction Control System

1. Thrusters
2. Oxidizer Tank
3. Fuel Tank
4. Helium Tank
5. Valves
6. Heaters
7. Selenoid Valves

H. Environmental Control System

1. Oxygen Control Assembly
2. Oxygen Surge Tank
3. Nitrogen Control Assembly
4. Backup Oxygen Tank

Spacecraft System's Components List
Table 13.4-1 (continued)

H. Environmental Control System (cont)

5. Main Shutoff Valve
6. Cabin Pressure Regulator
7. Fluid Tank Pressure Regulator
8. Cabin Pressure Relief Valves
9. Cyclic Accumulator Selector Valves
10. Suit Compressor
11. CO_2 and Odor Absorber
12. Suit Heat Exchanger
13. Oxygen Demand Pressure Regulator
14. Portable Water Shutoff Valve
15. Water Pressure Relief Valve
16. Waste Water Tank
17. Supplemental Water Tank
18. Water Chilling Assembly
19. Cabin Recirculation Blowers
20. Glycol Temperature Control Valve
21. Glycol Evaporator
22. Cabin Temperature Control Valve
23. Cabin Heat Exchanger
24. Glycol Pump Assembly
25. Lines, check valves, etc.

I. Electrical Power Distribution System

1. Batteries
2. Battery Charger
3. Series Regulator
4. Shunt Regulator
5. Invertor
6. DC-DC Inventor
7. Resistive Load Bank
8. Cables
9. Terminal Boards
10. Busses
11. Switch Selector
12. Power Monitor
13. Command and Control Package
14. Heaters

Spacecraft System's Components List
Table 13.4-1 (continued)